Injectable Nanoemulsions for the Delivery of Anticancer Agents

Loruthai, Orathai

Awarding institution:
King's College London

Injectable Nanoemulsions for the Delivery of Anticancer Agents

Orathai Loruthai

A thesis submitted in partial fulfillment of the requirements
for the degree of
Doctor of Philosophy

in the

Faculty of Life Sciences & Medicine

King's College London

November 2017

Abstract

Oil-in-water nanoemulsions (NE), comprising of an oil dispersed in a water and stabilised by a surfactant, have been increasingly explored as vehicles for the delivery of poorly-water soluble drugs. This interest stems from the ability of NE to increase the apparent aqueous solubility of such drugs. The aims of the current study were several fold and included the determination of the molecular architecture and physico-chemical properties of NE to determine their suitability as vehicles for the parenteral delivery of the hydrophobic drugs, testosterone propionate (TP), curcumin (CUR) and docetaxel (DTX) and establishing the cytotoxicity of NE towards CT26 and HeLa cancer cell lines. Finally a folate derived surfactant was synthesised to explore targeting of the NE.

The study involved the preparation and physico-chemical characterisation of NE stabilised by a range of nonionic surfactants, sometimes in combination with another surfactant and/or cosurfactant. The systems studied included Brij O10 (B), Tween 80 (T), Tween 80 with the cosurfactant, Dermosoft GMCY (TD), and Tween 80 with Dermosoft GMCY and lecithin (TDL). The NE contained as oil, either one of a series of triglyceride oils (namely tripalmitin (hTPN), soybean oil (hSBO), triolein (hGTO), and tristearin (hGTS)) or one of a series of ethyl ester of fatty acid oils (namely ethyl oleate (hEO) and ethyl stearate (hES)). A range of physico-chemical techniques including the phase inversion temperature (PIT), photon correlation spectroscopy (PCS), small angle neutron scattering (SANS), and UV spectroscopy, were used to characterise the NE in terms of their size and shape and ability to solubilise drug.

The Brij O10 NE containing hSBO (B20-hSBO), hTPN (B20-hTPN), hGTO (B20-hGTO) and hEO (B20-hEO) exhibited a larger area of NE formation whereas those containing GTS (B20-hGTS) and ES (B20-hES) produced only a small area of NE existence. The TDL NE incorporated only small amounts of SBO (TDL25-hSBO), while in contrast TD-stabilised NE were found to incorporate high amounts of the oil, EO (TD25-98hEO). The PIT and PCS studies recorded an increase in the PIT and apparent hydrodynamic size upon the addition of oil, suggesting that large molecular volume oils formed a distinct oil core in the NE. A significant enhancement in TP solubilisation in B20 NE was seen with an increase in the amount of oil in the following clear or slightly hazy NE, namely B20-hSBO, B20-85hTPN, B20-99hTPN, B20-99hGTO and B20-98hEO. However, there was a dramatic decrease in TP solubilisation when the B20-

hSBO, B20-85hTPN and B20-99hTPN NE were either cloudy or milky. Interestingly the addition of oil to B20, TD25 and TDL25 micelles did not significantly improve the solubility of CUR and DTX. Solubilisation and PIT studies suggested that both CUR and DTX tended to sit in the surfactant shell. After fitting the SANS data for the all of the NE studied, it was clear that the model which consistently provided the best fit was that of an oblate ellipsoid in which the radius of core of the NE increased with oil content. In addition, the shape of the NE became considerably more elongated as the oil content increased, explaining the decrease in TP solubilisation observed in the cloudy or milky NE.

The cytotoxicity of NE in HeLa and CT26 cell lines suggested that blank B20 NE were toxic while blank TD25 and TDL25 NE were far less toxic. TD25 NE containing 98hEO and TDL25 NE containing hSBO did not show any difference in toxicity in the absence and absence of CUR (a high-dose anticancer agent). As a consequence therefore, DTX (a low-dose anticancer drug) was selected for further study. TDL25 NE containing hSBO in the presence of DTX exhibited a significant different in cytotoxicity when compared to blank TDL25-hSBO NE. In order to selectively deliver DTX to solid tumours expressing folate receptor, folate derived BO10 was successfully synthesised and characterised.

In conclusion, these results suggest that the NE containing a large molar volume oil are the most suitable for the parenteral administration of a poorly water-soluble drug. However, before use the morphology of the NE and the nature of the drug to be solubilised should be carefully examined as both have an effect on the level of solubilisation in the NE.

Acknowledgements

My deepest gratitude goes to my supervisor, Professor Jayne Lawrence for the opportunity, resources and support to complete the work for this thesis. Without her guidance, patience and encouragement, the work presented in this thesis would not be possible.

I also would like to acknowledge my second supervisor, Professor Khuloud Al-Jamal for providing direction and discussion for the cell culture experiments and for the docetaxel. Many thanks to Dr. Julie Tzu Wen Wang and Izzat Bin Mohamed Suffian for their help with the cytotoxicity tests.

I am also grateful to Professor Robert Hider, Dr. Vincenzo Abbate and Junpei Li for their help with the synthesis and analysis of folate derived Brij O10.

Many thanks to the Rutherford Appleton Labs (RAL) for providing neutron beam time for this work. Special thanks to Dr. Ann Terry for offering her expertise without hesitation on instrument setup and neutron data analysis. I would also like to thank Dr. Peixun Li who synthesised the deuterated triolein (dGTO).

I wish to thank all members of the Pharmaceutical Biophysics Group who are always friendly and helpful, especially Yuvared Luangwitchajaroen, Lili Cui, Yussif Saaka, and Yanan Shao.

I would love to acknowledge the Royal Thai Government Scholarship for providing the financial support for this research. I am indebted to the National Nanotechnology Center (NANOTEC) for nominating me for the scholarship and granting me educational leave to undertake my research.

Finally, I would like to thank my family for their love and support. I am more thankful that they continue to share their prayers and keep me constantly motivated.

Table of Contents

List of Figures

List of Tables

Abbreviation

$(\partial\Sigma/\partial\Omega)$	differential scanning cross-section
ΔA	increase in the interfacial area
ΔS	change in entropy of the system
60hEO	protiated ethyl oleate (purity >60 %)
60hGTS	protiated tristeatin (purity >60 %)
65hGTO	protiated triolein (purity 65 %)
85hTPN	protiated tripalmitin (purity 85 %)
98.6dTPN	deuterated tripalmitin ($–d_{98}$, 98.6 atom%D)
98dGTO	deuterated triolein ($–d_{51}$, 98 atom%D)
98hEO	protiated ethyl oleate (purity 98 %)
99hES	protiated ethyl stearate (purity 99 %)
99hGTO	protiated triolein (purity 99 %)
99hGTS	protiated tristearin (purity 99 %)
99hTPN	protiated tripalmitin (purity 99 %)
Å	Angstrom
a	major semi-axis
A	area
b	minor semi-axis
B	Brij O10
BCS	Biopharmaceutics Classification System
b_i	coherent neutron scattering length of nucleus i
B_i	incoherent background scattering
Brij 35	polyoxyethylene (23) lauryl ether
Brij 99	polyoxyethylene-20- oleyl ether, $C_{18:1}E_{20}$
Brij O10	polyoxyethylene (10) oleyl ether, $C_{18:1}E_{10}$, Brij 97, Brij 96

cmc	critical micelle concentration
CP	cloud point
CPP	critical packing parameter
CT26	murine colon cell line
CUR	curcumin
D	Dermosoft GMCY
D	bulk density of the molecule
D	diffusion coefficient
d	molecular length scale
DCC	dicyclohexylcarbodiimide
D_h	hydrodynamic diameter
DLS	dynamic light scattering
DMF	dimethylformamide
DMSO	dimethylsulphoxide
DTX	docetaxel
ε_c	axial ratios of core
ε_s	axial ratios of shell
F(Q)	single particle form factor
FR	folate receptor
g	gram
h	hour
HeLa	folate-expressing cervical-tumour-derived cell line
HLB	hydrophile−lipophile balance
hSBO	protiated soybean oil
I(Q)	neutron flux
I(Q)	intensity of scattering
ILL	Institut Laue Langevin

Abbreviation	
IPM	isopropyl myristate
k	Boltzmann constant
k_i	incident wave vector
K_m	weight mixing ratio
k_s	scattered wave vector
L	lecithin
Log P	partition coefficient in octanol−water
L_{sd}	distance of 2-dimensional detector from the sample
m	mass
m	metre
ME	microemulsion
min	minute
mol vol	molecular volume
MTT	3-(4, 5-dimethylthiazol-2-yl)-2, 5-diphenyltetrazolium bromide
MW	molecular weight
n	neutron refractive index
n	number of carbon atom in the hydrocarbon chain
n	number of polyoxyethylene groups
n	mole fraction
N_A	Avogadro’s constant
N_{agg}	aggregation number
NE	nanoemulsion
NMR	nuclear magnetic resonance
o/w	oil-in-water
P(Q)	form factor
PBS	phosphate buffer saline
PCS	photon correlation spectroscopy

Abbreviation	
PEG	polyethyleneglycol
PES	polyethersulfone
PIT	phase inversion temperature
POE	polyoxyethylene
POP	polyoxypropylene, POE-polyoxypropylene
Q	scattering vector
R_1	core equatorial radius
RAL	Rutherford-Appleton Laboratory
R_c	radius of core
r_{det}	radial distance
R_s	radius of shell
S(Q)	interparticle structure factor
SANS	small angle neutron scattering
SAXS	small angle X−ray scattering
SLD	scattering length density
SSE	sum of squared errors
T	temperature
T	Tween 80
TP	testosterone propionate
TPN	triplamitin
Tween 20	polyoxyethylene sorbitan monolaurate
Tween 80	polyoxyethylene sorbitan monostearate
UPW	ultrapure water
UV	ultraviolet-visible spectroscopy
V_{core}	volume of core
V_m	molar volume
V_{med}	volume of growth medium

V_{shell}	volume of shell
V_{sp}	volume of cell suspension
w/o	water-in-oil
X	axial ratio
x	core axial ratio
γ	interfacial tension
$\Delta G_{formation}$	free energy of emulsion formation
ΔG_I	interfacial free energy
η	viscosity
η	packing-density parameter
θ	scattering angle
λ	wavelength
ρ	density
ρ	scattering length density of solute
ρ_0	density of solvent
ρ_c	scattering length density of core
ρ_m	scattering length density of medium
ρ_s	scattering length density of shell
ρ_{SLD}	scattering length density
$\rho_{solvent}$	scattering length density of solvent
Φ	volume fraction

Chapter 1
General Introduction

1.1 Background

Recent advances in drug discovery such as combinatorial chemistry and high throughput screening have led to the identification of large numbers of compounds with good therapeutic potential, however many of these compounds have extremely poor water solubility and fall into class II or IV of the Biopharmaceutical Classification Scheme (BCS) (Lipinski et al., 2001). Poor-water solubility is one of the major obstacles for drugs attempting to reach the biological compartments. The definition of drug solubility is shown in **Table 1.1**.

Table 1.1 The definition used in statements of approximate solubilities (British Pharmacopoeia, 2013).

Definitions	Approximate volume of solvent in mL per gram of solute
Very soluble	Less than 1
Freely soluble	From 1 to 10
Soluble	From 10 to 30
Sparingly soluble	From 30 to100
Slightly soluble	From 100 to 1000
Very slightly soluble	From 1000 to 10000
Practically insoluble	More than 10000

The poor aqueous solubility is a particular problem if the drug is intended for intravenous administration, and as such as might be the cause of failure in the treatment of cancers. In previous studies, a wide variety of techniques have been attempted to improve the aqueous solubility of drugs intended for intravenous administration including using water-soluble organic solvents, cyclodextrin complexation, micelle, microemulsions (ME), nanoemulsions (NE), nanoparticles, liposome, niosomes or nanosuspensions (Strickley, 2004; Gulati and Gupta, 2011; Hamman and Steenekamp, 2012; Savjani et al., 2012). Nanoemulsions have attracted a lot of attention due to the number of potential benefits of nanoemulsions including improved stability, high optical clarity and the increased

bioavailability of any encapsulated lipophilic compounds and the less cytoxicity compared to micellce formulations (McClements, 2012; Warisnoicharoen et al., 2003).

Another major obstacle in drugs reaching the biological compartment(s) in which they act, is their limited transport across a range of biological barriers. These biological barriers can include the reticulo-endothelial system, endothelial or epithelial membranes, a complex network of blood vessels and abnormal flow of blood. These barriers are particularly problematic for biomolecules where they represent limiting steps in the delivery of such molecules to their intended site of action (**Figure 1.1**).

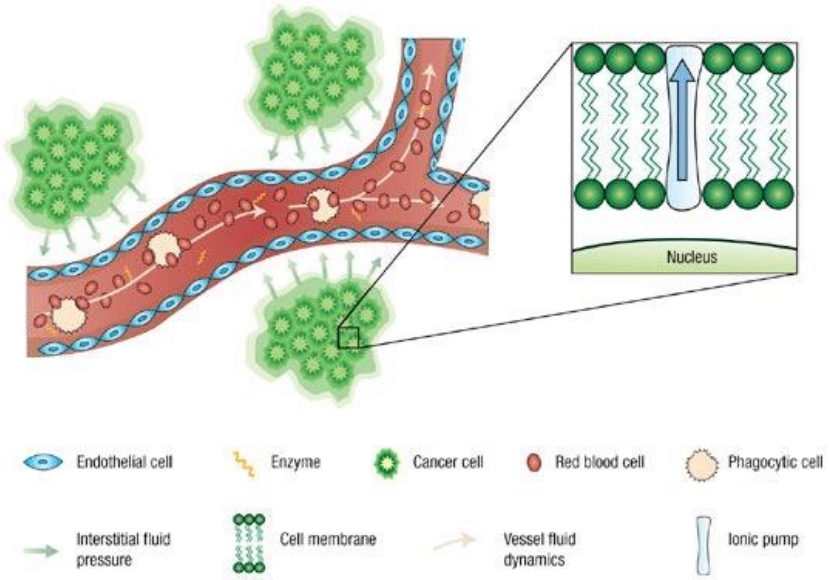

Figure 1.1: Obstacles or biological barriers that prevent injected chemicals, biomolecules, drug carriers and other foreign agents from reaching their intended site of action. (Copied from Sanhai et al., 2008)

In this study, nanoemulsions intended for the delivery of poorly-water soluble drugs, such as testosterone propionate (TP), curcumin (CUR) and docetaxel (DTX) will be formulated. The formulations will be prepared from nonionic surfactants including polyoxyethylene surfactants, Brij O10 or Polysorbate surfactants, Tween 80 in the absence or presence of cosurfactant and triglyceride/ethyl ester in water. All materials used in the preparation of NE are pharmaceutically acceptable and safe for intravenous use (Strickley, 2004; Date and Nagarsenker, 2008). In order to develop and design NE suitable for delivering a drug to its intended site of action, it is essential to understand the morphology of the NE. The physico-chemical characterisation of the drug-free and drug-containing formulations will also be examined using a range of techniques such as photon correlation spectroscopy (PCS), phase inversion temperature (PIT), small angle neutron scattering (SANS). The ability of NE to solubilise drugs is also important and will be performed using UV spectroscopy. The cytotoxicity of the resulting drug-containing

nanoemulsion formulations will be tested *in vitro* using HeLa (folate-expressing cervical-tumour-derived cell line) and CT26 (murine colon carcinoma) cell lines. It is also possible to attach a targeting group to the surface of NE to directly target NE to its intended site of action in the body and achieve drug targeting. Therefore, folate derived Brij O10 in which folate is covalently attached to Brij O10 via a polyethyleneglycol (PEG) linker will be synthesised. It has been reported that the folate receptor (FR) is frequently elevated in epithelial, ovarian, cervical, lung, kidney, colorectal and breast cancer (Praveen Kumar and Divya, 2015). Therefore, this receptor-targeting strategy has been exploited in the present study in the delivery of anticancer agents, and can be used as an ideal receptor to specifically target.

1.2 Nanoemulsions

1.2.1 Definition

Nanoemulsions (NE) are emulsions with an extremely small droplet size. In the current scientific literature, there is significant confusion about the use of the terms NE and "microemulsions" (ME) (Gutierrez et al., 2008; McClements, 2012) because of the prefixes used to describe them. The term of "micro-" means 10^{-6}, while the term of "nano" means 10^{-9}, which suggests that the particle size of ME is 1000 times larger on average than that of NE. However, the fact is the particle size of ME are smaller than that of the NE. The reason for this confusion is that the word ME was used before the particle size of the particles could be measured and had become well-established before the nanotechnology was introduced.

In addition, there are many similarities between both types of colloidal dispersions. For example, both of them typically comprise of an oil phase, a water phase, a surfactant, and sometimes a cosurfactant. In terms of size, recent literature has stated that the upper particle size of NE droplets could be as large as 500 nm (Anton et al., 2008), although upper limits of 200 nm (Tadros et al., 2004; Solans et al., 2005; Huang et al., 2010) and 100 nm (Rao et al., 2012) have all been widely quoted. Recently McClements (2012) has suggested that an upper limit of 100 nm would lead to a number of potential benefits of NE including improved stability, high optical clarity and the increased bioavailability of any encapsulated lipophilic compounds. Although there is some variability in the size range quoted for NE, a particle size range of 20-200 nm is most typically seen (Solans et al., 2005), in contrast to the widely quoted size range of 5-100 nm for ME. Normally, the physical appearance of a ME is clear, while that of a NE can be clear, translucent, or

cloudy. In this context it is worth noting that the appearance of a colloidal system is generally transparent or translucent when the dispersed particle size is less than 30 nm (Wooster et al., 2008). In addition to size and appearance, there is another major difference between ME and NE, that is ME are thermodynamically stable while NE are thermodynamically unstable, although they can be kinetically stable (Anton and Vandamme, 2011). As a result, ME are spontaneously formed by simply admixing the required ingredients, while NE need to be produced by adding energy. The difference between the property of microemulsion and nanoemulsion was shown in the **Table 1.2**.

Table 1.2 The difference between nanoemulsion and microemulsion

Property	Nanoemulsion	Microemulsion
Size	20-200 nm	5-100 nm
Appearance	Clear, translucent, or cloudy	Clear
Stability	Thermodynamic unstable but kinetically	Thermodynamic unstable
Preparation	Simply admixing	Addition of energy

1.2.2 Structure

NE are typically composed of oil, water, surfactant and possibly a cosurfactant. Oil-in-water (o/w) NE possess a disperse phase of oil which is separated from the aqueous phase by a monolayer of surfactant. The hydrophobic portion of surfactant is in contact with the disperse oil phase whereas the surfactant's hydrophilic head groups are in contact the continuous aqueous phase. On the other hand, water-in-oil (w/o) NE similarly contain an interfacial surfactant monolayer but show a reversed configuration in which the surfactant head groups are the centre of the droplets containing the aqueous phase, while the hydrocarbon chains of the surfactant are expressed on the exterior and contact the non-polar phase (Izquierdo et al., 2005; Morales et al., 2006; Sadtler et al., 2010,).

In this study, only an o/w NE, i.e. a system suitable for encapsulating hydrophobic drug in an oil phase, are of interest. o/w NE, consisting of oil surrounded with surfactant molecules dispersed in an aqueous phase, were examined for their ability to solubilise poorly water-soluble drugs. As a NE possesses an oily core, they should be able to increase apparent aqueous solubility over the corresponding micelles, assuming the drug has a good solubility in the relevant oil. **Figure 1.2** shows schematic diagram of NE containing oil, water and surfactant.

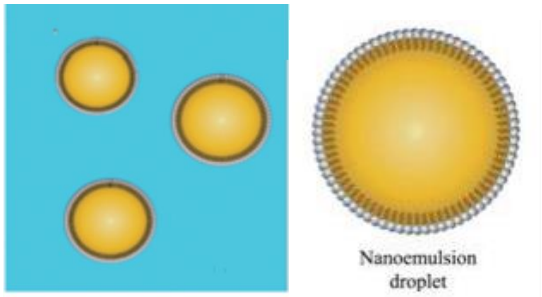

Figure 1.2: Schematic diagram of nanoemulsions and microemulsions containing oil, water and surfactant (modified from McClements, 2012).

1.2.3 Composition

Nonionic surfactants are used in various pharmaceutical formulations including micelles, ME and NE (Matsuyama et al., 2006; Feng et al., 2009; Maali and Mosavian, 2013) since they exhibit better compatibility, improved stability, and reduced toxicity when compared to ionic, or amphoteric surfactants (Jiao, 2008). As surfactants poses a polar head group and nonpolar hydrocarbon chain they exhibit a wide range of interfacial activities and functions as emulsifiers (Kumar and Rajeshwarrao, 2011). Due to the uncharged head group present in nonionic surfactants, these surfactants are less sensitive than ionic surfactants to salt, changes in pH and ionic strength of the water phase, although they are quite sensitive to temperature changes (Li et al., 2009). The surface tension at the concentration that polyethoxylated nonionic surfactants can form aggregates (i.e. the critical micelle concentration) is usually higher than that of ionic surfactants (Jiao, 2008). This tends to make the nonionic surfactants less destructive towards cell membranes and therefore less toxic and less irritating. Moreover, as nonionic surfactants are usually more bulky in size, they tend to be less well adsorbed onto surfaces and are less polar, therefore they tend to associate together at a lower cmc to reduce the free energy of the system (Jiao, 2008).

Polyoxyethylated nonionic surfactants are widely employed in various pharmaceutical applications. Examples of this class of surfactant are the polysorbates, polyoxyethylene sorbitan, Tyloxapol, poloxamers, Brij and Cremophor EL (Jiao, 2008). These surfactants are generally defined as polymeric ethers because all of them contain as their hydrophilic moiety, polyoxyethylene or polyethylene glycol. This polymer is a repeated structure of polyoxyethylene, $(CH_2CH_2O)_n$ where n is the number of polyoxyethylene groups. The most common polyoxyethylene nonionic surfactant is described as being an ethylene oxide alkyl ether type and is represented as C_mE_n, where m and n are the number of the

carbon atoms in the hydrocarbon chain, and the number of oxyethylene groups, respectively (Inoue and Yamakawa, 2011). The solubility of these nonionic surfactants in water depends on the length of alkyl chain and the number of oxyethylene groups in their structure. According to the HLB system, the higher percentage weight of the polyoxyethylene, the higher HLB value of the surfactant, the higher its solubility in water (Jiao, 2008). In the present study, the use of the polyoxyethylene nonionic surfactant, polyoxyethylene 10-oleyl ether ($C_{18:1}E_{10}$) to stabilise the NE is attractive because it is possible to use it to produce ME without recourse to a cosurfactant and, as well, it is possible to use it for the microemulsification of many oils (Malcolmson et al., 1997; Ko et al., 2003).

When formulating a NE to deliver drug, it is very important to determine which oils can form NE with a given surfactant. The choice of the oil is crucial because the oil has an effect on both the area of nanoemulsion existence and the solubilisation capacity of the NE (Malcolmson et al., 1997; Warisnoicharoen et al., 2000a; Djekic and Primorac, 2008). Frequently, amphiphilic oils such as the medium- or long-chain triglyceride and the fatty acid ester are utilised in the pharmaceutical, food and cosmetic industries because they are compatible with biological systems and are more environmentally friendly compared to hydrocarbon oils. Medium-chain and long-chain triglycerides from vegetable oils are usually used in commercial applications because these oils can provide desirable physical and drug absorption properties (Hauss, 2007). For example lymphatic transport can be promoted by long-chain triglycerides to deliver drug into the lymph before entering the systemic circulation to avoid hepatic first-pass metabolism (Khoo et al., 2003). Note that triglycerides are made up of three fatty acids and a glycerol backbone. The length of their carbon atom chains and the number of double bonds can be varied by the fatty acids that compose the structure of the triglycerides. Long-chain triglycerides tend to be solubilised to a lower extent by PEG-8 caprylic/capric glycerides surfactant than their medium-chain triglycerides counterparts (Djekic and Primorac, 2008). On the other hand, previous studies have shown that Brij O10 containing NE can, surprisingly, solubilise more long-chain triglycerides than medium- or short-chain triglycerides (Warisnoicharoen et al., 2000a). Therefore, the formation of NE depends on both the structure of oils and surfactants.

1.2.4 Formation

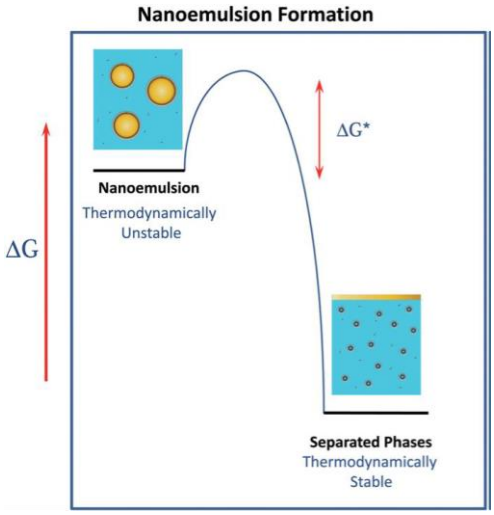

Figure 1.3: Differences in the free energy of NE systems compared with their phase separated state (bulk oil and water phases) (copied from McClements, 2012).

Oil, water, surfactant and an in-put of energy are needed to prepare emulsions. **Figure 1.3** shows the differences in the free energy of NE systems compared with their phase separated states (i.e. bulk oil and water phases). Nanoemulsions have a higher free energy than the phase separated state. The free energy of emulsion formation ($\Delta G_{formation}$) is considered to depend on the interfacial free energy (ΔG_I) and the configuration entropy term ($-T\Delta S$) which is illustrated by following equation (Tadros et al., 2004):

$$\Delta G_{formation} = \Delta G_I - T\Delta S$$

where ΔS is the change in entropy of the system, effectively the dispersion entropy, and T is the temperature. The interfacial free energy (ΔG_I) is equal to the increase in the interfacial area between the oil and the aqueous phases (ΔA) multiplied by the interfacial tension (γ) at the oil-water interface at constant temperature, pressure and interfacial chemical potential:

$$\Delta G_I = \Delta A\gamma$$

In addition, the interfacial free energy term (ΔG_I) is usually positive as increasing the contact area and the interfacial tension both require the input of energy. Therefore, this term always opposes NE formation. The free energy of the preparation of an emulsion can be considered from the energy required to expand the interface, $\Delta A\gamma$ (where ΔA is the change of interfacial area upon emulsification when the bulk oil with area A_1 produces a large number of oil droplets with area A_2, and the value of A_2 is much higher than that of A_1). Since γ is positive, the energy to expand the interface is large and positive.

The configuration entropy (-TΔS) is dependent upon the number of different arrangements of the oil within the system. The configuration entropy is always negative because the number of possible arrangements of the oil phase in an emulsified state is much greater than in a non-emulsified state, and therefore the configuration energy always favours the formation of a colloidal (emulsified) dispersion.

It was known that the interfacial tension of the system depends on the curvature of the surfactant monolayer. NE are formed when the interfacial tension at the oil-water boundary in the emulsified system is similar to the interfacial tension at a planar oil-water interface. However, upon decreasing particle size, the interfacial free energy becomes increasingly less negative or more positive (i.e. unfavourable to the formation of a colloidal dispersion) due to an increasing contact area, while the configuration free energy becomes more negative (i.e. favourable to the formation of a colloidal dispersion) as the oil droplets increase the number of different ways in which the oil can be organised. Overall, the total free energy change becomes increasingly positive because the interfacial free energy term dominates over the configuration entropy term. This results in NE formation which although is a thermodynamic unstable system, possess sufficient kinetic stability to be used as a drug delivery vehicle (Girard et al., 1997; Tadros et al., 2004).

1.2.5 Preparation

In terms of preparation, NE always require the input of external energy to convert the separated oil and water phases into a (thermodynamically unstable) colloidal dispersion. NE are usually prepared by the input of external energy, the power of which depends upon the physico-chemical mechanism of the droplet disruption. Generally, one of the techniques to produce NE are the high-energy emulsification procedures, such as microfluidizers, high-pressure homogenizers, sonicators and ultrasound generators (Schultz et al., 2004; Kentish et al., 2008; Gaikwad and Pandit, 2008; McClements, 2013). On the other hand, NE can be prepared by low-energy emulsification procedures such as phase inversion temperature (PIT), phase inversion composition and self-emulsifying methods (Izquierdo et al., 2005; Maestro et al., 2008; McClements, 2013). In these cases, smaller NE droplets are formed when the system undergoes a phase inversion in response to a change in either composition and/or temperature (Mason et al., 2006). Indeed, PIT is one of the low energy methods used to produce nanoemulsions (Forgiarini et al., 2001a; Forgiarini et al., 2001b; Izquierdo et al., 2002).

Phase inversion temperature (PIT)

Nonionic surfactants of the polyethoxylene type used in the preparation of NE have been studied by Shinoda and co-workers (Shinoda et al., 1969). The behaviour of these surfactants is very dependent on the experimental temperature and they become hydrophobic with increasing temperature due to the dehydration of the polyoxyethylene head groups. In fact o/w NE, of very small and uniform droplet size, stabilised by nonionic surfactants are typically prepared by the PIT method (Morales et al., 2003; Izquierdo et al., 2004; Rao et al., 2010). When an o/w emulsion prepared using this type of surfactant is heated at a phase inversion temperature, the emulsion converts to a w/o emulsion. By rapid cooling of the emulsion that is prepared at a temperature near the PIT, the transition of w/o emulsion to o/w emulsion occurs. In addition, very stable and small emulsion droplets can be produced (Tadros et al., 2004).

In the present study, NE will be prepared using the phase inversion temperature (PIT) method, which results in the formation of optically transparent colloidal dispersions by heating a mixture of oil, water and surfactant (and possibly cosurfactant or second surfactant) to just above the phase inversion temperature of the system and then cooling the mixture to ambient with continuous and vigorous stirring.

1.2.6 Application of nanoemulsions in drug delivery

The interest in NE in terms of their application in drug delivery application has increased in recent years, as evidenced by the many publications and the fact that some NE are commercialised and are on the market. **Table 1.2** lists some commercially available NE formulations (Gulati and Gupta, 2011). The attraction of NE for pharmaceutical applications is increasing because their many beneficial properties including their transparency, their small droplet size, high surface area which makes them suitable for the efficient delivery of active ingredients, their ease of preparation, their highly kinetically stability and their ability to be sterilised by filtration as well as their solubilising capacity which can improve the apparent aqueous solubility of a wide range of drug molecules, especially poorly-water soluble drugs (Kentish et al., 2008; Maestro et al., 2008; Shah et al., 2010). Indeed the potential ability of NE to increase drug solubility and stability are among some of the most important reasons why NE are attractive drug delivery systems (Brime et al., 2002; Shafiq et al., 2007; Date and Nagarsenker, 2007). The ability of NE to increase drug solubilisation over the

corresponding micelles is considered to be a consequence of the fact that drug is soluble in the oil that comprises the micelle core.

Table 1.3 Commercially available nanoemulsion formulations (Gulati and Gupta, 2011).

Drug	**Brand**	**Company**	**Indication**
Propofol	Diprivan®	Astra Zeneca	Anesthetic
Dexamethasone	Limethason®	Mitsubishi Pharmaceuticals	Steroid
Flurbiprofen axetil	Ropion®	Mitsubishi Pharmaceuticals	Non-steroidal analgesic
Vitamin A, D, E, K	Vitalipid®	Fresenius Kabi	Parenteral nutrition

O/w NE have been widely employed for their ability to increase the solubilisation and bioavailability of hydrophobic drug molecules. NE have been shown to enhance the oral bioavailability of a wide range of drugs (Shafiq et al., 2007; Singh and Vingkar, 2008). There have been a number of studies into the application of NE as drug carriers for a whole range of administration routes including intravenous (Ahmed et al., 2008), transdermal (Dixit et al., 2008), and pulmonary (Bivas-Benita et al., 2004). In an o/w NE, it is widely considered that hydrophobic drug molecules are solubilised within the oil core while more hydrophilic drug molecules are located at a boundary between the hydrophobic chains of the surfactant and the surfactant head group depending on their hydrophilicity (Torchilin, 2001). The primary locus of drug solubilisation depends on drug hydrophobicity and its interaction with the oil, surfactant and/or cosurfactant.

1.2.6.1 NE for parenteral administration

NE are used as injectable drug delivery vehicles for a variety of purposes including the administration of nutrition (fats, carbohydrates or vitamins), for controlled drug release, targeting of drugs to specific sites in body and the delivery of vaccines or as gene carriers (Pan et al., 2003; Tamilvanan et al., 2004). The benefit of NE in the parenteral administration of drugs is partly due to the small droplet size of these formulations - a strict requirement of this route of administration.

Oils used in the parenteral administration

The choice of oils used in NE formulations is a crucial factor for the preparation of o/w NE as an oil with a maximum solubilising potential for the selected drug(s) can help to achieve the maximum drug loading in NE. In addition, the ability of the selected oil to

yield systems with a large NE existence region is also important. The oily components available for parenteral NE range from fixed oils (e.g. soybean oil, castor oil), medium chain triglycerides (e.g. triglycerides of capric/caprylic acids), fatty acid esters (e.g. ethyl oleate, isopropyl myristate, isopropyl palmitate) (Date and Nagarsenkar, 2008).

Surfactants used in the parenteral administration

The selection of surfactant is important for the formulation of NE. The surfactant or combination of surfactants used should favour nanoemulsification of the oil phase and possess good solubilizing potential for the selected drugs. It should be noted that no surfactant is completely harmless. For instance, PEG-35-castor oil, a surfactant with very good parenteral acceptability can cause a range of adverse effects including anaphylactic shock and histamine release (Tije et al., 2003). Such adverse effects must be considered when selecting a type and the concentration of surfactant to use. The choice of the surfactant is also governed by the type of the NE to be formulated. Low HLB surfactants such as the sorbitan monoesters (Span) are preferred for w/o NE whereas high HLB surfactants such as Tween 80 are preferred for o/w NE. In several cases, a mixture of lipophilic (low HLB) and hydrophilic (high HLB) surfactant may be required to formulate a NE or ME. The various class of surfactant that can be used for the parenteral ME range from the polysorbates (Tween 20, Tween 80), the sorbitan esters (e.g. Span 20), the PEO–PPO-block copolymers (Poloxamer 188), the polyoxyethylene alkyl ethers (POE-10-oleyl ether), POE castor oil (POE-35-castor oil), POE hydrogenated castor oil (Cremophore RH 40, Cremophore RH 60), POE-stearate (PEG-660-12-hydroxystearate) and phospholipids (soybean lecithin, egg lecithin, diolelyl phosphatidyl choline, distearoyl phosphatidyl glycerol, PEGylated phospholipids, dimyristoyl phosphatidyl choline). Among the various surfactants that are available for producing NE and ME, the lecithins, poloxamers and polysorbates are the most preferred (Strickley, 2004).

1.3 Physico-chemical characterisation of micelles and nanoemulsions

As NE have attracted attention as potential drug delivery systems, the relationship between their solubilisation capacity and physicochemical properties needs to be fully explored. There are a wide range of different techniques that can be used to characterise NE. NE have been characterised with respect to their composition by establishing the phase behaviour, the size and shape of the NE droplets (Yuan et al., 2008; Kuntsche et al., 2011, Sharma and Warr, 2012). An excellent understanding of the influence of the

physicochemical properties of the NE droplets is required for the best application and use of NE.

1.3.1 Phase behaviour

The study of phase behaviour is used to determine the types of NE formed and their area of existence, as well as stability, all of which is related to the composition of the three main components; oil, surfactants and water. Phase diagrams are prepared simply and can show a large amount of information relating to the phase behaviour of a NE system. Each apex of the triangle represents 100% of that component. The region can be separated into w/o or o/w NE by simply considering the amount of water and oil in the composition. **Figure 1.4** illustrates some of the possible structures that are usually formed by a mixture of oil, surfactant and water including micelles, NE, ME and bilayers (Talegaonkar et al., 2008).

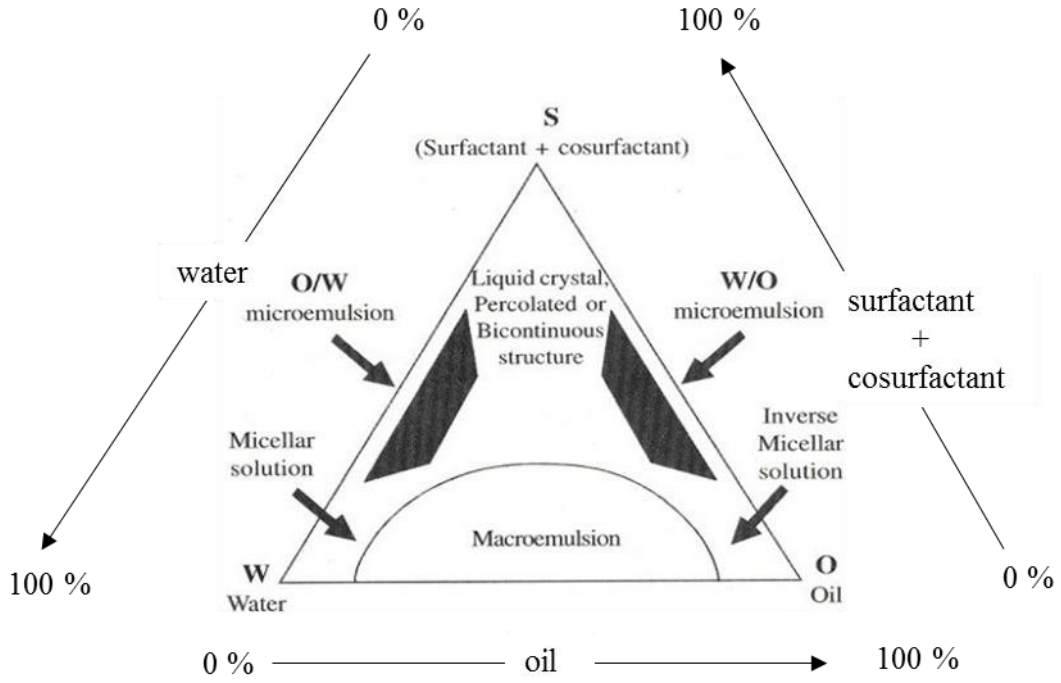

Figure 1.4: Schematic diagram illustrating the phase behaviour of oil/water/surfactant systems. (modified from Talegaonkar et al., 2008).

1.3.2 Phase inversion temperature (PIT)

In NE prepared using a nonionic surfactant, the transition from o/w to w/o NE typically occurs upon altering either the phase volume and/or temperature. It is known that most nonionic surfactants, especially the polyoxyethylene surfactants, form aqueous micellar solutions which exhibit a phase inversion temperature (PIT) when heated (Corti et al., 2002). Once the temperature of o/w NE reaches the PIT, the NE turns from clear to cloudy

and vice versa, as the temperature is increased and decreased, respectively. However, note that it is not possible to observe the PIT of a cloudy NE. The PIT occurs because the interactions between the surfactant molecules in the aggregate change from repulsive to attractive forces at higher temperature. For example, increasing the temperature of polyoxyethylene ether surfactant solutions in water causes the dehydration of ethylene oxide head groups. These changes lead to a decrease in the area of the effective surfactant head group and the shape of the aggregate which may become elongated or bicontinuous. Finally, the formation of w/o structure occurs which depends on the surfactant: oil ratio (Tadros, 2005). The data obtained from the PIT experiments can be used to give indirect information of the location and arrangement of the oil within the surfactant aggregate. Typically, the changes in PIT are explained in terms of the way in which oils of different molecular volume/weight are solubilized within the droplets (Schubert and Kaler, 1996). When there is a decrease in PIT of NE compared to the cloud point (CP) of the corresponding micelle, it can be assumed that the aggregates of micelle are probably slightly asymmetric and have become even more asymmetric on the addition of oil, probably because of the oil chains mixing with the surfactant chains, in much the same way as a cosurfactant does (Wasutrasawat, 2011). In contrast, an increase in the PIT with an increasing amount of oil present, suggests that the oil is forming a core in the centre of the droplet and, as a consequence, more spherical NE aggregates (Aveyard et al., 1990; Malcolmson et al., 1998).

1.3.3 Photon correlation spectroscopy (PCS)

In a photon correlation spectroscopy (PCS) or dynamic light scattering (DLS) study, time-dependent fluctuations of the light intensity from NE droplets are measured enabling the determination of a NE diffusion coefficient. It is generally assumed that the shape of particles are spherical and in doing so the diffusion coefficient of the NE can be used to calculate a hydrodynamic particle size (Aveyard et al., 1989). Due to the random motion of the colloidal aggregates in solution (Brownian motion), these fluctuations can be analysed in terms of the variation in the intensity of the scattered light with time. The motion of the colloidal particles in the solution is inversely proportional to their particle size. Large particles will move more slowly and as consequence cause lower intensity fluctuations. By measuring the fluctuations over period of time, it is possible to determine an autocorrelation function, and therefore the diffusion coefficient of the particles. The

information about the diffusion coefficient (D) can then be used to calculate size, hydrodynamic diameter (D_h) using the Stokes-Einstein equation (Tadros, 2005):

$$D_h = \frac{kT}{3\pi\eta D}$$

where D_h is hydrodynamic diameter, k is Boltzmann constant, T is absolute temperature (K), D is diffusion coefficient and η is viscosity of the medium. PCS measures an 'equivalent particle diameter' which is known as the apparent hydrodynamic diameter of the particles dispersed in solution.

PCS is widely used to determine the size distribution of small particles and assess the stability profile of systems by measuring the variation in the diameter of the particles as a function of time. Its popularity is partly because it is a rapid measurement technique and requires only a small amount of sample (Anton et al., 2007; Nobbmann and Morfesis, 2009). In addition, it is possible to measure particle size in a wide variety of suspending liquids. For example, in the study of Izquierdo et al. (2005) PCS was used to investigate the stability of o/w NE containing water, mixed nonionic surfactants and isohexadecane. The results in this study showed that Ostwald ripening led to an instability of the NE. Moreover, PCS measurement can illustrate the effect of varying the amounts of components present in the NE system of interest. For instance, Sadurni et al. (2005) reported that the NE droplet size increased from 14 to 39 nm when the oil/surfactant ratios were changed from 10/90 to 40/60, respectively. However, there are a few drawbacks to this technique. First, this technique does not provide the information about the shape of particles. In addition, a small amount of dust can make the measurements and their subsequent interpretation difficult (Tscharnuter, 2006), although the present of dust can be avoided by the use of filtered water to prepare the samples.

1.3.4 Small angle neutron scattering (SANS)

Small angle neutron scattering (SANS) is a diffraction technique that exploits the neutron wave and its unique nuclear properties to provide information on particle morphology including the size and shape of a molecule, such as a surfactant, and its assemblies, such as a micelle (King, 1999). SANS is one of the most important techniques used to determine the structure, interaction and phase transition in micellar and ME systems (Chen, 1986). Despite these significant advantages, this technique has a number of

disadvantages. For example, it is slow and expensive as the experiment takes several days and must be performed at large international facilities.

However, SANS is probably the best technique to measure the internal architecture of small and colloidal particles. There are two ways to produce neutrons. Firstly, neutrons are produced by the nuclear fission of a heavy atom such as uranium-235 in a reactor, i.e. a continuous or steady-state source. The example neutron sources using the reactor source are the Institute Laue Langevin (ILL), Grenoble, France and the National Institute of Standard and Technology (NIST). The second way to produce neutrons is using a pulsed or spallation neutron source, where particle accelerators and synchrotrons are used to generate intense, high-energy, proton beams which are directed at a target composed of heavy nuclei to produce a beam of neutrons (King, 1999). After producing a beam of neutrons, the beam is moderated by passing through a material such as liquid hydrogen to decrease its velocity and to produce neutrons of the required wavelength for the experiment. An example of a pulsed neutron source is the ISIS facility, Rutherford-Appleton Laboratory (RAL), Didcot, UK, which is used in the present study. At ISIS, time of flight techniques are used to obtain the energy and wavelength of each neutron, and allowing fixed scattering geometries to be used by recording the time neutron takes for travelling from the target to the detectors (Rogers et al., 2009).

Light scattering and small angle X-ray scattering (SAXS) provide the same information for the sample as small angle neutron scattering. However, the difference between neutron and other scattering techniques is that neutrons are scattered by the nucleus and is not dependent upon atomic number, while light and X-ray are scattered by the electron cloud around the atom, and are therefore dependent upon atomic number and vary in intensity with atomic number of the atom. It is significant that neutrons are scattered differently by different isotopes of the same element due to the fact that an isotope's neutron scattering ability is determined by its scattering length. For instance, H and D have very different coherent scattering lengths which are -3.741×10^{-15} and 6.671×10^{-15} $Å^{-2}$, respectively. Due to this property, the part of a structure of interest can be highlighted by selective deuteration and thereby making part of the system invisible to neutrons, a technique known as contrast matching.

Moreover, light scattering especially PCS is used widely to determine the particle size of a colloidal sample, however there are limitations to the technique because the wavelength of light (4000-8000 Å) restricts the ability of light scattering to determine the shape of small aggregates. Additionally, SAXS is limited in that the X-ray beam may irreversibly

damage the sample, especially for biological samples such as proteins and lipids (King, 1999).

In contrast, neutron scattering possess many advantages over light and X-ray scattering, such as the fact that neutrons can penetrate into a sample without damaging it and that it is possible to specifically highlight the part of the system of interest by altering the scattering length of the sample (i.e. contrast matching). As a consequence of these, and other advantages, small angle neutron scattering (SANS) was used in the present study to determine the size and morphology of the NE droplets in the absence and presence of drugs.

1.3.4.1 Theory of small angle neutron scattering (SANS)

The scattering vector

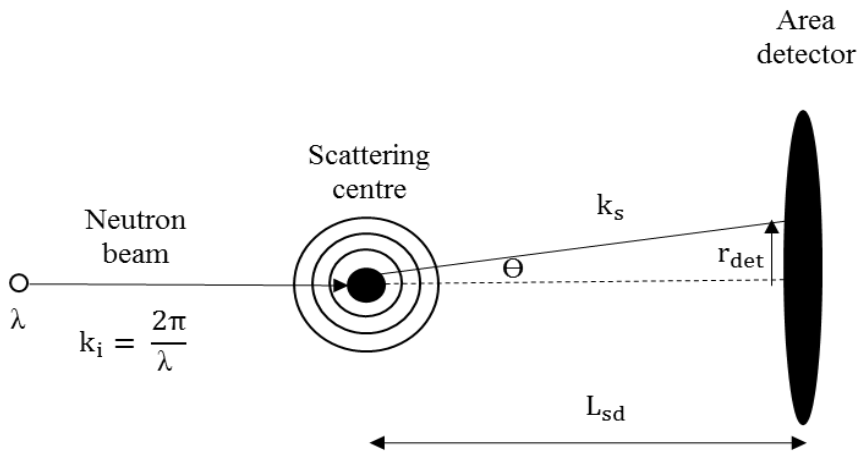

Figure 1.5: Scattering of neutrons by a sample (King, 1999).

The geometry of a SANS experiment is shown in **Figure 1.5**. Neutron waves are spherically symmetrically scattered by the nuclei of the sample. The fraction of the neutron scattered by the particles at a particular scattering angle are then recorded on a 2-dimensional detector at a distance L_{sd} from the sample at a radial distance r_{det}. The momentum transfer or wave vector transfer is known as the scattering vector (Q). Q is described by the relationship between the incident (k_i) and the scattered (k_s) wave vectors. Q has dimensions of $(length)^{-1}$ and is quoted in the units of either nm^{-1} (SI units) or, more typically $Å^{-1}$. The magnitude of scattering vector (Q) can be defined as:

$$Q = |Q| = |k_s - k_i| = \frac{4\pi n \sin(\frac{\theta}{2})}{\lambda}$$

when n is "neutron" refractive index, θ is the scattering angle and λ is the incident neutron wavelength. In practise, n is found to be slightly less than unity. Neutrons of the right wavelength are totally externally reflected from an interface so that n can be approximated to ~1. By substituting the equation above into Bragg's law of diffraction:

$$\lambda = 2d \sin(\frac{\theta}{2})$$

It is possible to obtain the very useful and simple expression:

$$Q = \frac{2\pi}{d}$$

where the d-spacing of plane (d) is obtained at a particular Q. This equation allows the ready determination of the molecular length scale (d) in a sample from the position of any diffraction peak in Q space (King, 1999).

1.3.4.2 Scattering length density and contrast matching

One of the important factors when determining particle size and morphology using light scattering technique is the difference in the refractive index of the solute and solvent. The same principle applies in SAXS, although the difference in this technique is due to the difference in electron density, while the difference in SANS is a consequence of the difference in scattering length density. The scattering length density (ρ_{SLD}) of a molecule with i atoms may be readily calculated from the simple expression:

$$\rho_{SLD} = \sum_i b_i \frac{DN_A}{MW}$$

where b_i is the coherent neutron scattering length of nucleus i, D is the bulk density of the molecule, N_A is Avogadro's constant and MW is molecular weight. The scattering length density normally has dimensions of $(\text{length})^{-2}$ and is expressed in units of 10^{10} cm^{-2} or 10^{-6} $Å^{-2}$.

Contrast matching is a powerful tool and useful in neutron scattering studies containing multicomponent samples. In any experiment, the contrast term is described as the square of the difference in the scattering length density between the solute (ρ) and the surrounding medium (ρ_m), ($(\Delta\rho)^2 = (\rho-\rho_m)^2$). At the contrast match point which is the point that the difference in scattering length density is zero ($(\Delta\rho)^2 = (\rho-\rho_m)^2 = 0$), there is no neutron scattering observed from the part of the sample of interest, which becomes "invisible" to neutrons. In neutron scattering studies, the difference in scattering length density between a proton and a deuterium is widely exploited in contrast match studies.

For example, using a mixture of D_2O (ρ = 6.39 x 10^{-6} Å^{-2}) and H_2O (ρ = -0.56 x 10^{-6} Å^{-2}) is often possible to match the scattering length density of the medium to the scattering region of interest and therefore making it "invisible" as is illustrated in **Figure 1.6**.

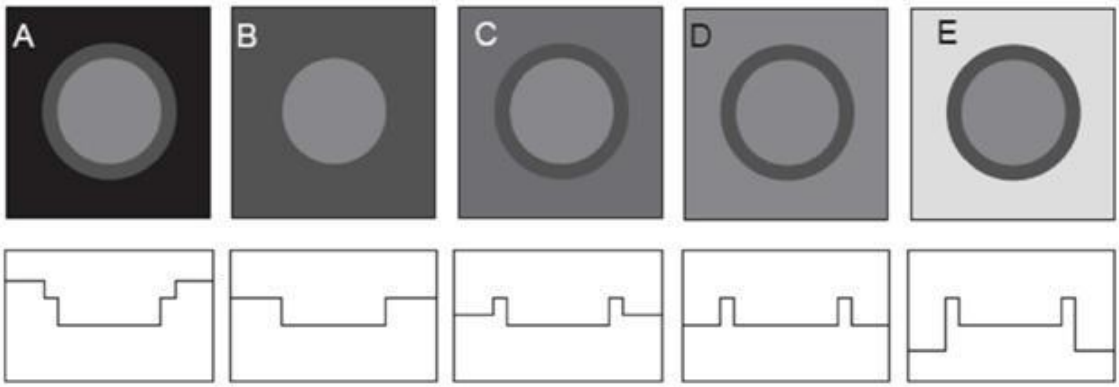

Figure 1.6: Schematic representation of a contrast variation experiment using different D_2O/H_2O mixtures to study core shell nanoparticles. The second row of figures schematically show the scattering length density profile across the core shell structure (Rübe et al., 2005).

1.3.4.3 SANS data interpretation

The differential scattering cross−section, ($\partial\Sigma/\partial\Omega$) is the dependent variable measured in a SANS experiment and is often referred to as the intensity of scattering, I(Q). The absolute SANS intensity of scattering I(Q) is expressed by the form factor, P(Q) and the structure factor, S(Q);

$$(\partial\Sigma/\partial\Omega) = \mathrm{I(Q)} = \mathrm{N_p P(Q) S(Q)}$$

where N_p is the average number density of the scattering droplets. The form factor, P(Q) is also known as the shape factor, which is a dimensionless function which describes how ($\partial\Sigma/\partial\Omega$) is modulated by interference effects between radiation scattered by different parts of the same scattering centres (King, 1999). As a consequence, the term of ($\partial\Sigma/\partial\Omega$) depends on both the size and shape of the scattering centre in the absence of interference effects. The structure factor, S(Q) represents the effect of interference due to neighbouring scatterers and depends on their relative positions. In the diluted system, this S(Q) parameter is approximately 1 which suggests that the interaction between the droplets is negligible and the scattering intensity is mainly dependent on the form factor, P(Q).

1.3.4.4 The form factor, P(Q)

A core-shell model is widely used to describe the scattering data obtained from micelles or NE, where the core is considered to consist of the tails of the surfactant for micelles or

the oil core for NE, while the shell is composed of the surfactant head groups for micelle or whole surfactant molecule for NE. Pedersen (1997) found that micelles or ME could be well fitted by assuming one of two shapes, namely a sphere or an ellipsoid. The form factor is weighted by the relative volumes of the core and shell of the droplets as well as their scattering length densities. This form factor is described by (Chen, 1986):

$$P(Q) \equiv \langle |F(Q)|^2 \rangle = \int_0^1 |F(u)|^2 d\mu$$

where F(Q) is the single particle form factor.

The form factor for a core shell model of homogeneous spherical particle is:

$$F(Q) = \frac{4}{3}\pi R_c^3(\rho_c - \rho_s)\frac{3j_i(QR_c)}{QR_c} + \frac{4}{3}\pi R_s^3(\rho_s - \rho_{solvent})\frac{3j_i(QR_s)}{QR_s}$$

where, $j_i(x) = \frac{\sin x - x\cos x}{x^2}$ is the first order spherical Bessel function, R_c and R_s are the radius of core and shell, ρ_c, ρ_s and $\rho_{solvent}$ are the scattering length densities of core, shell and solvent.

In addition, the form factor for ellipsoidal droplets is written as:

$$[F(Q)^2]_0 = \int_0^{\frac{\pi}{2}} \left(V_c(\rho_c - \rho_s)F_1\left(qR_c\sqrt{\sin^2\theta + \varepsilon_c^2\cos^2\theta}\right) + (V_c + V_s)(\rho_s - \rho_0)F_1 \times \left(qR_c\sqrt{\sin^2\theta + \varepsilon_c^2\cos^2\theta}\right)^2 \right)^2 \sin\theta d\theta$$

where V_c and V_s are the volumes of core and shell, ρ_c, ρ_s and ρ_0 are the scattering length densities of core, shell, and solvent, R_c and R_s are the semi-axes of core and shell, and ε_c and ε_s are the axial ratios of core and shell.

1.3.4.5 The structure factor, S(Q)

The structure factor, S(Q), describes how ($\partial\Sigma/\partial\Omega$) is modulated by interference effects between neutrons scattered by different scattering bodies (King, 1999). Consequently, it is dependent on the degree of local order in the sample and increases with the concentration of scattering bodies in the system.

Many previous studies have found that a hard-sphere model can satisfactorily describe the structure factor for many NE and ME (Arleth et al., 2001; Preu et al., 1999) and in particular, when a nonionic surfactant is used to prepare the system (Nagao et al., 2005).

Therefore, in this present study, the structure factor derived by using the Percus-Yevick approximation was used for the analysis of the NE stabilised by nonionic surfactant. The equation is used as following (Ashcroft et al., 1966):

$$S(q) = \frac{1}{1 - nc(qR_s)}$$

$$c(qR_s) = -4\pi R_s^3 \int_0^1 dss^2 \frac{\sin sqR_s}{sqR_s} (\alpha + \beta_s + \gamma_s^2)$$

where $c(qR_s)$ is the direct correlation function and

$$\alpha = \frac{(1+2\eta)^2}{(1-\eta)^4}$$

$$\beta = -\frac{6\eta\left(1+\frac{\eta}{2}\right)^2}{(1-\eta)^4}$$

$$\gamma = \frac{\frac{1}{2}\eta(1+2\eta)^2}{(1-\eta)^4}$$

η is a packing-density parameter and it is related to the concentration of spheres (φ) as follows:

$$\eta = \left(\frac{\pi}{6}\right)\varphi R_s^3$$

1.4 Aim of the current project

The first aim of this present study was to formulate o/w NE stabilised by the nonionic surfactant, Brij O10 or Tween 80 in the absence and presence of cosurfactant: lecithin and Dermosoft GMCY and containing pharmaceutical acceptable oils either triglycerides or ethyl esters to study the effect of surfactant, cosurfactant and oil on the formation of NE. A study of the physicochemical properties of NE such as their phase behaviour, their phase inversion temperature, and particle size (as characterised by light scattering and small angle neutron scattering) was undertaken to examine the architecture of the NE. The ability of the NE to solubilise poorly water soluble drugs, testosterone propionate (TP), curcumin (CUR) and docetaxel (DTX) was determined by UV/vis spectroscopy and allowed the establishment of whether it is possible to solubilise poorly water soluble drug in NE in high loading.

The second aim of this study was to investigate the cytotoxicity and efficacy of NE in the absence and presence of either CUR or DTX to deliver anticancer drug to HeLa and CT26 cancer cell lines. Moreover, the ultimate purpose in cancer therapy was to deliver anticancer drugs to tumour tissue with reduced toxicity to normal cells. This resulted in

the synthesis of folate receptor-targeting surfactant in order to specifically increase the intracellular uptake of anticancer drugs encapsulated in NE within cancer cells.

Chapter 2
Experimental

Part 1 The physicochemical properties of nanoemulsions

2.1.1 Materials

2.1.1.1 Surfactants and co-surfactants

Brij O10 (polyoxyethylene-10-oleyl ether, $C_{18:1}E_{10}$, Brij 97, Brij 96), Brij 99 (polyoxyethylene-20-oleyl ether, $C_{18:1}E_{20}$), Triton X-100, Tyloxapol were purchased from Sigma-Chemicals Ltd. (Dorset, UK). Lutrol F68 was supplied by BASF (New Jersey, USA) while Brij 35 (polyoxyethylene-23-dodecyl ether) was obtained from MP Biomedicals LLC (Ohio, USA). Tween 20, Tween 80, Span 20, Span 60 and Span 80 were purchased from Merck KGaA (Darmstadt, Germany). Tween 60 was purchased from Acros Organics (Geel, Belgium). Dermosoft GMCY (glyceryl caprylate) was a gift from Infinity Ingredients (Berkshire, UK). L-α-phosphatidylcholine from soy bean (lecithin) was purchased from Avanti Polar lipids (Alabama, USA). The structures of surfactants studied are shown in **Table 2.1**.

Table 2.1 Surfactants used in the preparation of the nanoemulsions.

Surfactant	Chemical Formula
Brij O10 ($C_{18:1}E_{10}$, Brij 97, Brij 96 or polyoxyethylene-10-oleyl ether)	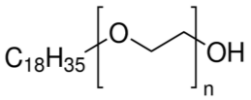 n = 10
Brij 99 ($C_{18:1}E_{20}$ or polyoxyethylene-20-oleyl ether)	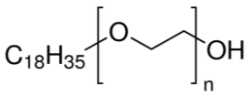 n = 20
Brij 35 ($C_{12}E_{23}$ or polyoxyethylene-23-lauryl ether)	$CH_3(CH_2)_{10}(OCH_2CH_2)_{23}OH$

Table 2.1 Surfactants used in the preparation of nanoemulsions (cont.).

Surfactant	Chemical Formula
Triton X-100	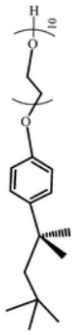
Tyloxapol	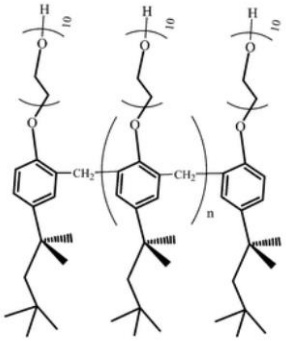
Tween 20	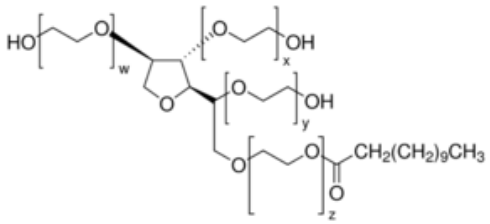 w+x+y+z = 20
Tween 60	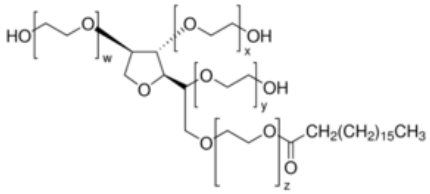 w+x+y+z = 20
Tween 80	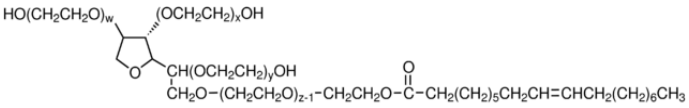 w+x+y+z = 20

Table 2.1 Surfactants used in the preparation of the nanoemulsions (cont.).

Surfactant	Chemical Formula
Span 20	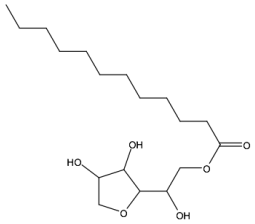
Span 60	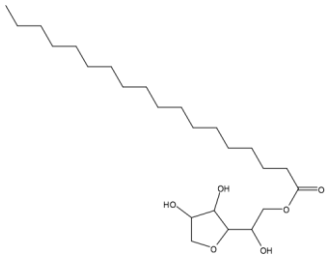
Span 80	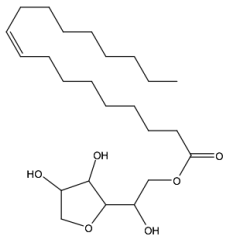
Lutrol F68	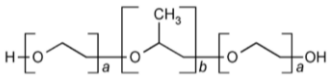 a = 80, b = 27
Dermosoft GMCY	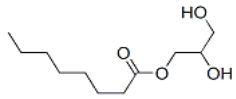
Lecithin (L-α-phosphatidylcholine from soy bean)	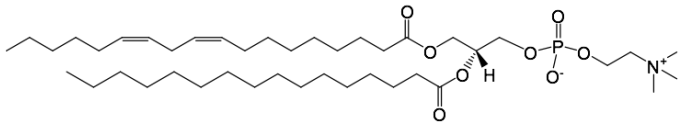

2.1.1.2 Oils

The oils employed in this study include a range of triglyceride oils, ethyl esters of fatty acids and hydrocarbon oils (**Table 2.2**). (Protiated) soybean oil ((*h*-)SBO), a mixture of predominately (i.e. > 75 %) $C_{18:1}$ and $C_{18:2}$ triglycerides, was supplied by Alfa Aeser (Lancashire, UK). It is noted that the precise chemical structure of (*h*-)SBO varies due to the natural source of the material. (Protiated) tripalmitin of >85 % purity (85(*h*-)TPN) was

purchased from Sigma-Chemicals Ltd. (Dorset, UK) while (protiated) tripalmitin of purity 99 % (99(*h*-)TPN), (protiated) triolein of 99% purity (99(*h*-)GTO) were obtained by Acros Organic (New Jersey, USA). (Protiated) triolein of purity 65 % (65(*h*-)GTO) and (protiated) tristearin of 99% purity (99(*h*-)GTS) were from Sigma-Chemicals Ltd. (Dorset, UK). (Protiated) tristearin of purity >60 % (60(*h*-)GTS), (protiated) ethyl oleate of purity >60 % (60(*h*-)EO), (protiated) ethyl oleate of 98% purity (98(*h*-)EO), (protiated) ethyl stearate of purity 99 %, (99(*h*-)ES), and (protiated) hexadecane of 99% purity were purchased from Aldrich Chemical (Dorset, UK). (Protiated) 1-hexadecene (purity 92%) was supplied by Merck KGaA (Darmstadt, Germany). The chemical structure of the various triglyceride oils (i.e. (*h*-)SBO, 65(*h*-)GTO, 99(*h*-)GTO, 85(*h*-)TPN, 99(*h*-)TPN, 60(*h*-)GTS, 99(*h*-)GTS) and ethyl ester oils (i.e. 60(*h*-)EO, 98(*h*-)EO and 99(*h*-)ES) was confirmed by dissolving the oil in chloroform-d (99.8 atom %D) and performing ^{1}H NMR spectroscopy (Bruker Avance DRX 400 MHz NMR spectrometer) (Bruker, Coventry, UK). The fully deuterated form of tripalmitin (–d_{98}, 98.6 atom%D) ((*d*-)TPN) was obtained from CDN Isotopes (Quebec, Canada) whereas the terminal chain deuterated form of triolein (–d_{51}, 98 atom%D) (*d*-)GTO) was synthesised by the Oxford Isotope Facility (Oxford, UK).

Table 2.2 Structure and melting point of the triglyceride, ethyl ester and hydrocarbon oils.

Oil (and where available its purity)	Structure	Melting point (˚C) [a]
Triglyceride		
Soybean oil (*h*-SBO)	-	< 0
Triolein, purity >65 % (65*h*-GTO)	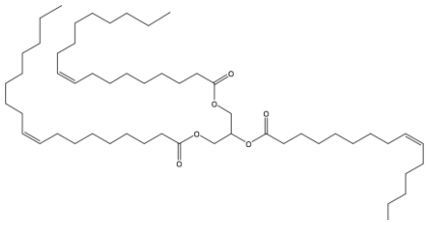	< 0
Triolein, purity 99 % (99*h*-GTO)		< 0
Triolein (*d*-GTO)		< 0
Tripalmitin, purity >85 %, (85*h*-TPN)	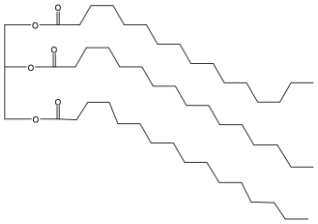	66-67
Tripalmitin, purity 99 %, (99*h*-TPN)		65-68
Tripalmitin – d_{98} (*d*-TPN)		63-64
Tristearin, purity >60 % (60*h*-GTS)	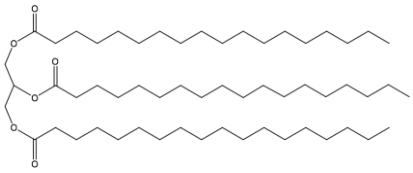	72
Tristearin, purity 99 % (99*h*-GTS)		72
Ethyl ester oils		
Ethyl oleate, purity >60 % (60*h*-EO)	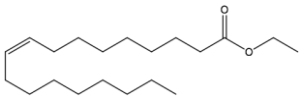	-32
Ethyl oleate, purity 98 % (98*h*-EO)		-32
Ethyl stearate, purity 99 % (99*h*-ES))	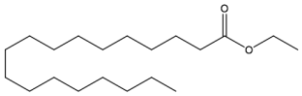	33-36
Hydrocarbon oils		
Hexadecane	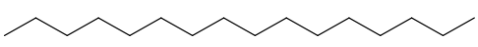	18
1-hexadecene	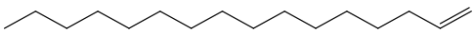	2.2

[a] from manufacturer

2.1.1.3 Solvents

Ultrapure water (UPW), supplied by a well-seasoned, all glass still (D4000 Distinction, Sterling, UK) was used throughout. Sodium chloride, extra pure was purchased from Acros Organics (Geel, Belgium) and used to prepare a 0.9 %w/v NaCl solution in water. Isopropanol was obtained from Fisher Scientific (Leicestershire, UK). D_2O (99.9 atom %D) was supplied by from Aldrich Chemical Company (Dorset, UK) while chloroform-d (99.8 atom %D) containing 0.03 %v/v TMS was from Acros Organics (Geel, Belgium).

2.1.1.4 Drugs

Testosterone propionate (TP) was purchased from Sigma-Chemicals Ltd. (Dorset, UK). Curcumin, purity 98 % (CUR) was obtained from Alfa Aeser (Lancashire, UK). Docetaxel (DTX) was supplied by Apollo Scientific Ltd (UK). The chemical structures of testosterone propionate (TP), curcumin (CUR) and docetaxel (DTX) are given in **Table 2.3**.

Table 2.3 Structure of drugs used in this study.

Drug	Structure
Testosterone propionate	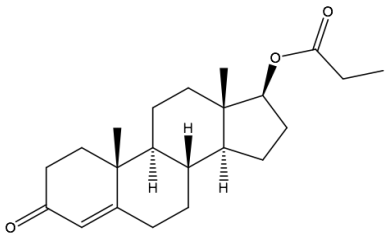
Curcumin	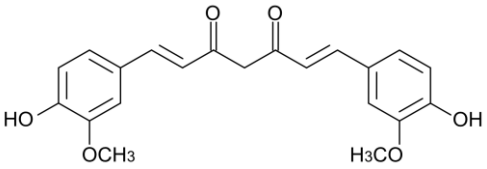
Docetaxel	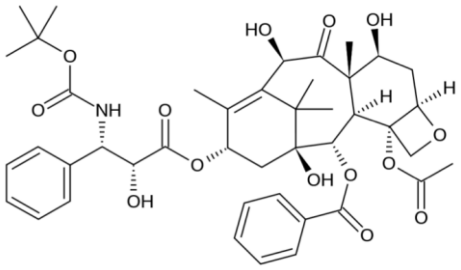

2.1.2 Sample nomenclature

In order to make it easier to know the composition of the sample under the study, a sample nomenclature has been devised (**Figure 2.1**). The first letter (**A** in **Figure 2.1**) is used to denote the surfactant used. This is immediately followed some numbers (**B** in **Figure 2.1**) denoting the concentration of surfactant used in its preparation (in %w/w). Thus far the code is the same for micelles and nanoemulsions (NE). In the case of NE, the letters **A/B** are followed by **C/D**, which are the codes for the nature and amount (in %w/w) of oil present, respectively. **C/D** are obviously omitted in the case of micelles. Finally, if a drug is present in either the micelles or NE, the code used to indicate the drug follows, either **C/D** in the case of a NE or **A/B** in the case of micelles. The full code used to denote the micelles and NE is shown in **Figure 2.1.** Note that in the final code a hyphen separates **A/B** from **C/D** and **C/D** from **E**. The codes used for the various surfactants, oils and drugs are tabulated in **Table 2.4**. For example the code, B20-hSBO2 means that the NE contains 20 %w/w Brij O10 and 2 %w/w SBO.

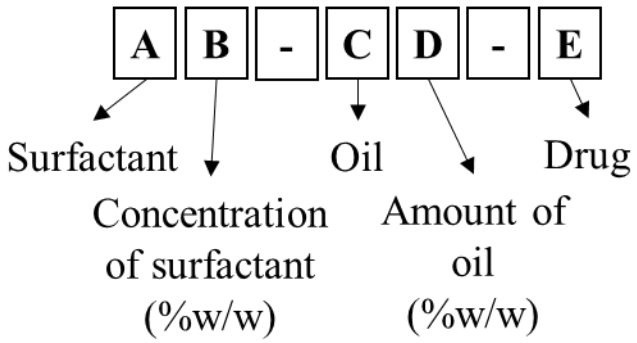

Figure 2.1: Sample nomenclature used for micelles and nanoemulsions.

Table 2.4 Code of surfactants, oils and drugs used in the preparation of the micelles and nanoemulsions**.**

Chemicals (and where available purity)	Code
Surfactants (A)	
Brij O10	B
Tween 80	T
Dermosoft GMCY	D
Lecithin	L
Oils (B)	
Soybean oil	hSBO
Triolein, purity >65 % (65*h*-GTO)	65hGTO
Triolein, purity 99 % (99*h*-GTO)	99hGTO
Triolein (*d*-GTO)	98dGTO
Tripalmitin, purity >85 %, (85*h*-TPN)	85hTPN
Tripalmitin, purity 99 %, (99*h*-TPN)	99hTPN
Tripalmitin – d98 (*d*-TPN)	98.6dTPN
Tristearin, purity >60 % (60*h*-GTS)	60hGTS
Tristearin, purity 99 % (99*h*-GTS)	99hGTS
Ethyl oleate, purity >60 % (60*h*-EO)	60hEO
Ethyl oleate, purity 98 % (98*h*-EO)	98hEO
Ethyl stearate, purity 99 % (99*h*-ES))	99hES
Drugs (E)	
Testosterone propionate	TP
Curcumin	CUR
Docetaxel	DTX

2.1.3 Methods

2.1.3.1 Preparation of nanoemulsions by phase inversion temperature method

Nanoemulsions (NE) were individually prepared by the phase inversion temperature (PIT) method using H_2O or an aqueous solution of 0.9 %w/v NaCl. The required amounts of oil, surfactant and water or aqueous 0.9 %w/v NaCl solution making a total of 2 g of sample were

weighed. The list of all formulations studied is shown in **Appendix A**, **Table A.1** which illustrates the amount of material in the unit of %w/w. To illustrate the example of measurement for the preparation of NE, B20-SBO2 NE containing 2 %w/w SBO, 20 %w/w Brij O10 and 78 %w/w water was weighed 0.4 g of SBO, 0.04 g of Brij O10 and 1.56 g of water to prepare 2 g of sample. The order of materials weighed was oil, surfactant/cosurfactant and water, respectively. A magnetic stirrer was added to the sample and the sample heated for 10 min at 70 - 80 ˚C and then cooled to room temperature with vigorous stirring throughout. Micellar solutions were prepared in the same method but with no added oil. After preparation, all the samples were placed in tightly sealed glass bottles and stored at room temperature unless otherwise stated.

2.1.3.2 Determination of phase diagrams

The area of existence for the NE were determined by individually preparing a large number of compositions. Samples were routinely visually (including through cross polars) inspected for stability immediately after preparation, after one day, one week, and one month. Specifically, the samples were visually examined for any physical changes such as the changing from clear to cloudy or undergoing a phase separation. Those samples which remained completely clear, non-birefringent (isotropic) when observed through crossed polars, one-phase and fluid after one month were denoted as a NE and included within the NE area of existence. Samples that were clear (or indeed turbid), non-birefringent but did not change their meniscus after tilting to an angle of 90° were classified as gels and were not studied further. Samples that were fluid and exhibited phase separation or birefringence were denoted to lie outside the NE area.

Each area of NE existence was determined using triplicate samples to ensure an accuracy of the boundary to better than ± 1 %w/w for each component. The composition of stable NE formulations was plotted as a partial triangular phase diagram. Each apex of the triangular plot in 3-component systems represents 100 % of one of the components (**Figure 2.2**). In the present study, the 3 components are oil (triglyceride or ethyl ester), surfactant and water. Each point within the triangle represents a different composition of the three components. The point shown in **Figure 2.2a** has a composition of 20 %w/w surfactant, 5 %w/w oil, and 75 %w/w water.

In the present study, stable, clear NE are described as Region A NE, while bluish or translucent NE as Region B NE and cloudy or milky NE as Region C NE. The boundaries of each of the resulting areas of NE existence were drawn. The partial triangular diagram in **Figure 2.2b** represents an example of a NE that contains Regions A, B and C.

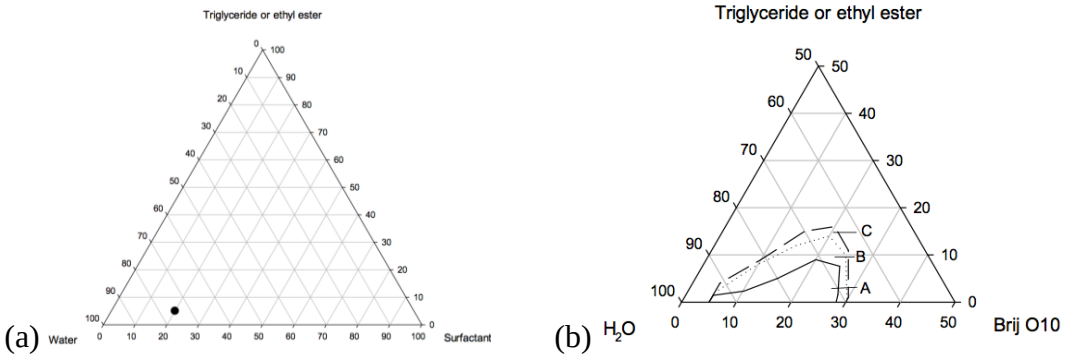

Figure 2.2: a) Tertiary phase diagram for a 3-component system and b) partial tertiary phase diagram showing Region A nanoemulsions (i.e. clear nanoemulsions), Region B nanoemulsions (bluish or translucent nanoemulsions) and Region C nanoemulsions (cloudy or milky nanoemulsions).

2.1.3.3 Dilutability of nonionic o/w nanoemulsions

Nanoemulsion was diluted with water from a range of surfactant concentrations, namely 20-25 %w/w, down to 1-2 %w/w surfactant. The diluted NE samples were kept at room temperature and visually inspected for stability immediately after dilution, after one day, one week, and one month.

2.1.3.4 Cloud point and phase inversion temperature determination

The phase inversion temperatures (PIT) of the clear Region A NE, and the cloud point (CP) of the corresponding micelles were determined by placing a thermometer inside a glass bottle which contained the sample, which was itself placed in a water bath on a hot plate. The samples were heated until they became turbid and thereafter cooled to ambient, both heating and cooling at a rate of about 1 ˚C/min with constant, vigorous throughout stirring. The temperatures at which the onset of turbidity (upon heating) and the appearance of clarity (upon cooling) occurred were recorded. The reported PIT of the NE, and the CP of the corresponding micellar solutions, are the average of 3 temperature and cooling cycles, i.e. six individual measurements.

2.1.3.5 Particle size measurement by photon correlation spectroscopy

Photon correlation spectroscopy (PCS) was employed to investigate the apparent hydrodynamic size of micelles and oil-in-water (o/w) NE samples. Specifically, either a Brookhaven ZetaPlus particle sizer v2.29 (Brookhaven Instruments Corporation, UK) or a Malvern Nano ZS Zetasizer (Worcestershire, UK) was used. The former instrument used a scattering angle of 90° while the latter exploited a scattering angle of 173°, both instruments used a red laser of wavelength 633 nm and a temperature of 25 ± 0.1 °C. The PCS measurement used a value of refractive index of 1.33 and a viscosity of 0.89 cP or 1.10 cP for water and deuterium oxide, respectively. The water used to dilute the samples under study was clarified by filtration through a 0.2 μm polyethersulfone (PES) filter (Jet biofil, Guangzhou, China). All samples were stored in the concentrated form and freshly diluted to a surfactant concentration of 1 %w/w immediately before the PCS measurement in order to avoid the effects of multiple scattering, likely to be present at higher surfactant concentrations. Unless otherwise stated, all diluted samples were stable for at least a month. The diluted samples were filtered through a 0.45 μm polyethersulfone (PES) filter (Jet biofil, Guangzhou, China) immediately before examination by PCS to avoid the presence of dust. The diluted samples were allowed to equilibrate at the experimental temperature for 10 minutes before measuring by PCS. In order to determine sample stability over 1 month, samples were measured immediately after their preparation, after 1 day, 1 week and 1 month storage at room temperature, unless otherwise stated. The particle size of three individual samples was measured and the results expressed as the average and standard deviation of the mean apparent hydrodynamic size. The apparent hydrodynamic size and polydispersity of each sample were determined assuming that the particles were spherical. The relationship between the visual appearance of the sample and the results of the light scattering study were noted. The variation, if any, in the apparent hydrodynamic size of the micelles and NE with surfactant concentration for samples in different NE Regions of the phase diagram was determined.

2.1.3.6 Solubilisation of the hydrophobic drugs

The incorporation of testosterone propionate (TP) was determined in both the micelles and the NE in Regions A, B, and C, while that of curcumin (CUR) and docetaxel (DTX) were determined only in the micelles and in Region A NE. Samples for solubilisation studies were

prepared in the absence of drug as described in **section 2.1.3.1** and a known excess of drug added to 3 x 1 mL aliquots of the micelles and the NE contained in eppendorf tubes, which were tightly closed and covered in foil to protect the samples they contained from light. The samples were equilibrated at room temperature on a circular rotating wheel for 5 or 7, 10, and 14 days to ensure that the drugs have reached their maximum solubility. Excess drug was removed by centrifugation (6500 rpm Biofuge pico, Heraeus, Osterode, Germany) for 20 minutes. A blank sample (i.e. either the corresponding micelles or the NE without drug) was treated in the same way.

The solubility of drug in the micelles and NE samples was assessed by diluting an aliquot of the supernatant obtained by centrifugation in isopropanol. Only the 85hTPN and 99hTPN NE containing TP and their corresponding blanks needed sonication in order to help the TPN dissolve in isopropanol. After dilution of each sample, the drug concentration in the resulting clear isopropanol solutions was determined by UV analysis, subtracting the absorbance of the isopropanol diluted blank containing the equivalent concentration of surfactant and oil, and comparing the resultant absorbance with the corresponding calibration curves for that drug. The levels of drug incorporation obtained in the micelles and the o/w NE were compared. CUR solubility also was similarly determined in the various bulk oils and distilled water, in this case excess CUR was removed from the samples by filtration through 0.2 µm polyethersulfone (PES) filters (Jet biofil, Guangzhou, China). Filtration was used to separate excess CUR from the solvent under tested (either an oil or water) due to the fact that centrifugation could not separate the CUR from oil because of the high viscosity of the oils.

2.1.3.6.1 Calibration curve of testosterone propionate in isopropanol

A calibration curve for TP was obtained by dissolving a precisely known quantity of TP (approximately 40 mg) in 20 mL isopropanol. This stock solution was then serially diluted by taking 50, 100, 150, 200, 250 and 300 µL aliquots and making up to 20 mL with isopropanol. Dilutions were performed in triplicate. The UV spectra of the TP containing standard solutions in a 1-cm path length cuvette was then measured and the value at a lambda max of 240 nm determined (UV/Vis Spectrophotometer LAMBDA 35, Perkin-Elmer, USA). The blank in all cases was isopropanol.

2.1.3.6.2 Calibration curve of curcumin in isopropanol

A calibration curve for CUR was obtained by dissolving a precisely known quantity of CUR (approximately 5 mg) in 10 mL isopropanol. This stock solution was then serially diluted by taking 7, 14, 28, 42, 56 and 70 µL aliquots and making up to 5 mL with isopropanol. The dilutions were performed in triplicate. The UV spectra of the CUR containing standard solutions in 1-cm path length cuvette was then measured and the value at a lambda max of 428 nm determined (UV/Vis Spectrophotometer LAMBDA 35, Perkin-Elmer, USA). The blank was isopropanol.

2.1.3.6.3 Calibration curve of docetaxel in isopropanol

A calibration curve for DTX was obtained by dissolving an accurately known quantity of DTX (approximately 2 mg) in 2 mL isopropanol. This stock solution was then serially diluted by taking 25, 75, 125, 175 and 225 µL aliquots and making up to 5 mL with isopropanol. The dilutions were performed in triplicate. The UV spectra of the DTX containing standard solutions in 1-cm path length cuvette was then measured and the value at a lambda max of 229 nm determined (UV/Vis Spectrophotometer LAMBDA 35, Perkin-Elmer, USA). The blank was isopropanol.

2.1.3.7 Characterization of drug-loaded nanoemulsions

The effect of the incorporation of the maximum amount of drug on the stability, size, and PIT of the NE droplets was determined by visual observation, light scattering (PCS), heating and cooling of the NE to determine PIT, as well as by small angle neutron scattering (SANS).

2.1.3.8 Small-angle neutron scattering

Small angle neutron scattering (SANS) studies were performed on the SANS2d small-angle diffractometer at the ISIS Pulsed Neutron Source (STFC Rutherford-Appleton Laboratory, Didcot, Oxford) (Heenan, 2011). Neutrons of wavelengths from 2 to 14 Å were used for SANS2d and were separated by time-of-flight technique. The SANS2d instrument gives a scattering vector, Q, where $Q = (4\pi/\lambda) \sin(\theta/2)$, in the range of 0.0045 to 0.8 $Å^{-1}$. SANS measurements were performed at 25 ± 0.1 or 37 ± 0.1 ºC using a 12-mm diameter neutron

beam. The pattern of scattering of neutrons after passage through the sample were recorded on two $^{3}He\text{-}CF_4$ filled ORDELA 96.5 x 96.5 cm^2, two-dimensional detectors of resolution of 5 mm, and rear detector was positioned at either 4 m from the clear micelle and NE samples and typically 8 m from the bluish/translucent and cloudy/milky NE samples because of their larger size and therefore greater scattering.

Wavelength dependent corrections were made to allow for the incident spectrum, detector efficiencies and measured sample transmissions in order to create a composite SANS pattern. Comparisons with scattering from a partially deuterated polystyrene standard allowed the absolute scattering cross section to be determined, with an error of ~ ± 2 %. All the samples were contained in 1 or 2 mm path length Hellma quartz cuvettes, depending on whether the solvent of the sample was predominately H_2O or D_2O, respectively. The transmission and scattering runs of sample and solvents were simultaneously measured and accumulated. An empty cell was used as direct beam.

Each raw scattering data set was corrected for detector efficiencies, sample transmission and background scattering and converted to the scattering cross-section ($\partial\Sigma/\partial\Omega$) as a function of Q using the instrument-specific software, Mantid, before being converted into "scattered intensity" (I(Q)) as a function of Q. These data were placed on an absolute scale (cm^{-1}) using the scattering from a standard sample (a solid blend of hydrogenous and perdeuterated polystyrene) in accordance with established procedures.

2.1.3.8.1 Preparation of samples for SANS studies

As a rule all NE and micellar samples studied by SANS were individually prepared by weighing the required amount of h- or d-triglyceride or ethyl ester, h-surfactant and either ultrapure water (H_2O) or deuterated water (D_2O) at room temperature, depending upon the contrast required (**Appendix A.1a)-A.1h)**). For each sample, a total of 1 g was prepared. A small magnetic stirrer was placed into the sample vial and the sample heated to 70-80 ºC for 10 minutes before cooling to room temperature with vigorous stirring throughout.

Due to the small amount of dGTO that was synthesised, the core and shell contrasts of the B20-98dGTO NE were individually prepared only at the highest concentration of oil. NE containing lower amounts of oil were then prepared by taking a small amount of the NE containing the highest concentration oil and diluting with surfactant solution. The resulting

mixture was re-heated for 10 min and then stirred at room temperature until cool to prepare the NE containing lower concentration of oil. In all experiments that necessitated the use of deuterated material, the weight of the deuterated material to be added was corrected for the difference in density compared to its protiated counterpart to ensure the same volume/number of molecules of each component was present in the final samples. It is worth noting that NE containing hSBO, 98hEO, hGTS could be prepared only as drop contrasts as there was no commercially available deuterated form of hSBO.

Once prepared, the samples were stored in tightly sealed containers after flushing with nitrogen in an attempt to reduce D to H exchange. Typically, both deuterated and protiated triglycerides and water were used, along with the normal (protiated) surfactant, as d-oil/h-surfactant/H_2O (D/H/H), d-oil/h-surfactant/D_2O (D/H/D) and h-oil/h-surfactant/D_2O (H/H/D) combinations of triglyceride oil or ethyl ester oil/surfactant/water for the core, shell and drop contrast, respectively (**Table 2.5**). The protiated and deuterated chemicals used were selected to highlight specific parts of the NE droplets when studying using SANS.

Table 2.5 Composition of protiated and deuterated chemicals for contrast matching.

Composition	Drop	Core	Shell
Protiated 	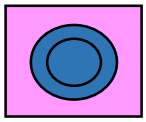	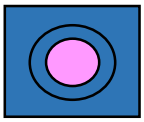	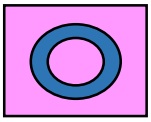
Deuterated 			
Oil	h-oil	d-oil	d-oil
Surfactant	h-surfactant	h-surfactant	h-surfactant
Solvent	D_2O	H_2O	D_2O

In order to avoid the existence of strong interactions between the micelles and NE droplets when examining by SANS, a stock solution was diluted to the required surfactant concentration immediately prior to its measurement. It was necessary to produce a stock solution as it was often not possible to prepare the required (low concentration surfactant) NE compositions directly. The list of sample nomenclature for SANS contrast matching experiments were listed in **Table 2.6** (a-i). All of the NE samples for the SANS experiments

were diluted to 2 %w/w surfactant concentration. Note that when a stock solution had been diluted 10 times for the Brij O10 NE and 12.5 times for the TD and TDL NE. "B2-hSBO0.2" means that the stock "B20-hSBO2" (which contains 20 %w/w Brij O10 and 2 %w/w SBO) had been diluted 10 times. Testosterone propionate (TP) or/and curcumin (CUR) saturated NE were prepared by adding an excess of TP or/and CUR to the concentrated NE which were then left to rotate on a wheel, generally for 1 week, following which time any excess TP or CUR was removed by centrifugation. When a sample was saturated with drug in this manner, a -TP was added to the end of the code such that B2-hSBO0.2-TP means a diluted stock NE which contains 2 %w/w Brij O10 and 0.2 %w/w hSBO and is saturated with TP.

In order to study the effect of temperature on the physico-chemical properties of micelles/ NE, B2-hSBO NE, TD2-98hEO NE and TDL2-hSBO NE was performed at 25 ºC and 37 ºC. When a sample was measured at 37 ºC overtime, a -37C was added to the end of the code such that B2-hSBO0.6-37C means that the measurement was performed at 37 ºC.

The drop contrast of B2-hSBO NE, TD2-98hEO NE was prepared by PIT method and the SANS experiments were performed at 37 ºC in the presence of complete media by dilution the sample with an equal volume of complete media to order to investigate if there was any interaction of the micelles or NE with complete media. When the sample under study was mixed with complete media and measured using SANS, the scattering intensity was determined overtime, namely immediately (t0), 2.5 hours (2.5h)/3 hours (3h)/3.5 hours (3.5h), 6 hours (6h), and 11 hours (11h)/12 hours (12h). In this case after mixing, a –DM and time point were added to the middle and end of the sample code such that B2-hSBO0.6-DM-37C-t0 means a sample was performed at 37 ºC and immediately measured after mixing with complete media.

Table 2.6 List of sample nomenclature for SANS contrast matching experiments in the absence and presence of drug (TP, CUR, CUR-TP).

2.6a) Brij O10 micelles (B micelles) in the absence and presence of drug.

Contrast	**B0.1**	**B0.2**	**B0.5**	**B1**	**B1.5**	**B2**	**B5**	**B10**	**B15**	**B20**
Droplet	B0.1d	B0.2d	B0.5d	B1d	B1.5d	B2d	B5d	B10d	B15d	B20d
Droplet with drug	-	-	-	-	-	B2d-TP	-	-	-	-
	-	-	-	-	-	B2d-CUR	-	-	-	-
	-	-	-	-	-	B2d-CUR-TP	-	-	-	-

2.6b) Brij O10 and soybean oil nanoemulsions (B-SBO NE) in the absence and presence of drug.

Contrast	**B2-SBO0.2**	**B2-SBO0.4**	**B2-SBO0.6**	**B2-SBO0.8**
Droplet	B2-hSBO0.2d	B2-hSBO0.4d	B2-hSBO0.6d	B2-hSBO0.8d
Droplet with drug	B2-hSBO0.2d-TP	B2-hSBO0.4d-TP	B2-hSBO0.6d-TP	B2-hSBO0.8d-TP
	B2-hSBO0.2d-CUR	B2-hSBO0.4d-CUR	B2-hSBO0.6d-CUR	B2-hSBO0.8d-CUR
	B2-hSBO0.2d-CUR-TP	-	-	B2-hSBO0.8d-CUR-TP

2.6b) Brij O10 and soybean oil nanoemulsions (B-SBO NE) in the absence and presence of drug (cont.).

Contrast	**B2-SBO0.9**	**B2-SBO1.0**	**B2-SBO1.2**	**B2-SBO1.4**	**B2-SBO1.6**
Droplet	B2-hSBO0.9d	B2-hSBO1.0d	B2-hSBO1.2d	B2-hSBO1.4d	B2-hSBO1.6d
Droplet with drug	B2-hSBO0.9d-TP	B2-hSBO1.0d-TP	B2-hSBO1.2d-TP	B2-hSBO1.4d-TP	B2-hSBO1.6d-TP
	B2-hSBO0.9d-CUR	-	-	-	-
	B2-hSBO0.9d-CUR-TP	-	-	-	-

2.6c) Brij O10 and triolein nanoemulsions (B-GTO NE) in the absence and presence of drug.

Contrast	**B2-GTO0.05**	**B2-GTO0.1**	**B2-GTO0.2**	**B2-GTO0.4**	**B2-GTO0.6**
Core	B2-98dGTO0.05c	B2-98dGTO0.1c	B2-98dGTO0.2c	B2-98dGTO0.4c	B2-98dGTO0.6c
Shell	B2-98dGTO0.05s	B2-98dGTO0.1s	B2-98dGTO0.2s	B2-98dGTO0.4s	B2-98dGTO0.6s
Droplet	B2-65hGTO0.05d	B2-65hGTO0.1d	B2-65hGTO0.2d	-	-
	B2-99hGTO0.05d	B2-99hGTO0.1d	B2-99hGTO0.2d	B2-99hGTO0.4d	B2-99hGTO0.6d
Droplet with drug	B2-65hGTO0.05d-TP	B2-65hGTO0.1d-TP	B2-65hGTO0.2d-TP	-	-
	B2-99hGTO0.05d-TP	B2-99hGTO0.1d-TP	B2-99hGTO0.2d-TP	B2-99hGTO0.4d-TP	B2-99hGTO0.6d-TP

2.6c) Brij O10 and triolein nanoemulsions (B-GTO NE) in the absence and presence of drug (cont.).

Contrast	**B2-GTO0.8**	**B2-GTO1.0**	**B2-GTO1.2**	**B2-GTO1.5**
Core	B2-98dGTO0.8c	B2-98dGTO1.0c	B2-98dGTO1.2c	B2-98dGTO1.5c
Shell	B2-98dGTO0.8s	B2-98dGTO1.0s	B2-98dGTO1.2s	B2-98dGTO1.5s
Droplet	-	-	-	-
	B2-99hGTO0.8d	B2-99hGTO1.0d	B2-99hGTO1.2d	B2-99hGTO1.5d
Droplet with drug	-	-	-	-
	B2-99hGTO0.8d-TP	B2-99hGTO1.0d-TP	B2-99hGTO1.2d-TP	B2-99hGTO1.5d-TP

2.6d) Brij O10 and tripalmitin nanoemulsions (B-TPN NE) in the absence and presence of drug.

Contrast	**B2-TPN0.2**	**B2-TPN0.4**	**B2-TPN0.6**	**B2-TPN0.8**
Core	B2-98.6dTPN0.2c	B2-98.6dTPN0.4c	B2-98.6dTPN0.6c	B2-98.6dTPN0.8c
Shell	B2-98.6dTPN0.2s	B2-98.6dTPN0.4s	B2-98.6dTPN0.6s	B2-98.6dTPN0.8s
Droplet	B2-85hTPN0.2d	B2-85hTPN0.4d	B2-85hTPN0.6d	B2-85hTPN0.8d
	B2-99hTPN0.2d	B2-99hTPN0.4d	B2-99hTPN0.6d	B2-99hTPN0.8d
Core with drug	B2-98.6dTPN0.2c-TP	B2-98.6dTPN0.4c-TP	B2-98.6dTPN0.6c-TP	B2-98.6dTPN0.8c-TP
Shell with drug	B2-98.6dTPN0.2s-TP	B2-98.6dTPN0.4s-TP	B2-98.6dTPN0.6s-TP	B2-98.6dTPN0.8s-TP
Droplet with drug	B2-85hTPN0.2d-TP	B2-85hTPN0.4d-TP	B2-85hTPN0.6d-TP	B2-85hTPN0.8d-TP
	B2-99hTPN0.2d-TP	B2-99hTPN0.4d-TP	B2-99hTPN0.6d-TP	B2-99hTPN0.8d-TP

2.6d) Brij O10 and tripalmitin nanoemulsions (B-TPN NE) in the absence and presence of drug (cont.).

Contrast	**B2-TPN1.0**	**B2-TPN1.2**	**B2-TPN1.4**	**B2-TPN1.6**
Core	B2-98.6dTPN1.0c	B2-98.6dTPN1.2c	B2-98.6dTPN1.4c	B2-98.6dTPN1.6c
Shell	B2-98.6dTPN1.0s	B2-98.6dTPN1.2s	B2-98.6dTPN1.4s	B2-98.6dTPN1.6s
Droplet	B2-85hTPN1.0d	B2-85hTPN1.2d	B2-85hTPN1.4d	B2-85hTPN1.6d
	B2-99hTPN1.0d	B2-99hTPN1.2d	B2-99hTPN1.4d	B2-99hTPN1.6d
Core with drug	B2-98.6dTPN1.0c-TP	B2-98.6dTPN1.2c-TP	B2-98.6dTPN1.4c-TP	B2-98.6dTPN1.6c-TP
Shell with drug	B2-98.6dTPN1.0s-TP	B2-98.6dTPN1.2s-TP	B2-98.6dTPN1.4s-TP	B2-98.6dTPN1.6s-TP
Droplet with drug	B2-85hTPN1.0d-TP	B2-85hTPN1.2d-TP	B2-85hTPN1.4d-TP	B2-85hTPN1.6d-TP
	B2-99hTPN1.0d-TP	B2-99hTPN1.2d-TP	B2-99hTPN1.4d-TP	B2-99hTPN1.6d-TP

2.6e) Brij O10 and tristearin nanoemulsions (B-GTS NE) in the absence and presence of drug.

Contrast	**B2-GTS0.1**	**B2-GTS0.2**	**B2-GTS0.4**	**B2-GTS0.6**	**B2-GTS0.8**	**B2-GTS1.0**	**B2-GTS1.2**	**B2-GTS1.3**
Droplet	B2-99hGTS0.1d	B2-99hGTS0.2d	B2-99hGTS0.4d	B2-99hGTS0.6d	B2-99hGTS0.8d	B2-99hGTS1.0d	B2-99hGTS1.2d	B2-99hGTS1.3d

2.6f) Brij O10 and ethyl oleate nanoemulsions (B-EO NE) in the absence and presence of drug.

Contrast	**B2-EO0.2**	**B2-EO0.4**	**B2-EO0.6**	**B2-EO0.8**
Droplet	B2-98hEO0.2d	B2-98hEO0.4d	B2-98hEO0.6d	B2-98hEO0.8d
Droplet with drug	B2-98hEO0.2d-TP	B2-98hEO0.4d-TP	B2-98hEO0.6d-TP	B2-98hEO0.8d-TP

2.6g) Tween 80 (T micelle), Tween 80:Dermosoft GMCY (weight ratio 3:1) (TD micelles) and Tween 80:Dermosoft GMCY: lecithin (weight ratio 7.5:2.5:1) micelles (TDL micelle) in the absence and presence of drug.

Contrast	**T2**	**TD2**	**TDL2**
Droplet	T2d	TD2d	TDL2d
Droplet with drug	-	TD2d-CUR	TDL2d-CUR
	-	TD2d-CUR-TP	TDL2d-CUR-TP

2.6h) Tween 80:Dermosoft GMCY (weight ratio 3:1) micelles and ethyl oleate nanoemulsions (TD-EO NE) in the absence and presence of drug.

Contrast	**TD2-EO0.64**	**TD2-EO0.72**
Droplet	TD2-98hEO0.64d	TD2-98hEO0.72d
Droplet with drug	TD2-98hEO0.64d-CUR	TD2-98hEO0.72d-CUR
	TD2-98hEO0.64d-CUR-TP	TD2-98hEO0.72d-CUR-TP

2.6i) Tween 80:Dermosoft GMCY (weight ratio 3:1) micelles and soybean oil nanoemulsions (TD-SBO NE) and Tween 80:Dermosoft GMCY: lecithin (weight ratio 7.5:2.5:1) micelles and soybean oil nanoemulsions (TDL-SBO NE) in the absence and presence of drug (cont.).

Contrast	**TD2-EO0.8**	**TDL2-SBO0.24**
Droplet	TD2-98hEO0.8d	TDL2-hSBO0.24d
Droplet with drug	TD2-98hEO0.8d-CUR	TDL2-hSBO0.24d-CUR
	TD2-98hEO0.8d-CUR-TP	TDL2-hSBO0.24d-CUR-TP

2.1.3.8.2 Analysis of SANS data

The FISH and SASView program were used to analyse the SANS data (Heenan, 1989; www.sasview.org). Before fitting the SANS data, the SLD of the various ingredients was calculated from **Equation 2.1**:

$$SLD = (\sum n_i b_i)/V_m \qquad \textbf{Equation 2.1}$$

where b_i is the bound coherent scattering length of n_i atoms in a molecule with molecular volume, V_m. In addition, the volume fraction of NE's was calculated. For SLD of mixture of solvent or surfactant, SLD of mixture was calculated by **Equation 2.2**:

$$SLD \text{ of mixture} = ((n_x b_x)+(n_y b_y))/((n_x V_{mx})+(n_y V_{my})) \qquad \textbf{Equation 2.2}$$

where n_x is the mole fraction of chemical x, b_x is the bound coherent scattering length of chemical x while n_y is the mole fraction of chemical y, by is the bound coherent scattering length of chemical y. V_{mx} and V_{my} are the molar volume of chemical x and y, respectively. The SLD of the various ingredients is tabulated in **Table 2.7 and 2.8**.

The data was analysed using solid-body models which allow for the ready construction of various possible models of the micelles and NE including spherical, oblate, prolate or triaxial ellipsoid and rod-shaped. In particular, the modelling of the micelles and NE using a core/shell model was explored. Here it was assumed that micelle core contained the surfactant tails and shell contained the surfactant head group and associated water of hydration while in the case of NE, the core consisted of oil while the shell consisted of the whole surfactant and associated water of hydration.

Table 2.7 Scattering length densities (SLDs) and related physicochemical parameters of the solvents and surfactants used for SANS measurements.

Composition	Molecular Formula	Molecular Weight (g/mol)	Density [a] (g/cm^{-3})	Molar Volume ($Å^3$)	SLD ($Å^{-2}$) x 10^{-6}
Solvent	H_2O	18.01	1.00	29.99	-0.561
	D_2O	20.03	1.107	29.99	6.393
	H_2O:D_2O (1:1)	-	-	29.99	2.916 [b]
hBrij O10 whole	$C_{38}H_{76}O_{11}$	708.94	1	1143.34	0.273
hBrij O10 tail	$C_{18}H_{35}$	251.47	0.75	556.97	-0.20
hBrij O10 head	$C_{20}H_{41}O_{11}$	457.47	1.30	586.38	0.74
hTween 80 whole	$C_{64}H_{124}O_{26}$	1309.65	1.07	2031.79	0.554
hTween 80 tail	$C_{17}H_{33}$	237.44	0.77	513	-0.204
hTween 80 head	$C_{47}H_{91}O_{26}$	1072.21	1.17	1518.79	0.808
hDermosoft GMCY whole	$C_{11}H_{22}O_4$	218.29	1.0	362.36	0.405
hDermosoft GMCY tail	C_7H_{15}	99.19	0.759	217	-0.441
hDermosoft GMCY head	$C_4H_7O_4$	119.10	1.36	145.36	1.625
hLecithin whole	$C_{42}H_{80}NO_8P$	758.06	1.012	1244	0.329
hLecithin tail	$C_{32}H_{62}$	446.83	0.824	900	-0.213
hLecithin head	$C_{10}H_{18}NO_8P$	311.23	1.502	344	1.75
hTween 80: hDermosoft GMCY (weight ratio3:1) whole	-	-	-	918.28	0.510
hTween 80: hDermosoft GMCY (weight ratio3:1) tail	-	-	-	315.57	-0.415
hTween 80: hDermosoft GMCY (weight ratio 3:1) head	-	-	-	602.71	0.941
hTween 80: hDermosoft GMCY: hLecithin (weight ratio 7.5: 2.5: 1) whole	-	-	-	942.48	0.493
hTween 80: hDermosoft GMCY: hLecithin (weigh ratio 7.5: 2.5: 1) tail	-	-	-	357.25	-0.370
hTween 80: hDermosoft GMCY: hLecithin (weight ratio 7.5: 2.5: 1) head	-	-	-	585.23	0.974

[a] from manufacturer
[b] SLD of the mixture of D_2O and H_2O in 1:1 volume ratio was calculated from the ratio of D_2O and H_2O by volume.

Table 2.8 Scattering length densities and related physicochemical parameters of the oils used for SANS measurements.

Composition	Molecular Formula	Molecular Weight (g/mol)	Density [a] (g/cm^{-3})	Molar Volume ($Å^3$)	SLD ($Å^{-2}$) x 10^{-6}
hSBO	-	885.5	0.924	1563	0.154
65hGTO	$C_{57}H_{104}O_6$	885.43	0.91	1609.91	0.153
99hGTO	$C_{57}H_{104}O_6$	885.43	0.913	1609.91	0.154
98dGTO [b]	$C_{57}D_{52.92}H_{51.08}O_6$	938.78	1.060	1609.91	3.916
85hTPN	$C_{51}H_{98}O_6$	807.29	0.92	1457.62	0.050
99hTPN	$C_{51}H_{98}O_6$	807.32	0.92	1457.62	0.050
98.6dTPN [c]	$C_{51}D_{96.63}H_{1.37}O_6$	905.93	1.03	1457.62	6.951
99hGTS	$C_{57}H_{110}O_6$	891.48	0.856	1728.8	0.013
98hEO	$C_{20}H_{38}O_2$	310.52	0.87	600	0.041

[a] from manufacturer
[b] Deuterated assumes 51% replacement of H for GTO.
[c] Deuterated assumes 98.6 % replacement of H for TPN.

Part 2 Study of nanoemulsion cytotoxicity

2.2.1 Materials

Advanced RPMI-1640 media (Roswell Park Memorial Institute), fetal bovine serum (FBS), penicillin-streptomycin (100X), trypsin-EDTA (0.05%, 1X) with phenol red, Glutamax^{TM} supplement and phosphate buffered saline (PBS, 10X, pH 7.4) were all obtained from Gibco, Invitrogen (UK). Trypan blue solution (0.4 %w/v), dimethylsulphoxide (DMSO) and 3-(4, 5-dimethylthiazol-2-yl)-2, 5-diphenyltetrazolium bromide (MTT) were purchased from Sigma-Chemical Co. Ltd. (Dorset, UK). Double distilled water were used to prepare autoclaved water and dilute PBS (10X) to prepare PBS (1X).

2.2.2 Methods

The determination of the cytotoxicity of the micelles and NE was performed using the MTT assay. The experiment was performed in a Howorth Airtech safety cabinet (Model SC II, class 2, Farnworth, UK).

2.2.2.1 Cell culture

The cervical-tumour-derived cell line, HeLa (HeLa; ATCC, CCL-2) and the murine colon carcinoma cell line, CT26, (CT26; ATCC, CRL-2638TM), were cultured in a complete media (i.e. advanced RPMI-1640 media supplemented with 10 % FBS, 50 U/mL penicillin, 50 μg/mL streptomycin, and 1 %v/v of 200 mM L–glutamine) in a humidified atmosphere at 37 °C in 5 % CO_2 and 95 % air. Cells were routinely grown in 75 cm^2 canted-neck tissue culture flask. The cells were passaged twice weekly when they had reached ~80 % confluency by removing the growth medium, washing the cell monolayer with PBS (1x), which prepared from PBS (10x) diluted 10 times using DI water, in order to remove any traces of serum which would inhibit the action of trypsin, while completely covering the monolayer of cells with trypsin-EDTA (0.05 %) and incubating the cells for approximately 2 minutes until more than 90% of cells had detached from the flask. After the incubation period, growth medium was added to inhibit any further activity of trypsin and cells were re-suspended by gently pipetting the cell suspension in and out of a Stripette Serological Pipette to break up any clumps of cells. The cell suspension was then divided between 75 cm^2 canted-

neck tissue culture flasks containing growth medium for further culturing or used in the MTT assay as described below.

2.2.2.2 Preparation of the cells for MTT assay

After the cells were washed with PBS (1x) which was prepared from PBS (10x) diluted 10 times using DI water and trypsinised, they were re-suspended in growth medium to obtain a known volume (V_{sp}) of cell suspension, normally 10 mL. Typically a 20 uL aliquot of this cell suspension was removed and 20 uL of trypan blue (0.4 %w/v) added to stain any dead cells dark blue. The hemocytometer and cover slip was cleaned and dried. Once the coverslip was fixed in the position, 20 uL of cells was added to the hemocytometer. The number of living, clear cells within 4 squares of the hemocytometer was then determined and the volume of growth medium required to re-suspend the cells (V_{med}) at the desired cell count per mL (C_{cell}) calculated as **Equation 2.3**.

$$V_{med} = (\text{total cell count}/4) \times 2 \times (10^4/C_{cell}) \times V_{sp} \qquad \textbf{Equation 2.3}$$

where the factor 2 accounts for the dilution of 20 uL of cell suspension with 20 uL trypan blue solution. Dividing the total cell count by 4 gives the average number of cells in a single square of the hemocytometer since the volume contained in each square is 0.1 mm^3 or 10^{-4} mL, a multiplication factor of 10^4 is used.

Once diluted using advanced RPMI-1640 media to the required cell count, the cell suspension was then dispensed into a 96-well flat bottom tissue culture plate (0.2 mL per well) using a multichannel pipette. The 96-well tissue culture plate was then incubated overnight in a humidified incubator at 37 ˚C and 5 % CO_2, 95 % air.

2.2.2.3 Sample preparation for the MTT assay

The HeLa and CT26 cells was seeded in 96-well plates at 5 x 10^3 cells/ well in a complete media for 24 or 72 hours in a humidified incubator at 37 ˚C and 5 % CO_2, 95 % air. The outer wells of the plate were not used to avoid any edge effects and filled with PBS. The cells were then incubated with 200 uL of different concentration surfactant micelles or NE dispersions

in the presence or absence of different concentrations of CUR or DTX. The autoclaved water and DMSO were the negative and positive controls, respectively, achieved by incubating the cells with 20 uL of either autoclaved water or DMSO and 180 uL of complete media.

The 5 mg/mL of MTT solution was prepared by reconstituting the MTT powder in 1x sterile PBS and subsequently filtered to sterilise this solution using a 0.22-um sterile filter. The MTT solution was stored at −20°C and protected from light until use. Before using, the MTT solution was diluted with complete media at a volume ratio of 1:6. At the end of the incubation period, the complete media was removed at the required time and replaced with 120 μL of the mixture of complete media and MTT solution. Cells were incubated for 3 hours at 37 °C and 5 % CO_2. At the end of the incubation period, formazan was dissolved in 200 μL of DMSO and the wells in the plate were read at 570 nm (A_{570nm}) using a FLUO star OPTIMA plate reader (BMG Labtech). The results were expressed as percentage cell survival (mean ± SD), calculated using **Equation 2.4** and expressed as mean ± S.D., (n=5):

$$\% \text{ Cell survival} = (A_{570nm} \text{ of treated cells}/A_{570nm} \text{ of untreated control cells}) \times 100\ \%.$$

Equation 2.4

Part 3 Synthesis

2.3.1 Materials

Brij O10, hydrochloric acid 37 % (HCl), poly(ethylene glycol) bis(3-aminopropyl) terminated (bis(3-aminopropyl) terminated PEG), dicyclohexylcarbodiimide (DCC), HEPES, ninhydrin, Sephadex G-25 and pyridine were all obtained from Sigma-Aldrich (Dorset, UK). Folic acid, crystalline was purchased from Alfa Aesar (Lancashire, UK), while 2, 2, 2-trifluoroethanesulfonyl chloride (tresyl chloride) was supplied by Acros organics (Geel, Belgium). Absolute ethanol was from VWR international (Leicestershire, UK). Dimethylsulfoxide, anhydrous dimethylsulfoxide (DMSO), dichloromethane and anhydrous dimethylformamide (DMF) was purchased from Fisher Scientific (Loughborough, UK). Deuterium oxide was supplied by Goss Scientific Instruments (Cheshire, UK). Dimethylsulfoxide ($-d_6$) was obtained from Cambridge Isotope Laboratories (Massachusetts, USA). Ultrapure water (MilliQ, Millipore, Spain) and double distilled water were used throughout all experiments.

2.3.2 Methods

2.3.2.1 Synthesis of PEG bis(3-aminopropyl) terminated-folate

2.3.2.1.1 Preparation of PEG bis(3-aminopropyl) terminated-folate

2.250 mg (1.5 mmol) bis(3-aminopropyl) terminated PEG was reacted with 661.5 mg (1.5 mmol) folic acid in DMSO (50 mL) containing one molar equivalent of DCC and 100 uL of pyridine. The reaction mixture was stirred 2 days in the dark at room temperature. Water (100 mL) was added and the insoluble by-product, dicyclohexylurea, removed by filtration through Whatman glass microfiber filter, grade GF/F. The filtrate was then evaporated and kept in the fridge until use. The filtrate was dissolved in water and then passed through a Sephadex G-25 column, previously equilibrated with water. The filtrate was eluted with water at a flow rate of 2 mL/min, and 10-mL fractions were collected from first yellow elute was eluted. This collection was repeated until all of the yellow eluates had been eluted, typically 15 x 10-mL fractions. Each fraction was analysed for folate content by determining its absorbance at 364 nm and for $-NH_2$ content by the ninhydrin assay as described below. The synthesis of PEG bis(3-aminopropyl) terminated-folate was showed in **Figure 2.3**.

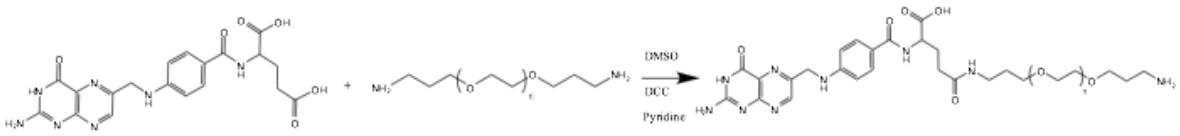

Figure 2.3: Synthesis of PEG bis(3-aminopropyl) terminated-folate

2.3.2.1.2 Analysis of PEG bis(3-aminopropyl) terminated-folate

The diagram of analysis of PEG bis(3-aminopropyl) terminated-folate was shown in **Figure 2.4**.

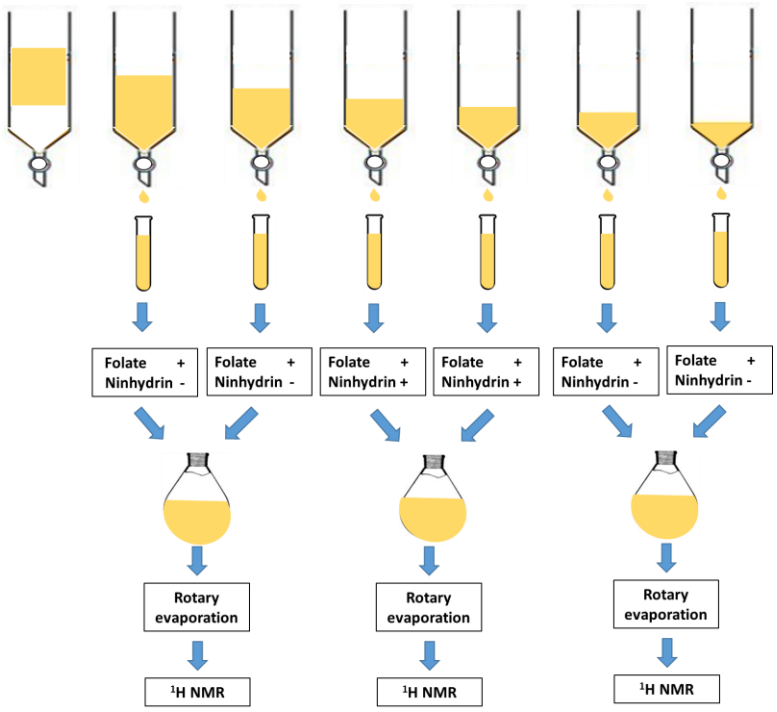

Figure 2.4: Diagram shown the process of synthesis and analysis of PEG bis(3-aminopropyl) terminated-folate.

Analysis of PEG bis(3-aminopropyl) terminated-folate using UV-vis spectroscopy

A calibration curve of folate was prepared by first making a stock folic acid solution by dissolving folic acid in ethanol at a concentration of 0.13 mg/mL. The stock solution was diluted with ethanol to prepare a number of solutions of folic acid concentration ranging from 0.0065 to 0.065 mg/mL. The folate content of each fraction was determined.

Analysis of PEG bis(3-aminopropyl) terminated-folate using ninhydrin reaction

To qualitatively analyse the amount of $–NH_2$ present in each fraction, a 2 %w/v ninhydrin stock solution was prepared by dissolving 2 g ninhydrin in ethanol and adjusting volume to 100 mL with ethanol. For the assay, 200 uL of ninhydrin solution was added to 100 uL of each fraction in glass vial. This mixture was heated by a heat gun for 5 minutes and the change in colour of mixture was examined by eye. In this test, bis(3-aminopropyl) terminated PEG and folic acid were positive and negative controls, respectively. 100 uL of the positive control was reacted with 200 uL of ninhydrin and a purple colour was detected. On the other hand, 100 uL of negative control was reacted with 200 uL of ninhydrin and a colour of the mixture remained yellow.

Analysis of PEG bis(3-aminopropyl) terminated-folate using proton nuclear magnetic resonance spectroscopy (^{1}H NMR)

After each fraction was analysed for its folate and $–NH_2$ content, the fractions which showed same results for the ninhydrin reaction and the folate analysis were pooled together and evaporated using a rotary evaporator.

The chemical structure of dry product of the various pooled fractions, i.e. the first fractions which are positive to folate only, the fractions which are positive for both folate and ninhydrin and finally the last group fractions of fractions which are positive to folate, was determined using ^{1}H NMR spectroscopy (Bruker Avance DRX 400 MHz NMR spectrometer) (Bruker, Coventry, UK). Each dry product was dissolved in a D_2O or DMSO system prior to analysis by ^{1}H NMR spectroscopy. The chemical shifts (δ) were expressed as parts per million (ppm). Data from synthetic procedures was analysed using MestReNova software (Mestrelab Research SL, Spain).

Analysis of PEG bis(3-aminopropyl) terminated-folate for folate and $–NH_2$ ratio

To quantitatively determine the folate content in the final product, the dry product of fractions that contained PEG bis(3-aminopropyl) terminated-folate was diluted in HEPES buffer to prepare a solution at a concentration of 0.368 mg/mL and the absorbance at 364 nm measured (LAMBDA 2 UV/Vis Spectrophotometer, Perkin-Elmer, USA). Ethanol was used as the blank.

In order to quantitatively determine -NH_2 content, 10 mg of bis(3-aminopropyl) terminated PEG was weighed and water added up to 10 mL to obtain a stock solution. Solutions were prepared as illustrated in **Table 2.9**. Both standard and samples were gently mixed and heated in boiling water for 15 min, after which time the samples were cooled to room temperature and 5 mL of 50 %v/v ethanol was added. The UV absorbance of each sample was measured at 570 nm (LAMBDA 2 UV/Vis Spectrophotometer, Perkin-Elmer, USA). The blank in this study was the mixture of 1 mL of water, 1 mL of 2 %w/v ninhydrin solution and 5 mL of 50 %v/v ethanol, heated in the same way as the sample.

Table 2.9 Composition of samples used to prepare the calibration curve.

Chemical	Amount of chemicals (mL)					
	1	2	3	4	5	6
bis(3-aminopropyl) terminated PEG stock solution	0.3	0.4	0.6	0.7	0.9	1.0
water	0.7	0.6	0.4	0.3	0.1	0
2 %w/v ninhydrin solution	1	1	1	1	1	1
50 %v/v ethanol	5	5	5	5	5	5

Consequently the folate and -NH_2 content of the PEG bis(3-aminopropyl) terminated-folate was determined from the calibration curve obtained for both of the chemicals using the absorbance measured for both chemicals.

2.3.2.2 Synthesis of tresylated Brij O10

2.3.2.2.1 Preparation of tresylated Brij O10

The synthesis of tresylated Brij O10 is shown in **Figure 2.5**.

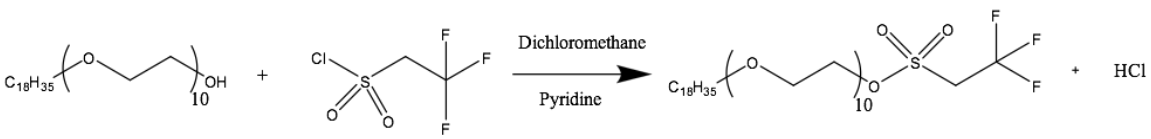

Figure 2.5: Synthesis of tresylated Brij O10.

The method used for tresylation of Brij O10 was a modification of the method used to tresylate Brij 78 (Jain et al., 2010). In brief, Brij O10 (2.84 g, 4mmol) was dissolved in 10 mL dichloromethane and incubated at 0 ˚C. Tresyl chloride (480 uL, 8 mmol) and 1 mL pyridine were then added dropwise to the Brij O10 solution with stirring. Once the addition was complete, the reaction was allowed to continue at room temperature with constant stirring for 2 days under nitrogen atmosphere. After which time the solution was rotary evaporated under reduced pressure and the resultant precipitate re-dissolved in 240 mL ethanol with 1 mL HCl. The solution was kept overnight at −20 ˚C and the precipitate formed centrifuged at 3000 rpm for 2 min. The supernatant was discarded and the resultant pellet was re-suspended in 50 mL ethanol acidified with 50 uL HCl. The centrifugation and the re-suspension in a mixture of ethanol and HCl were repeated until pyridine was removed as verified by a minimum and constant absorbance (around 0.1) at 255 nm. The solid tresylated Brij O10 was stored at -20 ˚C under nitrogen.

2.3.2.3 Synthesis of folate derived Brij O10

2.3.2.3.1 Preparation of folate derived Brij O10

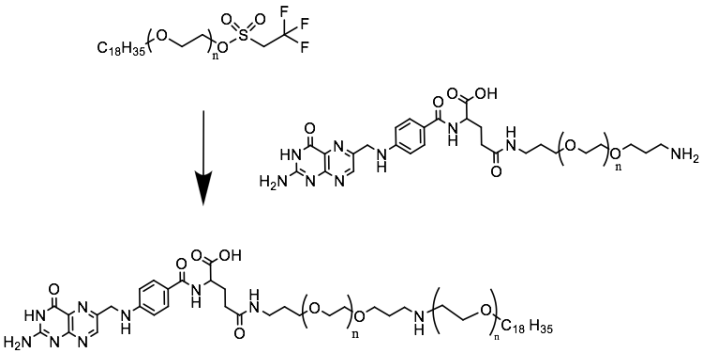

Figure 2.6: Synthesis of folate derived Brij O10.

PEG bis(3-aminopropyl) terminated-folate (0.165 mmol, 1.63 mL of a 194.39 mg/mL in anhydrous dimethylformamide) was added to tresylated Brij O10 (424.9 mg, 0.495 mmol) and the mixture allowed to react overnight at room temperature. The reaction mixture was then evaporated using the rotary evaporator to remove dimethylformamide and the resulting product dissolved in 15 mL of DI water and subjected to chromatography using a Sephadex G-25 column previously equilibrated with water. The sample was eluted with water at a flow

rate of 2 mL/min, and 10-mL fractions were collected from the first yellow elute. This collection was repeated until all of the yellow material had been eluted, typically this needed 16 x 10-mL fractions. Each fraction was analysed for folate content by determining its absorbance at 364 nm and for -NH_2 content using the ninhydrin assay described below. The synthesis of the folate derived Brij O10 is shown in **Figure 2.6**.

2.3.2.3.2 Analysis of folate derived Brij O10

The diagram of analysis of PEG bis(3-aminopropyl) terminated-folate is shown in **Figure 2.7**.

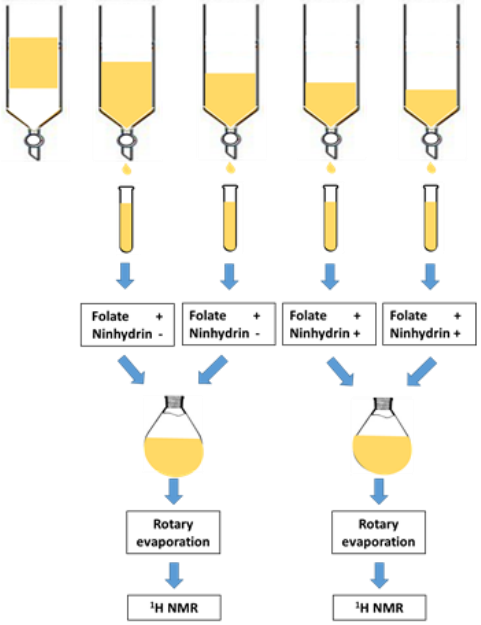

Figure 2.7: The diagram of analysis of folate derived Brij O10.

Analysis of folate derived Brij O10 using UV-vis spectroscopy

In order to determine the folate content of the final product, each fraction was analysed for folate content by measuring its absorbance at 364 nm. Blank was ethanol (LAMBDA 2 UV/Vis Spectrophotometer, Perkin-Elmer, USA).

Analysis of folate derived Brij O10 using ninhydrin reaction

To examine the presence of $–NH_2$ in the product, 2 %w/v ninhydrin solution was prepared by dissolving 2 g ninhydrin in ethanol and adjusting its volume to 100 mL with ethanol. For the assay, 200 uL of ninhydrin solution was added to 100 uL of each fraction in a glass vial. This mixture was heated and the colour of the mixture examined. In this test, bis(3-aminopropyl) terminated PEG and folic acid were the positive and negative controls, respectively. 100 uL of the positive control was reacted with 200 uL of ninhydrin and a purple colour was detected. Reacting 100 uL of the negative control with 200 uL of ninhydrin resulted in the mixture remaining yellow.

Analysis of folate derived Brij O10 using proton nuclear magnetic resonance spectroscopy (^{1}H NMR)

The chemical structure of folate derived Brij O10 after elution through Sephadex G-25 column was obtained using ^{1}H NMR spectroscopy (Bruker Avance DRX 400 MHz NMR spectrometer) (Bruker, Coventry, UK). Each dry sample was dissolved in a D_2O or DMSO system prior to analysis. Chemical shifts (δ) were expressed in parts per million (ppm).

Chapter 3
Preparation of Brij O10 nanoemulsions

3.1 Introduction

3.1.1 Background

Over the last two decades, many researchers have attempted to develop improved delivery systems for challenging drug candidates, in particular those candidates belonging to either Class II or IV of the biopharmaceutical classification system (BCS) (**Table 3.1**) (Amidon et al., 1995, Lobenberg and Amidon, 2000). Drug substances presenting with very poor aqueous solubility generally fall into Class II or IV of the BCS as a consequence of their low solubility, which results in a very poor *in vivo* absorption. In order to overcome the problem of the very poor water solubility of many drugs and drug candidates, new delivery systems are urgently required.

Table 3.1 Biopharmaceutical classification system (Amidon et al., 1995).

Class	Solubility	Permeability	Description
I	High	High	Well absorbed, absorption rate is usually higher than excretion rate.
II	Low	High	Bioavailability is limited by solvation rate. A correlation can be found between the *in vivo* bioavailability and the *in vitro* solvation rate.
III	High	Low	Although the drug is solvated quickly, absorption is limited by permeation rate.
IV	Low	Low	Those compounds have a poor bioavailability. Usually they are not well absorbed across the intestinal mucosa and thus a high variability is expected.

Over the last decade, there has been considerable interest in the use of nanoemulsions (NE) as drug delivery vehicles for poorly-water soluble drugs. This interest stems largely from the potential of NE to increase drug solubility, particularly in comparison to the corresponding micelles (Shafiq et al., 2007; Date and Nagarsenker, 2007). The ability of

NE to increase drug solubilisation is a consequence of the core of oil present in the NE, always assuming that is the drug is soluble in the oil. Despite the fact that NE have considerable potential as drug delivery vehicles, they have not been widely commercialised to date. This lack of exploitation is most probably a consequence of the requirement for advanced physico-chemical techniques such as laser light and neutron scattering, to both characterise and determine their stability, although almost all papers on NE suggest that it is possible to formulate them with stability lasting many years (Malcolmson, 1993; Solan et al., 2005; Maruno and Rocha-Filho, 2009).

An understanding of the detailed internal structure of a NE is important because of the correlation between structure, drug solubilisation capacity and ultimately drug bioavailability. The increase in bioavailability achievable with a NE is attributed to their small droplet size, which provides a large surface area for drug release (Charman et al., 1992, Shah et al., 1994). In addition, the amount and nature of the oil present in the NE have been shown to effect the physico-chemical properties of the NE, including the ability of the NE to solubilise drug. A previous study within our group has shown that NE containing the polyoxyethylated nonionic surfactant, $C_{18:1}E_{10}$ (Brij O10), and very low levels of the triglyceride soybean oil can significantly increase the apparent aqueous solubility of the hydrophobic drug, testosterone propionate, when compared to the corresponding Brij O10 micelles (Malcolmson et al., 1998). This increase in solubility was attributed to the large molecular volume of the soybean oil which resulted in the oil forming a core in the centre of the microemulsion (ME) droplets, thereby creating an extra locus of solubilisation of the testosterone propionate.

The present study examines the formation and detailed physico-chemical characterisation of oil-in-water (o/w) nanoemulsions (NE) prepared using the nonionic surfactant, Brij O10 in either water or an aqueous solution of 0.9 %w/v NaCl at room temperature. The polyoxyethylene nonionic surfactant, Brij O10 ($C_{18:1}E_{10}$), was chosen for this study because it has been shown in many studies to form NE without the need for cosurfactant (Malcolmson and Lawrence, 1995, Warisnoicharoen et al., 2000a; Wasutrasawat et al., 2013). Moreover, it is currently used in a range of pharmaceutical and cosmetic preparations (Porter, 1991). Furthermore, all oils used in this study are pharmaceutically acceptable. The phase inversion temperature of the polyoxyethylene nonionic surfactant, Brij O10, was determined in order to ensure the absence of any phase change around the

temperatures of interest, namely 25 and 37°C. In addition, the particle size of the NE was examined to ensure the stability of the NE over time.

3.1.2 Aim of the study

The aim of the study was to investigate the detailed molecular architecture and the physico-chemical properties of the NE in order to establish their capacity for two poorly-water soluble drugs, namely testosterone propionate (TP) and curcumin (CUR), alone or in combination. A range of physico-chemical techniques have been employed to achieve this aim.

3.2 Micelle and nanoemulsion without drug

3.2.1 The area of existence of Brij O10 nanoemulsions

Three component o/w NE were prepared and examined for their ability to remain stable at room temperature using a commercially available triglyceride or ethyl ester, the nonionic surfactant Brij O10 ($C_{18:1}E_{10}$) and either distilled water or an aqueous solution of 0.9 %w/v NaCl. In previous studies, it was found that both triglyceride and ethyl ester oils, possessing a high molar volume, could produce a large area of existence of NE using Brij O10 in water (Malcolmson et al., 1998; Warisnoicharoen et al., 2000a; Wasutrasawat et al., 2013). As a consequence triglyceride and ethyl ester oils with high molar volumes were chosen for the present study. The triglycerides used were selected from either the liquid triglycerides, soybean oil (hSBO) or triolein (two purities studied - 65hGTO and 99hGTO) or the solid triglycerides, tripalmitin (two purities studied - 85hTPN and 99hTPN) or tristearin (two purities studied - 60hGTS and 99hGTS). The high molar volume ethyl ester oils studied were either the liquid ethyl ester, ethyl oleate (two purities tested - 60hEO and 98hEO) or the solid ethyl ester, ethyl stearate (99hES). The area of NE existence was determined by varying the composition of each sample and plotting the results, on a weight basis, on a partial ternary phase diagram in order to understand the phase behaviour of the NE formulations (**Figures 3.1, 3.2 and 3.3**).

Triglyceride	Solvent	
	H_2O	0.9 %w/v NaCl
SBO	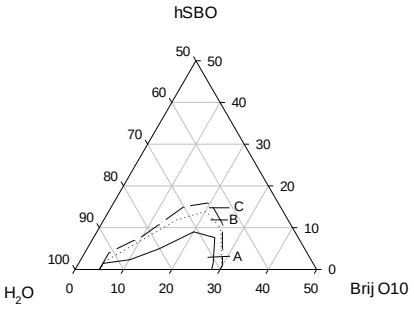	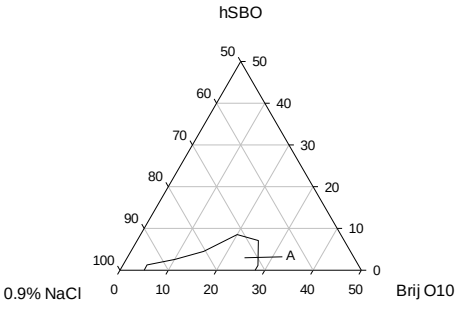

Figure 3.1: Partial ternary phase diagrams obtained for the oil-in-water nanoemulsions prepared using hSBO, Brij O10 and water or an aqueous solution of 0.9 %w/v NaCl after 1 month storage at room temperature. Clear NE are described as Region A NE, while bluish or translucent NE are called Region B NE and the cloudy or milky NE were denoted as Region C NE.

Triglyceride	Triglyceride purity	
	Low purity	High purity
GTO	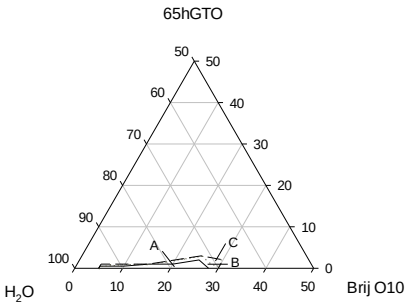	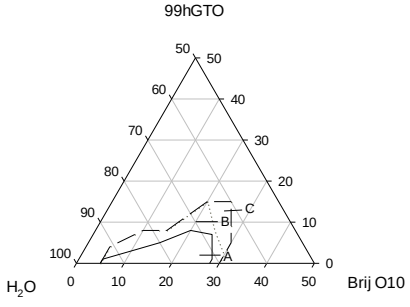
TPN	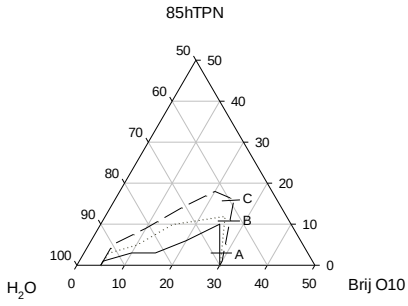	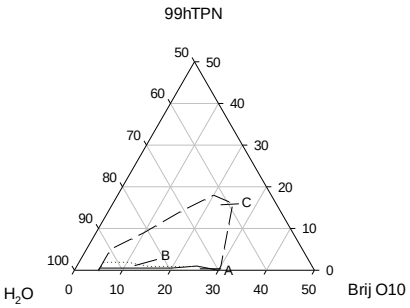
GTS	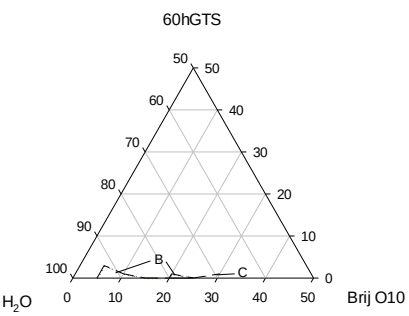	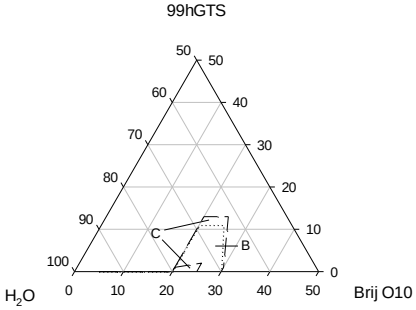

Figure 3.2: Partial ternary phase diagrams of the oil-in-water nanoemulsions prepared using triglyceride, Brij O10 and water after 1 month storage at room temperature. Clear NE are described as Region A NE, while bluish or translucent NE are called Region B NE and the cloudy or milky NE were denoted as Region C NE.

Ethyl ester	Ethyl ester purity	
	Low purity	High purity
EO	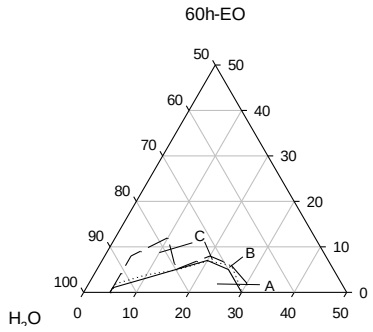	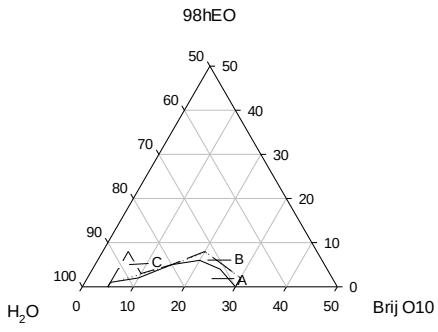
ES	Low purity ES was not available commercially.	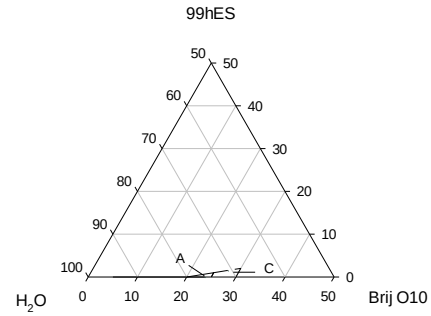

Figure 3.3: Partial ternary phase diagrams for the oil-in-water nanoemulsions prepared using ethyl ester, Brij O10 and water after 1 month storage at room temperature. Clear NE are described as Region A NE, while bluish or translucent NE are called Region B NE and the cloudy or milky NE were denoted as Region C NE.

On the abscissa, surfactant concentration (in %w/w) increases from left to right while on the ordinate, oil concentration (in %w/w) increases from bottom to top. A (partial) phase diagram is used regularly to observe the NE formation (Djekic et al., 2011; Lawrence and Rees, 2012). In the present study, only the region of the phase diagram at lower and intermediate surfactant concentrations of up to ~ 50 %w/w surfactant was determined. In previous studies the appearance of the individual NE after one month storage at room temperature was plotted on the phase diagrams. The present study focused on the one phase o/w NE region immediately, 1 day, 1 week and 1 month after preparation when stored at room temperature. **Figure 3.4** shows the appearance of 1 month old, stable NE. It can be seen that the appearance of these NE samples altered from transparent samples in Region A, the bluish/translucent samples of Region B, to the cloudy/milky samples of Region C as oil concentration increased.

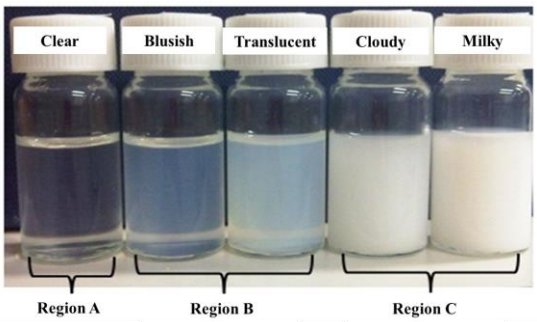

Figure 3.4: The appearance of oil-in-water nanoemulsions in Region A (clear), Region B (bluish/translucent) and Region C (cloudy/milky).

As can be seen in **Figures 3.1, 3.2 and 3.3**, the Brij O10 concentrations that formed NE ranged from 5-30 %w/w. Furthermore, when using hSBO, 85hTPN and 99hGTO, NE of all types of NE, i.e. Regions A, B and C NE, could be formed, with largest region of NE existence being Region A. In addition, the maximum level of oil incorporation observed occurred in the 20-25 %w/w range of surfactant. The formation of gels was observed at Brij O10 concentrations above 30 %w/w and when high amounts of oil were present. (Note that gels do not fall under the definition of a NE.) Indeed, many samples containing oils at a level greater than those recorded in Region C were gels or else they formed two phase systems and were therefore not studied any further. For comparative purposes, the upper limit of the amount of oil (%w/w) incorporated into stable, NE in Regions A, B and C are shown in **Table 3.2**.

Table 3.2 Upper limit of the amount of oil (%w/w) incorporated into Brij O10 containing oil-in-water nanoemulsions in Regions A, B and C which were stable for 1 month.

Type	Appearance of oil	Sample	5% Brij O10			10% Brij O10			15% Brij O10			20% Brij O10			25% Brij O10			30% Brij O10		
			A	B	C	A	B	C	A	B	C	A	B	C	A	B	C	A	B	C
Triglyceride	Liquid	hSBO, H_2O	1.4	2	4	2.3	7	8	5	12	15	9	14	16	7.5	10	11	-	0.5	1
		hSBO, 0.9 %w/v NaCl	1.4	N	N	2.3	N	N	5	N	N	9	N	N	7.5	N	N	-	N	N
		65hGTO, H_2O	0.5	-	1	0.5	1	-	1	-	-	1	2	-	2	3	-	-	0.5	2
		99hGTO, H_2O	1	3	4	3	7	8	5	8	-	8	15	-	6	8	15	-	2	5
	Solid	85hTPN, H_2O	1	3	5	3	5	9	3	10	14	6	11	18	10	12	16	-	-	1
		99hTPN, H_2O	0.5	2	5	0.5	2	9	0.5	1	14	0.5	1	18	1	-	16	-	-	1
		60hGTS, H_2O	-	3	-	-	1	-	-	-	-	-	1	-	-	-	-	-	-	1
		99hGTS, H_2O	-	-	-	-	-	-	-	-	-	-	11	1, 12-13	-	11	1-2, 12-13	-	-	1
Ethyl ester	Liquid	60hEO, H_2O	1	2	8	3	4	12	5	-	-	7	-	8	5	6	-	-	-	2
		98hEO, H_2O	1	-	8	2	3	-	5	-	-	6	8	-	4	5	-	-	2	-
	Solid	99hES, H_2O	-	-	-	-	-	-	-	-	-	1	-	-	1	-	-	-	-	2

- means the NE was not formed.
N means the experiment was not performed.

The area existence of clear Region A NE formed by hSBO, shown in **Figure 3.1**, occurred between 5-30 %w/w Brij O10, with a maximum oil incorporation of 9 %w/w hSBO, which occurred at ~ 20 %w/w Brij O10. The highest hSBO concentration obtainable in the bluish/translucent Region B NE was 14 %w/w which occurred at a Brij O10 concentration of 20 %w/w. In comparison the highest hSBO concentration achievable in the NE formed in cloudy/milky, Region C was 16 %w/w, which again occurred at 20 %w/w Brij O10.

The presence of electrolytes in the aqueous phase of micellar or NE formulations has been known to affect, generally reduce, the extent of hydration of the polyoxyethylene head group and may, as a consequence, reduce the extent of the area of NE existence (Schott and Royce, 1984). In the present study, the effect of electrolytes on the level of oil incorporation in NE at 22 °C was examined by the use of an aqueous solution containing 0.9 %w/v NaCl solution in place of water. A 0.9 %w/v aqueous NaCl solution was selected for study because it is isotonic and is commonly used in pharmaceutical preparations intended for intravenous administration. It was clear from **Figure 3.1** that the phase behaviour of NE prepared using Brij O10 and the aqueous 0.9 %w/v NaCl solution at 22 °C was very similar to that seen when water was used as solvent, suggesting that at this experimental temperature, the phase behaviour of the surfactants is not very sensitive to the presence of this concentration of electrolyte.

Based on previous work it was anticipated that NE prepared using a large molar volume oil would produce a large area of NE existence in the phase diagramm. However, some of NE prepared using the same oil but of differing purity did not produce NE of comparable area existence. Specifically, the area existence of NE containing 65hGTO, 99hTPN and 60hGTS were much smaller than those obtained using the corresponding oils of differing purity, namely 99hGTO, 85hTPN and 99hGTS, respectively (**Figure 3.2**), although interestingly, in all cases, the maximum level of oil incorporation occurred at approximately 20 %w/w Brij O10. For example, the maximum amount of oil incorporated into the area existence of clear, Region A and bluish/translucent, Region B, NE containing 65hGTO was 1 and 2 %w/w, respectively, while in contrast the maximum level of incorporation of GTO of 99% purity (99hGTO) in the corresponding regions was much higher at 8 and 15 %w/w, respectively. The maximum level of incorporation of 85hTPN in the clear, Region A and bluish/translucent, Region B NE was 6 and 11 %w/w, respectively while only 0.5 and 1 %w/w of the higher purity TPN, namely 99hTPN, respectively was incorporated into the corresponding A and B

Regions. Differences were also observed in the cloudy/milky Region C NE. For example a maximum oil incorporation of 13 %w/w 99hGTS was observed in this region while NE containing 60hGTS did not exhibit the formation of any cloudy/milky NE. On the other hand, the area existence of Region C NE obtained using 60hEO as oil was not significantly different from that prepared using 98hEO.

While, the differences observed in the extent of NE formation was clearly a consequence of the purity of the various oils, there was no obvious correlation between purity and the extent of NE formation. The purity of the oils used in the present study was assessed by determining their ^{1}H NMR spectra in chloroform-d **(Appendix B.1-B.10)**. It was established that the ^{1}H NMR spectra obtained was broadly in agreement with the reported composition of the oil, although there was the presence of some impurities which could potentially affect the formation of NE. The ^{1}H NMR spectra of both 85hTPN and 99hGTS exhibited a signal at δ = 3.5 ppm, which Joyce et al. (2016) have proposed is due to the presence of a glyceryl group of monoglyceride or diglycerol. In contrast the corresponding oils, 99hTPN and 60hGTS, did not exhibit the same signal at δ = 3.5 ppm. It has been established that the presence of Imwitor 308, i.e. glyceryl caprylate, can increase the area of ME existence as a consequence of Imwitor 308 penetrating into the interfacial surfactant region, acting as a cosurfactant (Zargar-Shoshtari et al., 2010). Further, the higher amount of Imwitor 308 contained in ME, the greater the area of ME existence (Zargar-Shoshtari et al., 2010). Considering this information, it would be expected therefore that the presence of a monoglyceride and/or a diglycerol in 85hTPN and 99hGTS NE would be the reason why these oils exhibited a larger area of NE existence than was seen when the oils, 99hTPN and 60hGTS, were used. In addition, the level of saturation of a fatty acid has been also found to have an effect on the formation of NE (Almeida et al., 2010). Almeida et al. (2010) illustrateed that the particle size of NE containing cholesteryl stearate (C18:0) exhibited the greatest particle size and greater size variation than NE containing either cholesteryl oleate, C18:1, or cholesteryl linoleate, C18:2, respectively. In the present study, 65hGTO contained a lower amount of unsaturated fatty acid than 99hGTO, resulting in a smaller area of NE formation in the 65hGTO-containing systems. However, clear NE stabilised by 20 %w/w Brij 96 NE showed a maximum incorporation of tributyrin (C4:0) at 4 %w/w (Warisnoicharoen et al., 2000a) while a maximum incorporation of 10 %w/w trilaurin (C12:0) occured at the same concentration of surfactant (Wasutrasawat et al., 2013). Consequently, the degree of saturation of a fatty acid did not show the clear relationship with the area existence of NE. Interestingly, while 60hEO exhibited a

signal at δ = 2.8 ppm, suggesting that 60hEO contained the impurity CH=CH-C**H**$_2^*$-CH=CH (Miyake et al., 1998; Knothe and Kenar, 2004), 98hEO contained a monoglyceride/glycerol impurity. As a consequence of both oils containing impurities, the effect of which balanced each other out, lead to a similarity in the area of NE existence of the 60hEO and 98hEO containing systems.

As expected, NE prepared using either triglyceride or ethyl ester possessing long, (C18) saturated chains, namely 60hGTS, 99hGTS and 99hES formed only very small areas of NE existence. Both 60hGTS and 99hGTS could not form clear, Region A, NE while 99hES formed a clear Region A NE containing only 1% oil. This observation can be explained by the fact that 60hGTS, 99hGTS and 99hES are expected to be crystallisation at room temperature, and hence it may be inferred that at higher concentrations of oil, the formation of fat crystals might disturb surfactant formation of the NE. Calligaris et al. (2016) reported that systems containing hGTS and 30 %w/w Tween 80 in 0.8 M NaCl only formed transparent ME (diameter ~25 nm) at or below 5 %w/w oil content; whereas turbid dispersions were generated at hGTS concentrations of 7.5 %w/w or above. Lyon et al. (1990) have also reported the formation of opalescent systems (which the authors termed ME) containing ES and the surfactant, Teric X10 or Triton X100, at oil:surfactant ratios of 0.8:1, 1:1 and 1.6:1. These systems become milkier is appearance over several hours before creaming and finally separating into oily layers and transparent aqueous layers. Interestingly, the 99hGTS containing systems formed cloudy NE at an oil concentration of only 1%, while at the higher oil concentrations of 2-11%, the NE became bluish/translucent (Region B) and at 12-13% oil content appeared cloudy. This result suggested that the shape and size of NE changed at each boundary. In order to confirm this hypothesis, it was necessary to use SANS to establish the presence of shape changes in the 99hGTS-containing systems as a function of oil concentration.

The results obtained in the present studies of the formation of a clear NE area at low surfactant concentrations (**Figures 3.1, 3.2 and 3.3**) are in contrast to those reported by Kale and Allen (1989) who determined that it was not possible to produce ME using light mineral oil, Brij 96 and water without the presence of a cosurfactant. Encouragingly however, the area existence of Brij O10 NE found in the present study covered a similar range of concentrations to those reported by Gradzielski et al. (1990) for the formation of isotropic, water-continuous phase (L_1 phase) by paraffin/Brij 96/water. Although, in contrast to the studies of Gradzielski et al. (1990) the area of NE observed in this study does not extend to the water apex. This difference could be

explained by the greater number of compositions prepared at low surfactant concentrations in the present study, allowing the extent of NE existence in this region to be more closely defined. It was also observed that the NE compositions individually produced within the Region A of the three-phase diagram shown in **Figures 3.1, 3.2 and 3.3** could be diluted with water to produce compositions closer to the water apex which, although outside the experimentally determined NE region, remained clear for at least a month.

Compositions outside the Region A towards the water apex, exhibited varying degrees of turbidity, eventually separating into two phases. The boundary of NE with higher surfactant concentrations was not as easy to define. Clear and fluid NE systems tended to increase in viscosity with increasing Brij O10 content until gels were formed. These gels, although initially clear, fluid systems could also form some time after preparation. The gels sometimes produced a ring upon tapping, and frequently exhibited birefringence. A region of a clear gel directly adjacent to the NE region, at a minimum Brij O10 concentration of approximately 30%, has also been reported by other researchers (Provost and Kinget, 1988; Gradzielski et al., 1990).

Due to the large size of the oil molecules and the long alkyl chains of the triglyceride or ethyl ester studied, it is not expected that oil will significantly penetrate into the hydrophobic chain region of the interfacial surfactant monolayer (Aveyard and Lawless, 1986). Therefore, it is expected that the core of the o/w NE droplet will consist of only oil and that this core is surrounded by the oleyl chains of the interfacial Brij O10 monolayer. The outer region of the NE is composed of ethylene oxide chains, the hydration of which increases as the distance from the core increases. In addition, previous studies (Malcolmson et al., 1998; Warisnoicharoen et al., 2000a; Wasutrasawat et al., 2013) have reported that NE prepared using large molecular volume triglycerides and stabilised by Brij O10 tend to form the large o/w NE region. The reason for this may be due to the fluid, long hydrophobic chain of the surfactant which assist in the incorporation of both long-chained oils and large volume triglyceride oils into the o/w NE droplets. These earlier studies (Malcolmson et al., 1998; Warisnoicharoen et al., 2000a; Wasutrasawat et al., 2013) reported the preparation of o/w NE using hSBO, 85hTPN and 98hEO using the same surfactant, $C_{18:1}E_{10}$ as studied here. It should be noted that Brij 96 and Brij 97 are the oldest and the previous version, respectively of Brij O10 ($C_{18:1}E_{10}$) and are no longer commercially produced.

At 20 %w/w surfactant, Brij O10 NE could incorporate 9 %w/w hSBO while Brij 96 and Brij 97 NE incorporated slightly lower levels of SBO, namely 6.5 and 7 %w/w hSBO, respectively (Malcolmson et al., 1995; Warisnoicharoen et al., 2000a). Obviously, the phase behaviour of the three versions of $C_{18:1}E_{10}$ was slightly different and this showed that the commercially polyoxyethylene surfactants contain a polydispersity of head group that has an effect on a variation of the phase diagram between different batches of surfactant. Besides the oil molecular volume, NE formation also depends on other factors such as chemical structure of the oils, the hydrophilic-lipophilic balance of surfactants and oils used, the surfactant molecular structure, the shape of micellar solution, etc.

3.2.2 Dilutability of nonionic o/w nanoemulsions containing Brij O10

The ability of NE to be diluted is essential for their use as drug delivery vehicle, particularly for oral delivery, because they will be diluted by body fluids after administration. The dilutability of NE also allows their physicochemical properties to be investigated with no change of the integrity of the system; which assures that the appearance of the clear NE remains clear, fluid and non-birefringent upon dilution. It should be noted that the ratio of oil to surfactant of the o/w NE stabilised by nonionic surfactant is expected to remain constant upon dilution (Attwood, 1994).

Dilutability experiments on Brij O10 NE showed that the NE stabilised by Brij O10 and prepared in water could be readily diluted from a range of surfactant concentrations, namely 15-25 %w/w, down to 1-2 %w/w surfactant, and that these diluted NE remained stable for at least a month at room temperature. These results suggest that the ability of the nonionic o/w NE prepared (without a cosurfactant) in the present study, to be readily diluted offers advantage for pharmaceutical purposes. In contrast, it has been established that ME containing cosurfactants cannot be diluted without altering the ME and in many cases, destroying them (Attwood, 1994). ME containing cosurfactant (typically a short chain alcohol) are frequently destroyed upon dilution due to the cosurfactant partitioning out from the interfacial monolayer of the ME droplet into the continuous phase (Lawrence, 1994).

3.2.3 Cloud point and phase inversion temperature

One of the characteristic properties of nonionic surfactants is their cloud point (CP). In general, the phase behaviour of nonionic surfactant micellar solutions especially of the polyoxyethylene surfactants depends on the experimental temperature. For example, increasing the temperature of a solution containing a water soluble nonionic surfactant frequently results in a phase separation of the micelles into surfactant-rich and surfactant-lean phases at a temperature known as the cloud point (CP) (Aveyard et al., 1989, Strey, 1996).

The phase inversion temperature (PIT) is defined as the temperature below which a surfactant preferentially partitions into water, and at which an o/w NE is transformed into a w/o NE. The PIT also corresponds to the temperature of the minimum value in o/w interfacial tension (Ruckenstein, 1997) and the temperature at which the uptake of oil and water into the surfactant-rich phase is equal (Billman and Kaler, 1991). The presence of a CP or a PIT in a surfactant system, especially if their temperature is close to that at which the micellar solution and NE will be used, can cause problems with their exploitation as a drug delivery vehicle because of the changes in physical behaviour and appearance that may occur upon routine temperature fluctuations. As a consequence it is therefore necessary to determine the CP and PIT of the Brij O10-containing micelles and NE.

3.2.3.1 The effect of micelle concentration on cloud point

The CP of Brij O10 micellar solutions was determined over a 1 – 20 %w/w concentration range of Brij O10 (**Figure 3.5**). The results show that the CP increases slowly with increasing nonionic surfactant concentration at concentrations above the critical micelle concentration (CMC). Similar trends in the variation of CP have been reported for the nonionic surfactant, Triton X-100 (Sadaghiania and Khan, 1991). The CP of 15, 20 and 25 %w/w Brij O10 micellar solutions were recorded in the present study as 67.4 ± 0.5, 69.3 ± 0.8, and 73.3 ± 0.7 °C respectively. Similar trends in the variation of the CP with Brij O10 concentration have been reported previously (Malcolmson et al., 1998; Warisnoicharoen et al., 2000a). However, the CP (and PIT) measured in this study were lower than those recorded for Brij 96, the oldest version of Brij O10, (Malcolmson et al., 1998) and higher than those recorded for Brij 97, the previous version of Brij O10, (Warisnoicharoen et al., 2000a). This observation might suggest that while Brij O10 was a less hydrophilic surfactant than Brij 96, it was more

hydrophilic surfactant than Brij 97. It is worth noting that the commercially polyoxyethylene surfactants contain a polydisperse head group. Any variation in the polydispersity of the head group has an effect on the CP leading to potential differences between different batches of surfactant. It has been suggested that the CP is more sensitive to impurities than the area of NE existence (Malcolmson et al., 1998; Warisnoicharoen et al., 2000a).

The CP of a nonionic surfactant system is the temperature at which the total effective forces between micelles changes from being repulsive to attractive (Mukherjee et al., 2011). This change results from either an increase in the attractive forces due to van der Waals forces of attraction and hydrophobic interactions between hydrophobic surfaces, or a decrease in repulsive forces because of a reduction in hydration forces at higher temperature and/or electrostatic double-layer forces, or a combination of both effects (Sadaghiania and Khan, 1991), in addition to related changes in micelle size and shape (Aveyard et al., 1990). With ethylene oxide surfactants such as Brij O10, an increase in experimental temperature results in a dehydration of the ethylene oxide head groups causing a reduction of the cross-sectional area of a polyoxyethylene head group (a_o). This dehydration results in an increase in the critical packing parameter (CPP) of the surfactant, and the formation of more elongated aggregates such as rods or discs of decreased curvature, all possessing higher aggregation numbers (Kjellander, 1982; Aveyard et al., 1990; Shigeta et al., 2001). However, this change is reversible when the system is cooled to a temperature below the CP with the system becoming a clear, single phase solution once again.

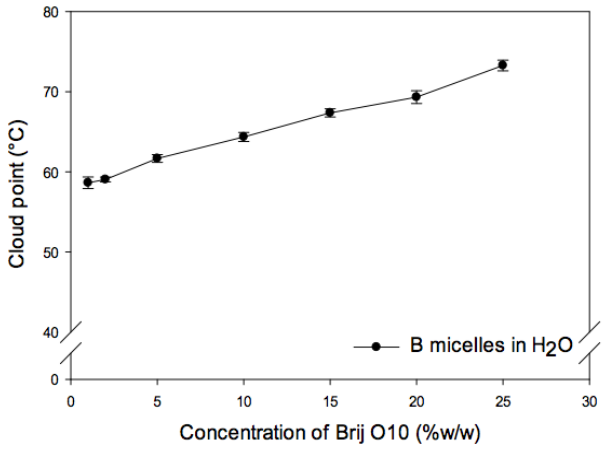

Figure 3.5: The cloud point of Brij O10 micellar solutions as a function of surfactant concentration (%w/w).

3.2.3.2 The effect of oil on the phase inversion temperature (PIT)

The CP of a micellar surfactant solution can be altered by the presence of additives such as oils. Note that the corresponding temperature of a NE is termed a phase inversion temperature (PIT) (Shinoda and Arai, 1964). The results of the CP experiments for the Brij O10/water systems and of the PIT experiments for the NE containing various triglycerides or ethyl esters as a function of oil concentration are shown in **Figures 3.6, and 3.7**.

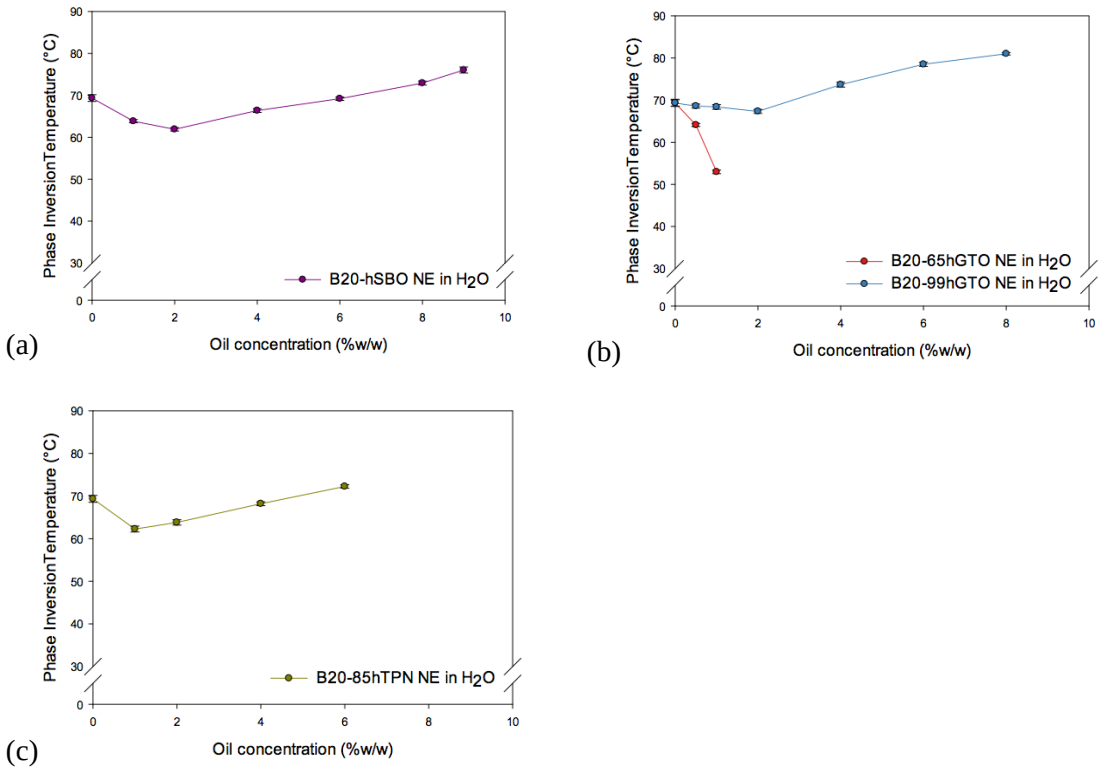

Figure 3.6: The phase inversion temperature of the oil-in-water nanoemulsions containing triglyceride (a) hSBO, (b) hGTO, and (c) hTPN and containing 20 %w/w Brij O10 in H2O (mean ± S.D.). Error bars in some cases contained within the symbols.

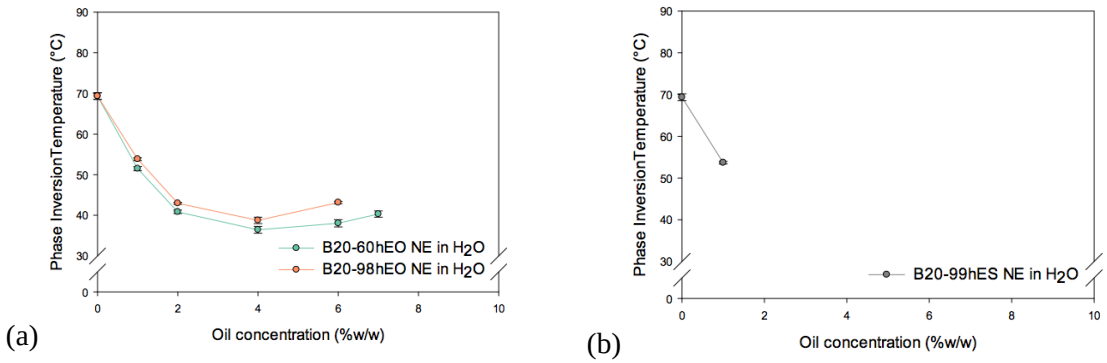

Figure 3.7: The phase inversion temperature of the oil-in-water nanoemulsions containing ethyl ester, (a) hEO and (b) hES, and containing 20 %w/w Brij O10 in H_2O (mean ± S.D.). Error bars in some cases contained within symbols.

The values determined for the PIT illustrated the complex and concentration-dependent way in which PIT varies with the nature and the amount of oil incorporated. According to the results obtained in the present study, the PIT of the Brij O10 NE containing the larger molecular volume oils first decreased and then increased as the concentration of oil increased. For example, NE systems containing more than 4 %w/w hSBO and 20 %w/w Brij O10 showed an increased PIT compared to the corresponding NE containing 2 %w/w hSBO. The decrease and then increase in PIT as the amount of oil increases suggests that the micellar aggregates were originally asymmetric in shape and became more spherical with oil concentration.

In order to interpret the results of the PIT studies, it is proposed that Brij O10 forms asymmetric rather than spherical micelles in the absence of oil. When a low level of oil is incorporated, it is proposed that the oil penetrates the interfacial surfactant monolayer, encouraging the formation of even more asymmetric micelles resulting in a PIT of the NE that is below the CP of the micelle. When an even higher content of oil is added, an increase in the PIT of the NE is observed. This increase can be explained by the fact that the oil can cause a transformation of asymmetric into spherical aggregates and the formation of a core of oil. It is clear from the PIT studies that only low level of triglyceride, namely 2 %w/w hSBO, 2 %w/w 99hGTO and, 1 %w/w 85hTPN was required to promote the transformation of the aggregates from asymmetric to spherical droplets, while larger amount of ethyl ester, namely 4 %w/w 60hEO and 4 %w/w 98hEO, was needed to effect the same transformation. This result is not surprising when considering the relative molecular volume of oils, shown in **Table 2.8**. The results of an earlier light scattering study (Warisnoicharoen et al., 2000b) support the hypothesis proposed here, and show that the asymmetric Brij 97 aggregates became more spherical

upon the addition of oil, with the oil forming a core. The hypothesis that the presence of a sufficient amount of a large molecular volume oil will cause a change in the shape can ideally be studied using small angle neutron scattering (SANS) in combination with contrast variation to determine the size and shape of the NE.

As the reduction of PIT was greatest for the smallest molecular volume oils, hEO and hES, it is likely that the smaller molecular volume oil penetrated the interfacial surfactant monolayer furthest forming the most asymmetric droplets. Indeed, the behaviour of small molecular volume oils may reasonably be likened to cosurfactant, sitting alongside the surfactant in the interfacial monolayer as opposed to forming a core of oil. On the other hand, the larger the molecular volume of the oil, the lower the extent of its penetration into the interfacial surfactant monolayer, the more symmetric the droplet becomes and the greater the increase in PIT. The order of the PIT measured in the present study was 99hGTO > 85hTPN > hSBO > 65hGTO >> 98hEO = 60hEO = 99hES. Based on the similarity in the value of the molecular volume (V_m) of the following oils, it would be anticipated that the PIT of NE containing either of the three triglycerides, namely hGTO (V_m = 1610 Å^3), hSBO (V_m = 1563 Å^3) or hTPN (V_m = 1458 Å^3), and the two ethyl esters, namely hEO (V_m = 600 Å^3) or hES (V_m = 596 Å^3) would be comparable. Correspondingly, the PIT of NE containing hGTO, hSBO or hTPN was expected to be higher than those containing hEO or hES. The PIT of 65hGTO is also much lower than that of 99hGTO which suggests that 65hGTO contained smaller molecular volume impurities than 99hGTO.

Moreover, the changes in PIT are typically explained in terms of the solubilisation of the oils of differing volume into the NE droplets. For example, oils with a large molecular volume are expected to form a core in the centre of the droplet. (Evans et al., 1986). A large core of oil in the centre of a NE droplet can provide an additional site to solubilise poorly-water soluble drug. It was therefore expected that the higher the molar volume of oil-contained in the NE, the greater the solubilisation of drug.

3.2.4 Light scattering investigations by photon correlation spectroscopy

Calculation of the hydrodynamic radius of a particle from the measured value of the diffusion coefficient obtained from photon correlation spectroscopy (PCS) only gives a true assessment of size at infinite dilution. The measurement of highly concentrated particles leads to problems with the interpretation of the data due to the presence of inter-particulate forces and/or the presence of multiple scattering of the laser beam

(Muller and Muller, 1984). The consequence of these effects is typically a higher diffusion coefficient, and a correspondingly smaller particle radius (Muller and Muller, 1984; Cheung, 1987). As a consequence therefore, all micelles and NE examined in the present study by PCS were diluted in order to increase the distance between droplets and decrease the interaction between individual particles (Ganz and Boeger, 1985). However, it is worth noting that dilution in (some) NE may change the interfacial composition of droplets, leading to a change in the structure or stability of the system (Siano et al., 1987) and the possible disappearance of the NE (Hermansky and Mackay, 1979; Richtening et al., 1988). This was not thought to be a problem in the present study due to the absence of a cosurfactant, coupled with the fact that the Brij O10 surfactant used could prepare the NE exhibited a low cmc. Due to the fact that the micelles and NE were not being measured at infinite dilution, the measured Z mean diameter is therefore referred to as the apparent hydrodynamic size or diameter (D_h).

3.2.4.1 Effect of Brij O10 concentration on particle size of micelle

The variation in the D_h of the Brij O10 micellar solutions at different concentrations of Brij O10, diluted to 1 %w/w Brij O10, without any added oil were examined by PCS (**Figure 3.8**). For Brij O10 surfactant solutions, the size of the micelles were found to be fairly constant at about between 13 – 15 nm. This constant size would be expected if the diluted micelles were acting as non-interacting aggregates. In all following studies, samples were diluted to 1 %w/w Brij O10 for determination of particle size, unless otherwise stated.

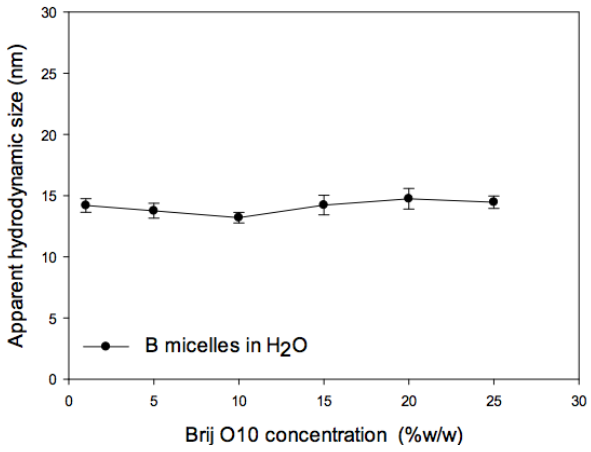

Figure 3.8: The mean hydrodynamic droplet size of the Brij O10 micellar solution without SBO (mean ± S.D.) at 25 °C. All samples were diluted to 1 %w/w Brij O10 for measurement.

3.2.4.2 Stability of nanoemulsions

A range of compositions within the NE area of existence were examined visually for any physical change immediately after preparation and after storage for periods of up to a month at room temperature. The NE were also examined by PCS for periods of up to 1 month. The apparent hydrodynamic size showed a good correlation between with NE appearance.

Figures 3.9 and 3.10 give graphs of the variation in the apparent hydrodynamic size measured at 25 ºC with varying oil concentration with time after preparation. The PCS measurements indicated that, because D_h did not exhibit any significant change, most of the samples were stable for at least 1 month. The only exceptions were 85hTPN NE containing greater than 12 %w/w oil, 99hTPN NE containing 2 %w/w oil and 99hGTS NE containing 1 %w/w oil, where there was a big increase in the apparent hydrodynamic size due to the fact that these NE became cloudy/milky (Region C).

Triglyceride	Triglyceride purity	
	Low purity	High purity
SBO	Low purity SBO was not available commercially.	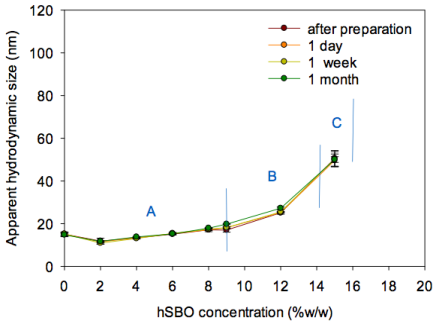 a)
GTO	b) 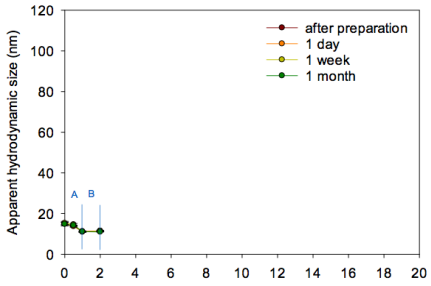	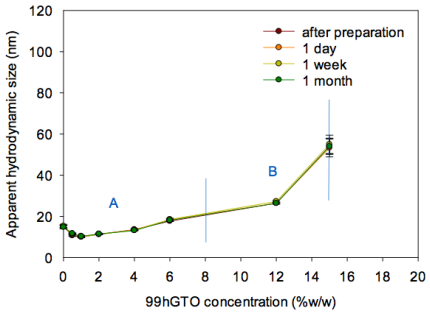 c)
TPN	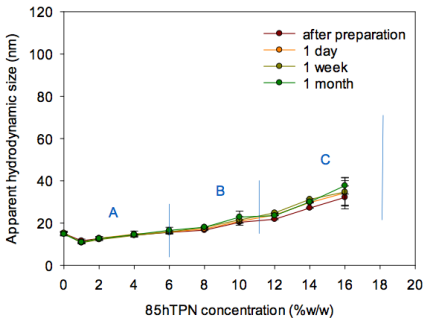 d)	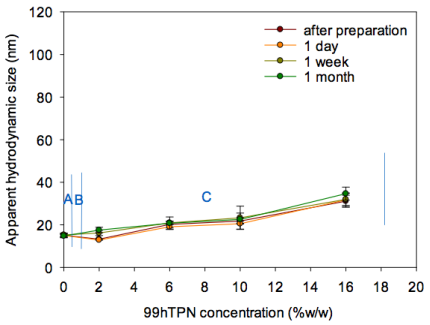 e)
GTS	Low purity GTS was not examined.	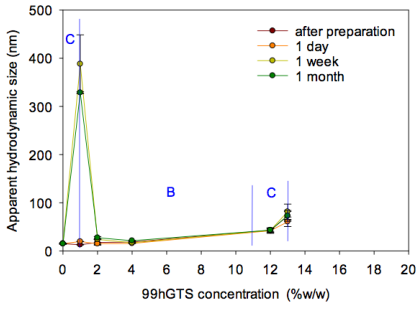 f)

Figure 3.9: The mean apparent hydrodynamic droplet size of the oil-in-water nanoemulsions containing 20 %w/w Brij O10 and containing either (a) hSBO, (b) 65hGTO, (c) 98hGTO, (d) 85hTPN, (e) 99hTPN, or (f) 99hGTS at different triglyceride concentrations over a period of up to a month (mean ± S.D.) at 25 °C. Samples were diluted to 1 %w/w Brij O10 for measurement. Error bars in some cases contained within the symbols.

Ethyl ester	Ethyl ester purity	
	Low purity	High purity
EO	Low purity EO was not examined.	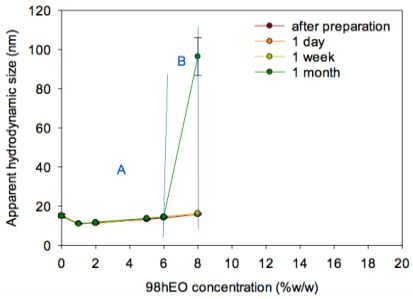

Figure 3.10: The mean apparent hydrodynamic droplet size of the oil-in-water nanoemulsions containing 20 %w/w Brij O10 and containing 98hEO (diluted to 1 %w/w Brij O10 for measurement) at different triglyceride concentrations over a period of up to a month (mean ± S.D.) at 25 °C. Samples were diluted to 1 %w/w Brij O10 for measurement. Error bars in some cases contained within the symbols.

Note that while the appearance and apparent hydrodynamic size of NE containing 8 %w/w 98hEO changed over time - becoming translucent (from bluish) and larger in size - this composition is on the phase boundary between Regions B and C. NE with greater than 8 %w/w were not stable and exhibited a phase separation over time.

3.2.4.3 Effect of oil on the particle size of nanoemulsions

The apparent hydrodynamic droplet size (D_h) of the NE with increasing oil concentration was examined at a Brij O10 concentration of 20 %w/w and a temperature of 25ºC (diluted to 1 %w/w for measurement). Regardless of the nature and amount of oil present, the D_h of the NE droplets fell well within the size range quoted for a NE (i.e. an upper limit of 200 nm) with sizes of up to a 100 nm being recorded for NE with an oil content within the upper boundary of Region C (**Figures 3.11 and 3.12**) (Solan et al. 2005; Gutierrez et al., 2008). More, however that NE containing 1 %w/w 99hGTS and prepared using 20 %w/w Brij O10 exhibited a D_h of 325 nm.

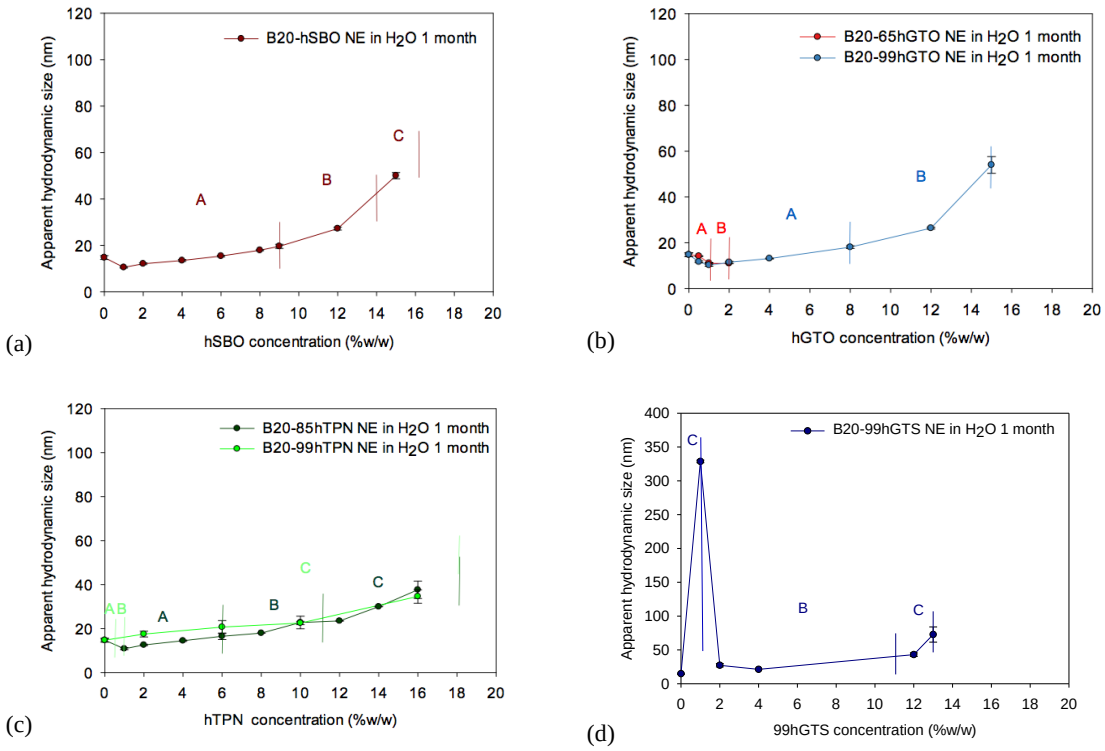

Figure 3.11: The mean hydrodynamic droplet size of the 1-month old oil-in-water nano emulsions containing 20 %w/w Brij O10 and containing triglyceride either (a) hSBO, (b) hGTO, (c) hTPN, or (d) 99hGTS at different triglyceride concentrations (mean ± S.D.) at 25 °C. All samples were diluted to 1 %w/w Brij O10 for measurement. Error bars in some cases contained within the symbols.

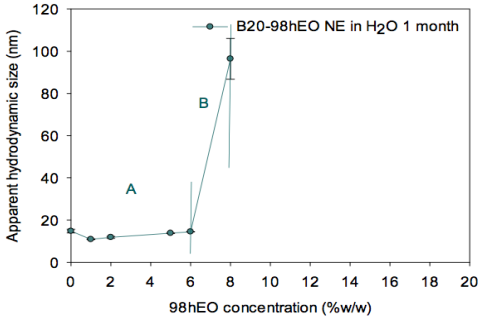

Figure 3.12: The mean hydrodynamic droplet size of the 1-month old oil-in-water nanoemulsions stabilised by 20 %w/w Brij O10 and containing ethyl ester, 98hEO at different concentrations (mean ± S.D.) at 25 °C. All samples were diluted to 1 %w/w Brij O10 for measurement. Error bars in some cases contained within the symbols.

It is of note that, regardless of the oil, NE droplets in Region A tended to be less than 25 nm in size while those that were in Region B were either bluish or transparent and exhibited a size in the range of 25 – 60 nm. For example, the D_h of one-month-old samples measured by PCS and prepared using 20 %w/w Brij O10 and containing the highest amount of oil in Region A were 19.6 ± 0.9 nm (at 9 %w/w hSBO), 11.1 ± 0.3

nm (at 1 %w/w 65hGTO), 18.1 ± 0.6 nm (at 8 %w/w 99hGTO), 22.8 ± 2.9 nm (at 10 %w/w 85hTPN) and 14.5 ± 0.1 nm (at 6 %w/w 98hEO).

The corresponding NE, prepared using the same concentration of Brij O10, and containing the highest amount of oil in Region B were 27.2 ± 0.6 nm (at 12 %w/w hSBO), 11.0 ± 0.1 nm (at 2 %w/w 65hGTO), 54.0 ± 3.7 nm (at 15 %w/w 99hGTO), 22.8 ± 2.9 nm (at 10 %w/w 85hTPN), 21.2 ± 0.1 nm (at 4 %w/w 99hGTS) and 96.4 ± 9.7 nm (at 8 %w/w 98hEO) in size. The corresponding NE containing the highest amount of oil in Region C were 50.1 ± 1.3 nm (at 15 %w/w hSBO), 37.7 ± 4.0 nm (at 16 %w/w 85hTPN), 34.6 ± 3.1 nm (at 16 %w/w 99hTPN) and 72.7 ± 11.2 nm (at 13 %w/w 99hGTS).

It is clear that the particle size of NE containing a triglyceride of large molecular volume and ethyl ester exhibited first a decrease in apparent hydrodynamic size followed by an increase in apparent hydrodynamic size as the level of oil increased **(Figures 3.11 and 3.12**). This fall and subsequent rise in apparent hydrodynamic size upon increasing oil concentration is indicative of a change in the shape of the surfactant aggregates from ellipsoidal aggregates at low oil concentrations to increasingly spherical at higher oil concentrations. The transformation of asymmetric or ellipsoid aggregates at low oil concentrations to spherical ones at higher oil concentrations has been observed with ME formed by both nonionic and ionic surfactants (Hoffmann and Ulbright, 1989).

The apparent hydrodynamic size of the NE varied approximately linearly with triglyceride or ethyl ester concentration in Region A suggesting that a bigger oil core was formed upon increasing oil concentration. Interestingly, for NE in Region B and C, the apparent hydrodynamic size either slightly increased or sharply increased. For example, the apparent hydrodynamic size increased from ~ 20 to 60 nm for NE containing either hSBO, 98hGTO, 85hTPN or 99hTPN while the size changed from 20 to ~ 100 nm for NE containing 99hGTS and 98hEO. This dramatic change in the size of the NE between Region B and Region C is indicative of a change in the structure of the NE found in Region A, most probably as a consequence of a larger amount of oil being present. It is thought that the higher amount of oil in Region B and C leads either to the formation of a larger oil core in the centre of NE droplet compared to the NE in Region A and/or the formation of a totally different NE structure from the structure of NE in Region A. It might reasonably be expected that in the larger sized NE, the interfacial surfactant monolayer represents a smaller portion of the NE volume, and as a

consequence the oil is more likely to behave a bulk oil. Interestingly, the particle size of NE in Region C containing either hSBO or 85hTPN and prepared using 20 %w/w Brij O10 were smaller than the corresponding NE examined in an earlier study (Wasutrasawat et al., 2013). This result suggested that the batch-to-batch variation of the Brij O10 surfactant had an effect on particle size.

3.3 Micelle and nanoemulsion in the presence of hydrophobic drugs

In order to examine the advantage of a NE as a delivery system, two hydrophobic drugs, testosterone propionate (TP) and curcumin (CUR), were chosen as drugs. In the present study, it is hoped not only to increase the apparent aqueous solubility of both drugs by formulating them as o/w NE but also to increase their bioavailability.

It is worth noting that NE are not inert vehicles for drug because the presence of drug may alter NE size, shape and/or stability. This is particularly true if the drug is surface active and sits in the interfacial surfactant region as it may disrupt the packing of surfactant in this region (Narang et al., 2007).

3.3.1 The incorporation of testosterone propionate

To investigate the incorporation of hydrophobic drug into a NE, the water-insoluble steroid, testosterone propionate (aqueous solubility of 0.0009 ± 0.002 %w/w), of log P_{oct} 4.78 was selected as drug (Malcolmson et al., 1998; Craig, 1990). Earlier studies reported that Brij 96 ME containing SBO were unaffected by the presence of an excess of TP (Malcolmson, 1993). In contrast, however, the presence of the drug, Tacrolimus, has an effect on NE particle (Borhade et al., 2008). In the present study, the effect of the addition of TP on NE stability was investigated by saturating the NE prepared using 20 %w/w Brij O10 containing varying amounts of oil with excess TP. After 7, 10 and 14 days incubation, excess TP was removed from the NE by centrifugation. TP was selected for study here as our group have shown that it is possible to prepare ME in which its apparent aqueous solubility was increased by careful selection of the components used to make the ME (Satra et al., 1995; Malcolmson et al., 1998). Example of licensed pharmaceutical formulation for TP include testosterone propionate ointment (2 %w/w) and testosterone propionate (50 mg/ml) in ethyl ester for intramuscular use (Virormone ®) (Lund W., 1994), both of which were prepared as oil-

based formulations. The solubility of TP in Brij O10 micelles and 3-component o/w NE were compared, and the effect of the drugs on the area of NE existence, apparent hydrodynamic size and phase inversion temperature of the NE droplets determined. The solubilisation of TP was determined in a range of oil types - namely triglycerides, ethyl esters and hydrocarbon oils (**Table 3.3**). The results of this study suggested that TP is preferentially solubilised in the triglycerides or ethyl esters of relatively high polarity in comparison to the hydrocarbon oils with relatively low polarity in which the TP is poorly soluble.

Table 3.3 The solubilisation of testosterone propionate in water and various oils (Malcolmson et al, 1998).

Sample		**Drug solubilisation (%w/v)**
DI water		0.0009 ± 0.0002
Triglycerides	tributryin	8.78 ± 0.51
	Miglyol 812	6.20 ± 0.44
	Soybean oil	3.42 ± 0.29
Ethyl esters	Ethyl butyrate	18.64 ± 0.45
	Ethyl caprylate	12.17 ± 0.68
	Ethyl oleate	5.79 ± 0.40
Hydrocarbon oils	Hexadecane	1.70 ± 0.10
	Hexadecane	1.74 ± 0.13
	1-octadecene	1.51 ± 0.01

3.3.1.1 Effect of testosterone propionate on the area of NE existence

A large number of samples were prepared using Brij O10 and containing varying amounts of either triglyceride or ethyl ester. The samples were all within the o/w NE region as shown in **Figures 3.1, 3.2 and 3.3.** When the samples were saturated with the drug, their physical appearance did not appear to be affected by the presence of TP, this was particularly true for samples in Region A. Furthermore, in no case did the presence of TP cause the NE to become cloudy/milky if the NE was initially bluish/translucent or to become bluish/translucent if the NE was initially clear.

It is important to note that, from visual observation, there was no evidence of the centrifugation resulting in the precipitation in any NE, either in the presence and absence of TP. Stability studies showed that the TP saturated NE prepared with either hSBO, 65hGTO, 99hGTO or 98hEO were stable for at least 2 months. In contrast, when

TP was added to NE samples containing 85hTPN and 99hTPN they became unstable. For example TP-loaded NE containing 14-16 %w/w of either 85hTPN or 99hTPN were precipitated within three weeks after preparation, while those containing 8-12 %w/w oil were unstable within four weeks and those containing 4-6 %w/w oil within six weeks. Significantly, the TP-loaded NE containing either 85hTPN or 99hTPN manifested their instability more quickly than the corresponding TP-free NE. The only exceptions to this were the TP-loaded NE containing relatively small amounts of TPN, namely 1-2 %w/w, which remained stable for at least 2 months, suggesting that the NE containing the lower concentrations of triglyceride were more stable. On the other hand, the NE containing the higher triglyceride concentrations might not be able to re-arrange to accommodate both the TP and triglyceride within their structure. Previous PCS results suggested that the 85hTPN incorporated into NE containing 20 %w/w Brij O10 and between 2-3 %w/w oil were in a 'liquid-like' state (Wasutrasawat et al., 2013). Wasutrasawat et al. (2013) showed that NE containing either fluid triglycerides exhibited a better long term stability, both in the absence and presence of the lipophilic TP drug, when compared to NE containing 'solid-like' triglycerides particularly when a high amount of solid triglyceride was present and the NE loaded with TP. The high stability of NE containing either hSBO, 99hGTO or 98hEO NE, coupled with the relatively large NE region exhibited by the NE containing these oils, suggests that these NE offer considerable potential as drug delivery vehicles.

3.3.1.2 Effect of testosterone propionate on cloud point and phase inversion temperature

The cloud points (CP) and the variation in the phase inversion temperature (PIT) of drug-loaded micellar solutions and NE followed the trend of the corresponding samples prepared in the absence of TP (**Figures 3.13 and 3.14**) suggesting that (some of) TP was probably located at the boundary between the hydrophobic and hydrophilic regions of the interfacial surfactant monolayer. The differences in the PIT of NE containing either hSBO, 65hGTO or 98hEO NE with and without TP was around 5 ºC ($p < 0.05$). A similar difference was also seen between the CP of TP-free micellar solutions and the CP of TP-loaded micellar solutions ($p < 0.05$). On the basis of these results, it is proposed therefore that TP was solubilised in the surfactant micelles in a similar way to NE containing the oils, hSBO, 65hGTO or 98hEO NE.

<table>
<tr><th rowspan="2">Triglyceride</th><th colspan="2">Triglyceride purity</th></tr>
<tr><th>Low purity</th><th>High purity</th></tr>
<tr><td>SBO</td><td>Low purity SBO was not available commercially.</td><td> 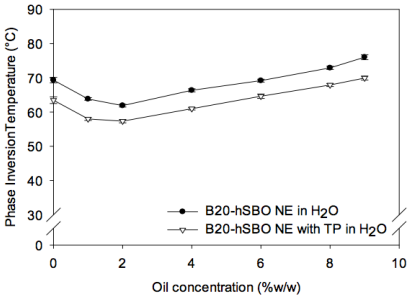

a)</td></tr>
<tr><td>GTO</td><td> 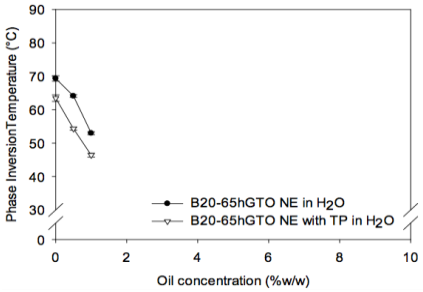

b)</td><td> 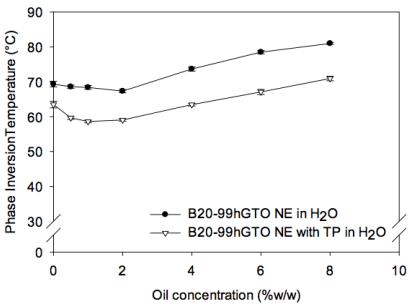

c)</td></tr>
<tr><td>TPN</td><td> 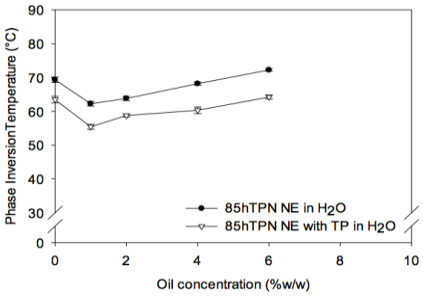

d)</td><td>High purity TPN was not examined.</td></tr>
</table>

Figure 3.13: The phase inversion temperature of oil-in-water nanoemulsions containing triglyceride, (a) hSBO, (b) 65hGTO, (c) 99hGTO and (d) 85hTPN and stabilised by 20 %w/w Brij O10 in H_2O and in the absence and presence of testosterone propionate (TP) (mean ± S.D.). Error bars in some cases contained within the symbols.

Ethyl ester	Ethyl ester purity	
	Low purity	High purity
EO	Low purity EO was not examined.	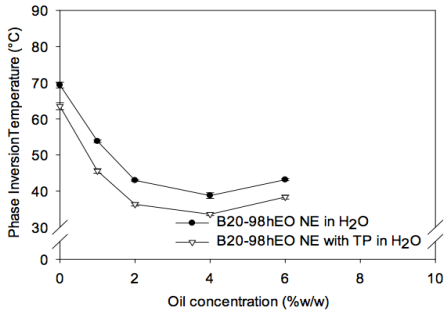

Figure 3.14: The phase inversion temperature of oil-in-water nanoemulsions containing ethyl ester, 98hEO, and stabilised by 20 %w/w Brij O10 in H_2O and in the absence and presence of testosterone propionate (TP) (mean ± S.D.). Error bars in some cases contained within the symbols.

The decrease in PIT of 99hGTO containing NE loaded with TP compared with the corresponding NE in the absence of TP was greater than the difference between the measured CP for the TP-free and TP-loaded micellar solutions. This result suggested that the amount of TP solubilised in the interfacial surfactant monolayer of 99hGTO containing NE was higher than the amount of TP solubilised in the same region in the drug-free micelles, possibly as a consequence of the solubility of TP in GTO being so low such that more TP tended to sit in the interfacial surfactant monolayer of the NE (Wasutrasawat et al, 2013).

In the case of 85hTPN containing NE, the difference in PIT in NE with and without TP was ~ 5 ºC, suggesting that again TP was solubilised at the boundary between the hydrophobic and hydrophilic portions of the surfactant monolayer in the TPN-NE. The difference between PIT with and without TP increased with increasing content of 85hTPN (4-6 %w/w 85hTPN). Hence the core of NE containing a higher amount of 85hTPN were more solid as evidenced by the results of DSC experiments (Wasutrasawat et al., 2013). Consequently, the ability of TP to solubilise in the oil core were decreased as the amount of 85hTPN increased and thus more TP tends to sit at the boundary between the hydrophobic and hydrophilic region of the interfacial surfactant monolayer (Wasutrasawat et al, 2013).

3.3.1.3 Effect of testosterone propionate on the particle size of Brij O10 micelle and nanoemulsions

Light scattering investigations by photon correlation spectroscopy (PCS) were carried out on six NE systems in which a saturation amount of TP had been added in order to examine the effect of the TP on the apparent hydrodynamic size of NE containing either hSBO, 65hGTO, 99hGTO, 85hTPN, 99hTPN or 98hEO. PCS investigations of the equivalent drug-free NE have been previously reported **(Figures 3.15 and 3.16)**. Light scattering analysis of the TP saturated NE prepared using 20 %w/w Brij O10 and containing the six oils were performed 7 days after the addition of TP, with the excess TP being removed by centrifugation.

Triglyceride	Triglyceride purity	
	Low purity	High purity
SBO	Low purity SBO was not available commercially.	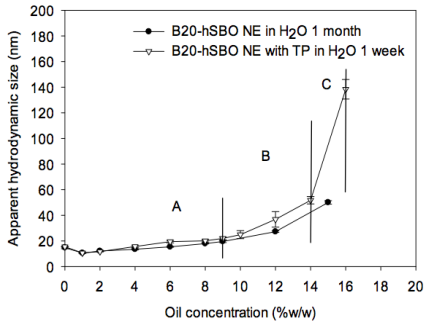 a)
GTO	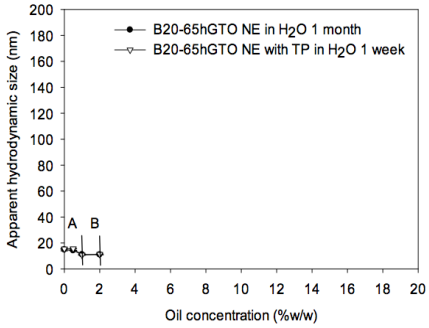 b)	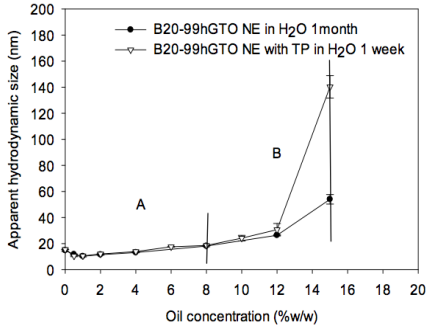 c)
TPN	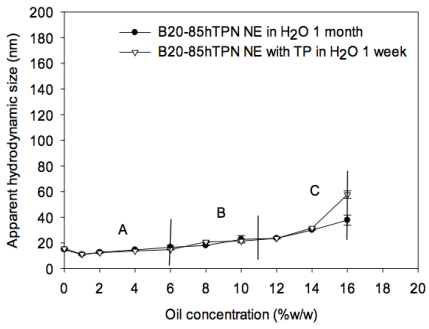 d)	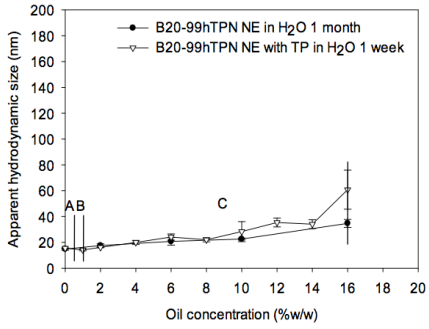 e)

Figure 3.15: The mean hydrodynamic droplet size of the 1-month old oil-in-water nanoemulsions stabilised by 20 %w/w Brij O10 and containing triglyceride either (a) hSBO, (b) 65hGTO, (c) 99hGTO, (d) 85hTPN, or (e) 99hTPN at different concentrations in the absence and presence of testosterone propionate (TP) (mean ± S.D.) at 25 °C. Samples were diluted to 1 %w/w Brij O10 for measurement. Error bars in some cases contained within the symbols.

Ethyl ester	Ethyl ester purity	
	Low purity	High purity
EO	Low purity EO was not performed.	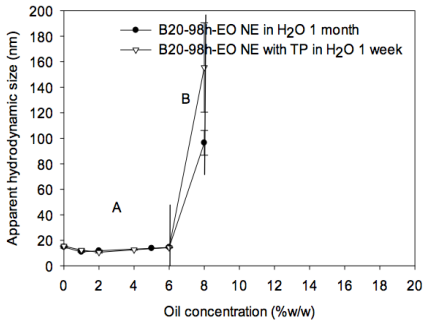

Figure 3.16: The mean hydrodynamic droplet size of the 1-month old oil-in-water nanoemulsions stabilised by 20 %w/w Brij O10 and containing ethyl ester, (a) 98hEO at different concentrations in the absence and presence of testosterone propionate (TP) (mean ± S.D.) at 25 °C. Samples were diluted to 1 %w/w Brij O10 for measurement. Error bar in some cases contained within the symbols.

Results of the PCS investigations are shown in **Figures 3.15 and 3.16**. The apparent hydrodynamic size of the NE with and without TP, are plotted as a function of oil concentration. In all Region A NE, the apparent hydrodynamic size (D_h) of NE containing a saturation amount of TP were slightly larger in those prepared in its absence. In region B the only exception was the measured D_h of 99hGTO and 98hEO containing NE where there was a significant increase in particle size of TP-saturated NE ($p < 0.05$). In Region C, NE containing either hSBO, 85hTPN or 99hTPN NE were significantly larger in the presence of TP ($p < 0.05$). This increase in size was anticipated due to the presence of drug within the NE droplet. However, it must also be noted that (because the added TP had replaced an equivalent weight of water found in the drug-free compositions) the volume fraction of the TP-loaded NE droplets was larger than the corresponding TP-free compositions increasing the possibility of a greater degree of interaction between NE droplets.

However, the increase in NE size observed in this study was much less than the dramatic increase reported by Wasutrasawat et al. (2013) who stated that the D_h of TP saturated 85hTPN NE containing 16 %w/w oil was 183.3 ± 3.8 nm compared to the 71.8 ± 0.3 nm size determined for the corresponding TP-free 85hTPN NE. This result showed the effect of batch-to-batch variation of surfactant.

3.3.1.4 The solubility of testosterone propionate in micelle and nanoemulsions

The level of TP incorporation after saturation was investigated in Brij O10 micelles and o/w NE containing six oils, namely hSBO, 85hTPN, 99hTPN, 65hGTO, 99hGTO and 98hEO (**Figures 3.17 and 3.18**). It can be seen that saturation solubilisation of TP was achieved by 7 days. In addition, the results clearly showed that there was a significant increase in the amount of TP solubilised in the hSBO, 99hGTO, 85hTPN or 99hTPN containing NE system prepared using 20 %w/w Brij O10 compared to corresponding micellar systems. It has been reported that the differences in the location of solubilised steroid molecules in surfactant micelles depend upon the polarity of the drug (Tomida et al., 1978; Lundberg et al., 1979).

Triglyceride	Triglyceride purity	
	Low purity	High purity
SBO	Low purity SBO was not available commercially.	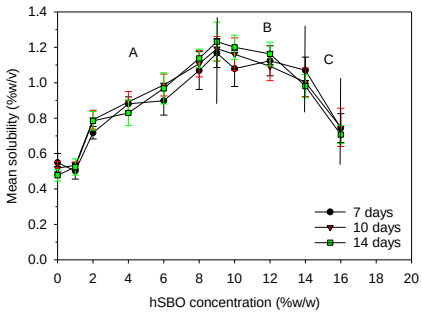 a)
GTO	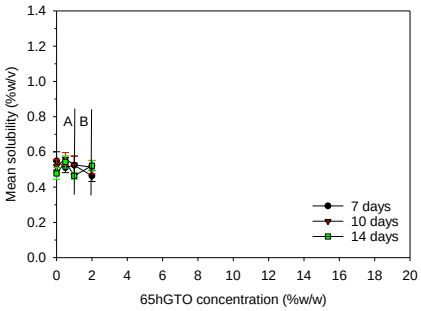 b)	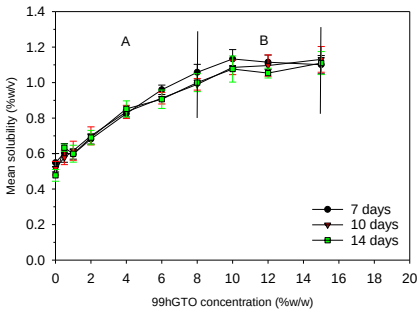 c)
TPN	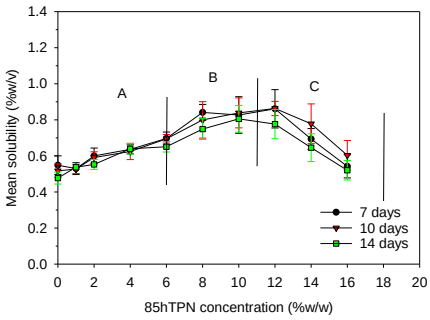 d)	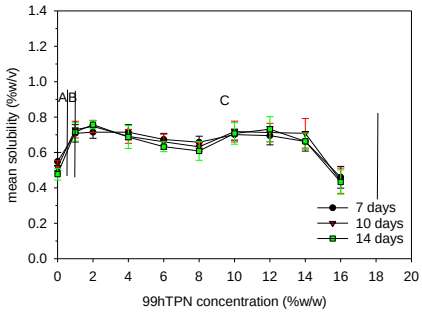 e)

Figure 3.17: The solubilisation of testosterone propionate in micelles and oil-in-water nanoemulsions stabilised using 20 %w/w Brij O10 and containing triglyceride either (a) hSBO, (b) 65hGTO, (c) 99hGTO, (d) 85hTPN or (e) 99hTPN at different concentrations (mean ± S.D.) at 25 °C. Error bars in some cases contained within the symbols.

Ethyl ester	Ethyl ester purity	
	Low purity	High purity
EO	Low purity EO was not performed.	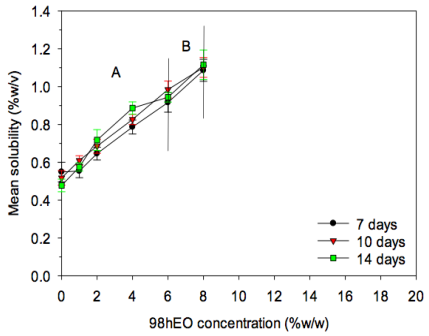

Figure 3.18: The solubilisation of testosterone propionate in micelles and oil-in-water nanoemulsions stabilised using 20 %w/w Brij O10 and containing ethyl ester, 98hEO at different concentrations (mean ± S.D.) at 25 °C. Error bars in some cases contained within the symbols.

As can be seen, a significant increase in TP solubilisation was observed with increasing triglyceride or ethyl ester concentration in Region A NE. In NE containing 2 %w/w triglyceride or ethyl ester, the solubility of TP in the oil phase was deemed insufficient to affect any significant increase in TP loading. The only NE containing 2 %w/w oil that exhibited a much higher level of incorporation of TP was the NE containing 99hTPN. In contrast the solubility of TP in NE containing higher amount of oil was large enough to allow a significant increase in the amount of TP in the NE when compared to the parent micelles. The increase in TP continued with oil concentration until Region B, where solubilisation levelled off, whereas in Region C solubilisation dramatically decreased (**Figures 3.17a, 3.17d and 3.17e**). The levelling off in Region B and decrease in TP solubilisation in the Region C was unexpected. It had been anticipated that NE in these regions would exhibit an increase in TP solubilisation due to the high solubility of TP in the oil coupled with the large apparent hydrodynamic size of the NE. Possible changes in the structure of the NE at higher triglyceride/ethyl ester concentrations maybe responsible for this observation. In particular the results may indicate a significant change in the internal structure of the NE resulting in it becoming a less favourable environment for TP solubilisation. Small angle neutron scattering therefore was used to probe the internal structure of the NE.

In the PIT experiments, it was seen that the oil with the higher molecular volume caused the greatest increase in the PIT, ultimately forming a large oil core in the centre of the NE providing an additional locus to solubilise TP. On the basis of these results, it was anticipated that the high molar volume oil containing NE would exhibit a greater

level of TP solubilisation. The results obtained for TP solubilisation agree with this assumption; TP solubilisation was greater in 99hGTO containing NE, which in turn were greater than hSBO containing NE, which in turn are greater than the 85hTPN containing NE. However, it was unexpected that TP solubilisation in 98hEO containing NE was higher than that seen in 85hTPN containing NE.

Table 3.4 gives a comparison of the experimentally measured TP solubilisation with that calculated from the solubilisation of TP in the Brij O10 micelles coupled with the amount of oil incorporated in the NE. This comparison shows that the experimentally measured TP solubilisation in the NE was higher than the calculated solubilisation, which shows the advantage of NE over micelles in improving the apparent TP solubilisation. This observation suggests that oil was incorporated in the NE in such a way as to improve the solubilisation of TP.

Table 3.4 Comparison of expected TP solubilisation.

Sample	Region	Experimental TP solubilisation (%w/v)	Expected TP solubilisation (%w/v)[a]
B20	-	0.48 ± 0.03	-
B20-hSBO1	A	0.50 ± 0.05	0.51
B20-hSBO2		0.72 ± 0.04	0.55
B20-hSBO4		0.88 ± 0.04	0.62
B20-hSBO6		0.90 ± 0.08	0.69
B20-hSBO8		1.10 ± 0.11	0.75
B20-hSBO9		1.17 ± 0.08	0.79
B20-hSBO10	B	1.08 ± 0.10	0.82
B20-hSBO12		1.12 ± 0.08	0.89
B20-hSBO14		1.07 ± 0.07	0.96
B20-hSBO16	C	0.74 ± 0.08	1.03
B20-98hEO1	A	0.55 ± 0.04	0.54
B20-98hEO2		0.65 ± 0.03	0.60
B20-98hEO4		0.79 ± 0.04	0.71
B20-98hEO6		0.92 ± 0.05	0.83
B20-98hEO8	B	1.09 ± 0.06	0.94

[a] calculated from the experimental TP solubilisation in micelle and oil according to amount of oil and surfactant in the samples. The solubility of TP in 20 %w/w Brij O10 was 0.48 ± 0.03 %w/v at 25 ^{0}C while the solubility of TP in hSBO and 98hEO was 3.42 ± 0.29 and 5.79 ± 0.40 %w/v at 25 ^{0}C (Malcolmson et al., 1993; Malcolmson et al., 1998).

3.3.2 The incorporation of curcumin

In order to investigate the incorporation of hydrophobic drug into the NE, the water insoluble drug, curcumin was selected. The solubilisation of CUR was determined in a range of oils - namely triglycerides, ethyl esters and hydrocarbon oils (**Table 3.5**). The results suggest, that even though CUR is water-insoluble drug, it does not dissolve at high levels in the various oils studied. The results indicate that CUR was preferentially solubilised in the triglycerides or ethyl esters (i.e. oils with relatively high polarity) in comparison to the hydrocarbon oils (i.e. oils with relatively low polarity). Moreover, the limited results available suggests that the purity of material had an effect on CUR solubilisation in the oil as CUR solubilisation in 60hGTO was higher than that in 99hGTO. Because the triglycerides and ethyl esters, hSBO and 98hEO respectively, exhibited the highest level of CUR solubilisation, both oils were selected for further study.

Table 3.5 The solubilisation of curcumin in water and various oils (mean ± S.D.), n = 3.

Sample		**Drug solubilisation (%w/v)**		
		7 days	**10 days**	**14 days**
DI water		< 0.0007	-	-
Triglycerides	hSBO	0.18 ± 0.03	0.19 ± 0.01	0.20 ± 0.02
	60hGTO	0.12 ± 0.00	-	-
	99hGTO	0.07 ± 0.02	-	-
Ethyl ester	60hEO	0.14 ± 0.01	-	-
	98hEO	0.14 ± 0.03	-	-
Hydrocarbon oils	Hexadecane	< 0.0007	-	-
	Hexadecene	< 0.0007	-	-

The effect of the addition of CUR on the stability of the NE containing varying amounts of oil was investigated by saturating Brij O10 micelles and NE with an excess of CUR. The excess CUR was removed from contact with either micelles or NE after either 7, 10 or 14 days by centrifugation. The effect of the presence of a saturation amount of CUR on the area of NE existence, the phase inversion temperature, and the apparent hydrodynamic size was determined. In addition, the solubility of CUR in Brij O10 micelles and 3-component o/w NE were established.

3.3.2.1 Effect of curcumin on the area of NE existence

A large number of samples of varying hSBO or 98hEO content, all from within Region A of the o/w NE area of existence, were prepared in the presence of a saturation amount of CUR (**Figures 3.1 and 3.3**). It is worth commenting that, from visual observation, there was no evidence of instability in any of the CUR containing micelles or NE, before or after removal of excess CUR. Most of the CUR-containing Brij O10 NE were completely clear in Region A (**Figure 3.19**). Furthermore, most of the CUR saturated NE prepared using hSBO or 98hEO were stable for at least 1 month. However, in the presence of CUR all the Brij O10 micelles, regardless of surfactant concentration, as well as B20-hSBO9-CUR, B20-98hEO1-CUR and B20-98hEO2-CUR NE transformed, within 2 weeks of preparation, from clear to turbid. This observation suggests that the physical appearance of Brij O10 micelles and Region A, 3-component o/w NE produced from hSBO or 98hEO and Brij O10, were affected by the presence of CUR, possibly by affecting/disrupting the packing of surfactant and the long term stability of the micelles and NE.

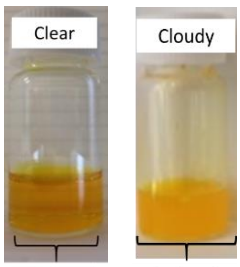

Figure 3.19: The appearance of a) clear nanoemulsions and b) cloudy nanoemulsions in the presence of curcumin.

3.3.2.2 Effect of curcumin on cloud point and phase inversion temperature

The cloud point of B20-CUR micelles at different concentrations of surfactant is reported in **Figure 3.20**. The micelles saturated with CUR showed a decrease in the measured cloud point, the precise depression being dependent upon the surfactant concentration - in general the difference between the CUR containing and the CUR free micelles was around 10 ºC ($p < 0.05$). These observations suggest that CUR was solubilised at the boundary between the hydrophobic and hydrophilic portions of the Brij O10 surfactant. Indeed it has been reported, based on ^{1}H NMR spectroscopy and confirmed by using transmission electron microscopy (TEM), that the location of CUR molecules in the cationic and nonionic mixed surfactant aggregates was predominately

in the head region of mixed surfactant system, particularly when compared to core of mixed micelle (Kumar et al., 2016).

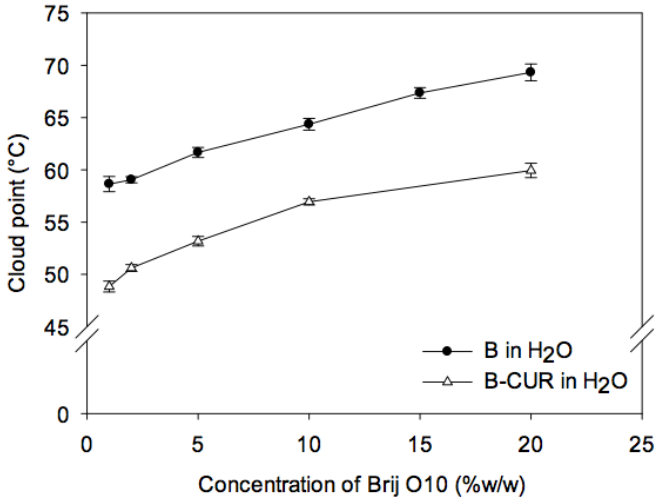

Figure 3.20: The cloud point of Brij O10 micelles at different surfactant concentrations in the absence and presence of CUR (mean ± S.D.), n=3.

The differences in PIT between the SBO-containing NE, B20-hSBO-CUR NE, and ethyl oleate-containing NE, B20-98hEO-CUR NE, are shown in **Figure 3.21**. The PIT of B20-hSBO-CUR exhibited a small increase in the PIT upon the increasing amount of oil, although surprisingly any increase was extremely small or non-existent when compared to the PIT recorded for the drug-free NE, B20-hSBO NE ($p > 0.05$) (**Figure 3.21a**). The absence of any effect of CUR on the PIT of B20-hSBO-CUR suggested that CUR might not sit at the boundary between the NE core and head group region and it may instead sit in the NE core due to its solubility in SBO. This result was in contradiction to that seen for CUR in Brij O10 micelles where the drug was believed to sit at the boundary of the core and head group region in the NE. Upon the addition of more oil, an increase in the PIT of the CUR-containing NE was observed, which is most likely due to the oil resulting in the formation of less ellipsoidal/more spherical aggregates.

The PIT of B20-98hEO-CUR first decreased and then increased upon the increasing the amount of EO present. Overall, while the data obtained for the CUR-containing NE followed the trend in the variation in PIT with EO content observed for the CUR-free NE, there was a small decrease in PIT, of around 2-3 ºC ($p < 0.05$) (**Figure 3.21b**). These observations suggest that CUR is solubilised in the surfactant boundary of B20-98hEO, in agreement with the results obtained for the Brij O10 micelles. However, it is likely that the amount of CUR present in the core/head group boundary of the NE is

lower than that of CUR in the Brij O10 micelles. The decrease and then increase in the PIT of the various NE implies that the micellar aggregates were asymmetrical shape. In fact, when a low level of oil was incorporated, it is likely that it penetrated the interfacial surfactant monolayer, encouraging the formation of asymmetric aggregates, which lower the PIT of the NE below that of the corresponding micelle. Upon the addition of a further amount of oil, an increase in the PIT of the NE was observed, due to the added oil resulting the transformation of asymmetric to spherical aggregates.

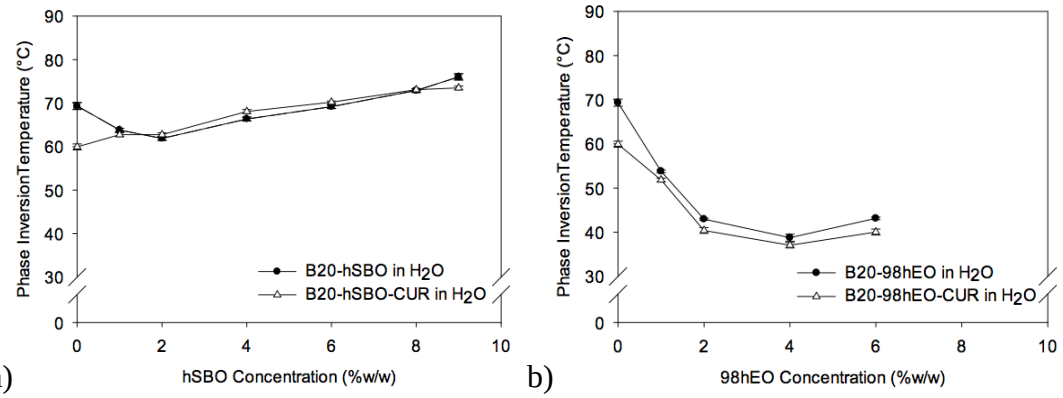

Figure 3.21: The variation in the phase inversion temperature of nanoemulsions stabilised by 20 %w/w Brij O10 and containing varying amounts of either hSBO or 98hEO and in the absence and presence of curcumin (CUR) (mean ± S.D.). Error bars in some cases contained in symbol.

3.3.2.3 Effect of curcumin on the particle size of Brij O10 micelle and nanoemulsions

The apparent hydrodynamic size (D_h) of micelles with varying Brij O10 concentrations and B20-hSBO and B20-98hEO NE in the presence and absence of CUR was obtained using Brookhaven ZetaPlus particle sizer (**Figure 3.22**). Unexpectedly, the D_h of Brij O10 micelles as well as B20-hSBO and B20-98hEO NE exhibited a significant increase in D_h in the presence of CUR as assessed using the Brookhaven ZetaPlus particle sizer, even though the diluted samples containing CUR were completely clear by eye. The measured D_h of B20-CUR was 8 to 9 times larger than that of the corresponding B20 micelles (**Figure 3.22a**). Moreover, the measured increase in D_h of both B20-hSBO-CUR and B20-98hEO-CUR NE did not follow the expected trend of exhibiting an increase in size with increasing oil concentration, instead D_h exhibited an irregular fluctuation with increasing oil (**Figure 3.22b** and **3.22c**).

To explore the origin of this unexpected result, the diluted samples were re-filtered through a 0.45 um polyethersulfone (PES) filter (Jet biofil, Guangzhou, China) before

re-examination by PCS to ensure the absence of dust in the samples, however the D_h of micelles or NE samples still exhibited an irregular variation in size (data was not shown). As the Brookhaven nanosizer was fitted with a red laser, it was necessary to ensure that the yellow, CUR-containing samples were not absorbing the beam by checking that the beam remained as a thin red line as it passed through the NE. In addition, the clear, 4-sided, 10-mm path length disposable polystyrene cuvette typically used for PCS measurements was replaced by a 4-sided, 1-cm path length quartz cuvette, normally used for fluorescence spectroscopy, to ensure that a chemical reaction was not occurring between the samples and the container which might affect particle size. `however, none was seen and the measured D_h varied in an irregular manner as before. Finally, size measurement of the samples was performed using the Malvern Nano ZS Zetasizer, which exploited a scattering angle of 173° while the Brookhaven ZetaPlus particle sizer used a scattering angle of 90°.

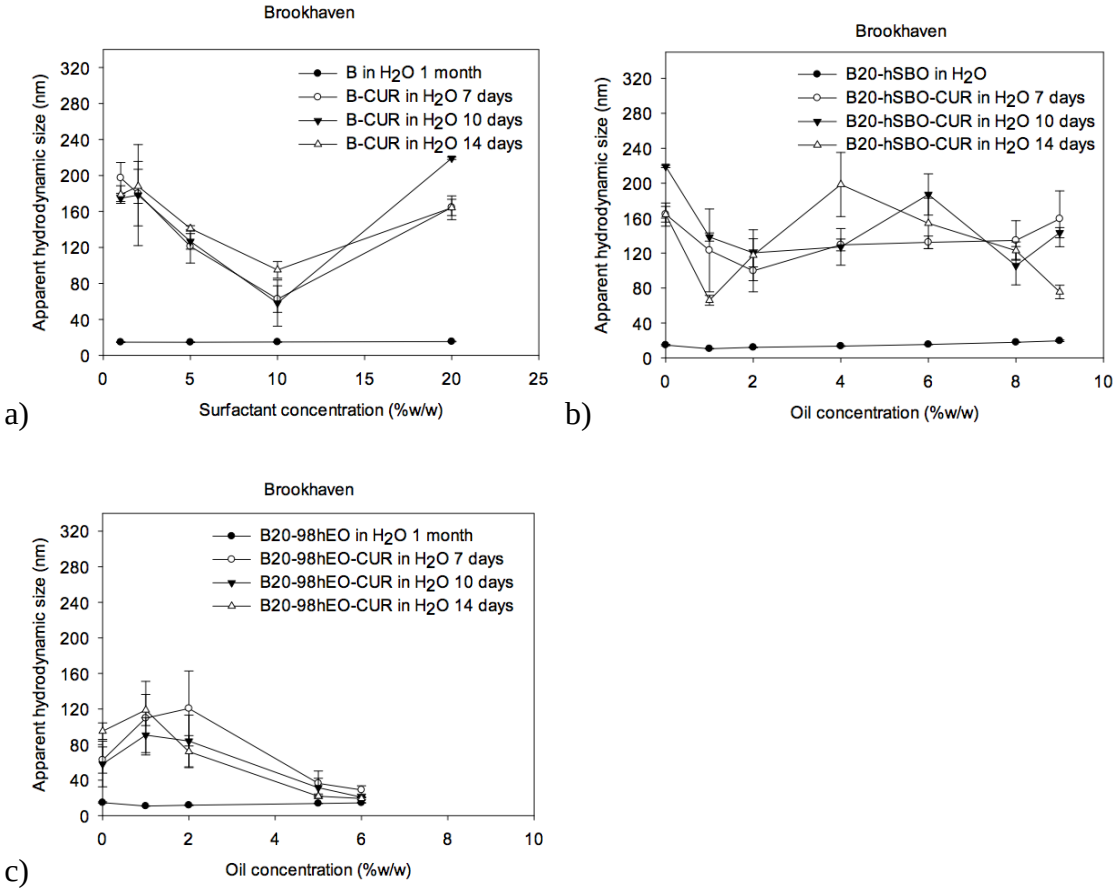

Figure 3.22: The mean hydrodynamic droplet size measured using a Brookhaven ZetaPlus particle sizer of a) Brij O10 micelles prepared using different surfactant concentrations and nanoemulsions prepared using 20 %w/w Brij O10 and different concentrations of either b) hSBO or c) 98hEO in the absence and presence of curcumin (CUR) (mean ± S.D.). Error bars in some cases contained in symbol.

The apparent hydrodynamic size (D_h) of Brij O10 micelles with varying surfactant concentration as well as B20-hSBO, and B20-98hEO NE prepared in the absence and presence of curcumin using Malvern Nano ZS Zetasizer is shown in **Figure 3.23**. While, the D_h of the Brij O10 micelles, and B20-hSBO and B20-98hEO NE containing CUR still exhibited a fluctuation in the value D_h, these fluctuations were less than those seen with the Brookhaven nanosizer. This observation might suggest that CUR could interact with Brij O10 resulting in an increase in the size of the micelles and NE. An alternative explanation is that CUR might be incorporated into and link 2 micelle or 2 NE droplets leading to a miss-interpretation of the PCS data leading to a larger apparent size. As a consequence of these results it was decided to perform small-angle neutron scattering (SANS) studies on the systems to try and understand these randomly variable results.

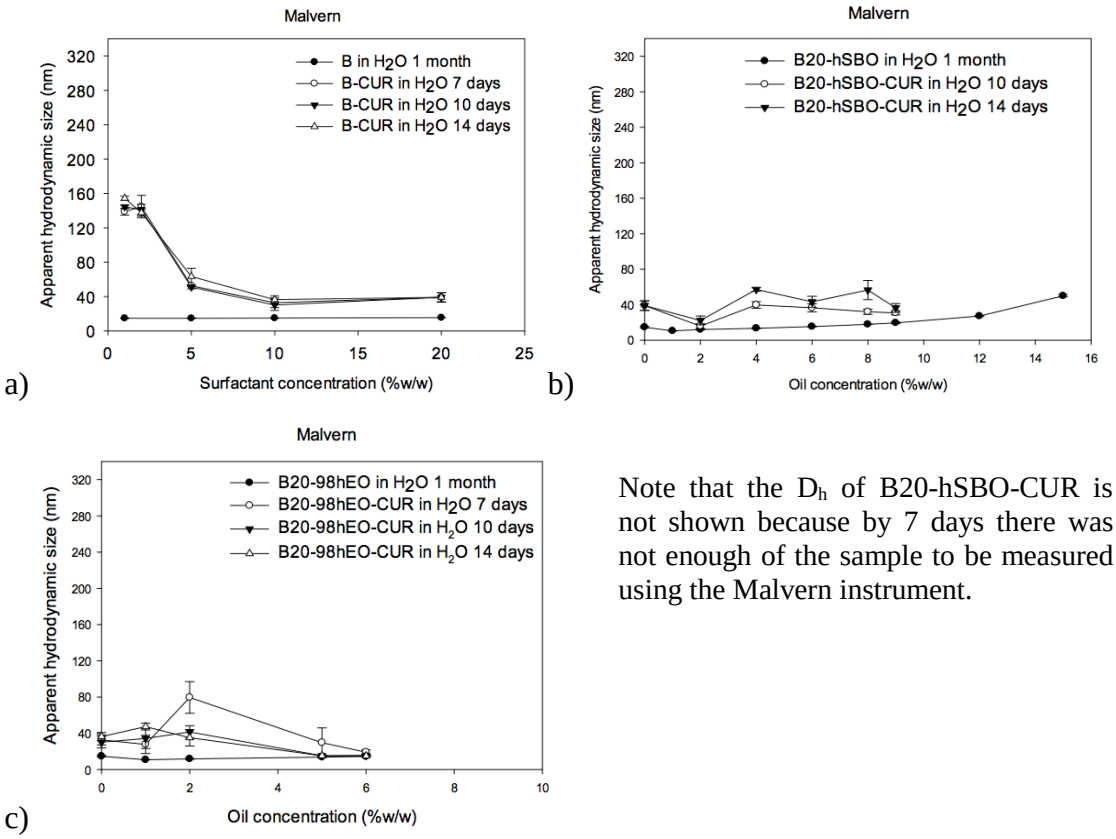

Note that the D_h of B20-hSBO-CUR is not shown because by 7 days there was not enough of the sample to be measured using the Malvern instrument.

Figure 3.23: The mean hydrodynamic droplet size measured using a Malvern Nano ZS Zetasizer of a) Brij O10 micelles prepared using different surfactant concentrations and nanoemulsions prepared using 20 %w/w Brij O10 and different concentrations of either b) hSBO or c) 98hEO in the absence and presence of curcumin (CUR) (mean ± S.D.). Error bars in some cases contained in symbol.

3.3.2.4 The solubility of curcumin in micelle and nanoemulsions

The solubilisation of curcumin (CUR) in micelles prepared using different surfactant concentrations is shown in **Figure 3.24**. It is clear that the CUR reached saturation level in the micelles by 7 days, solubilisation at earlier times were not measured. Furthermore, the solubility of CUR increased, in an approximately linear fashion, with increasing Brij O10 concentration up to 20 %w/w.

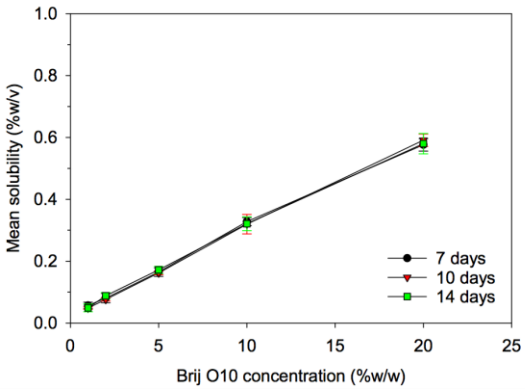

Figure 3.24: Variation in the level of solubilisation of curcumin in Brij O10 micelles of different surfactant concentration (mean ± S.D.). Error bars in some cases contained within symbol.

The variation in the solubilisation of CUR in different concentrations of Brij O10 micelles, B20-hSBO and B20-98hEO NE is shown in **Figure 3.25**. Again the results indicated that CUR saturated the samples within 7 days, shorter time courses were not measured. Surprisingly, the solubilisation of CUR in the NE did not increase significantly, over the corresponding micelles suggesting that the presence of oil did not have positive effect on the solubilisation of CUR. This observation can be explained by the low level of CUR solubility in both of the oils, hSBO and 98hEO, meaning that there was no benefit in the addition of oil, in terms of solubilisation.

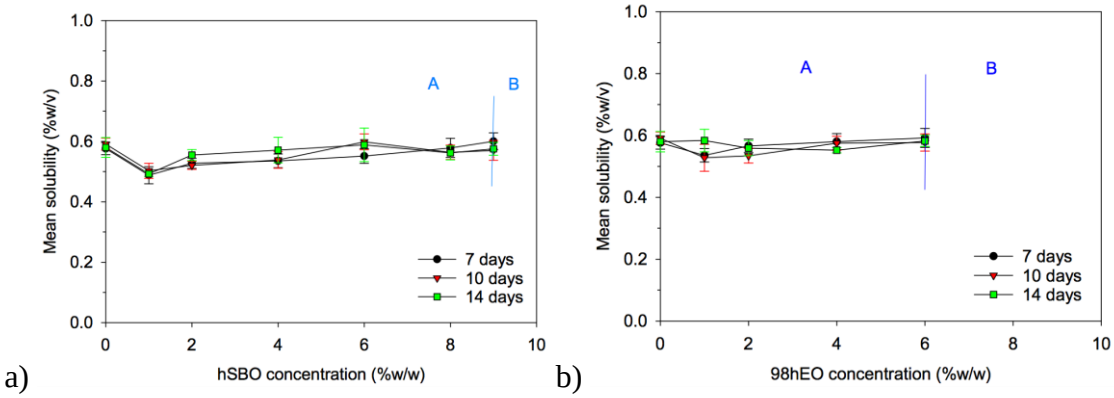

Figure 3.25: Variation in the solubilisation of curcumin in 20 %w/w Brij O10 micelles and nanoemulsions prepared using 20 %w/w Brij O10 and containing varying amounts of either a) hSBO or b) 98hEO (mean ± S.D.). Error bars in some cases contained in symbol.

Table 3.6 Comparison of experimentally obtained and predicted curcumin (CUR) solubilisation

Sample	Region	Experimentally measured CUR solubilisation in B20-hSBO-CUR (%w/v)	Predicted CUR solubilisation in B20-hSBO-CUR (%w/v) [a]
B20	-	0.58 ± 0.02	-
B20-hSBO1	A	0.49 ± 0.03	0.58
B20-hSBO2		0.53 ± 0.02	0.58
B20-hSBO4		0.54 ± 0.02	0.59
B20-hSBO6		0.55 ± 0.02	0.59
B20-hSBO8		0.58 ± 0.03	0.59
B20-hSBO9		0.60 ± 0.03	0.60
B20-98hEO1	A	0.54 ± 0.02	0.58
B20-98hEO2		0.57 ± 0.02	0.58
B20-98hEO4		0.58 ± 0.03	0.59
B20-98hEO6		0.59 ± 0.03	0.59

[a] calculated from the experimental CUR solubilisation in the Brij O10 micelles and oil according to amount of oil and surfactant contained in the samples. The solubility of CUR in 20 %w/w Brij O10 was 0.58 ± 0.02 %w/v at 25 °C while the solubility of CUR in hSBO and 98hEO was 0.18 ± 0.03 and 0.14 ± 0.03 %w/v at 25 °C.

As it was possible to predict the expected level of CUR solubilisation in the NE from a knowledge of the level of solubilisation of CUR in B20-CUR and its solubility in the oils of interest, here SBO and EO (**Table 3.6**) it is possible to compare the predicted solubilisation with that experimentally measured. This comparison showed that the experimental CUR solubilisation in NE containing a small amount of oil was less than the predicted solubilisation. This result indicated that formulation of CUR in NE did not

yield the anticipated advantages, most probably because the oil was incorporated in NE in a manner that did not lead to an improved solubilisation of CUR. It is therefore useful to perform small angle neutron scattering studies to establish the internal structure of the NE.

3.3.3 The incorporation of curcumin and testosterone propionate

To investigate the behaviour of two hydrophobic drugs when incorporated into the same NE, curcumin (CUR) and testosterone propionate (TP) were selected as drugs. The effect of the addition of CUR and TP on the stability of the NE containing varying amounts of hSBO as a representative oil, was investigated by saturating B20-hSBO with CUR and TP. Excess drug was removed from the NE after 7, 10 and 14 days by centrifugation allowing the solubility of CUR and TP in Brij O10 micelles solutions and B20hSBO-CUR-TP to be established. The effect of the presence of both drugs on the area of NE existence, phase inversion temperature and particle size of the NE were also determined.

3.3.3.1 Effect of curcumin and testosterone propionate on the area of NE existence

A large number of NE of varying hSBO content within Region A were produced containing saturation amounts of both CUR and TP (**Figures 3.1**). It is important to note that, from visual observation, there was no evidence of the precipitation in any of the NE, either in the presence and absence of CUR and TP, after centrifugation suggesting that presence of both drugs did not immediately de-stabilise the NE. In addition, the physical appearance of the B20hSBO-CUR-TP NE did not appear to be detrimentally affected by the presence of CUR and TP as they were stable for at least 1 month. The NE in Region A containing as saturation amount of CUR and TP were completely clear systems, suggesting that it was possible to incorporate a saturation amount of CUR and TP without any visible effect the area of NE existence. The high stability of the B20-hSBO-CUR-TP NE and the relatively large NE region they exhibited supports the potential of B20-hSBO NE as drug delivery vehicles. Interestingly, while B20-hSBO-CUR-TP NE exhibited good stability of NE, the B20-hSBO-CUR NE did not, suggesting that the presence of TP stabilised the NE.

3.3.3.2 Effect of curcumin and testosterone propionate on cloud point and phase inversion temperature

The CP of B20-CUR-TP micelles and the PIT of B20-hSBO-CUR-TP NE at various hSBO concentrations are shown in **Figure 3.26**. The B20-CUR-TP NE exhibited a decrease in cloud point, in comparison with the corresponding CUR-TP-free micelles which was around 13 ºC less than the CP of CUR-TP-free micelles and indeed the solution and CUR-TP-saturated micelles ($p < 0.05$).. This finding indicates that CUR and possibly TP were solubilised at the boundary between the hydrophobic and hydrophilic portions of the Brij O10 surfactant micelle.

The differences in PIT of B20-hSBO-CUR-TP NE are shown in **Figure 3.26**. The PIT of B20-hSBO-CUR-TP NE containing hSBO concentrations of 2 %w/w and above, was only slightly less than the PIT recorded for the CUR-TP-free samples ($p < 0.05$). As with the micelles, this result suggests that CUR and possibly, TP might sit at the hydrophilic and hydrophobic boundary of the surfactant monolayer. Finally, the observed increase in the PIT suggested that more spherical aggregates of NE were formed as the amount of oil increased.

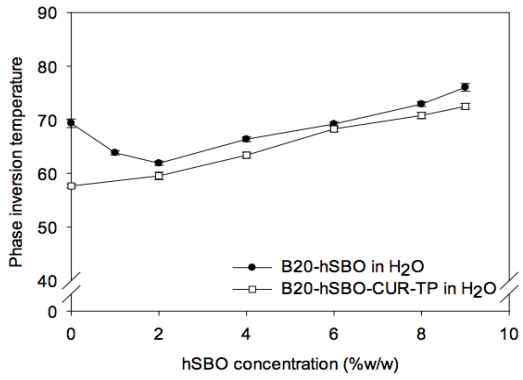

Figure 3.26: Cloud point of 20 %w/w Brij O10 micelles and phase inversion temperature of corresponding nanoemulsions containing varying amounts of hSBO in the absence and presence of curcumin (CUR) and testosterone propionate (mean ± S.D.). Error bars in some cases contained in symbol.

3.3.3.3 Effect of curcumin and testosterone propionate on the particle size of Brij O10 micelles and nanoemulsions

The apparent hydrodynamic size (D_h) of micelles of varying Brij O10 concentration as well as B20-hSBO NE in the absence and presence of CUR and TP measured using Brookhaven ZetaPlus particle sizer and Malvern Nano ZS Zetasizer is shown in **Figure**

3.27. The D_h of the hSBO-containing NE measured using the Brookhaven ZetaPlus particle sizer demonstrated a significant increase in the D_h measured for CUR-containing samples at low oil concentrations, namely 4-6 %w/w hSBO. At higher oil concentrations, the D_h of CUR-containing samples started to decrease (i.e. size increased), even though the diluted samples containing CUR were completely clear. Indeed the D_h of the B20-hSBO4-CUR-TP and B20-hSBO6-CUR-TP NE was 6 to 8 time larger than that of the micelles in the absence of the two drugs (**Figure 3.27a**).

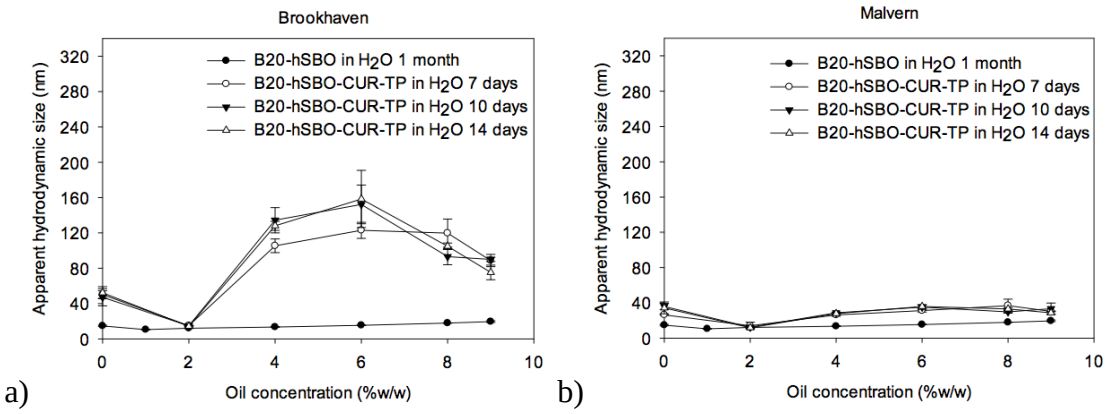

Figure 3.27: The variation in the mean hydrodynamic droplet size with the surfactant concentration of the Brij O10 micelles and nanoemulsions prepared using 20 %w/w Brij O10 and containing different concentrations of hSBO in the absence and presence of curcumin and testosterone propionate (mean ± S.D.) using a) Brookhaven ZetaPlus particle sizer and b) Malvern Nano ZS Zetasizer. Error bars in some cases contained in symbol.

As before, the diluted samples were re-filtered through a 0.45 um polyethersulfone (PES) filter (Jet biofil, Guangzhou, China) to ensure the absence of dust in the samples before their re-examination by PCS. However, the D_h of micelles or NE stills showed the significant increase (data not shown). As before, the laser was checked to ensure that it remained thin and red upon passage through the yellow coloured NE. Additionally, the clear, 4-sided, 10-mm path length disposable polystyrene cuvette generally used for PCS measurement was exchanged with a 4-sided clear 1-cm path length quartz cuvette used for fluorescence spectroscopy measurements, to ensure that there was no chemical reaction occurring between the NE and the container which would have affected the measurement of NE size. The D_h of the NE remained high and variable suggesting that the plastic nature of the measurement cells was not the reason for the irreproducible size measurements. Once again, NE size was measured using the Malvern Nano ZS Zetasizer, which exploited a scattering angle of 173° as opposed to the usual Brookhaven ZetaPlus particle sizer which utilised a scattering angle of 90°.

The apparent hydrodynamic size (D_h) of the B20 micelles and B20-hSBO NE in the absence and presence of CUR and TP, measured using a Malvern Nano ZS Zetasizer is shown in **Figure 3.27b**. As was seen when using the Brookhaven particle sizer, the D_h of the drug containing micelles, B20-CUR-TP and drug containing B20-hSBO-CUR-TP NE exhibited an increase when measured using a Malvern Nano ZS Zetasizer. In order to gain a fuller understanding of these unpredictable size effects, the size of B20-hSBO-CUR-TP NE will be assessed using small-angle neutron scattering (SANS).

3.3.3.4 The solubility of curcumin and testosterone propionate in micelle and nanoemulsions

The ultra-violet (UV) absorbance spectra of CUR and TP in isopropanol is shown in **Figure 3.28**. It was clear that both CUR and TP absorbed UV light at 240 nm while in contrast only CUR absorbed UV light at 428 nm. Here UV-vis spectroscopy was used to analyse the amount of CUR and TP in the micelle and NE in the presence of CUR and TP.

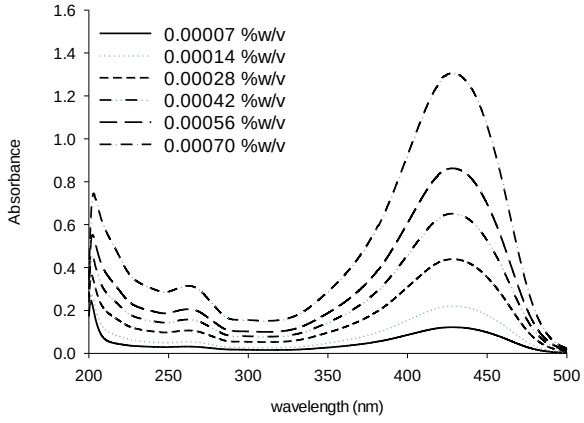

a)

b)

Figure 3.28: Ultra-violet absorbance spectra of a) curcumin (CUR) and b) testosterone propionate (TP) in isopropanol (n = 9 at each concentration studied).

Figure 3.29 shows the variation in absorbance of curcumin over the concentration range of 0.00007-0.00070 %w/v in isopropanol at wavelengths of 240 nm (Figure 3.29a) and 428 nm (Figure 3.29b). The calculated extinction coefficient for CUR in isopropanol at wavelengths of 240 and 428 nm were 13509 and 54445 M^{-1} cm^{-1}, respectively. The extinction coefficient of CUR in isopropanol obtained in this study of 55445 M^{-1} cm^{-1} at wavelength of 428 nm was similar to the extinction coefficient reported in previous studies (Waranyoupalin et al., 2009; Zsila et al., 2003; Jasim and Ali, 1989). Specifically an extinction coefficient of 49,370 $M^{-1}cm^{-1}$ for CUR in in methanol/H_2O (1:1 v/v) of at wavelength of 428 nm have been reported by Waranyoupalin et al. (2009). Zsila et al (2003) noted an extinction coefficient of 55,000 M^{-1} $cm^{-1}$for CUR in ethanol at wavelength of 429 nm while Jasim and Ali (1989) quoted values of 67,680 and 54,954 M^{-1} cm^{-1} in methanol and ethanol, respectively at 428 nm. **Figure 3.30** shows the variation in the absorbance of testosterone propionate over the concentration range of 0.0005-0.0030 %w/v in isopropanol at wavelength of 240 nm. The extinction coefficient of 16722 M^{-1} cm^{-1} determined in this study for TP in isopropanol at wavelength of 240 nm, was reassuring similar to an extinction coefficient of 17400 M^{-1} cm^{-1} reported for TP in ethanol by Sigma Aldrich.

In order to determine the solubilisation of CUR and TP in samples containing both drugs, the absorbance of CUR at 428 nm was used to estimate the incorporation of CUR in the B20-hSBO-CUR-TP NE after which the absorbance of TP at 240 nm was estimated by subtracting from the total absorbance at this wavelength, the predicted absorbance for CUR at 240 nm, calculated using the ratio of 0.25 for the absorbance of CUR at 240:428 nm. A ratio of 0.25 was calculated by dividing the extinction coefficient of CUR at a wavelength of 240 nm by the extinction coefficient of CUR at wavelength of 428 nm.

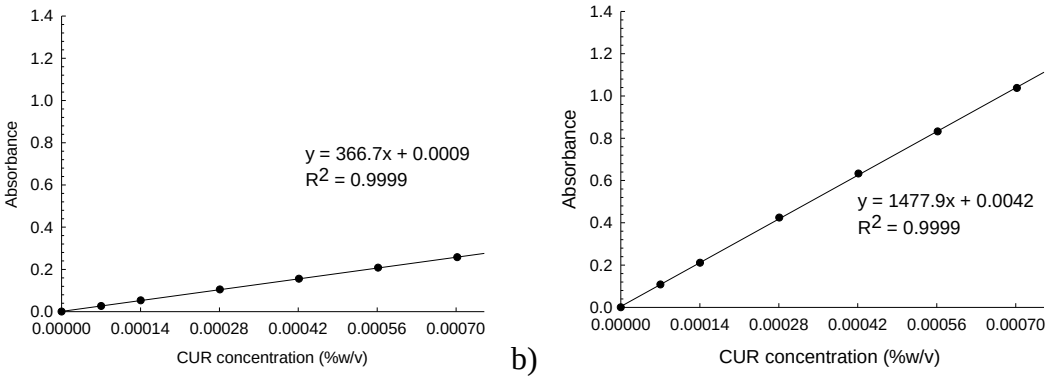

Figure 3.29: The absorbance of curcumin concentration in isopropanol at 0.00007-0.00070 %w/v at the wavelength of a) 240 nm and b) 428 nm, respectively (n = 9 at each concentration studied). Extinction coefficient of curcumin at 240 and 428 nm were 13509 and 54445 M^{-1} cm^{-1}, respectively. Error bars in some cases contained within the symbols.

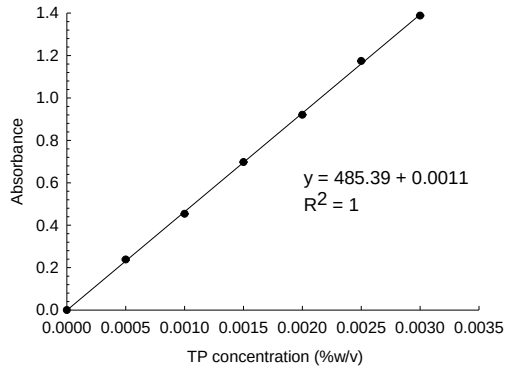

Figure 3.30: The absorbance of testosterone propionate concentration in isopropanol at 0.0005-0.0030 %w/v at the wavelength of a) 240 nm (n = 9 at each concentration studied). Extinction coefficient of testosterone propionate at 240 nm was 16722 M^{-1} cm^{-1}. Note that TP does not absorb UV light at 428 nm. Error bars in some cases contained within the symbols.

The solubilisation of CUR and TP in B20-hSBO after saturation with both drugs for 7, 10 and 14 days are shown in **Figure 3.31**. The results showed that the CUR could saturate in all samples within 7 days (shorter time periods not measured), while TP could reach the saturation between 10-14 days. **Figure 3.32** shows the solubility of (a) CUR measured in the absence and presence of TP and (b) TP measured in the absence and presence of CUR in B20-hSBO NE saturation with drug for 7 days. It was clear that B20-hSBO NE containing saturation amounts of both CUR and TP could incorporate more CUR than could be incorporated in B20-hSBO NE in the absence of TP. Similarly much less TP was solubilised in B20-hSBO NE containing CUR compared to those in which CUR was absent. Taken together these results suggest that the presence of TP had a positive effect on the solubilisation of CUR in NE.

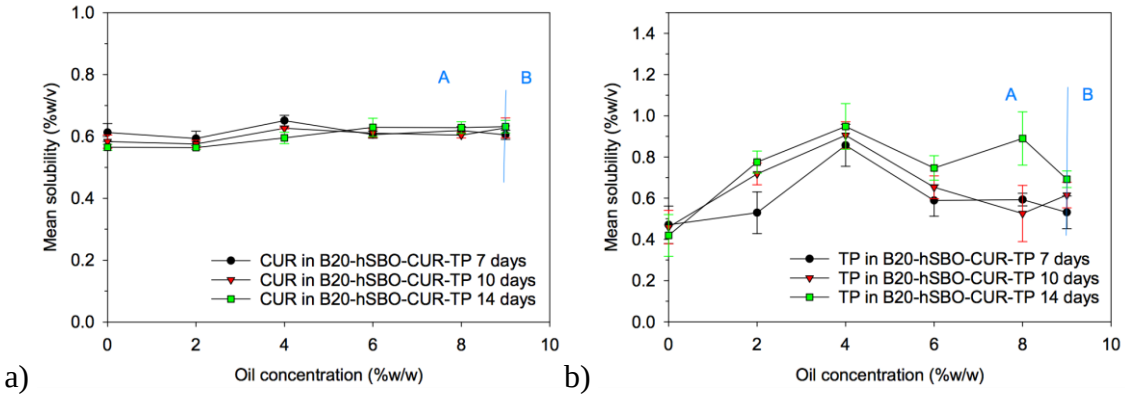

Figure 3.31: Solubilisation over time of a) curcumin (CUR) and b) testosterone propionate (TP) in hSBO-containing NE prepared using 20 %w/w Brij O10 and containing varying amounts of hSBO and saturated with both curcumin and testosterone propionate (mean ± S.D.). Error bars in some cases contained within symbol.

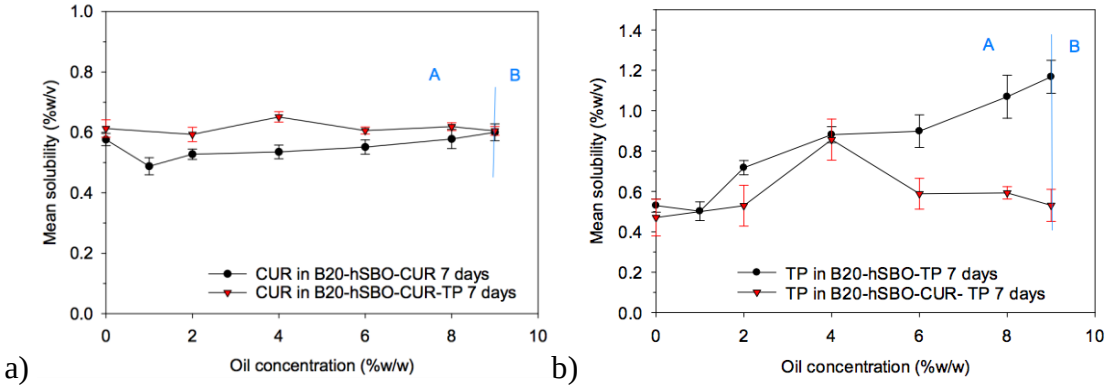

Figure 3.32: Solubilisation at 7 days of a) curcumin (CUR) and b) testosterone propionate (TP) in hSBO-containing NE prepared using 20 %w/w Brij O10 and containing varying amounts of hSBO and saturated with both curcumin and testosterone propionate (mean ± S.D.). Error bars in some cases contained within the symbol.

Table 3.7 shows the comparison between the experimentally measured TP and CUR solubilisation with the expected level of solubilisation of TP and CUR. The expected level of TP or CUR solubilisation was calculated from the level of TP and CUR solubilisation in B20 and their solubility in the oils that comprise the NE is shown in **Table 3.7**. This comparison showed that the experimentally measured TP solubilisation in B20-hSBO NE containing both saturated amount of CUR and TP and containing low levels of hSBO (2-4 %w/w) was greater than that predicted. These results show that CUR-containing NE improve the solubilisation of TP. At higher hSBO concentrations, namely 6-9 %w/w, the experimentally determined TP solubilisation in NE was lower than that predicted, which showed that the presence of CUR could affect the amount of TP solubilised in the NE.

On the other hand, the experimentally measured level of CUR solubilisation in B20-hSBO NE saturated with both CUR and TP and containing a low level of oil incorporated was similar to that level predicted for CUR solubilisation in NE. This observation indicated that formulation in a NE did not an advantageous effect on the solubilisation of CUR in NE and that the presence of hSBO did not improve the solubilisation of CUR. Interestingly, however, the level of CUR solubilisation in B20-hSBO NE containing saturation amounts of both CUR and TP was higher than in the corresponding NE containing only CUR, indicating that the presence of TP could improve the solubility of CUR in the NE. On the basis of these solubilisation studies, it is likely that performing SANS studies would be beneficial in that they would enable the internal structure of the NE to be probed.

Table 3.7 Comparison of the experimentally determined and predicted testosterone propionate and curcumin solubilisation in nanoemulsions containing both curcumin and testosterone propionate

Oil concentration (%w/w)	Experimentally determined TP solubilisation in B20-hSBO-CUR-TP (%w/v)	Predicted TP solubilisation in B20-hSBO-CUR-TP (%w/v) [b]	Experimentally determined CUR solubilisation in B20-hSBO-CUR-TP (%w/v)	Predicted CUR solubilisation in B20-hSBO-CUR-TP (%w/v) [a]
0	0.48 ± 0.08	-	0.61 ± 0.03	-
2	0.66 ± 0.11	0.51	0.58 ± 0.04	0.58
4	0.90 ± 0.08	0.55	0.65 ± 0.03	0.59
6	0.59 ± 0.08	0.62	0.61 ± 0.05	0.59
8	0.59 ± 0.03	0.69	0.62 ± 0.03	0.59
9	0.53 ± 0.08	0.75	0.61 ± 0.04	0.60

[a] calculated from the experimentally determined solubilisation of CUR in a micelle and the bulk oil according to amount of oil and surfactant in the NE. The solubility of CUR in 20 %w/w Brij O10 was 0.58 ± 0.02 %w/v at 25 ^{0}C while the solubility of CUR in hSBO was 0.18 ± 0.03 %w/v at 25 ^{0}C.

[b] calculated from the experimentally determined TP solubilisation in a micelle and the bulk oil according to amount of oil and surfactant in the NE. The solubility of TP in 20 %w/w Brij O10 was 0.48 ± 0.03 %w/v at 25 ^{0}C while the solubility of TP in hSBO was 3.42 ± 0.29 %w/v at 25 ^{0}C (Malcolmson et al., 1993; Malcolmson et al., 1998).

3.3.4 Comparison of physico-chemical properties of NE in the absence and presence of hydrophobic drugs

The cloud point of B20 micelles and the phase inversion temperature of B20-hSBO NE, both dispersed in H_2O, in the absence and presence of TP, CUR and both TP and CUR are shown in **Figure 3.33. Table 3.8** gives the solubility of TP and CUR in B20 micelles and B20-hSBO NE containing different amounts of hSBO. It was found that

the CP of the micelles increased in the order of B20-CUR-TP < B20-CUR < B20-TP < B20, whereas the level of drug solubility in micelles was CUR solubility (0.61 %w/v) and TP solubility (0.48 %w/v) in B20-CUR-TP > CUR solubility (0.58 %w/v) in B20-CUR > TP solubility (0.48 %w/v) in B20-TP > B20. The decrease in the cloud point of the micelles was due to the incorporation of hydrophobic drugs, most likely at the boundary between the micelle core and its head group. The results of the CP and drug solubilisation studies indicated that the presence of both CUR and TP had an effect on the CP of the micelle.

In contrast, the order of the PIT of the NE was B20-hSBO-TP < B20-hSBO-CUR-TP < B20-hSBO-CUR = B20-hSBO. The PIT studies indicated that only TP in NE decreased the PIT of NE while in contrast the presence of CUR in NE had little or no effect on the PIT of NE. The order of drug solubility in the NE was CUR solubility (0.58 %w/v) and TP solubility (0.66 %w/v) in B20-hSBO2-CUR-TP > TP solubility (0.72 %w/v) in B20-hSBO2-TP NE > CUR solubility (0.53 %w/v) in B20-hSBO2-CUR > B20-hSBO2. Taken together the PIT and drug solubilisation studies imply that the site of incorporation of CUR and TP in micelles might result in differences in the phase behaviour of NE.

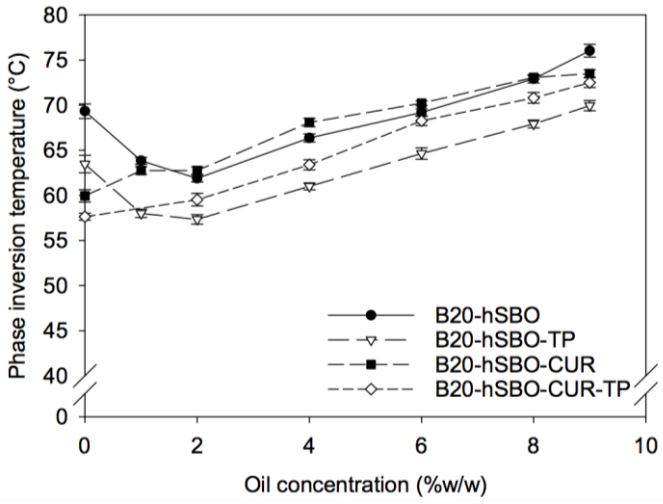

Figure 3.33: The cloud point of 20 %w/w Brij O10 micelles and phase inversion temperature of nanoemulsions containing hSBO and prepared using 20 %w/w Brij O10 and in the absence and presence of testosterone propionate (TP), curcumin (CUR), and both testosterone propionate (TP) and curcumin (CUR) (mean ± S.D.). Error bars in some cases contained within the symbol.

Table 3.8 The solubility of testosterone propionate and curcumin in micelles and nanoemulsions prepared using 20 %w/w Brij O10 and containing different amounts of hSBO (mean ± S.D).

Oil concentration (%w/w)	The solubilisation of TP in B20-hSBO-TP (%w/v)	The solubilisation of CUR in B20-hSBO-CUR (%w/v)	The solubilisation of TP in B20-hSBO-CUR-TP (%w/v)	The solubilisation of CUR in B20-hSBO-CUR-TP (%w/v)
0	0.48 ± 0.03	0.58 ± 0.02	0.48 ± 0.08	0.61 ± 0.03
2	0.72 ± 0.04	0.53 ± 0.02	0.66 ± 0.11	0.58 ± 0.04
4	0.88 ± 0.04	0.54 ± 0.02	0.90 ± 0.08	0.65 ± 0.03
6	0.90 ± 0.08	0.55 ± 0.02	0.59 ± 0.08	0.61 ± 0.05
8	1.10 ± 0.11	0.58 ± 0.03	0.59 ± 0.03	0.62 ± 0.03
9	1.17 ± 0.08	0.60 ± 0.03	0.53 ± 0.08	0.61 ± 0.04

3.4 Effect of deuterated materials on the physico-chemical properties of Brij O10 micelles and nanoemulsions

It has been reported that there is a significant isotope effect observed on the cloud point and phase boundary when H_2O is replaced with D_2O in a solution containing a mixed alkylglucoside surfactant (Whiddon and Soderman, 2001). Subsequent to the exchange of H for D on the hydroxyl groups of the surfactant's glucose head groups, the combination of the increased hydrophobicity of the surfactant in D_2O and changes in the hydrogen bond strength and length result in an isotope effect. In case a similar effect was occurring in the micelles and NE under examination here, a series of studies on the physico-chemical properties of micelles and NE in D_2O was performed and the results compared to those obtained in NE in H_2O. These studies included determining the area of NE existence, the cloud point/phase inversion temperature and particle size. It was important that these isotope studies were performed prior to the small angle neutron scattering experiments.

3.4.1 Effect of deuterated water on the area of existence of Brij O10 nanoemulsion

Three component NE systems were prepared using commercially available protiated triglyceride/ethyl ester and Brij O10 ($C_{18:1}E_{10}$) in D_2O and their stability examined at room temperature. The area of NE existence was determined by varying the amount of each component and plotting the results on a weight basis on a ternary phase diagram in

order to understand the phase behaviour of the NE formulations in D_2O (**Figures 3.34-3.35 and Table 3.9**). On the abscissa, surfactant concentration (in %w/w) increases from left to right while on the ordinate, oil concentration (in %w/w) increases from bottom to top. It can be seen that the appearance of NE samples prepared in D_2O is the same area of NE existence as that of NE prepared in H_2O, suggesting that under the conditions of the study the area of NE existence is unaffected by solvent deuteration.

Triglyceride	Solvent	
	D_2O	H_2O
hSBO	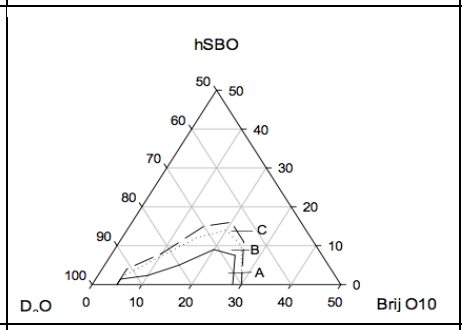	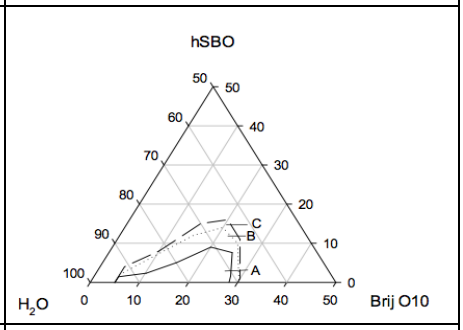
65hGTO	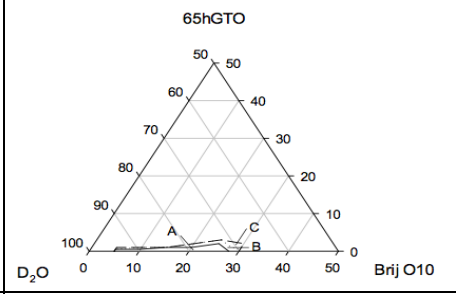	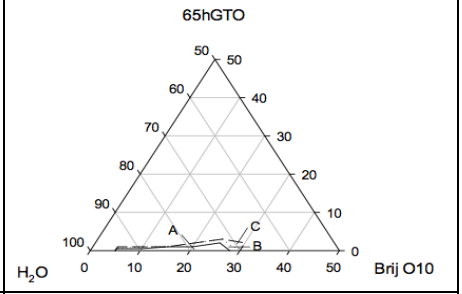
99hGTO	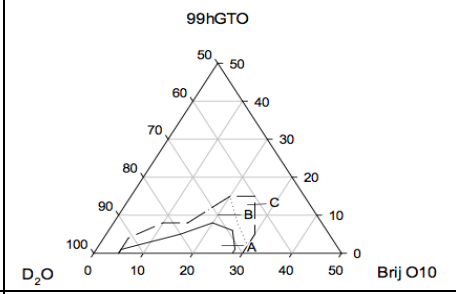	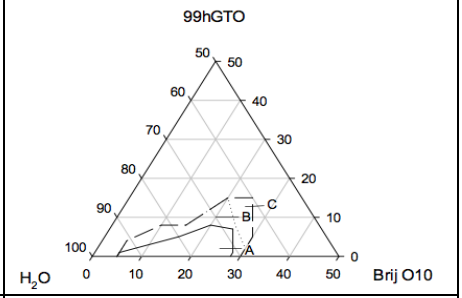
85hTPN	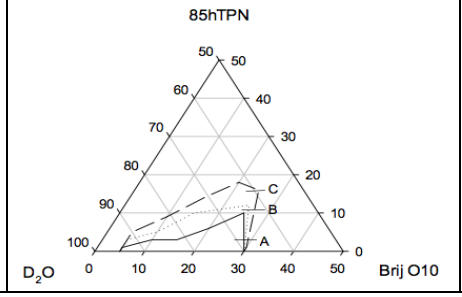	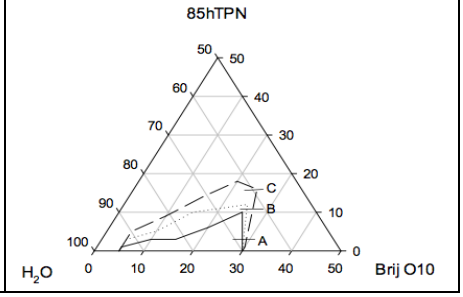

Figure 3.34: Partial ternary phase diagrams for o/w nanoemulsions formed using protiated triglyceride and Brij O10 in either D_2O or H_2O after 1 month storage at room temperature. Clear NE are described as Region A NE, while bluish or translucent NE as Region B NE and cloudy or milky NE as Region C NE.

Ethyl ester	Solvent	
	D_2O	H_2O
99hEO	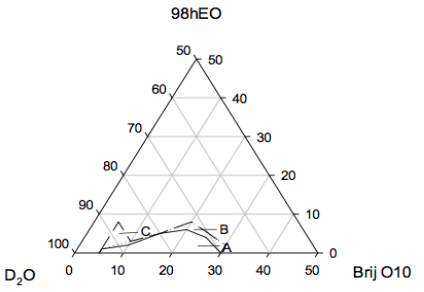	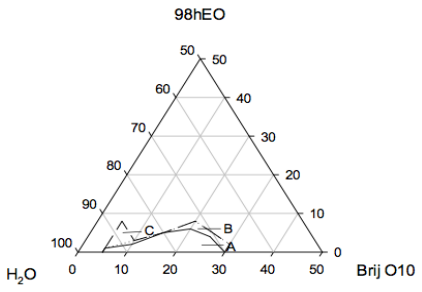

Figure 3.35: Partial ternary phase diagrams for o/w nanoemulsion formed with ethyl ester and Brij O10 in either D_2O or H_2O after 1-month storage at room temperature. Clear NE are described as Region A NE, while bluish or translucent NE are called Region B NE, and the cloudy or milky NE were denoted as Region C NE.

Table 3.9 The upper limit of oil (%w/w) incorporation into nanoemulsions prepared using Brij O10 and D_2O in Regions A, B and C which were stable for 1 month

Type	Sample	5% Brij O10			10% Brij O10			15% Brij O10			20% Brij O10			25% Brij O10			30% Brij O10		
		A	B	C	A	B	C	A	B	C	A	B	C	A	B	C	A	B	C
Triglyceride	hSBO, D_2O	1.4	2	4	2.3	7	8	5	12	15	9	14	16	7.5	10	11	-	-	-
	65hGTO, D_2O	-	0.5	1	0.5	1	-	1	-	-	1	2	-	2	3	-	-	0.5	2
	99hGTO, D_2O	1	3	4	3	7	8	5	8	-	8	15	-	6	8	15	-	2	5
	85hTPN, D_2O	1	3	5	3	5	9	3	10	14	6	11	18	10	12	16	-	-	1
Ethyl ester	98hEO, D_2O	1	-	8	2	3	-	5	-	-	6	8	-	4	5	-	-	2	-

- means the NE was not formed.

3.4.2 Effect of deuterated water on the cloud point and phase inversion temperature

Pandit and Caronia studied the effect on the cloud point of Triton X-100 of replacing H_2O with D_2O (Pandit and Caronia, 1987) and reported that while the trend of the cloud points measured in H_2O and D_2O were similar, the value of the cloud points determined in D_2O were consistently ~ 4 °C lower than those measured in H_2O. These results were in agreement with those reported by other workers who found that replacing H_2O with

D_2O leads to a widening of the miscibility gap, i.e. the region of composition or temperature in which a composition of mixtures form two phases (Schon et al., 1986).

The same phenomena of a widening miscibility gap is exhibited by many polyoxyethylated nonionic surfactant systems. For example the CP of the $C_{12}E_5$ in D_2O was 2 K lower than the same surfactant in H_2O (Martin et al., 1996). In addition, a similar effect of deuteration on clouding temperature was exhibited by the zwitterionic surfactant, 2-decyldimethylammonioethane sulphate (DES), where it was found that the CP of DES in D_2O was 8 °C higher than that measured in H_2O (Nilsson et al., 2004). Note that zwitterionic surfactants cloud upon decreasing temperature as opposed to increasing temperature as recorded for nonionic surfactants. This observation suggests that H_2O and D_2O have a different effect on the conformation of the self-assembled surfactant structures. As a consequence, it is necessary to study the effect of H_2O and D_2O on the CP of the micelles and the phase inversion temperature of NE prior to SANS measurements.

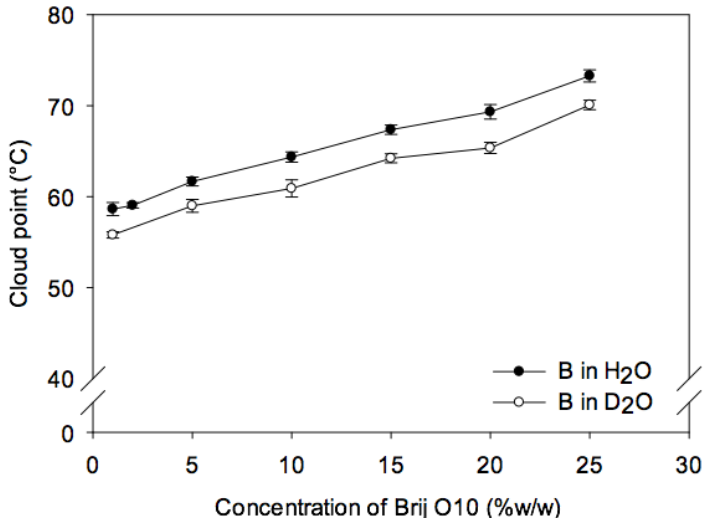

Figure 3.36: The cloud point of Brij O10 micelles as a function of concentration (%w/w) in D_2O.

The CP of different concentrations of Brij O10 micelles prepared in D_2O is shown in **Figure 3.36**. As anticipated the same variation in the trend in the cloud point was seen when replacing H_2O with D_2O in that the CP of Brij O10 micelle in D_2O increases with the increasing surfactant concentration (**Figure 3.5**). Furthermore, in agreement with the results of Pandit and Caronia (Pandit and Caronia, 1987), the value of the CP recorded for D_2O and H_2O were different, with the CP of the surfactant in D_2O being ~ 3 °C lower than that recorded in H_2O ($p < 0.05$).

The phase inversion temperature (PIT) of 20 %w/w Brij O10 NE containing different amounts of either hSBO, 65hGTO, 99hGTO, 85hTPN, or 98hEO are shown in **Figures 3.37 and 3.38**. Again the trend in the variation of the PIT of the NE prepared in D_2O was comparable with that of the corresponding NE prepared in H_2O (**Figures 3.6 and 3.7**). The PIT of Brij O10 NE in D_2O first decreased with increasing oil concentration and then increased upon the addition of further oil. Again, as anticipated there was a difference in the value of the PIT reported for the NE prepared in D_2O and H_2O, with the NE dispersed in D_2O exhibiting the lower cloud point ($p < 0.05$). However, the use of D_2O in place of H_2O is not thought to affect the morphology of the NE which was important for the SANS experiments, which were predominately performed at 25 °C, although a few NE containing hSBO, were measured at 37 °C, because the CP of the micelle and the PIT of NE is significantly higher than the experimental temperature used.

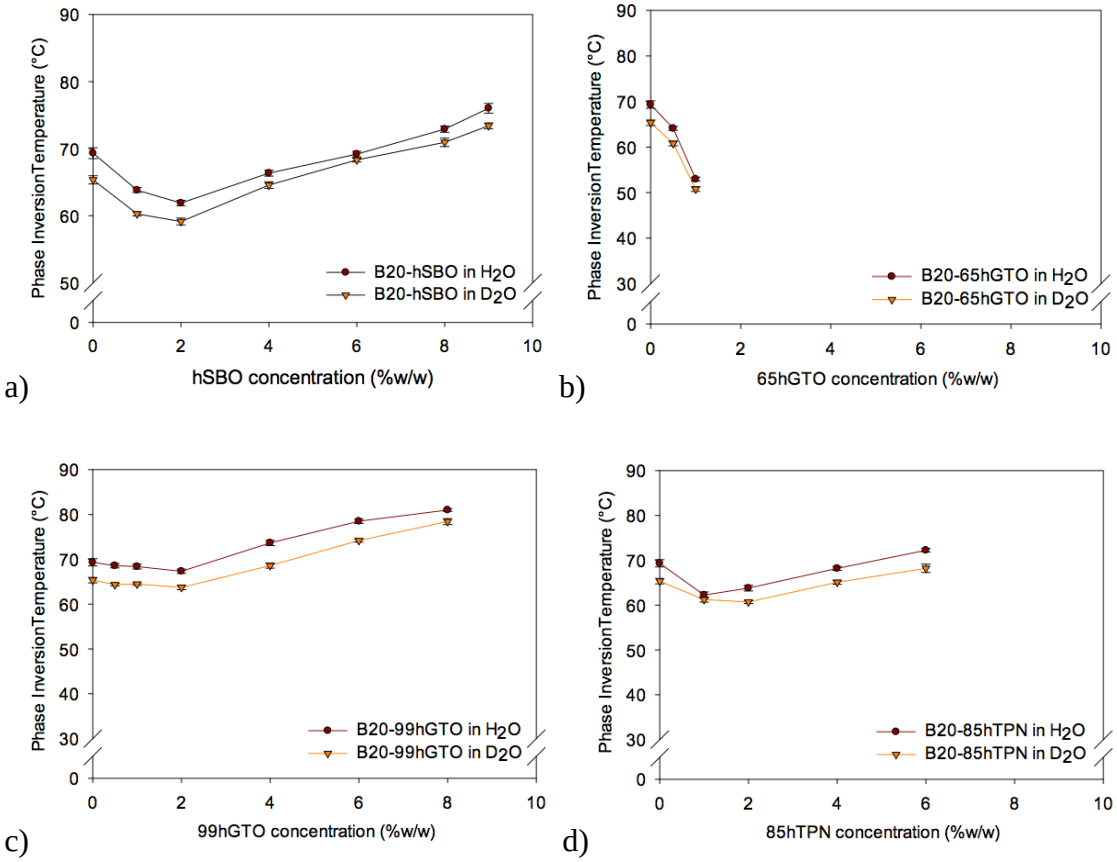

Figure 3.37: The variation in the phase inversion temperature of nanoemulsion prepared using 20 %w/w Brij O10 and containing a triglyceride, (a) hSBO, (b) 65hGTO, (c) 99hGTO and (d) hTPN and in either D_2O or H_2O (mean ± S.D.). Error bars in some cases contained within the symbol.

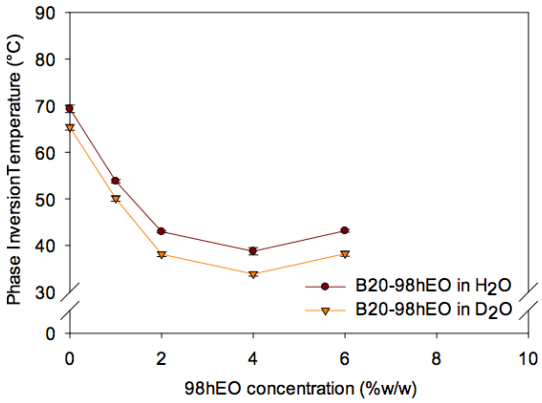

Figure 3.38: The variation in the phase inversion temperature of nanoemulsion prepared using 20 %w/w Brij O10 and containing the ethyl ester oil, 98hEO in either D_2O or H_2O (mean ± S.D.). Error bars in some cases contained within the symbol.

3.4.3 Effect of deuterated water on the particle size determined by photon correlation spectroscopy (PCS)

In order to ensure that D_2O does not grossly change the morphology of the micelle and NE, the size of the micelles and NE by PCS at 25 °C. Such measurements were important because it has been reported that substitution of H_2O by D_2O can affect micelle size, such as was reported for micelles formed by the alkyl glycoside surfactant, n-nonyl-β-D-glucoside (β-C_9G_1) (Ericsson et al., 2004). The same research group also studied the aggregation of the related sugar surfactant, *n*-tetradecyl-β-D-maltoside ($C_{14}G_2$), determining particle size using photon correlation spectroscopy (PCS), and again found that the particle size of the micelles in D_2O were larger than those in H_2O (Ericson et al., 2005).

Therefore, to evaluate the effect of D_2O on the particle size of the aggregates prepared in the present study, PCS was employed to measure the particle size of all micelles and NE prior to their study by SANS. **Figures 3.39 and 3.40** shows the apparent hydrodynamic size of the NE in D_2O at 25 °C after 1-month storage and compares their size to that obtained for the samples prepared in H_2O and measured under the same conditions. It was clear that replacing the H_2O with D_2O did not significantly affect the particle size, or indeed stability, of micelles and NE as determined by PCS.

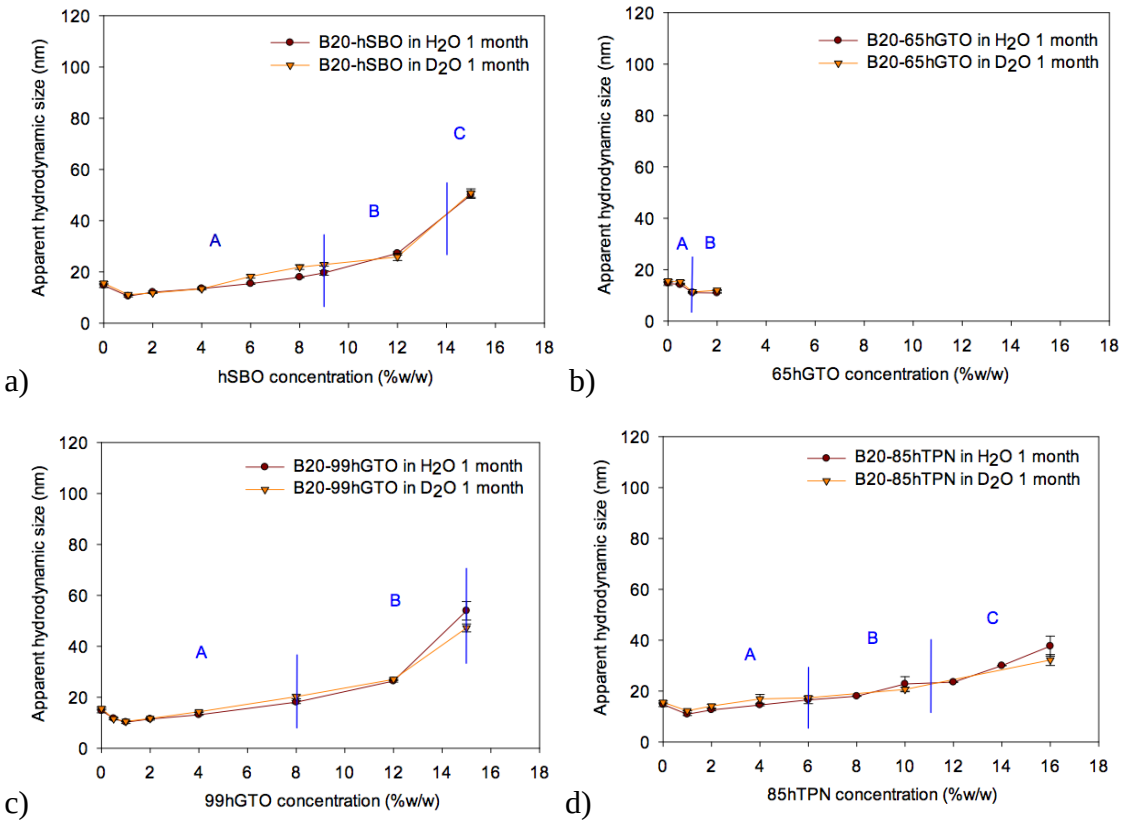

Figure 3.39: The variation in the mean apparent hydrodynamic droplet size of 1 month old nanoemulsions prepared using 20 %w/w Brij O10 and containing a triglyceride, (a) hSBO, (b) 65hGTO, (c) 99hGTO and (d) hTPN and in either D_2O or H_2O (mean ± S.D.). Error bars in some cases contained within the symbol.

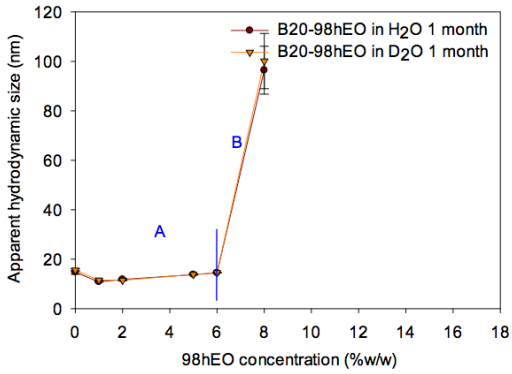

Figure 3.40: The variation in the mean apparent hydrodynamic droplet size of 1 month old nanoemulsions prepared using 20 %w/w Brij O10 and containing the ethyl ester, 98hEO and in either D_2O or H_2O (mean ± S.D.). Error bars in some cases contained within the symbol.

3.5 Small angle neutron scattering data

The first step in the analysis of SANS data is an initial estimation of the shape of the NE particles. The SANS data were therefore analysed using a range of different form factors, P(Q), in order to determine the shape of the aggregates. The different form

factors selected to fit that SANS data for the micelles and NE where a sphere, an oblate or a prolate ellipsoid (**Figure 3.41**). In all these models, the interparticulate structure factor, S(Q), used was the Percus-Yevick approximation to account for hard-sphere interactions present in the system. In order to analyse the SANS data, the micelles and NE were assumed to be monodisperse and of a uniform scattering length density (SLD).

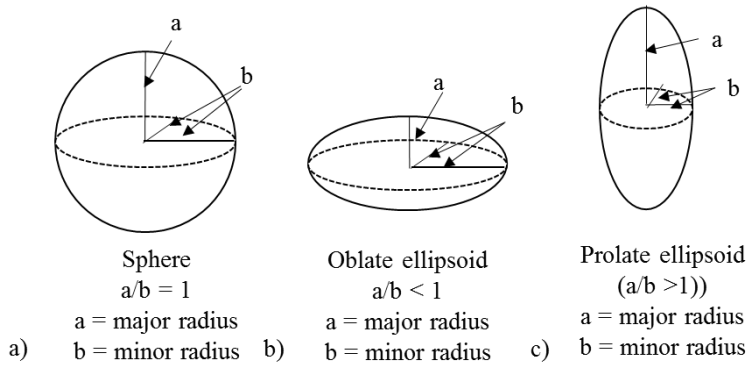

Figure 3.41: Schematic representation of a) a sphere, b) an oblate ellipsoid and c) a prolate ellipsoid.

The model used for the micelles examined in this study assumes the existence of a core-shell particle, with the core containing the hydrocarbon chains of the surfactant only and a shell composed of the surfactants polar head groups together with some solvent molecules. In contrast, the model used for the NEs, where more than one contrast was frequently available, was slightly different in that it was assumed that the core of the NE consisted only of oil, while the shell consisted of the whole surfactant molecule along with any associated solvent. In this case each contrast was fitted separately but the parameters used had to be consistent with the other models.

Clearly, the SANS data could not be satisfactorily fitted using simple form factors such as spheres, while in contrast, the data could be reasonably well fitted using prolate ellipsoids for the Brij O10 micelles and oblate ellipsoids for the Brij O10 NEs. It is clear from this preliminary study that the particles were not spherical but rather were ellipsoidal in nature. As a consequence of these preliminary results, a core-shell ellipsoid model was chosen as standard to analyse this SANS data in the present study as it appeared to be the most appropriate way to describe the SANS data, yielding statistically better results in comparison to the spherical model.

3.5.1 SANS studies of Brij O10 micelle in the presence and absence of drug

A series of the best fits to the data were obtained using the core-shell ellipsoidal model for the Brij O10 micelles at various concentration, as shown in **Figure 3.42**. Note that Q

and I(Q) are scattering vector and the intensity of the scattered neutron radiation, respectively. As can be seen, the scattering intensity increased with the increasing surfactant concentration. Furthermore the shape of the curve maintained a similar shape at a surfactant concentration up to 5 %w/w. Above this concentration, a peak appears in the scattering curve at a Q value of 0.06 $Å^{-1}$, which is indicative of the presence of strong inter-particulate interactions. In addition the apparent volume of the micelles decreased as the Brij O10 concentration increased. However, the structure factor, S(Q), obtained from samples at Brij O10 concentration above 2 %w/w was not equal to 1, which further indicates the presence of inter-particulate interactions at higher concentrations. Taken together this information suggests that, at concentrations above 2 %w/w, the interactions were too strong and too long range to be described by the simple hard-sphere model, and/or also possibly because of an elongation of the micelles, the model fails to describe the interactions present in the elongated micelles present at the higher surfactant concentrations. As a consequence therefore, a Brij O10 concentration of 2 %w/w was used to prepare NE for the remaining part of the SANS study.

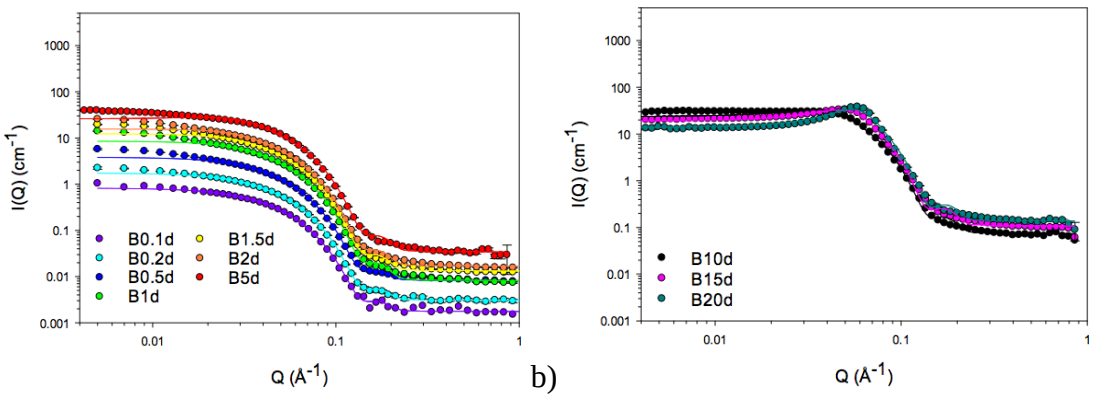

Figure 3.42: Drop contrast of SANS data and the 'best' fits for Brij O10 micelle droplets with increasing surfactant concentration from a) 0.1 to 5 %w/w and b) 10 to 20 %w/w at 25 ˚C using a core-shell ellipsoid model together with a hard sphere model for interactions.

The dimensions obtained from the best fits to the SANS data for the Brij O10 micelles, namely, the core equatorial radius, the minor radius, the major radius and the shell thickness are listed in **Table 3.10**. It is noteworthy that there was no remarkable difference result observed between the different surfactant concentrations, in that the micelles remained the same size and shape between Brij O10 concentrations of 0.1-5 %w/w Brij O10 when the core equatorial radius was around 22.5-23.0 Å and the core axial ratio of ~ 3.0, suggesting that the Brij O10 micelles were prolate ellipsoid in shape. The shell thickness obtained from these fits was 10.5-11.0 Å with 30 % of the shell being D_2O, while the minor and major radii were 33.0-33.5 Å and 76.0-83.0 Å,

respectively. Overall, the size of the Brij O10 micelles at concentrations of between 1-5 %w/w remained similar with the trend seen upon increasing surfactant concentration being the same as that seen with the variation in apparent hydrodynamic size of the micelles determined using PCS. The aggregation number of Brij O10 micelles were in the range 254-276, while the equivalent hard sphere (SPH) radius was 82.0-93.0 Å. A schematic representation of the ellipsoidal Brij O10 micelles seen at a concentration of 2 %w/w is shown in **Figure 3.43**. At Brij O10 concentrations of above 10 %w/w, where the inter-particulate interactions where greatest, the micelles surprisingly became more spherical, while the core equatorial radius remained the same, the core axial ratio decreased to 1.6.

Table 3.10 Parameters obtained for the best fit to the SANS data for 0.1, 0.2, 0.5, 1, 1.5, 2, 5, 10, 15, 20 %w/w Brij O10 micelles in the absence of drugs using a core-shell ellipsoid model together with a hard sphere structure factor S(Q). The modelling of the SANS data was constrained using Vshell(dry)/Vcore, along with the percentage of solvent in shell at 30%.

sample	core equatorial radius (R_1,Å)	core axial ratio (x)	core axial radius (R_1x,Å)	shell thickness (Å)	minor radius (Å)	major radius (Å)	axial ratio (X)	micelle volume (Å^3)	sphere radius (Å)	hydration (%)	N_{agg}	surfaces area of surfactant (Å^2)	sum of squared error (SSE)
B0.1d	22.6	2.9	66.2	10.5	33.1	76.6	2.3	350701	83.3	30	254	61	526
B0.2d	22.7	3.0	67.8	10.6	33.3	78.4	2.4	364972	83.8	30	262	60	1440
B0.5d	23.0	2.9	65.5	10.6	33.6	76.2	2.3	361059	87.7	30	261	60	8552
B1d	22.8	3.0	69.0	10.9	33.7	79.9	2.4	379742	87.9	30	270	60	22917
B1.5d	22.7	3.1	70.7	11.0	33.7	81.8	2.4	389705	81.7	30	274	60	35868
B2d	22.6	3.2	72.0	11.0	33.6	83.0	2.5	393141	92.7	30	276	60	43473
B5d	22.1	3.3	73.0	10.9	33.0	83.8	2.5	382361	86.8	30	269	61	35316
B10d	23.0	2.1	48.5	10.3	33.3	58.8	1.8	272491	65.0	30	192	62	42416
B15d	23.3	1.7	39.7	9.9	33.2	49.5	1.5	228472	51.5	30	162	63	24440
B20d	22.7	1.6	35.6	9.7	32.4	45.3	1.4	199171	47.9	30	138	65	72778

Estimated uncertainty for R_1 and x were ± 0.2 and ± 0.05, respectively.

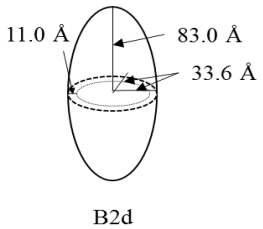

Figure 3.43: Schematic representation of the ellipsoidal 2 %w/w Brij O10 micelles.

Surprisingly, the prolate ellipsoid shape of Brij O10 micelles determined in the present study was in direct contrast to the oblate ellipsoids previously reported by Wasutrasawat (2011). This observation might be the result of batch-to-batch variations in the $C_{18:1}E_{10}$ surfactant. However, the volume of one Brij O10 micelle at 25 °C was calculated to be ~ 350-393 nm^3, which was a little bigger than the volume of 271-302 nm^3 at 25 °C calculated by Wasutrasawat (2011) and 324 nm^3 at 20 °C reported by Prak et al. (2011). This observation showed that even though the shape of Brij O10 micelles were different in each study, but the volume of micelles were comparable.

The SANS data and the best fits for 2 %w/w Brij O10 micelles in the presence of a saturated amount of drug, namely testosterone propionate (TP), curcumin (CUR), and curcumin in combination with testosterone propionate (CUR-TP) are shown in **Figure 3.44** and **Table 3.11**. A schematic representation of the ellipsoidal Brij O10 micelles together with either TP, CUR, or CUR-TP is shown in **Figure 3.45**. It is found that the presence of TP and CUR-TP slightly affected the size and shape of the micelles. According to the best fits, the core radius increased from 22.6 ± 0.2 Å for the micelles (B2d) to 23.0 ± 0.4 Å for the micelles containing a saturation amount of TP (B2d-TP) and 23.4 ± 0.4 Å for micelles containing a saturation amount of CUR and TP (B2d-CUR-TP), while the minor radius very slightly changed from 33.6 Å for B2d to 34.3 Å for B2d-TP and 34.6 Å for B2d-CUR-TP, the major radius increased from 83.0 Å for B2d to 87.0 Å for B2d-TP and 88.0 Å for B2d-CUR-TP. The very small change in the axial ratio (x) from 3.2 ± 0.05 for B2d to 3.3 ± 0.05 for B2d-TP and 3.3 ± 0.05 for B2d-CUR-TP shows that the shape of micelle was not greatly affected by the addition of TP or CUR-TP. In addition, the shell thickness remained relatively constant at ~ 11.0 Å for B2d, B2d-TP and B2d-CUR-TP. Interestingly, the small increase in size of B2d-CUR-TP as determined by SANS is not in good agreement with the large increase in size observed for the CUR and TP containing B2d micelles determined by PCS. This apparent discrepancy may suggest a limitation of PCS to measure particle size and/or the absence of any correction for inter particulate interactions.

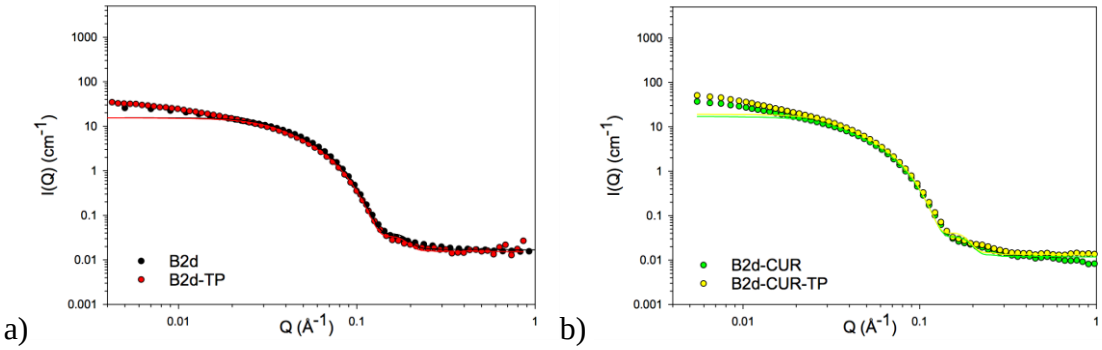

Figure 3.44: SANS curves obtained for drop contrast of 2 %w/w Brij O10 micelles a) in the absence and presence of TP, b) in the presence of either CUR or CUR-TP, along with the 'best' fits to the data.

In contrast, the presence of CUR alone significantly affected the shape of B2 micelles according to the SANS measurements. According to the best fits to the SANS data, there was a large change in the axial ratio of the micelles from 3.2 ± 0.05 to 3.7 ± 0.05 in the presence of CUR, while the core radius remained approximately the same at 22.5 Å for B2d micelles to 22.7 ± 0.2 Å for B2d-CUR micelles as did the shell thickness, which was ~ constant at 11.0 Å for both B2d and B2d-CUR micelles. In addition, the minor radius stayed constant at ~ 33.5 Å for B2d and B2d-CUR micelles, although the major radius increased from 83.0 Å for B2d micelles to 94.5 Å for B2d-CUR micelles. Taken together these results suggest that the presence of CUR affects the shape of the B2 micelles. The change in shape of the B2d micelles in the presence of CUR measured with SANS might suggest the reason why the measured PCS indicated an increase in the size of the micelles containing CUR. This result might be a consequence of the fact that the PCS measurements assumed the presence of spherical micelles, while the SANS measurements clearly indicated that the shape of the B2d-CUR micelles were oblate ellipsoid.

Table 3.11 Parameters obtained for the best fit to the SANS data for 2 %w/w Brij O10 micelles in the presence of drugs using a core-shell ellipsoid model together with a hard sphere structure factor S(Q). The modelling of the SANS data was constrained using Vshell(dry)/Vcore, along with the percentage of solvent in shell at 30%.

sample	core equatorial radius (R_1,Å)	core axial ratio (x)	core axial radius (R_1x,Å)	shell thickness (Å)	minor radius (Å)	major radius (Å)	axial ratio (X)	micelle volume (Å^3)	sphere radius (Å)	hydration (%)	N_{agg}	surfaces area of surfactant (Å^2)	sum of squared error (SSE)
B2d-TP	23.0	3.3	75.7	11.3	34.3	87.0	2.5	428894	92.8	30	302	59	51192
B2d-CUR	22.7	3.7	83.6	11.1	33.7	94.7	2.8	450887	98.2	30	323	59	25903
B2d-CUR-TP	23.4	3.3	76.8	11.2	34.6	88.0	2.5	441479	98.4	30	317	58	59207

Estimated uncertainty for R_1 and x were ± 0.4 and ± 0.05, respectively.

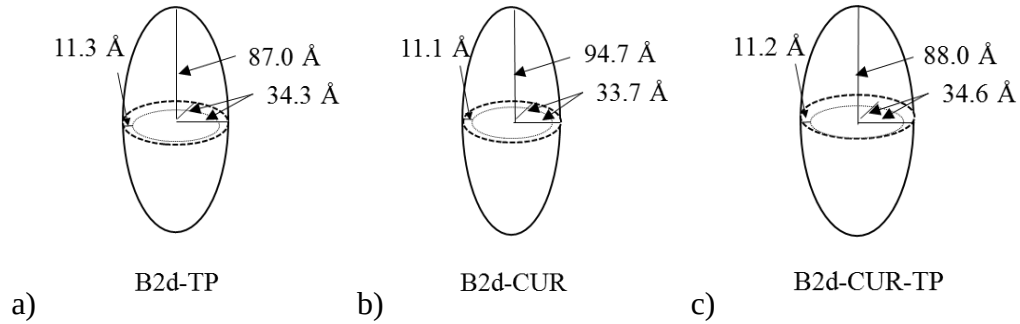

Figure 3.45: Schematic representation of the ellipsoidal 2 %w/w Brij O10 micelles containing with either a) TP, b) CUR or c) CUR and TP.

The parameters obtained for the best fit to the SANS data for NE in the absence and presence of drugs are shown in **Tables 3.12-3.15** for the SBO NE, **Tables 3.17-3.18** for the GTO NE, **Table 3.20-3.21** for the TPN NE, **Table 3.23** for the GTS NE and **Table 3.24-3.25** for the EO NE. The parameters obtained for the best fit to the SANS data for the NE performed at 37 °C are shown in **Table 3.27**, while those for NE incubation in the presence of cell culture media at 37 °C are shown in **Table 3.28-3.29**.

3.5.2 SANS studies of Brij O10 nanoemulsions

3.5.2.1 SANS studies of Brij O10 nanoemulsions containing soybean and drug

A range of models (form factors) were used to fit the drop contrasts of the B2-hSBO NE (prepared using hSBO, hBrij O10, D_2O) at different concentration of hSBO in Regions A, B and C. It was clear from the preliminary modelling that the best fit to the SANS data was an ellipsoid, with an axial ratio of the core of less than 1, suggesting the presence of an oblate ellipsoid, the same shape as reported for SBO NE in an earlier study (Wasutrasawat, 2011). The SANS data and the 'best' fits of the B2-hSBO NE obtained using the core-shell ellipsoid model are shown in **Figure 3.46** while **Table 3.12** shows the parameters obtained from the 'best' fits of the SANS data.

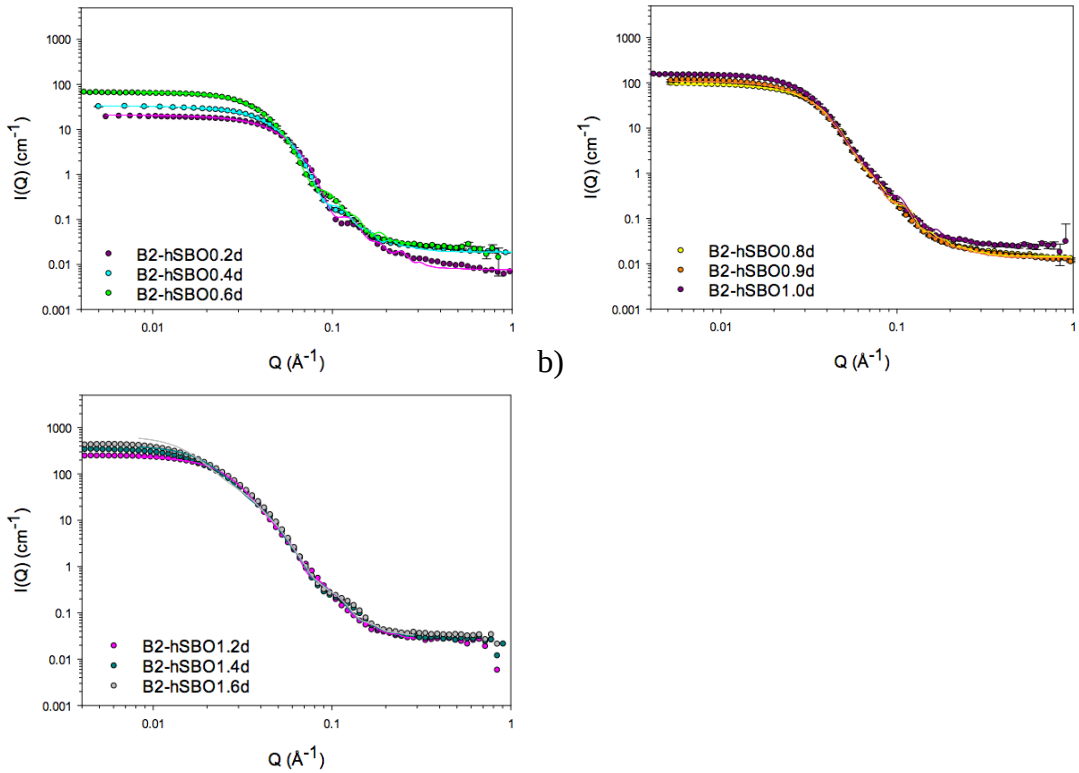

Figure 3.46: SANS data and 'best' fits using the oblate ellipsoid model for the drop contrast of NE prepared using 2 %w/w Brij O10 and containing various concentration of hSBO from a) 0.2 - 0.6 %w/w, b) 0.8 - 1.0 %w/w and c) 1.2-1.6 %w/w in the absence of drug. SANS data of NE performed on SANS2D with the rear detector positioned at 8 m showed a wider Q range than that of NE performed on SANS2D with the rear detector positioned at 4 m.

Table 3.12 Parameters obtained for the 'best' fit of the SANS data to 2 %w/w Brij O10 and hSBO nanoemulsions in the absence of drug using a core-shell ellipsoid model together with a hard sphere structure factor S(Q). The modelling of the SANS data was constrained using Vshell(dry)/Vcore.

sample	region	core equatorial radius (R_1,Å)	core axial ratio (x)	core axial radius (R_1x,Å)	shell thickness (Å)	minor radius (Å)	major radius (Å)	axial ratio (X)	NE volume (Å^3)	sphere radius (Å)	hydration (%)	N_{agg}	surfaces area of surfactant (Å^2)	sum of squared error (SSE)
B2-hSBO0.2d	A	27.0	0.4	10.5	24.8	51.8	35.3	0.7	397912	55.7	20	256	74	5347
B2-hSBO0.4d		36.1	0.4	16.1	22.6	58.7	38.7	0.7	559854	58.5	15	351	78	13950
B2-hSBO0.6d		46.7	0.5	21.9	22.2	68.9	44.1	0.6	878496	73.0	10	534	73	3816
B2-hSBO0.8d		60.4	0.4	25.0	22.3	82.7	47.3	0.6	1353642	82.7	10	764	71	7301
B2-hSBO0.9d		66.9	0.4	26.1	22.0	88.9	48.1	0.5	1591197	95.9	10	868	72	9978
B2-hSBO1.0d	B	71.8	0.4	28.1	21.9	93.7	50.0	0.5	1839135	91.9	10	970	72	4689
B2-hSBO1.2d		91.1	0.3	29.0	21.8	112.9	50.8	0.5	2712089	116.1	10	1342	72	15191
B2-hSBO1.4d		124.6	0.2	28.1	21.8	146.3	49.9	0.3	4475604	150.4	10	2085	73	42635
B2-hSBO1.6d	C	165.5	0.2	27.2	21.3	186.7	48.5	0.3	7089159	192.5	10	3134	76	84407

Estimated uncertainty for R_1 was ± 0.2 for B2-hSBO0.2d to B2-hSBO0.8d and then increased to ± 1.5 for B2-hSBO1.6d in the absence of drug.
Estimated uncertainty for x were ± 0.01.

The results obtained suggest that no significant interactions occurred between the diluted NE droplets as expected. As can be seen the core equatorial radius of the NE increased with hSBO content, a trend which was similar to that seen with dynamic light scattering. The shell thickness obtained from the 'best' fits were in the range 21.5-25.0 Å. After attempting to fit the SANS data using various levels of hydration of the B2-hSBO NE, the best value of shell hydration for the various hSBO-containing NE was found to decrease with an increase in SBO from 20 % for hSBO1 NE to 10 % for hSBO0.5 NE and higher SBO concentrations. Surprisingly, the shape of the NE became more elongated as the oil content increased. **Figure 3.47** gives a schematic representation of the NE containing the upper limit possible of hSBO in a) Regions A, b) Region B and c) Region C in the absence of drug.

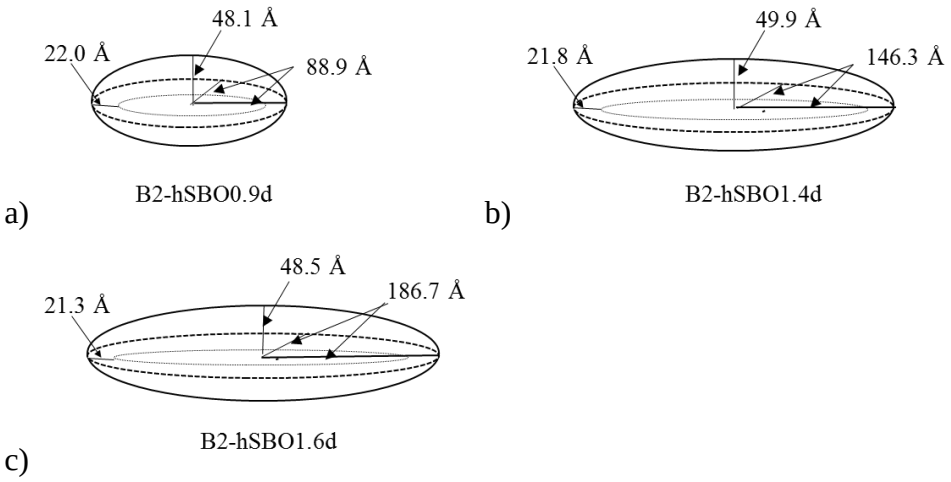

Figure 3.47: Schematic representation of ellipsoidal 2 %w/w Brij O10 NE containing the upper limit possible of hSBO incorporated in a) Regions A, b) Region B and c) Region C in the absence of drug.

The major radius of B2-hSBO NE in Region A NE increased from 35.5 Å for B2-hSBO0.2d NE to 48.0 Å for B2-hSBO0.9d NE, while the minor radius of B2-hSBO NE in Region A NE increased with increasing hSBO concentration from 52.0 Å for B2-hSBO0.2d NE to 89.0 Å for B2-hSBO0.9d NE. However, the major radius of B2-hSBO NE in Regions B and C NE stayed constant at around 50 Å, while the minor radius of B2-hSBO NE in Region B and C NE increased with the increasing hSBO concentration from 93.5 Å for the B2-hSBO1.0d NE to 187.0 Å for the B2-hSBO1.6d NE.

After using a range of form factors to try to individually fit the drop contrast of B2-hSBO-TP, B2-hSBO-CUR and B2-hSBO-CUR-TP NE containing different concentrations of hSBO in Regions A, B and C for B2-hSBO-TP NE and in Region A

for B2-hSBO-CUR and B2-hSBO-CUR-TP NE, it was clear that there was no difference in the shape and size of the NE in the absence and presence of drug. The SANS data and 'best' fits of the NE with the upper limit of amount of hSBO incorporated into NE denoted in Regions A, B and C are shown in **Figure 3.48**.

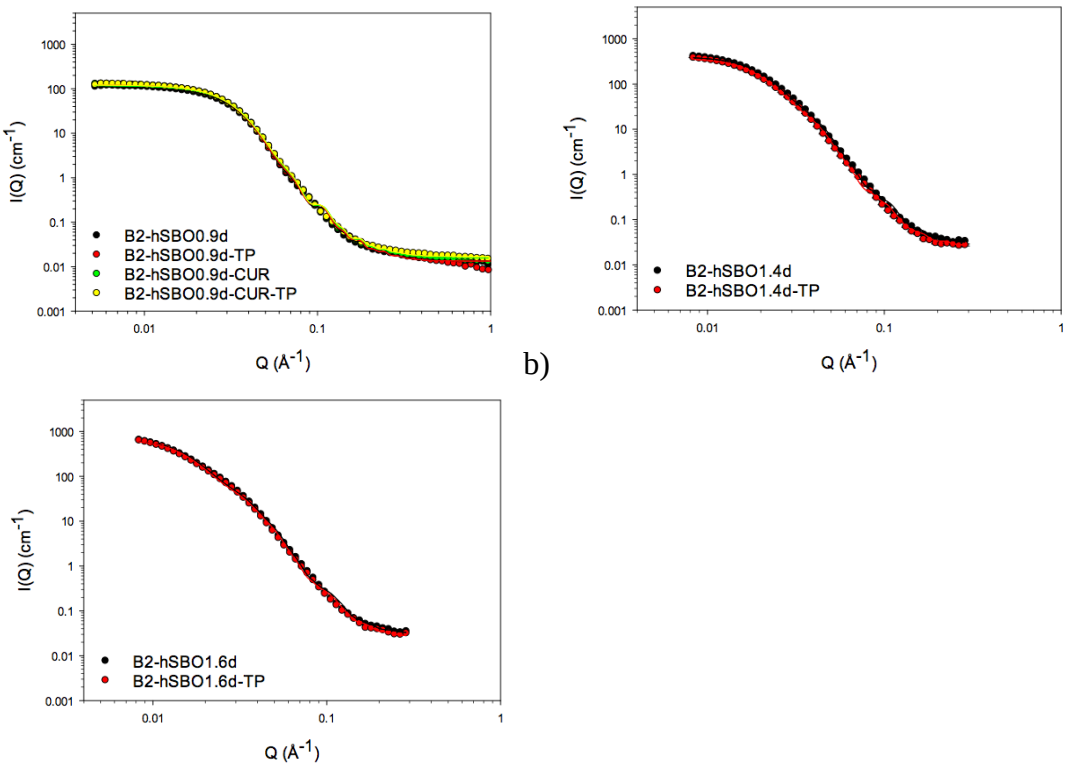

Figure 3.48: SANS data together with the 'best' fits using oblate ellipsoid model obtained for the drop contrast of 2 %w/w Brij O10 NE containing the upper limit of hSBO incorporated in a) Region A, b) Region B, and c) Region C in the absence and presence of drug.

The SANS data and 'best' fits obtained for B2-hSBO-TP, B2-hSBO-CUR and B2-hSBO-CUR-TP NE using the core-shell ellipsoid model are shown in **Figures 3.49, 3.50** and **3.51**, respectively. The parameters obtained for the 'best' fits to the B2-hSBO-TP, B2-hSBO-CUR and B2-hSBO-CUR-TP NE are shown in **Tables 3.13, 3.14** and **3.15**. The results suggest that no significant interaction occurred between droplets as was expected in the diluted NE system.

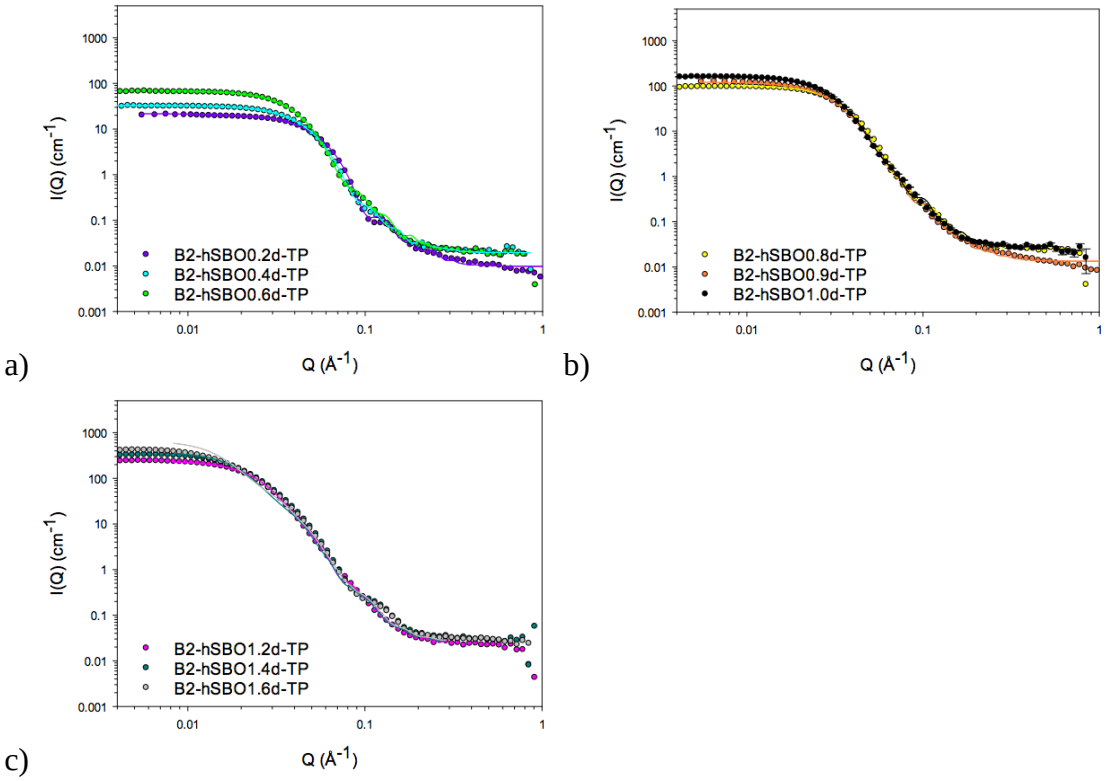

Figure 3.49: SANS data and corresponding 'best' fits to the drop contrast of 2 %w/w Brij O10 and hSBO nanoemulsions with increasing hSBO content from a) 0.2 - 0.6 %w/w, b) 0.8 - 1.0 %w/w and b) 1.2 - 1.6 %w/w in the presence of TP.

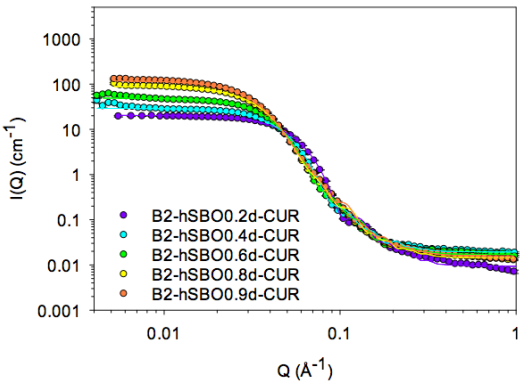

Figure 3.50: SANS data and the corresponding 'best' fits to the drop contrast for 2 %w/w Brij O10 and hSBO nanoemulsions with increasing hSBO content from 0.2 - 0.9 %w/w in the presence of CUR.

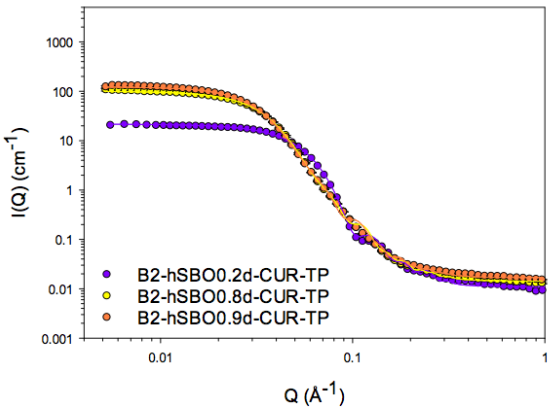

Figure 3.51: SANS data and the corresponding 'best' fits to the drop contrast for 2 %w/w Brij O10 and hSBO nanoemulsions with increasing hSBO content from 0.2 - 0.9 %w/w in the presence of CUR and TP.

Table 3.13 Parameters obtained for the 'best' fit of the SANS data to 2 %w/w Brij O10 and hSBO nanoemulsions in the presence of TP using a core-shell ellipsoid model together with a hard sphere structure factor S(Q). The modelling of the SANS data was constrained using Vshell(dry)/Vcore.

sample	region	core equatorial radius (R_1,Å)	core axial ratio (x)	core axial radius (R_1x,Å)	shell thickness (Å)	minor radius (Å)	major radius (Å)	axial ratio (X)	NE volume (Å^3)	sphere radius (Å)	hydration (%)	N_{agg}	surfaces area of surfactant (Å^2)	sum of squared error (SSE)
B2-hSBO0.2d-TP	A	26.9	0.4	10.4	24.5	51.1	34.8	0.7	401462	56.6	20	245	75	4521
B2-hSBO0.4d-TP		38.2	0.4	15.5	23.0	61.1	38.4	0.6	601965	71.9	15	377	76	1644
B2-hSBO0.6d-TP		48.5	0.4	21.4	22.4	70.9	43.8	0.6	923486	75.5	10	561	72	2720
B2-hSBO0.8d-TP		59.7	0.4	25.9	22.5	82.2	48.4	0.6	1370239	90.6	10	774	70	1631
B2-hSBO0.9d-TP		68.5	0.4	26.1	22.3	90.9	48.4	0.5	1675591	95.3	10	914	70	9594
B2-hSBO1.0d-TP	B	71.8	0.4	29.0	22.5	94.3	51.5	0.5	1918142	98.5	10	1016	69	6200
B2-hSBO1.2d-TP		93.6	0.3	29.8	22.4	116.0	52.2	0.5	2943671	115.9	10	1456	69	14861
B2-hSBO1.4d-TP		129.1	0.2	29.0	22.5	151.6	51.5	0.3	4961346	151.7	10	2312	70	38118
B2-hSBO1.6d-TP	C	169.4	0.2	27.9	21.8	191.2	49.7	0.3	7615899	198.7	10	3353	74	78879

Estimated uncertainty for R_1 remained at ± 0.2 for B2-hSBO0.2d-TP to B2-hSBO0.8d-TP and then increased to ± 1.5 for B2-hSBO1.6d-TP.
Estimated uncertainty for x were ± 0.01.

Table 3.14 Parameters obtained for the 'best' fit of the SANS data to 2 %w/w Brij O10 and hSBO nanoemulsions in the presence of CUR using a core-shell ellipsoid model together with a hard sphere structure factor S(Q). The modelling of the SANS data was constrained using Vshell(dry)/Vcore.

sample	Region	core equatorial radius (R_1,Å)	core axial ratio (x)	core axial radius (R_1x,Å)	shell thickness (Å)	minor radius (Å)	major radius (Å)	axial ratio (X)	NE volume (Å^3)	sphere radius (Å)	hydration (%)	N_{agg}	surfaces area of surfactant (Å^2)	sum of squared error (SSE)
B2-hSBO0.2d-CUR	A	26.0	0.4	10.8	24.6	50.6	35.3	0.7	379227	56.1	20	244	75	2825
B2-hSBO0.4d-CUR		37.9	0.4	15.9	23.2	61.1	39.1	0.6	610497	67.2	15	383	75	1601
B2-hSBO0.6d-CUR		49.0	0.4	20.9	22.3	71.3	43.2	0.6	920774	73.5	10	559	72	1684
B2-hSBO0.8d-CUR		60.9	0.4	24.4	22.1	83.0	46.4	0.6	1340070	83.8	10	757	72	6812
B2-hSBO0.9d-CUR		67.5	0.4	25.3	21.8	89.3	47.1	0.5	1573771	95.0	10	858	73	11073

Estimated uncertainty for R_1 and x were ± 0.3 and ± 0.01, respectively.

Table 3.15 Parameters obtained for the 'best' fits of the SANS data to 2 %w/w Brij O10 and hSBO nanoemulsions in the presence of CUR and TP using a core-shell ellipsoid model together with a hard sphere structure factor S(Q). The modelling of the SANS data was constrained using Vshell(dry)/Vcore.

sample	Region	core equatorial radius (R_1,Å)	core axial ratio (x)	core axial radius (R_1x,Å)	shell thickness (Å)	minor radius (Å)	major radius (Å)	axial ratio (X)	NE volume (Å^3)	sphere radius (Å)	hydration (%)	N_{agg}	surfaces area of surfactant (Å^2)	sum of squared error (SSE)
B2-hSBO0.2d-CUR-TP	A	26.7	0.4	10.7	24.9	51.6	35.6	0.7	396259	55.8	20	255	73	4282
B2-hSBO0.8d-CUR-TP		62.1	0.4	23.8	22.0	84.1	45.8	0.5	1358766	87.4	10	767	72	7648
B2-hSBO0.9d-CUR-TP		69.1	0.4	24.8	21.8	91.0	46.6	0.5	1615925	97.6	10	881	73	10969

Estimated uncertainty for R_1 and x were ± 0.3 and ± 0.01, respectively.

As can be seen from the 'best' fit parameters obtained using an oblate ellipsoid, the SANS results showed a slight difference in the size and shape of the NE in the presence and absence of TP (**Table 3.13**). As expected, the equatorial core radius of the B2-hSBO-TP NE increased with hSBO content, exhibiting a similar trend to that seen in the B2-hSBO NE. After fitting the SANS data with varying levels of shell hydration, the shell hydration of the hSBO NE was found to decrease from 20 % at B2-hSBO0.2d-TP NE to 10 % at B2-hSBO0.6d-TP NE and remained at 10 % for higher hSBO concentrations. The shell thickness obtained from the 'best' fits was in the range 21-24.5 Å.

As the concentration of hSBO increased within Regions A and B, the solubilisation of TP in the B2-hSBO-TP NE also increased, no doubt because of the larger equatorial core radius and the high solubility of TP in the hSBO comprising the core. The shape of the Region C NE containing TP and a high amount of hSBO was unexpected as it became more elongated as the content of hSBO increased as it was anticipated that NE would be more spherical in shape due to their high hSBO loading and the anticipated low penetration of the large molecular volume oil, SBO, into the interfacial surfactant monolayer. Interestingly, however, this change in morphology explains the decrease in observed TP solubilisation in Region C - because in this Region there is less of a distinct core of oil in which TP can be solubilised.

Within Region A, the major radius of B2-hSBO-TP NE increased upon increasing hSBO concentration from 35.0 Å for B2-hSBO0.2d-TP NE to 48.5 Å for B2-hSBO0.9d-TP NE, while the minor radius of B2-hSBO-TP NE changed from 51.0 Å for B2-hSBO0.2d-TP NE to 91.0 Å for B2-hSBO0.9d-TP NE for the same increase in hSBO concentration. In Regions B and C, the major radius of B2-hSBO-TP NE was unaltered by the amount of hSBO present, staying constant at ~ 50 Å while the minor radius increased with increasing hSBO content from 94.5 Å for B2-hSBO1.0d-TP NE to 191.0 Å for B2-hSBO1.6d-TP NE. When comparing the SANS data there was no difference in shape and/or size of TP-free and TP-containing NE, a result that was in direct contrast to the results obtained from PCS experiments. It is worth noting, that in this context, the analysis used for the PCS measurements assumed that the NE droplets were spherical, although from the SANS data the shape of B2-hSBO-TP NE were not spherical. The assumption of sphericity in the case of PCS, might explain the discrepancy between the two techniques, in particular the apparently larger size of the

B2-hSBO-TP NE in Regions B and C when compared with the size of the B2-hSBO NE when assessed by PCS.

In order to illustrate the change in shape reduces the capacity of NE to solubilise hydrophobic drug, the volume and the surface area of the equivalent ellipsoid and sphere are shown in **Table 3.16**. In this study it was reasonably assumed that TP would sit in the oil core and at the surfactant interface. As a consequence therefore the volume in which TP could be solubilised is the volume of the oil core and the volume of the surfactant hydrocarbon tails. **Figure 3.52** shows the schematic representation of an ellipsoidal SBO NE droplet.

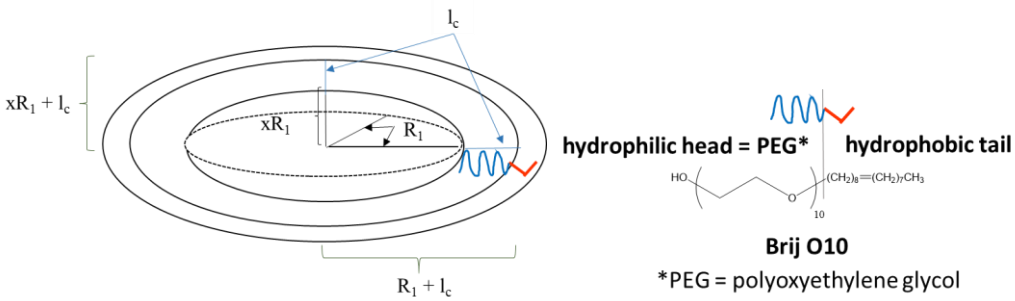

Figure 3.52: The schematic representation of ellipsoidal nanoemulsion containing soybean oil with the equatorial radius of the core (R_1), major radius of ellipsoid core (xR_1) and the length of the surfactant hydrocarbon tail (l_c)

The minor radius of equivalent ellipsoid is the sum of the length of the equatorial radius of the core (R_1) and the length of the surfactant hydrocarbon tail (l_c) calculated to be 17.3 Å by Malcolmson et al. (1995), i.e. R_1+l_c. The major radius of ellipsoid is the length of the axial radius of the core (xR_1) and the length of surfactant hydrocarbon tail ($xR_1 + l_c$). Both of these values were used to calculate the volume of oblate ellipsoid in which the drug was solubilised. The volume and surface area of ellipsoid were calculated using the following formula:

$$\text{Volume of ellipsoid} = \frac{4}{3}\pi(xR_1 + l_c)(R_1 + l_c)(R_1 + l_c)$$

Surface area of ellipsoid

$$= 4\pi\left(\frac{((R_1 + l_c)^p(R_1 + l_c)^p + (R_1 + l_c)^p(xR_1 + l_c)^p + (R_1 + l_c)^p(xR_1 + l_c)^p)}{3}\right)^{\frac{1}{p}},$$

$$p = 1.6075$$

The radius of the equivalent sphere is the equatorial radius of the core (R_1) obtained from the fitting of the SANS data for NE and the length of the surfactant hydrocarbon

tail (l_c) calculated to be 17.3 Å by Malcolmson et al. (1995), i.e. R_1+l_c. The volume and surface area of sphere were calculated using the following formula:

$$\text{Volume of sphere} = \frac{4}{3}\pi(R_1 + l_c)^3$$

$$\text{Surface area of sphere} = 4\pi(R_1 + l_c)^2$$

It is clear from the volume and surface area of the equivalent ellipsoid were much lower than those of the corresponding sphere, suggesting that a change in the shape of the NE from sphere to ellipsoid would affect the drug solubilisation capacity of NE (**Table 3.16**).

Table 3.16 The comparison of the volume and the surface area of ellipsoid and sphere of 2 %w/w Brij O10 and hSBO nanoemulsions in the presence of TP

sample	region	ellipsoid		sphere	
		volume of oil core and tail of surfactant (Å^3)	surface area of ellipsoid (Å^3)	volume of oil core and tail of surfactant (Å^3)	surface area of sphere (Å^3)
B2-hSBO0.2d-TP	A	228535	18808	361448	24542
B2-hSBO0.4d-TP		421872	28671	713973	38636
B2-hSBO0.6d-TP		700744	40255	1191977	54374
B2-hSBO0.8d-TP		1073232	54035	1913810	74555
B2-hSBO0.9d-TP		1340183	64268	2649346	92605
B2-hSBO1.0d-TP	B	1540060	70009	2962491	99766
B2-hSBO1.2d-TP		2424482	100538	5708526	154487
B2-hSBO1.4d-TP		4154769	161133	13145636	269399
B2-hSBO1.6d-TP	C	6599747	248245	27262947	438118

As can be seen from the parameters obtained for the best fit, the SANS results showed a slight difference in size and shape of NE droplets in the presence and absence of CUR (**Table 3.14**). As expected, the core equatorial radius of the B2-hSBO-CUR NE increased with hSBO content - a trend which was similar to that seen for the corresponding B2-hSBO NE in the absence of CUR. The shell thickness obtained from the fits decreases from 24.5 to 22.0 Å with hSBO concentration. After attempting to fit the SANS data using a range of hydration levels, the best fits to the data yielded a shell hydration for hSBO-CUR NE which decreased from 20 % for B2-hSBO0.2d-CUR NE to 10 % for B2-hSBO0.6d-CUR NE whereafter it remained at 10 % regardless of any

increase in hSBO concentration. Again the model which provided the best fit to the SANS data was an ellipsoid. The axial ratio of the core suggested that the shape of B2-hSBO NE was an oblate ellipsoid. In Region A NE, the major radius of B2-hSBO-CUR NE increased from 35.5 Å for B2-hSBO0.2d-CUR NE to 47.0 Å for B2-hSBO0.9d-CUR NE, while the minor radius of B2-hSBO-CUR NE changed from 51.0 Å for B2-hSBO0.2d-CUR NE upon increasing hSBO concentration to 89.5 Å for B2-hSBO0.9d-CUR.

Interestingly, although the equatorial radius of the core of B2-hSBO-CUR NE increased with increasing hSBO content, the solubilisation of CUR in B2-hSBO-CUR remained unaltered. This observation may be explained by the poor solubility of CUR in hSBO, particularly when compared to the very much higher solubility of TP in hSBO. Moreover, the shape and size of the B2-hSBO-CUR NE obtained from the SANS experiments was not significantly different from that of B2-hSBO NE. On the other hand, using PCS the size of B2-hSBO-CUR NE were significantly larger and exhibited a fluctuation with increasing hSBO content. This observation suggests again that there is a limitation using PCS for the size measurement of CUR-containing hSBO NE.

As can be seen from the fitting parameters, the SANS results showed a slight difference in size and shape of NE droplets in the presence and absence of CUR-TP (**Table 3.15**). As expected, the core equatorial radius of the B2-hSBO-CUR-TP NE increased with hSBO content, a trend which was similar to B2-hSBO NE. After fitting SANS data with varying levels of the hydration in shell for each NE sample, the shell hydration of hSBO-CUR-TP NE was found to decrease from 20 % for B2-hSBO0.2d-CUR-TP NE and remained at 10 % at other higher hSBO concentrations. The shell thickness obtained from the fits stayed the same at about 25.0 Å to 22.0 Å. It was clear that the model that provided the best fit to the SANS data was an ellipsoid. The axial ratio of the core suggested that the shape of B2-hSBO-CUR-TP NE was an oblate ellipsoid. In Region A NE, the major radius of B2-hSBO-CUR-TP NE changed from 35.5 Å for B2-hSBO0.2d-CUR-TP NE to 46.5 Å for B2-hSBO0.9d-CUR-TP NE and the minor radius of B2-hSBO-CUR-TP NE increased from 51.5 Å for B2-hSBO0.2d-CUR-TP NE to 91.0 Å for B2-hSBO0.9d-CUR-TP NE with the increasing hSBO.

Even though the core equatorial radius of B2-hSBO-CUR-TP NE increased with increasing hSBO content, the level of CUR solubilisation in B2-hSBO-CUR-TP NE was little higher than that in B2-hSBO-CUR NE while the solubilisation of TP in B2-hSBO-CUR-TP NE was less than that that of TP in B2-hSBO-TP NE. The small

increase in CUR solubilisation could be explained by the low CUR solubility in hSBO while the presence of CUR could result in a decrease of TP solubilisation in B2-hSBO-CUR-TP NE. Moreover, the shape and size of B2-hSBO-CUR-TP NE obtained from SANS was not any larger than that of B2-hSBO NE. This observation suggests that there is a limitation of PCS in the measurement of the particle size of CUR and TP-containing hSBO NE.

3.5.2.2 SANS studies of Brij O10 nanoemulsions containing triolein in the absence and presence of drug

The use of a range of models to individually fit the three contrasts of B2-GTO NE at different concentration of GTO in Region A and B was explored. The SANS data and best fits to the SANS data for B2-GTO NE when fitted with a core-shell ellipsoid model are shown in **Figures 3.53-3.54**, while **Table 3.17** shows the parameters obtained from the best fits. The results indicated that no significant interaction occurred between the droplets as was expected in the diluted NE. As anticipated the core equatorial radius of the NE increased with GTO content, a trend which was similar to that seen with PCS. Fitting the SANS data for GTO NE using various levels of shell hydration, showed that shell hydration decreased from 35 % for GTO0.05 to 30 % for GTO0.2 to 20 % for GTO0.4 then to 15 % for GTO0.6 and remained at 10 % for GTO1.0 and higher GTO concentrations. The thickness of the shell determined for GTO NE from the best fit ranged from ~ 25.0-26.0 Å for B2-65hGTOd NE, 22.0-27.0 Å for B2-99hGTOd NE, 27.0-32.0 Å for B2-98dGTOc NE to 18.0-27.0 Å for B2-98dGTOs NE.

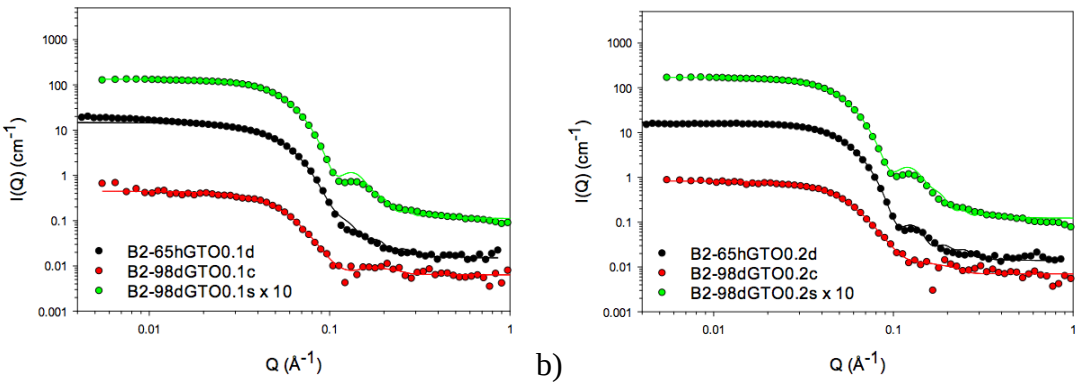

a) b)

Figure 3.53: SANS data and best fits to three contrasts for 2 %w/w Brij O10 NE containing the maximum amount of 65hGTO, in the absence of drug in a) Region A and b) Region B. Shell contrast for 2 %w/w Brij O10 NE containing 98dGTO was multiplied by the factor of 10.

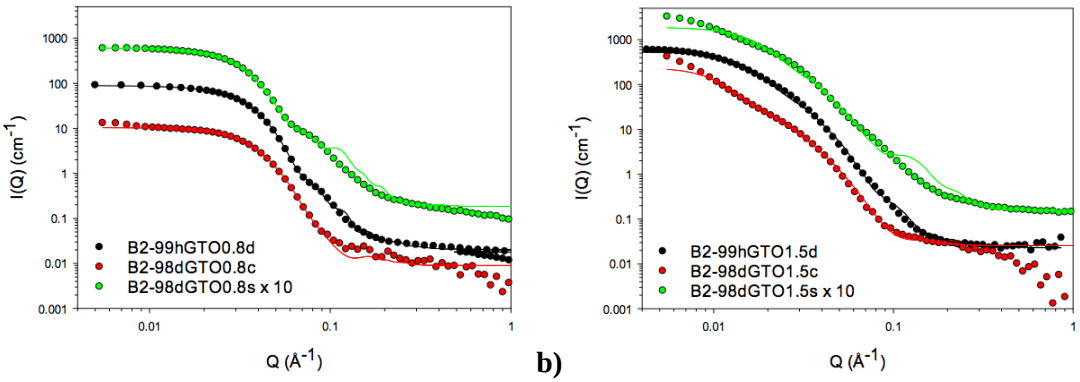

a) **b)**

Figure 3.54: SANS data and best fits to three contrasts for 2 %w/w Brij O10 NE containing the maximum amount of 99hGTO, in the absence of drug in a) Region A and b) Region B. Shell contrast for 2 %w/w Brij O10 NE containing 98dGTO was multiplied by the factor of 10. Note that best fits to shell contrast for 2 %w/w Brij O10 NE containing 0.8 %w/w 98dGTO and higher concentrations of 98dGTO were not well fitted to the SANS data.

Table 3.17 Parameters used to obtain the individual 'best fits' to the SANS results for 2 %w/w Brij O10 and GTO nanoemulsions in the absence of drug using a core-shell ellipsoid model in combination with a hard sphere structure factor S(Q). The modelling of the SANS data was constrained using Vshell(dry)/Vcore.

sample	region	core equatorial radius (R_1,Å)	core axial ratio (x)	core axial radius (R_1x,Å)	shell thickness (Å)	minor radius (Å)	major radius (Å)	axial ratio (X)	NE volume (Å^3)	sphere radius (Å)	hydration (%)	N_{agg}	surfaces area of surfactant (Å^2)	sum of squared error (SSE)
B2-65hGTO0.05d	A	25.0	0.1	2.1	25.8	50.7	27.8	0.5	300052	51.5	35	168	90	75874
B2-99hGTO0.05d		20.6	0.1	2.8	26.8	47.4	29.6	0.6	278353	50.7	35	155	82	2142
B2-98dGTO0.05c		19.3	0.2	4.0	30.9	50.3	34.9	0.7	369888	56.8	35	207	60	209
B2-98dGTO0.05s		19.5	0.1	2.8	26.6	46.1	29.4	0.6	262135	47.3	35	146	83	11450
B2-65hGTO0.1d		24.5	0.2	4.5	25.7	50.3	30.2	0.6	320548	51.9	35	176	88	6360
B2-99hGTO0.1d		20.2	0.3	6.2	26.6.	46.8	32.8	0.7	300820	50.7	35	165	82	1804
B2-98dGTO0.1c		22.9	0.3	7.1	31.0	53.9	38.1	0.7	464469	58.0	35	255	60	132
B2-98dGTO0.1s		20.8	0.3	5.5	26.4	47.1	31.8	0.7	296451	55.4	35	163	83	14653
B2-65hGTO0.2d	B	24.8	0.4	10.5	25.0	49.9	35.6	0.7	370308	55.8	30	210	83	1917
B2-99hGTO0.2d	A	26.2	0.4	10.5	25.9	52.0	36.4	0.7	412941	53.6	30	234	78	16260
B2-98dGTO0.2c		28.8	0.4	11.8	29.7	58.5	41.5	0.7	595487	61.7	30	339	60	231
B2-98dGTO0.2s		26.4	0.4	9.3	25.5	51.9	34.8	0.7	392682	63.7	30	224	81	17698
B2-99hGTO0.4d		36.7	0.5	17.3	24.1	60.8	41.4	0.7	640235	66.3	20	380	75	16587
B2-98dGTO0.4c		38.5	0.6	21.4	27.9	66.4	49.3	0.7	911350	72.2	20	545	58	312
B2-98dGTO0.4s		38.0	0.4	15.2	24.0	62.1	39.3	0.6	633915	71.3	20	379	75	35068

Estimated uncertainty for R_1 for B2-65hGTOd decreased from ± 0.9 for B2-65hGTO0.05d to ± 0.3 for B2-65hGTO0.2d, while those for B2-99hGTOd decreased from ± 0.4 for B2-99hGTO0.05d to ± 0.2 for B2-99hGTO0.8d and then increased to ± 1.5 for B2-99hGTO1.5d. Estimated uncertainty for R_1 for B2-98dGTOc decreased from ± 4 for B2-98dGTO0.05c to ± 0.3 for B2-98dGTO0.8c and then increased to ± 2.2 for B2-98dGTO1.5c, whereas those for B2-98dGTOs increased from ± 0.4 for B2-98dGTO0.05s to ± 2.6 for B2-98dGTO1.5s.
Estimated uncertainty for x of all B2-GTO NE were ± 0.01.

Table 3.17 Parameters used to obtain the individual 'best fits' to the SANS results for 2 %w/w Brij O10 and GTO nanoemulsions in the absence of drug using a core-shell ellipsoid model in combination with a hard sphere structure factor S(Q). The modelling of the SANS data was constrained using Vshell(dry)/Vcore (cont.).

sample	region	core equatorial radius (R_1,Å)	core axial ratio (x)	core axial radius (R_1x,Å)	shell thickness (Å)	minor radius (Å)	major radius (Å)	axial ratio (X)	NE volume (Å^3)	sphere radius (Å)	hydration (%)	N_{agg}	surfaces area of surfactant (Å^2)	sum of squared error (SSE)
B2-99hGTO0.6d	A	46.9	0.5	22.1	22.8	69.7	44.9	0.6	913182	70.8	15	527	74	16572
B2-98dGTO0.6c		48.9	0.6	28.1	26.8	75.7	54.9	0.7	1318925	76.9	15	771	57	268
B2-98dGTO0.6s		47.9	0.4	20.0	22.9	70.8	42.9	0.6	900730	84.7	15	527	74	83862
B2-99hGTO0.8d		57.0	0.5	25.8	22.3	79.3	48.1	0.6	1265395	82.3	15	680	75	14762
B2-98dGTO0.8c		62.1	0.5	32.3	26.9	89.0	59.2	0.7	1965715	90.6	15	1073	56	397
B2-98dGTO0.8s		61.4	0.4	21.9	22.4	83.9	44.4	0.5	1307297	91.9	15	714	75	119540
B2-99hGTO1.0d	B	75.1	0.4	30.1	22.7	97.8	52.7	0.5	2111980	105.5	10	1103	68	4830
B2-98dGTO1.0c		80.9	0.4	35.7	26.7	107.5	62.3	0.6	3018350	115.5	10	1607	54	1250
B2-98dGTO1.0s		80.5	0.2	19.8	19.7	100.3	39.6	0.4	1666482	117.0	10	887	85	137340
B2-99hGTO1.2d		94.9	0.3	30.5	22.3	117.2	52.8	0.5	3034349	120.2	10	1485	69	12355
B2-98dGTO1.2c		120.0	0.3	35.5	28.3	148.2	63.8	0.4	5876954	160.6	10	2939	51	6336
B2-98dGTO1.2s		101.3	0.2	20.4	19.1	120.4	39.5	0.3	2400822	132.1	10	1201	88	203830
B2-99hGTO1.5d		167.3	0.2	27.1	21.9	189.3	49.1	0.3	7367770	198.0	10	3293	74	96526
B2-98dGTO1.5c		256.0	0.1	35.8	31.9	288.0	67.8	0.2	23553358	296.2	10	10793	48	11259
B2-98dGTO1.5s		142.9	0.1	19.9	17.8	160.6	37.7	0.2	4070528	163.6	10	1865	97	345400

Estimated uncertainty for R_1 for B2-65hGTOd decreased from ± 0.9 for B2-65hGTO0.05d to ± 0.3 for B2-65hGTO0.2d, while those for B2-99hGTOd decreased from ± 0.4 for B2-99hGTO0.05d to ± 0.2 for B2-99hGTO0.8d and then increased to ± 1.5 for B2-99hGTO1.5d. Estimated uncertainty for R_1 for B2-98dGTOc decreased from ± 4 for B2-98dGTO0.05c to ± 0.3 for B2-98dGTO0.8c and then increased to ± 2.2 for B2-98dGTO1.5c, whereas those for B2-98dGTOs increased from ± 0.4 for B2-98dGTO0.05s to ± 2.6 for B2-98dGTO1.5s.
Estimated uncertainty for x of all B2-GTO NE was ± 0.01.

It is clear that the model that provided the best fit to the SANS data was an ellipsoid. The axial ratio of the core suggested that the shape of B2-GTO NE aggregates was an oblate ellipsoid because the axial ratio was less than 1. Interestingly, the core of the GTO NE became less ellipsoidal/more spherical in Region A as the GTO concentration increased as indicated by the increase in the core axial ratio from 0.1-0.5 - a result in agreement with the PIT study. Surprisingly, therefore the shape of the particles in Region B become more elongated as the oil content increases, as indicated by a change in the axial ratio obtained for the NE from the best fit data from 0.4 for drop and core contrasts and 0.2 for shell contrast to 0.2 for drop contrast and 0.1 for core and shell contrasts. Imaging of lipid NE droplets, composed of sphingomyelin/cholesterol/triolein in the molar ratio of either 1:1:4.7 or 4:1:11.7 revealed a rounded structure, similar to that of large unilamellar lipid vesicles (Vezocnik et al., 2015).

In Region A upon increasing GTO concentration, the major radius of the B2-GTO NE increased from 28.0 Å to 59.0 Å, while the minor radius increased from 46.0 to 89.0 Å. However, in Region B upon increasing GTO concentration, the major radius of B2-GTO NE stayed constant at around 40-60 Å while, in contrast, the minor radius of B2-GTO NE increased from 98.0 to 288.0 Å. Schematic representations of ellipsoid 2 %w/w Brij O10 NE containing the upper limit of either 65hGTO and 99hGTO, in both Regions A and B, in the absence of drug are shown in **Figures 3.55** and **3.56**, respectively.

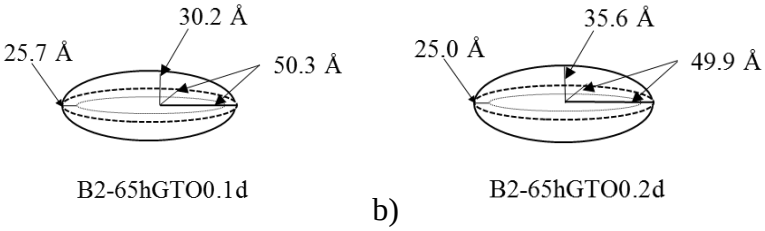

Figure 3.55: Schematic representation of the ellipsoidal 2 %w/w Brij O10 NE containing the maximum amount of 65hGTO in Region A for a) B2-65hGTO0.1d and in Region B for b) B2-65hGTO0.2d in the absence of drug.

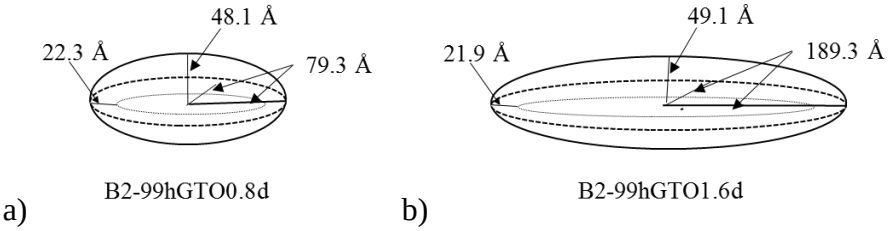

Figure 3.56: Schematic representation of the ellipsoidal 2 %w/w Brij O10 NE containing the maximum amount of 99hGTO in Region A for a) B2-99hGTO0.8d and in Region B for b) B2-99hGTO1.6d in the absence of drug.

When compared with the particle size of B2-65hGTO and B2-99hGTO NE obtained from SANS experiment, it was found that the core equatorial radius of B2-65hGTO0.05d NE was larger than that of B2-99hGTO0.05d NE, despite its possession of a comparable axial ratio. Although the radius of the core of B2-65hGTO0.1d NE was larger than that of B2-99hGTO0.1d NE, its core axial ratio was smaller, however the parameters obtained from the best fit to the SANS data resulted in particles of similar size. The trends in particle size of B2-65hGTO and B2-99hGTO NE obtained from the SANS experiments were reassuringly in agreement with those obtained from PCS, as well as being in line with the trends seen in the PIT experiments.

It was worth noting that there was the difference in parameters obtained for the three contrasts of the same NE. In Region A, the difference in the fit parameters were small, while in Region B, the thickness of the shell obtained from the core contrast was significantly larger than that the corresponding value obtained for the other contrasts. Furthermore, the fits to the shell contrast were not ideal and yielded smaller axial ratios that were obtained with the other fits. Due to the fact that many of the B2-GTO NE were run on multiple occasions and exhibited the same scattering, we are confident therefore that the SANS data were reproducible. In order to find out which factors were affecting the fitting, the level of deuteration of 98dGTO was first varied when fitting the SANS data using the core-shell ellipsoid model. However, the change in level of deuteration of 98dGTO did not improve the quality of the fitting. Next, another model contained in the program SASview, namely the triaxial ellipsoid model, was used to 'fit' the SANS data obtained for GTO. Again, however, no improvement was seen in the 'best fits' to the GTO SANS data. The triaxial ellipsoid model used in the present study is shown in **Figure 3.57**. As a consequence of this study it is proposed that the models currently available to analyse the SANS data might not be the most appropriate for B2-GTO NE.

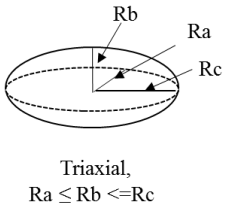

Figure 3.57: Triaxial ellipsoid model in SASview

Due to the small amount of 98dGTO synthesised, the drop contrast prepared using protiated GTO and surfactant, dispersed in D_2O was chosen to study the effect of the

drug, TP, on the size and shape of B2-GTO NE. As can be seen from the fitting parameters used to model the SANS2D data shown in **Figures 3.58-3.59** and given in **Table 3.18**, there was a slight difference in size and shape of NE droplets in the presence of TP. As expected, the equatorial core radius of the B2-GTO-TP NE increased with an increase in GTO content, a trend which was similar to that seen in the corresponding, drug-free B2-GTO NE. The hydration of the shell of the hGTO NE was found to decrease from 35 % in hGTO0.05d-TP NE to 10 % in hGTO1.0d-TP NE whereafter it remains at 10 % despite an increase in hGTO concentration. In all cases, the thickness of the fitted shell was in the range 22-27 Å. As with the drug-free TP NE, the model that provided the best fit to the SANS data was that an ellipsoid, with the axial ratio of the core suggesting that the shape of B2-hGTO-TP NE was an oblate ellipsoid.

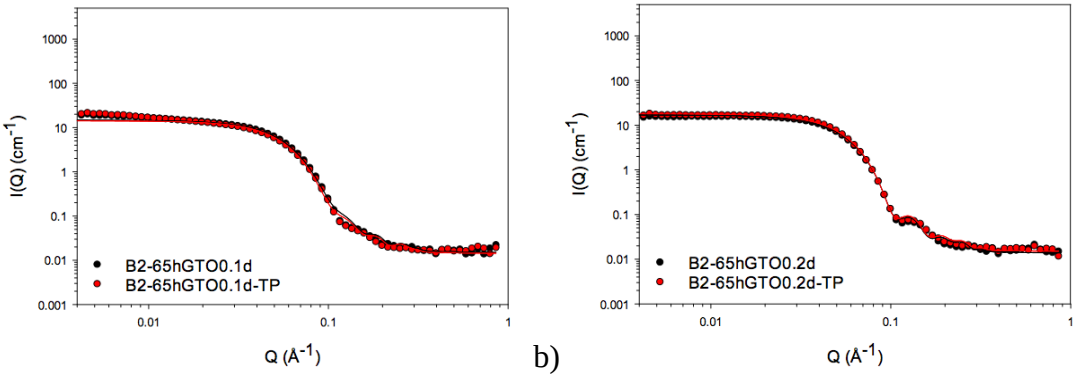

Figure 3.58: SANS data and best fits to drop contrast for 2 %w/w Brij O10 NE containing the maximum amount of 65hGTO in a) Region A and b) Region B in the absence and presence of TP.

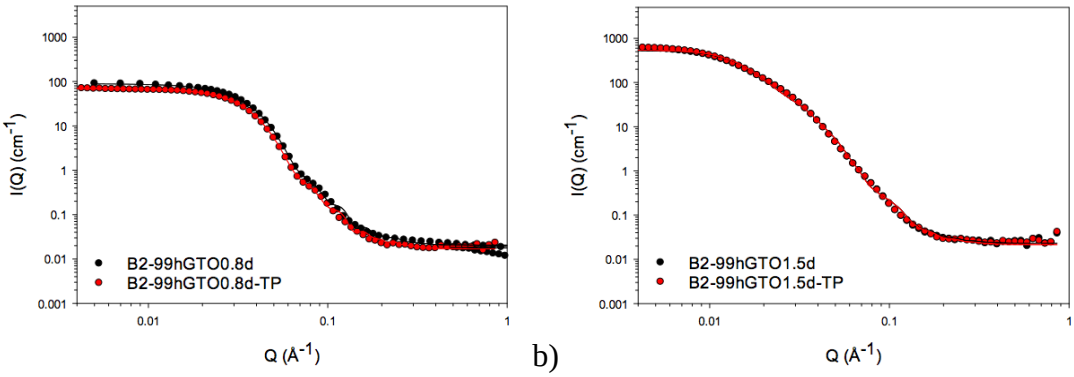

Figure 3.59: SANS data and best fits to drop contrast for 2 %w/w Brij O10 NE containing the maximum amount of 99hGTO in a) Region A and b) Region B in the absence and presence of TP.

Table 3.18 Parameters used to obtain the individual 'best fits' to the SANS results for 2 %w/w Brij O10 and GTO nanoemulsions in the presence of TP using a core-shell ellipsoid model in combination with a hard sphere structure factor S(Q). The modelling of the SANS data was constrained using Vshell(dry)/Vcore.

sample	region	core equatorial radius (R_1,Å)	core axial ratio (x)	core axial radius (R_1x,Å)	shell thickness (Å)	minor radius (Å)	major radius (Å)	axial ratio (X)	NE volume (Å^3)	sphere radius (Å)	hydration (%)	N_{agg}	surfaces area of surfactant (Å^2)	sum of squared error (SSE)
B2-65hGTO0.05d-TP	A	29.2	0.1	1.8	25.7	54.9	27.5	0.5	347559	56.0	35	194	90	37727
B2-99hGTO0.05d-TP		22.1	0.1	2.5	26.6	48.7	29.1	0.6	289427	48.8	35	162	84	4808
B2-65hGTO0.1d-TP		23.6	0.2	5.0	26.5	50.1	31.5	0.6	331886	52.6	35	182	83	10037
B2-99hGTO0.1d-TP		19.8	0.3	6.6	26.8	46.6	33.4	0.7	304478	52.7	35	167	80	2848
B2-65hGTO0.2d-TP	B	24.7	0.4	10.8	25.2	49.9	36.0	0.7	376655	53.0	30	214	82	2743
B2-99hGTO0.2d-TP	A	26.1	0.4	10.6	25.9	52.1	36.5	0.7	414979	56.8	30	235	78	3863
B2-99hGTO0.4d-TP		36.9	0.5	16.8	23.8	60.7	40.7	0.7	629042	69.6	20	373	76	4729
B2-99hGTO0.6d-TP		47.6	0.5	22.6	23.2	70.8	45.8	0.6	963278	75.2	15	556	72	4742
B2-99hGTO0.8d-TP		58.1	0.5	26.3	22.7	80.9	49.0	0.6	1343449	87.1	15	722	73	1682
B2-99hGTO1.0d-TP	B	76.2	0.4	29.8	22.7	98.9	52.6	0.5	2156393	108.9	10	1126	68	5953
B2-99hGTO1.2d-TP		95.3	0.3	30.3	22.3	117.6	52.6	0.4	3052169	134.8	10	1493	69	13239
B2-99hGTO1.5d-TP		168.1	0.2	27.3	22.1	190.1	49.4	0.3	7482387	207.4	10	3345	73	94599

Estimated uncertainty for R_1 for B2-65hGTOd-TP decreased from ± 1.7 for B2-65hGTO0.05d-TP to ± 0.3 for B2-65hGTO0.2d-TP, while those for B2-99hGTOd-TP decreased from ± 0.5 for B2-99hGTO0.05d-TP to ± 0.2 for B2-99hGTO0.8d-TP and then increased to ± 1.5 for B2-99hGTO1.5d-TP.
Estimated uncertainty for x of all B2-GTO-TP NE was ± 0.01.

Within Region A, the solubilisation of TP in B2-GTO-TP increased with GTO content because of the larger core equatorial radius. However, the TP-containing NE particles in Region B, became much more elongated with oil content. This change in morphology was unexpected as it had been anticipated that NE would become more spherical upon increasing GTO loading. This change in morphology can explain the plateau in TP solubilisation observed in Region B as there is less of an oil core in which the TP can be solubilised.

In Region A, the major radius of B2-hGTO-TP changed from 27.5 Å for B2-65hGTO0.05d-TP NE to 31.5 Å for B2-65hGTO0.1d-TP NE and 29 Å for B2-99hGTO0.05d-TP NE to 49 Å for B2-99hGTO0.8d-TP NE while the minor radius of B2-hGTO-TP NE changed from 55 Å for B2-65hGTO0.05d-TP NE to 50 Å for B2-65hGTO0.1d-TP NE and 49 Å for B2-65hGTO0.05d-TP NE to 81 Å for B2-99hGTO0.8d-TP NE. In Region B NE, the major radius of B2-99hGTO-TP NE remained approximately the same at ~ 50 Å, while the minor radius dramatically increased in size from ~ 99 Å for B2-99hGTO1.0d-TP NE to 190.0 Å for B2-99hGTO1.5d-TP NE. In contradiction to the results of the PCS experiments, the SANS data did not exhibit any difference in shape and size of the TP-free and TP-containing NE. It is of note that the analysis of the PCS data assumed that the NE were spherical, however it was clear from the SANS analysis that the shape of the B2-hGTO-TP NE in Region B was not spherical and may be the origin of the discrepancy between the SANS and PCS experiments as PCS indicated that the particle size of the B2-99hGTO-TP NE in Region B was much larger than that of B2-99hGTO NE.

The volume and the surface area of ellipsoid and sphere are shown in **Table 3.19** to illustrate the change in shape reduces the capacity of NE to solubilise hydrophobic drug. The PIT and TP solubility results suggested that TP would sit in oil core and surfactant interface, therefore the volume that TP could be solubilised is the volume of oil core and surfactant hydrocarbon tail. The schematic representation of ellipsoidal GTO NE is shown in **Figure 3.60**.

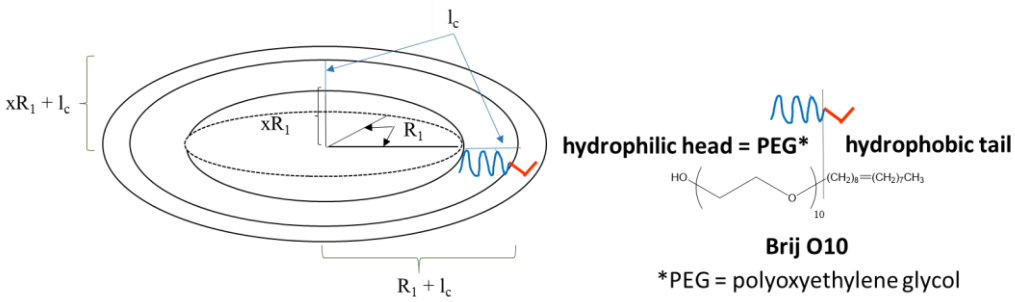

Figure 3.60: The schematic representation of ellipsoidal triolein nanoemulsion with the equatorial radius of the core (R_1), major radius of ellipsoid core (xR_1) and the length of the surfactant hydrocarbon tail (l_c)

The minor radius of ellipsoid is the length of the core equatorial radius (R_1) and the length of surfactant hydrocarbon tail (l_c) i.e. 17.3 Å (Malcolmson et al., 1995) (R_1+l_c), and the major radius of ellipsoid is the length of core axial radius (xR_1) and the length of surfactant hydrocarbon tail (xR_1+l_c) were used to calculate the volume of oblate ellipsoid, while the radius of the equivalent sphere is the equatorial radius of the core (R_1) obtained from the fitting of the SANS data for NE and the length of the surfactant hydrocarbon tail (l_c) calculated to be 17.3 Å by Malcolmson et al. (1995), i.e. R_1+l_c. The volume and surface of ellipsoid and sphere were calculated using the following formula:

$$\text{Volume of ellipsoid} = \frac{4}{3}\pi(xR_1 + l_c)(R_1 + l_c)(R_1 + l_c)$$

Surface area of ellipsoid

$$= 4\pi\left(\frac{((R_1 + l_c)^p(R_1 + l_c)^p + (R_1 + l_c)^p(xR_1 + l_c)^p + (R_1 + l_c)^p(xR_1 + l_c)^p)}{3}\right)^{\frac{1}{p}},$$

$$p = 1.6075$$

$$\text{Volume of sphere} = \frac{4}{3}\pi(R_1 + l_c)^3$$

$$\text{Surface area of sphere} = 4\pi(R_1 + l_c)^2$$

It is clear from the volume and surface area of the equivalent ellipsoid were much lower than those of the corresponding sphere, suggesting that a change in the shape of the NE from sphere to ellipsoid would affect the drug solubilisation capacity of NE (**Table 3.19**).

Table 3.19 The comparison of the volume and the surface area of ellipsoid and sphere of 2 %w/w Brij O10 and hGTO nanoemulsions in the presence of TP

sample	region	ellipsoid		sphere	
		volume of oil core and tail of surfactant ($Å^3$)	surface area of ellipsoid ($Å^3$)	volume of oil core and tail of surfactant ($Å^3$)	surface area of sphere ($Å^3$)
B2-65hGTO0.05d-TP	A	172077	17441	419696	27112
B2-99hGTO0.05d-TP		128994	13520	256557	19528
B2-65hGTO0.1d-TP		156484	15067	287015	21045
B2-99hGTO0.1d-TP		137273	13350	213494	17277
B2-65hGTO0.2d-TP	B	207446	17467	310075	22157
B2-99hGTO0.2d-TP	A	220251	18301	342937	23697
B2-99hGTO0.4d-TP		419841	28233	666791	36915
B2-99hGTO0.6d-TP		704624	40051	1146706	52988
B2-99hGTO0.8d-TP		1038279	52511	1797144	71493
B2-99hGTO1.0d-TP	B	1724884	76108	3420830	109807
B2-99hGTO1.2d-TP		2529929	103589	5984011	159418
B2-99hGTO1.5d-TP		6419664	244421	26675108	431797

3.5.2.3 SANS studies of Brij O10 nanoemulsions containing tripalmitin in the absence and presence of drug

A range of models were used to individually fit the three SANS contrasts obtained for B2-TPN NE containing different concentrations of TPN in Regions A, B and C. The SANS data and the ‘best fits’ for B2-TPN NE were obtained using a core-shell ellipsoid model, shown in **Figures 3.61-3.62** while **Table 3.20** gives the parameters used to obtain the best fits. The results suggested that no strong interactions occurred between droplets, as would be expected with a diluted NE system. Furthermore, upon increasing TPN content, there was an increase in the dimensions of the core equatorial radius of the NE - a similar increase in size with TPN content was seen with the dynamic light scattering results. The SANS data for the various NE was fitted using varying levels of shell hydration - the hydration was found to decrease from 30 % at TPN0.2 to 25 % at TPN0.4 and 20 % at TPN0.6 and 15 % at TPN1.0 whereafter it became at 10 % at TPN1.4 and remained at this level at higher TPN concentrations. The thickness obtained for the shell of TPN NE from the ‘best fits’ to the data were 19.0-25.5 Å for B2-85hTPNd NE, 19.5-25.5 Å for B2-99hTPNd NE, 23.0-29.5 Å for B2-98.6dTPNc NE and 20.0-25.5 Å for B2-98.6dTPNs NE.

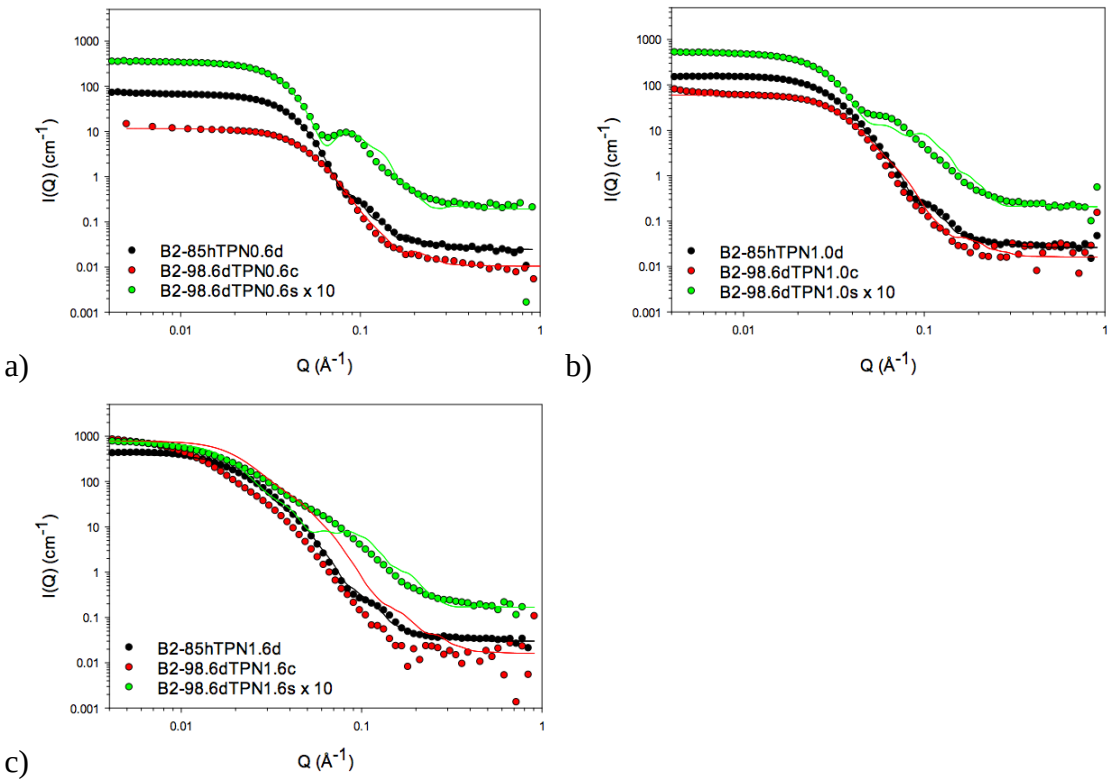

Figure 3.61: SANS data and best fits to three contrasts for 2 %w/w Brij O10 NE containing the maximum amount of 85hTPN in the absence of drug in a) Region A, b) Region B and c) Region C. Shell contrast for NE containing 98.6dTPN was multiplied by the factor of 10. Note that the best fits to shell contrast for 2 %w/w Brij O10 NE containing 0.4 %w/w 98.6dTPN and higher concentrations of 98.6dTPN were not well fitted to SANS data and the best fits to core contrast for 2 %w/w Brij O10 NE containing 0.8 %w/w 98.6dTPN and higher concentrations of 98.6dTPN were not fitted to SANS data.

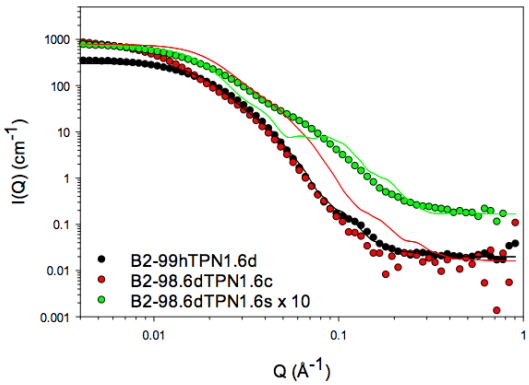

Figure 3.62: SANS data and best fits to three contrasts for 2 %w/w Brij O10 NE containing the maximum amount of 99hTPN in the absence of drug in a) Region C. Shell contrast for NE containing 98.6dTPN was multiplied by the factor of 10. Note that the best fits to shell contrast for 2 %w/w Brij O10 NE containing 0.4 %w/w 98.6dTPN and higher concentrations of 98.6dTPN were not well fitted to SANS data and the best fits to core contrast for 2 %w/w Brij O10 NE containing 0.8 %w/w 98.6dTPN and higher concentrations of 98.6dTPN were not fitted to SANS data.

Table 3.20 Parameters used for the best fits to the individual SANS data for 2 %w/w Brij O10 and TPN nanoemulsions in the absence of drug using a core-shell ellipsoid model together with a hard sphere structure factor S(Q). The modelling of the SANS data was constrained using Vshell(dry)/Vcore.

sample	region	core equatorial radius (R_1,Å)	core axial ratio (x)	core axial radius (R_1x,Å)	shell thickness (Å)	minor radius (Å)	major radius (Å)	axial ratio (X)	NE volume (Å^3)	sphere radius (Å)	hydration (%)	N_{agg}	surfaces area of surfactant (Å^2)	sum of squared error (SSE)
B2-85hTPN0.2d	A	25.4	0.4	10.7	25.6	51.0	36.3	0.7	395174	59.1	30	224	79	14542
B2-99hTPN0.2d	C	25.1	0.4	10.5	25.3	50.4	35.8	0.7	380802	58.8	30	216	81	11991
B2-98.6dTPN0.2c	A	27.1	0.4	11.8	29.6	56.6	41.4	0.7	555767	59.1	30	318	61	339
B2-98.6dTPN0.2s		24.6	0.4	9.4	25.5	50.1	34.9	0.7	367056	58.9	30	210	81	53029
B2-85hTPN0.4d	A	36.1	0.5	16.6	24.4	60.5	41.0	0.7	629622	64.0	25	354	78	13604
B2-99hTPN0.4d	C	36.0	0.5	16.6	24.4	60.4	40.9	0.7	625413	65.3	25	351	78	13293
B2-98.6dTPN0.4c	A	38.9	0.5	18.6	28.7	67.6	47.3	0.7	905073	74.9	25	516	59	2510
B2-98.6dTPN0.4s		35.6	0.4	14.9	24.8	60.4	39.7	0.7	607642	71.7	25	347	76	99268
B2-85hTPN0.6d	A	46.5	0.5	21.4	23.4	69.9	44.8	0.6	917022	80.3	20	506	76	3136
B2-99hTPN0.6d	C	48.3	0.4	21.0	23.7	71.9	44.6	0.6	967639	75.2	20	534	75	3850
B2-98.6dTPN0.6c	A	49.2	0.5	22.9	26.8	76.0	49.7	0.7	1204333	78.3	20	680	61	1711
B2-98.6dTPN0.6s		46.1	0.4	19.8	24.2	70.4	44.0	0.6	913540	80.6	20	516	72	28584
B2-85hTPN0.8d	B	58.9	0.4	23.2	22.7	81.6	45.9	0.6	1280144	90.5	20	659	78	5659
B2-99hTPN0.8d	C	59.8	0.4	22.9	22.7	82.6	45.6	0.6	1302971	84.9	20	671	78	5775
B2-98.6dTPN0.8c	B	63.9	0.4	27.1	27.5	91.5	54.6	0.6	1914576	92.9	20	1015	58	6733
B2-98.6dTPN0.8s		57.6	0.4	21.7	23.5	81.1	45.1	0.6	1243223	88.4	20	659	75	56191

Estimated uncertainty for R_1 for B2-TPNd increased from ± 0.2 for B2-TPN0.2d to ± 1.2 for B2-TPN1.6d, those for B2-98.6dTPNc decreased from ± 1.0 for B2-98.6dTPN0.2c to ± 0.3 for B2-98.6dTPN0.6c and then increased to ± 7.8 for B2-98.6dTPN1.6c, and those for B2-98.6dTPNs increased from ± 0.4 for B2-98.6dTPN0.2s to ± 4.5 for B2-98.6TPN1.6s.
Estimated uncertainty for x of all B2-TPN NE was ± 0.01.

Table 3.20 Parameters used for the best fits to the individual SANS data for 2 %w/w Brij O10 and TPN nanoemulsions in the absence of drug using a core-shell ellipsoid model together with a hard sphere structure factor S(Q). The modelling of the SANS data was constrained using Vshell(dry)/Vcore (cont.).

sample	region	core equatorial radius (R_1,Å)	core axial ratio (x)	core axial radius (R_1x,Å)	shell thickness (Å)	minor radius (Å)	major radius (Å)	axial ratio (X)	NE volume (Å^3)	sphere radius (Å)	hydration (%)	N_{agg}	surfaces area of surfactant (Å^2)	sum of squared error (SSE)
B2-85hTPN1.0d	B	73.5	0.3	25.4	21.6	95.2	47.0	0.5	1783419	106.8	15	898	78	16836
B2-99hTPN1.0d	C	72.2	0.3	25.0	21.3	93.5	46.3	0.5	1694898	103.8	15	854	80	10540
B2-98.6dTPN1.0c	B	78.7	0.4	28.9	26.0	104.7	54.9	0.5	2520604	115.4	15	1316	60	23710
B2-98.6dTPN1.0s		71.3	0.3	22.7	21.9	93.2	44.7	0.5	1627702	102.1	15	850	77	93182
B2-85hTPN1.2d	C	91.2	0.3	25.3	20.8	112.1	46.1	0.4	2425502	119.2	15	1148	82	31099
B2-99hTPN1.2d		87.9	0.3	26.1	20.8	108.7	46.9	0.4	2319561	113.8	15	1098	82	21132
B2-98.6dTPN1.2c		96.4	0.3	29.5	25.3	121.7	54.8	0.5	3401401	127.5	15	1676	62	123050
B2-98.6dTPN1.2s		87.5	0.3	24.6	22.0	109.5	46.6	0.4	2340426	123.7	15	1153	76	154100
B2-85hTPN1.4d	C	111.1	0.2	27.2	20.0	131.1	47.2	0.4	3401268	136.8	10	1570	81	73631
B2-99hTPN1.4d		107.5	0.3	27.2	19.7	127.2	46.9	0.4	3183783	133.7	10	1470	82	43050
B2-98.6dTPN1.4c		119.9	0.2	28.1	23.1	143.0	51.1	0.4	4379461	153.0	10	2116	68	756760
B2-98.6dTPN1.4s		96.8	0.3	25.5	19.9	116.7	45.4	0.4	2592750	123.2	10	1253	82	198790
B2-85hTPN1.6d	C	122.7	0.2	27.8	18.9	141.7	46.7	0.3	3929056	145.4	10	1713	86	135460
B2-99hTPN1.6d		132.2	0.2	27.3	19.3	151.5	46.7	0.3	4487618	157.9	10	1956	85	106340
B2-98.6dTPN1.6c		135.3	0.2	31.6	23.4	158.7	54.9	0.3	5795257	160.7	10	2654	66	31355000
B2-98.6dTPN1.6s		124.8	0.2	25.9	20.1	144.8	46.0	0.3	4041126	153.2	10	1851	81	396990

Estimated uncertainty for R_1 for B2-TPNd increased from ± 0.2 for B2-TPN0.2d to ± 1.2 for B2-TPN1.6d, those for B2-98.6dTPNc decreased from ± 1.0 for B2-98.6dTPN0.2c to ± 0.3 for B2-98.6dTPN0.6c and then increased to ± 7.8 for B2-98.6dTPN1.6c, and those for B2-98.6dTPNs increased from ± 0.4 for B2-98.6dTPN0.2s to ± 4.5 for B2-98.6TPN1.6s.
Estimated uncertainty for x of all B2-TPN NE was ± 0.01.

As with the other systems tested, it was clear that the model that best fit the SANS data was an ellipsoid. Furthermore, the axial ratio of the core obtained for B2-TPN NE was less than 1 indicating that these NE were oblate ellipsoids. However, as the concentration of TPN increased, the core of the NE became more spherical as indicated by the change in the axial ratio of the core from 0.4-0.5 in Region A of either B2-85hTPN, B2-98.6dTPNc or B2-98.6dTPNs and Region C of B2-99hTPN0.2d to B2-99hTPN0.8d - an observation in agreement with the PIT study. Surprisingly, however, the shape of the NE droplets in Region C become more elongated as the oil content increased as indicated by a change in the droplet axial ratio from 0.3 (for the drop and shell contrasts) and 0.4 (for the core contrast) to 0.2 for all contrasts at 1.6 % TPN. In Region A, the major and minor radii of B2-TPN NE increased from 35.0 to 50.0 Å and 50.0 to 76.0 Å, respectively upon increasing TPN concentration. However, in Regions B and C, the major radius of the B2-TPN NE remained constant at ~ 45.0-55.0 Å, while the minor radius increased from 45.0 to 159.0 Å with increasing TPN concentration. A schematic representation of ellipsoidal 2 %w/w Brij O10 NE containing the maximum amount of either 85hTPN or 99hTPN incorporated into the NE in Regions A, B or C in the absence of TP is given in **Figures 3.63–3.64**.

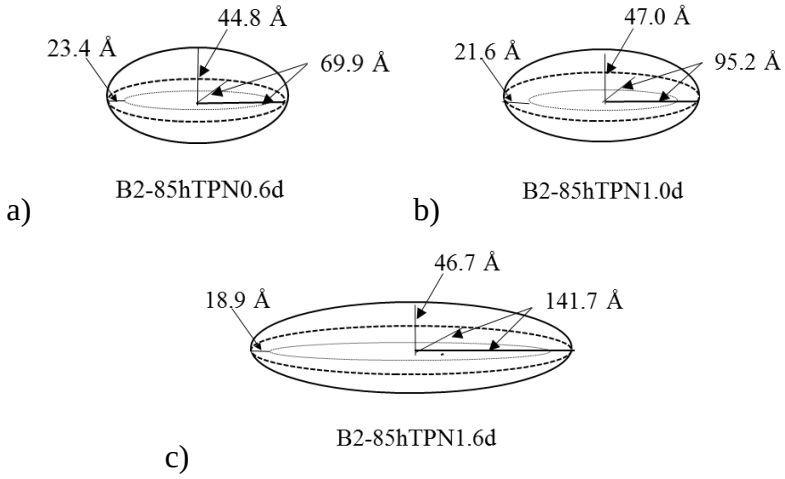

Figure 3.63: Schematic representation of the ellipsoidal 2 %w/w Brij O10 NE containing the maximum amount of 85hTPN incorporated into NE in a) Region A B2-85hTPN0.6d, b) Region B B2-85hTPN1.0d and c) Region C B2-85hTPN1.6d.

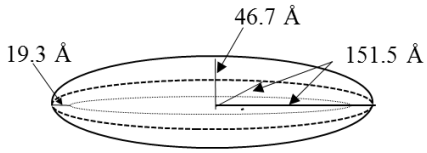

B2-99hTPN1.6d

a)

Figure 3.64: Schematic representation of the ellipsoidal 2 %w/w Brij O10 NE containing the maximum amount of 99hTPN incorporated into NE in a) Region C B2-99hTPN1.6d.

It has been reported that TPN suspensions stabilised by either purified soybean lecithin (S100), 1,2-dioleoyl-sn-glycero-3-phosphocholine (DOPC), or 1,2-dilauroyl-sn-glycero-3-phosphocholine (DLPC) formed individual, polydisperse, platelet-like particles with diameters ranging between 50 and 400 nm with some of the particles appearing to possess a rather elongated elliptic shape. The platelet-like shape of the particles are characteristic for the β-crystalline platelet form of tripalmitin which supports the findings from the WAXS measurement and TEM micrographs (Schmiele, 2013, Schmiele, 2014a and Schmiele, 2014b). No spherical tripalmitin nanoparticles in their α-crystal form were observed in the micrographs. At TPN concentrations above 4 %, the particles started to self-assemble in stacks as observed using cryo-TEM and freeze-fracture electron microscopy (Schmiele, 2013, Schmiele, 2014a and Schmiele, 2014b).

The size obtained from the SANS study for the core equatorial radius and the axial ratio of B2-85hTPN and B2-99hTPN NE were similar. This observation was in contrast to the results obtained from the PCS study where the particle size of B20-99hTPN4 NE were found to be larger than that of B20-85hTPN4 NE.

It was worth noting that there were the differences in the parameters used to fit the SANS data obtained for three contrasts. At low concentrations of TPN (i.e. below 0.6 %w/w) any differences in the parameters used for fitting the SANS data from all contrasts was small. Yet when the amount of TPN was 0.8% or higher, the thicknesses of the shell obtained from the core contrasts were significantly thicker than obtained from the other contrasts. Furthermore, it was not possible to obtain a good fit to the SANS data obtained for the core and shell contrasts, suggesting that the model did not perfectly describe the structure of the NE. Repeat SANS experiments confirmed that the data for these samples were reproducible as when the B2-TPN samples were run several different occasions, virtually identical scattering was obtained. To establish which factors affected the fitting, the level of deuteration of 98.6dTPN was varied when fitting

data using the core-shell ellipsoid model. Yet any change in the level of deuteration of 98.6dTPN did not improve the fitting of the data. Similarly any change in the hydration of the head group (manifested as a change in the SLD of the surfactant shell) did not improve the fitting. In addition, the use of different models, i.e. the triaxial, elliptical cylinder and core shell cylinder (illustrated in **Figure 3.65**), available in SASview, did not improve the fit to the SANS data. It is proposed here therefore that the models used to analyse data might not be the most appropriate for B2-TPN.

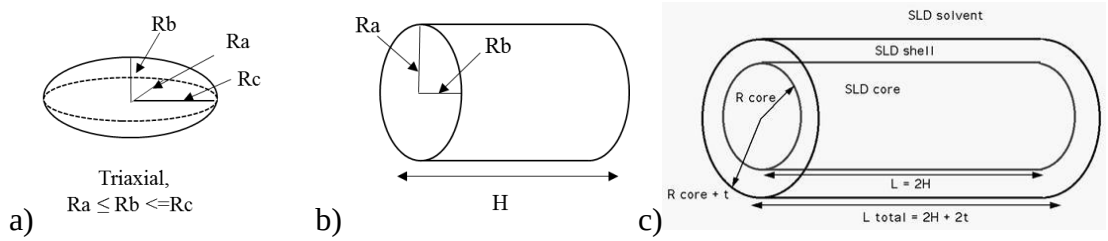

Figure 3.65: Triaxial ellipsoid, elliptical cylinder and core shell cylinder models from SASview.

As can be seen from the fitting parameters reported in **Table 3.21** and from **Figures 3.66-3.69**, the SANS results obtained for TPN NE droplets in the presence and absence of TP indicate that there were slight differences in the size and shape of the three contrasts. As expected, the core equatorial radius of the B2-TPN-TP NE increased with TPN content, a trend similar to that seen with TP-free B2-TPN NE. The shell hydration of TPN NE was found to decrease from 30 % for TPN0.2-TP NE to 10 % for TPN1.4-TP NE and thereafter remained at 10 % for all higher TPN concentrations, regardless of contrasts. The thickness of the shell obtained from the fits decreased from ~ 25 to 22 Å. It was clear from the axial ratio of the core that the model that provided the best fit to the SANS data was an oblate ellipsoid.

Table 3.21 Parameters used for the best fits to the individual SANS data for 2 %w/w Brij O10 and TPN nanoemulsions in the presence of TP using a core-shell ellipsoid model together with a hard sphere structure factor S(Q). The modelling of the SANS data was constrained using Vshell(dry)/Vcore.

sample	region	core equatorial radius (R_1,Å)	core axial ratio (x)	core axial radius (R_1x,Å)	shell thickness (Å)	minor radius (Å)	major radius (Å)	axial ratio (X)	NE volume (Å^3)	sphere radius (Å)	hydration (%)	N_{agg}	surfaces area of surfactant (Å^2)	sum of squared error (SSE)
B2-85hTPN0.2d-TP	A	24.5	0.5	11.4	25.8	50.3	37.1	0.7	393793	61.4	30	224	78	3830
B2-99hTPN0.2d-TP	C	24.8	0.4	10.8	25.4	50.2	36.2	0.7	382523	58.4	30	217	81	3045
B2-98.6dTPN0.2c-TP	A	26.9	0.4	11.8	29.4	56.3	41.2	0.7	547596	59.5	30	313	61	109
B2-98.6dTPN0.2s-TP		24.9	0.4	9.8	26.1	51.0	35.9	0.7	391082	58.3	30	224	77	8312
B2-85hTPN0.4d-TP	A	37.6	0.4	15.3	24.2	61.8	39.5	0.6	632267	70.1	25	355	79	3136
B2-99hTPN0.4d-TP	C	36.2	0.4	16.3	24.3	60.5	40.6	0.7	621819	69.1	25	349	79	4392
B2-98.6dTPN0.4c-TP	A	39.4	0.5	18.6	28.9	68.3	47.5	0.7	928839	70.3	25	530	58	475
B2-98.6dTPN0.4s-TP		36.0	0.4	14.5	24.7	60.7	39.2	0.6	605405	72.0	25	345	77	14021
B2-85hTPN0.6d-TP	A	47.1	0.4	21.1	23.4	70.5	44.5	0.6	928390	79.4	20	512	76	3080
B2-99hTPN0.6d-TP	C	48.5	0.4	19.9	23.1	71.6	43.0	0.6	922868	74.1	20	509	78	2995
B2-98.6dTPN0.6c-TP	A	51.6	0.5	23.2	27.7	79.3	50.9	0.6	1342679	83.4	20	758	58	1873
B2-98.6dTPN0.6s-TP		46.3	0.4	19.3	24.0	70.3	43.3	0.6	895047	79.6	20	505	74	30867
B2-85hTPN0.8d-TP	B	57.7	0.4	24.0	22.8	80.5	46.7	0.6	1267448	91.3	20	653	78	5173
B2-99hTPN0.8d-TP	C	61.0	0.4	22.3	22.7	83.7	45.0	0.5	1320183	84.5	20	680	79	2611
B2-98.6dTPN0.8c-TP	B	65.1	0.4	28.3	28.4	93.5	56.7	0.6	2076860	96.0	20	1101	56	4424
B2-98.6dTPN0.8s-TP		60.5	0.3	20.2	23.3	83.8	43.5	0.5	1280947	91.7	20	679	76	52387

Estimated uncertainty for R_1 for B2-TPNd-TP increased from ± 0.2 for B2-TPN0.2d-TP to ± 1.3 for B2-TPN1.6d-TP, those for B2-98.6dTPNc-TP decreased from ± 2.0 for B2-98.6dTPN0.2c-TP to ± 0.4 for B2-98.6dTPN0.6c-TP and then increased to ± 7.5 for B2-98.6dTPN1.6c-TP, and those for B2-98.6dTPNs-TP increased from ± 0.4 for B2-98.6dTPN0.2s-TP to ± 4.0 for B2-98.6TPN1.6s-TP. Estimated uncertainty for x of all B2-TPN-TP NE was ± 0.01.

Table 3.21 Parameters used for the best fits to the individual SANS data for 2 %w/w Brij O10 and TPN nanoemulsions in the presence of TP using a core-shell ellipsoid model together with a hard sphere structure factor S(Q). The modelling of the SANS data was constrained using Vshell(dry)/Vcore (cont.).

sample	region	core equatorial radius (R_1,Å)	core axial ratio (x)	core axial radius (R_1x,Å)	shell thickness (Å)	minor radius (Å)	major radius (Å)	axial ratio (X)	NE volume (Å^3)	sphere radius (Å)	hydration (%)	N_{agg}	surfaces area of surfactant (Å^2)	sum of squared error (SSE)
B2-85hTPN1.0d-TP	B	76.7	0.3	24.6	21.7	98.4	46.3	0.5	1879483	98.6	15	947	78	14654
B2-99hTPN1.0d-TP	C	74.0	0.3	25.1	21.6	95.5	46.6	0.5	1784438	101.0	15	899	78	11185
B2-98.6dTPN1.0c-TP	B	78.4	0.4	28.4	25.7	104.1	54.1	0.5	2457085	116.3	15	1283	61	31503
B2-98.6dTPN1.0s-TP		72.7	0.3	22.8	22.1	94.8	44.9	0.5	1691260	100.4	15	883	76	92300
B2-85hTPN1.2d-TP	C	90.8	0.3	25.7	21.0	111.7	46.7	0.4	2442626	125.6	15	1156	81	27897
B2-99hTPN1.2d-TP		88.2	0.3	26.2	20.9	109.1	47.0	0.4	2345035	115.8	15	1110	81	19227
B2-98.6dTPN1.2c-TP		95.2	0.3	31.0	25.8	121.0	56.8	0.5	3487027	127.9	15	1718	60	142690
B2-98.6dTPN1.2s-TP		89.1	0.3	23.5	21.6	110.8	45.1	0.4	2317995	124.0	15	1142	79	139620
B2-85hTPN1.4d-TP		112.3	0.2	26.3	19.7	132.0	45.9	0.3	3352375	142.3	10	1547	83	67425
B2-99hTPN1.4d-TP		120.0	0.2	26.7	20.5	140.4	47.2	0.3	3899776	145.7	10	1800	79	37915
B2-98.6dTPN1.4c-TP		112.7	0.2	27.0	22.0	134.7	49.0	0.4	3725813	139.4	10	1800	72	1572900
B2-98.6dTPN1.4s-TP		104.2	0.3	26.2	20.9	125.1	47.1	0.4	3089149	132.4	10	1493	77	218590
B2-85hTPN1.6d-TP		126.4	0.2	28.2	19.3	145.8	47.5	0.3	4229117	150.9	10	1843	84	136710
B2-99hTPN1.6d-TP		134.4	0.2	28.1	19.7	154.2	47.8	0.3	4761054	163.8	10	2075	82	98724
B2-98.6dTPN1.6c-TP		135.3	0.2	31.6	23.4	158.7	55.0	0.3	5799001	165.8	10	2656	66	24667000
B2-98.6dTPN1.6s-TP		120.3	0.2	22.8	18.3	138.6	41.1	0.3	3309804	141.4	10	1516	92	264600

Estimated uncertainty for R_1 for B2-TPNd-TP increased from ± 0.2 for B2-TPN0.2d-TP to ± 1.3 for B2-TPN1.6d-TP, those for B2-98.6dTPNc-TP decreased from ± 2.0 for B2-98.6dTPN0.2c-TP to ± 0.4 for B2-98.6dTPN0.6c-TP and then increased to ± 7.5 for B2-98.6dTPN1.6c-TP, and those for B2-98.6dTPNs-TP increased from ± 0.4 for B2-98.6dTPN0.2s-TP to ± 4.0 for B2-98.6TPN1.6s-TP. Estimated uncertainty for x of all B2-TPN-TP NE was ± 0.01.

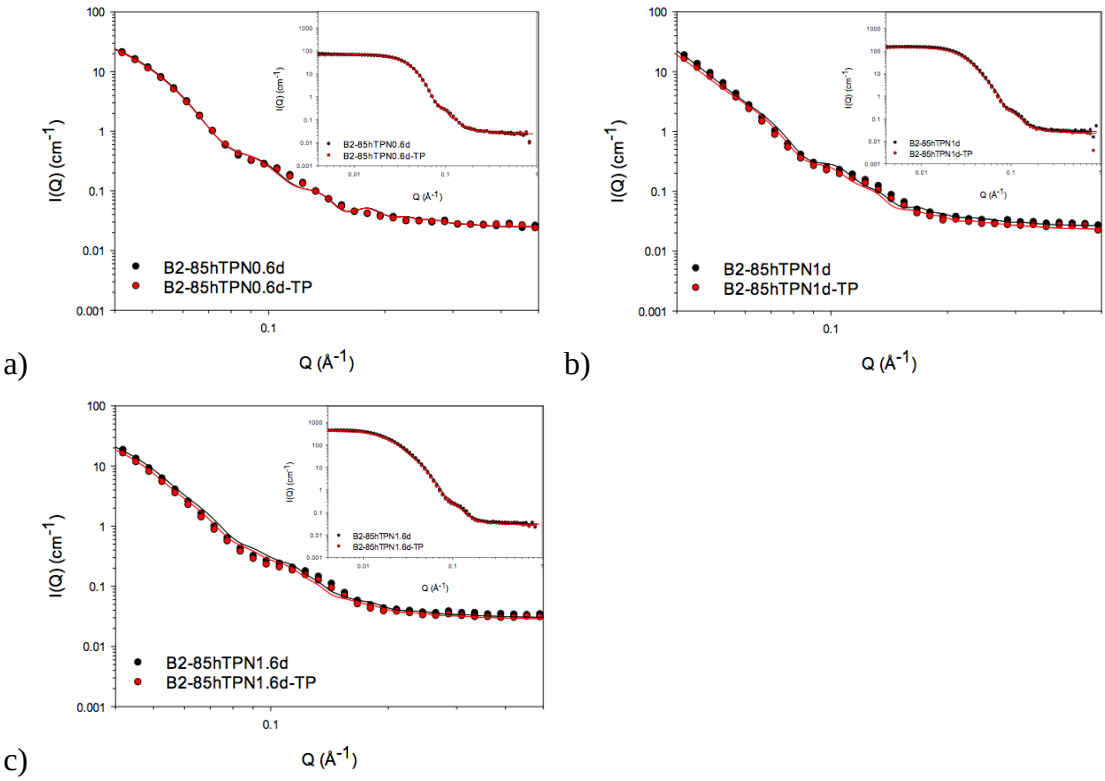

Figure 3.66: SANS data and best fits to the drop contrast for 2 %w/w Brij O10 NE containing the maximum amount of 85hTPN in the presence and absence of TP in a) Region A, b) Region B and c) Region C.

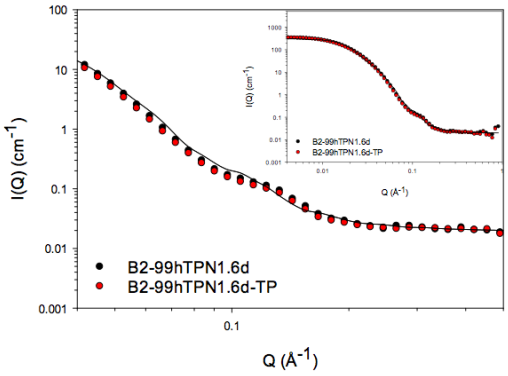

Figure 3.67: SANS data and best fits to the drop contrast for 2 %w/w Brij O10 NE containing the maximum amount of 99hTPN in the presence and absence of TP in a) Region C.

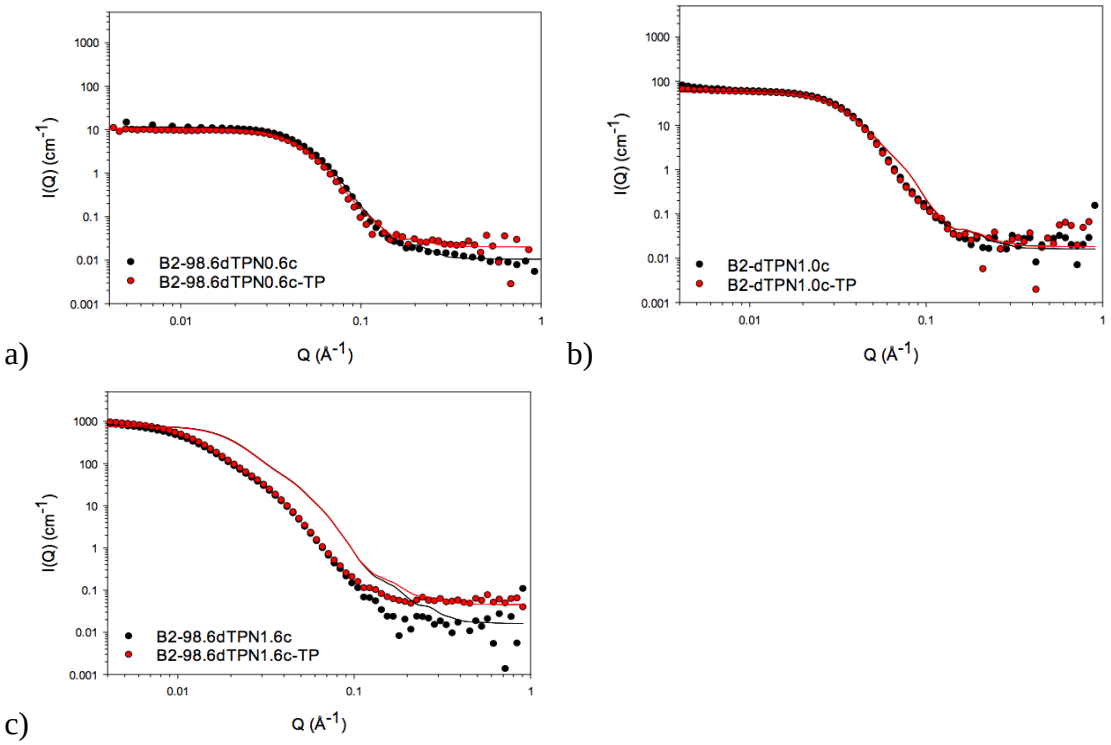

Figure 3.68: SANS data and best fits to the core contrast for 2 %w/w Brij O10 NE containing the maximum amount of 98.6dTPN in the presence and absence of TP in a) Region A, b) Region B and c) Region C. The best fits to core contrast for 2 %w/w Brij O10 NE containing 0.8 %w/w 98.6dTPN and higher concentrations of 98.6dTPN were not well fitted to SANS data.

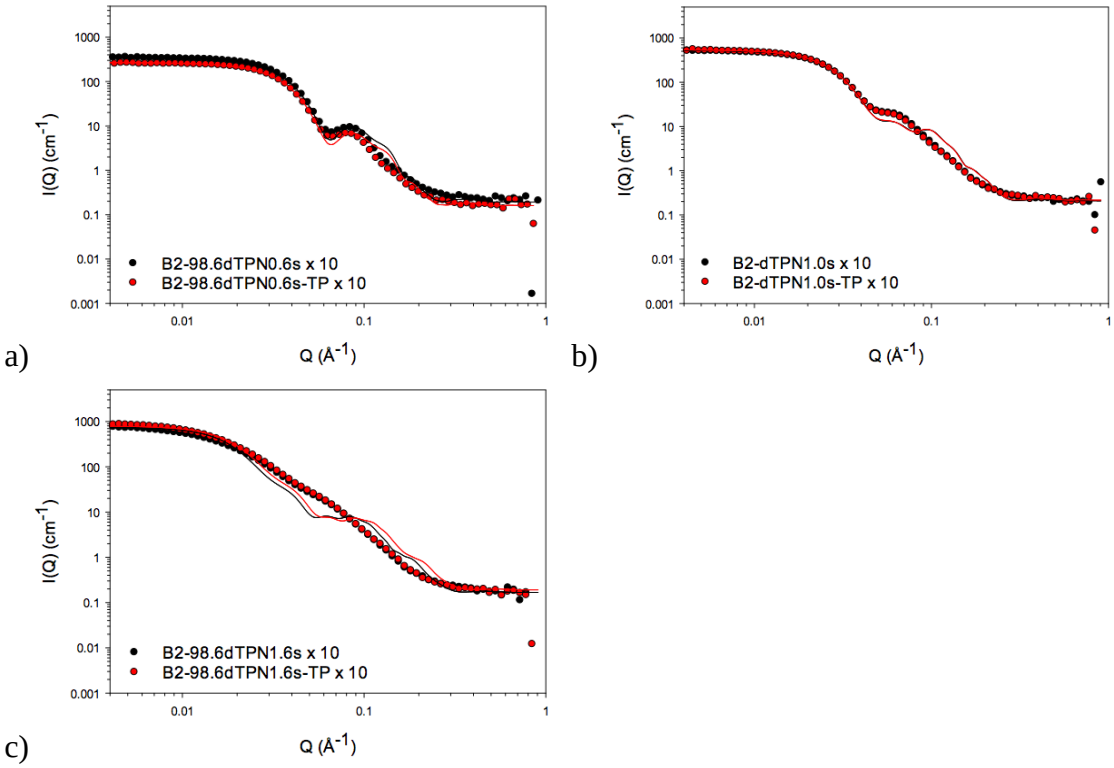

Figure 3.69: SANS data and best fits to the shell contrast for 2 %w/w Brij O10 NE containing the maximum amount of 98.6dTPN in the presence and absence of TP in a) Region A, b) Region B and c) Region C. Shell contrast for NE containing 98.6dTPN was multiplied by the factor of 10. Note that the best fits to shell contrast for 2 %w/w Brij O10 NE containing 0.4 %w/w 98.6dTPN and higher concentrations of 98.6dTPN were not well fitted to SANS data.

At low amounts of TPN, in Regions A and B, the solubilisation of TP in B2-TPN-TP NE resulted in an increase in the size of the core equatorial radius. Surprisingly, within Region C, a further increase in the amount of TPN present resulted in the production of elongated TP-containing particles. This change in morphology was unexpected as it had been anticipated that the NE would become more spherical upon increasing TPN content. This change in morphology and reduction in the size of the oil core could explain the decrease in TP solubilisation observed in Region C.

Upon increasing hTPN concentration in Region A, the major radius of B2-85hTPN-TP NE changed from 37.0 Å for B2-85hTPN0.2d-TP NE to 44.5 Å for B2-85hTPN0.6d-TP NE while the minor radius increased from 50.5 Å for B2-85hTPN0.2d-TP NE to 70.5 Å for B2-85hTPN0.6d-TP NE. In contrast, in Regions B and C, the major radius of the B2-85hTPN-TP NE remained constant at around 45-55 Å while the minor radius dramatically increased from 80.5 Å for B2-85hTPN0.8d-TP NE to 146.0 Å for B2-85hTPN1.6d-TP NE. In 99hTPN containing NE, within Region C, the major radius was 36.0 Å for B2-99hTPN0.2d-TP NE and increased to 45.0 Å for B2-99hTPN0.8d-TP NE, and then remained at 45-50 Å up to the limit of 99hTPN (i.e. B2-99hTPN1.6-TP NE) while the minor radius dramatically increased from 50.0 Å for B2-99hTPN0.2d-TP NE to 154.0 Å for B2-99hTPN1.6d-TP NE. In contrast to the PCS data, the SANS data did not show any difference in the size and shape of TP-free and TP-containing NE. This discrepancy may be due in part to the fact that analysis of the PCS assumed that the NE were spherical, however the shape of B2-hTPN-TP NE in Region C were clearly not spherical.

The volume and the surface area of ellipsoid and sphere are shown in **Table 3.22**. The PIT and TP solubility results suggested that TP would sit in oil core and surfactant interface, therefore the volume that TP could be solubilised is the volume of oil core and surfactant hydrocarbon tail. **Figure 3.70** shows the schematic representation of ellipsoidal TPN NE.

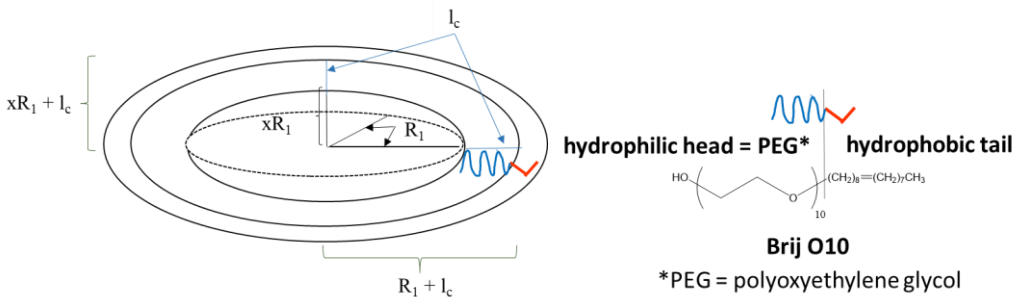

Figure 3.70: The schematic representation of ellipsoidal tripalmitin nanoemulsion with the equatorial radius of the core (R_1), major radius of ellipsoid core (xR_1) and the length of the surfactant hydrocarbon tail (l_c)

The minor radius of ellipsoid is the length of the core equatorial radius (R_1) and the length of surfactant hydrocarbon tail (l_c) i.e. 17.3 Å (Malcolmson et al., 1995) (R_1+l_c), and the major radius of ellipsoid is the length of core axial radius (xR_1) and the length of surfactant hydrocarbon tail (xR_1+l_c) were used to calculate the volume of oblate ellipsoid.

The radius of sphere is the sum of core equatorial radius (R_1) obtained from the fitting of NE and the length of surfactant hydrocarbon tail (l_c) i.e. 17.3 Å (Malcolmson et al., 1995) (R_1+l_c). The volume and surface area of ellipsoid were calculated using the following formula:

$$\text{Volume of ellipsoid} = \frac{4}{3}\pi(xR_1 + l_c)(R_1 + l_c)(R_1 + l_c)$$

Surface area of ellipsoid

$$= 4\pi\left(\frac{((R_1 + l_c)^p(R_1 + l_c)^p + (R_1 + l_c)^p(xR_1 + l_c)^p + (R_1 + l_c)^p(xR_1 + l_c)^p)}{3}\right)^{\frac{1}{p}},$$

$$p = 1.6075$$

The radius of the equivalent sphere is the equatorial radius of the core (R_1) obtained from the fitting of the SANS data for NE and the length of the surfactant hydrocarbon tail (l_c) calculated to be 17.3 Å by Malcolmson et al. (1995), i.e. R_1+l_c. The volume and surface area of sphere were calculated using the following formula:

$$\text{Volume of sphere} = \frac{4}{3}\pi(R_1 + l_c)^3$$

$$\text{Surface area of sphere} = 4\pi(R_1 + l_c)^2$$

It can be seen that the volume and surface area of ellipsoid were much lower than those of sphere which suggested that the change in NE shape from sphere to ellipsoid have an effect on the TP solubilisation in TPN NE (**Table 3.22**).

Table 3.22 The comparison of the volume and the surface area of ellipsoid and sphere of 2 %w/w Brij O10 and hTPN nanoemulsions in the presence of TP

sample	region	ellipsoid		sphere	
		volume of oil core and tail of surfactant ($Å^3$)	surface area of ellipsoid ($Å^3$)	volume of oil core and tail of surfactant ($Å^3$)	surface area of sphere ($Å^3$)
B2-85hTPN0.2d-TP	A	209695	17531.2	306131	21969
B2-99hTPN0.2d-TP	C	208107	17506.6	311304	22216
B2-98.6dTPN0.2c-TP	A	237864	19187.7	361685	24553
B2-98.6dTPN0.2s-TP		202206	17287.6	314923	22388
B2-85hTPN0.4d-TP	A	411890	28189.7	693751	37903
B2-99hTPN0.4d-TP	C	402256	27456.4	641164	35963
B2-98.6dTPN0.4c-TP	A	482856	30955	761827	40344
B2-98.6dTPN0.4s-TP		378137	26593.0	632775	35649
B2-85hTPN0.6d-TP	A	667586	38861.1	1119397	52143
B2-99hTPN0.6d-TP	C	672604	39505	1190446	54327
B2-98.6dTPN0.6c-TP	A	806050	44186	1370085	59663
B2-98.6dTPN0.6s-TP		618800	37222	1075667	50776
B2-85hTPN0.8d-TP	B	971564	50790	1766158	70669
B2-99hTPN0.8d-TP	C	1017396	53498	2013479	77121
B2-98.6dTPN0.8c-TP	B	1296462	61462	2340587	85263
B2-98.6dTPN0.8s-TP		950525	51784	1970335	76016
B2-85hTPN1.0d-TP	B	1548901	73416	3473779	110937
B2-99hTPN1.0d-TP	C	1478564	70307	3185646	104715
B2-98.6dTPN1.0c-TP	B	1752957	78092	3669256	115061
B2-98.6dTPN1.0s-TP		1357754	67275	3049501	101710
B2-85hTPN1.2d-TP	C	2103314	93520	5286392	146774
B2-99hTPN1.2d-TP		2024360	90073	4914962	139816
B2-98.6dTPN1.2c-TP		2558040	103829	5958550	158965
B2-98.6dTPN1.2s-TP		1934750	89677	5051448	142392
B2-85hTPN1.4d-TP		3061360	128121	9110167	210973
B2-99hTPN1.4d-TP		3475315	142175	10838671	236879
B2-98.6dTPN1.4c-TP		3136286	129407	9193586	212259
B2-98.6dTPN1.4s-TP		2690299	114645	7520586	185657
B2-85hTPN1.6d-TP		3934197	155330	12438600	259651
B2-99hTPN1.6d-TP		4373122	170867	14636968	289408
B2-98.6dTPN1.6c-TP		4769943	175638	14885721	292677
B2-98.6dTPN1.6s-TP		3181565	139788	10921409	238083

3.5.2.4 SANS studies of Brij O10 nanoemulsions containing tristearin in the absence of drug

A range of models were used in order to try and individually fit the drop contrast of B2-99hGTS NE at different 99hGTS concentrations within Regions B and C. The SANS data for the B2-99hGTS NE along with the best fits to the data, which was obtained using the core-shell ellipsoid model, are shown in **Figure 3.71** while **Table 3.23** shows the parameters obtained from the best fits to the SANS data.

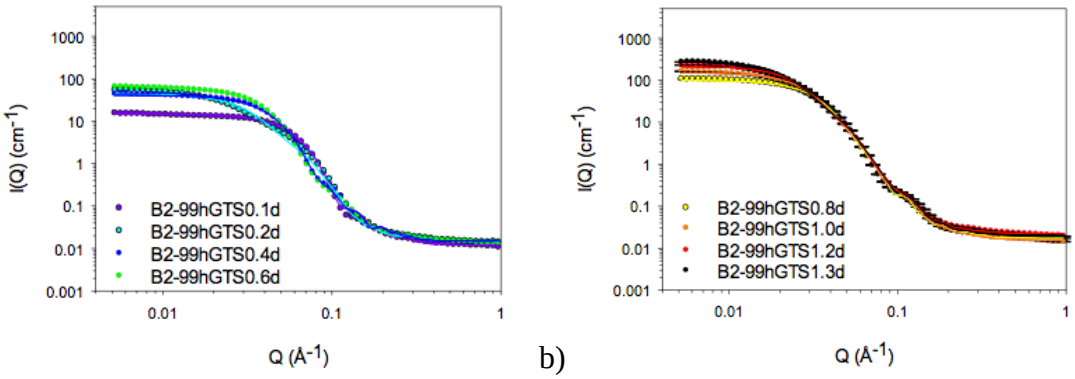

Figure 3.71: SANS data and best fits to the drop contrast for 2 %w/w Brij O10 NE upon increasing concentration of 99hGTS from a) 0.1-0.6 %w/w and b) 0.8-1.3 %w/w.

Table 3.23 Parameters used for the best fits to the individual SANS data for 2 %w/w Brij O10 and 99hGTS nanoemulsions in the absence of drug using a core-shell ellipsoid model together with a hard sphere structure factor S(Q). The modelling of the SANS data was constrained using Vshell(dry)/Vcore (cont.).

sample	Region	core equatorial radius (R_1,Å)	core axial ratio (x)	core axial radius (R_1x,Å)	shell thickness (Å)	minor radius (Å)	major radius (Å)	axial ratio (X)	NE volume (Å^3)	sphere radius (Å)	hydration (%)	N_{agg}	surfaces area of surfactant (Å^2)	sum of squared error (SSE)
B2-99hGTS0.1d	C	21.5	0.3	5.8	25.9	47.4	31.7	0.7	297661	50.0	35	163	86	18202
B2-99hGTS0.2d	B	65.6	0.1	4.2	24.6	90.2	28.9	0.3	984760	93.4	30	556	89	410200
B2-99hGTS0.4d		42.3	0.4	16.2	23.4	65.7	39.6	0.6	715844	73.5	15	442	73	19238
B2-99hGTS0.6d		50.3	0.4	21.2	22.2	72.5	43.4	0.6	956006	83.2	15	544	77	16335
B2-99hGTS0.8d		64.6	0.4	23.5	21.8	86.3	45.2	0.5	1411995	91.4	15	745	78	60184
B2-99hGTS1.0d		81.2	0.3	24.5	20.2	101.5	44.8	0.4	1932429	108.1	10	987	80	168260
B2-99hGTS1.2d	C	97.4	0.3	25.1	19.3	116.7	44.4	0.4	2535455	126.2	10	1210	85	333480
B2-99hGTS1.3d		111.4	0.2	25.2	19.2	130.6	44.4	0.3	3169667	136.9	10	1465	86	488930

Estimated uncertainty for the radius of the R_1 for either B2-99hGTS0.1d, B2-99hGTS0.4d, B2-99hGTS0.6d or B2-99hGTS0.8d were ± 0.3, that for either B2-99hGTS1.0d, B2-99hGTS1.2d or B2-99hGTS1.3d were ± 1.0 and that for B2-99hGTS0.2d were ± 0.3.
Estimated uncertainty for x of all B2-99hGTS NE was ± 0.01.

The results obtained indicate that there was no strong interaction occurring between droplets, as would be expected from a diluted NE. After attempting to fit the SANS data for each NE using various levels of hydration for the shell, the best levels of shell hydration for the 99hGTS NE were found to decrease from 35 % for 99hGTS0.1 to 10 % for hGTS1.0d whereafter it remained constant for all higher 99hGTS concentrations. The optimal value of the shell thickness was found to be in the range 19.2-25.9 Å. The axial ratio of the core, which was less than 1, suggested that the shape of B2-99hGTS NE were oblate ellipsoids. Surprisingly, the core equatorial radius of the NE varied irregularly with oil concentration, first increasing at low oil concentrations from 21.5 Å for B2-99hGTS0.1d to 65.6 Å for B2-99hGTS0.2d and finally decreasing to 42.3 Å for B2-99hGTS0.4d. This unusual variation could explain the change in the appearance of the 99hGTS NE from cloudy at B20-99hGTS1 to translucent at B20-99hGTS2. At 99hGTS concentrations of above 0.4 %w/w, the core equatorial radius of the NE increased with increasing 99hGTS content. The shape of the B2-99hGTS0.1d NE changed from an oblate ellipsoid to more elongated ellipsoids after the addition of 1 %w/w 99hGTS. After adding more 99hGTS, the shape of NE become more spherical in Region B and then surprisingly changed to become more elongated in Region C as indicated by the droplet axial ratio. A schematic representation of the ellipsoidal 2 %w/w Brij O10 NE containing the different amount of 99hGTS at the upper boundary of each Region in the absence of drug is shown in **Figure 3.72**.

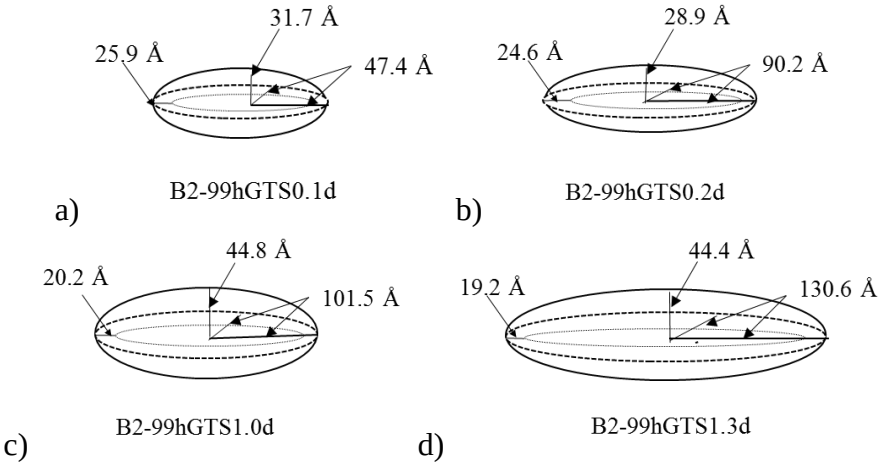

Figure 3.72: Schematic representation of the ellipsoidal 99hGTS NE a) B2-99hGTS0.1d in Region C, b) B2-99hGTS0.2d in Region B, c) B2-99hGTS1.0d NE in Region B and d) B20-99hGTS1.3d in Region C.

The major radius of B2-99hGTS NE only slightly changed for B2-99hGTS0.1d NE (31.7 Å) and B2-99hGTS0.2d NE (28.9 Å) while the minor radius increased from 47.4 Å to 90.2 Å for B2-99hGTS0.1d NE and B2-99hGTS0.2dNE, respectively. After the addition of more 99hGTS, the major radius of B2-99hGTS NE in Regions B and C NE increased from 39.6 Å for B2-99hGTS0.4d to 45 Å for B2-99hGTS1.3d while the minor radius of B2-99hGTS NE increased upon increasing 99hGTS concentrations from 65.7 Å for B2-99hGTS0.4d to 130.6 Å for B2-99hGTS1.3d.

3.5.2.5 SANS studies of Brij O10 nanoemulsions containing ethyl oleate in the absence and presence of drug

A range of models were used to individually fit the drop contrast of B2-98hEO NE at a range of different 98hEO concentrations of 98hEO in Regions A and B. The SANS data and best fits to B2-98hEO NE were obtained using a core-shell ellipsoid model and are shown in **Figure 3.73** while **Table 3.24** gives the parameters used to obtain the best fits. As expected the results indicated that there was no strong interaction between the diluted NE. Again as expected, the core equatorial radius of the NE increased with 98hEO content, a trend which was similar to that seen with dynamic light scattering.

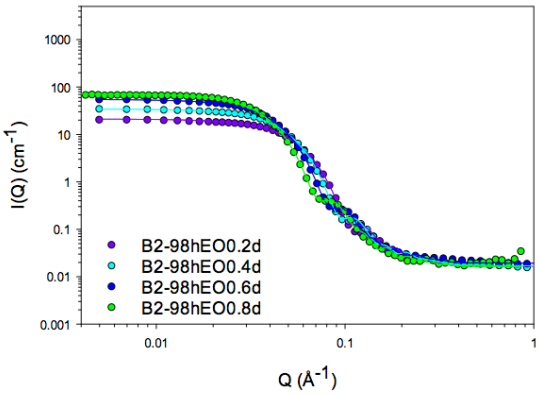

Figure 3.73: SANS data and best fits to the drop contrast for 2 %w/w Brij O10 NE upon increasing concentration of 98hEO from 0.2-0.8 %w/w.

Table 3.24 Parameters used for the best fits to the individual SANS data for 2 %w/w Brij O10 and 98hEO nanoemulsions in the absence of drug using a core-shell ellipsoid model together with a hard sphere structure factor S(Q). The modelling of the SANS data was constrained using Vshell(dry)/Vcore.

sample	Region	core equatorial radius (R_1,Å)	core axial ratio (x)	core axial radius (R_1x,Å)	shell thickness (Å)	minor radius (Å)	major radius (Å)	axial ratio (X)	NE volume (Å^3)	sphere radius (Å)	hydration (%)	N_{agg}	surfaces area of surfactant (Å^2)	sum of squared error (SSE)
B2-98hEO0.2d	A	27.3	0.4	10.6	23.9	51.2	34.4	0.7	378186	52.8	20	241	79	21207
B2-98hEO0.4d		34.8	0.5	17.5	22.6	57.4	40.0	0.7	552902	64.7	20	325	83	12030
B2-98hEO0.6d		43.8	0.5	23.1	22.3	66.1	45.5	0.7	832499	67.4	20	452	81	12454
B2-98hEO0.8d	B	53.3	0.6	29.4	21.8	75.0	51.2	0.7	1208160	79.1	15	638	77	3026

Estimated uncertainty for the radius of the R_1 and x were ± 0.3 and ± 0.01, respectively.

After attempting to fit the SANS data using a range of shell hydrations, the best fit for the shell hydration of 98hEO NE was found to decreased from 20 % at 98hEO0.2 to 15 % at 98hEO0.8. The thickness of the shell obtained from the fits were in the range 21.8-23.9 Å. It was clear that the model that provided the best fit to the SANS data was that of an oblate ellipsoid as the axial ratio was less than 1. Furthermore, the shape of the NE became more spherical as the oil content increased as suggested by the droplet axial ratio. A schematic representation of the oblate ellipsoids of 2 %w/w Brij O10 NE containing the maximum amount of 98hEO incorporated in a) Region A and b) Region B in the absence of drug is shown in **Figure 3.74**. The major radius of B2-98hEO NE in Regions A and B NE increased from 34.4 Å for B2-98hEO0.2d NE to 51.2 Å for B2-98hEO0.8d NE, while the minor radius increased from 51.2 Å for B2-98hEO0.2d NE to 75.0 Å for B2-98hEO0.8d NE upon increasing 98hEO concentration.

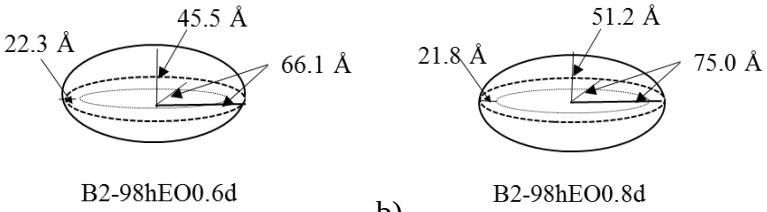

Figure 3.74: Schematic representation of the oblate ellipsoids of 98hEO NE for a) B2-98hEO0.6d in Region B and for b) B2-98hEO0.8d in Region B in the absence of drug.

A range of form factors were used to obtain individually the best fit to the SANS data obtained for the drop contrast of TP containing NE, namely B2-98hEO-TP, at different 98hEO concentrations in Region A. The upper limit of the amount of 98hEO incorporated into NE denoted in Regions A and B are shown in **Figure 3.75.** It is clear that there was no difference in the size and shape of the NE in the absence and presence of TP. The SANS data and best fits to TP-containing NE of B2-98hEO-TP were obtained using the core-shell ellipsoid model as shown in **Figure 3.76**. **Table 3.25** gives the values of the parameters used to obtain the best fits to the SANS data. As anticipated the results suggested that there was no significant interaction between the NE as anticipated with dilute NE.

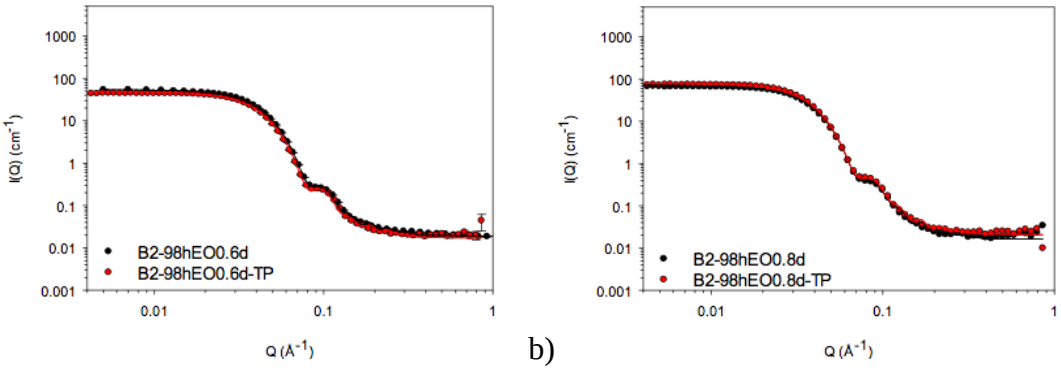

a) b)

Figure 3.75: SANS data and best fits to the drop contrast for 2 %w/w Brij O10 NE at the limit of 98hEO incorporation into NE in a) Region A and b) Region B in the absence and presence of TP.

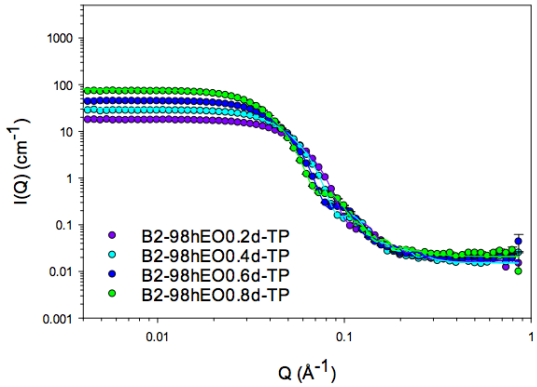

Figure 3.76: SANS data and best fits to the drop contrast for 2 %w/w Brij O10 NE upon increasing concentration of 98hEO from 0.2-0.8 %w/w in the presence of drug.

Table 3.25 Parameters used for the best fits to the individual SANS data for 2 %w/w Brij O10 and 98hEO nanoemulsions in the presence of TP using a core-shell ellipsoid model together with a hard sphere structure factor S(Q). The modelling of the SANS was constrained using Vshell(dry)/Vcore.

sample	Region	core equatorial radius (R_1,Å)	core axial ratio (x)	core axial radius (R_1x,Å)	shell thickness (Å)	minor radius (Å)	major radius (Å)	axial ratio (X)	NE volume (Å^3)	sphere radius (Å)	hydration (%)	N_{agg}	surfaces area of surfactant (Å^2)	sum of squared error (SSE)
B2-98hEO0.2d-TP	A	26.6	0.4	11.2	24.0	50.7	35.2	0.7	378691	51.7	20	242	78	3211
B2-98hEO0.4d-TP		35.2	0.5	17.9	22.9	58.1	40.9	0.7	578292	60.5	20	340	80	5305
B2-98hEO0.6d-TP		43.6	0.6	24.2	22.7	66.3	46.8	0.7	862471	71.8	20	469	70	4368
B2-98hEO0.8d-TP	B	53.7	0.6	29.8	22.0	75.7	51.8	0.7	1241806	78.4	15	656	76	5256

Estimated uncertainty for the radius of the R_1 and x were ± 0.3 and ± 0.01, respectively.

As can be seen from the parameters used for the fitting, the SANS results showed only a slight difference in size and shape of NE droplets in the presence and absence of TP. As expected, the core equatorial radius of the drug-containing NE, B2-98hEO-TP, increased with 98hEO content - a trend that was seen with B2-98hEO also. Attempts were made to fit the SANS data with varying levels of shell hydration, and it was found that the shell hydration of hEO NE decreased from 20 % in B20-98hEO0.2d-TP NE to 15 % in B20-98hEO0.8d-TP, while the thickness of the shell varied from 24 Å to 21 Å. It was clear that the model that provided the best fit to the SANS data was that of an oblate ellipsoid.

In Regions A and B, the solubilisation of TP in B2-98hEO-TP increased, most likely because of the bigger core equatorial radius together with the high solubility of TP in 98hEO. As anticipated that NE became less oblate/more spherical upon increasing their 98hEO loading, the change in morphology explaining the increase in TP solubilisation in both Region A and B.

In Regions A and B upon increasing 98hEO concentration, the major radius of the TP-containing NE, B2-98hEO-TP NE, increased from 35.2 Å for B2-98hEO0.2d-TP NE to 51.8 Å for B2-98hEO0.8d-TP NE while the minor radius of B2-98hEO-TP NE changed from 50.7 Å for B2-98hEO0.2d-TP NE to 75.7 Å for B2-98hEO0.8d-TP NE. The SANS data did not exhibit any difference in the size and shape of the TP-containing and TP-free NE - a result in contradiction to that obtained from the PCS experiment. The fact that PCS assumed that the NE were spherical, when clearly the SANS experiments indicated that the shape of the TP-containing NE, B2-98hEOd-TP NE, were not spherical, might be the reason why the PCS results suggested that the size of the TP-containing NE, B2-98hEO0.8d-TP NE, were larger than the drug-free, B2-98hEO0.8d NE.

Table 3.26 shows the volume and the surface area of ellipsoid and sphere. The PIT and TP solubilisation results of 98hEO NE suggested that TP would sit in oil core and surfactant interface, therefore the volume that TP could be solubilised is the volume of oil core and surfactant hydrocarrbon tail. The schematic representation of ellipsoidal EO NE is shown in **Figure 3.77**.

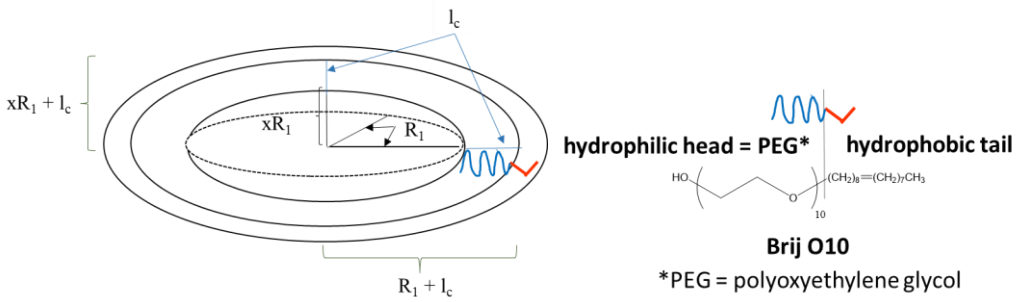

Figure 3.77: The schematic representation of ellipsoidal ethyl oleate nanoemulsion with the equatorial radius of the core (R_1), major radius of ellipsoid core (xR_1) and the length of the surfactant hydrocarbon tail (l_c)

The minor radius of ellipsoid is the length of the core equatorial radius (R_1) and the length of surfactant hydrocarbon tail (l_c) i.e. 17.3 Å (Malcolmson et al., 1995) (R_1+l_c), and the major radius of ellipsoid is the length of core axial radius (R_1x) and the length of surfactant hydrocarbon tail (R_1x+l_c) were used to calculate the volume of oblate ellipsoid, whereas the radius of sphere is the length of core equatorial radius (R_1) obtained from the fitting of the SANS data for NE and the length of the surfactant hydrocarbon tail (l_c) calculated to be 17.3 Å by Malcolmson et al. (1995), i.e. R_1+l_c. The volume and surface of ellipsoid and sphere were calculated using the following formula:

$$\text{Volume of ellipsoid} = \frac{4}{3}\pi(xR_1 + l_c)(R_1 + l_c)(R_1 + l_c)$$

Surface area of ellipsoid

$$= 4\pi\left(\frac{((R_1 + l_c)^p(R_1 + l_c)^p + (R_1 + l_c)^p(xR_1 + l_c)^p + (R_1 + l_c)^p(xR_1 + l_c)^p)}{3}\right)^{\frac{1}{p}},$$

$$p = 1.6075$$

$$\text{Volume of sphere} = \frac{4}{3}\pi(R_1 + l_c)^3$$

$$\text{Surface area of sphere} = 4\pi(R_1 + l_c)^2$$

Clearly, the volume and surface area of ellipsoid were much lower than those of sphere which suggested that the change in NE shape from sphere to ellipsoid resulted in the TP solubilisation in 98hEO NE.

Table 3.26 The comparison of the volume and the surface area of ellipsoid and sphere of 2 %w/w Brij O10 and 98hEO nanoemulsions in the presence of TP

sample	region	ellipsoid		sphere	
		volume of oil core and tail of surfactant ($Å^3$)	surface area of ellipsoid ($Å^3$)	volume of oil core and tail of surfactant ($Å^3$)	surface area of sphere ($Å^3$)
B2-98hEO0.2d-TP	A	229599	18786	354290	24217
B2-98hEO0.4d-TP		406156	27324	605152	34603
B2-98hEO0.6d-TP		644029	37079	946627	46630
B2-98hEO0.8d-TP	B	992711	49673	1497202	63299

3.5.3 Effect of temperature on Brij O10 nanoemulsions in the absence and presence of drug

In order to use Brij O10 NE as vehicles for the delivery of anticancer agents and to test their cytotoxicity using cell culture, it is essential to understand the effect of temperature, namely 37 °C (i.e. body temperature and the temperature used for cytotoxicity experiments) on the structure of the NE. It has been reported previously that the structure of the nonionic surfactant micelles formed by $C_{12}E_6$ did not change over a temperature of 25 and 31 °C when assessed using SANS (Zielinski wt al, 1995). Another SANS study over the wider temperature range of 30 to 75 °C showed that sizes of anionic, SDS micelles of 10 wt% decreased in size with an increase in temperature, while in contrast the size of micelles formed by the non-ionic surfactant, $C_{12}E_{10}$ at 10 %w/w increased in size. The SANS data of $C_{12}E_{10}$ exhibited a weak correlation peak, which shifted to smaller Q values with an increase in temperature, while there was an increase in the scattering cross-section on raising temperature (Aswal and Wagh, 2008). The present SANS study will therefore determine the effect of temperature on the properties of the Brij O10 NE. The oil selected for further study was SBO. The insight provided by this study should provide a better understanding of the potential of NE as vehicles for drug delivery.

A range of models were used to individually obtain the best fit to the drop contrast SANS data for B2-hSBO NE at either 0.6, 0.8 or 0.9 %w/w hSBO at 37 °C. The best fit model was obtained using core-shell ellipsoid model and are shown in **Figures 3.77-3.80**. **Table 3.27** gives the parameters used to obtain the best fits to the SANS data. As can be seen from the fitting parameters, the SANS results showed a small difference in size and shape of NE droplets at 25 and 37 °C, both in drug-free and drug-containing

NE. As expected, the core equatorial radius of the B2-hSBO-37C increased with hSBO content, a trend which was similar to that seen in the same NE at 25 °C. After fitting the SANS data with varying levels of shell hydration, the shell hydration of hSBO-CUR-TP was found to remain at 10 % for NE containing 0.6, 0.8 or 0.9 %w/w hSBO, regardless of the presence of drug. The thickness of the shell obtained from the fits remained constant at about 22.0-23.0 Å. The model that provided the best fit to the SANS data was an oblate ellipsoid.

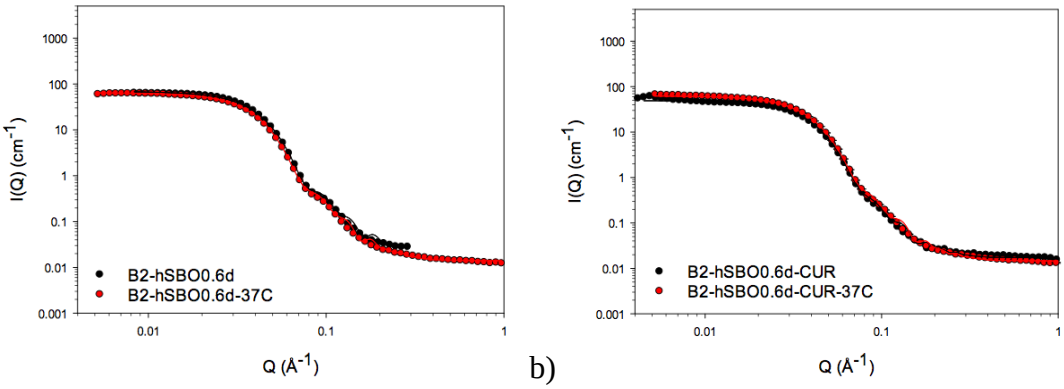

a) b)

Figure 3.78: SANS data and best fits to the drop contrast for 2 %w/w Brij O10 NE containing 0.6 %w/w hSBO with and without the presence of drug at 25 and 37 °C.

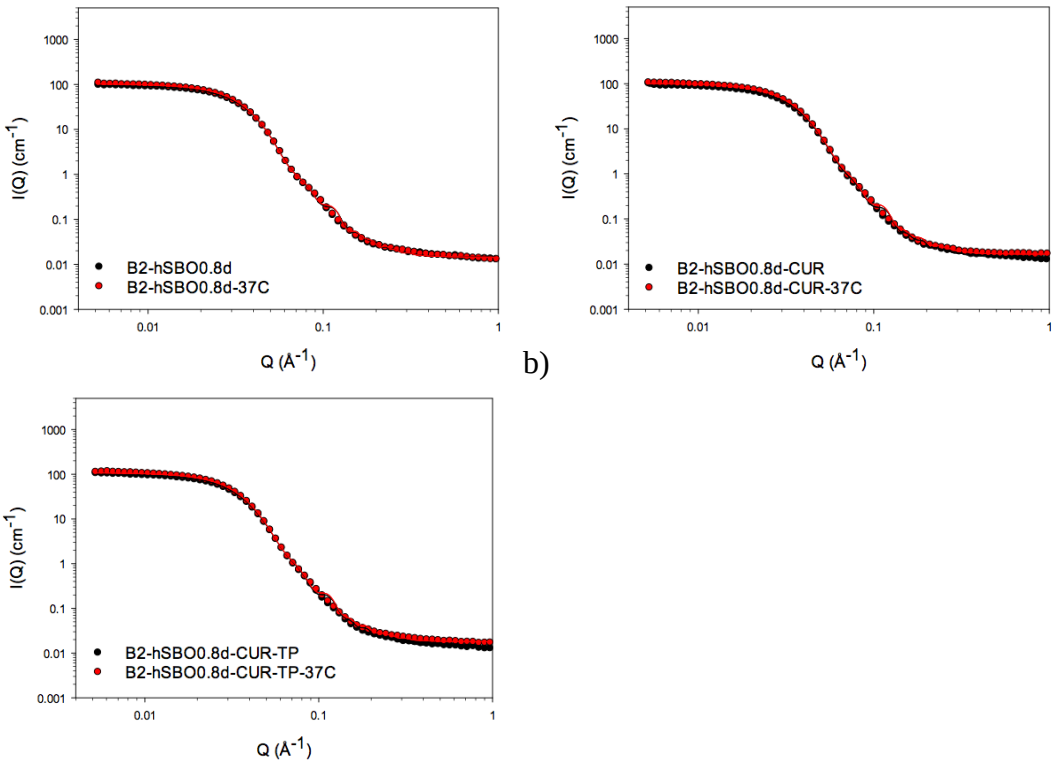

a) b)

c)

Figure 3.79: SANS data and best fits to the drop contrast for 2 %w/w Brij O10 NE containing 0.8 %w/w hSBO with and without the presence of drug at 25 and 37 °C.

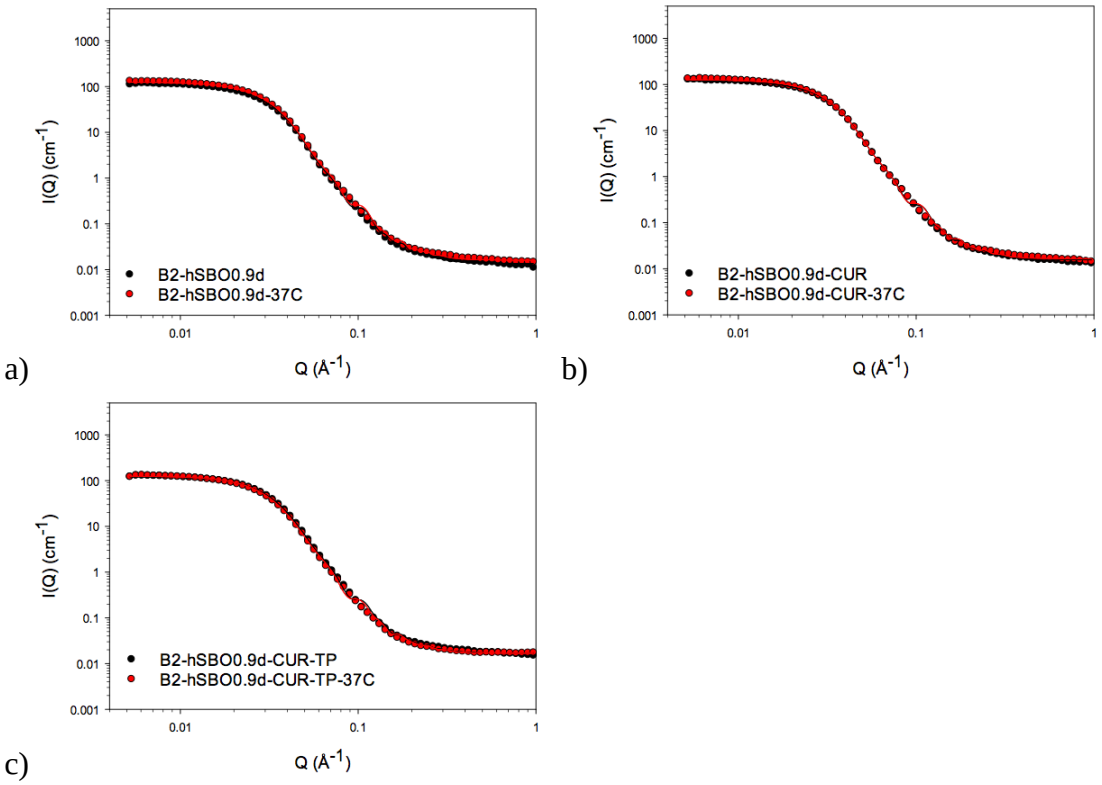

Figure 3.80: SANS data and best fits to the drop contrast for 2 %w/w Brij O10 NE containing 0.9 %w/w hSBO with and without the presence of drug at 25 and 37 °C.

The fact that there was no change in the size and shape of hSBO NE at the higher temperature of 37 °C was in agreement with the PIT studies on hSBO NE - the PIT is much higher than 37 °C. A similar result was seen in previous studies, using nonionic micelles (Degiorgio and Corti, 1984) and other nonionic ME systems (Aveyard et al., 1989), which concluded that at temperatures below the PIT the intensity of the scattered neutron radiation varies little with temperature and that only fairly weak interactions between NE exist.

Table 3.27 Parameters used for the best fits to the individual SANS data for 2 %w/w Brij O10 and hSBO nanoemulsions in the absence and presence of drug using a core-shell ellipsoid model together with a hard sphere structure factor S(Q) at 37 ˚C. The modelling of the SANS data was constrained using Vshell(dry)/Vcore.

sample	region	core equatorial radius (R_1,Å)	core axial ratio (x)	core axial radius (R_1x,Å)	shell thickness (Å)	minor radius (Å)	major radius (Å)	axial ratio (X)	NE volume (Å^3)	sphere radius (Å)	hydration (%)	N_{agg}	surfaces area of surfactant (Å^2)	sum of squared error (SSE)
B2-hSBO0.6d-37C	A	49.0	0.5	22.1	22.9	71.9	45.0	0.6	974078	70.7	10	592	69	6552
B2-hSBO0.6d-CUR-37C		49.8	0.4	21.2	22.7	72.4	43.9	0.6	964522	74.0	10	586	71	7017
B2-hSBO0.6d-CUR-TP-37C		50.4	0.4	21.1	22.8	73.2	43.9	0.6	986382	74.2	10	599	70	8112
B2-hSBO0.8d-37C		61.0	0.4	25.7	22.7	83.7	48.4	0.6	1419746	84.4	10	802	69	19603
B2-hSBO0.8d-CUR-37C		62.1	0.4	24.4	22.3	84.5	46.8	0.6	1399786	88.4	10	790	71	14794
B2-hSBO0.8d-CUR-TP-37C		62.1	0.4	24.3	22.3	84.4	46.6	0.6	1389929	88.3	10	785	71	6510
B2-hSBO0.9d-37C		68.6	0.4	26.0	22.2	90.8	48.2	0.5	1667050	97.5	10	909	71	12891
B2-hSBO0.9d-CUR-37C		69.2	0.4	25.5	22.1	91.3	47.6	0.5	1664286	97.4	10	908	71	13436
B2-hSBO0.9d-CUR-TP-37C		71.6	0.4	25.1	22.4	93.9	47.4	0.5	1754382	100.3	10	957	70	15300

Estimated uncertainty for R_1 and x were ± 0.3 and ± 0.01, respectively.

3.5.4 Effect of cell culture media on Brij O10 nanoemulsions in the absence and presence of drug

In order to use Brij O10 NE as vehicles for the delivery of anticancer agents and to test their cytotoxicity in cell culture, it is essential to understand the effect of plasma proteins, which are present in the bloodstream and in cell culture media, on the structure of the NE. It has been reported previously that the addition of either the anionic surfactant, SDS, or the cationic surfactant, CTAB, to protein bovine serum albumin (BSA) exhibits a binding to the protein which leads to a change in the size and structure of protein (Chodankar et al., 2007; Gull et al., 2008; Gull et al., 2009).

Although it is theoretically possible to use light scattering to observe any changes in the physical properties of the NE in the presence of electrolyte and/or plasma proteins, the wavelength of light (~ 500 nm) compared to the size (< 20 nm) of the NE droplets means that it will only be possible to detect gross changes in the NE without being able to attribute these changes to changes in the size and/or shape of the NE. Furthermore, such light scattering experiments are further complicated by the fact that the presence of plasma proteins, which themselves scatter light, and therefore complicate the analysis. Despite these problems, it is essential to determine the effect of serum on the NE if they are to be used as delivery vehicles intended for the intravenous administration. The aim of this part of the project is therefore to use SANS to determine the influence of the presence of plasma proteins on the physico-chemical properties of the Brij O10 NE and in particular their size and/or shape. Such a study should provide a better understanding of the potential of NE as vehicles for drug delivery.

A range of models were used to establish the best fit to the drop contrast of B2-hSBO NE at either 0.6 or 0.9 %w/w hSBO in the presence of cell culture media at 37 °C overtime. The SANS data and the best fits to B2-hSBO-DM-37C using the core-shell ellipsoid model are shown in **Figures 3.81-3.82** while **Tables 3.28-3.29** show the parameters used to obtain the best fits to the SANS data. As can be seen from the fitting parameters, the SANS results of B2-hSBO-DM-37C exhibited a lower scattering intensity due to the fact that these samples contained H_2O which has lower scattering density than D_2O and therefore resulted in lowering the overall SLD difference between the NE samples and the solvent which comprised of a 1:1 mixture of D_2O and cell culture media (DM). The parameters used to obtain the best fits to the data indicated that there were slight differences in the size and the shape of hSBO NE droplets at the temperature of 37 °C in the presence of cell culture media, regardless of the presence of

drug over 11 hours compared to size and shape of the corresponding hSBO NE at 25 °C. As anticipated the core equatorial radius of the B2-hSBO-37C NE increased with hSBO content, a trend which was similar to that seen for B2-hSBO NE at 25 °C. Attempts at fitting the SANS data using varying levels of shell hydration. The shell hydration of B2-hSBO-DM-37C was found to be 10 % for all NE containing either 0.6 or 0.9 %w/w hSBO, regardless of the presence of drugs. The thickness of the shell obtained from the fits remained constant at about 22.0-22.9 Å. It was clear that the model that provided the best fit to the SANS data was an oblate ellipsoid.

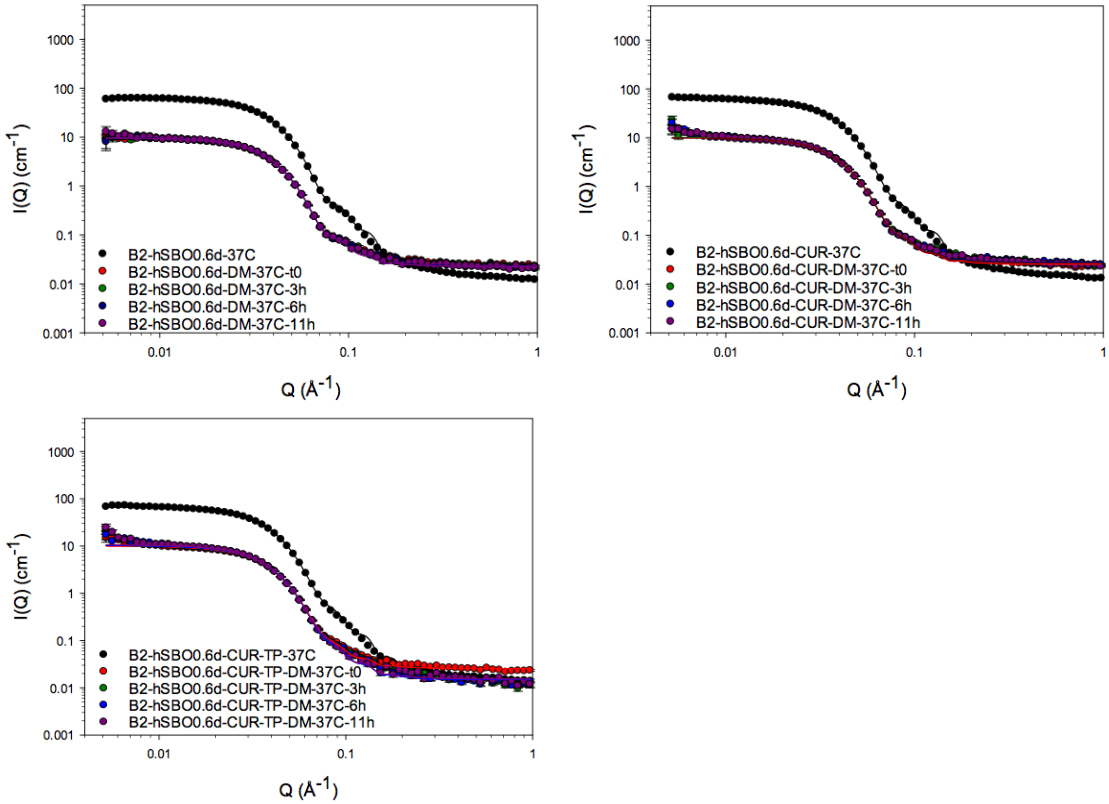

Figure 3.81: SANS data and best fits to the drop contrast for 2 %w/w Brij O10 NE containing 0.6 %w/w hSBO with and without drugs in the absence and presence of cell culture media (1:1 volume ratio) at 37 °C.

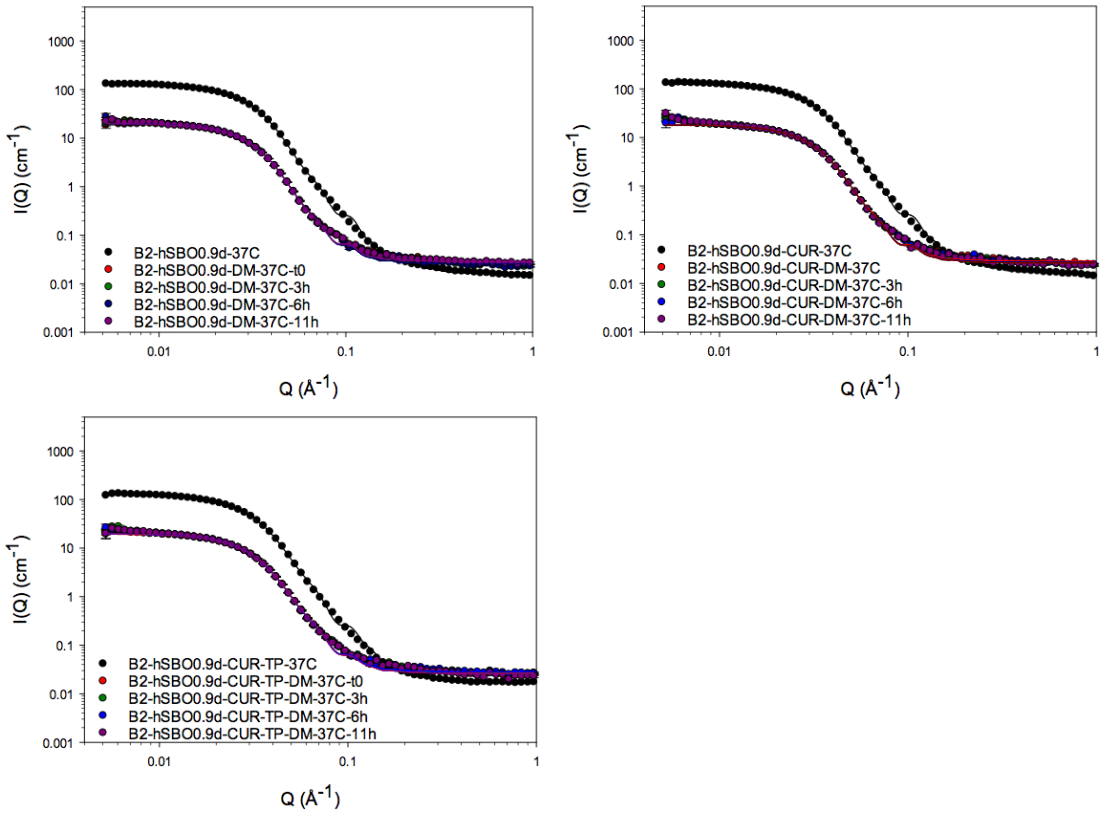

Figure 3.82: SANS data and best fits to the drop contrast for 2 %w/w Brij O10 NE containing 0.9 %w/w hSBO with and without drugs the presence of cell culture media (1:1 volume ratio) at 37 °C.

Table 3.28 Parameters used for the best fits to the individual SANS data for 2 %w/w Brij O10 and 0.6 %w/w hSBO nanoemulsions in the absence or presence of drugs and cell culture media using a core-shell ellipsoid model together with a hard sphere structure factor S(Q) at 37 ºC. The modelling of the SANS data was constrained using Vshell(dry)/Vcore.

sample	core equatorial radius (R_1,Å)	core axial ratio (x)	core axial radius (R_1x,Å)	shell thickness (Å)	minor radius (Å)	major radius (Å)	axial ratio (X)	NE volume (Å^3)	sphere radius (Å)	hydration (%)	N_{agg}	surfaces area of surfactant (Å^2)	sum of squared error (SSE)
B2-hSBO0.6-DM-37C-t0	49.4	0.4	21.3	22.6	72.0	43.9	0.6	954604	75.3	10	580	71	150
B2-hSBO0.6-DM-37C-3h	48.7	0.5	22.0	22.8	71.5	44.8	0.6	959652	77.3	10	583	70	138
B2-hSBO0.6-DM-37C-6h	49.2	0.4	21.9	22.9	72.1	44.8	0.6	975300	73.6	10	593	70	117
B2-hSBO0.6-DM-37C-11h	49.1	0.4	21.7	22.7	71.9	44.4	0.6	962490	78.7	10	585	70	122
B2-hSBO0.6-CUR-DM-37C-t0	49.6	0.4	20.7	22.4	71.9	43.0	0.6	933581	75.3	10	567	72	265
B2-hSBO0.6-CUR-DM-37C-3h	49.5	0.4	20.8	22.4	71.9	43.2	0.6	934733	80.9	10	568	72	273
B2-hSBO0.6-CUR-DM-37C-6h	48.8	0.4	21.2	22.4	71.2	43.6	0.6	927440	84.4	10	564	72	225
B2-hSBO0.6-CUR-DM-37C-11h	49.2	0.4	20.9	22.4	71.6	43.2	0.6	928161	83.4	10	564	72	210
B2-hSBO0.6-CUR-TP-DM-37C-t0	50.1	0.4	20.8	22.6	72.6	43.4	0.6	959085	78.9	10	583	71	355
B2-hSBO0.6-CUR-TP -DM-37C-3h	49.5	0.4	21.1	22.5	72.1	43.6	0.6	949914	76.3	10	577	71	428
B2-hSBO0.6-CUR-TP -DM-37C-6h	49.4	0.4	21.1	22.6	72.0	43.7	0.6	949459	77.9	10	577	71	355
B2-hSBO0.6-CUR-TP -DM-37C-11h	51.3	0.4	20.3	22.6	73.9	42.9	0.6	981588	77.7	10	596	71	250

Estimated uncertainty for R_1 and x were ± 0.3 and ± 0.01, respectively.

Table 3.29 Parameters used for the best fits to the individual SANS data for 2 %w/w Brij O10 and 0.9 %w/w hSBO nanoemulsions in the absence or presence of drugs and cell culture media using a core-shell ellipsoid model together with a hard sphere structure factor S(Q) at 37 ºC. The modelling of the SANS data was constrained using Vshell(dry)/Vcore.

sample	core equatorial radius (R_1,Å)	core axial ratio (x)	core axial radius (R_1x,Å)	shell thickness (Å)	minor radius (Å)	major radius (Å)	axial ratio (X)	NE volume (Å^3)	sphere radius (Å)	hydration (%)	N_{agg}	surfaces area of surfactant (Å^2)	sum of squared error (SSE)
B2-hSBO0.9-DM-37C-t0	68.4	0.4	26.1	22.2	90.6	48.3	0.5	1661527	92.6	10	906	71	519
B2-hSBO0.9-DM-37C-3h	69.2	0.4	25.8	22.3	91.4	48.1	0.5	1684786	98.5	10	919	71	543
B2-hSBO0.9-DM-37C-6h	68.8	0.4	26.1	22.3	91.1	48.5	0.5	1687578	98.9	10	920	70	528
B2-hSBO0.9-DM-37C-11h	68.7	0.4	26.3	22.4	91.1	48.8	0.5	1697234	93.7	10	926	70	347
B2-hSBO0.9d-CUR-DM-37C-t0	69.1	0.4	25.3	22.0	91.1	47.4	0.5	1646932	95.8	10	898	72	633
B2-hSBO0.9d-CUR-DM-37C-3h	68.8	0.4	25.6	22.1	90.9	47.7	0.5	1652925	93.6	10	902	71	479
B2-hSBO0.9d-CUR-DM-37C-6h	68.4	0.4	25.8	22.2	90.5	48.0	0.5	1647580	96.9	10	899	71	507
B2-hSBO0.9d-CUR-DM-37C-11h	68.8	0.4	25.6	22.1	90.9	47.7	0.5	1652389	96.3	10	901	71	514
B2-hSBO0.9-CUR-TP-DM-37C-t0	69.5	0.4	25.2	22.1	91.6	47.3	0.5	1661729	100.1	10	906	72	610
B2-hSBO0.9-CUR-TP-DM-37C-3h	70.3	0.4	25.4	22.3	92.6	47.6	0.5	1710677	95.3	10	933	71	466
B2-hSBO0.9-CUR-TP-DM-37C-6h	70.2	0.4	25.3	22.2	92.5	47.6	0.5	1705551	99.7	10	930	71	394
B2-hSBO0.9-CUR-TP-DM-37C-11h	71.2	0.3	24.9	22.2	93.4	47.1	0.5	1721092	94.2	10	939	71	479

Estimated uncertainty for R_1 and x were ± 0.4 and ± 0.01, respectively.

To sum up, the effect of amount of oils and the presence of drug on the SANS results of all micelles and NE are shown in **Table 3.30**, while the effect of temperature and the presence of cell culture media on the SANS results of B2-hSBO NE are shown in **Table 3.34**.

Table 3.30 SANS results of micelles and NE in the absence and presence of drugs at 25 °C.

Sample	Appearance of droplet
B2d	Prolate ellipsoid
B2d-TP	Prolate ellipsoid B2d-TP showed the slight difference in shape and size to drug-free B2d.
B2d-CUR	Prolate ellipsoid B2d-CUR showed the change in shape to drug-free B2d due to the increased axial ratio.
B2d-CUR-TP	Prolate ellipsoid B2d-CUR-TP showed the slight difference in shape and size to drug-free B2d.
B2-hSBOd	Oblate ellipsoid As the oil content increased, the shape of NE became more elongated with the increasing major radius in Region A and with the constant major radius in Region B and C.
B2-hSBOd-TP	Oblate ellipsoid The slight difference in the size and shape of NE droplets in the presence of drug.
B2-hSBOd-CUR	
B2-hSBOd-CUR-TP	
B2-65hGTOd	Oblate ellipsoid As the oil content increased, the shape of NE became more spherical in Region A and B.
B2-99hGTOd	Oblate ellipsoid As the oil content increased, the shape of NE became more spherical in Region A and more elongated with the constant major radius in Region B. Note that the best fits for shell contrast at some concentrations of oil were not well fitted to SANS data.
B2-98dGTOc	
B2-98dGTOs	
B2-65hGTOd-TP	Oblate ellipsoid The slight difference in the size and shape of NE droplets in the presence of drug. Note that the best fits for shell contrast at some concentrations of oil were not well fitted to SANS data.
B2-99hGTOd-TP	
B2-98dGTOc-TP	
B2-98dGTOs-TP	

Table 3.30: SANS results of micelles and NE in the absence and presence of drugs at 25 °C.

Sample	Appearance of droplet
B2-85hTPNd	Oblate ellipsoid As the oil content increased, the shape of NE became more spherical in Region A and more elongated with the constant major radius in Region B. Note that the best fits for core and shell contrasts at some concentrations of oil were not well fitted to SANS data.
B2-99hTPNd	
B2-98.6dTPNc	
B2-98.6dTPNs	
B2-85hTPNd-TP	Oblate ellipsoid The slight difference in the size and shape of NE droplets in the presence of drug. Note that the best fits for core and shell contrasts at some concentrations of oil were not well fitted to SANS data.
B2-99hTPNd-TP	
B2-98.6dTPNc-TP	
B2-98.6dTPNs-TP	
B2-99hGTSd	Oblate ellipsoid
B2-98hEO	Oblate ellipsoid As the oil content increased, the shape of NE became more spherical in Region A and B.
B2-98hEO-TP	Oblate ellipsoid The slight difference in the size and shape of NE droplets in the presence of drug.

Table 3.31 SANS results of micelles and NE at 37 °C and in the absence and presence of cell culture media.

Sample	Appearance of droplet
B2-hSBOd-37C	Oblate ellipsoid The slight difference in the size and shape of NE droplets at 37 °C.
B2-hSBOd-CUR-37C	
B2-hSBOd-CUR-TP-37C	
B2-hSBOd-DM-37C	Oblate ellipsoid The slight difference in the size and shape of NE droplets at 37 °C and in the presence of cell culture media.
B2-hSBOd-CUR-DM-37C	
B2-hSBOd-CUR-TP-DM-37C	

3.6 Chapter summary

Brij O10 NE stabilised by 20 %w/w Brij O10, non-ionic surfactant, and containing either a triglyceride or an ethyl ester of different but high molar volume and of different levels of oil purity were prepared by the phase inversion temperature (PIT) method. Clearly, the level of saturation of fatty acid in oils and the purity of oils have an effect on the extent of the area of NE existence. PIT experiments, particle size determination and SANS studies suggest that Brij O10 NE forms a distinct core of oil in the NE droplets.

In order to study the suitability of Brij O10 NE as drug delivery vehicles, two poorly water soluble drugs, TP and CUR, were selected as model drugs. The level of TP solubilisation obtained suggested that Brij O10 NE were suitable as drug delivery vehicles for TP in both the clear/transparent, Region A and bluish/translucent, Region B NE. In addition, the SANS studies explained the decrease in TP solubility observed in cloudy/milky, Region C NE which was due to their transformation in morphology, changing the shape of the aggregate from an oblate ellipsoid to more elongated ellipsoid as the oil content increased. On the other hand, CUR solubilisation suggested that Brij O10 NE are suitable to deliver CUR as they exhibit a high level of CUR solubilisation. However, the solubilisation of CUR did not show an increase upon increasing the amount of oil in the B20-hSBO and B20-98hEO NE. This is due to a small amount of CUR solubilised in both oils. While the solubilisation of CUR and TP in B20-hSBO NE exhibited an increase in CUR solubilisation, solubilisation of TP decreased compared to NE containing only one drug, which suggested that the presence of CUR affected TP solubilisation in the NE.

In the chapter 5, to determine the efficacy of NE as a delivery vehicle for anticancer drug, CUR, B20 micelle, B20-hSBO and B20-98hEO NE in the absence and presence of CUR will be tested their cytotoxicity in two cell lines, CT26 and HeLa.

Chapter 4
The preparation of nanoemulsions with other nonionic surfactants in the absence and presence of cosurfactant

4.1 Introduction

4.1.1 Background

The method of formation of nanoemulsions (NE) from ternary mixtures of oil, surfactant and water used in the present project involves the input of a low amount of energy in an approach known as the phase inversion temperature (PIT) method. In this method of NE preparation, which is only applicable to NE prepared using a POE-containing nonionic surfactant, the NE components are first heated to a temperature above the PIT of the system and then cooled back down to their original temperature with constant agitation generally required to produce the NE. Mostly, nonionic surfactants are chosen to achieve this goal because of their safety and pharmaceutical acceptability and the fact that they exhibit a PIT. Within this surfactant class, ethoxylated surfactants are mainly chosen because of their inherent ability to become more hydrophobic with increasing temperature over a reasonable temperature range (Izquierdo et al., 2004; Anton and Vandemme, 2011).

Factors affecting the area of nanoemulsion existence include the presence of cosurfactants, the relative proportion of each component, the chemical nature of surfactant, the molecular volume of the oil, and the experimental temperature. Recently, the addition of medium chain monoglycerides (MCM) into oil-in-water (o/w) NE formation has been studied. MCM are pharmaceutically acceptable and are used extensively in cosmetic products and in the pharmaceutical industry (Cornwell et al., 1998).

In this chapter, the phase behaviour (area of existence) of NE is studied and the results obtained are discussed. The area of NE existence is represented using ternary phase diagrams. When a mixture of surfactant and cosurfactant was examined in the present study, the resulting data were plotted on pseudoternary phase diagrams using a constant weight ratio of the surfactant:cosurfactant. Nonionic surfactants were investigated here

because of their low toxicity which makes them suitable for use in parenteral microemulsions (ME) (Strickley, 2004; Date and Nagarsenker, 2008). Monocaprylate (Dermosoft GMCY), a monoglyceride, and lecithin were used as cosurfactants in the NE formulations studied here, with the view of investigating the effect of added monoglyceride and/or lecithin on the phase behaviour of the nonionic surfactant NE. Oils, either the triglyceride, hSBO, or the ethyl ester, 98hEO, were added to the surfactant or the mixture of surfactant and cosurfactant. Both oils used in this study are pharmaceutically acceptable, being frequently used in parenteral formulations (Strickley, 2004; Date and Nagarsenker, 2008). The area of isotropic o/w NE existence and a range of the physico-chemical properties of the o/w NE; namely PIT and particle size were investigated. The PIT of the polyoxyethylene nonionic surfactants were studied in order to ensure the absence of any phase change at around the experimental temperature of 25 °C and to ensure that the particle size of the NE remained constant over time. The NE were finally studied using small angle neutron scattering to probe their internal structure at 25 and 37 °C to determine the effect of temperature on the shape and size of NE and in the presence of cell culture media to determine the effect of protein on the size and structure of the NE.

4.1.2 Aim of the study

The aim of the present study was to investigate the possibility of formulating o/w NE using pharmaceutical acceptable ingredients and to understand their molecular architecture and their physico-chemical properties in order to improve their capacity for poorly-water soluble drugs such as testosterone propionate (TP), curcumin (CUR) or docetaxel (DTX). A range of physico-chemical techniques have been employed to achieve this aim.

4.2 Micelle and nanoemulsion without drug

4.2.1 The area of existence of nanoemulsions

Formation of nonionic surfactant nanoemulsions

The phase behaviour of a number of pharmaceutically acceptable, POE-containing nonionic surfactants; namely the polyoxyethylene (POE) alkyl ethers, Brij 35 and Brij 99; the aryl alkyl polyoxyethylene ethers, Triton X-100 and Tyloxapol; the POE

sorbitan fatty acid, Tween 20, 60 and 80; and the POE-polyoxypropylene (POP) surfactants, Lutrol F68 in the presence of either the triglyceride, hSBO, or the ethyl ester, 98hEO, and water has been investigated. The appearance of the resulting one-phase NE ranged from transparent, where the samples were described as Region A, through bluish/translucent, when the samples were denoted as Region B, to cloudy/milky samples, which were termed Region C when plotted on the ternary phase diagram. The upper limits of the amount of oil incorporated into the NE prepared using the nonionic surfactants, denoted as Regions A, B and C, are shown in **Table 4.1**. Note that if NE did not form clear NE using 20 %w/w surfactant concentration or alternately formed NE containing only a very small amount of oil, no attempt was made to examine oil solubilisation levels for other concentrations of surfactants.

Table 4.1 Upper limit of the amount of oil (%w/w) incorporated into Regions A, B and C of nonionic nanoemulsions containing a single surfactant at room temperature.

Surfactant	Oil	5 %w/w surfactant			10 %w/w surfactant			15 %w/w surfactant			20 %w/w surfactant			25 %w/w surfactant			30 %w/w surfactant		
		A	B	C	A	B	C	A	B	C	A	B	C	A	B	C	A	B	C
Brij 35	hSBO	N	N	N	N	N	N	N	N	N	-	-	-	N	N	N	N	N	N
	98hEO	N	N	N	N	N	N	N	N	N	-	-	-	N	N	N	N	N	N
Brij 99	hSBO	N	N	N	N	N	N	N	N	N	-	-	-	N	N	N	N	N	N
	98hEO	N	N	N	N	N	N	-	-	-	1	-	-	1	-	-	-	1	-
Lutrol F68	hSBO	N	N	N	N	N	N	N	N	N	-	-	-	N	N	N	N	N	N
	98hEO	N	N	N	N	N	N	N	N	N	-	-	-	N	N	N	N	N	N
Triton X-100	hSBO	N	N	N	N	N	N	-	-	-	1	-	-	1	-	-	-	1	-
	98hEO	N	N	N	-	2	-	2	4	-	4	-	-	4	5	-	2	3	-
Tyloxapol	hSBO	N	N	N	N	N	N	N	N	N	-	-	-	N	N	N	N	N	N
	98hEO	N	N	N	N	N	N	N	N	N	-	-	-	N	N	N	N	N	N
Tween 20	hSBO	N	N	N	N	N	N	N	N	N	-	-	-	N	N	N	N	N	N
	98hEO	N	N	N	N	N	N	N	N	N	-	-	-	N	N	N	N	N	N
Tween 60	hSBO	N	N	N	N	N	N	N	N	N	-	-	-	N	N	N	N	N	N
	98hEO	N	N	N	N	N	N	N	N	N	-	-	-	N	N	N	N	N	N
Tween 80	hSBO	N	N	N	-	1	2	1	-	-	2	4	5	3	4	-	1	2	-
	98hEO	N	N	N	1	-	-	1	-	-	1	3	-	1	2	-	2	3	-

- means the NE was not formed.

N means the experiment was not performed.

As seen in **Table 4.1**, NE could not be formed using when using either Brij 35, Lutrol F68, Tyloxapol, Tween 20, or Tween 60 as surfactant and containing either hSBO or 98hEO as oil. Triton X-100 could form NE containing only a small amount of either hSBO or 98hEO. Similarly Brij 99 could form NE containing only a limited amount of 98hEO. It has previously been reported that, while Brij 99 could form clear o/w ME containing either heptane or 1-heptene, it formed only a very small ME area when using IPM as oil, and no ME when using oils possessing a longer chain hydrocarbon such as hSBO, hexadecane, 1-hexadecene, octadecane or 1-octadecene (Malcolmson et al., 1995), which suggested that Brij 99 NE could only form ME containing smaller molar volume oils at room temperature. This observation could be explained by the fact that when the smaller molecular volume oil molecules were used, they penetrated into hydrocarbon chains of the interfacial surfactant, acting in much the same was as a cosurfactant, increasing the effective CPP of the surfactants.

In contrast, out of the additional surfactants studied, only Tween 80 formed a reasonable size area of NE existence when using either hSBO or 98hEO as oil. Yet, in comparison to the NE formed by Brij O10, the NE formed by Tween 80 could only incorporate small amounts of oil. It was anticipated that, amongst the Tween surfactants tested, Tween 80 would be able to incorporate the highest amount of oil due to its possession of the longest of hydrophobic alkyl chain of all of the Tween surfactants and its subsequent ability to form the largest sized micellar aggregates (Tanford et al., 1977). **Figures 4.1a-4.1b** show the partial ternary phase diagrams for o/w Tween 80 NE formed using either 98hEO or hSBO in water. In fact, Tween 80 is already used as an emulsifying agent in the intravenous infusions, injections and oral formulations (Wade and Weller, 1994; Strickley, 2004; Date and Nagarsenker, 2008). For example, Cho et al. (2008) studied the formation of cosurfactant-free, o/w ME prepared using nonionic surfactants and showed that the transparent, liquid o/w Tween 80 ME could be formed using 20 %w/w Tween 80 and incorporating only 3 %w/w of the long chain triglyceride oil, canola. It has also been reported that the type of oil incorporated into the Tween 80 NE had an effect on particle size (Ostertag et al., 2012). For example, medium chain triglycerides formed NE with droplet small sizes while mineral or long chain triglyceride oils formed NE containing relatively large sized particles. This observation suggests that the long hydrocarbon chain oils make it difficult to incorporated into Tween 80-based NE. The addition of cosurfactants into the NE formulations was

therefore studied as it was hoped that the cosurfactant might alter the structure of the NE and encourage the formation of a larger area of NE existence.

Formation of nonionic surfactant nanoemulsions containing cosurfactant

In the following study, either Dermosoft GMCY (monocaprylate, C_8) and/or lecithin were added to the nonionic surfactant-based NE in order to study the effect of cosurfactants on their formation.

Firstly, Dermosoft GMCY was mixed at a constant weight ratio of surfactant (either Tween 20 or Tween 80) to cosurfactant (K_m). 98hEO was chosen as the model oil because it is a single chain oil with a high molar volume and is pharmaceutically acceptable. Furthermore, 98hEO is similar in structure to isopropyl myristate (IPM), which has been reported to form ME with either Tween 20 or Tween 80 in the presence of the monocaprylate, Imwittor 308 as cosurfactant (Jawhari, 1999). Moreover, the areas of ME existence obtained for cosurfactant-containing, lecithin-based ME incorporating either EO or IPM were very comparable, allowing the use of EO in place of IPM (Aboofazeli et al., 1993; Aboofazeli et al., 1995).

The upper limit of the amount of oil incorporated into Regions A, B and C NE prepared using a nonionic surfactant in the presence of Dermosoft GMCY are shown in **Table 4.2**. **Figure 4.1c** shows the partial ternary phase diagrams obtained for o/w NE prepared from Tween 80:Dermosoft GMCY and containing 98hEO. Clearly, it can be seen that a significantly higher level of oil incorporation was obtained in the Dermosoft GMCY-containing NE compared to the Dermosoft GMCY-free NE. Encouragingly, the amount of 98hEO incorporated either Tween 20 or Tween 80 NE containing Dermosoft GMCY at a range of K_m was similar to that reported for the Imwittor 308-containing NE by Jawhari (1999). The small differences reported in the level of oil incorporation between this and Jawhari's earlier study could be the result of one or more of a number of effects, including the polydispersity of either POE surfactants or the Dermosoft GMCY. Indeed Jawhari (1999) previously reported that there were effects on phase behaviour due to the polydispersity of thee surfactants studied and/or the cosurfactant.

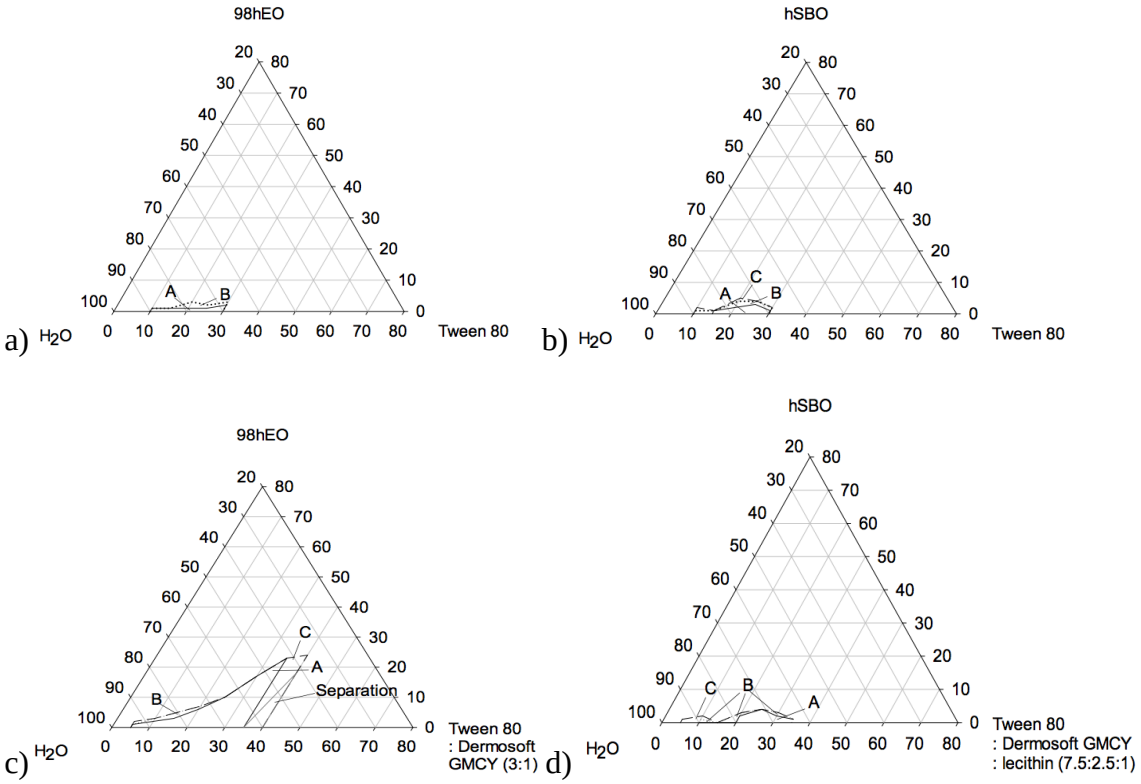

Figure 4.1: Partial ternary phase diagrams for o/w nanoemulsions prepared using a) Tween 80 and 98hEO; b) Tween 80 and hSBO; c) Tween 80:Dermosoft GMCY (K_m 3:1) and 98hEO; d) Tween 80:Dermosoft GMCY:lecithin (K_m 7.5:2.5:1) and hSBO after 1 months storage at room temperature. Clear NE are described as Region A NE, while bluish or translucent NE are called Region B NE and the cloudy or milky NE were denoted as Region C NE.

The preparation of nanoemulsions with other nonionic surfactants in the absence and presence of cosurfactant.

Table 4.2 Upper limit of the amount of oil (%w/w) incorporated into Regions A, B and C of nonionic nanoemulsions containing either single surfactant or the mixture of surfactant and cosurfactant at room temperature.

Surfactant with cosurfactant	Weight ratio (K_m)	Oil	5% surfactant			10% surfactant			15% surfactant			20% surfactant			25% surfactant			30% surfactant			35% surfactant		
			A	B	C	A	B	C	A	B	C	A	B	C	A	B	C	A	B	C	A	B	C
Tween 20 without cosurfactant	-	98hEO	N	N	N	N	N	N	N	N	N	-	-	-	N	N	N	N	N	N	N	N	N
Tween 20:Dermosoft GMCY	2:1		N	N	N	N	N	N	N	N	N	N	N	N	8	9	-	N	N	N	N	N	N
	3:1		N	N	N	N	N	N	N	N	N	N	N	N	6	7	-	N	N	N	N	N	N
	4:1		N	N	N	N	N	N	N	N	N	N	N	N	3	4	-	N	N	N	N	N	N
	5:1		N	N	N	N	N	N	N	N	N	N	N	N	3	-	-	N	N	N	N	N	N
Tween 80 without cosurfactant	-	98hEO	N	N	N	1	-	-	1	-	-	1	3	-	1	2	-	2	3	-	N	N	N
Tween 80:Dermosoft GMCY	2:1		N	N	N	N	N	N	N	N	N	N	N	N	2	8	-	N	N	N	N	N	N
	3:1		1	-	2	2	3	-	3	5	-	6	7	-	10	-	-	17	-	-	23	-	-
	4:1		N	N	N	N	N	N	N	N	N	N	N	N	7	8	-	N	N	N	N	N	N
	5:1		N	N	N	N	N	N	N	N	N	N	N	N	6	7	-	N	N	N	N	N	N

- means the NE was not formed.

N means the experiment was not performed.

The phase behaviour of NE could be explained by considering the action of Dermosoft GMCY as a cosurfactant within the interfacial surfactant region. Due to its low solubility in water, it is reasonable to assume that Dermosoft GMCY resides predominantly in the surfactant interfacial region and will act to increase the fluidity of the interfacial amphiphilic region, allowing more oil to penetrate the surfactant chains. It is anticipated that the incorporation of the hydrophobic amphiphile, Dermosoft GMCY into surfactant aggregates will result in an increase in the size of the aggregates, which in turn may increase the drug solubilising capacity of the NE (Saito and Shinoda, 1967). The increase in the size of NE is likely to depend on how much of the cosurfactant, Dermosoft GMCY is incorporated.

When using the saturated C_{12} surfactant, Tween 20, significant amounts of 98hEO were incorporated into NE when the Tween 20 was mixed with Dermosoft GMCY, the precise amount depending upon the mixing ratio (K_m). The highest levels of 98hEO incorporation occurred at a Tween 20:Dermosoft GMCY weight mixing ratio of 2:1 - a result in agreement with previous studies (Jawhari, 1999). These observations are most likely related to the oil's preferred site(s) of solubilisation. As a result of its relatively long hydrocarbon chain and its low polarity, when compared to Dermosoft GMCY (Malcolmson et al., 1998), 98hEO is considered to exhibit a low degree of penetration into the hydrocarbon chains of the interfacial surfactant monolayer, acting more like an oil than a cosurfactant, particularly at high concentrations of added 98hEO. As a consequence more 98hEO was solubilised when low weight mixing ratios were used, i.e. when there was a relatively high amount of cosurfactant present. When Tween 20 was used as surfactant, no gel phase was found. At a total of 25 %w/w Tween 20:Dermosoft GMCY and a K_m of 2:1, the highest amount of 98hEO incorporation was recorded, with an upper limit of 8 %w/w 98hEO being seen in the clear, Region A NE and 9 %w/w being recorded in the bluish/translucent Region B NE.

When the unsaturated $C_{18:1}$ chain surfactant, Tween 80, was used significant amounts of 98hEO were incorporated when it was mixed with Dermosoft GMCY, the precise amount being dependent upon the surfactant:cosurfactant weight mixing ratio (K_m). The highest levels of 98hEO incorporation were seen to occur at a Tween 80:Dermosoft GMCY weight mixing ratio of 3:1. It is significant that a large clear (Region A) NE was formed when using 98hEO as oil and Tween 80:Dermosoft GMCY, most probably

because the bulky $C_{18:1}$ chain in 98hEO was matched with the surfactant chains Tween 80, while the presence of the Dermosoft GMCY increases the fluidity of this region.

Lecithin was selected as a surfactant for the study because of its non-toxicity and biocompatibility. In this study, lecithin was added to the surfactant, Tween 80, at a range of surfactant:cosurfactant weight ratios of K_m. 98hEO and hSBO were chosen as the oils for study because they possess a high molar volume and are pharmaceutically acceptable. The appearance of the resultant samples varied from the clear/transparent, Region A, samples through bluish/translucent Region B samples to cloudy/milky (Region) samples, all of which were plotted on a ternary phase diagram. The maximum amount of oil incorporated into Regions A, B and C NE, prepared using the nonionic and lecithin surfactants, is shown in **Table 4.3**. Note, that if a composition did not form clear NE when using a total of 25 %w/w surfactant and incorporating a small amount (1-2 %w/w) of oil, no further attempt was made to examine higher levels of oil incorporation and/or other surfactant concentrations.

The preparation of nanoemulsions with other nonionic surfactants in the absence and presence of cosurfactant.

Table 4.3 Upper limit of the amount of oil (%w/w) incorporated into Regions A, B and C of nonionic nanoemulsions containing the mixture of surfactant and cosurfactant at room temperature.

Surfactant with cosurfactant	Weight ratio (K_m)	Oil	5% surfactant			10% surfactant			15% surfactant			20% surfactant			25% surfactant			30% surfactant			35% surfactant		
			A	B	C	A	B	C	A	B	C	A	B	C	A	B	C	A	B	C	A	B	C
Tween 80:lecithin	1:1	hSBO	N	N	N	-	-	-	N	N	N	N	N	N	-	-	-	N	N	N	N	N	N
		98hEO	N	N	N	-	-	-	N	N	N	N	N	N	-	-	1	-	-	-	N	N	N
	5:1	hSBO	N	N	N	-	-	-	N	N	N	N	N	N	-	2	-	N	N	N	N	N	N
		98hEO	N	N	N	N	N	N	N	N	N	N	N	N	-	-	1	N	N	N	N	N	N
	10:1	hSBO	N	N	N	-	-	-	N	N	N	N	N	N	1	-	-	N	N	N	N	N	N
		98hEO	N	N	N	N	N	N	N	N	N	N	N	N	1	-	-	N	N	N	N	N	N
	20:1	hSBO	N	N	N	-	-	-	N	N	N	N	N	N	1	-	-	N	N	N	N	N	N
		98hEO	N	N	N	N	N	N	N	N	N	N	N	N	1	-	-	N	N	N	N	N	N
	24:1	hSBO	N	N	N	-	-	-	N	N	N	N	N	N	1	-	-	N	N	N	N	N	N
		98hEO	N	N	N	N	N	N	N	N	N	N	N	N	1	-	-	N	N	N	N	N	N

- means the NE was not formed.

N means the experiment was not performed.

It was clear that Tween 80 in the presence of lecithin, at a range of different K_m, could form NE but only containing 1 %w/w of hSBO or 98hEO, which is less than the amount of oil incorporated in NE formed by Brij O10 and Tween 80 when used as sole surfactants. It was well known that lecithin is too lipophilic and its molecular geometry is not well suited to form the highly curved surfaces required to form an o/w NE, when it is used as sole surfactant. In order to form stable lecithin-containing NE, it is therefore necessary to adjust its effective HLB/modify its critical packing parameter (Klang, and Valenta, 2011). In the system containing both lecithin and Tween 80, it is expected that the effective CPP of lecithin will be reduced by the addition of the more hydrophilic, Tween 80 surfactant which consequently allows the interfacial surfactant film to be more flexible resulting in it taking up the curvature necessary for the formation of o/w NE (Trotta et al., 2002). Indeed, additional POE surfactants such as Tween 80 are frequently added to surfactants such as lecithin, not only for modification of the critical packing parameter of lecithin, but also to provide steric stabilisation (Yilmaz and Borchert, 2005; Hoellar et al., 2009). However, as the mixture of Tween 80 and lecithin in fact worsened the formation of NE, Dermosoft GMCY was added to the mixture to see if it can aid NE formation.

The formation of NE using Tween 80, Dermosoft GMCY and lecithin was then explored using a mixture of Tween 80:Dermosoft GMCY at a constant weight ratio of K_m 3:1 and adding to a 3:1 weight ratio of Tween 80:Dermosoft GMCY, lecithin in varying amounts from 5:1 to 24:1, which resulted in final weight ratios of Tween 80:Dermosoft GMCY:lecithin of 3.75:1.25:1 to 18:6:1. As before, hSBO and 98hEO were selected as oils for this study. The appearance of resultant samples varied from clear/transparent (Region A) samples through bluish/translucent (Region B) samples, to cloudy/milky (Region C) samples which were plotted on a ternary phase diagram. The maximum of amount of oil incorporated into Regions A, B and C NE containing the nonionic surfactant, Tween 80, lecithin and Dermosoft GMCY is shown in **Table 4.4**. Note, that if a composition of Tween 80, lecithin and Dermosoft GMCY at 25 %w/w total surfactant mixture did not form a clear NE when using a small amount (1-2 %w/w) of oil, no further attempt was made to examine either higher levels of oil solubilisation levels or different surfactant concentrations.

The preparation of nanoemulsions with other nonionic surfactants in the absence and presence of cosurfactant.

Table 4.4 Upper limit of the amount of oil (%w/w) incorporated into Regions A, B and C of nonionic nanoemulsions containing either single surfactant or the mixture of surfactant and cosurfactants at room temperature.

Surfactant with cosurfactant	Weight ratio of Tween 80: Dermosoft GMCY: soybean lecithin	Oil	5% surfactant			10% surfactant			15% surfactant			20% surfactant			25% surfactant			30% surfactant			35% surfactant		
			A	B	C	A	B	C	A	B	C	A	B	C	A	B	C	A	B	C	A	B	C
Tween 80:Dermosoft GMCY:lecithin	3.75:1.25:1	hSBO	N	N	N	N	N	N	N	N	N	-	-	-	-	-	1	N	N	N	N	N	N
		98hEO	N	N	N	N	N	N	N	N	N	N	N	N	-	-	-	N	N	N	N	N	N
	6:2:1	hSBO	N	N	N	N	N	N	N	N	N	-	-	-	-	-	1	N	N	N	N	N	N
		98hEO	N	N	N	N	N	N	N	N	N	N	N	N	N	N	N	N	N	N	N	N	N
	6.75:2.25:1	hSBO	N	N	N	N	N	N	N	N	N	N	N	N	-	-	1	N	N	N	N	N	N
		98hEO	N	N	N	N	N	N	N	N	N	N	N	N	N	N	N	N	N	N	N	N	N
	7.5:2.5:1	hSBO	-	-	1	-	1	2	-	-	-	2	3	-	4	-	-	2	3	-	1	-	-
		98hEO	N	N	N	N	N	N	N	N	N	N	N	N	-	-	-	N	N	N	N	N	N
	9.75:3.25:1	hSBO	N	N	N	N	N	N	N	N	N	-	-	-	4	-	-	N	N	N	N	N	N
		98hEO	N	N	N	N	N	N	N	N	N	N	N	N	N	N	N	N	N	N	N	N	N
	11.25:3.75:1	hSBO	N	N	N	N	N	N	N	N	N	-	-	-	3	-	-	N	N	N	N	N	N
		98hEO	N	N	N	N	N	N	N	N	N	N	N	N	1	-	2	N	N	N	N	N	N
	13.5:4.5:1	hSBO	N	N	N	N	N	N	N	N	N	-	-	-	N	N	N	N	N	N	N	N	N
		98hEO	N	N	N	N	N	N	N	N	N	N	N	N	N	N	N	N	N	N	N	N	N
	14.25:4.75:1	hSBO	N	N	N	N	N	N	N	N	N	N	N	N	3	-	-	N	N	N	N	N	N
		98hEO	N	N	N	N	N	N	N	N	N	N	N	N	1	-	-	N	N	N	N	N	N

- means the NE was not formed.

N means the experiment was not performed.

The preparation of nanoemulsions with other nonionic surfactants in the absence and presence of cosurfactant.

Table 4.4 Upper limit of the amount of oil (%w/w) incorporated into Regions A, B and C of nonionic nanoemulsions containing the mixture of surfactant and cosurfactants at room temperature (cont.).

Surfactant with cosurfactant	Weight ratio of Tween 80: Dermosoft GMCY:soybean lecithin	Oil	5% surfactant			10% surfactant			15% surfactant			20% surfactant			25% surfactant			30% surfactant			35% surfactant		
			A	B	C	A	B	C	A	B	C	A	B	C	A	B	C	A	B	C	A	B	C
Tween 80:Dermosoft GMCY:lecithin	15:5:1	hSBO	N	N	N	N	N	N	N	N	N	2	-	-	N	N	N	N	N	N	N	N	N
		98hEO	N	N	N	N	N	N	N	N	N	N	N	N	N	N	N	N	N	N	N	N	N
	18:6:1	hSBO	N	N	N	N	N	N	N	N	N	2	-	-	3	-	-	N	N	N	N	N	N
		98hEO	N	N	N	N	N	N	N	N	N	N	N	N	2	-	-	N	N	N	N	N	N

- means the NE was not formed.

N means the experiment was not performed.

Overall, a higher amount of oil was incorporated in the NE stabilised by Tween 80, Dermosoft GMCY and lecithin compared to NE stabilised by Tween 80 and lecithin. This suggested that Dermosoft GMCY could encourage the formation of NE, an observation which can be explained by the reduction in the effective CPP of lecithin (a CPP = 1/2 - 1 suggests the formation of a vesicle or bilayer) upon the addition of a short chain cosurfactant. A short chain cosurfactant can reduce the effective CPP of a surfactant to (a CPP = 1/3 – 1/2 suggests the formation of a cylindrical aggregate, while a CPP <1/3 suggests the formation of a spherical aggregate) by its incorporation into the interfacial film or by increasing the fluidity of the interfacial layer of lecithin, thereby reducing the tendency of lecithin to form a highly rigid film (Bink et al., 1989) and allowing the interfacial film sufficient flexibility to form a highly curved NE droplet. Interestingly, this particular combination of surfactant/cosurfactant prefers incorporating hSBO to 98hEO. The highest amount of hSBO incorporated occurred at a weight ratio of Tween 80:Dermosoft GMCY:lecithin of between 7.5:2.5:1 and 9.75:3.25:1. The weight ratio of 7.5:2.5:1 was chosen for further study because this ratio contained more lecithin and as a consequence it was anticipated to be less toxic towards cell lines (**Figure 4.1d**).

4.2.2 Dilutability of nonionic o/w nanoemulsions

The possibility of diluting a NE is important if it is to be used as a drug delivery vehicle. If a NE is to be administrated by intravenous injection then it will be subject to dilution by blood. The results obtained in this study show that the NE stabilised by 20 %w/w Tween 80 (T20) in the absence of cosurfactant could be readily diluted down to at least 1 %w/w surfactant, and that these diluted samples remained stable for at least four weeks when stored at room temperature. These results suggest that the use of nonionic o/w NE in the absence of cosurfactant offers an important benefit if they are to be used for drug delivery purposes because the NE stabilised solely by nonionic surfactants prepared in this study were able to be diluted without any change in their appearance.

In contrast, it is well established that the dilution of microemulsions (ME) containing cosurfactants can alter or destroy ME (Attwood, 1994). The ability of a NE containing a cosurfactant to be diluted is dependent on the nature of cosurfactant. For example, ME containing sorbitol, a hydrophilic cosurfactant, which resides predominantly in the

aqueous phase, cannot be infinitely diluted without undergoing a phase separation (Attwood et al., 1992). In addition, cosurfactant-containing ME, are frequently destroyed upon dilution due to a cosurfactant partitioning out from the interfacial monolayer of the ME droplet to the continuous phase (Lawrence, 1994). In contrast, however, it has been observed that ME stabilised by the mixture of lecithin and *N*,*N*-dimethyl alkyl amine *N*-oxides could be readily diluted (Satra, 1998). Taken together these results suggest that a suitable cosurfactant for incorporation into a NE intended for dilution would be one which will reside in the interfacial surfactant region, and which exhibits extremely low solubility in water, resulting in the ability to dilute the NE.

The monoglyceride used in the present study is well established to be water insoluble and therefore micelles prepared with a Tween surfactant in combination with Dermosoft GMCY should be dilutable. For all NE, containing Dermosoft GMCY, it proved possible to dilute the NE with water, however the duration for which the diluted NE remained stable varied and was dependent upon the composition of the NE. In the case of NE prepared from Tween 20:Dermosoft GMCY at a K_m of 2:1 and containing 98hEO, the diluted NE became cloudy within 2 hours and therefore, Tween 20:Dermosoft GMCY at a K_m of 2:1 NE containing 98hEO were not suitable for further investigation in the present study. In contrast, the same dilution (i.e. 1:25) of NE containing either 98hEO and 25 %w/w Tween 80:Dermosoft GMCY at a K_m of 3:1 (TD25) or containing hSBO and 25 %w/w Tween 80:Dermosoft GMCY:lecithin at a K_m of 7.5:2.5:1 (TDL25) were more stable than the Tween 20 NE containing Dermosoft GMCY, although the situation is complicated by the amount of oil incorporated into the NE, particularly true in the case of NE prepared in the absence of lecithin (**Table 4.5**).

Table 4.5 Stability (as assessed in days) of 25 %w/w Tween 80:Dermosoft GMCY at a K_m of 3:1 (TD) NE containing 98hEO and 25 %w/w Tween 80:Dermosoft GMCY:lecithin at a K_m of 7.5:2.5:1 (TDL) NE containing hSBO in the absence and presence of drug remained clear after diluted to 1 %w/w surfactant using water at room temperature.

Sample	Duration that NE remained clear after diluted (day)
TD25-98hEO8	2
TD25-98hEO9	1
TD25-98hEO10	1
TDL25-hSBO2	14
TDL25-hSBO3	14
TDL25-hSBO4	14

Compared to NE prepared with T20, it was clear from the results that the presence of Dermosoft GMCY or Dermosoft GMCY and lecithin in TD25 and TDL25 NE, respectively affected the appearance of diluted NE in that the diluted (i.e. Dermosoft GMCY and Dermosoft GMCY/lecithin free) T20 NE remained clear for longer than either of the diluted TD25 and TDL25 NE. Interestingly, dilution of the NE was associated with a dramatic decrease in the PIT for the TD25 and TDL25 NE (which contain, respectively around 17.1 and 18.8 %w/w Tween 80) by about ~ 30 °C from the CP of the Tween 80 micelles containing 20 %w/w (**Table 4.6)**. Furthermore, the diluted TDL25 NE were more stable than the diluted TD25 NE, which indicates a difference in the phase behaviour of Tween 80 and Dermosoft GMCY in the presence of lecithin.

In case of the TD25-98hEO NE, dilution with water was complicated by the oil penetrating into the hydrophobic chain region of the surfactant:cosurfactant monolayer, resulting in a depression of the PIT. It was considered that there were two reasons for the turbidity observed in these compositions, namely they are at the limit of the possible oil solubilisation and the depression of the PIT due to the presence of an increasing amount of 98hEO. The PIT of IPM-containing NE, prepared using Tween 80:Imwittor 308 at a surfactant:cosurfactant weight ratio of K_m 5:1 was determined by Jawhari (1999) who reported that dilution of a composition at the upper phase boundary, produced an unstable diluted NE, while dilution of a composition far from the phase boundary resulted in more stable NE. This behaviour is analogous to that observed in the present study and explains why the TD25-98hEO9 and TD25-98hEO10 became cloudier quicker than TD25-98hEO8.

In conclusion, the ability to dilute a Tween 20:Dermosoft GMCY containing NE was limited while that of the Dermosoft GMCY containing Tween 80 NE in the absence and presence of lecithin (TD25 and TDL25) was less restricted. The most readily diluted NE where those prepared solely with Tween 80 (T20). As a consequence therefore, only three systems of Tween 80-containing NE systems, namely T20, TD25 and TDL25 NE were further examined to establish their physico-chemical properties and drug solubilising ability.

4.2.3 Cloud point and phase inversion temperature

When nonionic surfactants containing a hydrophilic POE head group are dispersed in water they exhibit a temperature-dependent behaviour, which leads to their separation into surfactant-rich and surfactant-poor phases upon heating. The temperature at which the phase separation occurs is called the cloud point (CP) (Corti et al., 1984). The phase inversion temperature (PIT) is the corresponding temperature in oil/nonionic surfactant/water systems below which the surfactant partitions preferably into water, thus preferring to form o/w NE, and above which, the surfactant partitions preferably into oil, supporting the formation of w/o NE (Ruckenstein, 1997).

According to Conroy et al. (1990), the clouding of a solution of POE nonionic surfactant occurs upon increasing temperature as the result of dehydration of the POE head group. This dehydration is due to a decrease interaction between the hydrogen of water and the ether linkages of the POE head group, which reduce the area per surfactant head group, leading to an increase in the CPP (Corti et al., 1984; Lindman et al., 1989). Consequently, the intermicellar forces are changed from repulsive (hydration force) to attractive (Van der Waals and hydrophobic interactions), which allows a phase inversion to occur (Sadaghiania and Khan, 1991). Alternatively, raising the temperature of a surfactant solution has been linked to the transformation of a spherical micelle to a rod/disc shaped micelle (Conroy et al., 1990) eventually leading to the formation of liquid crystalline phase at a temperature above the PIT. Therefore, the type of NE formed and their stability is related to the PIT of the system, while the value and variations of the PIT can provide important information on the stability of the NE (Becher, 1984). The CP and PIT of T20, TD25 and TDL25 micelles and NE containing varying amounts of either hSBO or 98hEO are shown in **Table 4.6**.

Table 4.6 Variation in cloud point of micelles of 20 %w/w Tween 80, 25 %w/w Tween 80:Dermosoft GMCY at a K_m of 3:1 and 25 %w/w Tween 80:Dermosoft GMCY:lecithin at a K_m of 7.5:2.5:1 and the phase inversion temperature of their corresponding NE either various amounts of hSBO or 98hEO.

Samples	CP of micelles and PIT of NE (°C)	
	hSBO	98hEO
T20	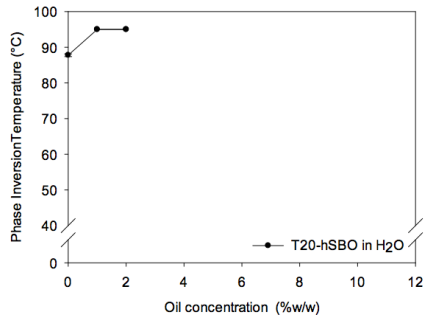	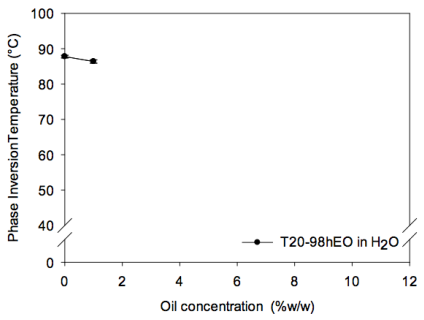
TD25	-	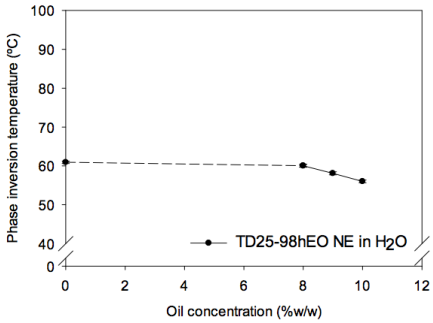
TDL25	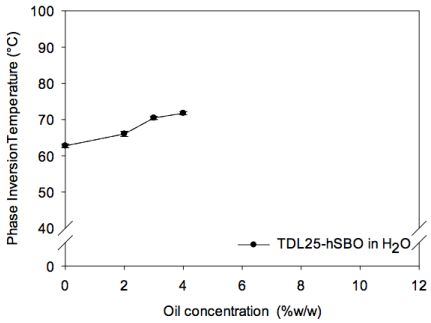	-

- means that samples were not performed the PIT measurement.

It is well established that the presence of a cosurfactant in a micelle can have an effect on the micelle's CP. The CP of 20 %w/w Tween 80 (T20) was ~ 90 °C, whereas the CP of TD25 and TDL25, which contain 17.1 and 18.8 %w/w Tween 80, respectively, exhibited a CP of ~ 60 °C. Clearly, the CP of cosurfactant-containing micellar solution was significantly lower than that of cosurfactant-free micellar solution. This effect is attributed to the action of more hydrophobic cosurfactants intercalating into the more hydrophilic surfactant interfacial monolayer.

The PIT of NE prepared using Tween 80 and H_2O in the absence or presence of Dermosoft GMCY exhibited different patterns in the variation in the PIT depending upon the nature (including molecular volume) and concentration of the incorporated oil. Due to the very low aqueous solubility of the oils studied, it is assumed that the added oil will be present within the NE droplets.

Regardless of the surfactant/combination of surfactants used, when the relatively low molar volume oil (V_m = 600 $Å^3$) 98hEO was incorporated into a NE, the PIT of the NE decreased with increasing oil content. This pattern of behaviour is consistent with the relationship predicted between the site of incorporation of the oil in an aggregate and the concentration of added oil, such that at low concentrations of added oil, it is more likely that the oil penetrates the hydrophobic region of the surfactant monolayer (Nagarajan, 1997). Surprisingly, TD25 NE containing higher amounts of 98hEO, exhibited, instead of the anticipated increase, a decrease in PIT which was the opposite trend to that seen in Brij O10 NE upon increasing amount of 98hEO (**section 3.2.3.1**, Malcolmson et al., 1998; Warisnoicharoen et al., 2000a). This result could be explained that it is reasonable to assume that the mixed micelles formed by Tween 80:Dermosoft GMCY (K_m 3:1) are slightly asymmetrical rather than spherical, therefore any oil penetrating the hydrophobic region of the surfactant monolayer would be expected to accentuate the asymmetrical aggregate shape, thus further lowering the PIT of the NE, possibly even below that of the corresponding micelles. As a consequence of the results obtained here, it can be concluded that 98hEO did penetrate the interfacial surfactant monolayer.

In contrast, the relatively large molecular volume oil (V_m = 1563 $Å^3$) hSBO, produced only an increase in the PIT, regardless of the about of hSBO added, although the PIT for Tween 80 NE-containing hSBO could not be determined due to the limited area over which NE containing hSBO could be produced. It could be explained by the hypothesis that hSBO, which because of its bulky structure and large molecular volume, would not be expected to penetrate the interfacial monolayer, preferring instead to reside within the droplet core forming spherical NE droplets. Indeed, hSBO-containing ME have been previously reported to show an increase in the PIT with increasing oil concentration (Malcolmson et al., 1998).

4.2.4 Light scattering investigations by photon correlation spectroscopy

The particle size of diluted T20, TD25 and TDL25 micelles and NE containing different concentrations of either hSBO or 98hEO were measured using PCS at a scattering angle of 90° is shown in **Table 4.7**.

Table 4.7 The variation in the apparent hydrodynamic size of micelles and nanoemulsions containing either 20 %w/w Tween 80, 25 %w/w Tween 80:Dermosoft GMCY (3:1) or 25 %w/w Tween 80:Dermosoft GMCY:lecithin (7.5:2.5:1) with hSBO or 98hEO content at 25 °C.

Surfactant	The variation in apparent hydrodynamic size of micelles and NE (nm)	
	hSBO	98hEO
T20	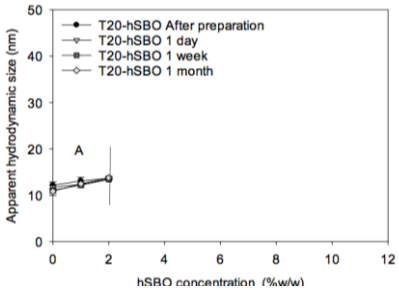	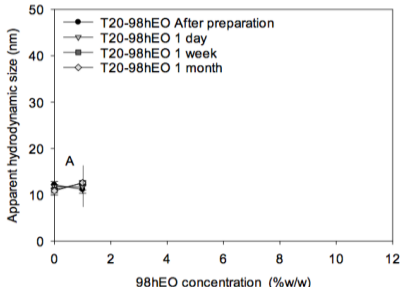
TD25	-	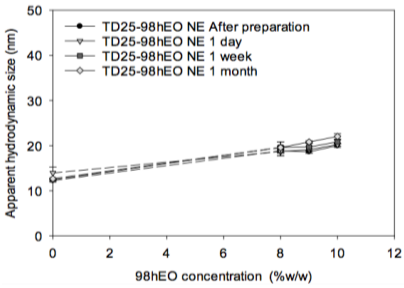
TDL25	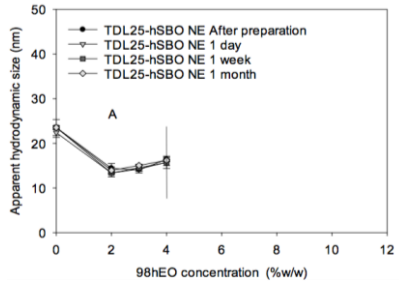	-

- means that samples were not performed the light scattering investigation.

It was clear that, over a month, the apparent hydrodynamic size of all Tween 80-stabilised micelles and NE was unchanged, therefore the preparations were stable over this period. In the present study, the measured hydrodynamic size of T20 micelles was ~ 10 nm, slightly larger than the size of Tween 80 of 8.7 nm reported by Jawhari (1999)

which was determined by extrapolation to zero surfactant concentration and is therefore a more accurate measurement of the size of the Tween 80 micelles. Although some of this observed difference in Tween 80 particle size could be explained by the batch-to-batch variation of POE surfactant.

On the other hand, the apparent hydrodynamic size of the mixed surfactant/surfactant: cosurfactant micellar solutions, i.e. TD25 and TDL25, was larger than that determined for T20 micelles. Specifically the micelle size recorded for T20 was 10 nm, whereas the sizes determined for micelles TD25 and TDL25 micelles were 13 and 20 nm, respectively. Satra et al. (1998) suggested the addition of Dermosoft GMCY to Tween 80 micelles changed the intermicellar forces for Tween 80 micelles from repulsive to attractive which is related to the change in shape of aggregates occurring in the presence of cosurfactant, leading to enhanced intermicellar interactions due to a lower interaction between the POE chains of the surfactant and water. Attractive intermicellar interactions increase for nonionic POE surfactants as the experimental temperature approaches the CP/PIT of the micellar solutions/NE (Aveyard et al., 1989). The addition of lecithin to Triton X-100 micelles resulted in the transformation of spherical micelles of Triton X-100 micelles to non-spherical mixed micelles of Triton X-100 and lecithin while NMR self-diffusion studies showed a decrease in the inter- and intramicellar repulsion in the mixed micelle system (Sadaghiania and Khan, 1991). However, it is not always easy to predict the effect of adding a second surface active compound will have on the micellar properties of the mixed aggregates because the effect will be dependent on the ability of the second surface active agent to partition into the micelles. For example, n-propanol, a short chain alcohol, will partition between the micellar and aqueous phase, lowering the hydrophilicity of the aqueous phase and therefore, indirectly influencing the micellar microstructure by altering the effective HLB of surfactant. Conversely, hexanol, an intermediate chain alcohol, will exert its effect by primarily locating itself at the micellar interface, changing the packing of the surfactant and causing the interfacial layer to expand (Muller and Muller, 1984).

In conclusion, the addition of Dermosoft GMCY to Tween 80 micelles results in an increase in the apparent hydrodynamic size of the micelles. It is likely that this increase in size is caused by an expansion of the interfacial layer because Dermosoft GMCY is expected to sit preferentially at the interface of the micelles. Note that due to its high lipophilicity, Dermosoft GMCY, is not expected to partition into the aqueous phase.

The effect of oil on the apparent hydrodynamic particle size of the T20, TD25 and TDL25 NE is shown in **Table 4.7**. It was clear that the apparent hydrodynamic particle size of the NE increased as the amount of oil, either hSBO or 98hEO, incorporated into the NE increased. Interestingly, the particle size of TDL25-hSBO NE exhibited first a decrease upon the addition of a small amount of hSBO, thereafter size increased upon the addition of further hSBO. From comparison with other studies on ME prepared using either ionic or nonionic surfactants (Hoffmann and Ulbright, 1989), the variation in the size of the TDL25 aggregates upon addition of the hSBO, it is suggested that the initial shape of the micelles and the NE containing a very small amount of hSBO were asymmetrical and that upon addition of more oil, the shape of the NE transformed into a more spherical shape.

Micelles formed by POE-containing surfactants are expected to show a phase separation at and above the PIT due to the dehydration of the POE head group (Mitchell et al., 1983; Corti et al., 1984). The changes in hydration taking place upon approach to the PIT generally result in an increase in the particle size of the micelle, with the aggregate shape becoming less highly curved and tending towards an ellipsoidal shape (Zulauf et al., 1985; Conroy et al., 1990). However, at a temperature far below the CP (i.e. more than 20-30 °C below the CP), the particle size of the micelle is constant and unaltered with any change in temperature. For example, the size of the C_8E_5 and $C_{12}E_8$ micelles were constant over the temperature range of 30-60 °C at a surfactant concentration range of 0-35 %w/w (Zulauf et al., 1985). In the present study, most of the systems investigated had a much higher CP than the temperature at which the PCS studies were performed. For example, the CP of T20 micellar solution was around 90 °C, although the addition of Dermosoft GMCY or lecithin lowered the CP to ~ 60 °C. Despite this lowering, the CP for all systems examined in the present study was still above the experiment temperature of 25 °C and therefore no complication arising from the proximity of the CP was expected to influence the results.

4.3 Micelle and nanoemulsion in the presence of hydrophobic drugs

4.3.1 The incorporation of testosterone propionate

The water-insoluble, hydrophobic steroid (0.0009 ± 0.002 %w/w, log P_{oct} 4.78 (Craig, 1990)), testosterone propionate (TP), was selected as a drug to investigate the

incorporation of drug in a NE (Craig, 1990; Malcolmson et al., 1998). On the basis of its solubility, it was anticipated that TP would be partially located at the interface between the hydrophobic and hydrophilic regions of the surfactant. While it has been reported that Brij 96 microemulsions containing SBO are unaffected by the presence of an excess of TP (Malcolmson, 1992), it has also been reported that some drugs do significantly affect the particle size of NE with some drugs causing precipitation upon dilution of the NE (Borhade et al., 2008). The effect of the addition of TP on NE containing varying amounts of oil was investigated in the present study by saturating with TP NE prepared using 25 %w/w Tween 80:Dermosoft GMCY (3:1) (TD25) and containing the oil 98hEO. Excess drug was removed from the NE after 7, 10 and 14 days by centrifugation. Other reasons why TP was selected for study include the fact that several studies have shown that it is possible to increase its apparent aqueous solubility by its formulation in a ME (Satra et al., 1998, Malcolmson et al., 1998). The solubility of TP in TD25 micelles and in NE containing 98hEO was measured, and the effect of TP on the area of NE existence, the apparent hydrodynamic size and phase inversion temperature of the NE determined.

4.3.1.1 Effect of testosterone propionate on the area of NE existence

TD25-98hEO samples within the o/w NE region prepared in the absence of a saturation amount of drug are shown in **Table 4.2** (**section 4.2.1**). Encouragingly, NE that where within Region A, in the absence of TP, remained completely clear in the presence of a saturation amount of drug and remained stable for at least 2 months. Furthermore, there was no visible change in the area of NE existence in the presence of saturation levels of TP. The high stability of the TP-containing TD25-98hEO NE, coupled with the large NE region they produced suggested that the TD25-98hEO NE offered considerable potential as drug delivery vehicles.

4.3.1.2 Effect of testosterone propionate on cloud point and phase inversion temperature

The cloud point (CP) and phase inversion temperature (PIT) of both drug-loaded and drug-free micelles and NE are recorded in **Figure 4.2**. It was clear that both the CP and PIT of TP-saturated samples were reduced in comparison to the corresponding TP-free samples suggesting that TP were partly located at the boundary between the

hydrophobic and hydrophilic portions of the surfactant ($p<0.05$). Interestingly, the PIT of TD25-98hEO8 and TD25-98hEO9 NE after saturation with TP for 7 days was much higher than that measured for samples after 10- or 14-days saturation with TP ($p<0.05$) (**Figure 4.2**). This result suggests that TD25-98hEO8 and TD25-98hEO9 NE saturated with TP for 7 days contained less TP than those saturated for 10- or 14-days, a result in agreement with the solubilisation studies which suggested that equilibrium solubilisation was achieved by 10-days.

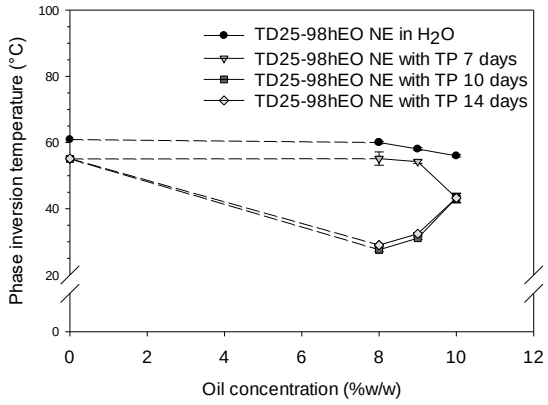

Figure 4.2: Variation in mean cloud point of micelles prepared at 25 %w/w Tween 80:Dermosoft GMCY at a K_m of 3:1 and the phase inversion temperature of nanoemulsions containing 98hEO and stabilised by 25 %w/w Tween 80:Dermosoft GMCY at a K_m of 3:1 in H_2O and in the absence and presence of testosterone propionate (TP). The data are the mean ± S.D. of triplicate measurements. Error bars in some cases contained within the symbols.

At day 7 of the TP equilibration, the difference in the PIT of TD25-98hEO8 and TD25-98hEO9 NE saturated with TP compared to the corresponding drug free samples was ~ 5 ºC - equivalent to the difference between the CP of the TP-free and the TP-loaded micelles. These findings suggest that the amount of TP solubilised in the TD25-98hEO8-TP and TD25-98hEO9-TP NE is similar to the amount of TP solubilised in the TD25-TP micelles. However, the decrease in the PIT of the TP-containing TD25-98hEO10 NE was greater than the differences recorded between the CP of the TP-free and TP-loaded micelles, suggesting that the amount of TP solubilised in the TD25-98hEO10 NE was greater than that solubilised in the TD25 micelles.

At days 10 and 14 of TP equilibration (i.e. the time by which TP saturation was reached), the decrease in the PIT of the TP-containing TD25-98hEO was much greater than the difference in the CP of the TP-free and TP-loaded micellar solutions. This observation suggested that the amount of TP was solubilised in the TD25-98hEO-TP NE was greater than that solubilised in the TD25-TP micelles.

4.3.1.3 Effect of testosterone propionate on the size of the micelle and nanoemulsions

Light scattering investigations by photon correlation spectroscopy (PCS) were performed on micelles prepared using a total of 25 %w/w Tween 80:Dermosoft GMCY at a K_m of 3:1 as well as the corresponding NE containing 98hEO and in which excess TP had been added in order to examine the effect of the addition of a saturation amount of TP on the apparent hydrodynamic size of TD25-98hEO NE. PCS investigations on the equivalent drug-free NE had previously been performed over a period of 1 month. Light scattering analysis of TDL25-98hEO-TP NE where also carried out 7, 10 and 14 days after the addition of TP, with the excess TP removed by centrifugation.

The variation in the apparent hydrodynamic size of NE saturated with TP for either 7, 10 or 14 days, assessed by PCS, plotted as a function of oil concentration is shown in **Figure 4.3**. As can be seen the apparent hydrodynamic size of TP-containing TD25-98hEO NE increased with increasing concentration of 98hEO. Furthermore, no difference was observable in the size of TP-containing NE measured at different days of TP saturation ($p>0.05$) (**Figure 4.3**). Indeed, when comparing all the Region A NE studied, it is clear that the apparent hydrodynamic size of NE with TP was the same size as that of TP-free NE.

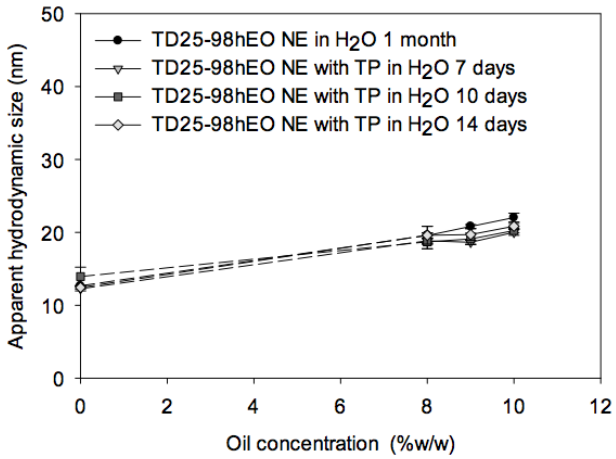

Figure 4.3: Variation in the mean apparent hydrodynamic size (as assessed using Brookhaven ZetaPlus particle sizer) of the nanoemulsions stabilised by 25 %w/w Tween 80:Dermosoft GMCY at a K_m of 3:1 and containing different concentrations of 98hEO in the absence and presence of testosterone propionate (TP) at 25 °C. The data are the mean ± S.D. of triplicate measurements. Error bars in some cases contained within the symbols.

4.3.1.4 The solubility of testosterone propionate in micelle and nanoemulsions

The level of TP incorporation in TD25 micelles and TD25-98hEO NE containing different concentrations of oil was determined (**Figure 4.4**). Clearly, TP solubilisation in TD25 micelles and in TD25-98hEO10 NE reached maximal levels by 7-day. In contrast, maximal TP solubilisation in NE containing 8 and 9 %w/w hEO (TD25-98hEO8 and TD25-98hEO9) was not achieved until after 10-day TP equilibration. These results suggest that in order for NE containing 8 and 9 %w/w 98hEO to be saturated with TP at least 10 days is required. These TP solubilisation results are in agreement with the results of the CP and the PIT studies of the micelle and NE which indicated that the amount of TP incorporated into the TD25-98hEO8 and TD25-98hEO9 NE after 7 days incubation was lower than that achieved at 10 days (**Figure 4.2**). This behaviour may be a consequence of the high viscosity of the NE causing a reduced rate of drug solubilisation, meaning that longer time was required to reach maximal TP solubilisation. However, the equilibrium solubility of TP in either Brij 97 or sodium dodecyl sulphate micelles and NE/ME was typically reached within 6 h for micelles and 24 h for NE/ME (Luangwitchajaroen, 2017). Finally, the results showed that there was a significant increase in the amount of TP solubilised in the TD25-98hEO NE when compared to corresponding micelles.

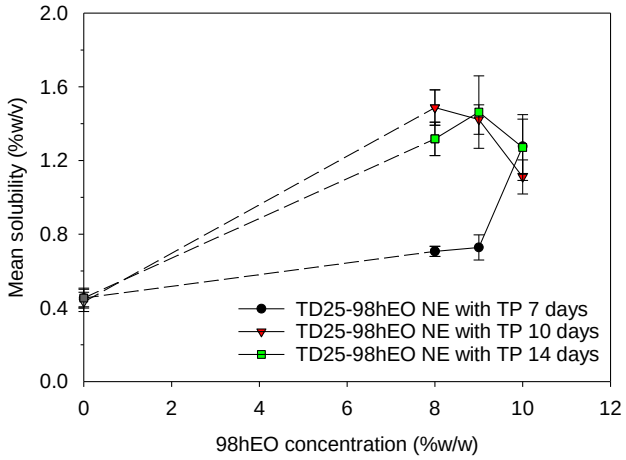

Figure 4.4: Variation in solubilisation of testosterone propionate in micelles and nanoemulsions prepared using 25 %w/w Tween 80:Dermosoft GMCY at a K_m of 3:1 and containing different amounts of 98hEO at 25 °C. The data are the mean ± S.D. of triplicate measurements. Error bars in some cases contained within the symbols.

It has been reported that the difference in the location of solubilised steroid molecules in surfactant micelles depends upon the polarity of the drug (Tomida et al., 1978; Lundberg et al., 1979). It has also been suggested that TP is more generally associated

with the head group region of an ethoxylated nonionic surfactant rather than with the surfactant's hydrophobic chains (Thakkar and Hall, 1967; Thakkar and Kuehn, 1968) and, in particular, is associated with the least hydrated polyoxyethylene region closest to the hydrocarbon core (Barry and El Eini, 1976). In the present study, it is suggested that, in the TD25 micelles, the TP is predominately solubilised in the dehydrated polyoxyethylene region of the surfactant, closet to the micelle core.

As can be seen, a significant increase in TP solubilisation with increasing oil concentration was seen for NE in Region A. The solubility of TP in NE containing a high amount of oil was enough to cause a significant increase in the amount of TP in the NE over the corresponding micelles. It is anticipated that NE in Region A would exhibit an increase in TP solubilisation due to their high oil loading and larger apparent hydrodynamic size, as assessed by PCS. According to the generally held view, oils with large molecular volumes form a core in the centre of the droplet. (Evans et al., 1986). It would be anticipated therefore, that an oil with a higher molecular volume would increase the PIT by forming a core in the centre of the NE which would be expected to provide an additional site for drug solubilisation.

Moreover, the comparison of the experimentally measured TP solubilisation with that predicted from that calculated by the addition of TP solubilisation in the corresponding micelles with the solubility of TP in the amount of oil incorporated in the NE is shown in **Table 4.8**. The comparison in **Table 4.8** shows that the experimental TP solubilisation in NE was higher than the predicted TP solubilisation, showing the advantage of NE to improve the apparent solubility of drug in water. This observation suggests that oil was incorporated in NE in such a way as to improve the solubilisation of drug.

Table 4.8 Comparison of experimentally determined and expected TP solubilisation in TD25 micelles and NE and after saturation with TP for 10 days at 25 °C.

Sample	Region	Experimental TP solubilisation (%w/v)	Expected TP solubilisation (%w/v) [a]
TD25	-	0.43 ± 0.05	-
TD25-98hEO8	A	1.49 ± 0.10	0.89
TD25-98hEO9		1.42 ± 0.08	0.95
TD25-98hEO10		1.11 ± 0.09	1.01

[a] calculated from the experimental TP solubilisation in micelle and oil according to amount of oil in the NE samples. The solubility of TP in 25 %w/w Tween 80:Dermosoft GMCY was 0.43 ± 0.05 %w/v at 25 ^{0}C while the solubility of TP in 98hEO was 5.79 ± 0.40 %w/v at 25 ^{0}C (Malcolmson et al., 1992; Malcolmson et al., 1998).

4.3.2 The incorporation of curcumin

A water insoluble, anticancer drug, curcumin (log P_{oct} 2.23 (Singh et al., 2010)), was selected as a second drug to investigate the incorporation of hydrophobic drug into NE systems. The effect of the addition of CUR on the stability of the NE containing varying amounts of oil was investigated in the present study by saturating either T20, TD25 or TDL25 NE with CUR. Excess drug was removed from the NE after 5 or 7, 10 and 14 days by centrifugation.

4.3.2.1 Effect of curcumin on the area of NE existence

Clear, Region A NE, T20-hSBO, T20-98hEO, TD25-98hEO and TDL25-hSBO NE were saturated with CUR (**Table 4.1, 4.2 and 4.4**). The area of all NE existence found with in the presence of CUR was identical to that found in its absence, suggesting that a saturation amount of CUR could be incorporated without any visible change on the area of existence. Furthermore, the CUR-saturated NE where stable for at least 2 months, longer periods were not observed. From visual observation, it is worth noting that no precipitation was seen in any NE after centrifugation, either in the absence or presence of CUR, further suggesting that the NE were stable. The stability of the Tween 80-containing NE in the presence of a saturation amount of CUR suggested that the NE offer potential as drug delivery vehicles.

4.3.2.2 Effect of the presence of curcumin on the cloud point and phase inversion temperature of Tween 80 containing nanoemulsions

The cloud point (CP) and phase inversion temperature (PIT) of CUR-loaded and CUR-free micelles and nanoemulsions prepared using Tween 80 and containing either SBO

and EO (i.e. T20-hSBO or T20-98hEO NE) are shown in **Figure 4.5**. It was clear that both the CP and most of the PIT were unchanged in the presence of a saturation amount of CUR. Such a lack of an effect may suggest that CUR is predominately located in the core of the Tween 80 micelles and their corresponding NE, although it should be noted that due to the low solubility of CUR in hSBO (0.18 %w/v) and 98hEO (0.14 %w/v) only a small amount of CUR would be expected to be located in the core. This result implies that if any of the CUR is in the head group region it does not alter the hydration of the polyoxyethylene chains. Only the PIT of T20-hSBO1-CUR was lower than the corresponding CUR-free NE ($p<0.05$) suggesting that in this case, sufficient CUR sits in the shell, thereby lowering the PIT of T20-hSBO1.

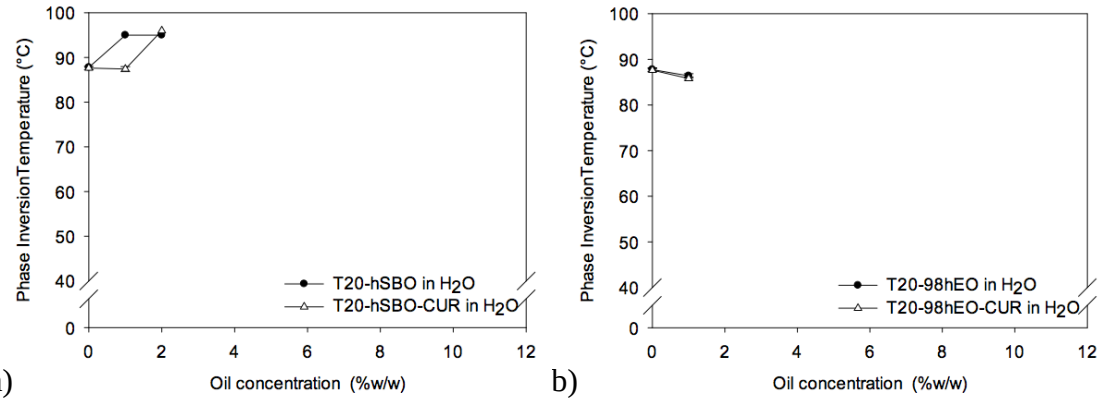

Figure 4.5: The variation in cloud point and the phase inversion temperature of micelles and nanoemulsion prepared using 20 %w/w Tween 80 and containing either a) hSBO or b) 98hEO in the absence and presence of curcumin (CUR) (mean ± S.D.). Error bars in some cases contained within the symbols.

The cloud point (CP) and phase inversion temperature (PIT) of CUR-loaded and CUR-free TD25 micelles and TD25-98hEO NE are shown in **Figure 4.6**. It was clear that CP of CUR-saturated micelle was little lower than the corresponding CUR-free micelles. This result suggests that CUR sits in the interfacial surfactant/cosurfactant region. However, no difference was seen in the PIT of TD25-98hEO8 in the absence and presence of CUR. Surprisingly, the PIT of CUR-saturated TD25-98hEO9 and TD25-98hEO10 NE was much higher than that of the corresponding CUR-free NE ($p<0.05$). Furthermore, this difference increased with increasing 98hEO concentration. This observation is thought to be a consequence of the penetration of Dermosoft GMCY into the surfactant interfacial resulting causing an increase the area of surfactant head group, an increase in the hydration and hydrophilicity of head group. In addition, the shape of

the CUR-containing TD25-98hEO NE at 9 and 10 %w/w 98hEO is expected to become more spherical upon increasing oil concentration.

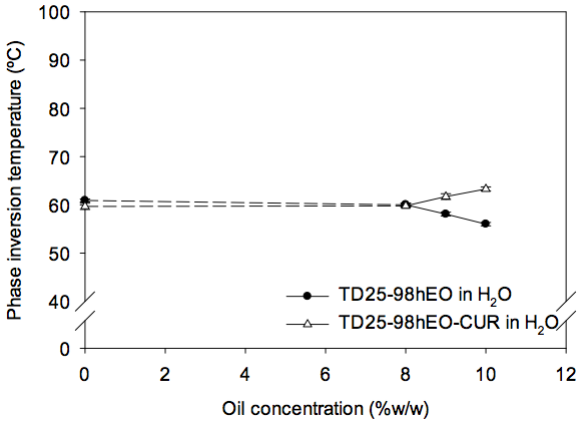

Figure 4.6: The variation in cloud point and the phase inversion temperature of micelles and nanoemulsion prepared using 20 %w/w Tween 80:Dermosoft GMCY (3:1) and containing 98hEO in the absence and presence of curcumin (CUR) (mean ± S.D.). Error bars in some cases contained within the symbols.

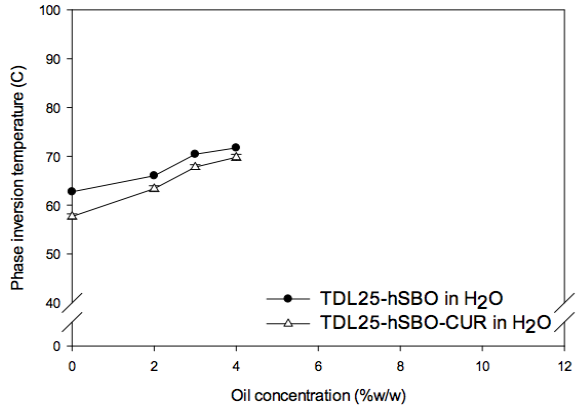

Figure 4.7: Variation in cloud point and the phase inversion temperature of micelles and nanoemulsions prepared using 20 %w/w Tween 80:Dermosoft GMCY:lecithin (7.5:2.5:1) and containing hSBO in the absence and presence of curcumin (CUR) (mean ± S.D.). Error bars in some cases contained within the symbols.

The cloud point (CP) and phase inversion temperature (PIT) of both CUR-loaded and CUR-free TDL25 micelles and TDL25-hSBO NE are shown in **Figure 4.7**. It was clear that the CP/PIT of the CUR-saturated samples is lower than the CUR-free samples ($p<0.05$). This suggests that CUR sits in the interfacial region of the surfactant/cosurfactant mixture and increases the hydrophobicity of surfactant. Note that although the log P of CUR was 2.23 (Singh et al., 2010) and its aqueous solubility was 0.00006 %w/v (Kurien et al., 2007), the solubility of CUR in octanol was low at only 0.00013 %w/v. The solubility of CUR in PEG 400 was 7 %w/v (Sood et al., 2014).

Based on these solubilities, it is suggested that CUR prefers sitting in the surfactant shell and in particular the dehydrated part close to the hydrocarbon core (Barry and El Eini, 1976). Furthermore, the fact that the difference in the PIT between the absence and presence of CUR decreased as the hSBO concentration increased suggests that the ability of the CUR to be solubilised in the core increases so that less of the drug sits in the interfacial boundary region between the hydrophobic and hydrophilic portions of the surfactant.

4.3.2.3 Effect of curcumin on the particle size of Tween 80-containing micelles and nanoemulsions

The apparent hydrodynamic size (D_h) of T20 micelles and T20-hSBO and T20-98hEO NE in the absence and presence of CUR, measured using the Brookhaven ZetaPlus particle sizer, is shown in **Figure 4.8**. The D_h of the T20 micelles and the T20-hSBO NE exhibited an increase in the CUR-containing micelles and NE with increasing hSBO concentration (**Figure 4.8a**). In contrast, the D_h of the T20-98hEO1 and T20-98hEO1-CUR where of comparable similar size (**Figure 4.8b**).

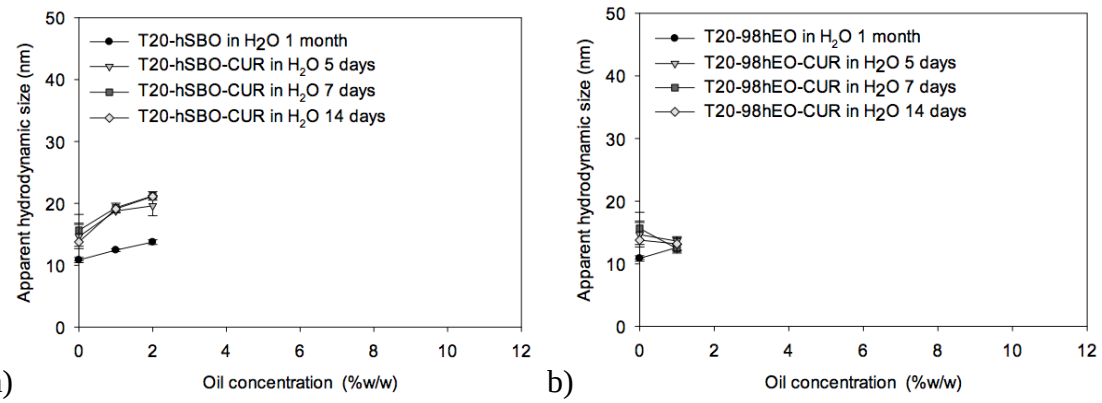

Figure 4.8: Variation in the mean hydrodynamic size (as assessed by the Brookhaven ZetaPlus particle sizer) of Tween 80 micelles and nanoemulsions prepared using 20 %w/w and containing either a) hSBO or b) 98hEO in the absence and presence of curcumin (CUR) (mean ± S.D.) at 25 °C. Error bars in some cases contained within the symbols.

The apparent hydrodynamic size (D_h) of TD25 micelles and TD25-98hEO NE in the absence and presence of curcumin is shown in **Figure 4.9**. While the D_h of the TD25 micelles and the TD25-98hEO8 NE, regardless of 98hEO concentration, showed an increase in size of the CUR-containing micelles and NE, the D_h of TD25-98hEO9-CUR

and TD25-98hEO10-CUR, in contrast, were of comparable size to the corresponding CUR-free NE.

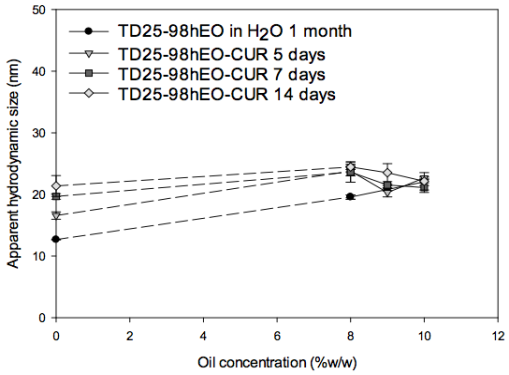

Figure 4.9: Variation in the mean hydrodynamic size (as assessed by the Brookhaven ZetaPlus particle sizer) of micelles and nanoemulsions prepared using 25 %w/w Tween80:Dermosoft GMCY (3:1) and containing 98hEO in the absence and presence of curcumin (CUR) (mean ± S.D.) at 25 °C. Error bars in some cases contained within the symbols.

The apparent hydrodynamic size (D_h) of TDL25 micelles and TDL25-hSBO NE in the absence and presence of curcumin is shown in **Figure 4.10**. The D_h of the TDL25 micelles and TDL25-hSBO NE, regardless of hSBO, showed a significant increase in size in the CUR-containing micelles and NE in comparison when compared to the corresponding CUR-free NE.

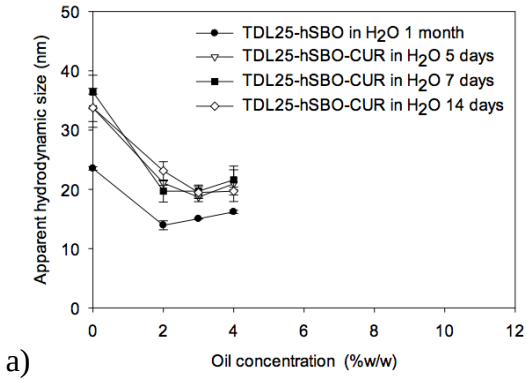

a)

Figure 4.10: Variation in the mean hydrodynamic size (as assessed by the Brookhaven ZetaPlus particle sizer) of micelles and nanoemulsions prepared using 25 %w/w Tween80:Dermosoft GMCY:lecithin (7.5:2.5:1) and containing varying amounts of hSBO in the absence and presence of curcumin (CUR) (mean ± S.D.) at 25 °C. Error bars in some cases contained within the symbols.

4.3.2.4 The solubility of curcumin in micelle and nanoemulsions

The incorporation of CUR into T20, TD25 and TDL25 micelles and T20-hSBO, T20-98hEO, TD25-98hEO and TDL25-hSBO NE as a function of oil concentration was

investigated (**Table 4.9**). Clearly, CUR solubilisation had reached equilibration by 5-day in T20 micelles, T20-hSBO and T20-98hEO NE, whereas CUR solubilisation in TD25 micelles, TD25-98hEO NE, TDL25 micelles and TDL25-hSBO NE only reached saturation after 10-days equilibration. Surprisingly, the amount of CUR incorporated into the NE did not increase over the corresponding micellar solution. This observation could be explained by the low solubility of CUR in either hSBO or 98hEO.

Table 4.9 Solubilisation of curcumin in micelles and nanoemulsions prepared using either 20 %w/w Tween 80, 25 %w/w Tween 80:Dermosoft GMCY (3:1) or 25 %w/w Tween 80:Dermosoft GMCY:lecithin (7.5:2.5:1) and containing different concentrations of either hSBO or 98hEO (mean ± S.D.) at 25 °C.

Sample	Drug Solubilisation (%w/v)			
	5 days	7 days	10 days	14 days
T20-CUR in H_2O	0.33 ± 0.01	0.33 ± 0.02	0.31 ± 0.01	0.31 ± 0.01
T20-hSBO1-CUR in H_2O	0.30 ± 0.01	0.33 ± 0.02	-	0.31 ± 0.02
T20-hSBO2-CUR in H_2O	0.33 ± 0.03	0.34 ± 0.03	-	0.32 ± 0.02
T20-98hEO1-CUR in H_2O	0.35 ± 0.03	0.32 ± 0.03	-	0.34 ± 0.01
TD25-CUR in H_2O	0.17 ± 0.02	-	0.21 ± 0.03	0.22 ± 0.02
TD25-98hEO8-CUR in H_2O	0.19 ± 0.03	-	0.22 ± 0.02	0.22 ± 0.02
TD25-98hEO9-CUR in H_2O	0.18 ± 0.01	-	0.19 ± 0.03	0.20 ± 0.02
TD25-98hEO10-CUR in H_2O	0.20 ± 0.02	-	0.20 ± 0.03	0.23 ± 0.03
TDL25-CUR in H_2O	0.18 ± 0.01	-	0.21 ± 0.02	0.20 ± 0.04
TDL25-hSBO2-CUR in H_2O	0.17 ± 0.01	-	0.17 ± 0.01	0.18 ± 0.01
TDL25-hSBO3-CUR in H_2O	0.16 ± 0.01	-	0.16 ± 0.01	0.19 ± 0.00
TDL25-hSBO4-CUR in H_2O	0.16 ± 0.01	-	0.18 ± 0.01	0.21 ± 0.01

Interestingly, the level of CUR solubilisation in T20 micelles and NE was higher than that obtained in TD25 and TDL25 micelles and NE (**Table 4.9**). The low amount of CUR solubilised in the cosurfactant-containing micelles and NE suggested that both Dermosoft GMCY and lecithin could affect the formation of micelles and NE causing a decrease in CUR solubilisation.

A comparison of the experimentally obtained CUR solubilisation and the expected CUR solubilisation in the various NE is shown in **Table 4.10**. The anticipated CUR solubilisation was calculated from the measured solubilisation of CUR in micelles and in oil. This comparison showed that, regardless of oil, the experimentally measured CUR solubilisation in T20 and TD25 NE was similar to the expected CUR

solubilisation in both NE while the experimentally determined CUR solubilisation in the TDL25 NE containing an amount of oil was less than the expected level of solubilisation. These results indicated that the NE do not possess an advantage over micelles in respect to solubilisation of CUR, which suggests that the oil was either incorporated into the NE in such a way as to not improve drug solubilisation and/or the solubilisation of CUR in oils was too low. In order to understand the effect of structure on solubilisation, small angle neutron scattering studies where undertaken.

Table 4.10 Comparison of experimentally determined and predicted CUR solubilisation in Tween 80-containing micelles and nanoemulsions at 25 °C.

Sample	Experimental CUR solubilisation in samples (%w/v)	Expected CUR solubilisation in samples (%w/v) [a]
T20-CUR in H_2O (7 days)	0.33 ± 0.02	-
T20-hSBO1-CUR in H_2O (7 days)	0.33 ± 0.02	0.31
T20-hSBO2-CUR in H_2O (7 days)	0.34 ± 0.03	0.31
T20-98hEO1-CUR in H_2O (7 days)	0.32 ± 0.03	0.31
TD25-CUR in H_2O (10 days)	0.21 ± 0.03	-
TD25-98hEO8-CUR in H_2O (10 days)	0.22 ± 0.02	0.22
TD25-98hEO9-CUR in H_2O (10 days)	0.19 ± 0.03	0.22
TD25-98hEO10-CUR in H_2O (10 days)	0.20 ± 0.03	0.22
TDL25-CUR in H_2O (10 days)	0.21 ± 0.02	-
TDL25-hSBO2-CUR in H_2O (10 days)	0.17 ± 0.01	0.21
TDL25-hSBO3-CUR in H_2O (10 days)	0.16 ± 0.01	0.22
TDL25-hSBO4-CUR in H_2O (10 days)	0.18 ± 0.01	0.22

[a] calculated from the experimental CUR solubilisation in micelle and oil according to amount of oil in NE samples. The solubility of CUR in T20, TD25 and TDL25 was 0.33 ± 0.02, 0.21 ± 0.03 and 0.21 ± 0.02 %w/v at 25^{0}C while the solubility of CUR in hSBO and 98hEO was 0.18 ± 0.03 and 0.14 ± 0.03 %w/v at 25 ^{0}C (**Table 3.4**).

4.3.3 The incorporation of curcumin and testosterone propionate

Curcumin (CUR) and testosterone propionate (TP) were selected as hydrophobic drugs to investigate the effect of the incorporation of two drugs into the same NE. The effect of the addition of both CUR and TP on the stability of the TD25-98hEO NE containing varying amounts of 98hEO was investigated by saturating TD25-98hEO with CUR and TP. Excess drug was removed from the NE after either 7, 10 or 14 days by centrifugation. The effect of the incorporation of both drugs on the area of NE existence for TD25-98hEO and the phase inversion temperature and particle size of the NE

droplets was determined, as well as the solubility of CUR and TP in TD25 micelles and TD25-98hEO-CUR-TP NE.

4.3.3.1 Effect of curcumin and testosterone propionate on the area of NE existence

Clear, Region A TD25-98hEO NE (**Table 4.2**) were used to study the effect on the area of existence on the incorporation of a saturation amount of both drugs. It was established that the area of NE existence was unchanged in the presence of saturation amounts of both drugs. Furthermore the drug-saturated NE, prepared with 98hEO, where all stable for at least 2 months. It is important to note that there was no evidence of the centrifugation precipitating in any of the NE, regardless of the absence or presence of CUR and TP. The high stability of the TD25-98hEO-CUR-TP NE and the relatively large NE region they exhibited suggests that the NE offer potential as drug delivery vehicles.

4.3.3.2 Effect of curcumin and testosterone propionate on cloud point and phase inversion temperature

The cloud point (CP) and phase inversion temperature (PIT) of CUR and TP-loaded and CUR and TP-free TD25 micelles and TD25-98hEO NE are shown in **Figure 4.11**. It was clear that both the CP and PIT of CUR-TP-saturated micelles and NE were lower than that of the corresponding CUR-TP-free samples ($p<0.05$). The lower recorded CP and PIT suggests that the CUR and/or TP sit in the surfactant interfacial region which is likely to increase the hydrophobicity of system leading to the observed decrease in CP and PIT of the CUR-TP-containing samples.

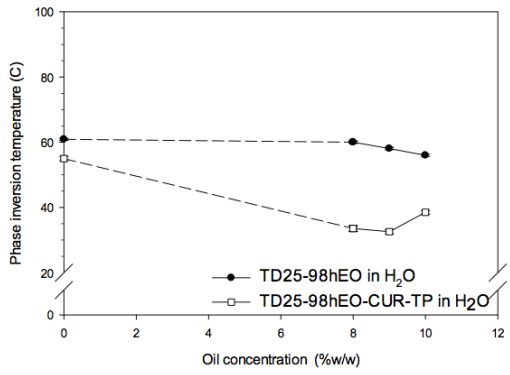

Figure 4.11: The cloud point and phase inversion temperature of micelles and nanoemulsions prepared using 25 %w/w Tween 80:Dermosoft GMCY (3:1) and containing 98hEO in the absence and presence of curcumin (CUR) and testosterone propionate (TP) (mean ± S.D.). Error bars in some cases contained within the symbols.

4.3.3.3 Effect of curcumin and testosterone propionate on the particle size of micelle and nanoemulsions

The apparent hydrodynamic size (D_h) of 25 %w/w Tween 80:Dermosoft GMCY (3:1) micelle and NE containing different concentration of 98hEO in the absence and presence of CUR and TP was measured using both the Brookhaven ZetaPlus particle sizer and Malvern Nano ZS Zetasizer (**Figure 4.12**). The measured D_h of the hSBO NE, obtained using the Brookhaven ZetaPlus particle sizer, showed a significant increase in size of the TD25-CUR-TP and TD25-98hEO8-CUR-TP NE, although apparently random fluctuations in D_h of CUR-TP-containing NE at 9 and 10 %w/w 98hEO were observed, even though the diluted samples containing CUR and TP were completely clear (**Figure 4.12a**). The laser in the Brookhaven was checked to ensure it did not blur after passing through the yellow sample, which it did not. Moreover, when the clear, 4-sided and 10-mm path length disposable polystyrene cuvette, normally used for PCS measurements, were exchanged for a 1-cm path length quartz cuvette normally used for fluorescent measurement to ensure that no chemical reaction occurred between samples and container - the particle size of the NE droplets still exhibited seemingly random fluctuations.

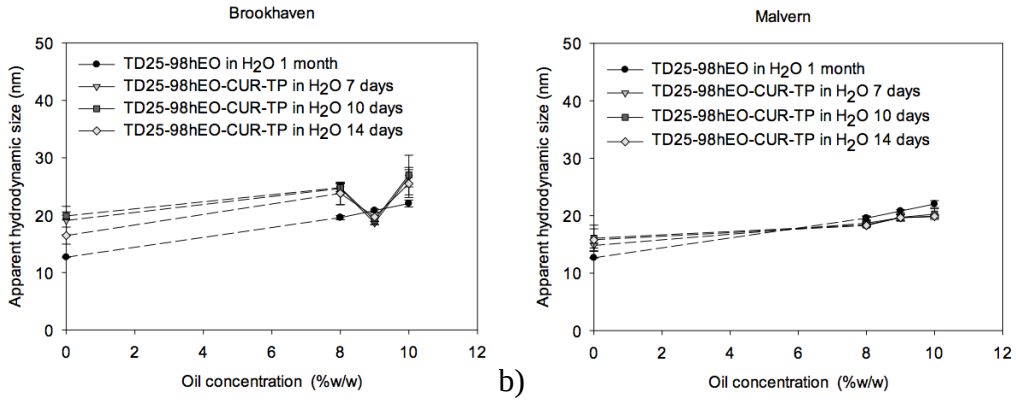

Figure 4.12: Variation in the mean hydrodynamic size of micelles and nanoemulsions prepared using 25 %w/w Tween80:Dermosoft GMCY (3:1) and Tween80:Dermosoft GMCY:lecithin (7.5:2.5:1) and containing varying amounts of 98hEO in the absence and presence of curcumin (CUR) and testosterone propionate (TP) using a) Brookhaven ZetaPlus particle sizer and b) Malvern Nano ZS Zetasizer (mean ± S.D.) at 25 °C. Error bars in some cases contained within the symbols.

When the particle size measurement of TD25 and TD25-98hEO in the absence and presence of CUR and TP was performed using Malvern Nano ZS Zetasizer (**Figure**

4.12b), the D_h of TD25-CUR-TP and TD25-98hEO-CUR-TP did not show an increase. Again small angle neutron scattering studies will be performed in TD25-98hEO-CUR-TP NE in order to probe the internal structure of NE.

4.3.3.4 Solubility of curcumin and testosterone propionate in micelle and nanoemulsions

The analysis of CUR and TP using UV-vis spectroscopy is shown in **section 3.3.3.4**. The solubilisation of CUR and TP in TD25-98hEO NE after incubation with both drugs for 7, 10 and 14 days are shown in **Figure 4.13**. The results showed that while CUR was equilibrated in all samples by 7 days, TP reached equilibration levels between 7-10 days. **Figure 4.14** shows the solubility of (a) CUR and (b) TP in TD25-98hEO-CUR NE in the absence and presence of either CUR or TP after incubation with drug for 14 days. It was clear that TD25-98hEO-CUR-TP NE could incorporate a slightly higher amount of CUR than the TD25-98hEO-CUR NE (i.e. TP-free NE). In contrast, far less TP was solubilisation was observed in TD25-98hEO-CUR-TP NE than in TD25-98hEO-TP NE. Interestingly, the level of TP solubilisation was lower in TD25-98hEO-CUR-TP NE than in TD25-98hEO-TP NE. These results suggest that the presence of CUR could affect TP solubilisation in NE.

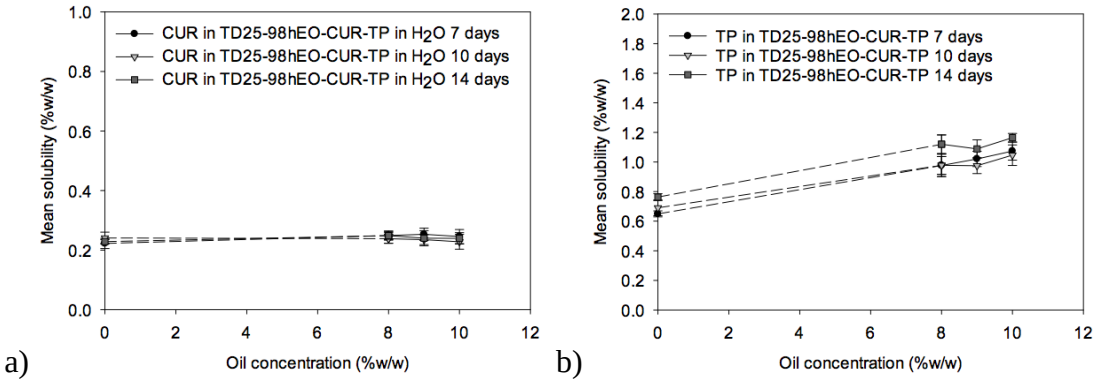

Figure 4.13: Solubilisation of a) curcumin (CUR) and b) testosterone propionate (TP) in 98hEO NE prepared using 25 %w/w Tween 80:Dermosoft GMCY (3:1) containing varying amounts of 98hEO and saturated with curcumin and testosterone propionate for 14 days (mean ± S.D.) at 25 °C. Error bars in some cases contained within the symbols.

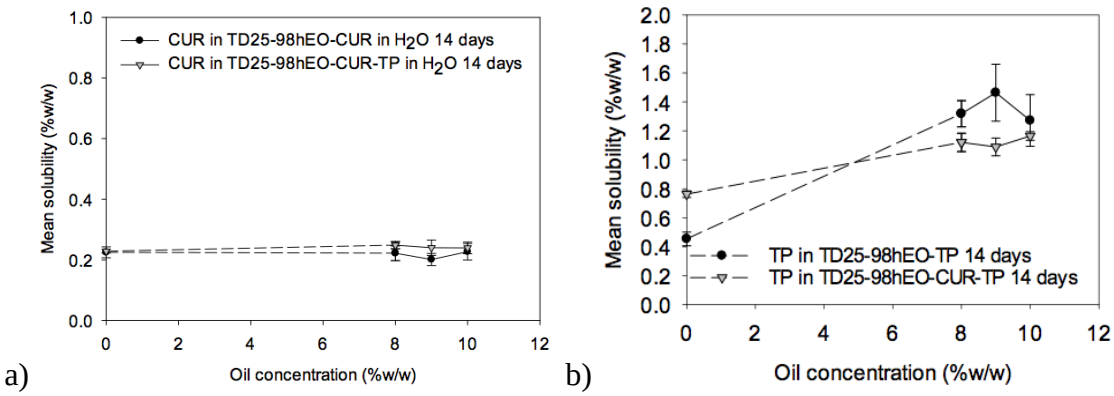

Figure 4.14: Solubilisation of a) curcumin (CUR) and b) testosterone propionate (TP) in 98hEO NE prepared using 25 %w/w Tween 80:Dermosoft GMCY (3:1) and saturated with curcumin and testosterone propionate and compared with CUR solubilisation in TD25-98hEO-CUR and TP solubilisation in TD25-98hEO-TP after 14 days saturation (mean ± S.D.) at 25 °C. Error bars in some cases contained within the symbols.

A comparison between the expected and experimentally determined TP and CUR solubilisation is shown in **Table 4.11**. The expected TP and CUR solubilisation was calculated using a knowledge of the solubilisation of TP or CUR in TD25 micelles and in the relevant bulk oils. This comparison showed that the experimentally measured CUR solubilisation in TD25-98hEO-CUR-TP NE was similar to that predicted but was not significantly different than that achieved in the corresponding micelles. This result demonstrated that NE did not possess any advantage over micelles in respect to CUR solubilisation - a result undoubtedly attributable to the poor solubility of CUR in hSBO. On the other hand, the experimentally measured solubilisation of TP in TD25-98hEO-CUR-TP NE was higher than the predicted TP solubilisation. These results showed that formulation of TP in a NE improves its solubilisation. Small angle neutron scattering (SANS) experiments should enable a greater understanding of reasons why NE are advantageous.

Table 4.11 Comparison of predicted curcumin and testosterone propionate solubilisation in TD25-98hEO-CUR-TP nanoemulsions after incubation with drugs for 14 days at 25 °C.

Oil concentration (%w/w)	Experimental CUR solubilisation in TD25-98hEO-CUR-TP (%w/v)	Expected CUR solubilisation in TD25-98hEO-CUR-TP (%w/v) [a]	Experimental TP solubilisation in TD25-98hEO-CUR-TP (%w/v)	Expected TP solubilisation in TD25-98hEO-CUR-TP (%w/v) [b]
0	0.23 ± 0.01	-	0.76 ± 0.02	-
8	0.25 ± 0.01	0.22	1.12 ± 0.06	0.89
9	0.24 ± 0.03	0.22	1.09 ± 0.06	0.95
10	0.24 ± 0.02	0.22	1.16 ± 0.03	1.01

[a] calculated from the experimental CUR solubilisation in micelle and oil according to amount of oil in NE samples. The solubility of CUR in 25% Tween 80:Dermosoft GMCY was 0.21 ± 0.03 %w/v at 25^{0}C while the solubility of CUR in 98hEO was 0.14 ± 0.03 %w/v at 25 ^{0}C (**Table 3.4**).
[b] calculated from the experimental TP solubilisation in micelle and oil according to amount of oil in NE samples. The solubility of TP in 25% Tween 80:Dermosoft GMCY was 0.43 ± 0.05 %w/v at 25^{0}C while the solubility of TP in 98hEO was 5.79 ± 0.40 %w/v at 25 ^{0}C (Malcolmson et al., 1992; Malcolmson et al., 1998).

4.3.4 The incorporation of docetaxel into micelles and nanoemulsions

The water insoluble anticancer drug, docetaxel (DTX), log P_{oct} 4.1 (Tang et al., 2015), was selected as a drug to investigate the incorporation of another hydrophobic drug into NE. The effect of the addition of DTX on the stability of the NE containing varying amounts of oil was investigated by saturating micelles prepared using 25 %w/w Tween 80:Dermosoft GMCY:lecithin (7.5:2.5:1) (TDL25) and NE varying amounts of 98hEO with DTX (TDL25-98hEO). Excess drug was removed from the NE after 7, 10 and 14 days by centrifugation.

4.3.4.1 Effect of docetaxel on the area of NE existence

DTX-saturated TDL25-hSBO NE containing varying amounts of hSBO from Region A are shown in **Table 4.4**. As can be seen the DTX-containing NE from Region A were clear, suggesting that there was no visible change in the area of existence. As previously reported, centrifugation either in the absence or presence of DTX, produced no evidence of precipitation. Furthermore, the DTX-saturated NE, prepared with hSBO, was stable for at least 2 months. The high stability of the TDL25-hSBO-DTX NE suggested that the TDL25-hSBO NE offer potential as drug delivery vehicles for hydrophobic drugs such as DTX.

4.3.4.2 Effect of docetaxel on cloud point and phase inversion temperature

The cloud point (CP) and phase inversion temperature (PIT) of DTX-saturated and DTX-free micelles and NE are shown in **Figure 4.15**. It was clear that both the CP and the PIT of DTX-saturated samples were reduced in comparison with the corresponding DTX-free samples ($p<0.05$), suggesting that DTX were located at the boundary between the hydrophobic and hydrophilic portions of the surfactant.

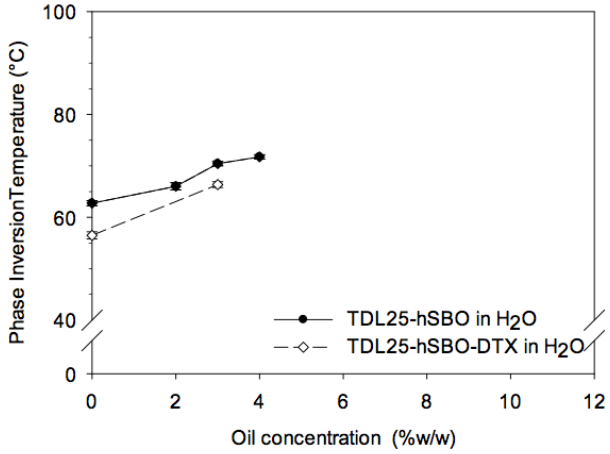

Figure 4.15: Cloud point and phase inversion temperature of micelles and nanoemulsions prepared using 25 %w/w Tween 80:Dermosoft GMCY:lecithin (7.5:2.5:1) and containing 98hEO in the absence and presence of docetaxel (DTX) (mean ± S.D.). Error bars in some cases contained within the symbols.

4.3.4.3 Effect of docetaxel on the particle size of micelle and nanoemulsions

Light scattering investigations using photon correlation spectroscopy (PCS) were performed on 25 %w/w Tween 80:Dermosoft GMCY:lecithin (7.5:2.5:1) micelles and the corresponding 98hEO NE in which DTX has been added to examine the effect of the addition of DTX on the apparent hydrodynamic size of TDL25-hSBO NE. PCS investigations of the equivalent drug-free NE had already been performed. Light scattering analysis of the TDL25-hSBO-DTX NE were performed after 7, 10 and 14 days incubation with excess DTX, which was removed by centrifugation. The apparent hydrodynamic sizes of the micelles and NE with and without DTX were investigated by PCS and the results plotted as a function of oil concentration (**Figure 4.16)**. No difference in the size of the DTX-containing NE at each of the different drug incubation times was observed. In all compositions studied, the apparent hydrodynamic size of the

micelles and the NE in the presence of DTX was the same size as the DTX-free micelles and NE.

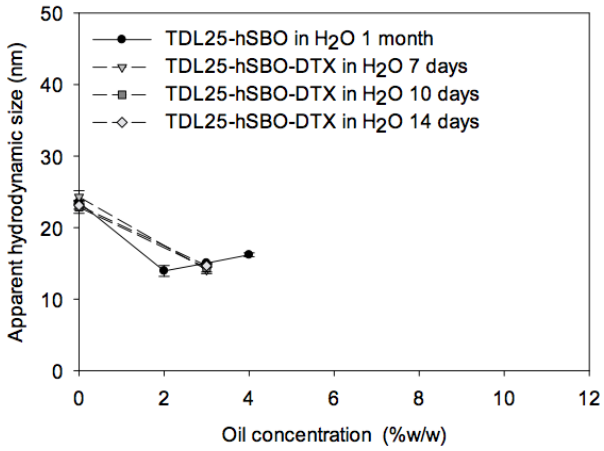

Figure 4.16: Variation in the mean hydrodynamic size of micelles and nanoemulsions prepared using 25 %w/w Tween80:Dermosoft GMCY:lecithin (7.5:2.5:1) and containing varying amounts of 98hEO in the absence and presence of docetaxel (DTX) at 25 °C. Error bars in some cases contained within the symbols.

4.3.4.4 The solubility of docetaxel in micelle and nanoemulsions

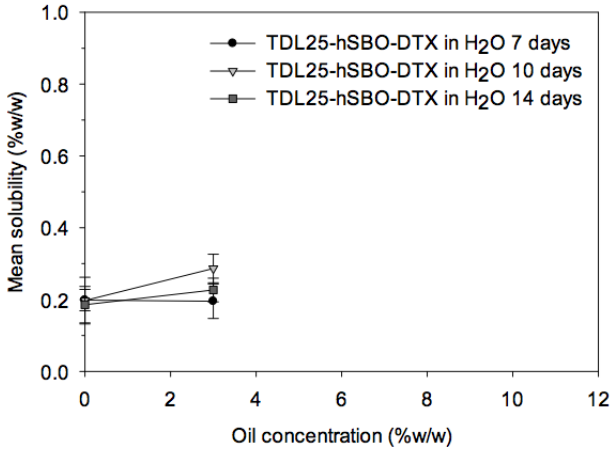

Figure 4.17: Solubilisation of docetaxel (DTX) in micelles and nanoemulsions prepared using 25 %w/w Tween 80:Dermosoft GMCY:lecithin (7.5:2.5:1) and containing different concentrations of hSBO after 7, 10 and 14 days saturation (mean ± S.D.) at 25 °C. Error bars in some cases contained within the symbols.

The incorporation of DTX in TDL25 micelles and TDL25-hSBO3 NE is shown in **Figure 4.17**. DTX solubilisation in TDL25 micelles had reached equilibrium by 7-day incubation. Equilibration in the TDL25-hSBO3 NE was much more variable but as the

data showed not clear no trend with incubation time, it is assumed here that saturation in the NE was also obtained by day 7. Taking a mean of the level of DTX incorporation achieved, suggested that there was no increase in DTX solubilisation in the TDL25-hSBO NE system when compared to the corresponding micelles. This result suggests that DTX is most likely preferentially associated with the interfacial surfactant layer, most probably in the dehydrated region close to the core, rather than with the oil.

A comparison between the experimentally determined DTX solubilisation and the calculated DTX solubilisation is shown in **Table 4.12**. The expected/calculated DTX solubilisation was obtained from a knowledge of the solubilisation of DTX in TDL25 micelles and the solubility of DTX in hSBO. This comparison showed that the experimentally measured level of DTX solubilisation in TDL25-hSBO-DTX NE was similar to that expected, indicating that there was not advantage formulating DTX in the NE under study.

Table 4.12 Comparison of the experimentally measured and expected/calculated docetaxel solubilisation in TDL25-hSBO-DTX nanoemulsions after incubation with excess drug for 14 days at 25 °C.

Oil concentration (%w/w)	Experimental DTX solubilisation in TDL25-hSBO-DTX (%w/v)	Expected CUR solubilisation in TDL25-hSBO-DTX (%w/v) [a]
0	0.20 ± 0.06	-
3	0.29 ± 0.05	0.26

[a] calculated from the experimental DTX solubilisation in micelle and oil according to amount of oil and surfactant in the samples. The solubility of DTX in 25% Tween 80:Dermosoft GMCY:lecithin (7.5:2.5:1) was 0.20 ± 0.06 %w/v at 25^0C while the solubility of DTX in hSBO was 1.94 ± 0.37 %w/v at 25 ^{0}C (Yao et al., 2012).

4.4 Small angle neutron scattering data

Analysis of the SANS data gave an excellent estimation of the shape of micelles and NE particles using different form factor P(Q) (i.e. a sphere, an oblate or a prolate ellipsoid (**Figure 4.18**). In analysis of the SANS data, the interparticulate structure factor was modelled as hard-sphere interactions using the Percus-Yevick approximation. Furthermore, it was assumed that the micelles and NE monodisperse, exhibiting a constant scattering length density (SLD) to analysis the SANS data.

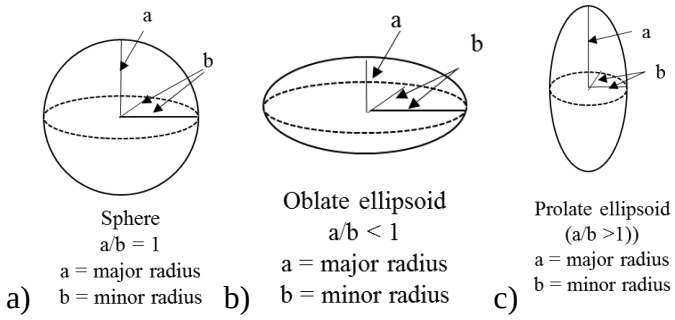

Figure 4. 18: Schematic representation of a) sphere, b) oblate ellipsoid and c) prolate ellipsoid.

In order to analyse the SANS data for the micelles, it was assumed that a core-shell particle of micelles contained 2 parts: a core composed of the hydrocarbon chains of Tween 80 surfactant (and the hydrocarbon chains of cosurfactants either Dermosoft GMCY or lecithin if micelles contain cosurfactants) and a shell containing the surfactant/cosurfactants polar head groups with some solvent molecules. On the other hand, the model used for the NE, where only drop contrast was available, was different and assuming that the core of the NE consisted only of the oil, and the shell consisted of the whole surfactant molecule (and whole cosurfactant molecule if cosurfactants present) and solvent molecule.

A preliminary fitting of SANS data, it showed that the SANS data could not be fitted using the simple spherical form factor, although it could be reasonably well fitted using an oblate ellipsoid for T2d micelles and a prolate ellipsoid for TD2d and TDL2d micelles. It is clear that the ellipsoid model was the best model to be used to fit SANS data. As a consequence therefore, a core-shell ellipsoid model was chosen to analyse SANS data in the present study due to the fact that it provided better fits to the experimentally obtained SANS data and yielded statistically better results were obtained in comparison with the sphere model.

4.4.1 SANS studies of Tween 80 micelle in the presence and absence of cosurfactant or drugs

A series of best fits were obtained assuming a core-shell ellipsoid shape for Tween 80-containing micelles as shown in **Figure 4.19** while **Table 4.13** gives the parameters obtained from the best fit to the Tween 80-containing micelles, namely, the core equatorial radius, the major and minor radii, and the shell thickness. Note that Q and I(Q) are the scattering vector and the intensity of the scattered neutron radiation,

respectively. The absence of an interaction peak in the SANS curves suggested that the Tween 80-containing micelles possessed no charge as expected. Furthermore, when a structure factor was used to explore the presence of interparticulate interactions in the samples at 2 %w/w surfactant concentration, it was found that there was no change to the fit suggesting that, at these concentrations, there were no interparticulate interactions.

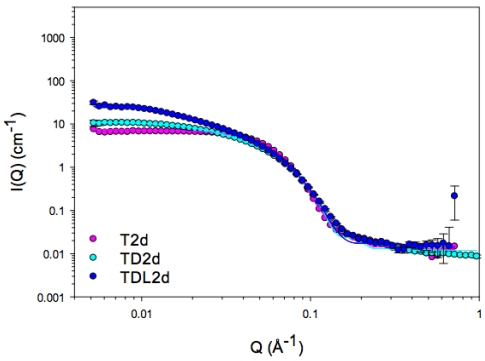

Figure 4.19: Drop contrast of SANS data and 'best' fits for 2 %w/w Tween 80, 2 %w/w Tween 80:Dermosoft GMCY (weight ratio 3:1) and 2 %w/w Tween 80:Dermosoft GMCY:lecithin (weight ratio 7.5:2.5:1) micelles in D_2O at 25 ˚C using a core-shell ellipsoid model together with a hard sphere model for interactions.

The preparation of nanoemulsions with other nonionic surfactants in the absence and presence of cosurfactant.

Table 4.13 Parameters obtained for the best fit to the SANS data for 2 %w/w Tween 80, 2 %w/w Tween 80:Dermosoft GMCY (weight ratio 3:1) and 2 %w/w Tween 80:Dermosoft GMCY:lecithin (weight ratio 7.5:2.5:1) micelles in the absence of drugs at 25 °C using a core-shell ellipsoid model together with a hard sphere structure factor S(Q). The modelling of the SANS data was constrained using Vshell(dry)/Vcore.

sample	core equatorial radius (R_1,Å)	core axial ratio (x)	core axial radius (R_{1x},Å)	shell thickness (Å)	minor radius (Å)	major radius (Å)	axial ratio (X)	micelle volume (Å^3)	sphere radius (Å)	Hydration (%)	N_{agg}	surfaces area of surfactant (Å^2)	sum of squared error (SSE)
T2d	32.0	0.4	13.4	14.7	46.7	28.2	0.6	257343	50.0	15	112	74	5272
TD2d	17.8	5.4	95.4	12.4	30.2	107.8	3.6	410801	115.8	15	401	42	4231
TDL2d	17.0	11.0	186.8	19.5	36.4	206.3	5.7	1147142	225.2	60	630	49	1857

Estimated uncertainty for R_1 were ± 0.15 for T2d, ± 0.1 for TD2d or ± 0.07 for TDL2d, respectively.
Estimated uncertainty for x were ± 0.01 for T2d and TD2d or ± 0.1 for TDL2d.

It was clear that the T2d micelles were oblate ellipsoid as indicated by the core axial ratio of less than 1. The core equatorial radius of 32.0 Å determined for T2d was, as expected, was bigger the 16.5 Å estimated for Tween 20 (Saaka, 2016), partially as a consequence of the elongation of the hydrophobic alkyl chain (Tanford et al., 1977). Moreover, Tween 80 has been shown to form the largest aggregates within the Tween series of surfactant (Atwood et al., 1992). The thickness of T2d shell was 14.7 Å which was thinner than that reported for 2 %w/w Tween 20 (a surfactant containing same number of ethylene oxide groups attached to the sorbitan head group as Tween 80) which was 19.1 Å (Saaka, 2016). The aggregation number (N_{agg}) of Tween 80 was 112, which was double that determined by Jawhari (1999) using static light scattering. The surface area of the Tween 80 micelles was calculated to be 74 $Å^2$, smaller than the value of 81.1 $Å^{2,}$ established using TILS and 86.5 $Å^2$ using surface tension measurements (Jawhari, 1999) and was similar to the value of 72 $Å^2$ determined by Yang et al. (2013) from surface tension experiments. The variation in the shell thickness, aggregation number and area per Tween 80 molecule could be explained by variation in the degree of ethoxylation (Penfold et al., 2015).

In this study, the effect of the addition of the cosurfactant, Dermosoft GMCY and the second (hydrophobic) surfactant, lecithin on the size and shape of the micelle is given in **Figure 4.19**. Clearly, the inclusion of either a cosurfactant or a cosurfactant and second (hydrophobic) surfactant had an effect on the shape of micelles which transformed from oblate ellipsoid, for T2d, to prolate ellipsoid for TD2d and TDL2d, respectively as shown by their possession of a core axial ratio greater than 1. The inclusion of a cosurfactant/second hydrophobic surfactant in a NE is known to have an influence on the size and shape of their aggregates. The core equatorial radius decreased from 32 Å for T2d to 17.8 Å for TD2d and 17.0 Å for TDL2d. Correspondingly, the micelle volume increased from 257 nm^3 for T2d to 410 nm^3 for TD2d and 1147 nm^3 for TDL2d. This result of the formation of larger aggregates after adding a cosurfactant or a cosurfactant/second hydrophobic surfactant is in agreement with the apparent hydrodynamic size (D_h) of micelles measured in this study using PCS which showed a slight increase in the D_h for TD25 micelles and a much larger increase in D_h of TDL25 micelle when compared to the site of the T20 micelles. When compared to T2d micelles, the N_{agg} of TD2d and TDL2d micelle was 4 and 6 times higher, respectively. The increase in N_{agg} due to the presence of cosurfactant or cosurfactant/second hydrophobic surfactant was the same trend in N_{agg} as that observed by Jawhari (1999)

upon adding Imwittor 308 (at a weight mixing ratio of 3:1 - 5:1) to Tween 80 micelles. **Table 4.14** shows the total aggregation number (N_{agg}), Tween 80 aggregation number (N_T), Dermosoft GMCY aggregation number (N_D) and lecithin aggregation number (N_L) in Tween 80-stabilised micelles in the absence and presence of either Dermosoft GMCY or Dermosoft GMCY and lecithin. In the presence of drug, it was clear that the increase in the N_{agg} of TD2d micelles occurred due to an mainly increase in the Dermosoft GMCY aggregation number (N_D) with a small increase in Tween 80 aggregation number (N_T) while the increase in N_{agg} of TDL2d occurred due to the major increase in Dermosoft GMCY aggregation number (N_D) with the a small increase in the N_T and lecithin aggregation number (N_L). **Figure 4.20** gives a schematic representation of the Tween 80 micelles in the absence and presence of cosurfactant.

Table 4.14 Number of surfactant and cosurfactant monomers comprising Tween 80 micelles in the presence of either Dermosoft GMCY or Dermosoft GMCY in combination with lecithin at 25 ˚C.

Composition	Ratio of surfactant: cosurfactant		Aggregate parameter			
	Weight ratio	Molar ratio	N_{agg}	N_T	N_D	N_L
T2d	0	0	112	112	0	0
TD2d	3:1	1:2	401	134	267	0
TD2d-CUR			433	148	295	0
TD2d-CUR-TP			586	195	391	0
TDL2d	7.5:2.5:1	4.4:8.8:1	630	195	390	45
TDL2d-CUR			769	238	477	54
TDL2d-CUR-TP			1068	331	662	75

N_{agg}, N_T, N_D and N_L are the total aggregation number, Tween 80, Dermosoft GMCY and lecithin aggregation number respectively.

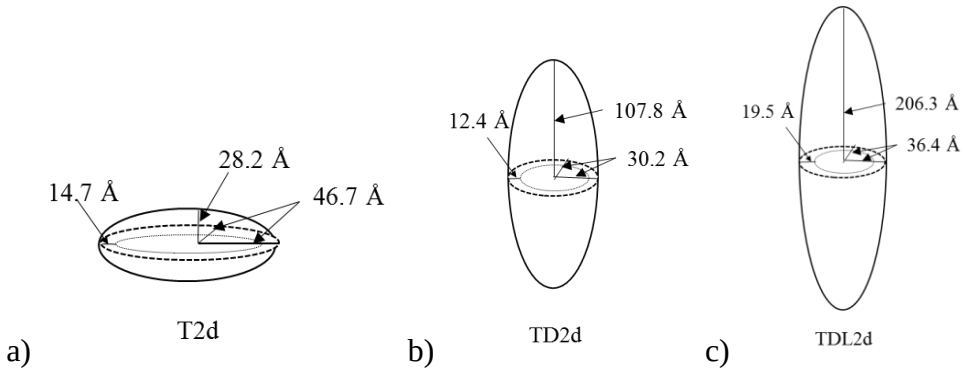

Figure 4.20: Schematic representation of the ellipsoidal a) 2 %w/w Tween 80 micelle, b) 2%w/w Tween 80:Dermosoft GMCY (weight ratio 3:1) micelle and c) 2%w/w Tween 80:Dermosoft GMCY:lecithin (weight ratio 7.5:2.5:1) micelle.

The SANS data for the Tween 80 micelles with cosurfactant or surfactant/second hydrophobic surfactant in the absence and presence of drug is shown in **Figure 4.21**. Saturation of TD2d and TDL2d with either CUR or CUR and TP resulted in a change in the intensity of scattering I(Q). For TD2d micelles (**Figure 4.21a** and **Table 4.15)**, the presence of a saturated amount of CUR slightly increased the core axial ratio from 5.4 for TD2d to 6.1 for TD2d-CUR with no change in the core equatorial radius (17.6-17.8 Å) or shell thickness (~12.4 Å). There was a small increase in the N_{agg} of the surfactant from 401 in TD2d micelles to 443 in the mixed TD2d-CUR micelles, although the surface area calculated for the surfactant remained constant at 42 $Å^2$. Moreover, the addition of a saturation amount of both CUR and TP dramatically increased the core axial ratio from 5.4 for TD2d micelles to 7.5 for the mixed TD2d-CUR-TP micelles, along with a very small change in the core equatorial radius from 17.8 Å to 18.1 Å for TD2d and TD2d-CUR-TP micelles, respectively. A small increase in the shell thickness to 13.0 Å was seen for TD2d-CUR-TP micelles along with a large increase in N_{agg} to 586, although the surface area in the presence of drug/drugs remains the same at ~ 41 $Å^2$. Interestingly, the presence of drugs resulted in the increase in the surfactant and cosurfactant aggregation number for TD2d system (**Table 4.13**).

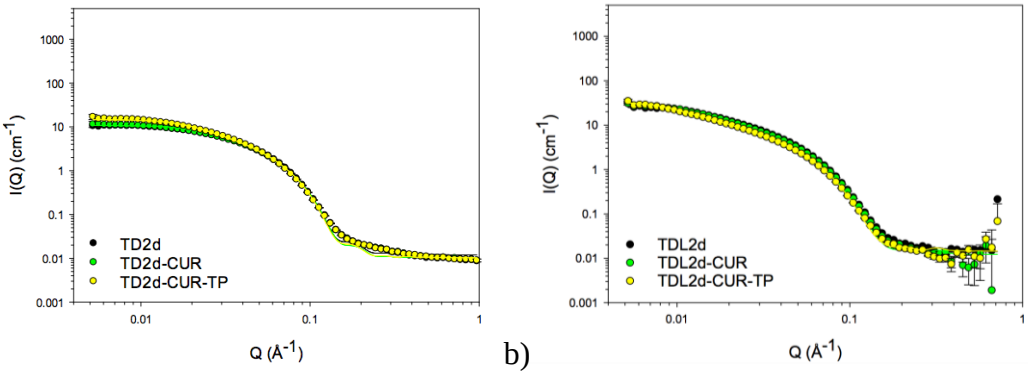

a) b)

Figure 4.21: SANS curve and 'best' fit to the data obtained for drop contrast of mixed micelles of 2 %w/w of a) Tween 80:Dermosoft GMCY (weight ratio 3:1) and b) Tween 80:Dermosoft GMCY:lecithin (weight ratio 7.5:2.5:1) in the absence and presence of drugs at 25 ˚C.

Table 4.15 Parameters obtained for the 'best' fit to the SANS data for 2 %w/w Tween 80:Dermosoft GMCY (weight ratio 3:1) and Tween 80:Dermosoft GMCY:lecithin (weight ratio 7.5:2.5:1) micelles in the presence of drugs at 25 °C using a core-shell ellipsoid model together with a hard sphere structure factor S(Q). The modelling of the SANS data was constrained using Vshell(dry)/Vcore.

sample	core equatorial radius (R_1,Å)	core axial ratio (x)	core axial radius (R_1x,Å)	shell thickness (Å)	minor radius (Å)	major radius (Å)	axial ratio (X)	micelle volume (Å^3)	sphere radius (Å)	Hydration (%)	N_{agg}	surfaces area of surfactant (Å^2)	sum of squared error (SSE)
TD2d-CUR	17.6	6.1	107.4	12.4	30.1	119.8	4.0	453691	124.1	15	443	42	4834
TD2d-CUR-TP	18.1	7.5	135.4	13.0	31.1	148.5	4.8	600891	154.3	15	586	41	3638
TDL2d-CUR	16.9	13.6	229.9	19.7	36.6	249.6	6.8	1399298	263.4	60	769	50	1410
TDL2d-CUR-TP	17.1	18.2	311.2	20.3	37.4	331.5	8.9	1943646	356.2	60	1068	49	774

Estimated uncertainty for R_1 of micelles in the presence of drug were ± 0.1 for TD2d and ± 0.5 for TDL2d, respectively.
Estimated uncertainty for x was ± 0.1.

The variation of the parameters obtained for the 'best' fit to the TDL2d system after the addition of either CUR or CUR and TP is shown in **Figure 4.21b** and **Table 4.15**. The core axial ratio of the mixed micelles of TDL2d-CUR increased from 11.0 Å for the TDL2d micelles to 13.6 Å in the presence of CUR with no change in the core equatorial radius, which remained constant at ~ 16.9-17.0 Å while the shell thickness was ~ 19.5-19.7 Å. An increase in the N_{agg} of surfactant and cosurfactant from 630 for TDL2d micelles to 769 for CUR-containing TDL2d micelles whereas the surface area of the surfactant remained constant at 50 $Å^2$. In addition, the addition of saturation amount of CUR and TP dramatically increased the core axial ratio from 11.0 for 'empty' TDL2d micelles to 18.2 for CUR and TP-containing TDL2d micelles with no difference in the core equatorial radius of either TDL2d or TDL2d-CUR-TP micelles, remaining constant at 17.1 Å for. In contrast, the shell thickness changed from 19.5 Å for TDL2d micelles to 20.3 Å for TDL2d-CUR-TP micelles with a corresponding large increase in N_{agg} to 1068, although the surface area of the surfactant of remained unchanged at 49 $Å^2$. Similar to the TD2d system, the presence of drug resulted in an increase in the N_T, N_D and N_L compared to empty micelles (**Table 4.13**). Schematic representations of the ellipsoid Tween 80 micelles, with and without cosurfactant, in the presence of drug are shown in **Figure 4.22**.

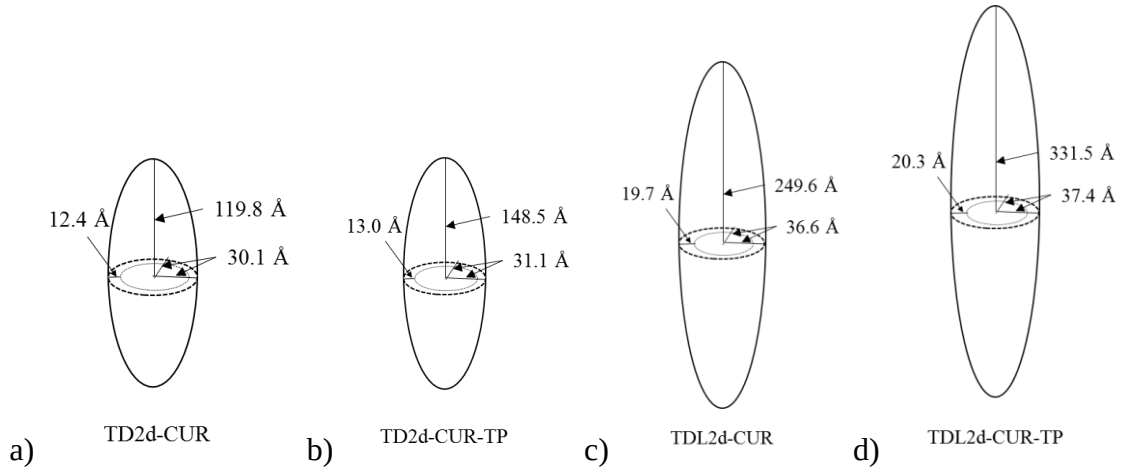

Figure 4.22: Schematic representation of the ellipsoidal 2 %w/w Tween 80:Dermosoft GMCY (weight ratio 3:1) micelle with either a) CUR or b) CUR and TP, and 2 %w/w Tween 80:Dermosoft GMCY:lecithin (weight ratio 7.5:2.5:1) micelle with either c) CUR or d) CUR and TP.

4.4.2 SANS studies of Tween 80 nanoemulsions containing triglyceride or ethyl ester and cosurfactant in the presence and absence of or drugs

A range of models was used to fit the drop contrast of TD2-98hEO NE at different concentrations of 98hEO in both the absence and presence of drugs. The resulting SANS data, along with the 'best' fits for the TD2-98hEO NE, fitted with core-shell ellipsoid model are shown in **Figure 4.23**, while **Table 4.16** shows the parameters obtained for the 'best' fits of SANS data.

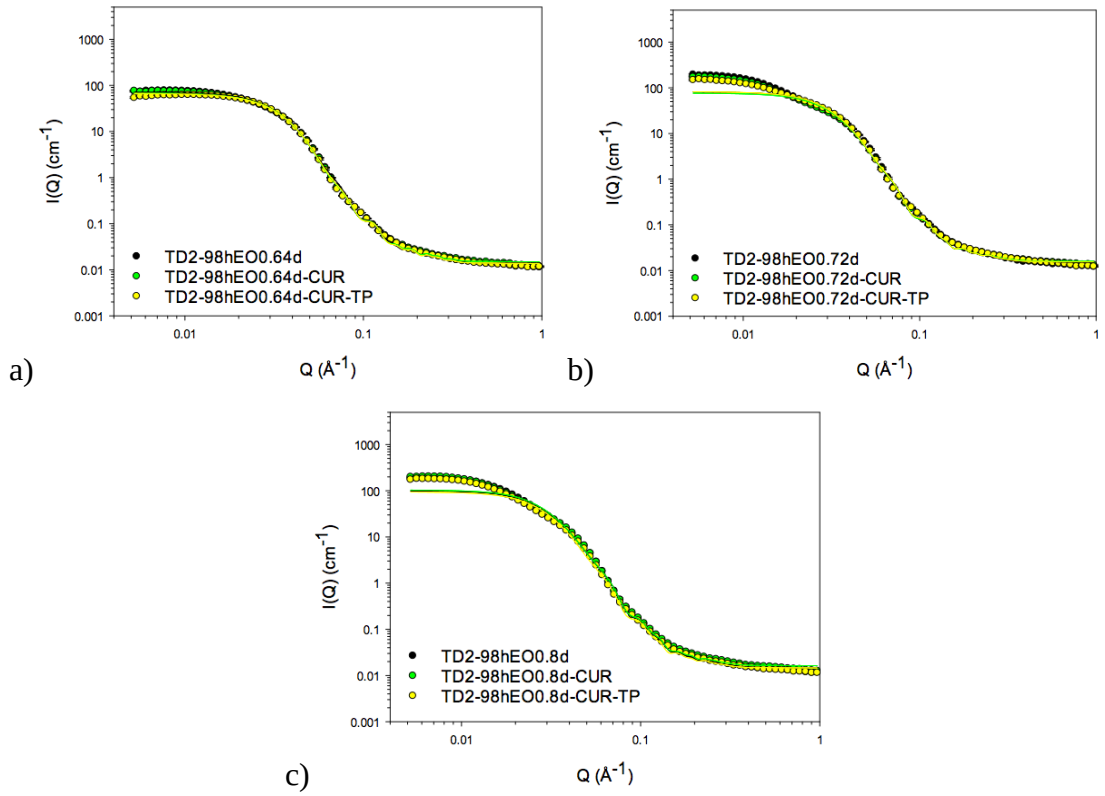

Figure 4.23: SANS data and 'best' fits using the oblate ellipsoid model for the drop contrast of NE prepared using 2 %w/w Tween 80:Dermosoft GMCY (weight ratio 3:1) and containing various concentrations of 98hEO from a) 0.6 %w/w, b) 0.72 %w/w and c) 0.8 %w/w in the absence and presence of drugs at 25 ˚C. Note that the best fits of TD2-98hEO0.72d and TD2-98hEO0.8d in the absence and presence of drug were not well fitted to SANS data at low Q.

The preparation of nanoemulsions with other nonionic surfactants in the absence and presence of cosurfactant.

Table 4.16 Individual SANS best fits results for 2 %w/w Tween 80:Dermosoft GMCY (weight ratio 3:1) and ethyl oleate nanoemulsions in the absence and presence of drug at 25 °C using a core-shell ellipsoid model together with a hard sphere structure factor S(Q). The data was constrained using Vshell(dry)/Vcore.

sample	core equatorial radius (R_1,Å)	core axial ratio (x)	core axial radius (R_1x,Å)	shell thickness (Å)	minor radius (Å)	major radius (Å)	axial ratio (X)	NE volume (Å^3)	sphere radius (Å)	hydration (%)	N_{agg}	surfaces area of surfactant (Å^2)	sum of squared error (SSE)
TD2-98hEO0.64d	63.0	0.3	21.6	23.9	86.9	45.4	0.5	1438156	95.9	15	999	50	85158
TD2-98hEO0.64d-CUR	60.6	0.4	23.0	24.1	84.7	47.2	0.6	1418259	92.4	15	985	49	63537
TD2-98hEO0.64d-CUR-TP	60.3	0.4	22.6	23.9	84.2	46.5	0.6	1381917	97.9	15	960	50	26343
TD2-98hEO0.72d	67.1	0.3	23.0	23.4	90.5	46.4	0.5	1589625	106.9	15	1070	52	375790
TD2-98hEO0.72d-CUR	67.4	0.3	22.3	23.1	90.5	45.4	0.5	1555576	105.0	15	1048	53	276400
TD2-98hEO0.72d-CUR-TP	67.7	0.3	22.6	23.3	91.0	45.9	0.5	1590893	105.2	15	1071	52	143490
TD2-98hEO0.8d	74.8	0.3	23.8	23.3	98.0	47.1	0.5	1897101	113.0	15	1240	52	222250
TD2-98hEO0.8d-CUR	75.8	0.3	23.8	23.4	99.2	47.2	0.5	1947306	116.4	15	1273	52	869860
TD2-98hEO0.8d-CUR-TP	75.7	0.3	25.0	24.0	99.7	49.0	0.5	2039364	116.0	15	1333	50	743900

Estimated uncertainty for R_1 of either 0.64, 0.72 or 0.8 %w/w 98hEO NE were ± 0.5, ± 1.5 or ± 2.0, respectively.
Estimated uncertainty for x were ± 0.02.

The results suggest that, as expected, no strong interaction exist between the droplets in the diluted NE system. It is worth noting, however, that the 'best' fits for TD2-98hEO0.72d and TD2-98hEO0.8d in the absence and presence of drug did not well fit to the SANS data at low Q. As expected, the core equatorial radius increased with increasing 98hEO content - being 63.0 Å for TD2-98hEO0.64d NE and 74.8 Å for TD2-98hEO0.8d NE. The increase in the core equatorial radius showed a similar trend to that seen for the hydrodynamic size assessed using PCS (**Table 4.7** in **section 4.2.4**) and is also in the agreement with that reported in the literature on the effect of oil on the aggregation properties of surfactant micelles. Similar trends have been previously reported by other researchers for both o/w and w/o ME (Baker et al., 1984; Attwood et al., 1992; Saint Ruth et al., 1995). After fitting SANS data for each NE with varying levels of shell hydration, a shell hydration of 15 % was found to fit TD2-98hEOd NE best. The thickness of the shell obtained from the best fits for the NE were in the range 23.1-24.1 Å. It was clear that the shape which provided the best fit to the SANS data was an ellipsoid. The axial ratio of the core suggested that the shape of TD2-98hEO NE was an oblate ellipsoid because the calculated core axial ratio was in the range 0.3-0.4. The shape of the NE droplets did not change as the oil content increased as indicated by the droplet axial ratio. This observation was not the trend suggested by the PIT result (**Table 4.6** in **section 4.2.3**) where the shape of TD25-98hEO NE droplets become more asymmetric with increasing 98hEO content. The increase in N_{agg} with increasing oil content probably encompass the increasing size of the oil core and this increase in N_{agg} was the cause of increase in N_T and N_D (**Table 4.17**).

Table 4.17 Number of surfactant and cosurfactant monomers comprising Tween 80 nanoemulsions in water in the presence of Dermosoft GMCY and/ or lecithin at 25 ˚C.

Composition	Ratio of surfactant: cosurfactant		Aggregate parameter			
	Weight ratio	Molar ratio	N_{agg}	N_T	N_D	N_L
TD2-98hEO0.64d	3:1	1:2	999	333	666	0
TD2-98hEO0.64d-CUR			985	328	657	0
TD2-98hEO0.64d-CUR-TP			960	320	640	0
TD2-98hEO0.72d			1070	357	713	0
TD2-98hEO0.72d-CUR			1048	349	699	0
TD2-98hEO0.72d-CUR-TP			1071	357	714	0
TD2-98hEO0.8d			1240	413	827	0
TD2-98hEO0.8d-CUR			1273	424	849	0
TD2-98hEO0.8d-CUR-TP			1333	444	889	0
TDL2-hSBO0.24d	7.5:2.5:1	4.4:8.8:1	369	114	229	26
TDL2-hSBO0.24d-CUR			368	114	228	26
TDL2-hSBO0.24d-CUR-TP			440	136	273	31

N_{agg}, N_T, N_D and N_L are the total aggregation number, Tween 80, Dermosoft GMCY and lecithin aggregation number respectively.

In the presence of a saturation amount of drug, either CUR or CUR and TP, it was clear that the size and shape of TD2-98hEO NE did not change. The observation from the SANS data that there was no change in the size of the TD2-98hEO-CUR NE droplets was not in the agreement with the PCS data which indicated that TD25-98hEO8-CUR NE were larger than TD25-98hEO8 NE (**Figure 4.9**). The PIT results suggested the TD25-98hEO-CUR NE droplets became more spherical as the amount of 98hEO incorporated increased, however the SANS data did not show the same trend (**Figure 4.6 and 4.11**). Moreover, no change in the N_{agg}, N_T or N_D was seen (**Table 4.17**) while the fitting results for drug-saturated NE imply that the level of solubilisation of CUR or CUR and TP was not enough to cause the change in head group region - believed to be the main locus of solubilisation leading to no change in the size, shape and aggregation number of NE. Schematic representations of the, Region A, TD2-98hEO NE, in the absence and presence of drug, is shown in **Figure 4.24**.

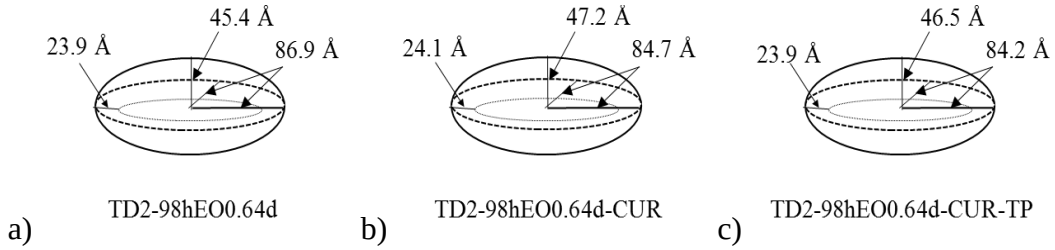

Figure 4.24: Schematic of the ellipsoidal 2 %w/w Tween 80:Dermosoft GMCY (weight ratio 3:1) NE containing 0.64 %w/w 98hEO with a) no drug, b) CUR and c) CUR and TP in D_2O.

After a range of shapes were used to fit the drop contrast of TDL2-hSBO0.24 NE in the absence and presence of drugs, the SANS data and best fits to the SANS data for TDL2-hSBO0.24 NE using a core-shell ellipsoid model are shown in **Figure 4.25** and **Table 4.18**. The results suggest that, as expected, no strong interaction existed between the droplets in the diluted NE system. It is worth noting that the SANS data was not well fitted at low Q. The core equatorial radius of 32.2 Å was for TDL2-hSBO0.24d NE and the axial ratio of the core of 0.3 suggested that the shape of TDL2-hSBO0.24d NE were oblate ellipsoid. After fitting the SANS data using various levels of shell hydration for each NE sample, a shell hydration of 25% for the TDL2-hSBO0.24d NE was found to produce the best fit to SANS data. The thickness of the shell under these conditions was found to be 25.7 Å. It was clear that the model which provided the best fit to the SANS data was that of an ellipsoid.

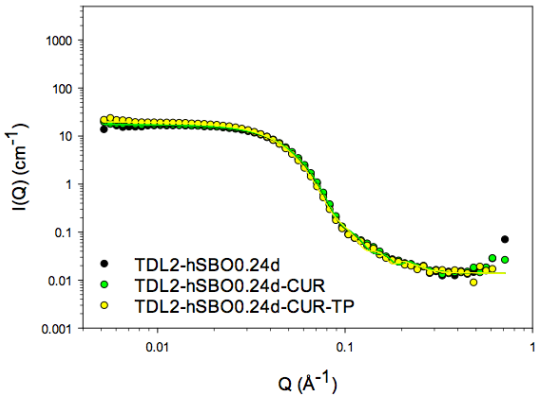

Figure 4.25: SANS data and 'best' fits using the oblate ellipsoid model for the drop contrast of 2 %w/w Tween 80:Dermosoft GMCY:lecithin (weight ratio 7.5:2.5:1) NE containing the upper limit of hSBO incorporated into Region A in the absence and presence of drugs at 25 °C. Note that the best fits of TDL2-hSBO0.24d in the absence and presence of drug were not well fitted to SANS data at low Q.

The preparation of nanoemulsions with other nonionic surfactants in the absence and presence of cosurfactant.

Table 4.18 Individual SANS best fits results for 2 %w/w Tween 80:Dermosoft GMCY (weight ratio 3:1) and soybean oil nanoemulsions in the absence and presence of drug at 25 °C using a core-shell ellipsoid model together with a hard sphere structure factor S(Q). The data was constrained using Vshell(dry)/Vcore.

sample	core equatorial radius (R_1,Å)	core axial ratio (x)	core axial radius (R_1x,Å)	shell thickness (Å)	minor radius (Å)	major radius (Å)	axial ratio (X)	NE volume (Å^3)	sphere radius (Å)	hydration (%)	N_{agg}	surfaces area of surfactant (Å^2)	sum of squared error (SSE)
TDL2-hSBO0.24d	32.2	0.3	10.7	25.7	57.9	36.3	0.6	510430	65.9	25	369	50	1074
TDL2-hSBO0.24d-CUR	32.3	0.3	10.6	25.6	57.9	36.2	0.6	508375	66.4	25	368	50	957
TDL2-hSBO0.24d-CUR-TP	35.7	0.3	10.4	26.8	62.5	37.2	0.6	607910	65.0	25	440	47	1463

Estimated uncertainty for R_1 and x were ± 0.2 and ± 0.01, respectively

In the presence of a saturation amount of drug, either CUR or CUR and TP, it was clear that neither the size, shape, N_{agg}, N_T, N_D nor N_L of the TDL2-hSBO0.24d-CUR NE changed. In contrast, those of TDL2-hSBO0.24d-CUR-TP NE because larger with an increase in the core equatorial from 32.2 Å for TDL2-hSBO0.24d NE to 35.7 Å for TDL2-hSBO0.24d-CUR-TP NE (**Table 4.17** and **4.18**). This SANS result suggests that the solubilisation of a saturation amount of CUR and TP caused the increase in size and aggregation of NE. A schematic representation of the Region A, TDL2-hSBO0.24d NE in the absence and presence of drugs is shown in **Figure 4.26**.

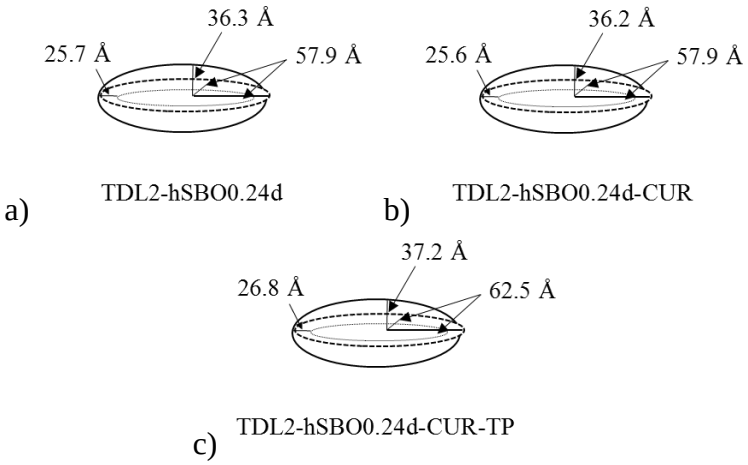

Figure 4.26: Schematic of the ellipsoidal 2 %w/w Tween 80:Dermosoft GMCY:lecithin (weight ratio 7.5:2.5:1) NE containing 0.24 %w/w hSBO with a) no drug, b) CUR and c) CUR and TP.

4.4.3 Effect of temperature on Tween 80 nanoemulsions in the present of cosurfactant and in the absence and presence of drug

It is essential to understand the effect of temperature and in particular the temperature of 37 °C (i.e. body temperature and the temperature of the cytotoxicity experiment) on the structure of NE containing hSBO or 98hEO as the disperse phase and the nonionic surfactant, Tween 80 alone or in the presence of cosurfactant with or without a second surfactant in order to successfully use the NE as vehicles for the delivery of drugs such as anticancer agents as well as being able to test their cytotoxicity using cell culture. Zielinski et al. (1995) reported that no change occurred in the structure of nonionic surfactant micelles formed by $C_{12}E_6$ over the temperature range of 25-31 °C when examined by SANS. In contrast, there was a 10% decrease in the size of SDS anionic micelles and a 10% increase in size of the $C_{12}E_{10}$, nonionic micelles over the

temperature range 30 to 75 °C when measured by SANS. The SANS data of $C_{12}E_{10}$ exhibited a weak correlation peak, which shifted to smaller Q values in conjunction with an increase in the scattering cross-section upon increasing the temperature (Aswal and Wagh, 2008). Therefore, it is worth performing a SANS experiment to determine the effect of temperature on the physico-chemical properties of the Brij O10 NE. The insight provided by such a study should provide a better understanding of the potential of Tween 80-stabilised NE in the absence and presence of cosurfactant as vehicles for drug delivery.

A range of models (form factors) were used to attempt to fit the drop contrast of TD2d and TDL2d micelles in the absence and presence of drugs at 37 °C. The SANS data along with the 'best' fits obtained for the TD2d and TDL2d micelles using a core-shell ellipsoid model are shown in **Figures 4.27-4.28** while **Table 4.19** shows the parameters used to obtain the best fits to SANS data.

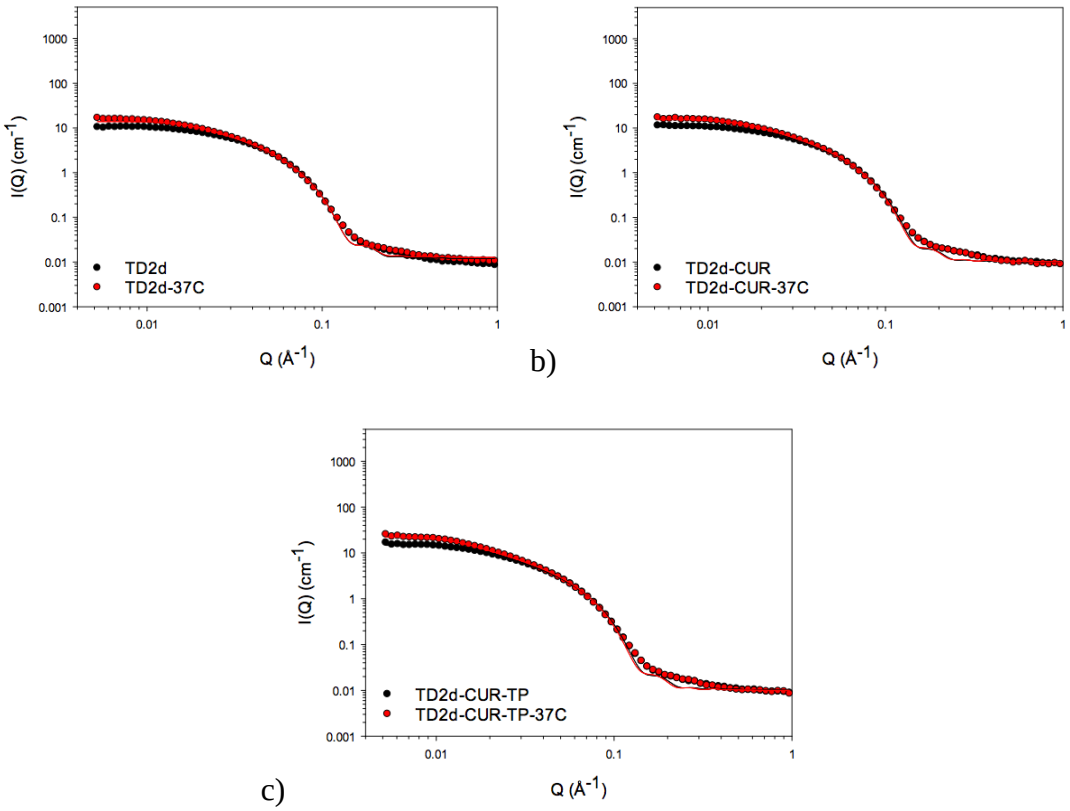

Figure 4.27: SANS data and best fits to the drop contrast for 2 %w/w Tween 80:Dermosoft GMCY (weight ratio of 3:1) micelles with and without the presence of drug at 25 and 37 ˚C.

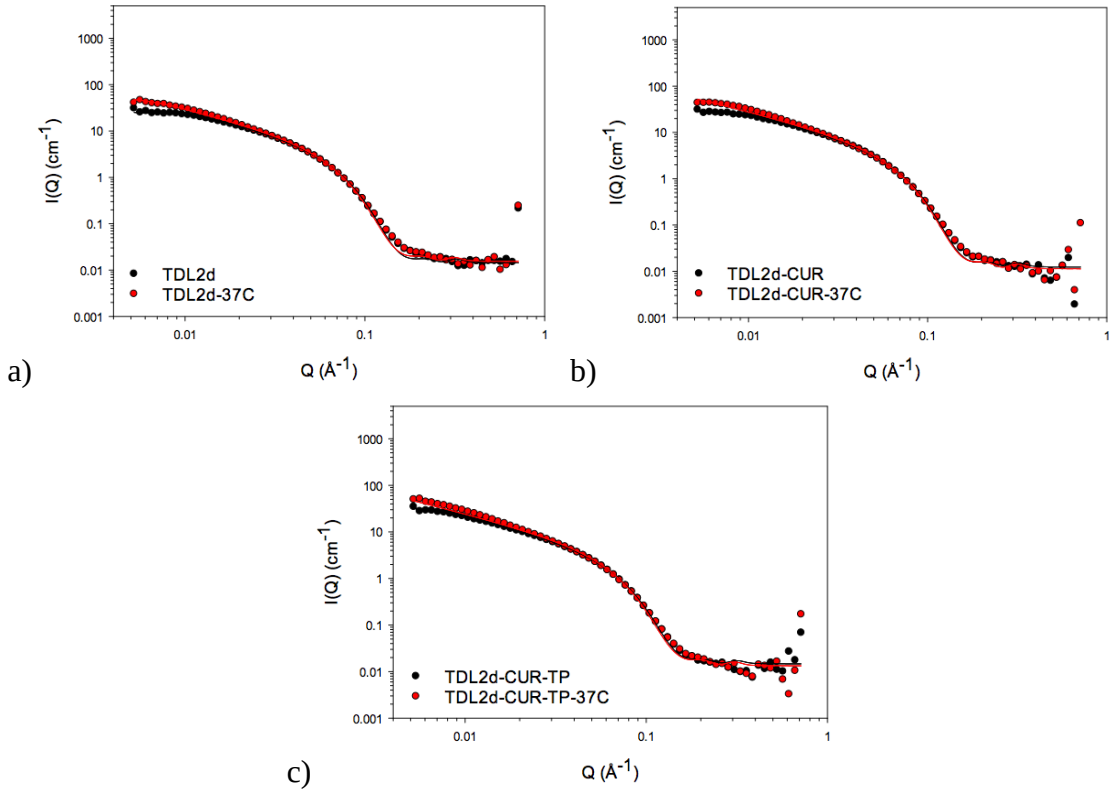

Figure 4.28: SANS data and best fits to the drop contrast for 2 %w/w Tween 80:Dermosoft GMCY:lecithin (weight ratio of 7.5:2.5:1) micelles with and without the presence of drug at 25 and 37 ˚C.

Table 4.19 Parameters used for the best fits to the individual SANS data for 2 %w/w Tween 80:Dermosoft GMCY (weight ratio 3:1) and Tween 80:Dermosoft GMCY:lecithin (weight ratio 7.5:2.5:1) micelles in the absence and presence of drug using a core-shell ellipsoid model together with a hard sphere structure factor S(Q) at 37 ˚C. The modelling of the SANS data was constrained using Vshell(dry)/Vcore.

sample	core equatorial radius (R_1,Å)	core axial ratio (x)	core axial radius (R_1x,Å)	shell thickness (Å)	minor radius (Å)	major radius (Å)	axial ratio (X)	NE volume (Å^3)	sphere radius (Å)	hydration (%)	N_{agg}	surfaces area of surfactant (Å^2)	sum of squared error (SSE)
TD2d-37C	18.1	7.0	126.1	12.9	31.0	139.1	4.5	560233	159.2	15	547	41	6309
TD2d-CUR-37C	18.0	8.2	147.2	13.1	31.1	160.3	5.2	647791	168.3	15	632	41	7313
TD2d-CUR-TP-37C	18.5	10.5	194.8	13.7	32.3	208.5	6.5	910367	215.6	15	888	40	10821
TDL2d-37C	17.3	21.4	369.8	20.7	38.0	390.5	10.3	2357829	400.1	60	1295	48	4122
TDL2d-CUR-37C	17.1	30.3	517.3	20.7	37.8	538.0	14.2	3221874	540.5	60	1770	49	5915
TDL2d-CUR-TP-37C	17.5	51.6	900.7	21.5	38.9	922.1	23.7	5859295	930.2	60	3219	48	5978

Estimated uncertainty for R_1 were ± 0.1.
Estimated uncertainty for x of either TD2d or TDL2d in the absence and presence of drugs were ± 0.1 or 0.5, respectively.

As can be seen from the parameters used to fit the micelles, there were only small differences in both the core equatorial radius and shell thickness but large differences in the shape of micelle at temperatures of 25 and 37 °C in both drug-free and drug-containing micelles. For example, the axial ratio of TD2d micelles was 5.4 at 25 ˚C but increased to 7.0 at 37 ˚C. Moreover, the change in the shape of the micelle in the presence of cosurfactant or cosurfactant and a second surfactant at 37 ˚C was due to an increase in the N_{agg} of micelle was due to an increase in both N_T and N_D for TD2d micelles and N_T, N_D and N_L for TDL2d micelles (**Table 4.20**).

Table 4.20 Number of surfactant and cosurfactant monomers comprising Tween 80 micelles in the presence of Dermosoft GMCY or Dermosoft GMCY and lecithin at 37 ˚C.

Composition	Ratio of surfactant: cosurfactant		Aggregate parameter			
	Weight ratio	Molar ratio	N_{agg}	N_T	N_D	N_L
TD2d-37C	3:1	1:2	547	182	365	0
TD2d-CUR-37C			632	211	421	0
TD2d-CUR-TP-37C			888	296	592	0
TDL2d-37C	7.5:2.5:1	4.4:8.8:1	1295	401	803	91
TDL2d-CUR-37C			1770	548	1097	125
TDL2d-CUR-TP-37C			3219	997	1994	227

N_{agg}, N_T, N_D and N_L are the total aggregation number, Tween 80, Dermosoft GMCY and lecithin aggregation number respectively.

This change in the shape of the TD2d and TDL2d micelles is in line with the decrease in the CP of the TD2d and TDL2d micelles. Fortunately the CP of the TD2d and TDL2d micelles were around 60 ˚C, ~ 30 ˚C higher than body temperature. The micelles in the presence of CUR and TP at 37 ˚C exhibited the biggest change in the shape of the micelles because the lowering in CP of micelles. For example, the CP of TD2d-CUR-TP at 25 ˚C was around 55 ˚C which was the lower CP than TD2d micelle in the absence and presence of CUR which occurred the CP at 60 ˚C (**Table 4.6, Figures 4.6 and 4.11**). Unfortunately, the CP of TDL2d-CUR-TP was not performed but it was expected that the CP of TDL2d-CUR-TP would decrease due to the presence of CUR and TP.

When fitting the SANS data for TD2d NE, a range of models were explored to individually fit the drop contrast of TD2-98hEO NE at either 0.64 or 0.8 %w/w 98hEO in the absence and presence of drugs at 37 °C. The best fits to the SANS data for TD2-98hEO where obtained when fitted using a core-shell ellipsoid model (shown in **Figures 4.29-4.30**).

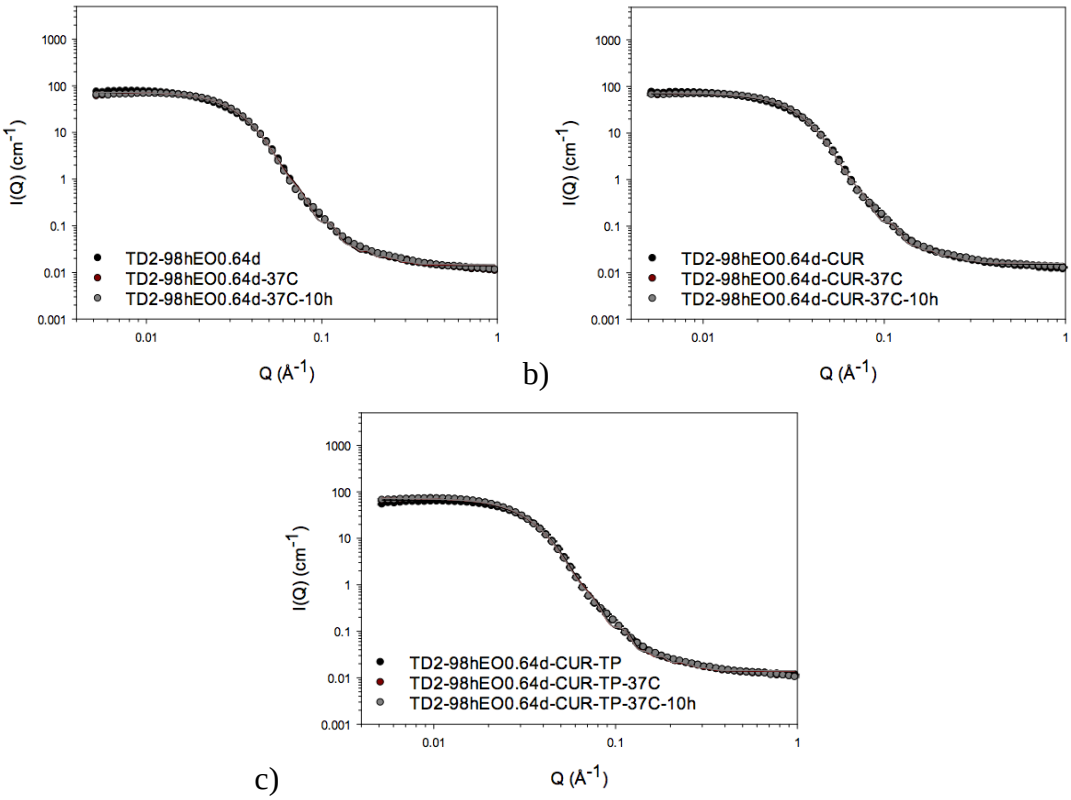

Figure 4.29: SANS data and best fits to the drop contrast for 2 %w/w Tween 80:Dermosoft GMCY (weight ratio 3:1) containing 0.64 %w/w 98hEO with and without the presence of drug at 25 and 37 ˚C.

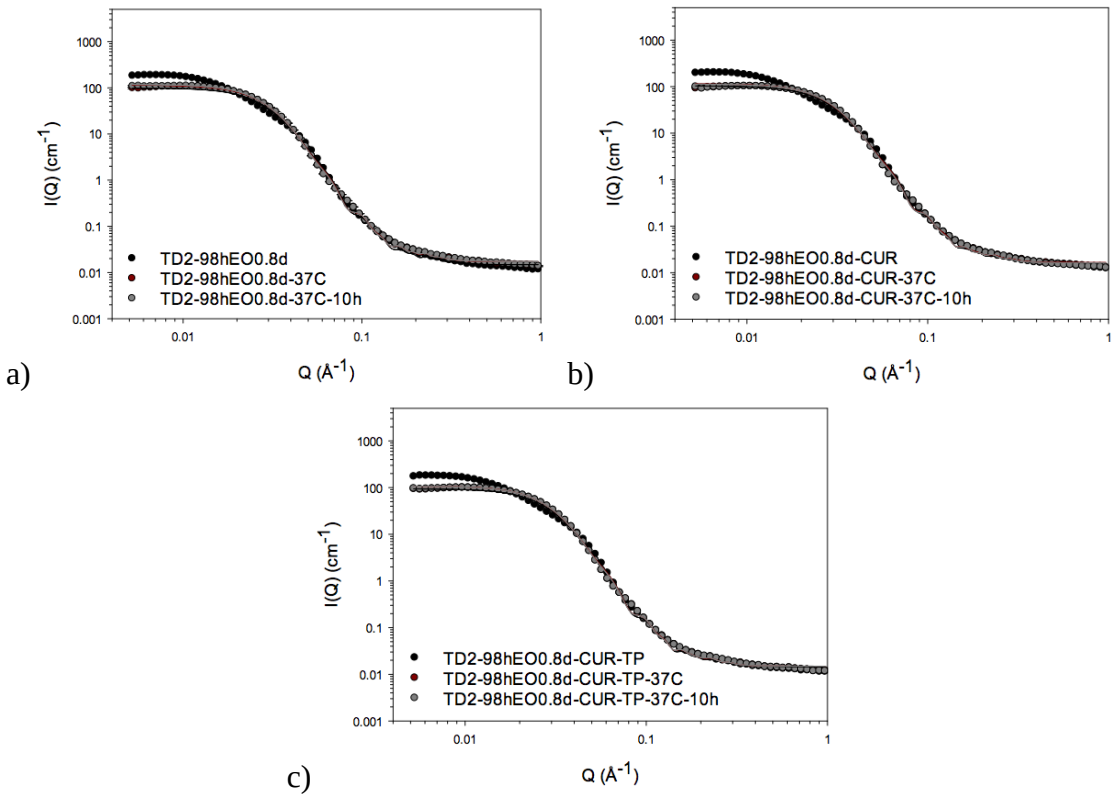

Figure 4.30: SANS data and best fits to the drop contrast for 2 %w/w Tween 80:Dermosoft GMCY (weight ratio 3:1) containing 0.8 %w/w 98hEO with and without the presence of drug at 25 and 37 ˚C.

Table 4.21 shows the parameters used for the best fits. It was clear from the fitting parameters that no difference in shape and/or size of TD2-98hEO0.64d-37C NE was observed in the absence and presence of drug at either 25 or 37 °C or even when the NE was stored at 37 °C for 10 hours, correspondingly the N_{agg} of TD2-98hEO0.64d-37C without drug and with drugs did not change (**Table 4.22**).

Table 4.21 Parameters used for the best fits to the individual SANS data for 2 %w/w Tween 80:Dermosoft GMCY (weight ratio 3:1) and 98hEO nanoemulsions in the absence and presence of drug using a core-shell ellipsoid model together with a hard sphere structure factor S(Q) at 37 ˚C. The modelling of the SANS data was constrained using Vshell(dry)/Vcore.

sample	core equatorial radius (R_1,Å)	core axial ratio (x)	core axial radius (R_1x,Å)	shell thickness (Å)	minor radius (Å)	major radius (Å)	axial ratio (X)	NE volume (Å^3)	sphere radius (Å)	hydration (%)	N_{agg}	surfaces area of surfactant (Å^2)	sum of squared error (SSE)
TD2-98hEO0.64d-37C-t0	61.5	0.4	22.4	24.0	85.5	46.4	0.5	1423209	99.8	15	988	49	16158
TD2-98hEO0.64d-37C-10h	61.4	0.4	22.8	24.2	85.6	47.0	0.5	1443940	93.9	15	1003	49	13918
TD2-98hEO0.64d-CUR-37C-t0	61.1	0.4	23.2	24.3	85.4	47.5	0.6	1451671	94.4	15	1008	48	11423
TD2-98hEO0.64d-CUR-37C-10h	61.1	0.4	23.3	24.4	85.4	47.7	0.6	1458163	92.3	15	1013	48	11859
TD2-98hEO0.64d-CUR-TP-37C-t0	62.3	0.4	23.1	24.5	86.8	47.6	0.5	1503500	97.5	15	1044	48	14657
TD2-98hEO0.64d-CUR-TP-37C-10h	61.5	0.4	23.6	24.6	86.1	48.2	0.6	1496906	99.2	15	1039	48	14110
TD2-98hEO0.8d-37C-t0	74.4	0.3	25.8	24.2	98.6	49.9	0.5	2034913	111.4	15	1330	49	29339
TD2-98hEO0.8d-37C-10h	74.3	0.4	26.4	24.4	98.8	50.8	0.5	2077701	117.7	15	1358	48	28479
TD2-98hEO0.8d-CUR-37C-t0	76.5	0.3	24.9	24.1	100.5	49.0	0.5	2074395	115.9	15	1356	50	56207
TD2-98hEO0.8d-CUR-37C-10h	74.7	0.3	25.8	24.2	99.0	50.0	0.5	2054002	113.3	15	1343	49	36880
TD2-98hEO0.8d-CUR-TP-37C-t0	76.7	0.3	25.8	24.6	101.3	50.4	0.5	2167841	119.1	15	1417	48	37524
TD2-98hEO0.8d-CUR-TP-37C-10h	76.3	0.3	26.4	24.8	101.0	51.1	0.5	2186670	113.1	15	1429	48	31077

Estimated uncertainty for R_1 and x were ± 0.5 and ± 0.01, respectively.

Table 4.22 Number of surfactant and cosurfactant monomers comprising Tween 80 micelles in water in the presence of Dermosoft GMCY and/ or lecithin at 37 ˚C.

Composition	Ratio of surfactant: cosurfactant		Aggregate parameter			
	Weight ratio	Molar ratio	N_{agg}	N_T	N_D	N_L
TD2-98hEO0.64d-37C-t0	3:1	1:2	988	329	659	0
TD2-98hEO0.64d-37C-10h			1003	334	669	0
TD2-98hEO0.64d-CUR-37C-t0			1008	336	672	0
TD2-98hEO0.64d-CUR-37C-10h			1013	338	675	0
TD2-98hEO0.64d-CUR-TP-37C-t0			1044	348	696	0
TD2-98hEO0.64d-CUR-TP-37C-10h			1039	346	693	0
TD2-98hEO0.64d-CUR-TP-DM-37C-t0			984	328	656	0
TD2-98hEO0.64d-CUR-TP-DM-37C-2.5h			990	330	660	0
TD2-98hEO0.64d-CUR-TP-DM-37C-6h			1021	340	681	0
TD2-98hEO0.64d-CUR-TP-DM-37C-12h			1023	341	682	0
TD2-98hEO0.8d-37C-t0			1330	443	887	0
TD2-98hEO0.8d-37C-10h			1358	453	905	0
TD2-98hEO0.8d-CUR-37C-t0			1356	452	904	0
TD2-98hEO0.8d-CUR-37C-10h			1343	448	895	0
TD2-98hEO0.8d-CUR-TP-37C-t0			1417	472	945	0
TD2-98hEO0.8d-CUR-TP-37C-10h			1429	476	953	0
TDL2-hSBO0.24d-37C	7.5:2.5:1	4.4:8.8:1	385	119	239	27
TDL2-hSBO0.24d-CUR-37C			399	124	247	28
TDL2-hSBO0.24d-CUR-TP-37C			465	144	288	33

N_{agg}, N_T, N_D and N_L are the total aggregation number, Tween 80, Dermosoft GMCY and lecithin aggregation number, respectively.

On the other hand, a lower intensity of scattering was observed for TD2-98hEO0.8d-37C at both time zero and ten hours of storage at 37 °C, regardless of the absence or presence of drug (**Figure 4.30**). Interestingly however, the values of the parameters used for fitting did not show any change in the size and shape of the NE (**Tables 4.16 and 4.21**), largely because the SANS data of samples at 25 °C were not well fitted at low Q. Interestingly, the N_{agg} of TD2-98hEO0.8d-37C without and with drugs (**Table 4.22**) increase compared to TD2-98hEO0.8d in the absence and presence of drugs at 25 °C (**Table 4.17**) which can be explained that the TD2-98hEO0.8d NE were on the boundary of Region A which tended to be easily altered.

As with the other NE studies, a range of models were used to fit the SANS data for the drop contrast of TDL2-hSBO0.24d NE in the absence and presence of drug at 37 °C. The 'best fit' to the SANS data of TDL2-hSBO0.24d NE at 25 and 37 °C were obtained using a core-shell ellipsoid model (**Figure 4.31**). **Table 4.23** gives the parameters used to obtain these best fits. From these results it was clear that there was no difference in shape and/or size of the TDL2-hSO0.24d-37C NE in the absence and presence of drug either at 25 or 37 °C, or even 10 hours storage of the samples at 37 °C. This result suggests that all of TDL2-hSBO0.24d NE system were stable on change in temperature. Note however the N_{agg} of TDL2-hSBO0.24d-37C NE slightly increased compared to TDL2-hSBO0.24d in the absence and presence of drugs due to an increase in N_D (**Tables 4.17 and 4.20**). In the absence of drug, N_{agg} of TDL2-hSBO0.24d-37C NE slightly increased from 369 for TDL2-hSBO0.24d to 385 for TDL2-hSBO0.24d-37C NE.

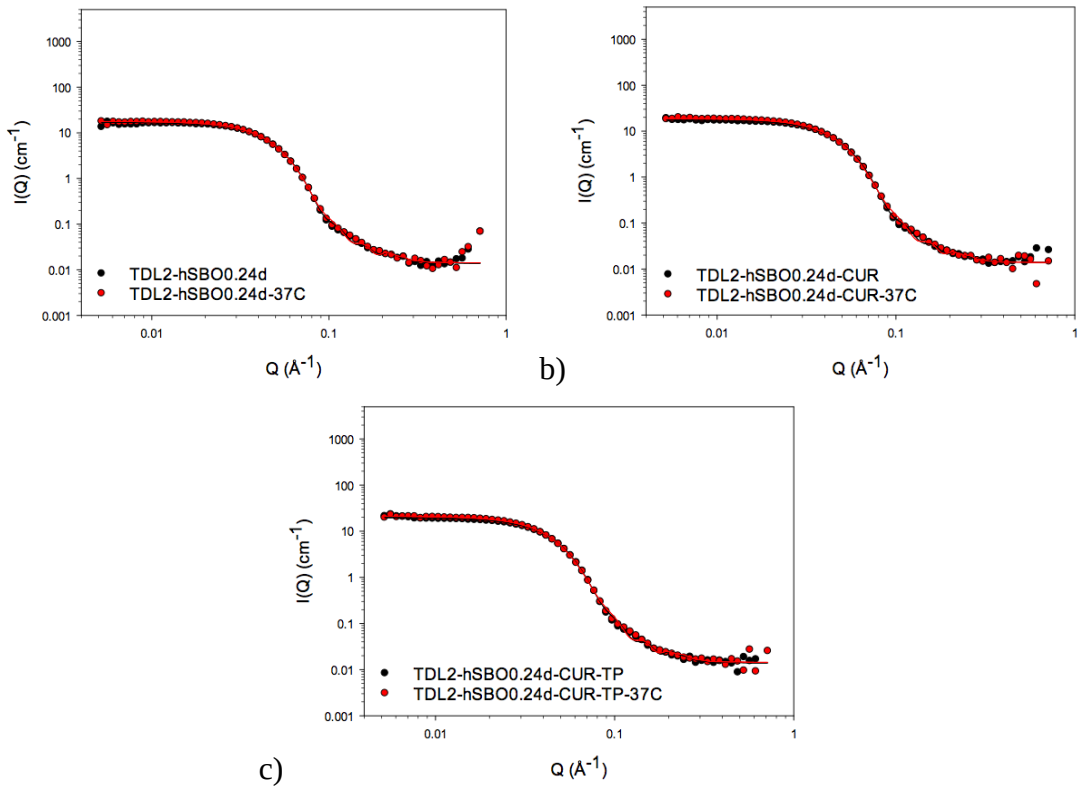

Figure 4.31: SANS data and best fits to the drop contrast for 2 %w/w Tween 80:Dermosoft GMCY:lecithin (weight ratio 7.5:2.5:1) containing 0.24 %w/w hSBO with and without the presence of drugs at 25 and 37 ˚C.

The preparation of nanoemulsions with other nonionic surfactants in the absence and presence of cosurfactant.

Table 4.23 Parameters used for the best fits to the individual SANS data for 2 %w/w Tween 80:Dermosoft GMCY:lecithin (weight ratio 7.5:2.5:1) and hSBO nanoemulsions in the absence and presence of drug using a core-shell ellipsoid model together with a hard sphere structure factor S(Q) at 37 ˚C. The modelling of the SANS data was constrained using Vshell(dry)/Vcore.

sample	core equatorial radius (R_1,Å)	core axial ratio (x)	core axial radius (R_1x,Å)	shell thickness (Å)	minor radius (Å)	major radius (Å)	axial ratio (X)	NE volume (Å^3)	sphere radius (Å)	hydration (%)	N_{agg}	surfaces area of surfactant (Å^2)	sum of squared error (SSE)
TDL2-hSBO0.24d-37C	34.0	0.3	10.0	25.7	59.7	35.7	0.6	532524	63.4	25	385	50	1321
TDL2-hSBO0.24d-CUR-37C	35.5	0.3	9.5	25.7	61.2	35.2	0.6	551666	64.5	25	399	51	1966
TDL2-hSBO0.24d-CUR-TP-37C	37.7	0.3	9.8	26.9	64.6	36.7	0.6	642982	66.9	25	465	47	2197

Estimated uncertainty for R_1 and x were ± 0.25 and ± 0.01, respectively.

4.4.4 Effect of cell culture media on Tween 80 nanoemulsions in the presence of cosurfactant in the absence and presence of drug

It is essential to understand the effect of plasma proteins, which are present in the bloodstream and cell culture media, on the structure of the NE, in order to best use the TD2-98hEO NE and TDL2-hSBO NE as vehicles for the delivery of therapeutic agents including anticancer agents and to test their cytotoxicity in cell culture. For example, the addition of either the anionic surfactant SDS or the cationic surfactant CTAB to the protein, bovine serum albumin (BSA) has been shown to result in its binding to the protein, causing a change in the size and structure of protein (Chodankar et al., 2007; Gull et al., 2008; Gull et al., 2009).

Although using light scattering to observe any changes in the physical properties of the NE in the presence of electrolyte and plasma proteins is theoretically possible, the wavelength of light (~ 500 nm) compared to the size (< 20 nm) of the NE droplets means that it will only be possible to detect changes in the whole system without being able to attribute these changes are due to changes in shape and/or size of the NE (and/or protein). Moreover, the light scattering experiments are more complicated in the presence of plasma proteins, which themselves scatter light, resulting in serious complications in the analysis of particle size. It is therefore essential to determine the effect of serum on the NE using SANS if the NE are to be used successfully as delivery vehicles intended for the intravenous administration. The aim of this part of the study was therefore to use SANS to determine the influence of the presence of plasma proteins on the physico-chemical properties of the TD2-98hEO and TDL2-hSBO NE. Significantly, it is possible to design a SANS study using contrast variation to make the proteins ‘invisible’ to the neutrons allowing only the behaviour of the NE to be observed. Fortunately in the present study, however, the cell culture media did not exhibit any scattering above that of it as a solvent, so it was not necessary to perform a contrast match study. Such a study should provide a better knowledge of the potential of cosurfactant-stabilised Tween 80 NE as vehicles for drug delivery.

A range of models were used in order to try and fit the drop contrast of TD2-98hEO0.64d and TD2-98hEO0.8d NE alone or with drugs in the presence of cell culture media at 37 °C overtime. The SANS data for the TD2-98hEO0.64d and TD2-98hEO0.8d NE, along with the best fits to the data, which were obtained using the core-shell ellipsoid model, are shown in **Figures 4.32-4.33**.

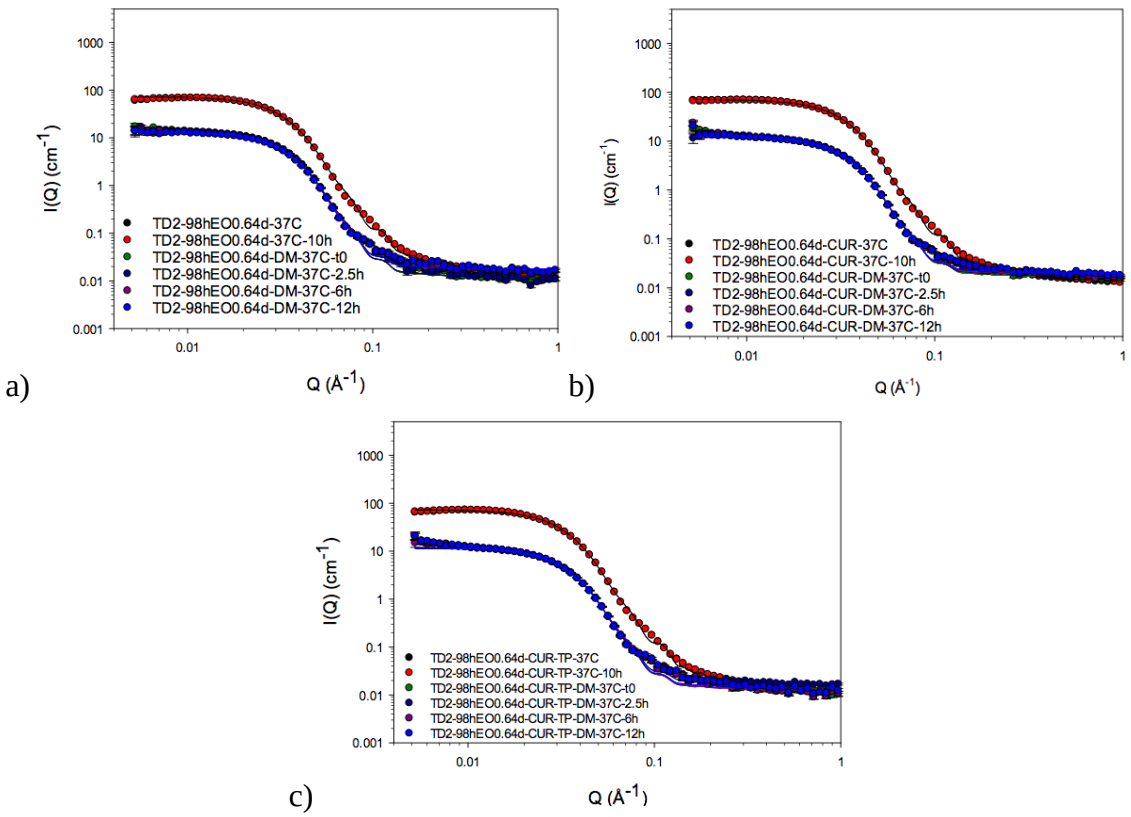

Figure 4.32: SANS data and best fits to the drop contrast for 2 %w/w Tween 80:Dermosoft GMCY (weight ratio 3:1) containing 0.64 %w/w 98hEO with and without drugs in the absence and presence of cell culture media (1:1 volume ratio) at 37 ˚C.

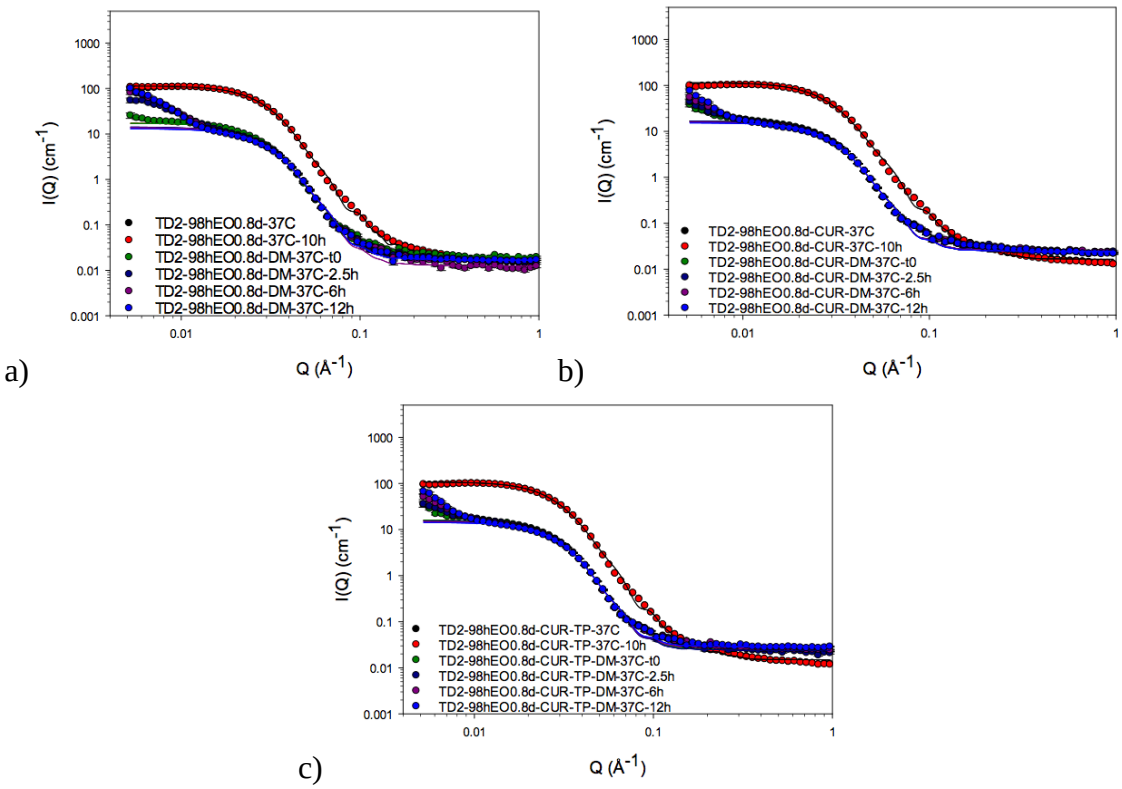

Figure 4.33: SANS data and best fits to the drop contrast for 2 %w/w Tween 80:Dermosoft GMCY (weight ratio 3:1) containing 0.8 %w/w 98hEO with and without drugs in the absence and presence of cell culture media (1:1 volume ratio) at 37 ˚C.

Tables 4.24-4.25 show the parameters obtained from the best fits to the SANS data. As can be seen from the fitting parameters, the SANS results obtained for the TD2-98hEO-DM-37C NE exhibited a lower scattering intensity than the NE dispersed in D_2O, due to the fact that cell culture media-added samples contained H_2O, which has a lower scattering density than D_2O and therefore reduces the overall scattering of the NE. Note that the intensity of scattering is a function of the square of the difference in the SLD between the scattering particles and the solvent.

Table 4.24 Parameters used for the best fits to the individual SANS data for 2 %w/w Tween 80:Dermosoft GMCY (weight ratio 3:1) and 0.64 %w/w 98hEO nanoemulsions in the absence and presence of drug and cell culture media using a core-shell ellipsoid model together with a hard sphere structure factor S(Q) at 37 ºC. The modelling of the SANS data was constrained using Vshell(dry)/Vcore.

sample	core equatorial radius (R_1,Å)	core axial ratio (x)	core axial radius (R_1x,Å)	shell thickness (Å)	minor radius (Å)	major radius (Å)	axial ratio (X)	NE volume (Å^3)	sphere radius (Å)	hydration (%)	N_{agg}	surfaces area of surfactant (Å^2)	sum of squared error (SSE)
TD2-98hEO0.64d-DM-37C-t0	60.4	0.4	22.4	23.8	84.1	46.1	0.5	1368160	94.3	15	950	50	797
TD2-98hEO0.64d-DM-37C-2.5h	60.9	0.4	21.8	23.6	84.5	45.4	0.5	1359423	92.6	15	944	51	577
TD2-98hEO0.64d-DM-37C-6h	60.7	0.4	22.0	23.6	84.4	45.7	0.5	1362515	96.1	15	946	51	472
TD2-98hEO0.64d-DM-37C-12h	59.5	0.4	22.9	23.8	83.4	46.7	0.6	1360527	95.9	15	945	50	267
TD2-98hEO0.64d-CUR-DM-37C-t0	59.8	0.4	22.7	23.8	83.5	46.5	0.6	1358969	88.4	15	944	50	400
TD2-98hEO0.64d-CUR-DM-37C-2.5h	60.6	0.4	22.8	24.0	84.6	46.8	0.6	1401722	88.3	15	973	49	536
TD2-98hEO0.64d-CUR-DM-37C-6h	60.6	0.4	22.4	23.8	84.4	46.2	0.5	1377242	89.6	15	956	50	413
TD2-98hEO0.64d-CUR-DM-37C-12h	60.9	0.4	22.6	24.0	84.8	46.6	0.5	1406532	88.7	15	977	49	318
TD2-98hEO0.64d-CUR-TP-DM-37C-t0	60.1	0.4	23.3	24.2	84.3	47.5	0.6	1416760	96.4	15	984	49	593
TD2-98hEO0.64d-CUR-TP-DM-37C-2.5h	60.1	0.4	23.5	24.3	84.4	47.7	0.6	1425143	93.4	15	990	48	567
TD2-98hEO0.64d-CUR-TP-DM-37C-6h	63.1	0.3	22.0	24.1	87.2	46.1	0.5	1469705	97.8	15	1021	49	684
TD2-98hEO0.64d-CUR-TP-DM-37C-12h	62.1	0.4	22.8	24.3	86.4	47.1	0.5	1472745	91.0	15	1023	49	467

Estimated uncertainty for R_1 and x were ± 0.4 and ± 0.01, respectively.

Table 4.25 Parameters used for the best fits to the individual SANS data for 2 %w/w Tween 80:Dermosoft GMCY (weight ratio 3:1) and 0.8 %w/w 98hEO nanoemulsions in the absence and presence of drug and cell culture media using a core-shell ellipsoid model together with a hard sphere structure factor S(Q) at 37 ºC. The modelling of the SANS data was constrained using Vshell(dry)/Vcore.

sample	core equatorial radius (R_1,Å)	core axial ratio (x)	core axial radius (R_1x,Å)	shell thickness (Å)	minor radius (Å)	major radius (Å)	axial ratio (X)	NE volume (Å^3)	sphere radius (Å)	hydration (%)	N_{agg}	surfaces area of surfactant (Å^2)	sum of squared error (SSE)
TD2-98hEO0.8d-DM-37C-t0	76.0	0.3	25.6	24.3	100.3	49.9	0.5	2105431	113.7	15	1376	49	992
TD2-98hEO0.8d-DM-37C-3.5h	72.4	0.3	24.6	23.3	95.7	47.9	0.5	1836991	102.0	15	1201	52	7543
TD2-98hEO0.8d-DM-37C-6h	73.1	0.3	23.5	22.9	95.9	46.3	0.5	1786846	109.0	15	1168	53	9935
TD2-98hEO0.8d-DM-37C-12h	71.5	0.3	23.8	22.8	94.3	46.6	0.5	1733362	100.6	15	1133	54	9219
TD2-98hEO0.8d-CUR-DM-37C-t0	73.8	0.3	25.2	23.8	97.6	49.0	0.5	1953677	113.3	15	1277	50	1338
TD2-98hEO0.8d-CUR-DM-37C-3.5h	73.4	0.3	25.5	23.9	97.3	49.4	0.5	1961504	108.4	15	1282	50	1212
TD2-98hEO0.8d-CUR-DM-37C-6h	72.7	0.3	25.3	23.7	96.4	49.0	0.5	1906928	104.7	15	1246	50	1605
TD2-98hEO0.8d-CUR-DM-37C-12h	71.9	0.3	25.1	23.5	95.3	48.6	0.5	1849918	111.4	15	1209	51	2187
TD2-98hEO0.8d-CUR-TP-DM-37C-t0	74.8	0.4	26.2	24.5	99.3	50.7	0.5	2093803	114.6	15	1369	48	943
TD2-98hEO0.8d-CUR-TP-DM-37C-3.5h	74.5	0.4	26.3	24.4	98.9	50.7	0.5	2080192	119.3	15	1360	48	1151
TD2-98hEO0.8d-CUR-TP-DM-37C-6h	74.2	0.4	26.2	24.4	98.5	50.6	0.5	2059141	106.3	15	1346	49	1557
TD2-98hEO0.8d-CUR-TP-DM-37C-12h	73.4	0.4	25.9	24.1	97.5	49.9	0.5	1989546	111.7	15	1300	49	2078

Estimated uncertainty for R_1 and x were ± 1.0 and ± 0.01, respectively.

Clearly, the neutron scattering intensity, I(Q), at low Q for TD2-98hEO0.64d-DM-37C NE did not show any significant change, while in contrast, that of TD2-98hEO0.8d-DM-37C kept increasing overtime suggesting that the presence of the cell culture media in TD2-98hEO0.8d-DM-37C resulted in an increase in size of the NE.

As can be seen from the fitting parameters, neither the size nor shape of TD2-98hEO0.64d-DM-37C NE droplets of the drug-free and drug-containing NE changed over 12 hours when compared to that of TD2-98hEO0.64d NE at 25 °C. In contrast, both drug-free and drug-containing TD2-98hEO0.8d-DM-37C NE demonstrated a decrease in the core equatorial radius over time when compared to the corresponding TD2-98hEO0.8d NE at 25 °C. As anticipated, the core equatorial radius of the TD2-98hEOd-37C NE increased with the concentration of 98hEO, a trend which was similar to that seen for TD2-98hEO NE at 25 °C. After fitting the SANS data using varying levels of shell hydration, the shell hydration of TD2-98hEO-DM-37C was found to be constant at 15% for NE containing either 0.64 or 0.8 %w/w 98hEO, regardless of the presence of drugs. The thickness of the shell obtained from the fits was in the range 22.0-26.2 Å. As with the other NE examined in the present study, it was clear that the model that provided the best fit to the SANS data was an oblate ellipsoid.

The effect of amount of oil and the presence of drug on the SANS results of micelles and NE is summarised in **Table 4.26**, while the effect of temperature and the presence of cell culture media on the SANS results of TD-98hEO and TDL-hSBO NE are shown in **Table 4.27**.

Table 4.26 SANS results of micelles and NE in the absence and presence of drugs at 25 °C.

Sample	Appearance of droplet
T2d	Oblate ellipsoid
TD2d	Prolate ellipsoid
TD2d-CUR	Prolate ellipsoid TD2d-CUR showed the slight difference in shape and size compared to drug-free TD2d.
TD2d-CUR-TP	Prolate ellipsoid TD2d-CUR-TP showed a change in shape compared to drug-free TD2d due to an increase in axial ratio.
TDL2d	Prolate ellipsoid

Table 4.26 SANS results of micelles and NE in the absence and presence of drugs at 25 °C.

Sample	Appearance of droplet
TDL2d-CUR	Prolate ellipsoid TDL2d-CUR showed a slight difference in shape and size compared to drug-free TDL2d.
TDL2d-CUR-TP	Prolate ellipsoid TDL2d-CUR-TP showed a dramatic change in shape compared to drug-free TDL2d due to an increase in axial ratio.
TD2-98hEOd	Oblate ellipsoid As the oil content increases, the size of NE become larger with no change in the shape of NE being noted. Note that the best fits obtained for both TD2-98hEO0.72d and TD2-98hEO0.8d did not fit the SANS data well.
TD2-98hEOd-CUR	Oblate ellipsoid No difference in the size and shape of NE droplets was noted in the presence of drug. Note that the best fits of TD2-98hEO0.72d and TD2-98hEO0.8d in the presence of either CUR or CUR-TP did not fit the SANS data well.
TD2-98hEOd-CUR-TP	
TDL2-hSBO0.24d	Oblate ellipsoid
TDL2-hSBO0.24d-CUR	Oblate ellipsoid TDL2d-hSBO0.24d-CUR no difference was seen in size compared to drug-free TDL2-hSBO0.24d.
TDL2-hSBO0.24d-CUR-TP	Oblate ellipsoid TDL2d-hSBO0.24d-CUR-TP showed a slight difference in size compared to drug-free TDL2-hSBO0.24d.

Table 4.27 SANS results of micelles and NE at 37 °C in the absence and presence of cell culture media.

Sample	Appearance of droplet
TD2d-37C	Prolate ellipsoid The large difference observed in the size and shape of NE droplets at 37 °C.
TD2d-CUR-37C	
TD2d-CUR-TP-37C	
TDL2d-37C	
TDL2d-CUR-37C	
TDL2d-CUR-TP-37C	
TD2d-98hEOd-37C	Oblate ellipsoid No difference in the size and shape of NE droplets at 37 °C.
TD2d-98hEOd-CUR-37C	
TD2d-98hEOd-CUR-TP-37C	
TDL2-hSBO0.24d-37C	Oblate ellipsoid No difference in the size and shape of NE droplets at 37 °C.
TDL2-hSBO0.24d-CUR-37C	
TDL2-hSBO0.24d-CUR-TP-37C	
TD2-98hEOd-DM-37C	Oblate ellipsoid No change in the shape and size of TD2-98hEO0.64d-DM-37C NE of at 37 °C while the TD2-98hEO0.8d-DM-37C NE showed change in shape with the increasing neutron scattering intensity, I(Q) overtime.

4.5 Chapter summary

Clearly, the addition of the cosurfactant, Dermosoft GMCY in the absence or presence of a second hydrophobic surfactant, namely lecithin, to Tween 80 NE lead to an increase in the area of NE existence, the formation of larger aggregates and a transformation of aggregate shape when to compared to NE prepared using solely Tween 80 NE as determined by PIT, PCS and SANS studies. The presence of a cosurfactant and second surfactant in NE has an effect on the dilutability of the NE which needs to be considered before continuing the further studies to exploit the NE for the purposes of drug delivery. The PIT experiments, particle size studies and SANS experiments suggested that Tween 80-containing NE in the absence and presence of cosurfactant contain a distinct oil core.

To examine the application of Tween 80 containing NE as drug delivery system, TP, CUR and DTX were chosen to be as poorly water soluble drugs. The solubility of TP in TD25-98hEO NE increased as the amount of oil present increased. On the other hand,

while T20, TD25-98hEO and TDL25-hSBO could solubilise a good level of CUR, the solubility of CUR did not increase as the amount of oil increased. In addition, the solubility of TP decreased in the presence of CUR. Furthermore, no improvement in DTX solubilisation was seen in TDL25-hSBO NE. Although it is hard to evaluate the advantage of NE over micelle in respect to DTX solubilisation due to the limited amount of hSBO incorporated in TDL25-hSBO NE.

In order to determine the cytotoxicity of the micelles and NE in the absence and presence of the anticancer drugs, CUR and DTX, T20-CUR, TD25-CUR, TDL25-CUR, TDL25-DTX micelles and T20-hSBO-CUR, TD25-98hEO-CUR, TDL25-hSBO-CUR and TDL25-hSBO-DTX NE were tested with CT26 and HeLa cell lines and the cytotoxicity results shown in Chapter 5.

Chapter 5
Toxicological evaluation of nonionic o/w nanoemulsions incorporating anticancer drugs

5.1 Introduction

5.1.1 *In vitro* cytotoxicity

The use of *in vitro* cell culture systems for the evaluation of cytotoxicity is very attractive, particularly as an alternative to the use of animals, i.e. *in vivo*, testing (Doke and Dhawale, 2015). *In vitro* cytotoxicity tests are generally more reliable, accurate, practical, environmentally friendly and economical than the use of animals (Ranganatha and Kuppast, 2012). Further, since cellular toxicity testing based on quantitative colourimetric assays has been widely used from about the mid 1990's so that the understanding of the methodology is good. Generally, the colourimetric assays provide information about some aspect of cellular metabolic function, and include resazurin (alamar blue) assay, neutral red incorporation (NRI) assay, adenosine triphosphate (ATP) content assay and tetrazolium-based assays (Bunel et al., 2014). Resazurin, for example, which is reduced to resorufin, is used to determine cell survival and proliferation, while the NRI assay measures the uptake and accumulation of neutral red (3-amino-*m*-dimethylamino-2-methyl-phenazine) in the lysosome. The ATP assay allows an estimate of the number of living cells (and by implication the number of the unviable cells) by measuring the production of adenosine triphosphate. The tetrazolium-based assays use a range of tetrazolium salts, including MTT, XTT, MTS or WST-1, as redox sensors that can only be reduced by metabolically active cells into formazan derivatives (Petty et al., 1995; Arechabala et al., 1999; Bunel et al., 2014).

Other assays which provide information about cell viability are based on plasma membrane integrity and include lactase dehydrogenase (LDH), trypan blue exclusion and fluorescence staining. The LDH assay measures lactase dehydrogenase (LDH) leakage from injured cells, while the trypan blue exclusion measures the penetration of trepan blue stain into the cytoplasm of dead cells and fluorescent staining measures the

extent of a fluorescent dye crossing the cell membrane of dying/dead cells and binds to DNA and/or RNA (Bunel et al., 2014).

5.1.1.1 MTT assay

As the NE formulated in this study are intended for intravenous administration for the treatment of cancer, the cytotoxicity of the formulations was examined in two cancer cell lines, namely the CT26 and HeLa cells lines, murine colon carcinoma and folate-expressing cervical-tumour-derived cells, respectively, using the MTT assay to assess their acute toxicity. The MTT assay, which was first described by Mosmann in 1983 has been modified by over the intervening years in order to improve its sensitivity and reproducibility, for example by using different tetrazolium salts (Wan et al., 1994; Goodwin et al., 1995). In the present study, the modified MTT protocol proposed by Klippstein et al. (2015) has been used.

The MTT assay (or thiazolyl blue assay) examines the reduction of MTT (3-(4,5-dimethylthiazol-2-yl)-2,5-diphenyltetrazolium bromide), a yellow and water soluble dye by mitochondrial succinic dehydrogenase present in viable cells, to form a purple, water insoluble product, formazan (Mosmann, 1983). The cleavage of the heterocyclic tetrazolium ring, by succinate-dehydrogenase enzymes present in viable cells, results in the production of the insoluble formazan (Stockert et al., 2012) (**Figure 5.1**).

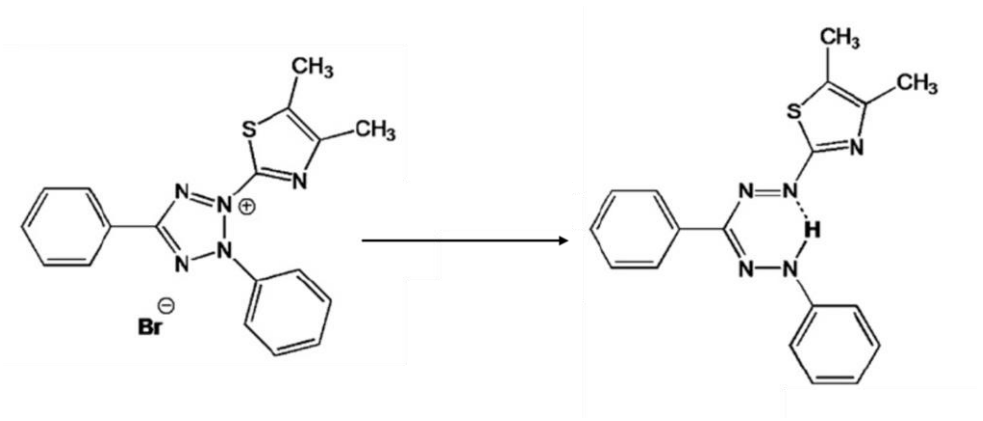

Figure 5.1: Chemical structure of MTT and formazan (modified from Stockert et al., 2012).

5.1.2 Interaction of surfactants with biological membrane

Cell membranes are comprised of a lipid bilayer, mainly composed of phospholipids possessing a heterogeneity of acyl chain lengths and head groups. Depending upon the particular cell membrane, these lipids frequently include: phosphatidylcholine, phosphatidylethanolamine, phosphatidylglycerol, sphingomyelin, glycolipids (glucosylceramide and galactosylceramide) and cholesterol (Swenson and Curatolo, 1992). In addition, cell membranes also contain molecules of protein imbedded in the lipid bilayer, while their external surface is covered by a polysaccharide-protein glycocalyx (Ratner, 1995).

A surfactant molecule can permeate across cell membrane in a variety of different ways. Possible routes of surfactant passage include the paracellular pathway (low concentrations of surfactant are thought to affect the integrity of the tight junctions between cells), the transcellular pathway, and 'gaps' in a (leaky) cell membrane caused by the denudation of cells at high surfactant concentrations (Anderberg et al., 1992). Due to the fact that surfactant molecules can directly affect the proteins and phospholipids of the cell membrane, they are sometimes used in pharmaceutical formulations as penetration enhancers of drugs (Swenson and Curatolo, 1992). Indeed, there is evidence of a correlation between enhanced permeability and cell damage. The study of Dimitrijevic et al. (2000) examined the effect of a range of nonionic surfactant, namely polysorbate 20, polysorbate 60, polysorbate 85 and Solulan C24, as absorption enhancers for the drug, metformin, by assessing transepithelial electrical resistance (TEER) and the viability of Caco-2 cells. The results showed an increase in TEER and in the permeability of metformin across the Caco-2 cell monolayer corresponding to a decrease in cell viability. In another study, Aungst (2012) showed that although sodium N-[8-(2-hydroxylbenzoyl)amino] caprylate increased the absorption of cromolyn across Caco-2 cell monolayers, a range of cytotoxicity assays, including lactate dehydrogenase, mitochondrial dehydrogenase activity, trypan blue exclusion, and neutral red binding, indicated that the molecule damage the membrane.

In general, the mechanism by which a surfactant can interact with a cell membrane depends upon the concentration of surfactant. At low concentrations of surfactant, the surfactant monomer may partition into the lipid bilayer. At higher surfactant concentrations, the formation of phospholipid-surfactant mixed micelles may be observed (Helenius and Simons, 1975; Lasch, 1995). The solubilisation of the phospholipid vesicles by surfactants has been widely studied for a better understanding

of the interaction between a surfactant and a biological membrane (Lichtenberg et al., 1983; Lasch, 1995; Heerklotz, 2008). **Figure 5.2** shows the transition of a lipid vesicle (A) to a swollen mixed vesicle (B) by the addition of surfactant. The addition of further surfactant can lead to the formation of small regions of local curvature (termed 'hump-backed' vesicles) (C) which can then 'bud off' to form sheets of mixed bilayer (D). It has been found that the complete transformation of vesicles to mixed micelles may occur when the effective molar ratio of surfactant to lipid in the bilayer exceeds the range 0.5 to 3.0 - the precise value being dependent upon the surfactant/lipid system of interest (Lichtenberg et al., 1983). The results of Pantaler et al. (2000) and Ahyayauch et al. (2010) confirmed the insertion of surfactant in the bilayer, supporting the proposed mechanism of Lichtenberg et al. (1983).

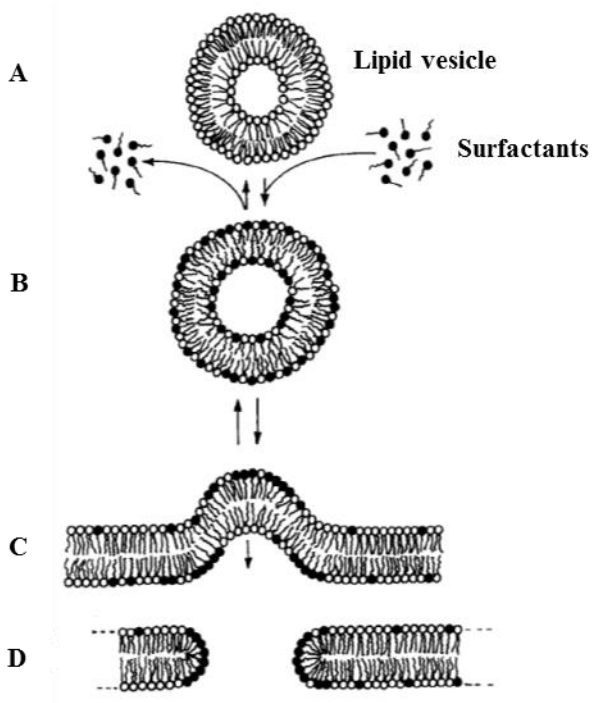

Figure 5.2: Schematic diagram of the solubilisation of a lipid vesicle by surfactants and transformation of lipid vesicles to mixed micelles: (=○) phospholipid, (—●) surfactant; (A) lipid vesicles, (B) swollen mixed bilayers, (C) humpbacked vesicles with surfactant at region of high curvature and (D) mixed bilayer sheets. In the steps of C to D, open flat bilayers and cylindrical mixed micelles form. (Reproduced from Lasch, 1995).

The interaction of the nonionic surfactant, Triton X-100, and the ionic surfactant, sodium dodecyl sulphate (SDS), with the Semliki Forest virus membrane glycoprotein have been studied (Helenius and Simons, 1975). These workers found that the disruption of the nucleocapsides and virus membrane was caused by the binding surfactant to the viral cell membrane followed by the formation of surfactant-lipid mixed micelles and surfactant-protein complexes. Recently, Mattei et al. (2017)

showed that the permeability of Triton X-100 to the vesicle was dependent on the lipid composition of the membrane. The membranes studied were composed of either of two phospholipids, namely palmitoyl oleoyl phosphatidylcholine (POPC) or sphingomyelin (SM), with and without 30 mol% of the steroid, cholesterol (chol). A fluorescence quenching assay showed that membranes composed of either POPC or SM alone, were completely solubilised by Triton X-100, whereas the presence of chol decreased the solubilisation of the lipid membranes by Triton X-100. In the case of POPC/chol membranes, the membrane was only partially solubilised by Triton X-100 whereas the membrane composed of SM/chol was virtually insoluble. In the case of erythrocytes, the penetration of surfactant molecules into the cell membrane induces the change its molecular organisation, its permeability and osmotic equilibrium, resulting in the eventual leakage of haemoglobin (Helenius and Simons, 1975; Manaargadoo-Catin et al., 2016).

The interaction of surfactants with the cell membrane has been proposed by Balgavy and Deveinsky (1996) to follow a free volume mechanism in which surfactant initially interacts with the cell membrane by means of its polar group interacting with the polar head group of phospholipid bilayer and the hydrocarbon chain of the surfactant inserting into the hydrophobic region of the phospholipid bilayer. Any mismatch between the hydrophobic parts of the surfactant and phospholipids results in the formation of free volume within the hydrophobic region of the bilayer which can only be eliminated by the trans-gauche isomerisation, the bending, or the hydrocarbon chain interdigitation of the hydrophobic chains of the bilayer. The effect of these interventions lead to a changes in the thickness and fluidity of the bilayer which are subsequently thought to result in the changes in cell membrane and cell function.

The possible mechanism of surfactant-induced bilayer to micelle transition depends on the solubilisation of phospholipid by the surfactants, which mainly depends on the trans-membrane motion of surfactant or “flip-flop” (Lichtenberg et al., 2013). The mechanism by which solubilisation occurs is different depending upon the fast and slow flipping of the surfactant. If the flipping of the surfactant to the inner monolayer is fast, solubilisation is rapid, whereas if the flipping of the surfactant is slow, solubilisation is slow. **Figure 5.3** shows the mechanism of the fast solubilisation of bilayers occurs by the trans-bilayer mechanism and the insertion of monomeric surfactant molecules into both the outer and inner membrane (Kragh-Hansen et al., 1998) resulting in the formation of open vesicles (Stuart and Boekema, 2007). In contrast, **figure 5.4** shows that the slow solubilisation results from either (a) the binding of micelles to the bilayers

(Kragh-Hansen et al., 1998) and the subsequent extraction of the membrane components from the outer bilayer into the surfactant micelles (Stuart and Boekema, 2007) or (b) vesicle-to-micelle transformation by the fragmentation of the closed phospholipid-surfactant mixed vesicles to form either thread-like, cylindrical or spherical micelles and ultimately small mixed micelles (Elsayed and Cevc, 2011).

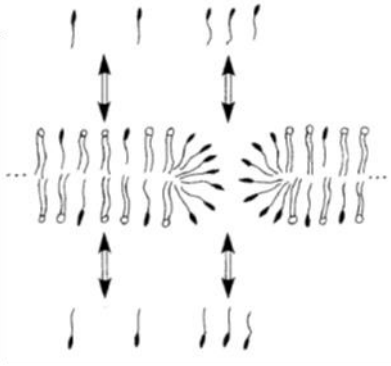

Figure 5.3: Schematic diagram of fast solubilisation of lipid membrane by surfactant (═○) phospholipid, (—●) surfactant by trans-bilayer mechanism (Reproduced from Kragh-Hansen et al., 1998).

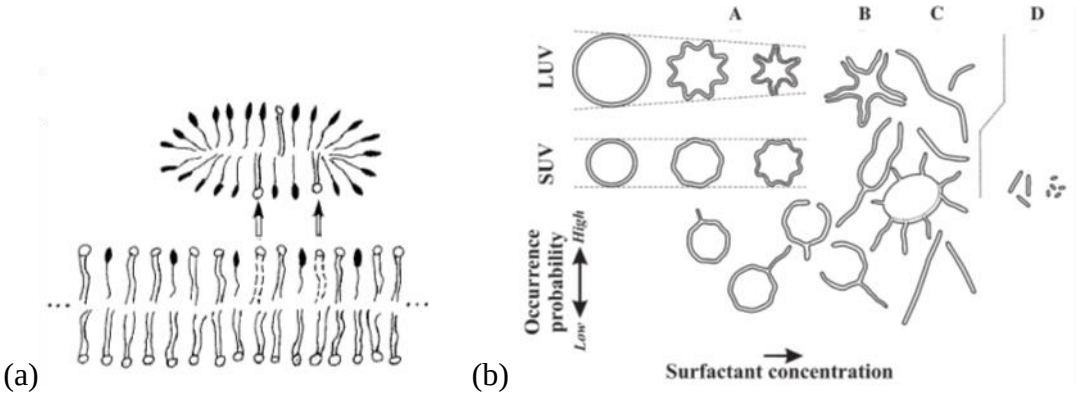

Figure 5.4: Schematic diagram of slow solubilisation of lipid membrane by surfactant (═○) phospholipid, (—●) surfactant and (┈○) phospholipid extracted from bilayer into a micelle by (a) the extraction of phospholipid from the outer bilayer into surfactant micelles and (b) vesicle-to-micelle transformation (Reproduced from Kragh-Hansen et al., 1998; Elsayed and Cevc, 2011).

In conclusion, the factors affecting the toxicity of the surfactants towards cells include the physicochemical properties of surfactants and/or the membrane properties of the cells themselves. It may be anticipated that the properties of the surfactants may be related to the value of their hydrophile-lipophile balance (HLB) and their critical micelle concentration (cmc) (Hofland et al., 1992).

5.2 Aim

The aim of this chapter is to investigate the cytotoxicity, using the MTT assay, of the o/w NE prepared using either Brij O10 or Tween 80 in the absence/presence of a cosurfactant (Dermosoft GMCY or lecithin). All the NE were examined in both in the absence and presence of the anticancer drugs, curcumin (CUR) and docetaxel (DTX), using one of two types of cancer cell lines, namely the CT26 and HeLa cells from murine colon carcinoma and folate-expressing cervical-tumour-derived cells, respectively.

5.3 Cytotoxicity of nonionic surfactant micellar solutions

The viability of CT26 and HeLa cells in the presence of Brij O10 (B), Tween 80 (T), Tween 80:Dermosoft GMCY at a 3:1 weight ratio (3:1) (TD) and Tween 80:Dermosoft GMCY:lecithin (7.5:2.5:1) (TDL) micelles was assessed with the MTT assay in the absence and presence of a saturation amount of either CUR or DTX, with CUR present at a concentration within the range 0.01 - 100 μM and DTX present at a concentration in the range 0.00001 - 100 μM (**Figure 5.5 and 5.6).** The drug-free micelles containing the same amount of surfactant as the drug-saturated micellar samples were tested in order to examine the cytotoxicity of drug-free and drug-containing formulations to both cell lines. It is worth noting that, due to the difference in the level of solubilisation of CUR and DTX in the micelles, the amount of either T, TD or TDL in the CUR-saturated micelles and the amount of TDL in the DTX-saturated TDL micelles were different (see **section 4.3.2.4** for the solubilisation of CUR in T-CUR, TD-CUR and TDL-CUR and **section 4.3.4.4** for the solubilisation of DTX in TDL-DTX). Regardless of the nonionic surfactant and cell line studied, a dose-dependent reduction in cell viability was seen. Due to the high toxicity of Brij O10 micelles, the B-CUR samples were not tested the cytotoxicity in the CT26 and HeLa cell lines. Unfortunately, however, no significant difference was seen in the viability of cells incubated for 72 hours with either CUR-free and CUR-saturated TD micelles ($p>0.05$). Only the cytotoxicity of T20-CUR micelles (at 2.4×10^{-1} and 2.4 %w/w T in CT26 cells) and TDL25-CUR micelles (at 5.2 %w/w TDL in HeLa cells) was significantly higher than that of CUR-free T20 and TDL25, respectively ($p<0.05$) suggesting that at high surfactant concentrations, the CUR containing systems exhibited a higher toxicity due to its presence. This experiment was repeated twice and the results showed the same trend. Surprisingly, the proliferation of cell lines in the presence of some CUR-

containing systems, namely T20 and TDL25 such as T20-CUR (at 2.4 %w/w T in HeLa cells) and TDL25-CUR (at 5.2 x 10^{-1} %w/w TDL in CT26 cells) was higher than in the corresponding CUR-free systems, namely T and TDL micelles ($p<0.05$). The reason for this proliferation is not known.

In contrast, it was clear that at the same time point of 72 hours, the viability of both the CT26 and HeLa cell lines in the presence of DTX-saturated TDL micelles at 10^{-2}, 10^{-1} and 10 %w/w TDL in CT26 cells and at 10^{-3}, 10^{-2} and 10^{-1} %w/w TDL in HeLa cells was significantly much lower than seen in the DTX-free TDL micelles ($p<0.05$). These results showed that the DTX was more potent against both the CT26 and HeLa cell lines than CUR, a result which is in agreement with a previous study showing that the IC_{50} of DTX (4.26 ± 0.51 nM) was much lower than that of CUR (10.25 ± 1.03 μM) in A549 cells from human lung cancer (Yin et al., 2012).

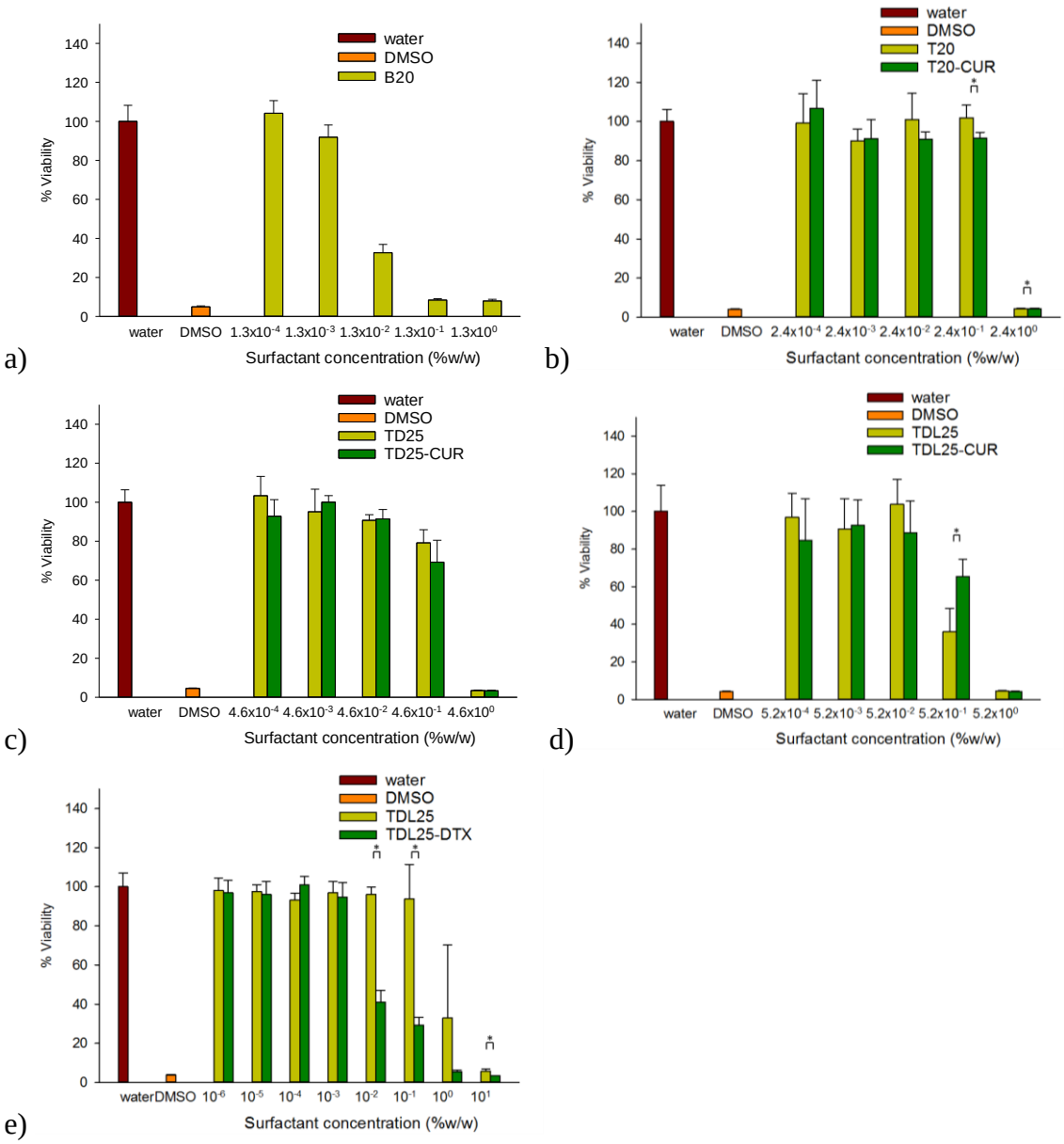

Figure 5.5: Viability of CT26 cells at 72 hours incubation in the presence of micelles: either a) Brij O10, b) Tween 80, c) Tween 80:Dermosoft GMCY (3:1) or d) Tween 80:Dermosoft GMCY:lecithin (7.5:2.5:1) in the absence and presence of a saturation amount of CUR and e) Tween 80:Dermosoft GMCY:lecithin (7.5:2.5:1) in the absence and presence of a saturation amount of DTX expressed as a percentage of control 'untreated' cells determined by MTT assay (mean ± S.D.; n=5; * $p<0.05$).

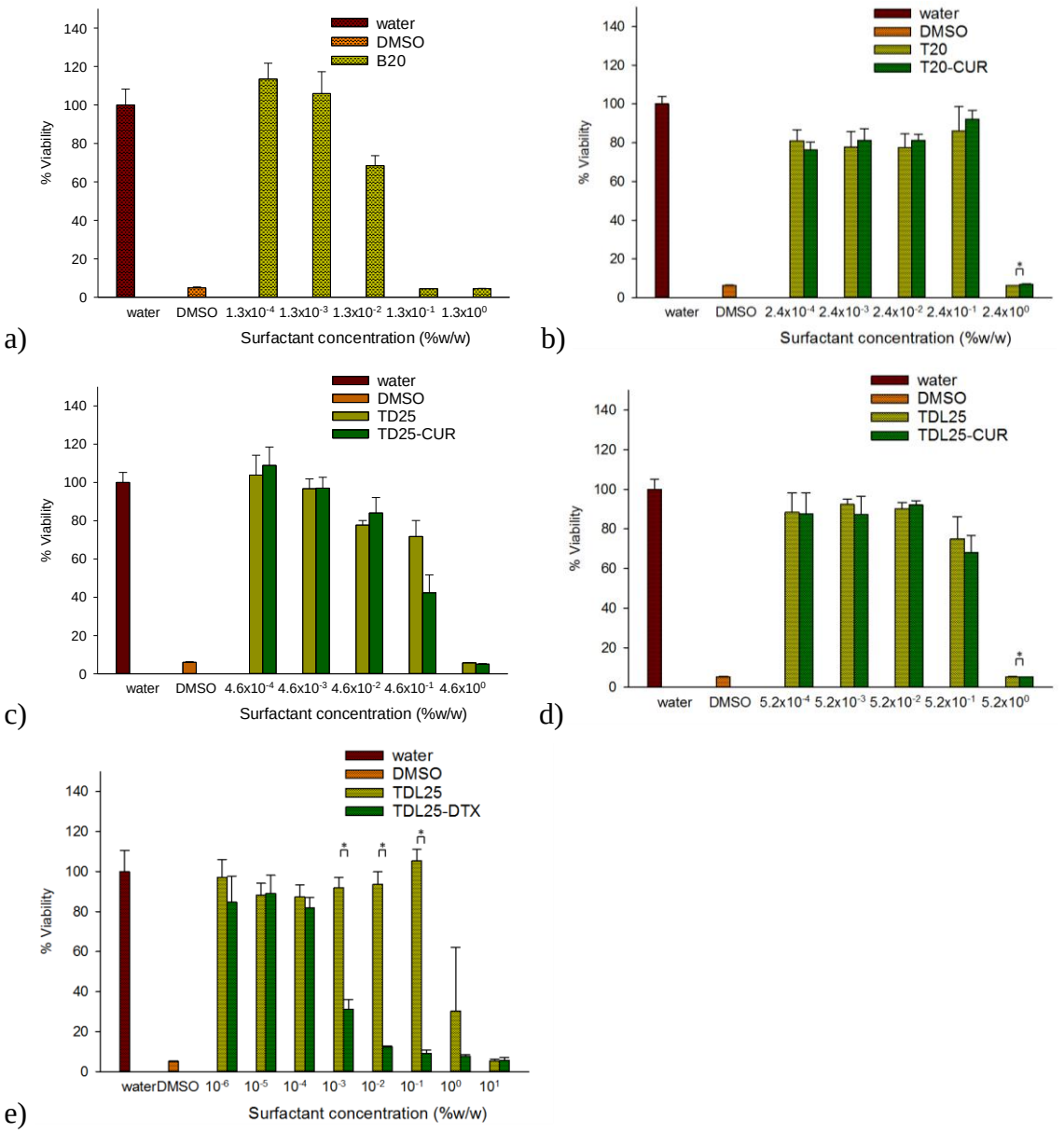

Figure 5.6: Viability of HeLa cells at 72 hours incubation in the presence of micelles: either a) Brij O10, b) Tween 80, c) Tween 80:Dermosoft GMCY (3:1) or d) Tween 80:Dermosoft GMCY:lecithin (7.5:2.5:1) in the absence and presence of a saturation amount of CUR and e) Tween 80:Dermosoft GMCY:lecithin (7.5:2.5:1) in the absence and presence of a saturation amount of DTX expressed as a percentage of control 'untreated' cells determined by MTT assay (mean ± S.D.; n=5; * $p<0.05$).

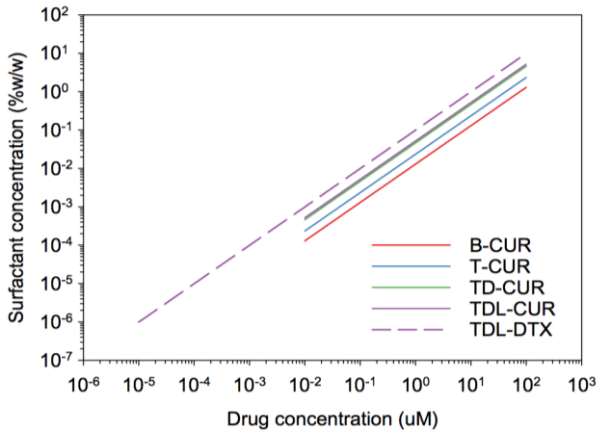

Figure 5.7: The surfactant concentration (%w/w) in the micellar solutions and oil-in-water nanoemulsions in the absence and presence of drug in the concentration range of 0.01-100 µM for CUR-saturated samples and 0.00001-100 µM for DTX-saturated samples.

At a surfactant concentration of 0.01 %w/w, the concentration of drug present in the micelles was 0.1 µM DTX and 0.2 µM CUR in TDL, 0.2 µM CUR in TD, 0.5 µM CUR in T and 1 µM CUR in B (**Figure 5.7,** see **section 3.3.2.4** for solubilisation of CUR in B-CUR, **section 4.3.2.4** for solubilisation of CUR in T-CUR, TD-CUR and TDL-CUR and **section 4.3.4.4** for solubilisation of DTX in TDL-DTX). At the same amount of surfactant, the drug-free Tween 80 micelles were seen to be less toxic to both types of cells than the corresponding Brij O10 micelles. This result is in agreement with that of Ohnishi and Sagitani (1993) when examining the haemolytic activity of Brij O10 and Tween 80.

As the HLB value of a surfactant is thought to be important in determining its toxicity, the relationship between the HLB of the surfactants and toxicity was examined (Hofland et al., 1992). Note that the HLB of Tween 80 and Brij O10, two surfactants used in the present study, is 15.0 and 12.4, respectively (Helenius and Simons, 1975). The haemolysis of POE-type nonionic surfactants (POE(n) oleyl ether and POE(n) monostrearate) was studied by Ohnishi and Sagitani (1993) who showed that haemolysis decreased as the HLB of surfactant increased. It has been reported that the ability of a surfactant to partition into a cell membrane is related to its hydrophobicity. A surfactant with a very high hydrophilicity will only poorly, if at all, partition into the lipid bilayer and therefore would be only expected to slightly, if at all, disrupt the cell membrane whereas a more hydrophobic surfactant will partition into the lipid bilayer causing damage to the membrane (Helenius and Simons, 1975). However, polyethylene glycol ester surfactants, such as polysorbate 20, polysorbate 60 and polysorbate 80 which posses a higher HLB exhibit a higher toxicity than the propylene glycol ester

surfactants, namely Capryol 90, Capryol PGMC and Lauroglycol 90 which posses a low HLB (Ujhelyi et al., 2012). This result indicates that the HLB of a surfactant is not a good parameter to indicate the toxicity.

The critical micelle concentration (cmc) of a surfactant is also considered to be an important parameter in determining membrane solubilisation power since the cmc is directly related, not only to the chemical potential of the surfactants, but also the thermodynamics of micelle formation (Tanford, 1972). The free energy of micelle formation (ΔG) can be expressed as $\Delta G = RT \ln (cmc)$ where R is the gas constant and T is the temperature (K) (Tanford, 1972). However, in the presence of biological membranes, there is also competition between micelle formation and surfactant partitioning into the lipid bilayer of a cell membrane. If the free energy of partitioning is greater than that of micelle formation, the surfactant prefers to partition into the membrane rather than form micelles (Becker et al., 1975). In addition, the binding of surfactant monomer to the membrane delays/prevents the formation of pure surfactant micelles as the concentration of free surfactant monomer is reduced (Helenius and Simons, 1975). The mixed micelles will only be formed when the free monomeric surfactant has reached its cmc.

If the surfactant exerts its toxicity by the interaction of the monomeric surfactant with the cell membrane, any membrane toxicity should occur at below the cmc of the surfactant. As a consequence therefore surfactants possessing a lower cmc should exhibit a lower toxicity due to the fact that less free surfactant monomer will be available to insert in the cell membrane (Singer et al., 1995). In the present study, the cmc of Brij 97 was 0.002 %w/w (Warisnoicharoen et al., 2003) while that of Tween 80 was 0.0128 %v/v (Ujhelyi et al., 2012). Based on the experimentally measured cmc of the surfactants, the expected relationship between the cytotoxicity and the cmc of surfactants was not observed. Hofland et al. (1991) found no correlation between either the HLB or the cmc of the polyoxyethylene surfactant vesicles containing cholesterol and either their ciliotoxicity or their effect on the proliferation of human keratinocytes. Indeed it was surprising that while the increase in the length of alkyl chain (from 12 to 18) or the decrease in the number of POE units (from 7 to 3) reduced ciliotoxicity, it had no effect on cellular proliferation. In addition, the bond by which the head group was linked to the alkyl chain exerted a very strong effect on toxicity in that the oleyl-EO5 ester surfactant was 10 times less toxic than oleyl-EO5 ether surfactant. This result may be a consequence of the fact that the oleyl-EO5 ester surfactant degrades at a much quicker rate than its ether counterpart. On the other hand, a linear relationship between

cmc and the solubilisation of protein released by the lysis of gill epithelial cells has been noted for several homologous series of surfactants, namely the n-alkyl sulphates, single and double chain tri/dimethylammonium bromides, cholates as well as the nonionic surfactants, n-octylglucoside and Trition X-100 (Partearroyo et al., 1991).

Unexpectedly in the present study, the addition of a small amount of lecithin into TD micelles did not significantly affect the cytotoxicity of CT26 and HeLa cell lines towards TDL micelles. This observation was not in agreement with previous studies by others, specifically Gould et al. (1994) and Trotta et al. (1996). For example studies by Gould et al. (1994) showed a decrease in haemolysis upon the addition of egg PC to Brij 96 micelles at egg PC:Brij 96 molar ratios between 0.1 and 2.0 while Trotta et al. (1996) noted that the addition of 5 mM lecithin to monoalkylphosphates, ranging from 120 mM hexylphosphate to 5 mM decylphosphate, and 15-80 mM polysorbate 60 also resulted in a decrease in haemolysis.

5.4 Cytotoxicity of nonionic nanoemulsions

Brij O10 NE systems

B20-98hEO NE in the presence of curcumin

CT26 and HeLa cell viability of B20-98hEO NE was assessed using the MTT assay in the absence and presence of CUR (**Figures 5.8 and 5.9**). The range of CUR present in this samples was 0.01 to 100 µM. The drug-free NE samples containing the same amount of surfactant as drug-saturated NE were tested in order to examine the cytotoxicity of comparable drug-free and drug-containing formulations to both cell lines. A dose-dependent reduction in cell viability was seen in both cell lines. Unfortunately, after 72 hours, there was no significant difference in cell viability between the CUR-free and the CUR-saturated NE ($p>0.05$). Only some of the CUR-containing B20-98hEO NE showed a significantly higher toxicity than CUR-free B20-98hEO NE ($p<0.05$), such as B20-98hEO1-CUR (observed at 1.3×10^{-1} %w/w B in CT26 and at 1.3×10^{-1} and 1.3 %w/w B in HeLa cells), B20-98hEO2-CUR (observed at 1.3 %w/w B in CT26 and at 1.3×10^{-1} and 1.3 %w/w B in HeLa cells), B20-98hEO4-CUR (observed at 1.3×10^{-4}, 1.3×10^{-1} and 1.3 %w/w B in HeLa cells) and B20-98hEO6-CUR (observed at 1.3×10^{-1} and 1.3 %w/w B in HeLa cells). Surprisingly, the proliferation of the cell lines when incubated with B20-98hEO-CUR NE was higher than that seen in the corresponding CUR-free B20-98hEO NE ($p<0.05$), for example

some CUR-containing B20-98hEO-CUR NE such as B20-98hEO1-CUR (seen at 1.3 x 10^{-2} %w/w B in CT26 cells and at 1.3 x 10^{-3} and 1.3 x 10^{-2} %w/w B in HeLa cells), B20-98hEO2-CUR (seen at 1.3 x 10^{-4} and 1.3 x 10^{-2} %w/w B in HeLa cells), B20-98hEO6-CUR (seen at 1.3 x 10^{-3}, 1.3 x 10^{-2}, 1.3 x 10^{-1} and 1.3 %w/w B in CT26 cells). In addition, due to the level of CUR solubilisation in the B20-98hEO-CUR NE as a function of 98hEO content being comparable, it is possible to test the various B20-98hEO-CUR NE at similar Brij O10 concentrations (see **section 3.3.2.4**). Surprisingly, the NE incorporating 98hEO did not reduce the toxicity towards the CT26 and HeLa cells when compared to the corresponding micelles (**Figures 5.5** and **5.6**). This observation is contrary to a previous cytotoxicity study performed on human bronchial (16-HBE14o-) epithelium cells (Warisnoicharoen et al., 2003) where $C_{18:1}E_{10}$ NE containing various amounts of large molar volume oils, such as soybean oil, ethyl oleate and Miglyol 812 exhibited lower cytotoxicity toward 16-HBE14o- cells than the corresponding surfactant micelles (Warisnoicharoen et al., 2003).

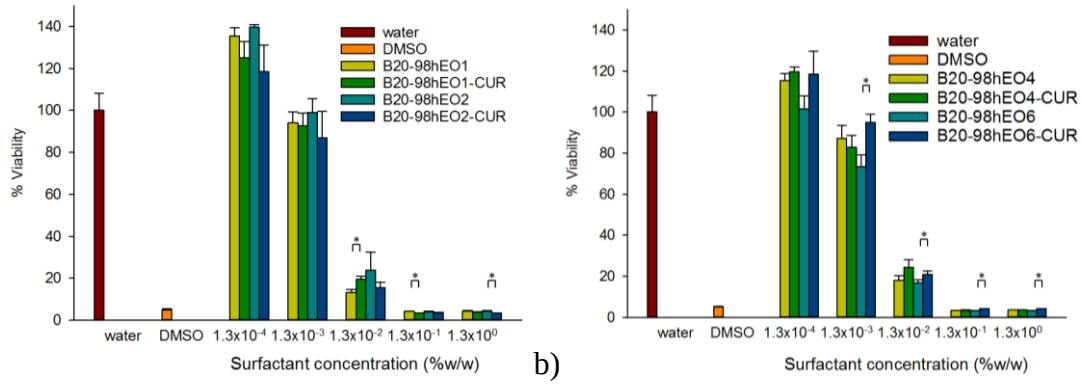

Figure 5.8: Viability of CT26 cells at 72 hours incubation of Brij O10 NE at the difference concentrations of 98hEO, a) 1-2 %w/w 98hEO and b) 4-6 %w/w 98hEO, expressed as a percentage of control 'untreated' cells in the absence and presence of curcumin determined by the MTT assay (mean ± S.D.; n=5; * $p<0.05$).

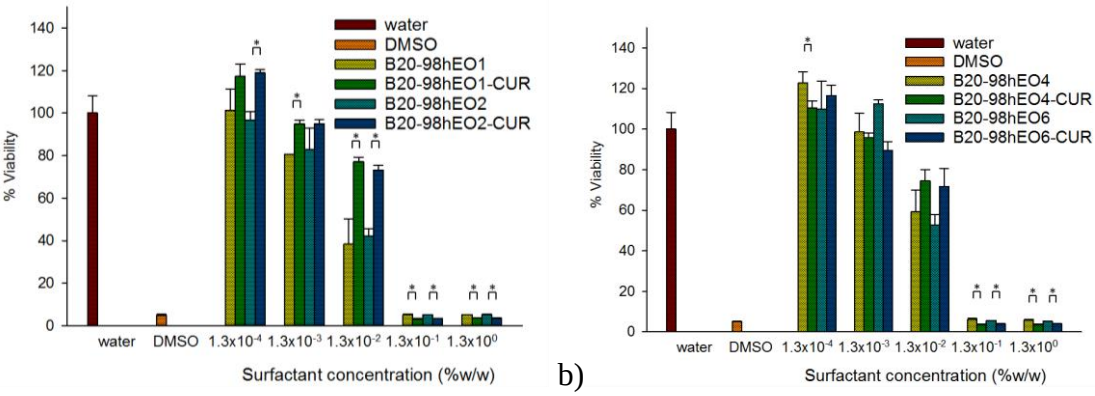

Figure 5.9: Viability of HeLa cells at 72 hours incubation of Brij O10 NE at the difference concentrations of 98hEO, a) 1-2 %w/w 98hEO and b) 4-6 %w/w 98hEO, expressed as a percentage of control 'untreated' cells in the absence and presence of curcumin determined by the MTT assay (mean ± S.D.; n=5; * $p<0.05$).

B20-hSBO NE in the presence of curcumin

The viability of CT26 and HeLa cells after incubation with B20-hSBO NE was assessed by the MTT assay in the absence and presence of CUR (**Figure 5.10**). The concentration of CUR in these samples was in the range of 0.01 to 100 μM. The drug-free NE samples containing the same amount of surfactant as the drug-saturated NE were tested in order to examine the cytotoxicity of the two types of formulation to both cell lines. A dose-dependent reduction in cell viability was seen in both cell lines. Unfortunately, no significant differences in cell viability between the CUR-free and CUR-saturated NE was observed at 72 hours ($p>0.05$). This experiment was repeated 3 times and each time the results showed the same trend. However, an increase in cell proliferation was seen after the incubation with some of the B20-hSBO-CUR NE. For example, proliferation was observed in cell lines incubated with B20-hSBO9-CUR (in CT26 cells NE containing either 1.3 x 10^{-1} or 1.3 %w/w B and in HeLa cells NE containing 1.3 %w/w B and was higher than in the cell lines incubated with CUR-free B20-hSBO9 NE ($p<0.05$).

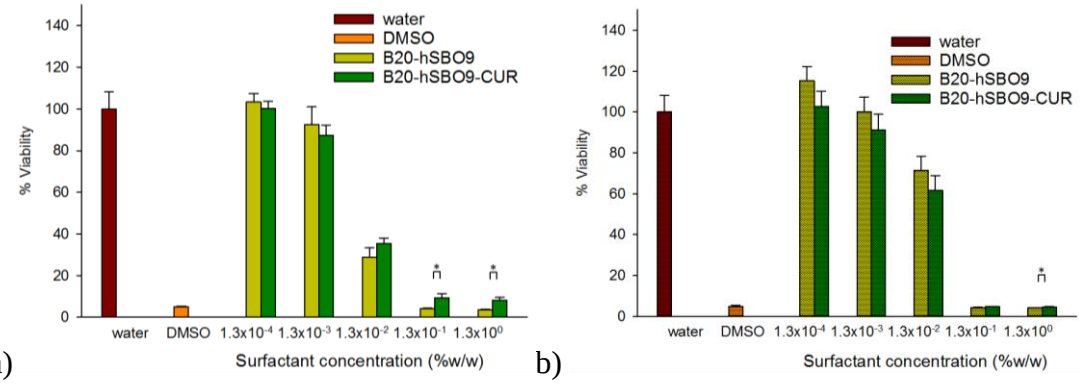

Figure 5.10: Viability of a) CT26 and b) HeLa cells at 72 hours incubation of Brij O10 NE at a concentration of 1 %w/w hSBO, expressed as a percentage of control 'untreated' cells in the absence and presence of curcumin determined by the MTT assay (mean ± S.D.; n=5; * $p<0.05$).

It is assumed the fact that was no difference in the toxicity of Brij O10 NE in the absence and presence of CUR was due to the quite high toxicity of Brij O10. As a consequence further studies used Tween 80 as the nonionic surfactant.

Tween 80 NE systems

T20-hSBO NE in the presence of curcumin

The viability of CT26 and HeLa cells in the presence of T20-hSBO1 NE was assessed using the MTT assay, both in the absence and presence of CUR (**Figure 5.11**). The concentration range of CUR used in these studies was 0.01 to 100 µM. The drug-free NE samples containing the same amount of surfactant as drug-saturated NE were also tested in order to examine the cytotoxicity of both types of formulation towards both cell lines. Notably a large reduction in cell viability was seen in both cell lines at the highest concentration of Tween 80 studied. Unfortunately, after 72 hours incubation, there was no significant difference in cell viability after incubation with CUR-free T NE and with CUR-saturated T NE, the latter of which contained 100 µM of CUR ($p>0.05$).

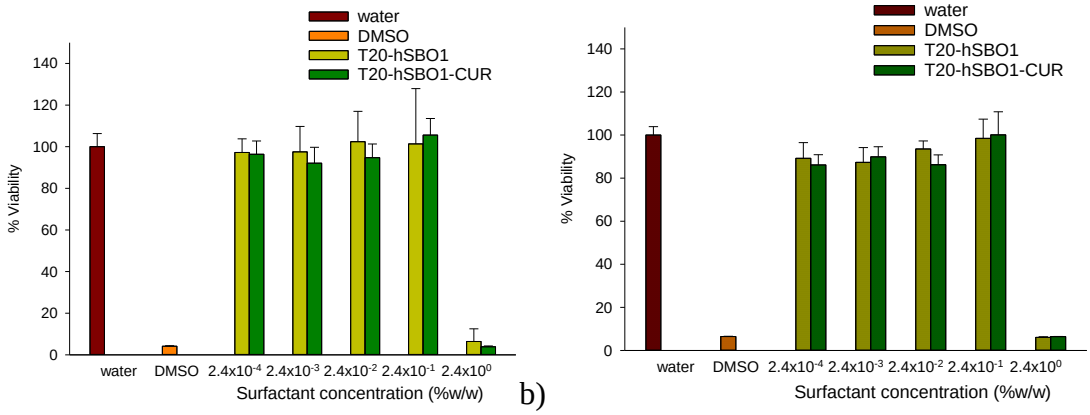

Figure 5.11: Viability of a) CT26 and b) HeLa cells at 72 hours incubation of Tween 80 NE containing 1 %w/w hSBO, expressed as a percentage of control 'untreated' cells in the absence and presence of curcumin determined by the MTT (mean ± S.D.; n=5; * $p<0.05$).

TD25-98hEO NE in the presence of curcumin

Due to the fact that Tween 80 alone could only incorporate a very small amount of oil, the cosurfactant, Dermosoft GMCY, was added in an attempt to increase the amount of oil incorporated into the Tween 80-containing NE. It is noteworthy that while Tween 80-containing NE in the presence of Dermosoft GMCY could increase the amount of 98hEO present, they could not increase the amount of hSBO incorporated and still form clear NE. As a consequence, the viability of CT26 and HeLa cells after incubation of 98hEO containing NE (i.e. TD25-98hEO NE) was assessed using the MTT assay in the absence and presence of CUR (**Figure 5.12**). The concentration of CUR used in this part of the study was in the range of 0.01 to 100 µM. The drug-free NE samples containing the same amount of surfactant as drug-saturated NE were tested in order to

examine the cytotoxicity of both types of formulation towards both cell lines. A dose-dependent reduction in cell viability was seen in both cell lines with a great reduction in viability between observed 10 and 100 µM of CUR, with the NE containing 100 µM CUR being prepared using the highest concentration of Tween 80. Unfortunately, no significant difference in cell viability between the CUR-free TD NE and CUR-saturated TD NE was seen at 72 hours incubation ($p>0.05$). Only the cytotoxicity of TD25-98hEO10-CUR (seen at 100 µM CUR in CT26 cells) was significantly higher than that of CUR-free TD25-98hEO NE ($p<0.05$). This experiment was repeated twice and each time the results showed the same trend. Surprisingly, the proliferation of cell lines in the presence of TD25-98hEO8-CUR (seen at 4.6 x 10^{-1} %w/w TD in HeLa cells) and TD25-98hEO10-CUR (observed at 4.6 x 10^{-1} and 4.6 %w/w TD in HeLa cells) was higher than that seen in the corresponding CUR-free TD25-98hEO NE ($p<0.05$).

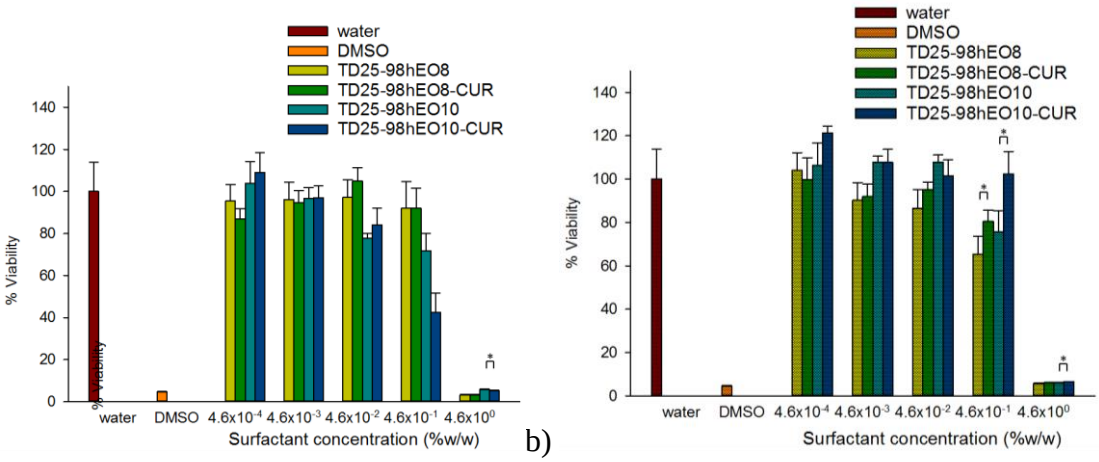

Figure 5.12: Viability of a) CT26 and b) HeLa cells at 72 hours incubation of Tween 80:Dermosoft GMCY (3:1) NE containing 8 and 10 %w/w 98hEO, expressed as a percentage of control 'untreated' cells in the absence and presence of curcumin determined by the MTT (mean ± S.D.; n=5; * $p<0.05$).

TDL25-hSBO NE in the presence of curcumin

The 'safer' surfactant, lecithin, was added to TD NE in an attempt to decrease the cytotoxicity of the NE. However, it was found that only a small amount of lecithin could be added for clear TDL NE be formed. Interestingly, a higher amount of hSBO could be incorporated into TDL NE than 98hEO. As a consequence therefore the viability of CT26 and HeLa cells was determined at by the MTT assay after incubation with TDL25-hSBO NE was assessed in the absence and presence of CUR (**Figures 5.13 and 5.14**). The concentration of CUR used in the study was in the range of 0.01 to 100 µM. Drug-free NE containing the same amount of surfactant as the drug-saturated NE

were tested to examine the cytotoxicity of both formulations in both cell lines. A reduction in cell viability was seen in both cells lines, with the reduction being more significant at 72 hours incubation compared to 24 hours incubation. Unfortunately, no significant differences in cell viability were observed between the CUR-free TDL-hSBO NE and the CUR-saturated TDL-hSBO NE at 24 and 72 hours ($p>0.05$). Only the cytotoxicity of TDL25-hSBO3-CUR (seen at 5.2×10^{-4} %w/w TDL in CT26 cells at 24 hours incubation) was significantly higher than that of the CUR-free TDL25-hSBO3 NE ($p<0.05$). Surprisingly, the proliferation of cell lines in the presence of TDL25-hSBO3-CUR (observed at 5.2×10^{-1} %w/w TD in both CT26 and HeLa cells at 72 hours incubation) was higher than that seen in CUR-free TDL25-hSBO3 NE ($p<0.05$).

It is generally noted that the cytotoxicity of a surfactant depends on exposure time, i.e. whether it is acute or prolonged exposure. For example, an increase in the cytotoxicity of surfactant towards human skin fibroblasts was seen at longer incubation times (Cornelis et al., 1991). Moreover, it was found that the IC_{50} value decreased upon increasing exposure time from 1 to 24 hours when using the LDH leakage test (Grant et al., 1992). Interestingly, however, there was no significant difference in the IC_{50} value observed after 1 and 24 hours when using either the NRI or the MTT assay (Grant et al., 1992). This apparent discrepancy is possibly due to the fact that the NRI and MTT tests require between 1-3 hours to complete after completion of the treatment of the cells with surfactant. During that period of time, the surfactant is still able to destroy the cells and consequently the toxicity observed (IC_{50}) in such cases is often considered to be representative of longer exposure times (Grant et al., 1992).

A clear reduction in cell viability was seen in both cell lines at the highest concentration of TDL, regardless of the presence of 100 μM CUR. Unfortunately, no significant difference in cell viability was seen after incubation with either CUR-free or CUR-saturated NE after 24 and 72 hours incubation ($p>0.05$).

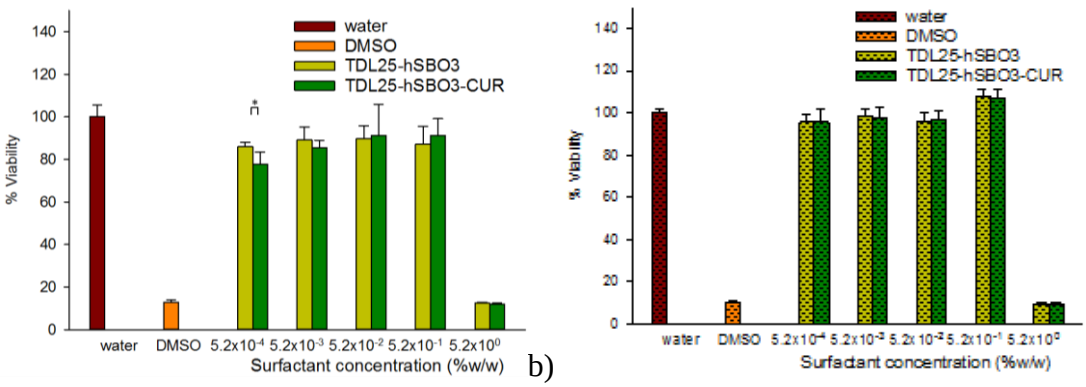

Figure 5.13: Viability of a) CT26 and b) HeLa cells at 24 hours incubation of Tween 80:Dermosoft GMCY:lecithin (7.5:2.5:1) NE containing 3 %w/w hSBO, expressed as a percentage of control 'untreated' cells in the absence and presence of curcumin determined by the MTT (mean ± S.D.; n=5; * $p<0.05$).

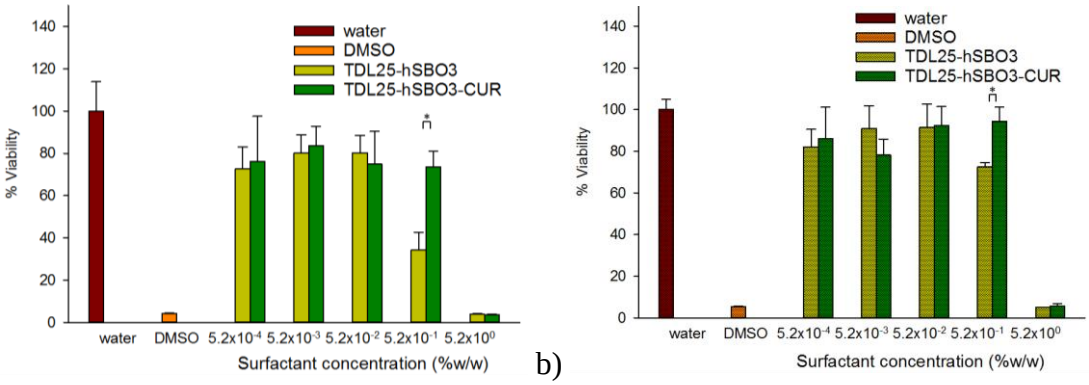

Figure 5.14: Viability of a) CT26 and b) HeLa cells at 72 hours incubation of Tween 80:Dermosoft GMCY:lecithin (7.5:2.5:1) NE containing 3 %w/w hSBO, expressed as a percentage of control 'untreated' cells in the absence and presence of curcumin determined by the MTT (mean ± S.D.; n=5; * $p<0.05$).

TDL25-hSBO NE in the presence of docetaxel

Another anticancer drug, DTX, was added at saturation levels to TDL NE in order to see whether it was possible to increase the cytotoxicity of the drug containing NE as it was felt that CUR was not toxic enough to allow a differentiation between the toxicity of the CUR-containing and the CUR-free NE. Such a differentiation was however seen for TDL-hSBO3 NE containing CUR (**Figure 5.14**) and TDL-hSBO3 NE containing DTX (**Figure 5.15**). The viability of CT26 and HeLa cells after TDL25-hSBO3 NE incubation was assessed using the MTT assay in the absence and presence of a saturation amount of DTX. The concentration range of DTX used in this part of the study was between 0.00001 and 100 μM. The drug-free NE samples containing the same amount of surfactant as the drug-saturated NE were tested in order to examine the cytotoxicity of both formulation types to both cell lines. The nonionic surfactants examined in the present study exhibited a clear dose-dependent cytotoxicity in both cell

lines in that a decrease in the number of viable cells was found with increasing surfactant concentration. Fortunately, however, a significant difference in cell viability was seen between the DTX-free and DTX-saturated NE at 72 hours. The cytotoxicity of TDL25-hSBO3-DTX (observed at 10^{-3}-10^{-1} %w/w TDL in CT26 cells and at 10^{-5}-1 %w/w TDL in HeLa cells) was significantly higher than that of DTX-free TDL-hSBO3 NE ($p<0.05$). This experiment was repeated twice and the results showed the same trend.

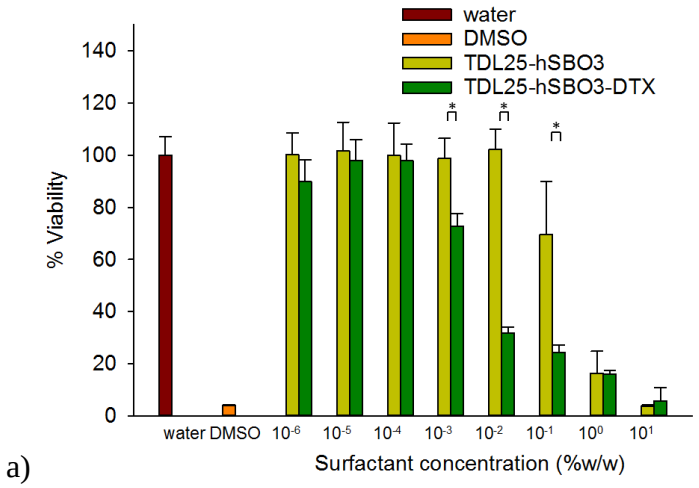

a)

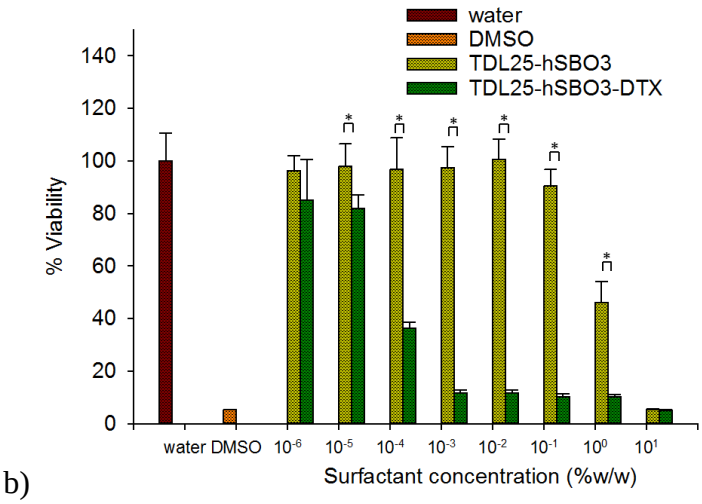

b)

Figure 5.15: Viability of a) CT26 and b) HeLa cells at 72 hours incubation of Tween 80:Dermosoft GMCY:lecithin (7.5:2.5:1) NE containing 3 %w/w hSBO, expressed as a percentage of control 'untreated' cells in the absence and presence of docetaxel determined by the MTT (mean ± S.D.; n=5; * $p<0.05$).

It is noteworthy that a similar decrease in toxicity attributable to a surfactant when formulated as an integral part of another type of aggregate has also been recorded by other workers. For example, the toxicity of the surfactant Solulan C24 (Cholesteryl

poly(24)oxyethylene ether) was decreased when formulated as a niosome compared to a micellar solution (Dimitrijevic et al., 1997). The components of the niosome were Solulan C24, cholesterol and sorbitan monostrearate (Span 80). Similarly, the haemolytic activity of monoalkylphosphate or polysorbate solutions were reduced when prepared in the presence of 5 mM lecithin (Trotta et al., 1996). Moreover, the addition of egg PC to Brij 96 and $C_{12}E_{10}$ micelles (Gould et al., 1994) and the addition of Epikuron 200 (soy lecithin) in NE solubilising ethyl butyrate and ethyl oleate (Satra, 1998) resulted in a decrease in the haemolytic effect of these preparations. In the latter case, the lower critical aggregation concentration of NE in the presence of Epikuron 200 tends to suggest that there was less free monomeric surfactant to cause haemolysis (Satra, 1998). In contrast however, lecithin showed no effect in reducing the toxicity of NE containing polysorbate (Tween) 60 (Trotta et al., 1996).

The IC_{50} values determined at 72 hours for incubation of micelles and NE with CT26 and HeLa cells are shown in **Tables 5.1** and **5.2**, respectively. Clearly, Brij O10-containing micelles and NE exhibited the lowest IC_{50} for both CT26 and HeLa cell lines. No difference in IC_{50} were seen either CUR-free and CUR-saturated micelles and NE, whereas the IC_{50} in the presence of DTX-saturated micelles and NE on both CT26 and HeLa cell lines were much lower than were seen for the DTX-free micelle and NE.

Table 5.1 IC_{50} Values of the micelles with CT26 and HeLa cell lines

Samples	Time (hours)	IC_{50} (%w/w)	
		CT26	HeLa
B20	72	7.2×10^{-3}	2.0×10^{-2}
T20	72	1.7	1.7
T20-CUR	72	0.7	1.8
TD25	72	9.4×10^{-1}	8.7×10^{-1}
TD25-CUR	72	7.6×10^{-1}	2.9×10^{-1}
TDL25	72	6.0×10^{-1}	9.2×10^{-1}
TDL25-CUR	72	5.5×10^{-1}	8.9×10^{-1}
TDL25-DTX	72	1.2×10^{-2}	5.1×10^{-4}
TD25-98hEO10-CUR	72	2.9×10^{-1}	1.5
TDL25-hSBO3	72	2.2×10^{-1}	8.6×10^{-1}
TDL25-hSBO3-CUR	72	2.2	3.8
TDL25-hSBO3-DTX	72	5.9×10^{-3}	6.4×10^{-5}

Table 5.2 IC_{50} Values of the nanoemulsions with CT26 and HeLa cell lines

Samples	Time (hours)	IC_{50} (%w/w)	
		CT26	HeLa
B20-98hEO1	72	3.6×10^{-3}	6.9×10^{-3}
B20-98hEO1-CUR	72	4.3×10^{-3}	2.4×10^{-2}
B20-98hEO2	72	5.1×10^{-3}	8.8×10^{-3}
B20-98hEO2-CUR	72	3.8×10^{-3}	2.3×10^{-2}
B20-98hEO4	72	4.1×10^{-3}	1.6×10^{-2}
B20-98hEO4-CUR	72	4.2×10^{-3}	2.3×10^{-2}
B20-98hEO6	72	3.1×10^{-3}	1.4×10^{-2}
B20-98hEO6-CUR	72	4.9×10^{-3}	2.3×10^{-2}
B20-hSBO9	72	6.7×10^{-3}	2.2×10^{-2}
B20-hSBO9-CUR	72	7.4×10^{-3}	1.8×10^{-2}
T20-hSBO1	72	1.8	1.8
T20-hSBO1-CUR	72	1.7	1.8
TD25-98hEO8	72	1.3	7.3×10^{-1}
TD25-98hEO8-CUR	72	1.4	1.1
TD25-98hEO10	72	8.7×10^{-1}	8.5×10^{-1}
TD25-98hEO10-CUR	72	2.9×10^{-1}	1.5
TDL25-hSBO3	72	2.2×10^{-1}	8.6×10^{-1}
TDL25-hSBO3-CUR	72	2.2	3.8
TDL25-hSBO3-DTX	72	5.9×10^{-3}	6.4×10^{-5}

5.5 Chapter summary

The cytotoxicity of all nonionic surfactant NE in HeLa (folate-expressing cervical-tumour-derived cells) and CT26 (murine colon carcinoma cells) suggested that drug-free B20-hSBO and B20-98hEO NE were toxic while drug-free T20-hSBO, TD25-98hEO and TDL20-hSBO NE were far less toxic. Furthermore, TD NE containing 98hEO and TDL NE containing hSBO did not exhibit any difference in toxicity of the NE in the absence and presence of CUR (a high-dose anticancer agent). On the other hand, TDL NE containing hSBO in the presence of DTX (a low-dose anticancer agent) exhibited a significant difference in cytotoxicity in both CT26 and HeLa cell lines when compared to the corresponding drug-free TDL-hSBO NE.

Chapter 6
Synthesis of folate derived Brij O10

6.1 Introduction

Various ligands for tumour-cell-specific receptors have been immobilised on the surface of nanoparticle systems in an attempt to direct 'target' the delivery vehicles to the desired cell type, where it is intended to deliver its payload. Folate receptor (FR)-derived drugs or delivery vehicles, in particular have shown considerable promise for the uptake, into target cells, of anticancer agents (Lee and Low, 1994; Lee and Low, 1995; Gabizon et al., 1995; Anderson et al., 2001), gene therapy products (Lee and Huang, 1996; Wang et al., 1995), and radiopharmaceuticals (Mathias et al., 1996) amongst other things. In order to achieve the selective targeting of the drug or drug carrier towards FR-positive tumour cells, folic acid is directly linked to the drug or drug carrier/vehicle. Such derivatized drugs/drug delivery systems frequently show FR-dependent cellular uptake and internalisation into FR-positive cells by the mechanism of endocytosis. The preparation of FR-derived liposomes has been previously reported. The covalent attachment of a folate moiety to anticancer drugs and liposomes has been previously used to target drug against tumours (Lee and Low, 1994; Lee and Low, 1995; Guo et al., 2000; Lu and Low, 2002). This targeting was achieved the linkage of folate to phospholipid or cholesterol using a polyethyleneglycol (PEG) spacer (Lu and Low, 2002; Lee and Low, 1995; Lee and Low, 1994; Guo et al., 2000). *In vitro* experiments using folate derived liposomes containing doxorubicin have shown that KB and HeLa cells, which highly overexpress the FR, significantly take-up the drug, whereas WI-38 fibroblast cells, which do not express the FR, showed minimal drug uptake (Lee and Low, 1995).

6.2 Aim of study

In the present study, folate derived Brij O10 was synthesised. The main objective of this part of the study was to synthesis a folate derived Brij O10 which could be incorporated into the NE in order to directly target to folate receptor embedded in the membrane of cancer cells.

During these studies the combined use of UV/vis spectroscopy, ninhydrin assay and ^{1}H NMR analysis was used employed to confirm the structure of the intermediates and final product.

6.3 The design folate targeting group

To selectively deliver anticancer drug to solid tumours expressing folate receptor, folate derived Brij O10 has been synthesised. **Figure 6.1** shows the design and the process of the preparation of the folate derived Brij O10.

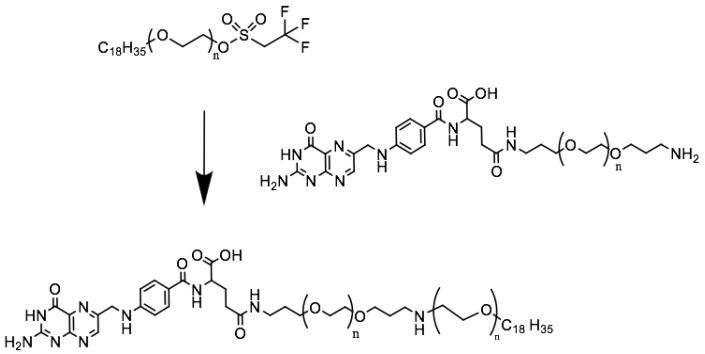

1. Tresylated Brij O10
2. PEG bis(3-aminopropyl) terminated-folate
3. Folate derived Brij O10

Figure 6.1: Design and the process of the preparation of folate derived Brij O10.

The first step is the preparation of PEG bis(3-aminopropyl) terminated-folate. The second step is the synthesis of tresylated-Brij O10. Lastly, folate derived Brij O10 was prepared by reacting PEG bis(3-aminopropyl) terminated-folate with the tresylated-Brij O10. A wide range of techniques, namely UV/vis spectroscopy, ninhydrin assay and ^{1}H NMR, were used to confirm the structure of the products in each step of the synthesis.

6.4 The synthesis of PEG bis(3-aminopropyl) terminated-folate

6.4.1 The preparation of PEG bis(3-aminopropyl) terminated-folate

The synthesis of PEG bis(3-aminopropyl) terminated-folate is outlined in **Figure 6.2**. Bis(3-aminopropyl) terminated PEG was reacted with folic acid in the presence of a coupling reagent (i.e. dicyclohexylcarbodiimide (DCC)), dimethylsulfoxide (DMSO) and pyridine to yield PEG bis(3-aminopropyl) terminated-folate.

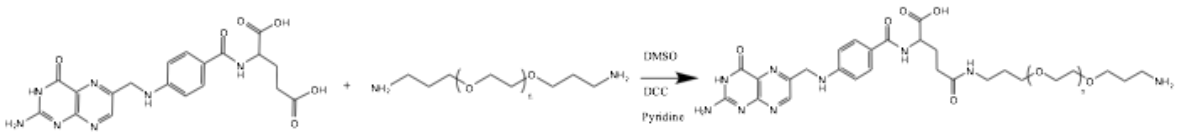

Folic acid Bis(3-aminopropyl) terminated PEG PEG bis(3-aminopropyl) terminated-folate

Figure 6.2: Synthesis of PEG bis(3-aminopropyl) terminated-folate.

The folate molecule (**Figure 6.3**) has two potentially reactive carboxyl groups, namely the α and γ carboxyl groups, which can be activated in the presence of DCC (Vortherms et al., 2008). As the α carboxyl group is more sterically hindered due to its position in the middle of the folic acid molecule, it is possible to select the experimental conditions to limit reaction at this site. In contrast, the (terminal) γ carboxylic acid group being more accessible and therefore more reactive can be selectively activated using DCC (Kim et al., 2007) before being reacted with the primary amine group of bis(3-aminopropyl) terminated PEG.

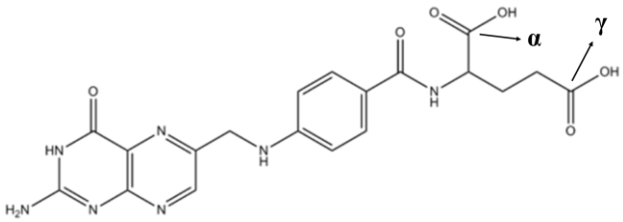

Figure 6.3: Structure of folic acid (modified from Vortherms et al., 2008).

Then water was added to the reaction mixture. Dicyclohexylurea, the by-product formed when using DCC, was insoluble in the organic solvent and water and precipitated out from the reaction mixture so this was removed by the filtration through a microfiber filter. The filtrate was evaporated to remove the solvent, however due to the high volume of filtrate, this filtrate was divided into 6 parts (each of about 10-15 mL). The purification of the remaining, crude PEG bis(3-aminopropyl) terminated-folate was achieved via size exclusion chromatography using Sephadex G-25. When each part of the filtrate was eluted through the Sephadex G-25 column it was called a separation. Finally, after the 6 parts of the filtrate had been passed through the column, separations 1 to 6 of products were called “the first separation” to “the sixth separation”. Such a separation was possible because of the increased molecular weight (MW) of the product. In fact, the MW of the PEG bis(3-aminopropyl) terminated-folate (MW = 1923) was sufficiently high to allow it to be separated from the low MW folate (MW = 441) and from the intermediate MW bis(3-aminopropyl) terminated PEG (MW = 1500). At this stage of the synthesis, the product, bis(3-aminopropyl) terminated

PEG-folate was more water soluble than folic acid, due to it being conjugated to the long PEG chain.

6.4.2 The analysis of PEG bis(3-aminopropyl) terminated-folate

After the crude PEG bis(3-aminopropyl) terminated-folate was eluted with water, the 10 mL fractions were collected from the first which contained a yellow material. This generally occurred at around fractions 15-16 (i.e. 150-160 mL of eluent). Collection of elute continued until all of the yellow colour had disappeared from the aliquots being collected, which generally occurred at around fractions 29-30 (i.e. 290-300 mL of eluent). **Figure 6.4** shows a schematic representation of the analysis of the PEG bis(3-aminopropyl) terminated-folate. As can be seen a combination of UV/vis spectroscopy, ninhydrin assay and ^{1}H NMR was used for characterisation. The folate content and -NH_2 content of each fraction were analysed by determining the UV absorbance at 364 nm (for folate content) and by ninhydrin (for -NH_2 content). The fractions which were positive for both folate and -NH_2 were pooled and evaporated using a rotary evaporator. In **Figure 6.4**, the dry product of first eluted fractions containing folate but no -NH_2 (i.e. negative to ninhydrin) are denoted as "1-A", while dry product of fractions containing both folate and -NH_2 was named as "1-B". Finally the dry product of fractions containing folate but no -NH_2 (i.e. negative to ninhydrin) but which were collected after the fractions which were positive to ninhydrin are described as "1-C". The chemical structure of the dry products, 1-A, 1-B and 1-C, was determined using ^{1}H NMR spectroscopy.

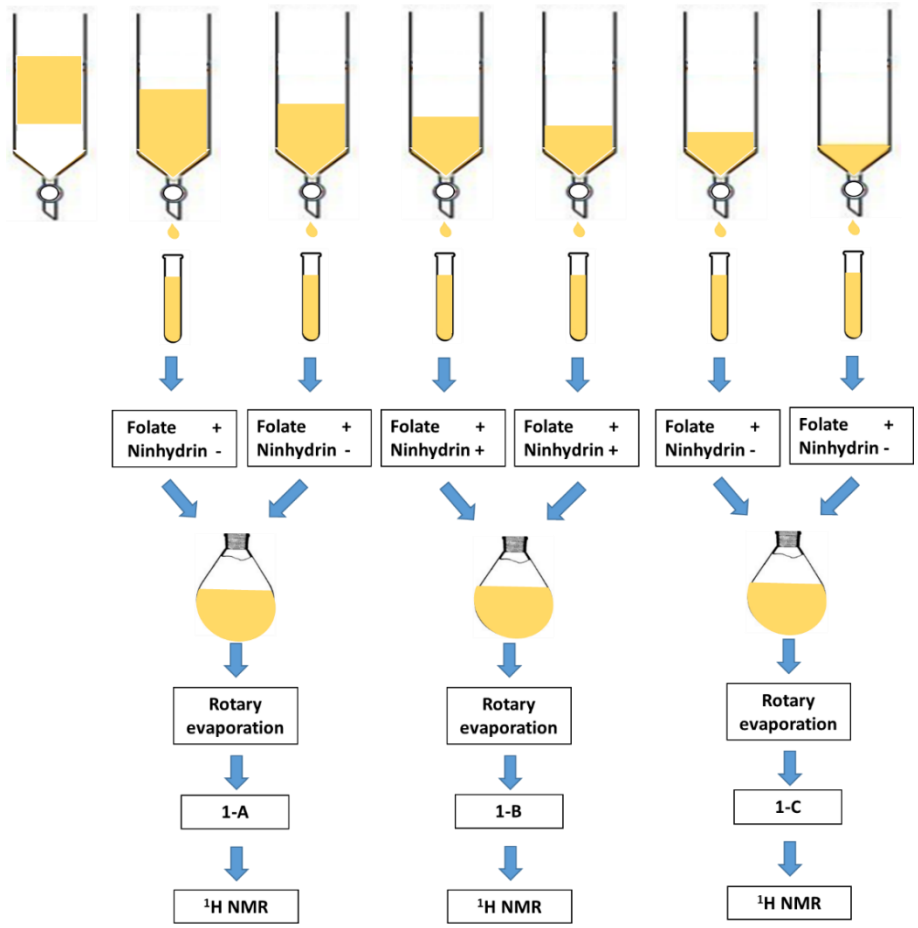

Figure 6.4: Flow diagram showing the process of analysis of the crude PEG bis(3-aminopropyl) terminated folate product using UV/vis spectroscopy, ninhydrin and proton nuclear magnetic resonance spectroscopy (^{1}H NMR).

6.4.2.1 Analysis of PEG bis(3-aminopropyl) terminated-folate using UV/vis spectroscopy

After elution of the filtrate of crude PEG bis(3-aminopropyl) terminated-folate obtained from the preparation of PEG bis(3-aminopropyl) terminated-folate through a Sephadex G-25, the amount of folic acid in each of the 'yellow' fractions from each separation was determined (**Figure 6.5**). It is clear that all the 'yellow' coloured fractions contained folate in some form.

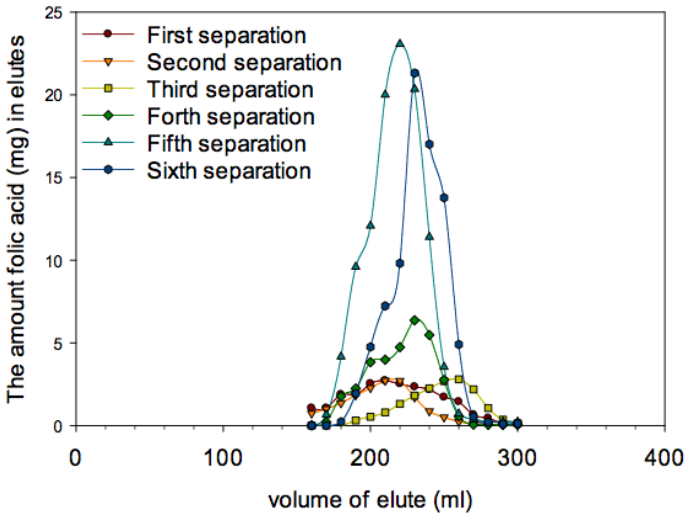

Figure 6.5: Amount of folic acid in the 10 mL 'yellow' coloured fractions eluted from the Sephadex G-25 column in the first separation to the sixth separation of PEG bis(3-aminopropyl) terminated-folate determined by the UV/vis spectroscopy using the absorbance at the wavelength of 364 nm.

6.4.2.2 Analysis of PEG bis(3-aminopropyl) terminated-folate using ninhydrin reaction

In the ninhydrin test, bis(3-aminopropyl) terminated PEG and folic acid were used as positive and negative controls, respectively. The bis(3-aminopropyl) terminated PEG reacted with ninhydrin to produce a purple coloured solution upon heating. On the other hand, when folic acid is reacted with ninhydrin the solution remains yellow in colour after heating. The reaction of each of the yellow coloured eluates with ninhydrin to produce a purple colour (or otherwise) upon heating was used to establish the presence (or otherwise) of $-NH_2$ in each of the eluates (**Table 6.1**).

Table 6.1 Reaction of each fraction in the synthesis of PEG bis(3-aminopropyl) terminated-folate to ninhydrin solution.

Sample	Order of separation					
	First	Second	Third	Forth	Fifth	Sixth
Bis(3-aminopropyl) terminated PEG (positive control)	Purple	Purple	Purple	Purple	Purple	Purple
Folic acid (negative control)	Yellow	Yellow	Yellow	Yellow	Yellow	Yellow
Fraction 1 at 150 - 160 ml	Yellow	Yellow	Yellow	Yellow	Yellow	Yellow
Fraction 2 at 160 - 170 ml	Yellow	Yellow	Yellow	Yellow	Yellow	Yellow
Fraction 3 at 170 - 180 ml	Yellow	Yellow	Yellow	*Purple*	*Purple*	Yellow
Fraction 4 at 180 - 190 ml	Yellow	*Purple*	Yellow	*Purple*	*Purple*	*Purple*
Fraction 5 at 190 - 200 ml	*Purple*	*Purple*	Yellow	*Purple*	*Purple*	*Purple*
Fraction 6 at 200 - 210 ml	*Purple*	*Purple*	Yellow	*Purple*	*Purple*	*Purple*
Fraction 7 at 210 - 220 ml	*Purple*	*Purple*	Yellow	*Purple*	*Purple*	*Purple*
Fraction 8 at 220 - 230 ml	*Purple*	*Purple*	*Purple*	*Purple*	*Purple*	*Purple*
Fraction 9 at 230 - 240 ml	*Purple*	*Purple*	*Purple*	*Purple*	*Purple*	*Purple*
Fraction 10 at 240 - 250 ml	*Purple*	*Purple*	*Purple*	*Purple*	*Purple*	*Purple*
Fraction 11 at 250 - 260 ml	Yellow	Yellow	*Purple*	Yellow	*Purple*	*Purple*
Fraction 12 at 260 - 270 ml	Yellow	Yellow	*Purple*	Yellow	Yellow	Yellow
Fraction 13 at 270 - 280 ml	Yellow	Yellow	*Purple*	Yellow	Yellow	Yellow
Fraction 14 at 280 - 290 ml	Yellow	Yellow	Yellow	Yellow	Yellow	Yellow
Fraction 15 at 290 - 300 ml	Yellow	Yellow	Yellow	Yellow	Yellow	Yellow

From the results of the UV/vis spectroscopy and ninhydrin assays, fractions 1-4 (first separation), fractions 1-3 (second separation), fractions 1-7 (third separation), fractions 1-2 (forth separation), fractions 1-2 (fifth separation), and fractions 1-3 (sixth separation) were found to contain folate but no $-NH_2$ (i.e. were negative in the ninhydrin assay) and were therefore pooled and the solvent evaporated using the rotary evaporation to obtain a dry product which was described as "1-A" (**Figure 6.4**).

In contrast, fractions 5-10 (first separation), fractions 4-10 (second separation), fractions 8-13 (third separation), fractions 3-10 (forth separation), fractions 3-11 (fifth separation), and fractions 4-11 (sixth separation) were found to contain folate and were positive in the ninhydrin assay (i.e. contained $-NH_2$) so these fractions were pooled together and evaporated using the rotary evaporation to obtain dry product which was denoted as "1-B" (**Figure 6.4**).

Finally, fractions 11-15 (first separation), fractions 11-15 (second separation), fractions 14-15 (third separation), fractions 11-15 (forth separation), fractions 12-15 (fifth separation), and fractions 12-15 (sixth separation) were also found to contain folate but no $-NH_2$ (i.e. were negative in the ninhydrin assay). As a consequence these fractions were pooled together and evaporated using the rotary evaporation to obtain dry product which was denoted as "1-C" (**Figure 6.4**).

Subsequently, the dry products, namely 1-A, 1-B and 1-C, were dissolved either in D_2O or DMSO in order to determine the chemical structure of each dry product using a 400 MHz ^1H NMR.

6.4.2.3 Analysis of PEG bis(3-aminopropyl) terminated-folate using proton nuclear magnetic resonance spectroscopy (^1H NMR)

All three dry products, namely 1-A, 1-B and 1-C were characterized by ^1H NMR spectroscopy to determine the structure of product (**Figures 6.6-6.8**).

Dry product 1-A

The ^1H NMR spectrum of the dry product, 1-A, which had previously showed an absorbance due to folate but was negative to ninhydrin solution, exhibited hydrogen resonances due to folate and bis(3-aminopropyl) terminated PEG (**Figure 6.6**). In particular the ^1H NMR spectrum exhibited a signal at 3.47 ppm (position l, m, n, o) corresponding to a methyl proton in the oxyethylene region of bis(3-aminopropyl) terminated PEG molecule while the signals at 2.80 ppm (position j, q), and 1.81 ppm (position k, p) were assigned to methylene of bis(3-aminopropyl) terminated PEG. In contrast, the signals at 6.63 ppm (position c, d) and 7.48 ppm (position e, f) corresponded to the para-aminobenzoic acid (PABA) of the folate, while the signal at 8.42 ppm (position a) corresponded to the protons in the pteridine moiety of the folate. Furthermore, the signal at 4.09 ppm (position b, g), and 2.05 ppm (position h, i) were assigned to the methylene of the folate.

In addition, the ^1H NMR results also indicated that the conjugation of folate and bis(3-aminopropyl) terminated PEG were present in a 2:1 ratio as determined from the ratio of the hydrogen peaks from the folate moiety and the bis(3-aminopropyl) terminated PEG and suggested the structure was folate-PEG bis(3-aminopropyl) terminated-folate (MW = 2346). This result was also supported by the time taken to elute the products from the Sephadex G-

25 column, in that fractions containing 1-A eluted first and before the fractions of the believed to contain the product 1-B, PEG bis(3-aminopropyl) terminated-folate, which is of a lower molecular weight (MW = 1923) than folate-PEG bis(3-aminopropyl) terminated-folate of fractions of product 1-A, folate-PEG bis(3-aminopropyl) terminated-folate, (MW = 2346). Moreover, product 1-A was not soluble in water and required a mixture of D_2O and DMSO (5:1) to prepare a clear solution for structure determination using ^1H NMR. The integral of the peaks attributed to the folate and bis(3-aminopropyl) terminated PEG of product 1-A indicate that product 1-A had higher amount of folate than product 1-B.

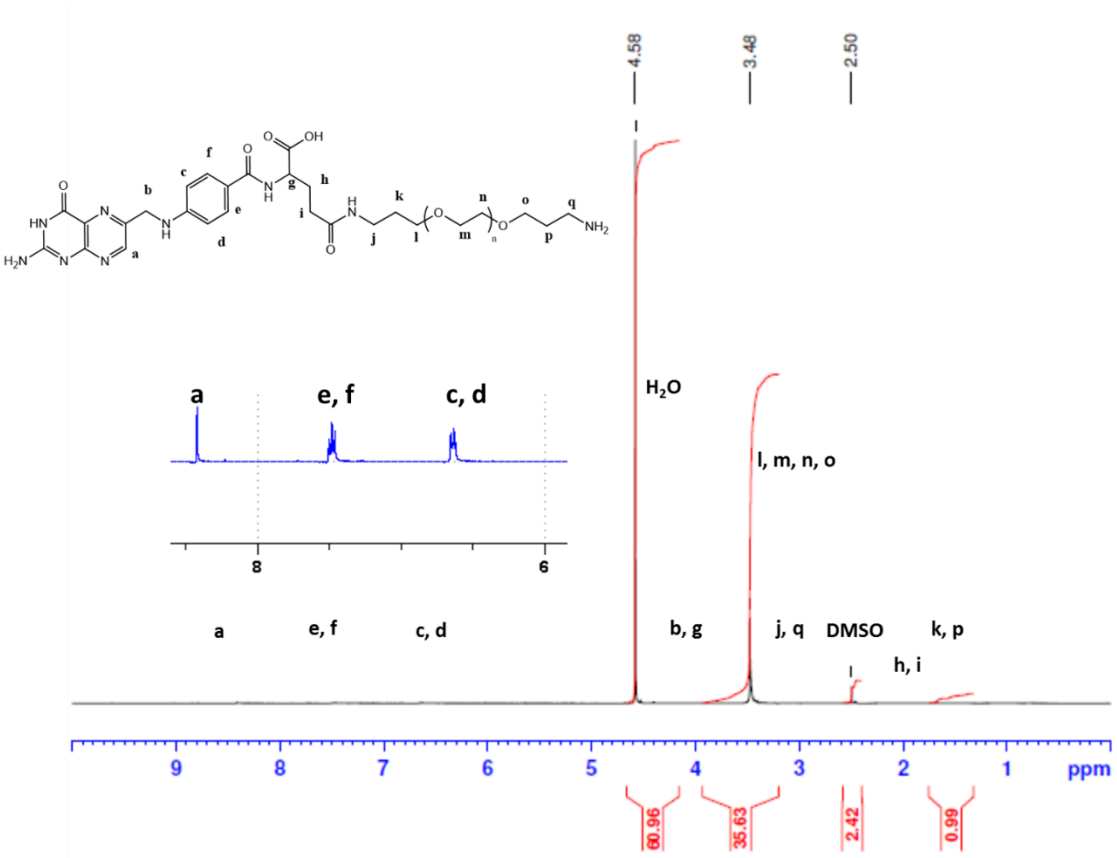

Figure 6.6: ^1H NMR spectrum of dry product 1-A (400 MHz, D_2O: DMSO (5:1)): δ 8.42, 7.48, 6.63, 4.09, 3.47, 2.80, 2.05, and 1.81 ppm.

Dry product 1-B

It is clear that the ^1H NMR spectrum of dry product 1-B which was positive to both folate and positive to ninhydrin solution, indicating the presence of -NH_2 exhibited ^1H NMR signals originating from both folic acid and the bis(3-aminopropyl) terminated PEG (**Figure 6.7**).

The ^{1}H NMR spectra exhibited a signal at 3.59 ppm (position l, m, n, o) corresponding to the methyl protons in the oxyethylene moieties of bis(3-aminopropyl) terminated PEG molecule while the signals at 3.00 ppm (position j, q), and 1.93 ppm (position k, p) could be assigned to the methylene of bis(3-aminopropyl) terminated PEG. In contrast, the signals at 6.56 ppm (position c, d) and 7.51 ppm (position e, f) corresponded to the para-aminobenzoic acid (PABA) moiety of the folate, while the signal at 8.57 ppm (position a) corresponds to the protons of the pteridine moiety of the folate. Finally, the signal at 4.22-4.39 ppm (position b, g), and 2.21 ppm (position h, i) was assigned to the methylene of the folate. The integrals of each hydrogen peak of the ^{1}H NMR spectra confirmed that both folate and bis(3-aminopropyl) terminated PEG were present and that they were associated in a 1:1 ratio. The percentage yield of product 1-B, PEG bis(3-aminopropyl) terminated-folate, was 40 %.

The human metabolome database (HMDB, http://www.hmdb.ca) showed that the ^{1}H NMR spectra of folic acid exhibited signals at 2.1 ppm (position h), 2.3 (position i), 4.3 (position g), 6.2 ppm (position c, d), 7.4 ppm (position e, f) and 8.4 (position a). This illustrated that the coupling of folic acid and bis(3-aminopropyl) terminated PEG affected the chemical shift of position i causing it to move upfield. In addition, mass spectral analyses (e.g. MALDI-TOF) could have been used in the analysis of PEG bis(3-aminopropyl) terminated-folate.

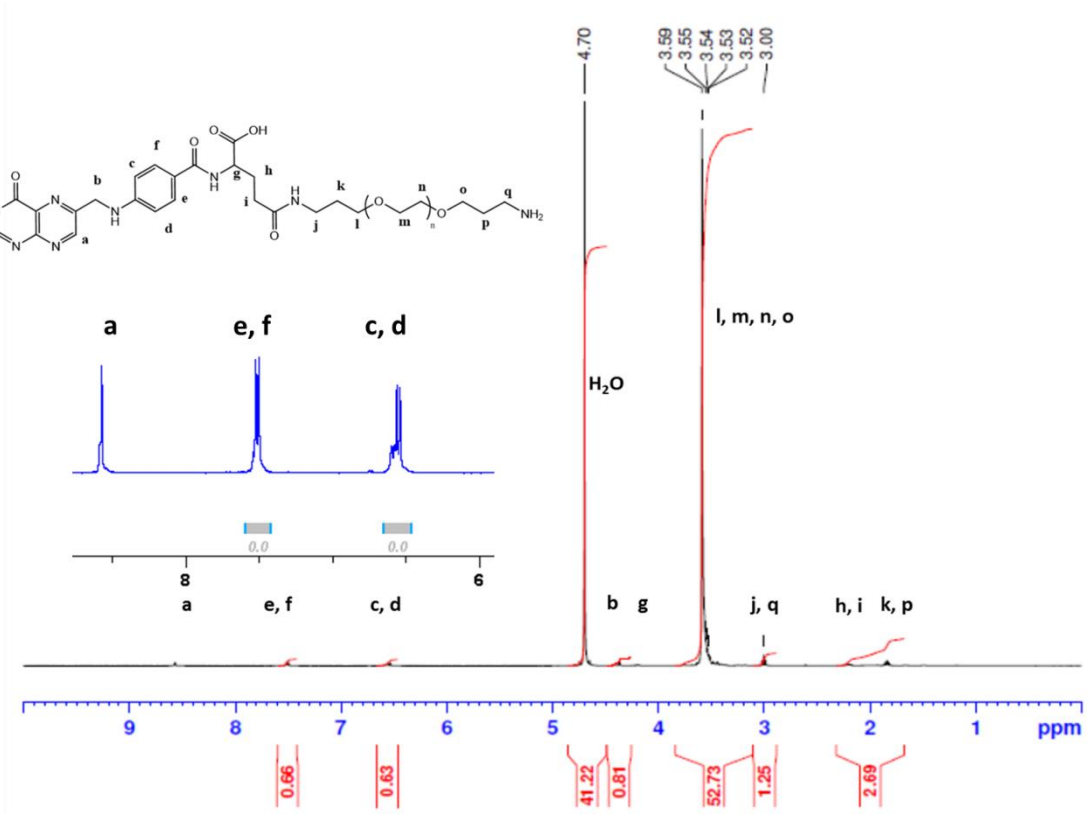

Figure 6.7: ^{1}H NMR spectrum of dry product 1-B (400 MHz, D_2O): δ 8.57, 7.51, 6.56, 4.39, 4.22, 3.59, 3.00, 2.21 and 1.93 ppm.

Dry product 1-C

The ^{1}H NMR spectrum of dry product 1-C (**Figure 6.8**), which was positive to folate but was negative to ninhydrin, suggests that the product 1-C was in fact folic acid. The ^{1}H NMR result showed signals at 6.51 ppm (position c, d) and 7.42 ppm (position e, f) corresponding to the para-aminobenzoic acid (PABA) moiety of folate, while the signals at 8.29 ppm (position a) corresponded to the protons of the pteridine moiety of the folate. Finally, the signals at 4.00-4.27 ppm (position b, g) and 1.46 ppm (position h, i) were assigned to methylene of folate. Surprisingly, the spectra indicated that bis(3-aminopropyl) terminated PEG was present as the signal at 3.29 ppm (position l, m, n, o), and 3.00 ppm (position j, q) and 1.10 ppm (position k, p) was assigned to the methylene of bis(3-aminopropyl) terminated PEG. So, despite the fact that qualitative analysis using ninhydrin assay had been negative result to the presence of -NH_2, ^{1}H NMR spectroscopy suggested the presence of a very small amount of bis(3-aminopropyl) terminated PEG in product 1-C. While ^{1}H NMR spectroscopy supported the presence of folate as the major product in dry product 1-C, size exclusion

spectroscopy also supported its presence due to the elution time – it would be expected to be more slowly eluted than the other possible products of the reaction. This is a consequence of the low MW of folic acid (MW = 441) when compared to bis(3-aminopropyl) terminated PEG (MW = 1500) and PEG bis(3-aminopropyl) terminated-folate (MW = 1923). In addition, the product 1-C was not soluble in water and so DMSO was used as a solvent to prepare the clear solution for structural determination of dry product 1-C using ^{1}H NMR.

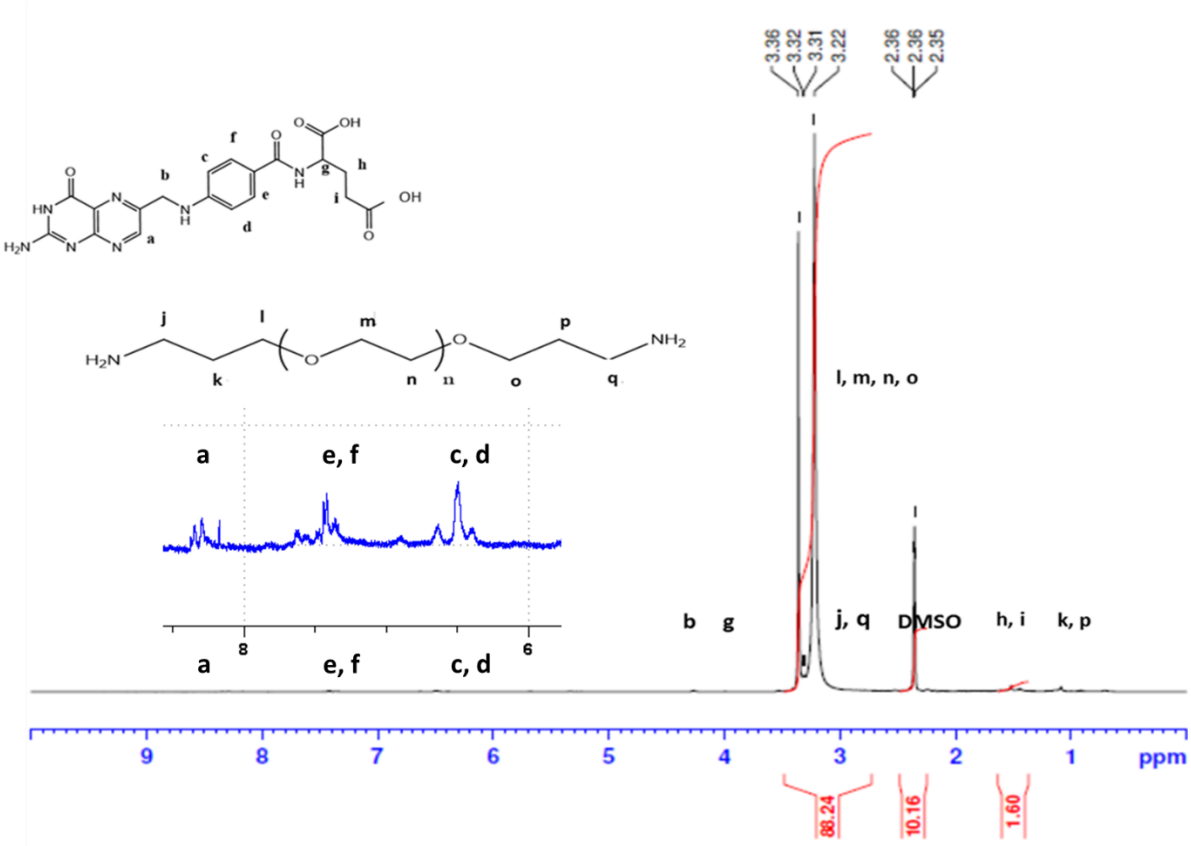

Figure 6.8: ^{1}H NMR spectrum of dry product 1-C (400 MHz, DMSO): δ 8.29, 7.42, 6.51, 4.27, 4.00, 3.29, 3.00, 1.46, and 1.10 ppm.

In previous study, it has been reported that in the ^{1}H NMR spectra of the folic acid conjugated to poly(ethylene glycol) (PEG)-modified dendrimers, the aromatic folate proton peaks could be observed at δ 6.65, 7.67, and 8.63 ppm, while the PEG protons were present at δ 3.58 ppm. (Chang, 2013). It was also reported that the ^{1}H NMR spectrum of folate-poly (PEG-cyanoacrylateco-cholesteryl cyanoacrylate) (FA-PEG-PCHL) exhibited a signal at 3.51 ppm which could be assigned to the methylene protons of the PEG backbone. In additions, signals at 2.00-2.40 ppm and 4.50 ppm were attributed to the methylene of folate. Finally the signals

at 6.61 ppm, 7.41 ppm, and 8.66 ppm were attributed to the protons of the aromatic ring of folate (Li et al., 2011).

6.4.2.4 The analysis of PEG bis(3-aminopropyl) terminated-folate for ratio of folate content and -NH_2 content

The folate content and -NH_2 content of product 1-B were assessed and used to calculate the molar ratio of folate and bis(3-aminopropyl) terminated PEG in its structure. In addition, the amount of folic acid present in product 1-B was also determined using UV/vis spectroscopy. The absorbance of the product 1-B, PEG bis(3-aminopropyl) terminated-folate, at a concentration of 0.368 mg/mL at a wavelength of 364 nm was determined to be 0.45. Therefore, the amount of folic acid in this sample was determined to be 0.032 mg.

The bis(3-aminopropyl) terminated PEG content was determined by preparing a 1.014 mg/mL stock solution of the PEG derivative which was then diluted with ethanol to yield working solutions of PEG derivative concentrations ranging from 0.043 to 0.145 mg/mL. The absorbance at 570 nm of each concentration of bis(3-aminopropyl) terminated PEG was plotted against concentration to get a standard curve.

<u>Ninhydrin assay of bis(3-aminopropyl) terminated PEG (Standard curve)</u>

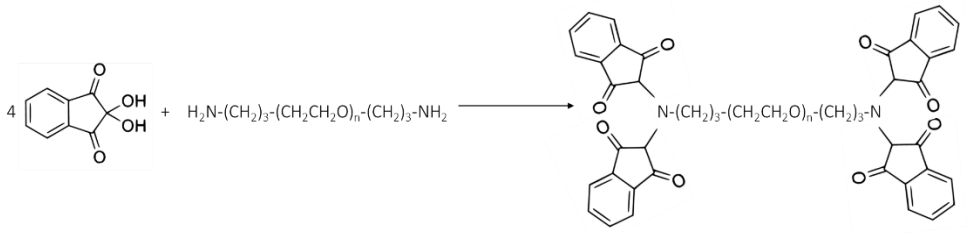

4 x ninhydrin + bis(3-aminopropyl) terminated PEG → (ninhydrin)$_4$-bis(3-aminopropyl) terminated PEG

<u>Ninhydrin assay of bis(3-aminopropyl) terminated PEG-folate</u>

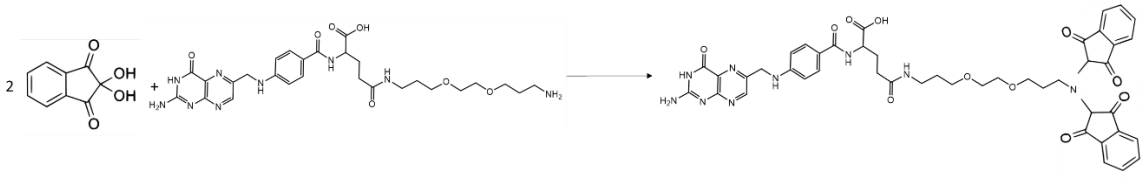

2 x ninhydrin + bis(3-aminopropyl) terminated PEG-folate → (ninhydrin)$_2$-bis(3-aminopropyl) terminated PEG-folate

In order to compare the amount of bis(3-aminopropyl) terminated PEG and bis(3-aminopropyl) terminated PEG-folate, the chemical reaction of ninhydrin assay with bis(3-aminopropyl) terminated PEG-folate should be multiplied with 2 in order that both reactions have used the same number of mole of ninhydrin.

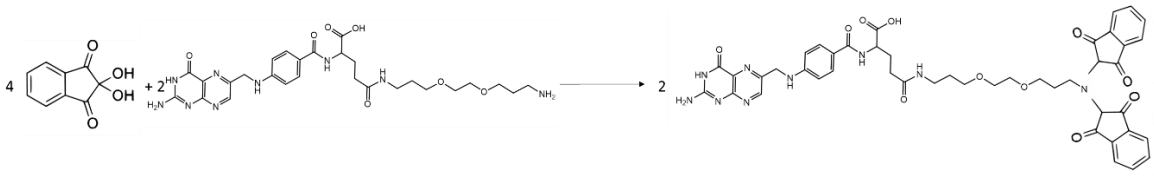

4 x ninhydrin + 2 x bis(3-aminopropyl) terminated PEG-folate → $(ninhydrin)_4$-bis(3-aminopropyl) terminated PEG-folate

As the same number of mole of ninhydrin (i.e. 4 mole) was used in both reactions; therefore, 1 mole of bis(3-aminopropyl) terminated PEG-folate is equivalent to 2 moles of bis(3-aminopropyl) terminated PEG-folate. The absorbance of a 0.368 mg/mL PEG bis(3-aminopropyl) terminated-folate solution at a wavelength of 570 nm was 0.25 which equivalent to 0.059 mg of bis(3-aminopropyl) terminated PEG obtained using the standard curve.

$H_2N\text{-}(CH_2)_3\text{-}(CH_2CH_2O)_n\text{-}(CH_2)_3\text{-}NH_2$ = 2 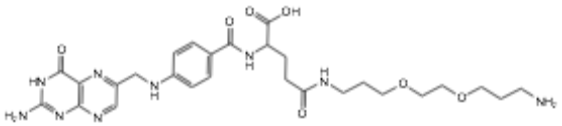

MW = 1500 MW=1923

if X is weight of bis(3-aminopropyl) terminated PEG-folate

$$0.059/1500 = (2X)/1923$$

$$X = 0.037 \text{ mg}$$

Therefore, the amount of bis(3-aminopropyl) terminated PEG-folate was 0.037 mg. Consequently, the UV/vis spectrophotometric results of folate and $-NH_2$ content verified both the presence of folate and $-NH_2$ in sample and indicated that the folate and $-NH_2$ were associated in the desired 1:1 ratio.

6.5 The synthesis of tresylated Brij O10

6.5.1 The preparation of tresylated Brij O10

In the preparation of tresylated Brij O10 (**Figure 6.9**), tresyl chloride (2,2,2-trifluoroethanesulfonyl chloride), an organic sulfonyl chloride, was reacted with Brij O10 dissolved in anhydrous dichloromethane. The synthesis of tresylated Brij O10 was performed in an anhydrous solvent in order to avoid the hydrolysis of the sulfonyl chloride ($-SO_2Cl$) in the tresyl chloride. Pyridine was added to neutralise the acidity of the reaction due to the HCl produced in the reaction. It is also known that Brij O10 has one terminal hydroxyl (OH) group. The terminal OH can then be activated with tresyl chloride. Tresyl chloride can then be coupled with the amine group of bis(3-aminopropyl) terminated PEG during the preparation in folate derived Brij O10. From this reaction, tresylated Brij O10, a white and waxy product, was produced. The percent yield of tresylated Brij O10 was 22%.

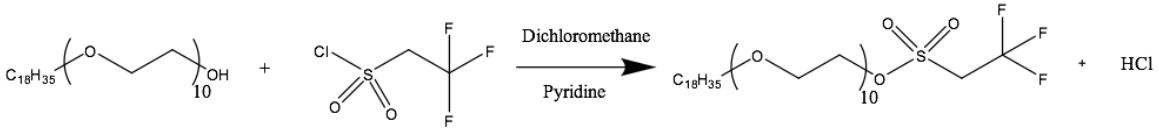

Brij O10 Tresyl chloride Tresylated Brij O10

Figure 6.9: Synthesis of tresylated Brij O10

In previous studies, a skilful method was developed for the activation of hydroxyl expressing supports such as agarose, cellulose, diol-silica, glycophase-glass or hydroxyethyl methacrylate using tresyl chloride such that a coupling reaction of proteins with a tresylated OH group was developed (Nilsson and Mosbach, 1981; Nilsson and Mosbach, 1984). In this method, tresyl chloride was used to convert a hydroxyl (OH) group to a sulfonate (RSO_3^-) - a good leaving group - which allowed the formation of linkages between the nucleophile and the hydroxyl group-carrying carbon. The activation and coupling of the ligand to the support involved the following steps:

Activation: support-CH_2OH + R-SO_2CI → support-CH_2OSO_2-R

Coupling: support-CH_2OSO_2-R + H_2N-ligand → support-CH_2-NH-ligand + $HOSO_2$-R

Analogous to this methodology both Brij 78 and Brij 700 have been reacted with tresyl chloride to prepare tresylated Brij 78 and tresylated Brij 700, respectively which were

subsequently conjugated to horseradish peroxidase to prepare solid lipid nanoparticles (Jain et al., 2010).

6.6 The synthesis of folate derived Brij O10

6.6.1 The preparation of folate derived Brij O10

The synthesis of folate derived Brij O10 is shown in **Figure 6.10**. Tresylated Brij O10 was prepared by the conversion OH group of Brij O10 into a sulfonate - a good leaving group - which allowed the formation of linkage between the nucleophile and the hydroxyl group-carrying carbon (Nilsson and Mosbach, 1981; Nilsson and Mosbach, 1984).

In the present study the support-CH_2OSO_2-R is the tresylated Brij O10, while the H_2N-ligand represents bis(3-aminopropyl) terminated PEG. Furthermore, the support-CH_2-NH-ligand is folate derived Brij O10. From this coupling reaction, it would be anticipated that PEG bis(3-aminopropyl) terminated-folate was coupled with tresylated Brij O10 to form folate derived Brij O10. The solvent was removed from the reaction mixture using rotary evaporation and the resulting dry product dissolved in water.

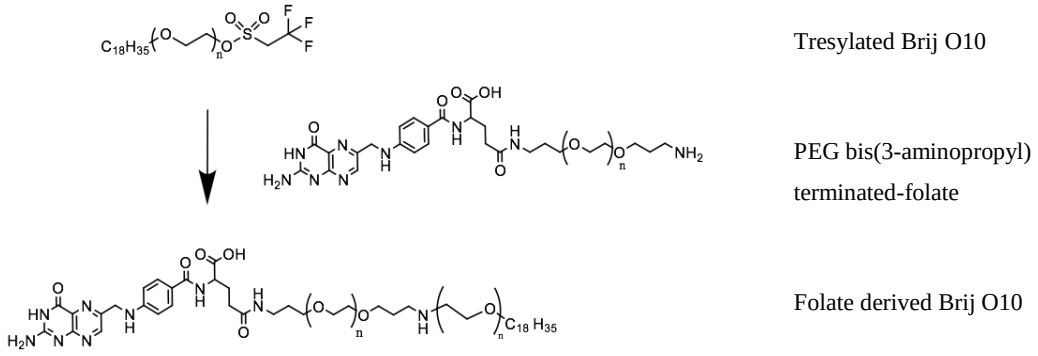

Figure 6.10: Synthesis of folate derived Brij O10

Due to the high amount of product used in the preparation of folate derived Brij O10, the product was divided into 3 separations. After that, each product solution was eluted through Sephadex G-25 to separate folate derived Brij O10 molecule from the uncoupled PEG bis(3-aminopropyl) terminated-folate according to their difference in molecular weight. The compound with higher molecular weight, namely the folate derived Brij O10 (MW = 2615) was eluted more quickly than the lower molecular weight parent molecule, namely PEG bis(3-aminopropyl) terminated-folate (MW = 1923) and tresylated Brij O10 (MW = 855).

The difference in molecular weight between the folate derived Brij O10 and the PEG bis(3-aminopropyl) terminated-folate and tresylated Brij O10 was enough to separate them.

6.6.2 The analysis of folate derived Brij O10

Figure 6.11 gives a schematic diagram of the analysis of folate derived Brij O10. The folate and -NH_2 content of each 10 mL fraction eluted through a Sephadex G-25 column were determined using UV absorbance at 364 nm and by the ninhydrin assay, respectively.

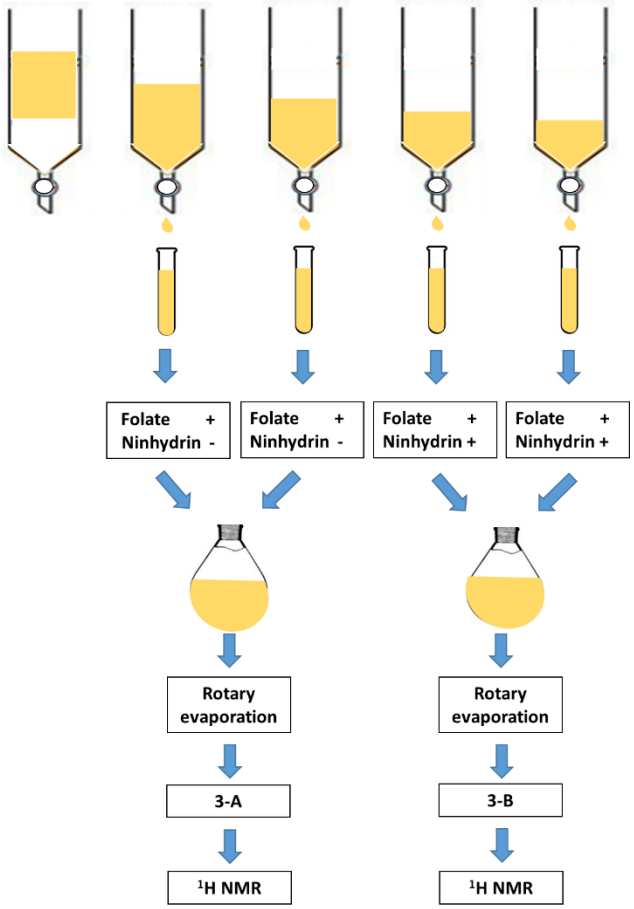

Figure 6.11: Diagram shows the process of the analysis of all fractions obtained from the preparation of folate derived Brij O10 by using UV/vis spectroscopy, ninhydrin reaction and proton nuclear magnetic resonance spectroscopy (^{1}H NMR).

The first yellow 10 mL fraction were collected starting at about 150-160 mL (fractions 15-16) and continued until the last yellow fraction, which eluted at ~ 300-310 mL (fractions 30-31). UV/vis spectroscopy and ninhydrin reaction were used to analyse all fractions obtained from the preparation of folate derived Brij O10 (**Figure 6.11**). 10 mL fractions which

exhibited the same result for the folate analysis and the ninhydrin reaction were pooled together and the solvent removed using a rotary evaporator. The dry product of fractions which contained folate but were negative to ninhydrin were denoted as "3-A", while the dry product of fractions positive to both folate and ninhydrin were described as "3-B". The chemical structures of dry product of 3-A and 3-B were separately determined using ^{1}H NMR spectroscopy.

6.6.2.1 The analysis of folate derived Brij O10 using UV/vis spectroscopy

All yellow coloured elutes from the Sephadex G-25 column were analysed using UV/vis spectroscopy to determine the amount of folic acid (**Figure 6.12**).

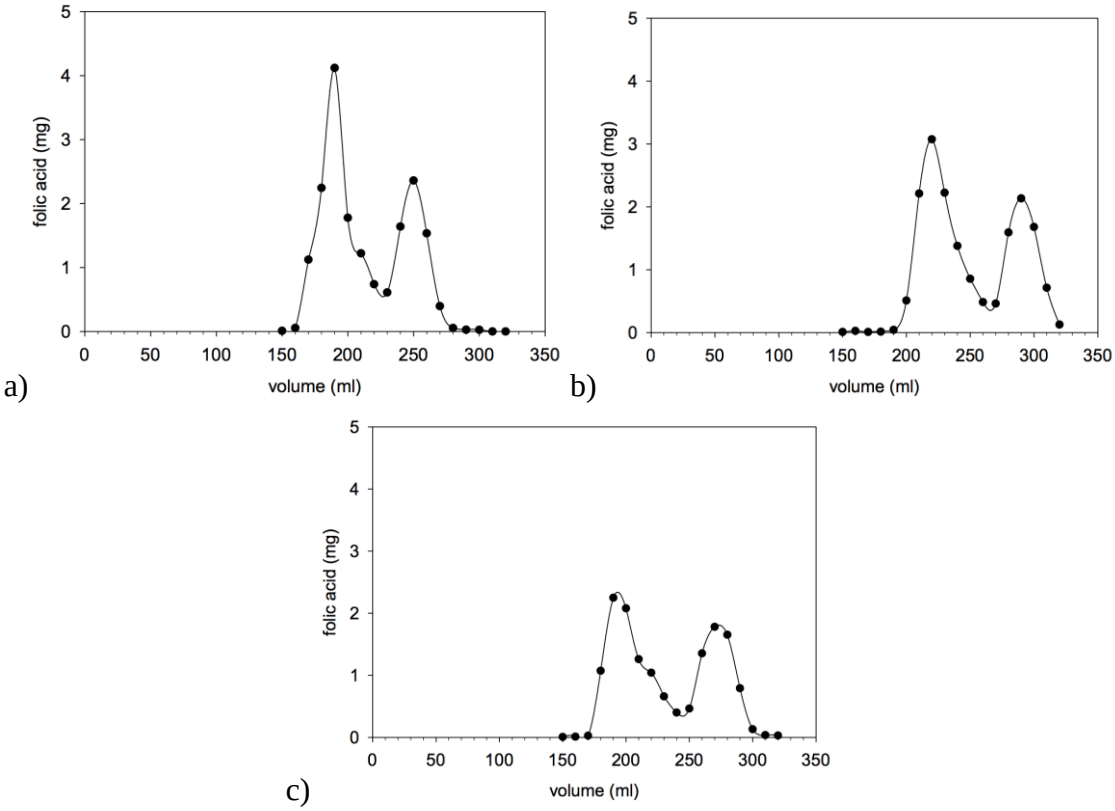

Figure 6.12: The amount of folic acid in the yellow 10 mL fractions eluted from Sephadex G-25 in the (a) first, (b) second and (c) third separation of the preparation of folate derived Brij O10 determined by the UV/vis spectroscopy using the absorbance at the wavelength of 364 nm.

6.6.2.2 The analysis of folate derived Brij O10 using ninhydrin reaction

Each fraction of yellow coloured elutes was analysed for the presence of -NH_2 group using the ninhydrin assay. In the ninhydrin assay, bis(3-aminopropyl) terminated PEG and folic acid were the positive and negative controls, respectively. The positive control, bis(3-aminopropyl) terminated PEG was mixed with ninhydrin and upon heating the colour of the mixture become purple. On the other hand, when the negative control, folic acid, was reacted with ninhydrin, the colour of the mixture remained yellow after heating. The result of ninhydrin assay performed on each yellow fraction is shown in **Table 6.2**.

Table 6.2 The reaction of each fraction in the synthesis of folate derived Brij O10 to ninhydrin solution

Sample	Order of separation		
	First	Second	Third
Bis(3-aminopropyl) terminated PEG (positive control)	Purple	Purple	Purple
Folic acid (negative control)	Yellow	Yellow	Yellow
Fraction 1 at 150 - 160 ml	Yellow	Yellow	Yellow
Fraction 2 at 160 - 170 ml	Yellow	Yellow	Yellow
Fraction 3 at 170 - 180 ml	Yellow	Yellow	Yellow
Fraction 4 at 180 - 190 ml	Yellow	Yellow	Yellow
Fraction 5 at 190 - 200 ml	Yellow	Yellow	Yellow
Fraction 6 at 200 - 210 ml	Yellow	Yellow	Yellow
Fraction 7 at 210 - 220 ml	Yellow	Yellow	Yellow
Fraction 8 at 220 - 230 ml	Yellow	Yellow	Yellow
Fraction 9 at 230 - 240 ml	*Purple*	Yellow	Yellow
Fraction 10 at 240 - 250 ml	*Purple*	Yellow	*Purple*
Fraction 11 at 250 - 260 ml	*Purple*	Yellow	*Purple*
Fraction 12 at 260 - 270 ml	Yellow	*Purple*	*Purple*
Fraction 13 at 270 - 280 ml	Yellow	*Purple*	*Purple*
Fraction 14 at 280 - 290 ml	Yellow	*Purple*	Yellow
Fraction 15 at 290 - 300 ml	Yellow	*Purple*	Yellow
Fraction 16 at 300 - 310 ml	Yellow	Yellow	Yellow

According to the results of the UV/vis spectroscopy and the ninhydrin assay, fractions 1-8 (first separation), fractions 1-11 (second separation) and fractions 1-9 (third separation) contained folate but were negative to ninhydrin assay (i.e. the fractions did not contain a -NH_2 group). Consequently these fractions were pooled together and evaporated using the rotary evaporation to obtain dry product which was called "3-A" (**Figure 6.11**).

On the other hand, fractions 9-11 (first separation), fractions 12-15 (second separation) and fractions 10-13 (third separation) all contained folate and were positive to ninhydrin indicating that these fractions contained -NH_2 group. Thus all these fractions were pooled together and evaporated using a rotary evaporator to obtain dry product which was called "3-B" (**Figure 6.11**).

According to the order of elution, it can be assumed that the structure of the compound contained in fractions 1-8 (first separation), fractions 1-11 (second separation) and fractions 1-9 (third separation) was likely to be folate derived Brij O10, whereas the compound present in fractions 9-11 (first separation), fractions 12-15 (second separation) and fractions 10-13 (third separation) was considered to be PEG bis(3-aminopropyl) terminated-folate. In order to confirm the structures contained in the dry products 3-A and 3-B, 400 MHz ^{1}H NMR spectroscopy was used.

6.6.2.3 Proton nuclear magnetic resonance spectroscopy (^{1}H NMR)

The molecular weight of folate derived Brij O10 and PEG bis(3-aminopropyl) terminated-folate were respectively, 2615 and 1923. The results of the UV/vis spectroscopy (**Figure 6.12**) and ninhydrin assays (**Table 6.2**) suggested that the dry product 3-A (the first peak in the three separations) was the desired product, the folate derived Brij O10, because of the absence of a -NH_2 group coupled with the fact that folate derived Brij O10 possess a higher molecular weight than bis(3-aminopropyl) terminated PEG as so will be expected to be eluted much quicker. The production of the desired conjugation product was confirmed by ^{1}H NMR spectroscopy as shown in **Figure 6.13**.

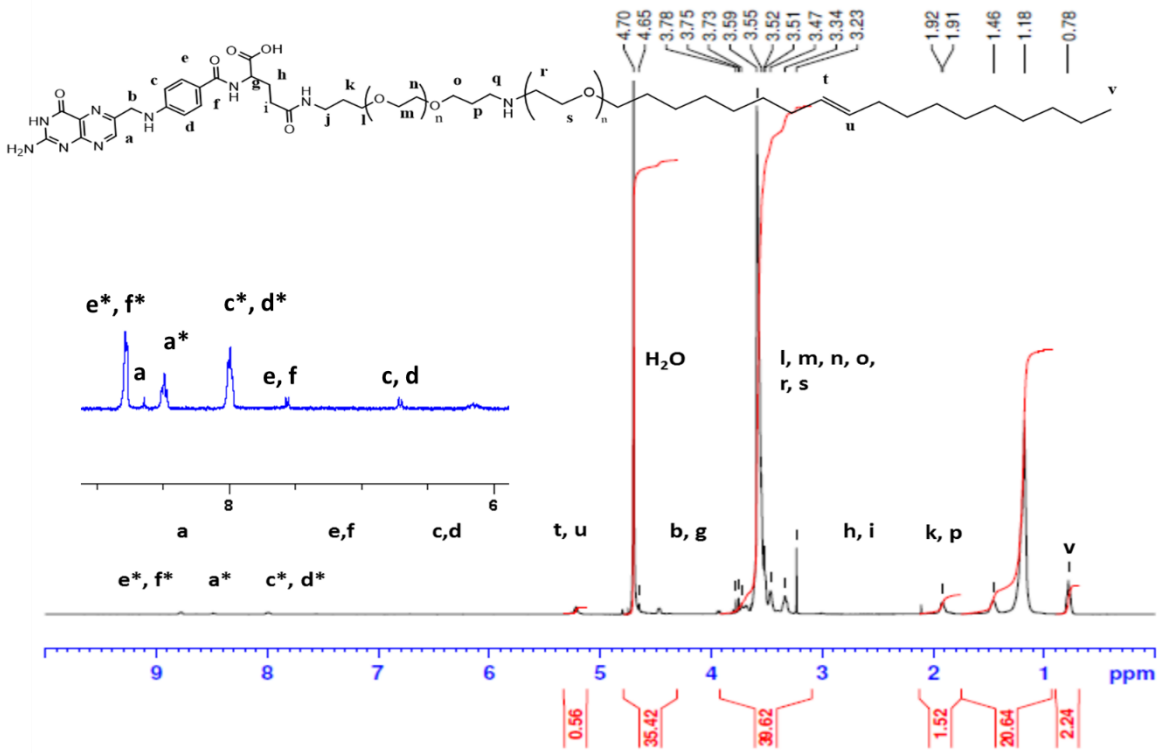

Figure 6.13: ^{1}H NMR spectrum of fraction 1-8 (first separation) (400 MHz, D_2O): δ 8.78, 8.64, 8.49, 8.00, 7.61, 6.73, 5.26, 4.23, 3.96, 3.56, 2.23, 1.97, 1.50, 1.22, and 0.82 ppm. (a*, c*, d*, e* and f* were protons of folate of folate derived Brij O10 while a, c, d, e and f were protons of folate of bis(3-aminopropyl) terminated PEG).

It is clear that the ^{1}H NMR spectrum of the folate derived Brij O10 contained signals arising from folic acid, bis(3-aminopropyl) terminated PEG and Brij O10. ^{1}H NMR results of the dry product 3-A showed the signal at 3.56-3.96 ppm (position l, m, n, o, r, s) corresponded to the methylene protons present in the PEG region of bis(3-aminopropyl) terminated PEG and the PEG in Brij O10 molecule. The signals at 8.00 ppm (position c*, d*) and 8.78 ppm (position e*, f*) corresponded to the para-aminobenzoic acid (PABA), and the signal at 8.64 ppm (position a*) corresponded to the pteridine moiety proton from the folate of folate derived Brij O10. The signal at 4.23 ppm (position b, g), and 2.23 ppm (position h, i) was assigned to the methylene of folate. The signal at 1.97 ppm (position k, p) was assigned to the methylene of bis(3-aminopropyl) terminated PEG. The signal at 5.26 ppm (position t, u) was belonged to double bond of Brij O10, and the signal at 0.82 ppm (position v) was assigned to methylene group of Brij O10. Consequently, ^{1}H NMR results confirmed the conjugation of PEG bis(3-aminopropyl) terminated-folate and tresylated Brij O10 to yield the desired product. The percentage yield of folate derived Brij O10 was 89%. However, the

signals at 6.73 ppm (position c, d) and 7.61 ppm (position e, f) corresponded to the para-aminobenzoic acid (PABA) in the folate of bis(3-aminopropyl) terminated PEG, while the signal at 8.66 ppm (position a) corresponded to protons from the pteridine moiety present in the folate of bis(3-aminopropyl) terminated PEG which suggested that this product contained a very small amount of bis(3-aminopropyl) terminated PEG.

On the other hand, the second peak of dry product 3-B in the preparation of folate derived Brij O10 was considered to be PEG bis(3-aminopropyl) terminated-folate because the fractions contained molecules possessing a -NH_2 group (i.e. they were positive to ninhydrin). This result is supported by the ^{1}H NMR results which indicate that there is no signal attributable to a double bond nor any methylene group of Brij O10 (**Figure 6.14**).

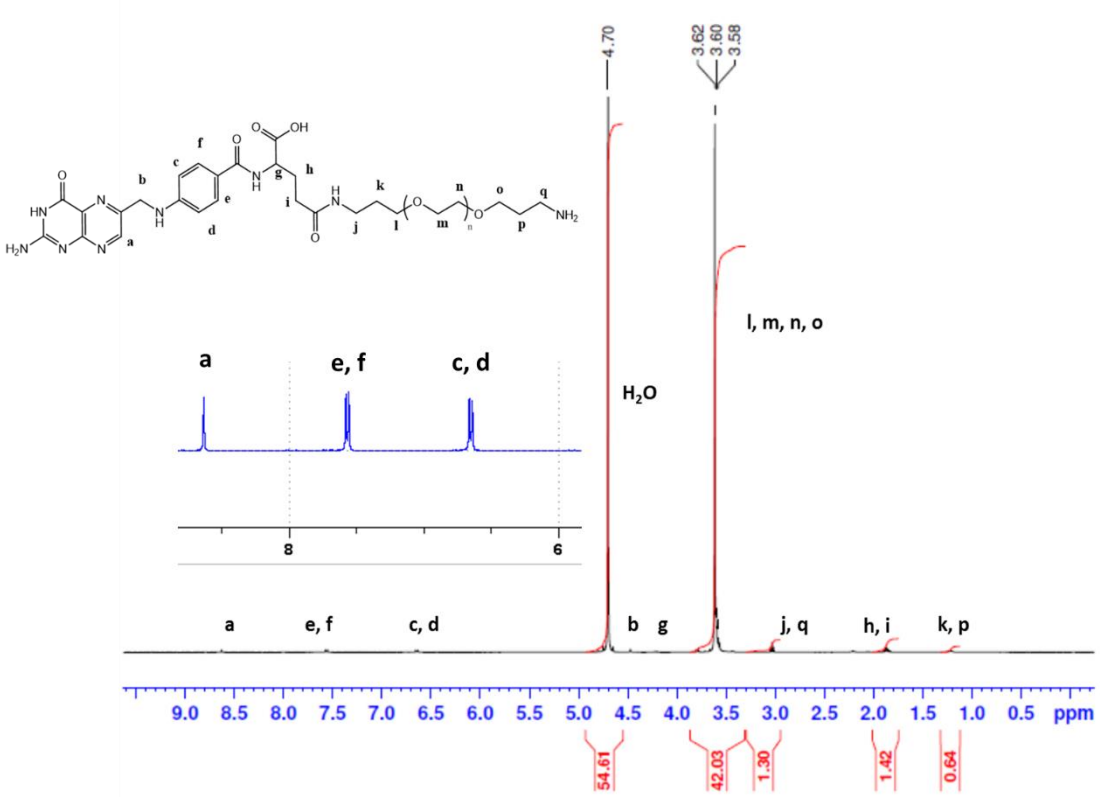

Figure 6.14: ^{1}H NMR spectrum of fraction 9-11 (first separation) (400 MHz, D_2O): δ 8.63, 7.55, 6.66, 4.47, 4.22, 3.60, 3.05, 1.88 and 1.20 ppm.

The product 3-B showed the signals originating from both the folic acid and the bis(3-aminopropyl) terminated PEG. The ^{1}H NMR results showed the signals at 3.60 ppm (position l, m, n, o) corresponded to the methylene protons in the bis(3-aminopropyl) terminated PEG molecule, while the signals at 6.66 ppm (position c, d) and 7.55 ppm (position e, f) corresponded to the para-aminobenzoic acid (PABA) from the folate, and the signal at 8.63

ppm (position a) to the protons of the pteridine moiety of the folate. The signals at 4.22-4.47 ppm (position b, g), and 1.88 ppm (position h, i) were assigned to methylene of the folate. The signals at 3.05 ppm (position j, q), and 1.20 ppm (position k, p) were assigned to methylene of bis(3-aminopropyl) terminated PEG. Moreover, mass spectral analyses (e.g. MALDI-TOF) could have been used in the analysis of folate derived Brij O10.

In addition, a comparison of the UV absorbance of the various fractions eluted from Sephadex G-25 column showed that folate derived Brij O10 eluted more quickly than the PEG bis(3-aminopropyl) terminated-folate because of the higher molecular weight of folate derived Brij O10 (**Figure 6.15**). The molecular weight of folate derived Brij O10 was 2615, while that of PEG bis(3-aminopropyl) terminated-folate was 1923. This observation also supported the hypothesis that the first peak eluted (i.e. product 3-A) was folate derived Brij O10, while the second peak eluted (i.e. product 3-B) was PEG bis(3-aminopropyl) terminated-folate.

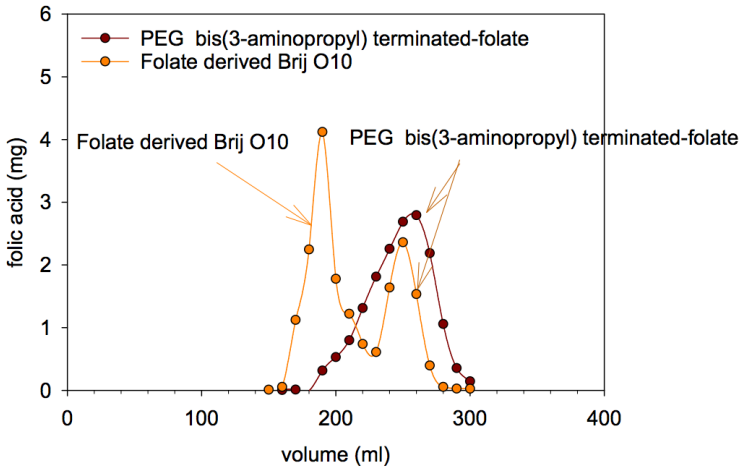

Figure 6.15: A comparison of the UV absorbance at the wavelength of 364 nm of fractions obtained from the synthesis of bis(3-aminopropyl) terminated-PEG folate and the synthesis of folate derived Brij O10.

6.7 Chapter summary

In order to selectively deliver anticancer drugs such as CUR and DTX to solid tumours expressing folate receptor, folate derived Brij O10 has been synthesised. Firstly, PEG bis(3-aminopropyl) terminated-folate was prepared by reacting bis(3-aminopropyl) terminated PEG with folic acid in dimethylsulfoxide containing dicyclohexylcarbodiimide and pyridine overnight in the dark. Secondly, tresylated-Brij O10 was prepared by dropwise addition at

0^{o}C of tresyl chloride in pyridine to Brij O10 in dichloromethane, after which the mixture was stirred under nitrogen. Finally, folate derived Brij O10 was prepared by reacting PEG bis(3-aminopropyl) terminated-folate in anhydrous dimethylformamide with tresylated-Brij O10 overnight. UV/vis spectroscopy, ninhydrin assay and ^{1}H NMR analysis were employed to confirm the structure of the intermediates and final product.

A ninhydrin assay and UV/vis spectroscopy showed that the product of the first reaction contained folate and an -NH_2 group while ^{1}H NMR confirmed the coupling of folate with bis(3-aminopropyl) terminated PEG. The white and waxy tresylated Brij O10 was synthesised. In the third step, the results of ninhydrin assay, UV/vis spectroscopy and ^{1}H NMR investigations showed that the product of third step was folate derived Brij O10 group while ^{1}H NMR confirmed the coupling of folate with bis(3-aminopropyl) terminated PEG. Therefore, it can be concluded that folate derived Brij O10 has been successfully synthesised and characterised. In addition, the mass spectral analyses (e.g. MALDI-TOF) could have been used in the analysis of the structure of the intermediates and the final product.

Chapter 7
Conclusion and Future Work

7.1 Conclusion

7.1.1 The preparation, characterisation and cytotoxicity of Brij O10 NE

Brij O10 NE was studied for the preparation of NE containing either a high molecular volume triglyceride or ethyl ester oil. The phase behaviour of Brij O10 NE showed the effect of the purity and the presence of saturation levels of oils on the extent of the area of NE existence. The PIT experiments, particle size determination and SANS studies suggest that Brij O10 NE forms a distinct core of oil in the NE.

To investigate the ability of Brij O10 NE to solubilise poorly water soluble drugs, TP and CUR, were chosen as drugs. The TP solubilisation suggested that the level of TP solubilisation in Brij O10 NE was noticeably higher than that observed in the Brij O10 micelles which indicated that the NE are suitable as drug delivery vehicles for TP. In particular, TP solubilisation exhibited an increase in TP solubility in the clear/transparent, Region A NE. However, TP solubilisation levelled off in bluish/translucent, Region B NE and dramatically decreased in the cloudy/milky, Region C NE. This levelling off and decrease in TP solubilisation was unexpected as it was anticipated that TP solubilisation in these regions would increase due to the high oil content. This unexpected solubilisation behaviour was explained by the SANS studies which indicated the transformation in the morphology of the aggregates upon increasing oil content from an oblate ellipsoid to a more elongated ellipsoid, which results in a decrease in the solubility of TP in the cloudy/milky, Region C NE. In addition, CUR solubilisation suggested that Brij O10 NE are suitable to deliver CUR as they exhibited a high level of CUR solubilisation. However, the solubilisation of CUR did not show the anticipated increase in CUR solubilisation in the clear/transparent, Region A NE as the amount of oil increased. This observation could be explained by a small amount of CUR solubilised in both hSBO and 98hEO. Moreover, the CUR and TP solubilisation in B20-hSBO NE showed an increase in CUR solubilisation and a decrease in TP solubilisation compared to the level of solubilisation obtained for a single drug in the corresponding NE, suggesting that the presence of CUR affected the level of TP solubilisation in NE. Taken together the results of the characterisation and solubilisation studies suggest that the ability of Brij O10 NE

to solubilise drug(s) depends on the nature of drug, the amount of oil in NE, the morphology of NE and the absence or presence of a second drug.

Unfortunately, the MTT assay showed the high level of cytotoxicity of the Brij O10 NEs towards HeLa (folate-expressing cervical-tumour-derived cell line) and CT26 (murine colon carcinoma) cells, suggesting that the pharmaceutical application of the Brij O10 NE was limited.

7.1.2 The preparation, characterisation and cytotoxicity of Tween 80 NE in the absence and presence of cosurfactant

Among the various nonionic surfactant NE systems that were studied, Tween 80 NE were seen to incorporate the highest amount of oil, which indicated that these NE were worthy of further study. However, relative to the Brij O10 NE, the Tween 80 NE (T20) could incorporate only small amounts of oil and were therefore not expected to exhibit a high level of drug solubilisation. Consequently, the addition of the cosurfactant, Dermosoft GMCY and the second surfactant, lecithin were considered for further studies. It was clear that the addition of Dermosoft GMCY and lecithin, in T20 NE resulted in a bigger area of NE existence as well as the formation of larger aggregates of TD25 and TDL25 NE as determined by PIT, PCS and SANS studies. Understanding the dilutability of the NE in the presence of the cosurfactant, Dermosoft GMCY, was important before performing any further studies as it is well known that the presence of cosurfactant could affect the stability of the diluted NE. The PIT experiments, the particle size studies and the SANS measurements suggested that, regardless of the presence of cosurfactant, the oil in the Tween 80-containing NE contained a distinct core of oil.

To examine the ability of the Tween 80 containing NE as drug delivery systems for the poorly water soluble drugs, TP, CUR and DTX were selected as poorly water soluble drugs. Clearly, T20-hSBO, T20-98hEO, TD25-98hEO and TDL25-hSBO NE could solubilise good levels of TP or CUR. The solubility of TP in TD25-98hEO NE showed an increase in TP solubilisation with the increasing oil content. In contrast, the solubility of CUR did not exhibit an increase in CUR solubilisation with increasing oil content. In addition, the presence of CUR in an NE was observed to decrease the solubility of TP in the NE. Surprisingly, no improvement in DTX solubilisation was observed in TDL25-hSBO NE. It is hard, however, to evaluate the advantage of NE over the corresponding micelles on DTX solubilisation because of the limited amount of hSBO (3 %w/w) incorporated into the TDL25-hSBO NE.

The cytotoxicity of T20-hSBO, TD25-98hEO and TDL25-hSBO NE towards the HeLa and CT26 cell lines suggested that 'drug-free' T20-hSBO, TD25-98hEO and TDL25-hSBO NE were far less toxic than the 'drug-free' B20-hSBO and B20-98hEO NE. Unfortunately, the NE containing CUR did not show any difference in cytotoxicity from the blank NE which suggested that the presence of CUR in NE did not enhance the cytotoxicity of NE in both cancer cell lines. On the other hand, the presence of DTX in TDL25-hSBO-DTX NE exhibited a significant enhancement in the cytotoxicity of NE in both CT26 and HeLa cell lines when compared to the 'drug-free' TDL25-hSBO NE, suggesting that the NE were potentially suitable delivery vehicles.

In order to selectively deliver NE containing DTX to solid tumours expressing the folate receptor, folate derived Brij O10 was synthesised. Folate derived Brij O10 was prepared by reacting PEG bis(3-aminopropyl) terminated-folate with tresylated Brij O10. UV/vis spectroscopy, a ninhydrin assay and ^{1}H NMR analysis were employed to confirm the structure of the intermediates of the synthesis as well as the final product. From the range of analytical techniques it was concluded that the folate derived Brij O10 was successfully synthesised.

7.2 Future work

The folate derivative, Brij O10 (FA-PEG-Brij) which contains a folate targeting group and is attached to Brij O10 via a short polyoxyethylene glycol chain is an attractive molecule to incorporate into the TDL25-hSBO3 NE to see if it is possible to specifically target cancer cells expressing folate receptors on their cell surface. However, before the ability of DTX containing NE incorporating the folate derived Brij O10 (FA-PEG-Brij-TDL25-hSBO3) to target to cancer cells is determined, the cytotoxicity of FA-PEG-Brij-TDL25-hSBO3 and FA-PEG-Brij-TDL25-hSBO3-DTX needs to be studied. Although the cytotoxicity studies of NE prepared from Brij O10 in CT26 and HeLa cells indicated that Brij O10 was quite toxic, the concentration of folate derived Brij O10 to be added to the TDL25-hSBO3-DTX NE to achieve targeting is likely to be very low. From **Figures 5.5, 5.6 and 5.7**, it can be seen that a concentration of 0.001 %w/w Brij O10 did not exhibit toxicity towards the CT26 and HeLa cell lines suggesting a concentration of 0.001 %w/w or less in the formulation would be satisfactory. NE formulations to be tested containing the Brij O10 derived folate targeting group are: (a) FA-PEG-Brij-TDL25-hSBO3; and (b) FA-PEG-Brij-TDL25-hSBO3-DTX. The cytotoxicity of these formulations will be compared to the cytotoxicity results obtained for TDL25-hSBO3 and

TDL25-hSBO3-DTX NE in the absence of targeting group, which is recorded in Chapter 5. It is anticipated that significant differences would be obtained between the targeted and nontargeted NE formulations when tested in HeLa cells, a positive cell line in this study, whereas the murine Colon Cancer CT26 cells, a negative cell line in this study, would be expected not to show a difference in the cytotoxicity obtained when treated with NE in the presence or absence of FA. These results are expected to confirm the benefit of the NE containing the FA-PEG-Brij targeting molecule. **Figure 7.1** gives a schematic of what the TDL25-hSBO NE may look like in the absence and presence of folate derived Brij O10.

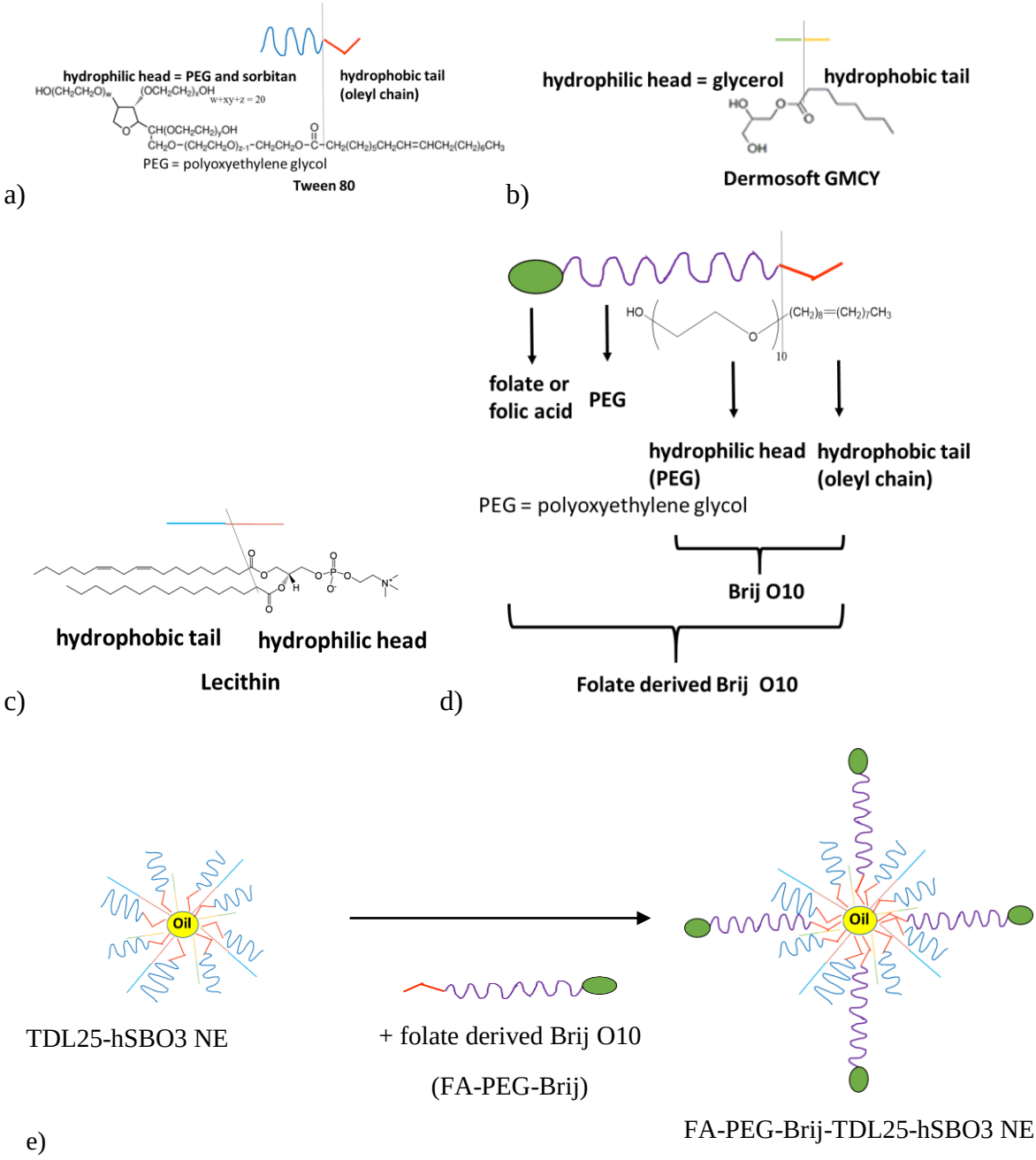

Figure 7.1: Schematic representative of a) Tween 80, b) Dermosoft GMCY, c) lecithin, d) folate derived Brij O10 and e) TDL25-hSBO NE in the absence and presence of folate derived Brij O10.

Moreover, to understand the mechanism behind the enhanced cytotoxicity of FA-PEG-Brij-TDL25-hSBO3 NE in comparison with blank TDL25-hSBO3 NE, the uptake of NE inside HeLa cell will be performed in NE labelled by incorporating the lipid soluble fluorescent dye, 1,1'-dioctadecyl-3,3,3',3'-tetramethylindocarbocyanine perchlorate (Dil) in the oil core of NE. The concentration of dye in the NE will be optimised so that the lowest concentration that can be detected will be present in the cell lysate. When the optimisation has been satisfactorily achieved, HeLa cells will be incubated with drug-free NE. In addition, the intracellular delivery to HeLa cells of the folate targeted NE will be studied by confocal laser scanning microscopy (CLSM). HeLa cells will be fixed and stained for F-actin (green) before examination by CLSM. The uptake of the NE will be further confirmed by the presence of red fluorescence of Dil inside the cells.

Finally, TDL25-hSBO3 NE in the absence and presence of FA-PEG-Brij will be examined by animal studies. In particular NE uptake by tumours in *in vivo* experiments will be established using hydrophobic fluorescent markers such as DiR (1,1'-Dioctadecyl-3,3,3',3'-tetramethylindocarbocyanine iodide) incorporated into the oil phase of the NE. Dil will be exchanged with DiR for the *in vivo* studies as it absorbs light in the near-infrared (NIR) region, thus allowing for better tissue penetration and a better signal-to-noise ratio. Female Athymic nude and SHrN mice aged-4-6 weeks (Harlan) will be used for the *in vivo* studies and inoculated subcutaneously with HeLa cells (5×10^6 cells in 0.1 mL PBS) in their lower flanks. When the tumours reach an appropriate size (600 mm^3), the mice will be maintained on a folate free diet (Test Diet) for one week prior to, and for the duration of the *in vivo* studies. Mice (n = 3) will be intravenously injected with the DiR-labelled TDL25-hSBO3 NE in the absence and presence of FA-PEG-Brij and the animals scanned at 1, 4, and 24 hours post injection. Animals will be anesthetized to maintain sedation during imaging. *Ex vivo* imaging will be performed immediately afterward by imaging excised major organs (heart, lung, liver, spleen and kidney) including the tumours. The tumours in the HeLa-bearing mice which were injected with Dil-labelled NE will be snap-frozen at 24 h post IV injection prior to examination by CLSM studies.

Appendix

Appendix A: Composition of stock micelle and nanoemulsion solutions for small-angle neutron scattering experiments

Usually 15 μA were accumulated during the scattering measurement for Brij O10 NE samples containing hSBO, 85hTPN and 99hTPN (namely B2-hSBO, B2-85hTPN, B2-99hTPN) in D_2O and 20 μA and 25 μA were accumulated during the scattering measurement for Brij O10 NE containing dTPN (i.e. B2-dTPN) in D_2O and H_2O, respectively. 10 μA was accumulated during the scattering measurement for Brij O10 micelles (B micelle) and Brij O10 NE containing 65hGTO, 99hGTO, dGTO, 99hGTS and 98hEO (namely B2-65hGTO, B2-99hGTO, B2-dGTO, B2-99hGTS, B2-98hEO) in D_2O or H_2O. 20 μA was accumulated during the scattering measurement for Tween 80 micelles (T micelle) in D_2O while 10 μA was accumulated during the scattering measurement for Tween 80:Dermosoft GMCY micelles (TD micelle) in D_2O. 5 μA was accumulated during the scattering measurements made for Tween 80:Dermosoft GMCY NE containing 98hEO (i.e. TD2-98hEO), Tween 80:Dermosoft GMCY:lecithin micelles (TDL micelle) and Tween 80:Dermosoft GMCY:lecithin NE containing hSBO (TDL-hSBO) in D_2O. Similarly, 5 μA was accumulated for Brij O10 NE containing hSBO, TD micelles and NE containing 98hEO and TDL micelles and NE containing hSBO (namely B2-hSBO-37C, TD2-37C, TD2-98hEO-37C, TDL2-37C and TDL2-hSBO-37C) prepared in D_2O and measured at 37 ºC and for Brij O10 NE containing hSBO and TD NE containing 98hEO samples (namely B2-hSBO-DM-37C and TD2-98hEO-DM-37C) prepared in a mixture of D_2O and complete media at 37 ºC. The compositions of stock micelle and nanoemulsion formulations are given in **Table A.1**.

Appendix

Table A.1 Composition of stock micelle and nanoemulsions
A.1a) Brij O10 micelles (B micelles)

Micelle composition (%w/w)	**B0.1**	**B0.2**	**B0.5**	**B1**	**B1.5**	**B2**	**B5**	**B10**	**B15**	**B20**
Brij O10 (B) (%w/w)	0.1	0.2	0.5	1	1.5	2	5	10	15	20
Aqueous phase (%w/w)	99.9	99.8	99.5	99	98.5	98	95	90	85	80

A.1b) Brij O10 and soybean oil nanoemulsions (B-SBO NE)

NE composition (%w/w)	**B20-SBO2**	**B20-SBO4**	**B20-SBO6**	**B20-SBO8**	**B20-SBO9**	**B20-SBO10**	**B20-SBO12**	**B20-SBO14**	**B20-SBO16**
Brij O10 (B) (%w/w)	20	20	20	20	20	20	20	20	20
Soybean oil (SBO) (%w/w)	2	4	6	8	9	10	12	14	16
Aqueous phase (%w/w)	78	76	74	72	71	70	68	66	64
Weight ratio of surfactant/oil	10:1	5:1	3.3:1	2.5:1	2.2:1	2:1	1.7:1	1.4:1	1.25:1

The maximum level of incorporation of hSBO in the clear, Region A, bluish/translucent, Region B and cloudy/milky, C NE was 9, 14 and 16 %w/w, respectively.

A.1c) Brij O10 and triolein nanoemulsions (B-GTO NE)

NE composition (% w/w)	**B20-GTO0.5**	**B20-GTO1**	**B20-GTO2**	**B20-GTO4**	**B20-GTO6**	**B20-GTO8**	**B20-GTO10**	**B20-GTO12**	**B20-GTO15**
Brij O10 (B) (%w/w)	20	20	20	20	20	20	20	20	20
Triolein (GTO)[a] (%w/w)	0.5	1	2	4	6	8	10	12	15
Aqueous phase (%w/w)	79.5	79	78	76	74	72	70	68	65
Weight ratio of surfactant/oil	40:1	20:1	10:1	5:1	3.3:1	2.5:1	2:1	1.7:1	1.3:1

[a] According to the ternary phase diagram of B20-65hGTO and B20-99hGTO NE, B20-65hGTO NE were prepared at oil concentrations of 0.5 and 1 %, while B20-99hGTO NE were prepared at oil concentrations of 0.5, 1, 2, 4, 6, 8, 10, 12 and 15%.

The maximum level of incorporation of 65hGTO in the clear, Region A and bluish/translucent, Region B NE was 1 and 2 %w/w, respectively while 8 and 15 %w/w of the 99hGTO, respectively was incorporated into the corresponding A and B Regions.

A.1d) Brij O10 and tripalmitin nanoemulsions (B-TPN NE)

NE composition (%w/w)	**B20-TPN2**	**B20-TPN4**	**B20-TPN6**	**B20-TPN8**	**B20-TPN10**	**B20-TPN12**	**B20-TPN14**	**B20-TPN16**
Brij O10 (B) (%w/w)	20	20	20	20	20	20	20	20
Tripalmitin (TPN) (%w/w)	2	4	6	8	10	12	14	16
Aqueous phase (%w/w)	78	76	74	72	70	68	66	64
Weight ratio of surfactant/oil	10:1	5:1	3.3:1	2.5:1	2:1	1.7:1	1.4:1	1.25:1

The maximum level of incorporation of 85hTPN in the clear, Region A, bluish/translucent, Region B and cloudy/milky, C NE was 6, 11 and 18 %w/w, respectively while 0.5, 1 and 18 %w/w of the 99hTPN, respectively was incorporated into the corresponding A, B and C Regions.

A.1e) Brij O10 and ethyl oleate nanoemulsions (B-EO NE)

NE composition (%w/w)	**B20-EO2**	**B20-EO4**	**B20-EO6**	**B20-EO8**	**B20-EO9**
Brij O10 (B) (%w/w)	20	20	20	20	20
Ethyl oleate (98hEO) (%w/w)	2	4	6	8	9
Aqueous phase (%w/w)	78	76	74	72	71
Weight ratio of surfactant/oil	10:1	5:1	3.3:1	2.5:1	2.2:1

The maximum level of incorporation of 60hEO in the clear, Region A and cloudy/milky, C NE was 7 and 8 %w/w, respectively while 6 and 8 %w/w of the 98hEO, respectively was incorporated into the corresponding A and B Regions.

A.1f) Brij O10 and tristearin nanoemulsion (B-GTS NE)

NE composition (%w/w)	**B20-GTS1**	**B20-GTS2**	**B20-GTS4**	**B20-GTS6**	**B20-GTS8**	**B20-GTS10**	**B20-GTS12**	**B20-GTS13**
Brij O10 (B) (%w/w)	20	20	20	20	20	20	20	20
Tristearin (99hGTS) (%w/w)	1	2	4	6	8	10	12	13
Aqueous phase (%w/w)	79	78	76	74	72	70	68	67
Weight ratio of surfactant/oil	20:1	10:1	5:1	3.3:1	2.5:1	2:1	1.7:1	1.5:1

The maximum level of incorporation of 60hGTS in the bluish/translucent, Region B NE was 1 %w/w while 11 and 13 %w/w of the 99hGTS, respectively was incorporated into the corresponding B and C Regions.

A.1g) Tween 80 (T micelle), Tween 80:Dermosoft GMCY micelles (3:1) (TD micelles), and Tween 80:Dermosoft GMCY:lecithin (7.5:2.5:1) (TDL micelle)

Micelle composition (%w/w)	**T20**	**TD25 (3:1)**	**TDL25 (7.5: 2.5: 1)**
Tween 80 (T) (%w/w)	20	18.75	17.05
Dermosoft GMCY (D) (%w/w)	-	6.25	5.68
Lecithin (L) (%w/w)	-	-	2.27
Aqueous phase	80	75	75

A.1h) Tween 80:Dermosoft GMCY (3:1) and ethyl oleate nanoemulsions (TD-EO NE) and Tween 80:Dermosoft GMCY:lecithin (7.5:2.5:1) and soybean oil nanoemulsion (TDL-SBO NE)

NE composition (%w/w)	**TD25-EO8**	**TD25-EO9**	**TD25-EO10**	**TDL25-SBO3**
Tween 80 (T) (%w/w)	18.75	18.75	18.75	17.05
Dermosoft GMCY (D) (%w/w)	6.25	6.25	6.25	5.68
Lecithin (L) (%w/w)	-	-	-	2.27
Ethyl oleate (EO) (%w/w)	8	9	10	-
Soybean oil (SBO) (%w/w)	-	-	-	3
Aqueous phase (%w/w)	67	66	65	-
Weight ratio of surfactant[b]/oil	3.1:1	2.8:1	2.5:1	8.3:1

[b] The surfactant and cosurfactant contained in TD25-EO8, TD25-EO9 and TD25-EO10 are Tween 80 and Dermosoft GMCY respectively, while TDL25-SBO3 contains the second surfactant lecithin.
The maximum level of incorporation of 98hEO in the clear, Region A NE was 10 %w/w for TD25-98hEO NE while 3 %w/w of hSBO was incorporated into the corresponding A Regions for TDL25-hSBO NE.

Appendix B: The results for the preparation of Brij O10 nanoemulsions

The structure of all oils was measured using ^{1}H NMR by diluting the oil in deutero-chloroform (**Figure B.1 – B.10**).

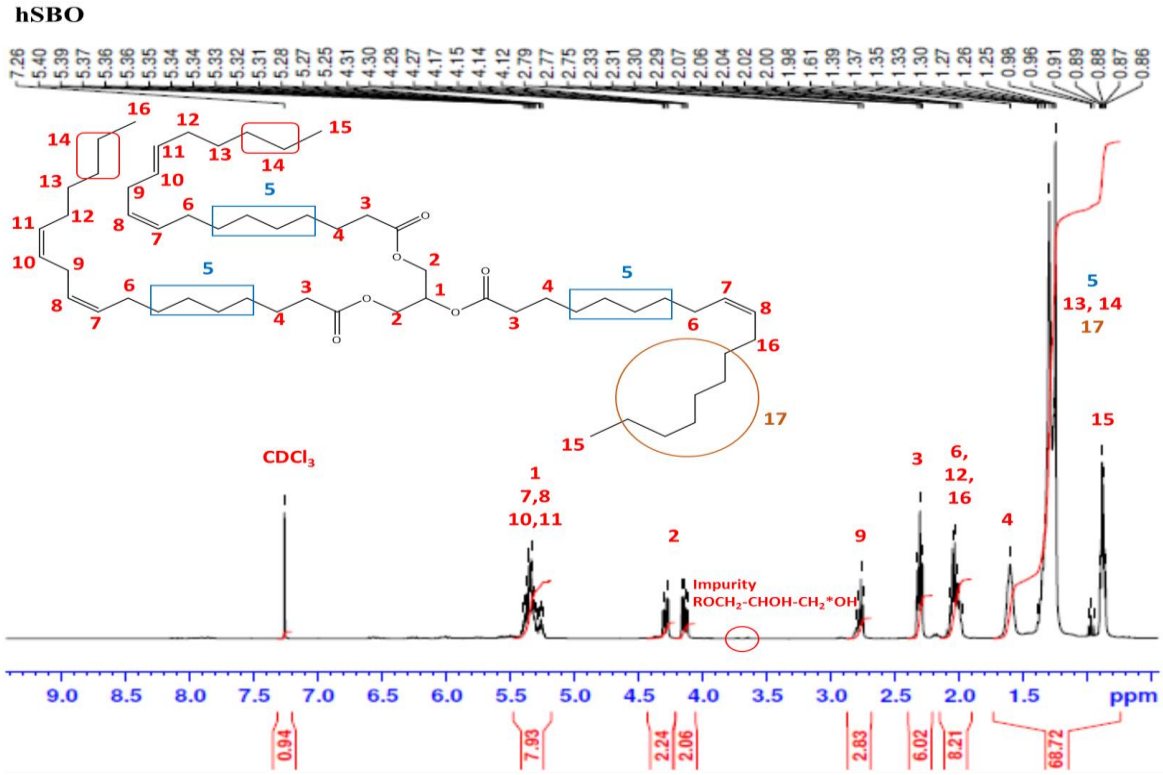

Figure B.1: ^{1}H NMR spectrum of hSBO (400 MHz, $CDCl_3$): δ 5.34, 4.29, 4.14, 2.77, 2.31, 2.16, 2.03, 1.60, 1.29, and 0.88 ppm.

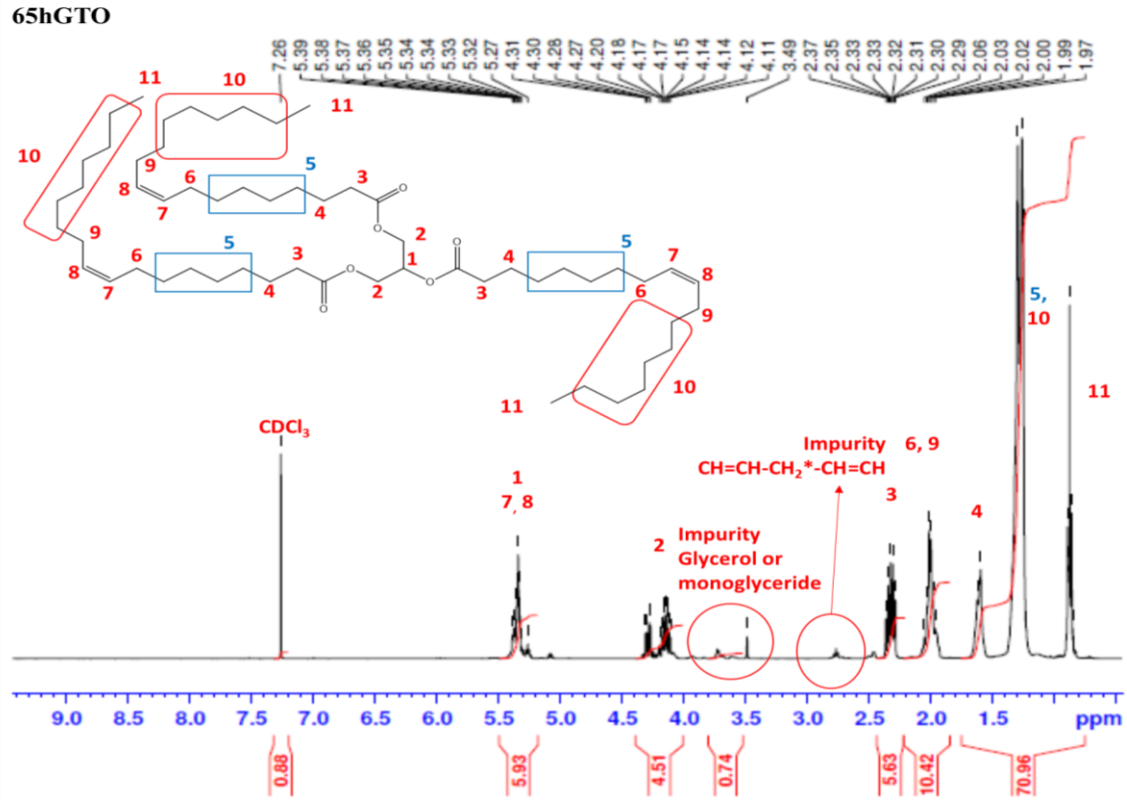

Figure B.2: ^{1}H NMR spectrum of 65hGTO (400 MHz, $CDCl_3$): δ 5.35, 5.08, 4.23, 4.16, 3.74, 3.49, 2.76, 2.48, 2.32, 2.00, 1.61, 1.28, and 0.88 ppm.

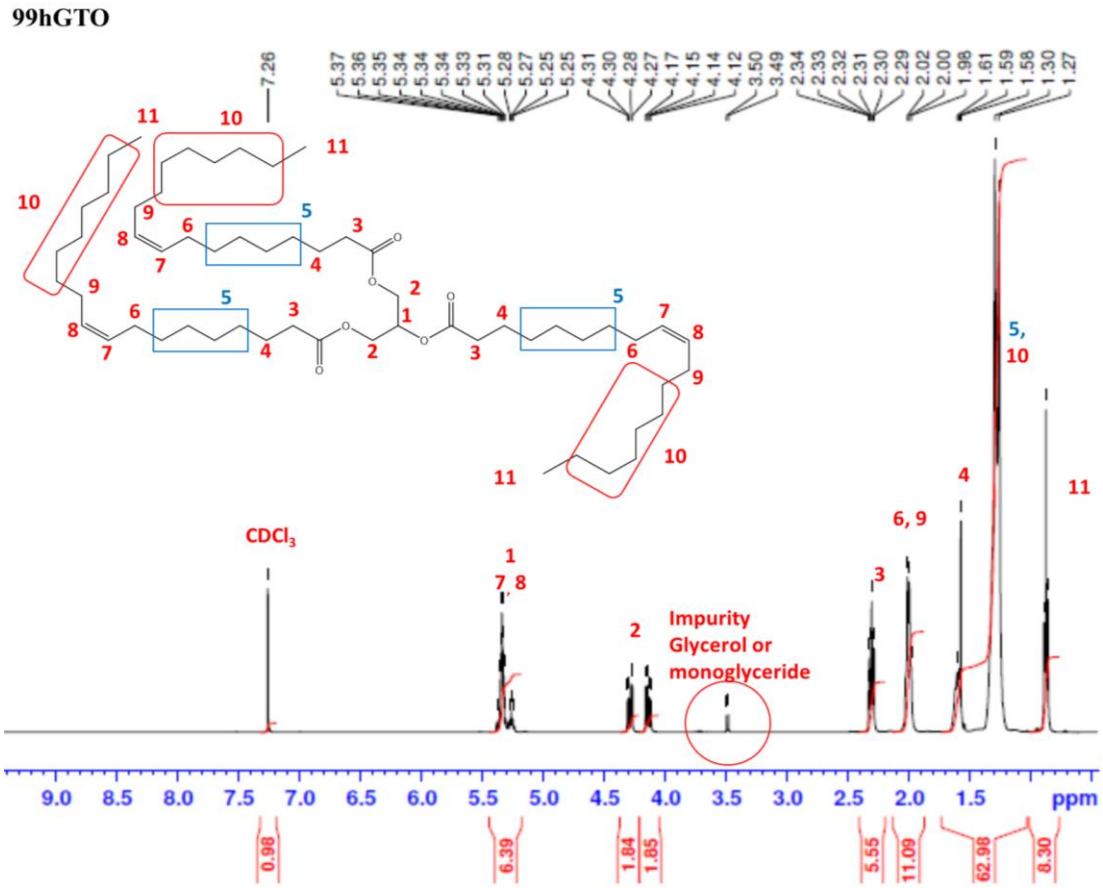

Figure B.3: ^{1}H NMR spectrum of 99hGTO (400 MHz, $CDCl_3$): δ 5.32, 4.29, 4.14, 3.49, 2.31, 2.01, 1.60, 1.28, and 0.88 ppm.

85hTPN

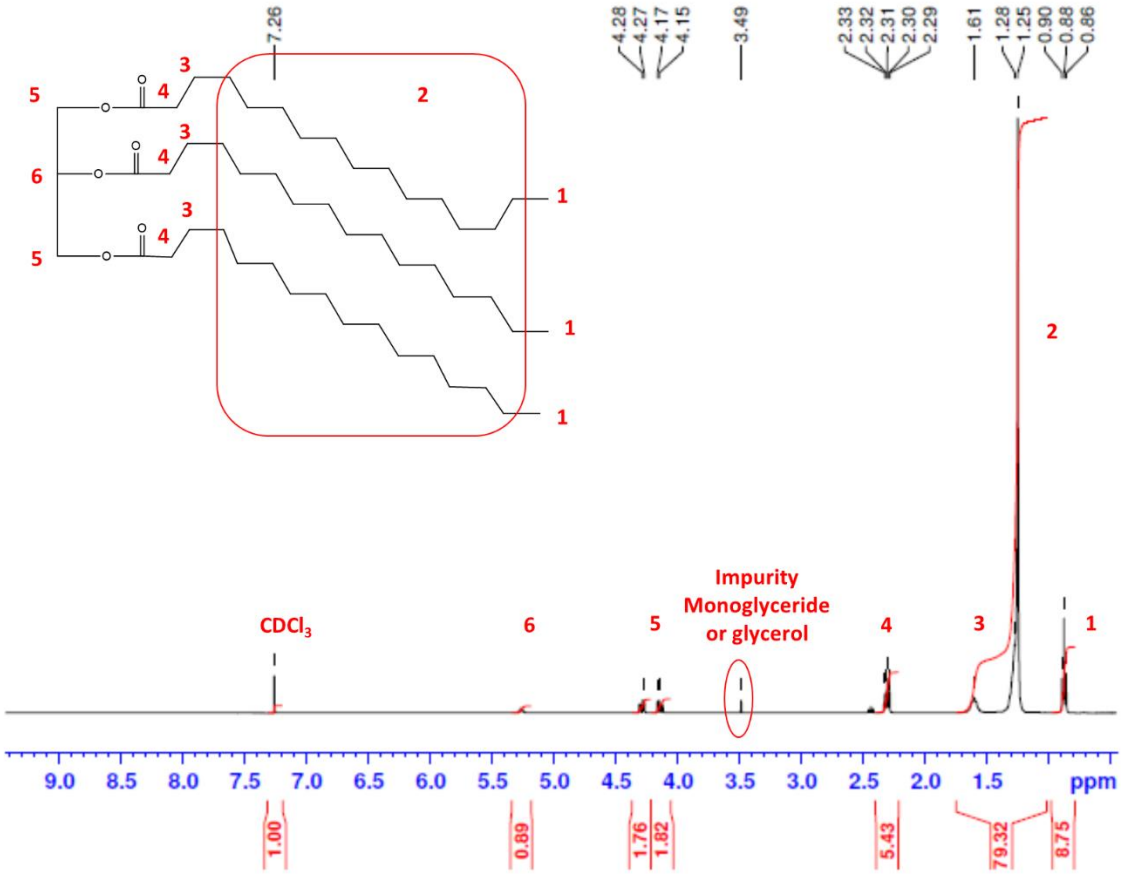

Figure B.4: ^{1}H NMR spectrum of 85hTPN (400 MHz, $CDCl_3$): δ 5.27, 4.29, 4.14, 3.49, 2.44, 2.31, 1.61, 1.25, and 0.87 ppm.

99hTPN

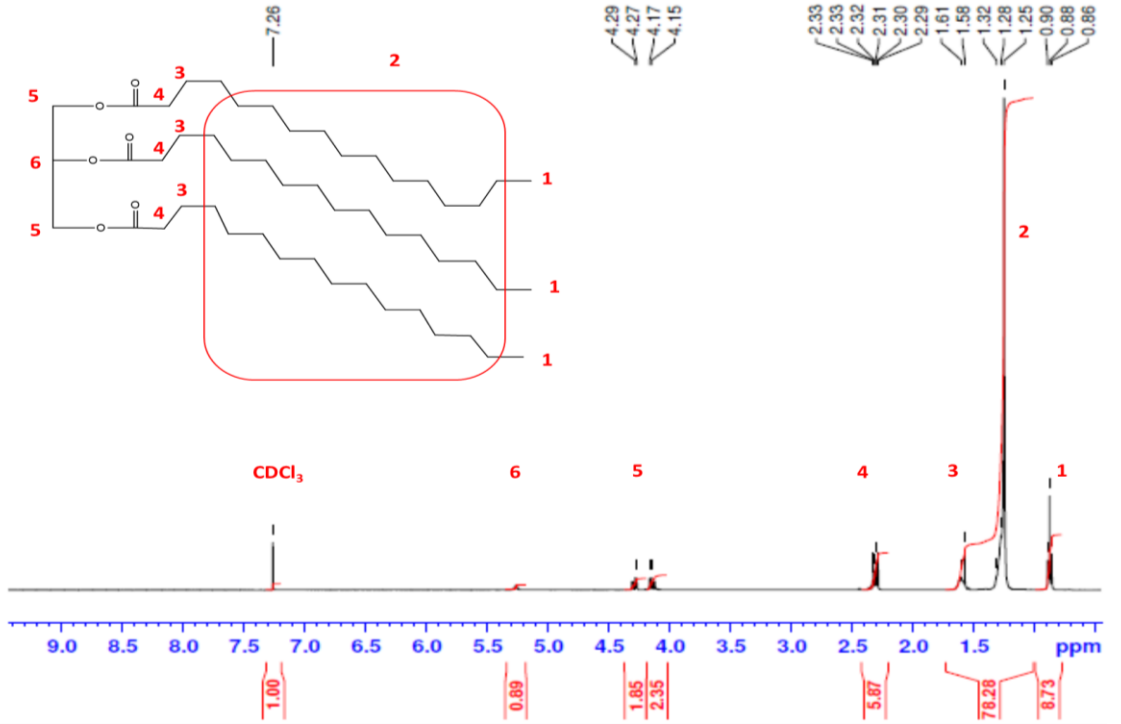

Figure B.5: ^{1}H NMR spectrum of 99hTPN (400 MHz, $CDCl_3$): δ 5.27, 4.29, 4.14, 2.31, 1.60, 1.25, and 0.88 ppm.

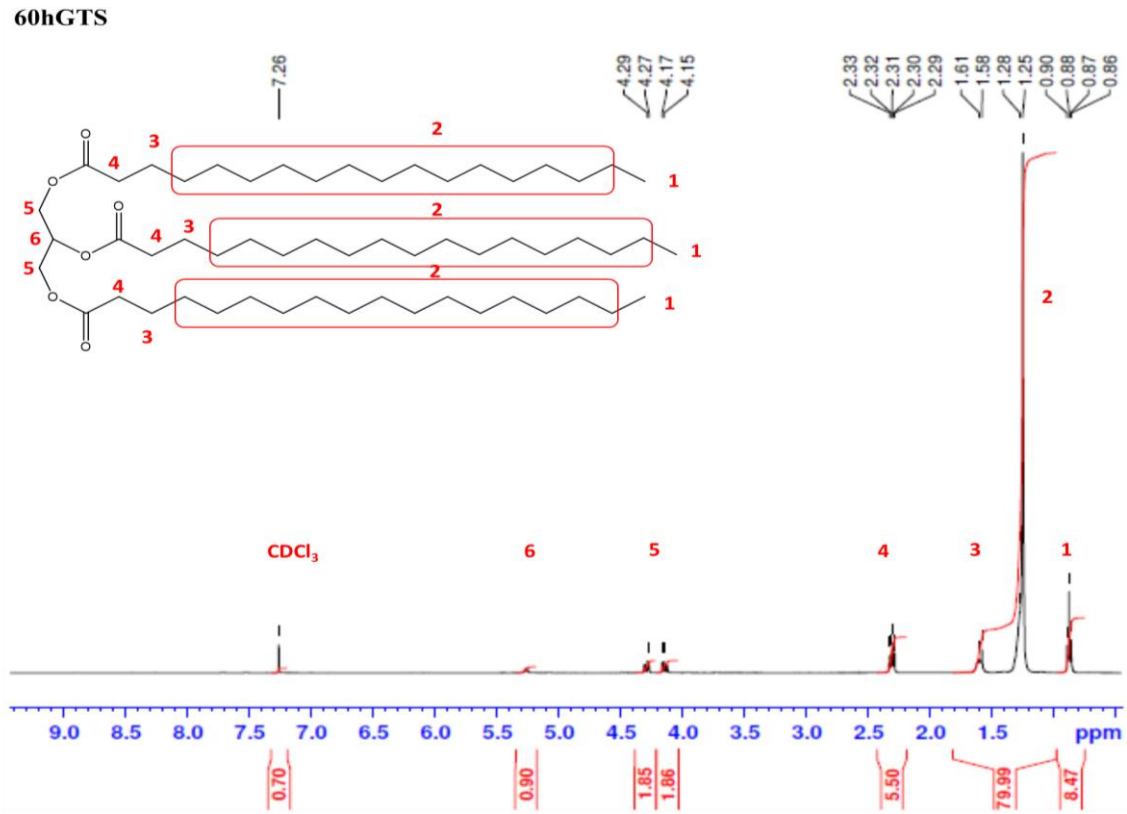

Figure B.6: ^{1}H NMR spectrum of 60hGTS (400 MHz, $CDCl_3$): δ 5.27, 4.29, 4.15, 2.31, 1.60, 1.25, and 0.88 ppm.

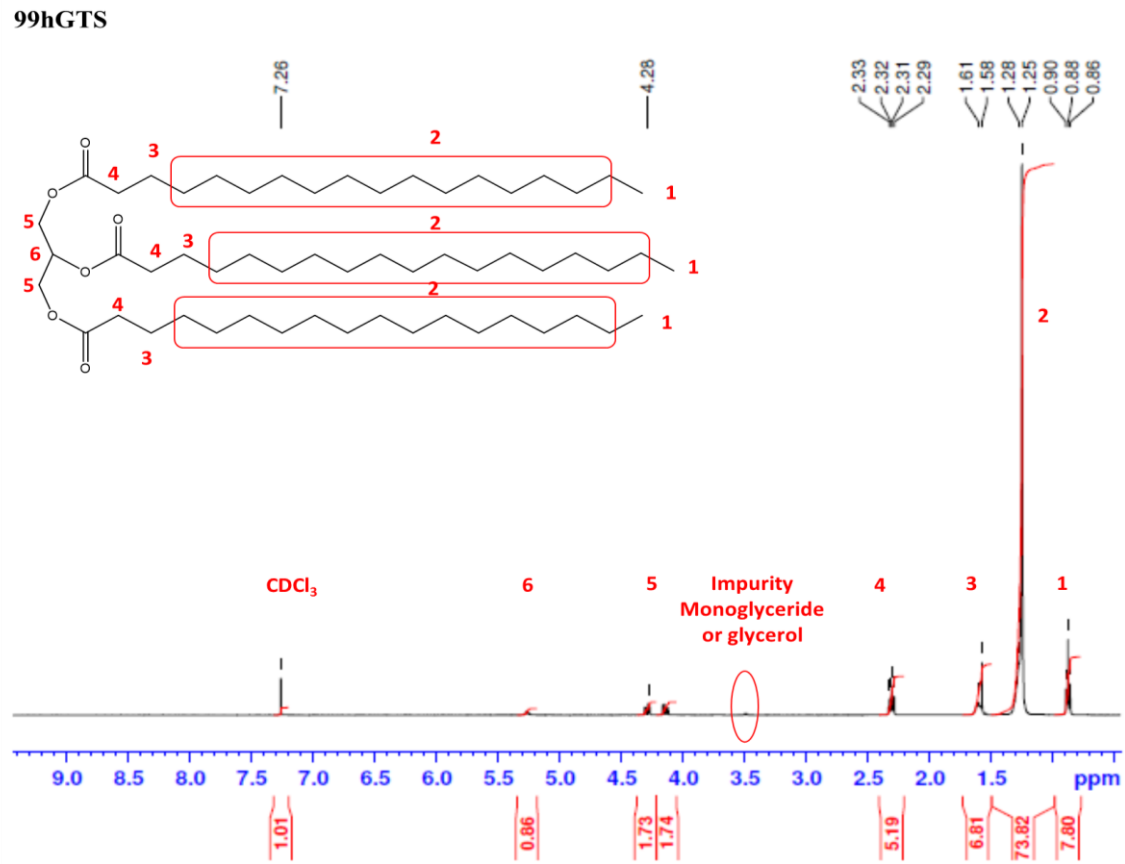

Figure B.7: ^{1}H NMR spectrum of 99hGTS (400 MHz, $CDCl_3$): δ 5.27, 4.29, 4.14, 3.49, 2.31, 1.60, 1.25, and 0.88 ppm.

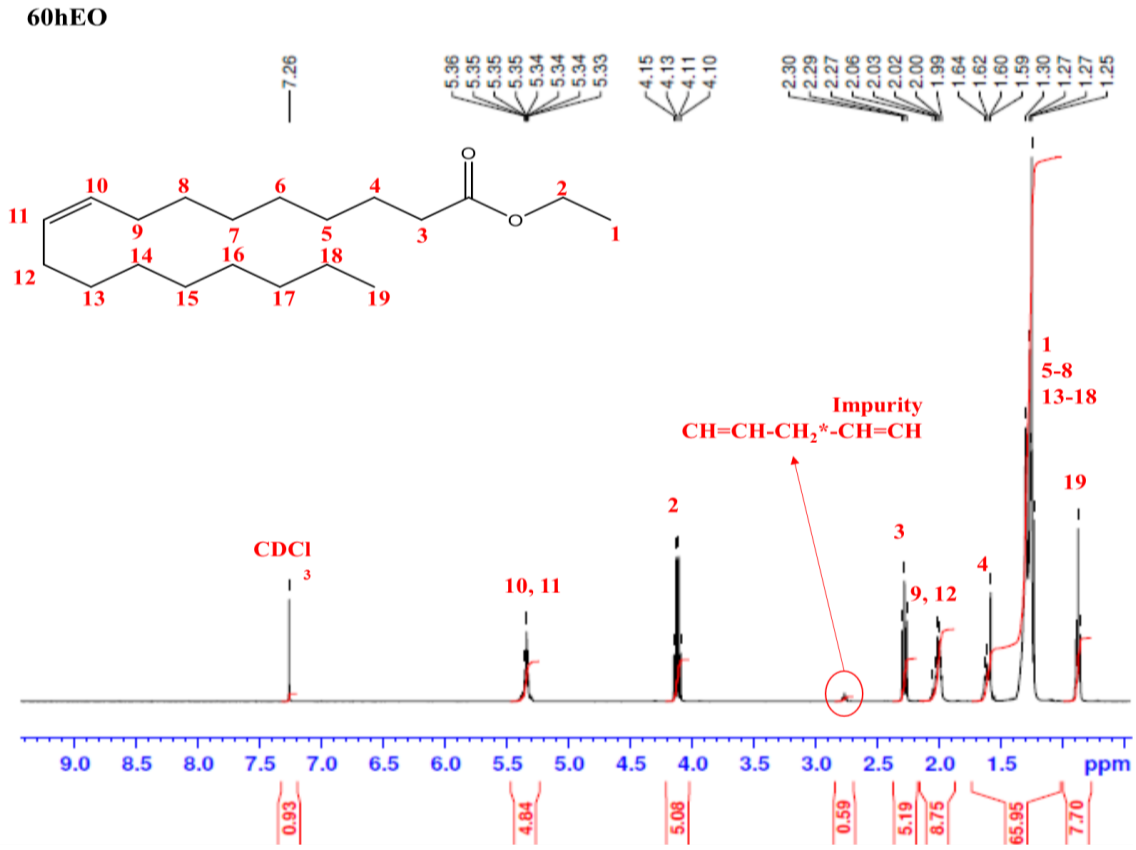

Figure B.8: ^{1}H NMR spectrum of 60hEO (400 MHz, $CDCl_3$): δ 5.34, 4.12, 2.77, 2.29, 2.01, 1.60, 1.27, and 0.88 ppm.

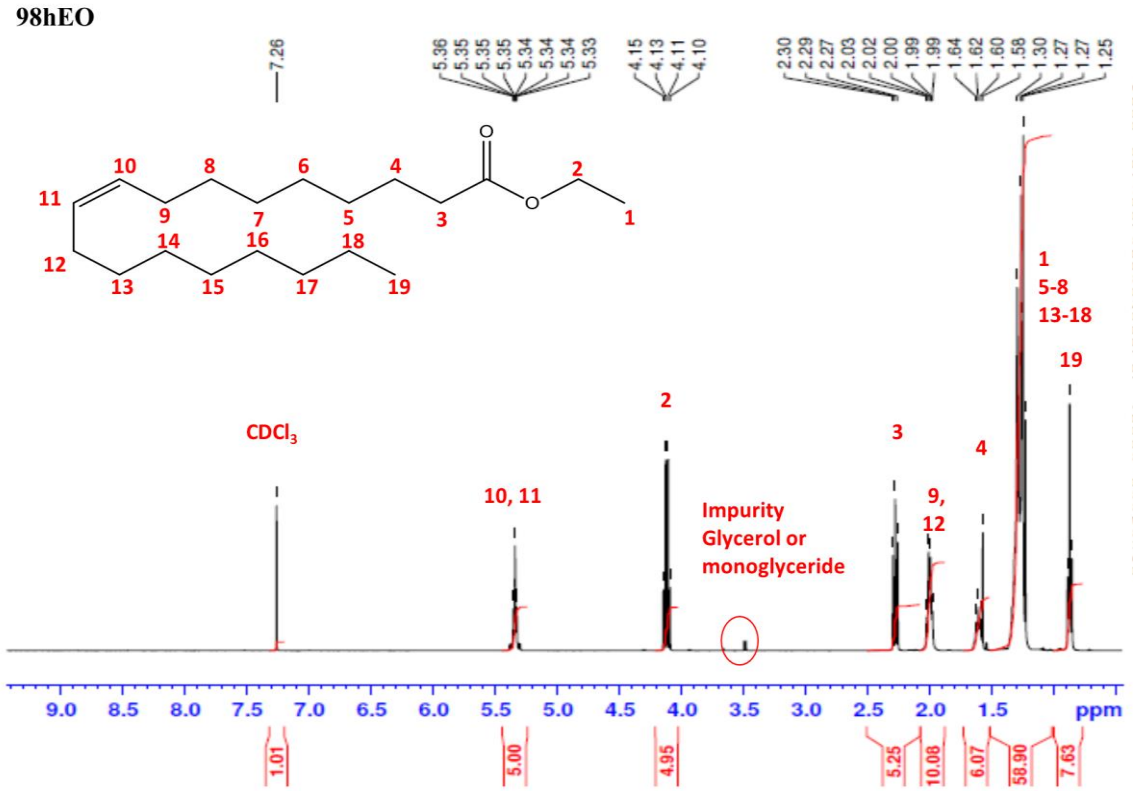

Figure B.9: ^{1}H NMR spectrum of 98hEO (400 MHz, $CDCl_3$): δ 5.34, 4.12, 3.49, 2.29, 2.01, 1.60, 1.27, and 0.88 ppm.

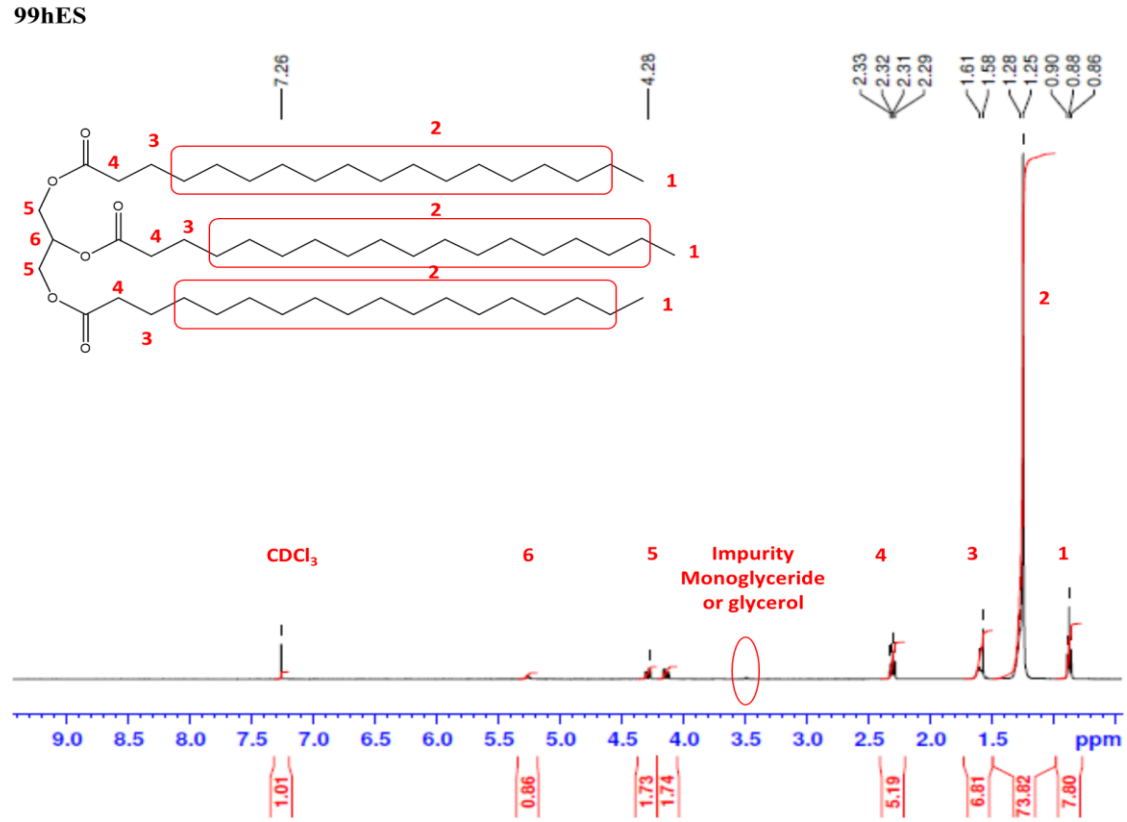

Figure B.10: ^{1}H NMR spectrum of 99hES (400 MHz, $CDCl_3$): δ 4.12, 2.28, 1.61, 1.26, and 0.88 ppm.

Table B.1 Variation in the cloud point of Brij O10 micelles prepared using either 1, 2, 5, 10, 15, 20 or 25 %w/w Brij O10 (mean ± S.D., n = 3).

Micelles	Cloud point (°C)
B1 in H_2O	58.6 ± 0.7
B2 in H_2O	59.1 ± 0.3
B5 in H_2O	61.7 ± 0.5
B10 in H_2O	64.4 ± 0.6
B15 in H_2O	67.4 ± 0.5
B20 in H_2O	69.3 ± 0.8
B25 in H_2O	73.3 ± 0.7

Table B.2 Variation in the phase inversion temperature of nanoemulsions prepared using 20 %w/w Brij O10 and containing varying amounts of oil (mean ± S.D., n = 3).

Oil concentration (%w/w)	Phase inversion temperature (°C)						
	B20-hSBO NE in H_2O 1 month	B20-65hGTO NE in H_2O 1 month	B20-99hGTO NE in H_2O 1 month	B20-85hTPN NE in H_2O 1 month	B20-60hEO NE in H_2O 1 month	B20-98hEO NE in H_2O 1 month	B20-99hES NE in H_2O 1 month
0.5	-	64.1 ± 0.4	68.6 ± 0.5	-	-	-	-
1	63.8 ± 0.4	53.0 ± 0.4	68.4 ± 0.6	62.3 ± 0.7	51.5 ± 0.5	53.8 ± 0.3	53.7 ± 0.3
2	61.9 ± 0.4	-	67.3 ± 0 .5	63.8 ± 0.6	40.8 ± 0.4	42.9 ± 0.2	-
4	66.4 ± 0.4	-	73.7 ± 0.6	68.2 ± 0.5	36.4 ± 0.8	38.8 ± 0.8	-
6	69.2 ± 0.4	-	78.5 ± 0.5	72.3 ± 0.4	38.0 ± 0.9	43.1 ± 0.3	-
8	72.9 ± 0.5	-	81.0 ± 0.3	-	40.3 ± 0.8	-	-
9	76.0 ± 0.7	-	-	-	-	-	-

Table B.3 Variation in the apparent hydrodynamic size of Brij O10 micelles prepared using either 1, 5, 10, 15, 20 or 25 %w/w Brij O10 after 1-month preparation. All samples were diluted to 1 %w/w of Brij O10 (mean ± S.D., n = 3).

Micelles	Hydrodynamic droplet size (nm)
	H_2O 1 month
B1 in H_2O	14.2 ± 0.6
B5 in H_2O	13.8 ± 0.6
B10 in H_2O	13.2 ± 0.4
B15 in H_2O	14.2 ± 0.8
B20 in H_2O	14.8 ± 0.8
B25 in H_2O	14.5 ± 0.5

Table B.4 Variation in the apparent hydrodynamic size of nanoemulsions prepared using 20 %w/w Brij O10 and containing varying amounts of oil 1-month after preparation. All samples were diluted to 1 %w/w of Brij O10 (mean ± S.D., n = 3).

Oil concentration (%w/w)	Hydrodynamic droplet size (nm)						
	B20-hSBO NE in H_2O 1 month	B20-65hGTO NE in H_2O 1 month	B20-99hGTO NE in H_2O 1 month	B20-85hTPN NE in H_2O 1 month	B20-99hTPN NE in H_2O 1 month	B20-99hGTS NE in H_2O 1 month	B20-98hEO NE in H_2O 1 month
0.5	-	14.2 ± 0.2	11.7 ± 0.4	-	-		-
1	10.5 ± 0.3	11.1 ± 0.3	10.2 ± 0.5	10.9 ± 0.5	-	328.7 ± 1.9	10.9 ± 0.2
2	12.1 ± 0.4	11.0 ± 0.1	11.5 ± 0.4	12.6 ± 0.3	17.5 ± 1.3	27.3 ± 2.5	11.8 ± 0.5
4	13.5 ± 0.4	-	13.1 ± 0.2	14.5 ± 0.3	-	21.2 ± 0.1	-
5	-	-	-	-	-		13.8 ± 0.2
6	15.4 ± 0.3	-	-	16.5 ± 1.5	20.7 ± 3.0		14.5 ± 0.1
8	17.9 ± 0.2	-	18.1 ± 0.6	18.0 ± 0.1	-		96.4 ± 9.7
9	19.6 ± 0.9	-	-	-	-		-
10	-	-	-	22.8 ± 2.9	22.6 ± 0.8		-
12	27.2 ± 0.6	-	26.4 ± 0.4	23.5 ± 0.1	-	43.1 ± 2.6	-
13						72.7 ± 11.2	
14	-	-	-	30.0 ± 0.1	-		-
15	50.6 ± 1.3	-	54.0 ± 3.7	-	-		-
16	-	-	-	37.7 ± 4.0	34.6 ± 3.1		-

Table B.5 Variation in cloud point of Brij O10 micelle prepared using 20 %w/w Brij O10 in the presence of testosterone propionate after 7-days saturation (mean ± S.D., n = 3).

Micelles	Cloud point (°C)
B20 with TP in H_2O 7 days	63.5 ± 1.0

The CP of TP-saturated micelles was significant lower than the CP of TP-free micelles ($p<0.05$).

Table B.6 Variation in phase inversion temperature of nanoemulsions prepared using 20 %w/w Brij O10 and containing varying amounts of oil in the presence of testosterone propionate after 7-days saturation (mean ± S.D., n = 3).

Oil concentration (%w/w)	Phase inversion temperature (°C)				
	B20-hSBO NE with TP in H_2O 7 days	B20-65hGTO NE with TP in H_2O 7 days	B20-99hGTO NE with TP in H_2O 7 days	B20-85hTPN NE with TP in H_2O 7 days	B20-98hEO NE with TP in H_2O 7 days
0.5	-	54.3 ± 0.5	59.7 ± 0.5	-	-
1	58.0 ± 0.5	46.4 ± 0.6	58.6 ± 0.4	55.4 ± 0.7	45.6 ± 0.6
2	57.3 ± 0.5	-	59.1 ± 0.3	58.8 ± 0.5	36.3 ± 0.5
4	61.0 ± 0.4	-	63.4 ± 0.4	60.3 ± 1.0	33.6 ± 0.4
6	64.6 ± 0.6	-	67.1 ± 0.7	64.2 ± 0.6	38.3 ± 0.5
8	67.9 ± 0.4	-	70.9 ± 0.6	-	-
9	69.9 ± 0.6	-	-	-	-

The PIT of TP-saturated NE was significant lower than the PIT of TP-free NE ($p<0.05$).

Table B.7 Variation in the apparent hydrodynamic size of Brij O10 micelle prepared using 20 %w/w Brij O10 in the presence of testosterone propionate after 7-days saturation. All samples were diluted to 1 %w/w of Brij O10 (mean ± S.D., n = 3).

Micelles	Hydrodynamic droplet size (nm)
B20 with TP in H_2O	15.5 ± 0.2

Table B.8 Variation in the apparent hydrodynamic size of nanoemulsions prepared using 20 %w/w Brij O10 and containing varying amounts of oil in the presence of testosterone propionate after 7-days saturation. All samples were diluted to 1 %w/w of Brij O10 (mean ± S.D., n = 3).

Oil concentration (%w/w)	Hydrodynamic droplet size (nm)					
	B20-hSBO NE with TP in H_2O 7 days	B20-65hGTO NE with TP in H_2O 7 days	B20-99hGTO NE with TP in H_2O 7 days	B20-85hTPN NE with TP in H_2O 7 days	B20-99hTPN NE with TP in H_2O 7 days	B20-98hEO NE with TP in H_2O 7 days
0.5	-	15.6 ± 0.2 *	10.4 ± 0.5	-	-	-
1	10.6 ± 0.2	10.7 ± 0.2 *	10.6 ± 0.1	11.1 ± 0.2	14.1 ± 0.7	12.3 ± 0.2 *
2	11.7 ± 0.2	11.3 ± 0.3	12.0 ± 0.6	12.4 ± 0.7	16.1 ± 0.3	10.6 ± 0.6
4	15.6 ± 0.7	-	13.8 ± 0.1 *	13.7 ± 0.1	19.9 ± 1.6	12.6 ± 0.3
6	19.4 ± 1.0 *	-	17.5 ± 0.2	14.8 ± 0.3	24.1 ± 2.4 *	14.3 ± 0.3
8	20.1 ± 0.9 *	-	18.5 ± 0.2	20.7 ± 0.6	22.0 ± 1.6	155.5 ± 35.0
9	22.0 ± 1.0	-	-	-	-	-
10	24.9 ± 3.1	-	24.2 ± 2.1	21.4 ± 1.0	28.3 ± 7.7	-
12	36.8 ± 6.0	-	30.6 ± 4.7	23.6 ± 0.5	35.4 ± 3.5	-
14	51.8 ± 2.9	-	-	31.5 ± 0.3	34.0 ± 3.4	-
15	-	-	140.3 ± 8.6 *	-	-	-
16	138.4 ± 7.6	-	-	57.6 ± 2.9 *	60.8 ± 15.1	-

* The particle size of TP-saturated NE was larger than that of TP-free NE ($p<0.05$).

Table B.9 Solubilisation of testosterone propionate in micelles and nanoemulsions stabilised using 20 %w/w Brij O10 and containing varying amounts of oil at room temperature (mean ± S.D., n = 3) after 7-days saturation.

Oil concentration (%w/w)	TP solubilisation (%w/v)					
	B20-hSBO NE with TP in H_2O 7 days	B20-65hGTO NE with TP in H_2O 7 days	B20-99hGTO NE with TP in H_2O 7 days	B20-85hTPN NE with TP in H_2O 7 days	B20-99hTPN NE with TP in H_2O 7 days	B20-98hEO NE with TP in H_2O 7 days
0	0.48 ± 0.03	0.48 ± 0.03	0.48 ± 0.03	0.48 ± 0.03	0.48 ± 0.03	0.48 ± 0.03
0.5	-	0.51 ± 0.03	0.60 ± 0.05	-	-	-
1	0.50 ± 0.05	0.52 ± 0.05	0.60 ± 0.03	0.53 ± 0.03	0.71 ± 0.05	0.55 ± 0.04
2	0.72 ± 0.04	0.46 ± 0.03	0.68 ± 0.03	0.60 ± 0.04	0.72 ± 0.03	0.65 ± 0.03
4	0.88 ± 0.04	-	0.83 ± 0.02	0.64 ± 0.02	0.72 ± 0.04	0.79 ± 0.04
6	0.90 ± 0.08	-	0.96 ± 0.03	0.70 ± 0.04	0.67 ± 0.03	0.92 ± 0.05
8	1.10 ± 0.11	-	1.06 ± 0.05	0.84 ± 0.04	0.66 ± 0.03	1.09 ± 0.06
9	1.17 ± 0.08	-	-	-	-	-
10	1.08 ± 0.10	-	1.13 ± 0.05	0.83 ± 0.10	0.70 ± 0.03	-
12	1.12 ± 0.08	-	1.12 ± 0.04	0.86 ± 0.11	0.70 ± 0.05	-
14	1.07 ± 0.07	-	-	0.69 ± 0.06	0.66 ± 0.05	-
15	-	-	1.10 ± 0.05	-	-	-
16	0.74 ± 0.08	-	-	0.54 ± 0.06	0.46 ± 0.06	-

Table B.10 Solubilisation of curcumin in micelles and nanoemulsions stabilised using 20 %w/w Brij O10 and containing varying amounts of hSBO at room temperature (after 7-days saturation with curcumin and testosterone propionate (mean ± S.D., n = 3).

Oil concentration (%w/w)	Curcumin solubilisation (%w/v)
	B20-hSBO NE with CUR and TP in H_2O 7 days
0	0.61 ± 0.03
2	0.58 ± 0.04
4	0.65 ± 0.03
6	0.61 ± 0.05
8	0.62 ± 0.03
9	0.61 ± 0.04

Table B.11 Solubilisation of testosterone propionate in micelles and nanoemulsions stabilised using 20 %w/w Brij O10 and containing varying amounts of hSBO at room temperature after 7-days saturation with curcumin and testosterone propionate mean ± S.D., n = 3).

Oil concentration (%w/w)	TP solubilisation (%w/v)
	B20-hSBO NE with CUR and TP in H_2O 7 days
0	0.48 ± 0.08
2	0.66 ± 0.11
4	0.90 ± 0.08
6	0.59 ± 0.08
8	0.59 ± 0.03
9	0.53 ± 0.08

Table B.12 Variation in cloud point of Brij O10 micelles prepared using either 1, 5, 10, 15, 20 or 25 %w/w Brij O10 in D_2O (mean ± S.D., n = 3).

Sample	Cloud point (°C)
B1 in D_2O	55.8 ± 0.3
B5 in D_2O	59.0 ± 0.7
B10 in D_2O	60.9 ± 0.9
B15 in D_2O	64.2 ± 0.5
B20 in D_2O	65.4 ± 0.6
B25 in D_2O	70.1 ± 0.5

The PIT of B20 micelle in D_2O was significant lower than the PIT of B20 micelle in H_2O ($p<0.05$).

Table B.13 Variation in phase inversion temperature of nanoemulsions prepared using 20 %w/w Brij O10 and containing varying amounts of oils in D_2O (mean ± S.D., n = 3).

Oil concentration (%w/w)	Phase inversion temperature (°C)				
	B20-hSBO NE in D_2O	B20-65hGTO NE in D_2O	B20-99hGTO NE in D_2O	B20-85hTPN NE in D_2O	B20-98hEO NE in D_2O
0.5	-	60.8 ± 0.5	64.4 ± 0.3	-	-
1	60.3 ± 0.3	50.8 ± 0.5	64.5 ± 0.3	61.3 ± 0.6	50.1 ± 0.6
2	59.1 ± 0.5	-	63.7 ± 0.5	60.7 ± 0.4	38.1 ± 0.5
4	64.6 ± 0.5	-	68.6 ± 0.6	65.1 ± 0.4	33.9 ± 0.4
6	68.3 ± 0.3	-	74.2 ± 0.3	68.2 ± 0.9	38.2 ± 0.5
8	70.9 ± 0.6	-	78.4 ± 0.7	-	-
9	73.4 ± 0.4	-	-	-	-

The PIT of NE in D_2O was significant lower than the PIT of NE in H_2O ($p<0.05$).

Table B.14 Variation in the apparent hydrodynamic size of Brij O10 micelles prepared using 20 %w/w Brij O10 in D_2O after 1-month preparation. All samples were diluted to 1 %w/w Brij O10 for measurement (mean ± S.D., n = 3).

Sample	Hydrodynamic droplet size (nm)
B1 in D_2O 1 month	15.8 ± 0.4
B5 in D_2O 1 month	15.0 ± 0.5
B10 in D_2O 1 month	15.6 ± 0.8
B15 in D_2O 1 month	14.4 ± 0.4
B20 in D_2O 1 month	15.6 ± 0.6
B25 in D_2O 1 month	15.4 ± 0.5

Table B.15 Variation in the apparent hydrodynamic size of nanoemulsions prepared using 20 %w/w Brij O10 and containing varying amounts of oil in D_2O after 1-month after preparation. All samples were diluted to 1 %w/w Brij O10 for measurement (mean ± S.D., n = 3).

Oil concentration (%w/w)	Hydrodynamic droplet size (nm)				
	B20-hSBO	B20-65hGTO	B20-99hGTO	B20-85hTPN	B20-98hEO
0.5	-	15.3 ± 0.5	11.5 ± 0.4	-	-
1	11.1 ± 0.2	11.4 ± 0.2	10.5 ± 0.1 *	12.3 ± 0.1	11.5 ± 0.1
2	11.8 ± 0.1	12.0 ± 0.2 *	11.7 ± 0.2	14.1 ± 0.7 *	11.5 ± 0.1
4	13.4 ± 0.3	-	14.3 ± 0.3 *	16.9 ± 1.7	-
5	-	-	-	-	13.8 ± 0.3
6	18.2 ± 0.7 *	-	-	17.4 ± 0.5	14.6 ± 0.1
8	21.9 ± 0.9 *	-	20.2 ± 0.8 *	-	100.1 ± 11.2
9	22.9 ± 0.6	-	-	-	-
10	-	-	-	20.7 ± 0.9	-
12	25.8 ± 1.4	-	27.0 ± 0.4	-	-
14	-	-	-	-	-
15	50.8 ± 1.6	-	47.2 ± 1.5 *	-	-
16	-	-	-	32.2 ± 2.1	-

* The particle size of NE in D_2O was larger than that of NE in H_2O ($p<0.05$).

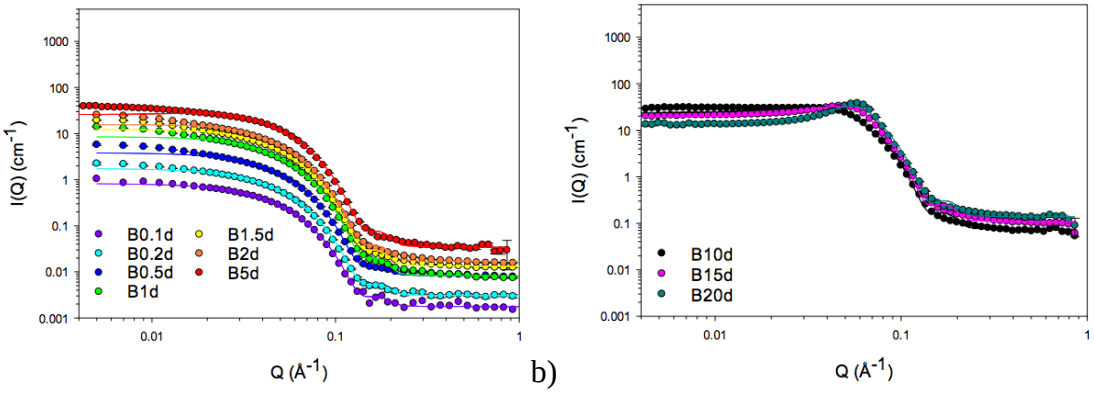

a) b)

Figure B.11: Drop contrast of SANS data and 'best' fits for Brij O10 micelle droplets with increasing surfactant concentration from a) 0.1 to 5 %w/w and b) 10 to 20 %w/w at 25 ˚C using a core-shell ellipsoid model together with a hard sphere model for interactions.

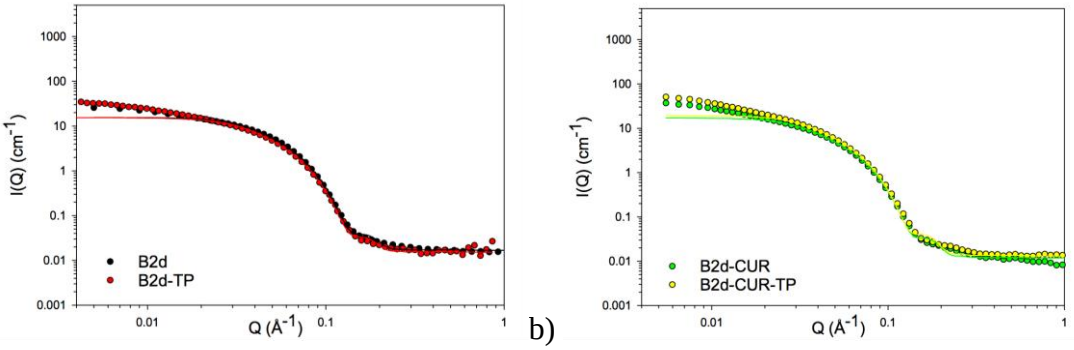

a) b)

Figure B.12: SANS curves obtained for drop contrast of 2 %w/w Brij O10 micelles a) in the absence and presence of TP, b) in the presence of either CUR or CUR-TP, along with the 'best' fits to the data.

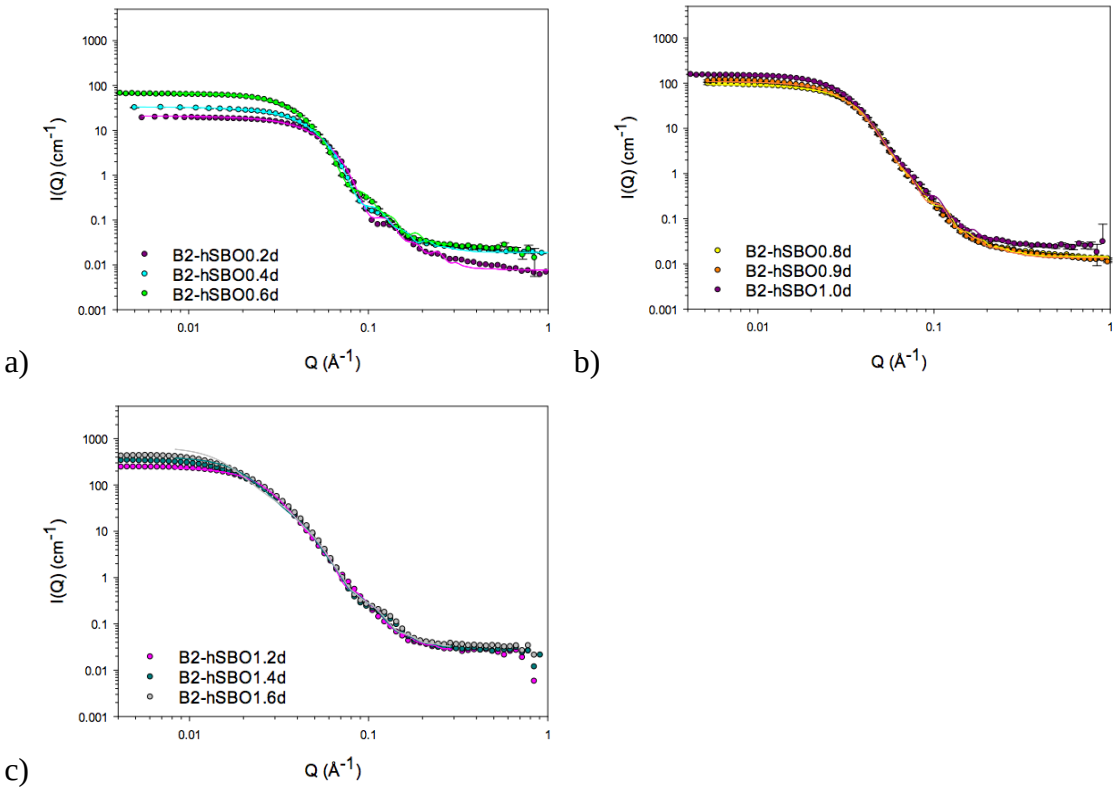

Figure B.13: SANS data and 'best' fits using the oblate ellipsoid model for the drop contrast of NE prepared using 2 %w/w Brij O10 and containing various concentration of hSBO from a) 0.2 - 0.6 %w/w, b) 0.8 - 1.0 %w/w and c) 1.2-1.6 %w/w in the absence of drug. SANS data of NE performed on SANS2D with the rear detector positioned at 8 m showed a wider Q range than that of NE performed on SANS2D with the rear detector positioned at 4 m.

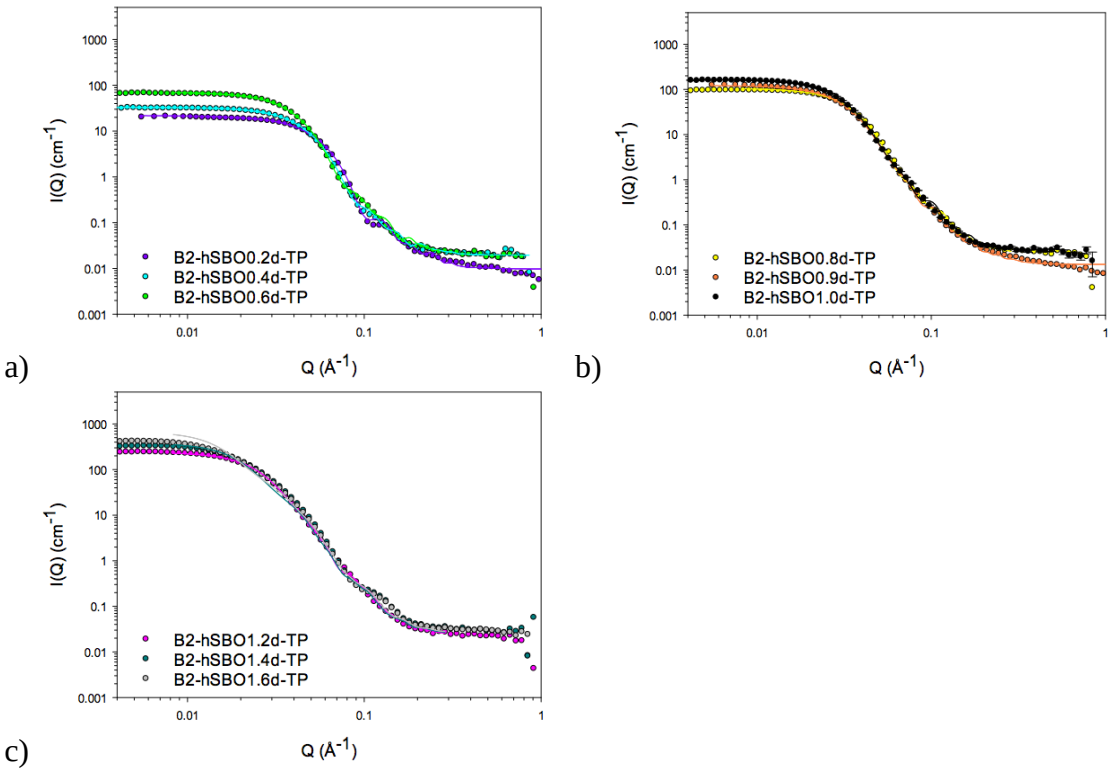

Figure B.14: SANS data and corresponding 'best' fits to the drop contrast of 2 %w/w Brij O10 and hSBO nanoemulsions with increasing hSBO content from a) 0.2 - 0.6 %w/w, b) 0.8 - 1.0 %w/w and b) 1.2 - 1.6 %w/w in the presence of TP.

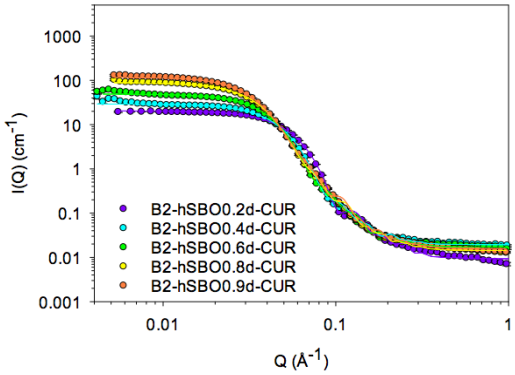

Figure B.15: SANS data and the corresponding 'best' fits to the drop contrast for 2 %w/w Brij O10 and hSBO nanoemulsions with increasing hSBO content from 0.2 - 0.9 %w/w in the presence of CUR.

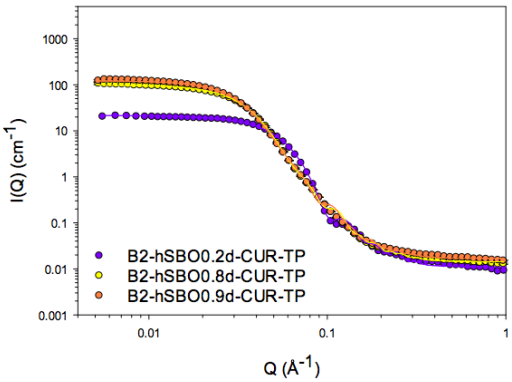

Figure B.16: SANS data and the corresponding 'best' fits to the drop contrast for 2 %w/w Brij O10 and hSBO nanoemulsions with increasing hSBO content from 0.2 - 0.9 %w/w in the presence of CUR and TP.

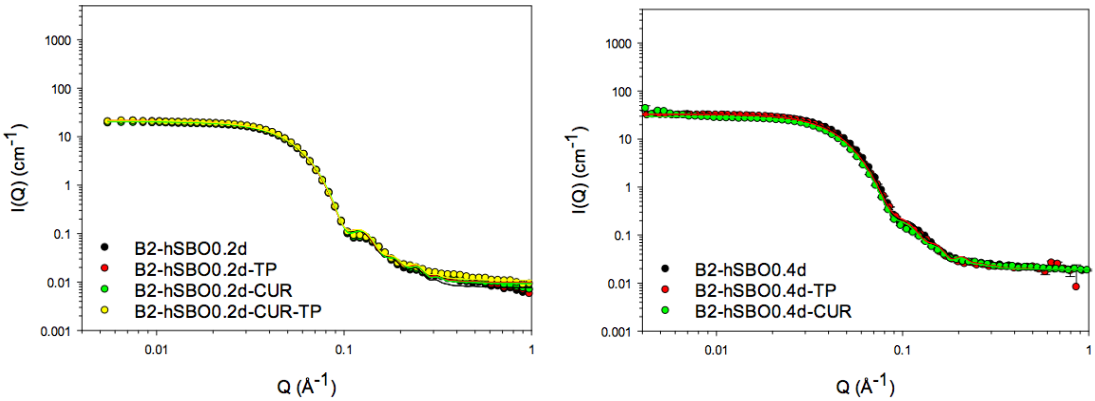

Figure B.17: SANS data and the corresponding 'best' fits to the drop contrast for 2 %w/w Brij O10 and hSBO nanoemulsions with increasing hSBO content from 0.2 – 1.6 %w/w in the absence and presence of drug.

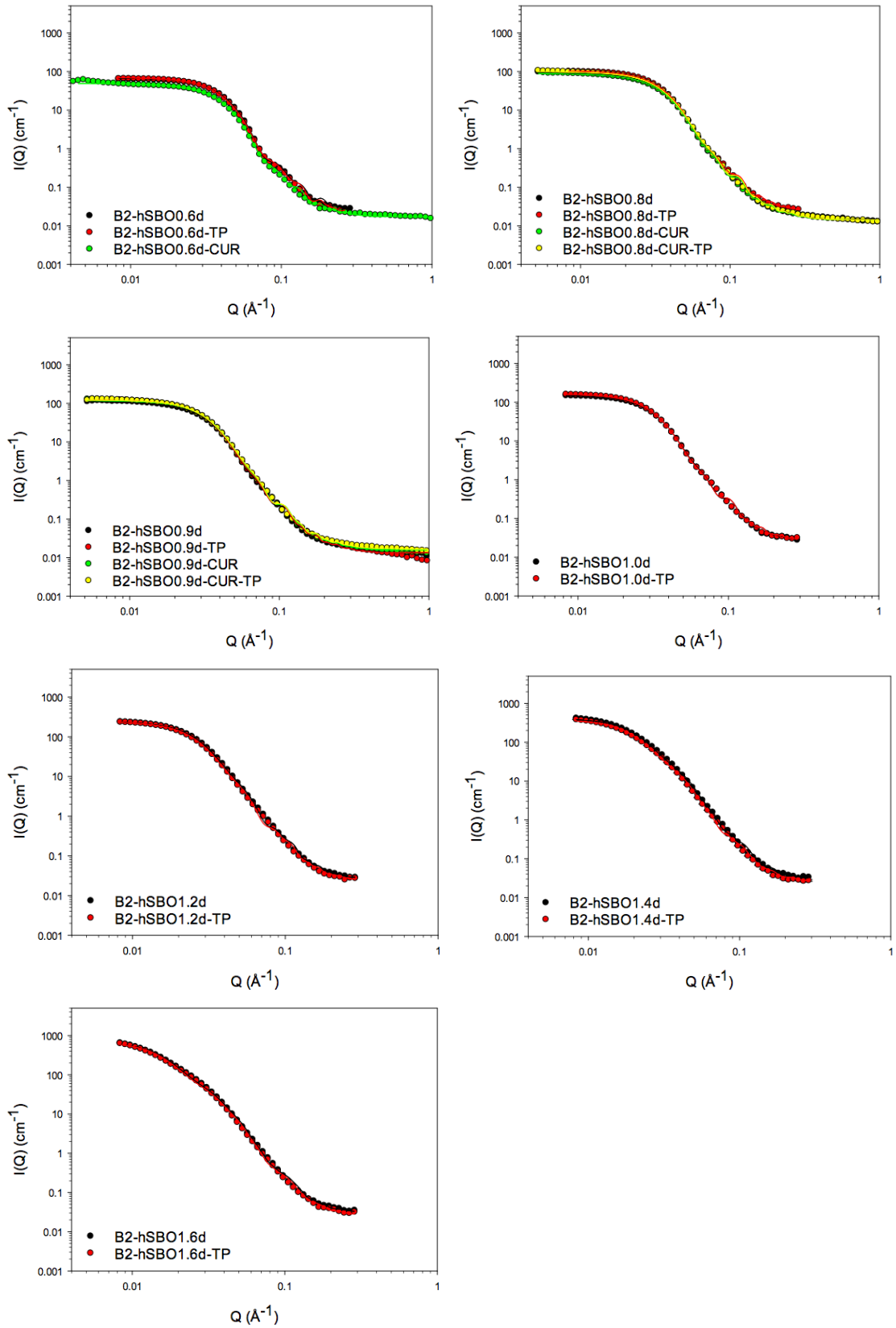

Figure B.17: SANS data and the corresponding 'best' fits to the drop contrast for 2 %w/w Brij O10 and hSBO nanoemulsions with increasing hSBO content from 0.2 – 1.6 %w/w in the absence and presence of drug (cont.).

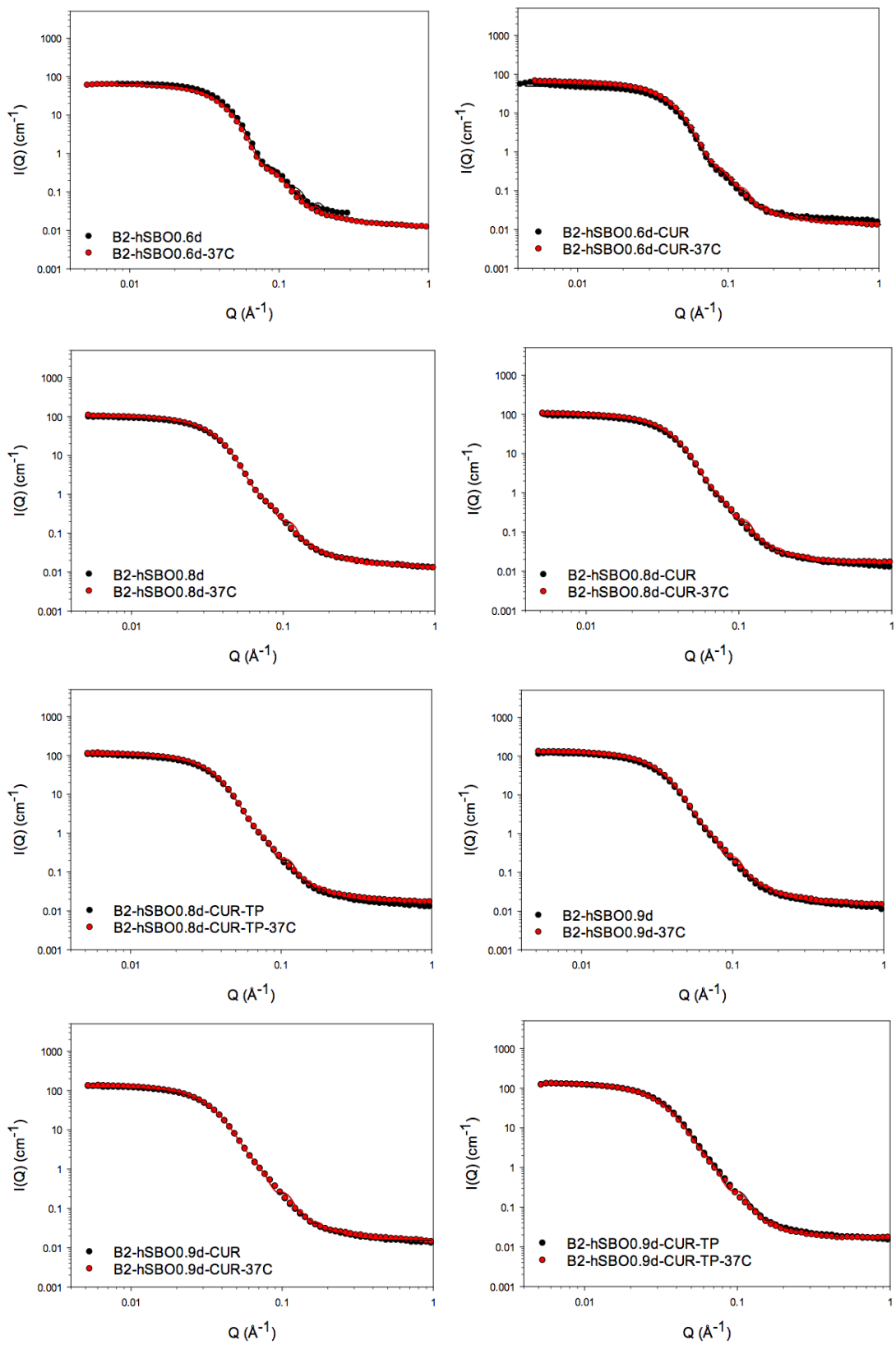

Figure B.18: SANS data and best fits to the drop contrast for 2 %w/w Brij O10 NE containing either 0.6, 0.8 or 0.9 %w/w hSBO in the absence and presence of drug at 25 and 37 °C.

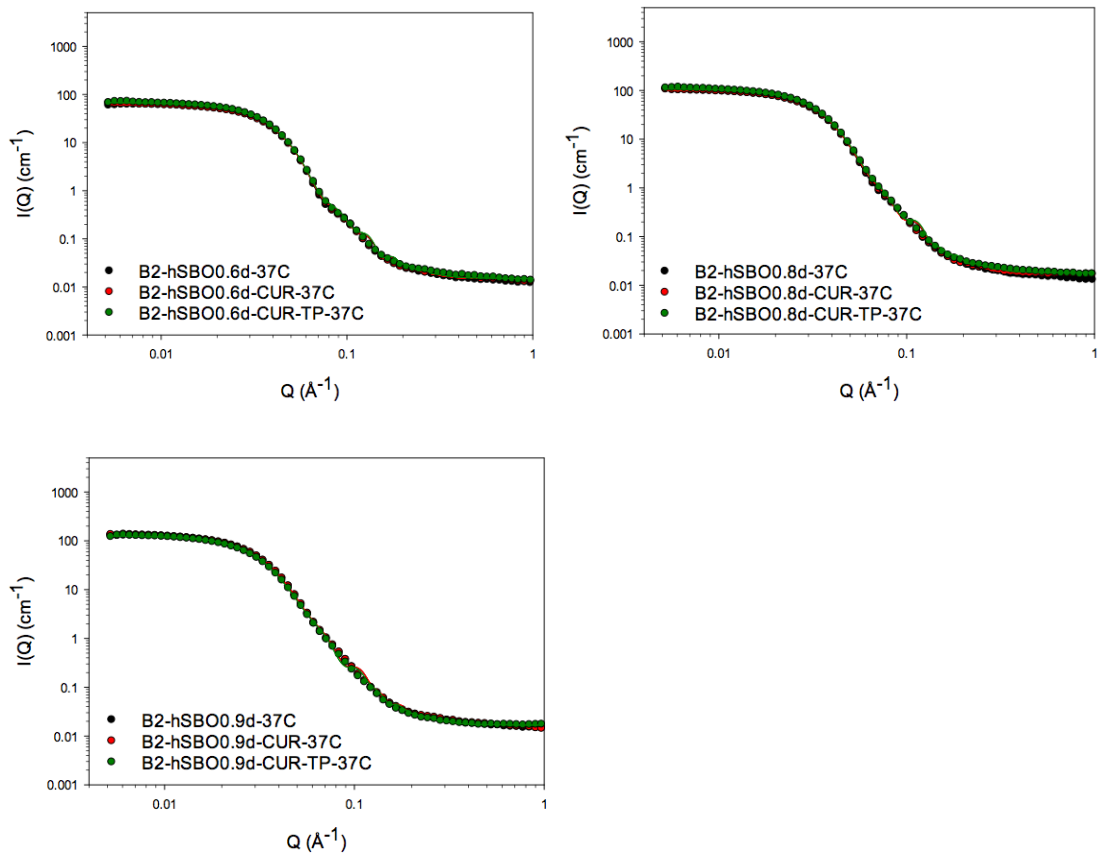

Figure B.19: SANS data and best fits to the drop contrast for 2 %w/w Brij O10 NE containing either 0.6, 0.8 or 0.9 %w/w hSBO in the absence and presence of drug at 37 °C.

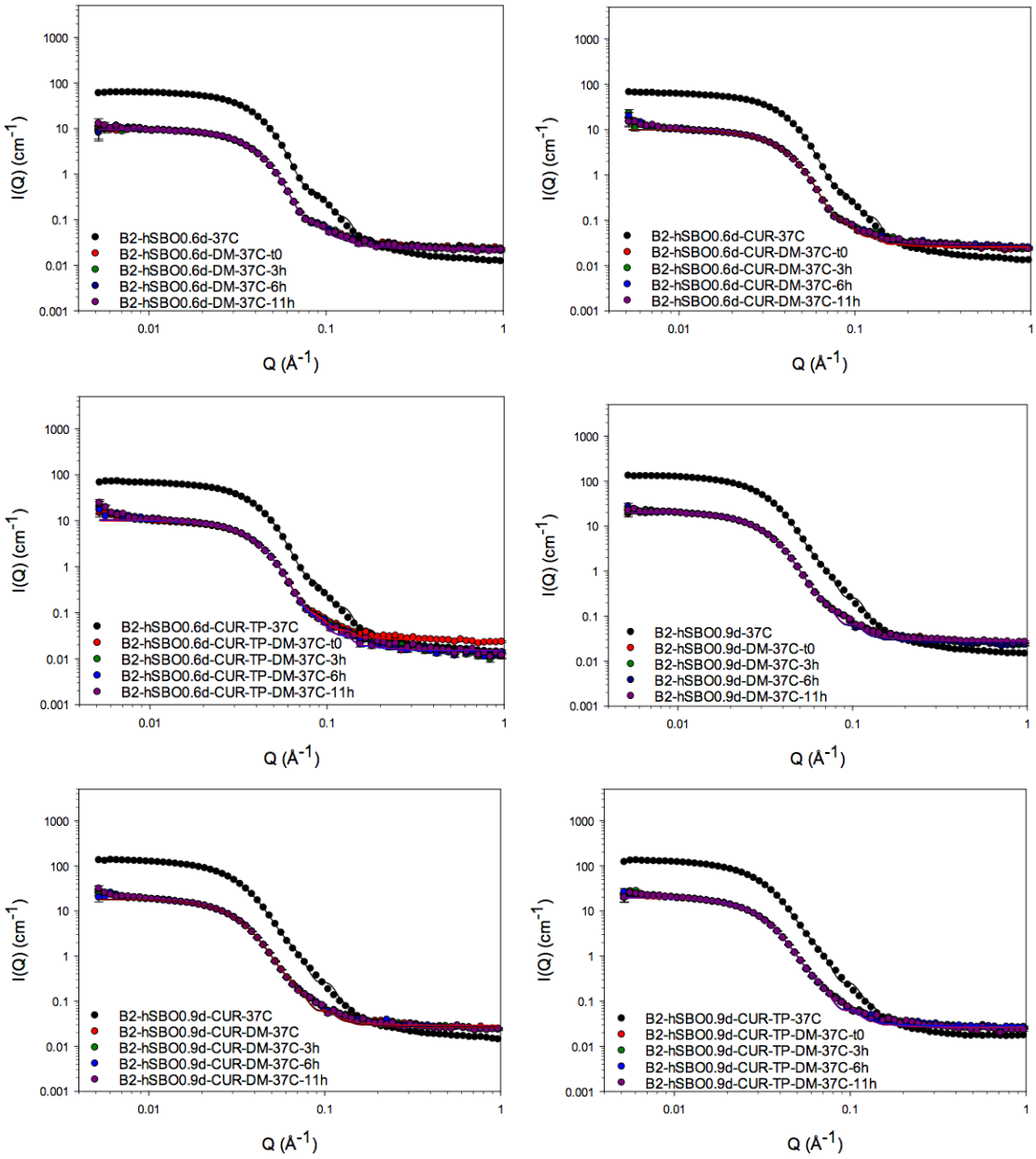

Figure B.20: SANS data and best fits to the drop contrast for 2 %w/w Brij O10 NE containing either 0.6 or 0.9 %w/w hSBO with and without drugs in the absence and presence of cell culture media at 37 °C.

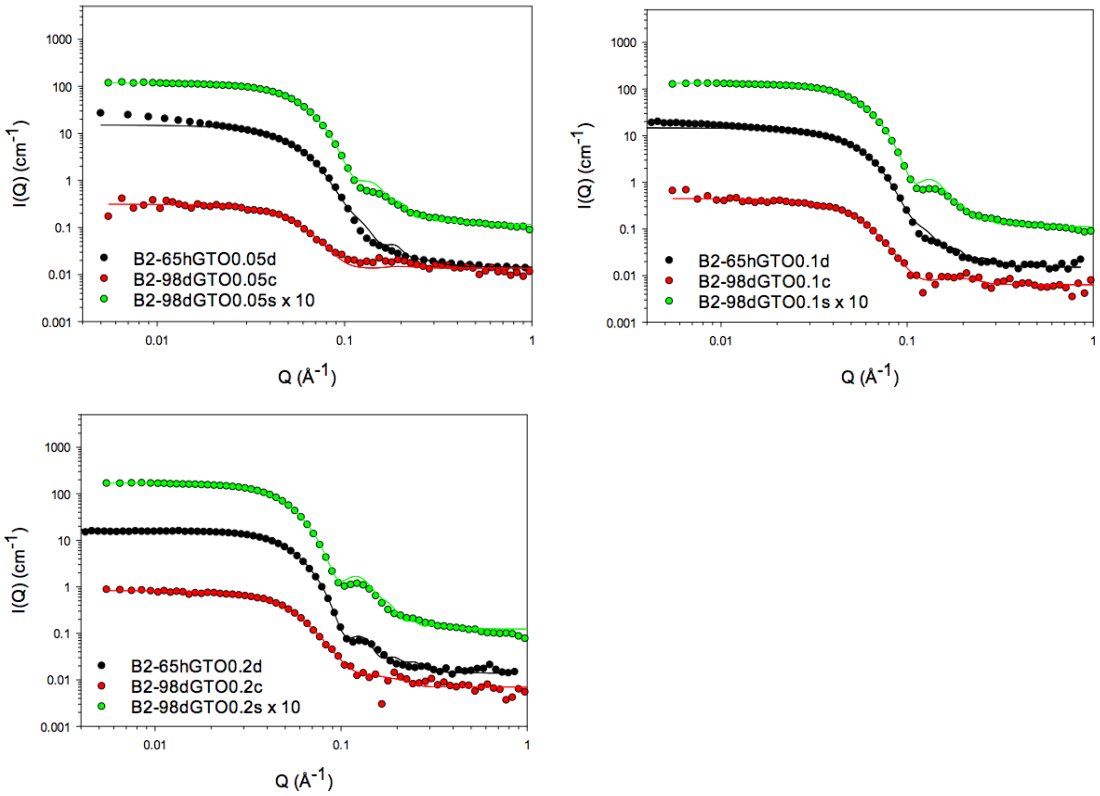

Figure B.21: SANS data and best fits to three contrasts for 2 %w/w Brij O10 NE containing varying amounts of 65hGTO in the absence of drug. Shell contrast for 2 %w/w Brij O10 NE containing 98dGTO was multiplied by the factor of 10.

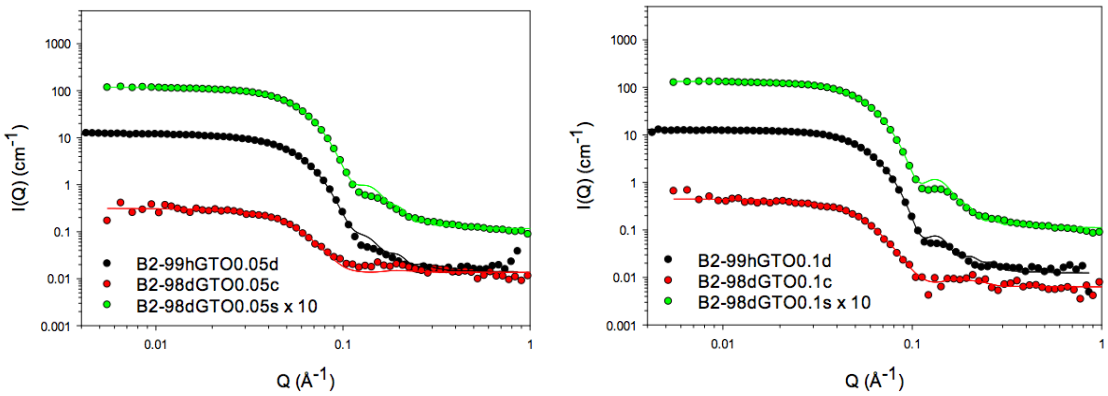

Figure B.22: SANS data and best fits to three contrasts for 2 %w/w Brij O10 NE containing varying amounts of 99hGTO in the absence of drug. The shell contrast for 2 %w/w Brij O10 NE containing 98dGTO was multiplied by the factor of 10. Note that the best fits to the shell contrast for 2 %w/w Brij O10 NE containing 0.8 %w/w 98dGTO and higher concentrations of 98dGTO were not well fitted to the SANS data.

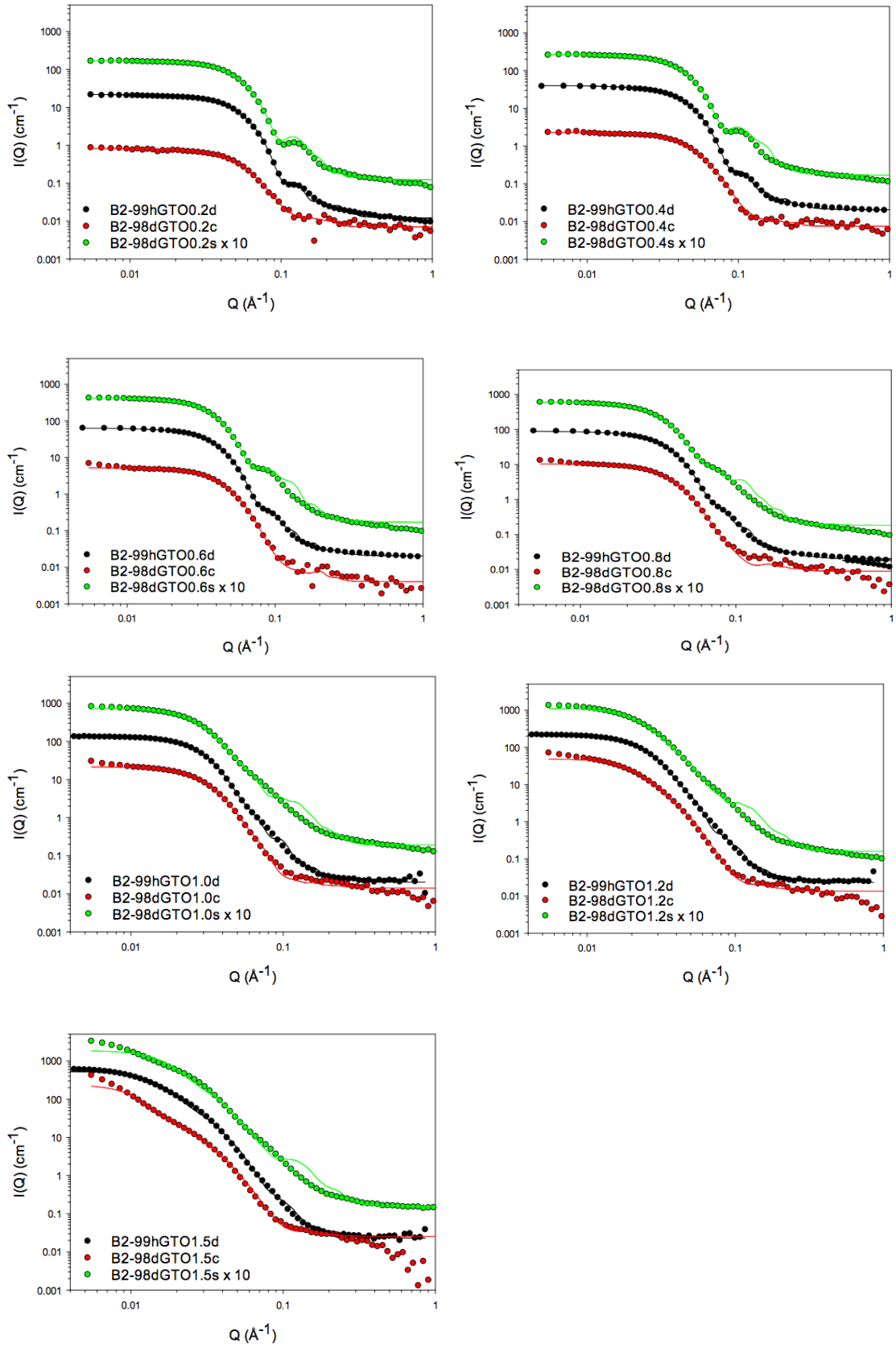

Figure B.22: SANS data and best fits to three contrasts for 2 %w/w Brij O10 NE containing varying amounts of 99hGTO in the absence of drug. The shell contrast for 2 %w/w Brij O10 NE containing 98dGTO was multiplied by the factor of 10. Note that the best fits to the shell contrast for 2 %w/w Brij O10 NE containing 0.8 %w/w 98dGTO and higher concentrations of 98dGTO were not well fitted to the SANS data (cont.).

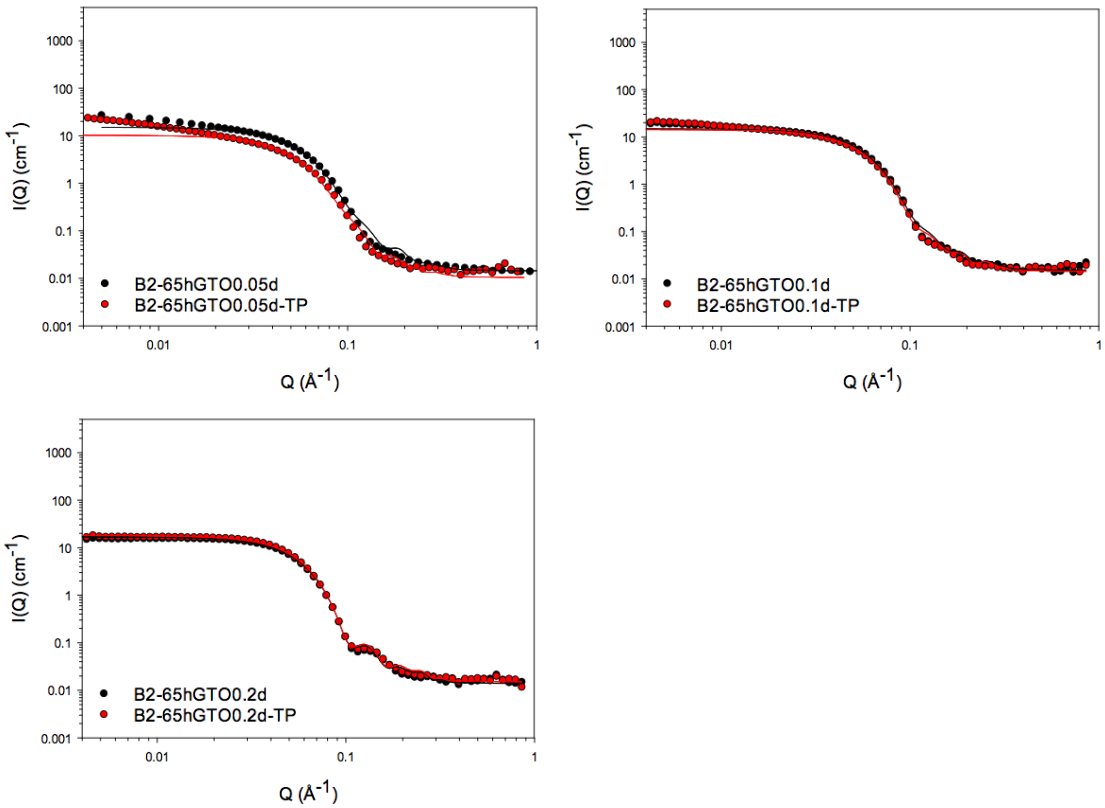

Figure B.23: SANS data and best fits to the drop contrast for 2 %w/w Brij O10 NE containing varying amounts of 65hGTO in the absence and presence of TP.

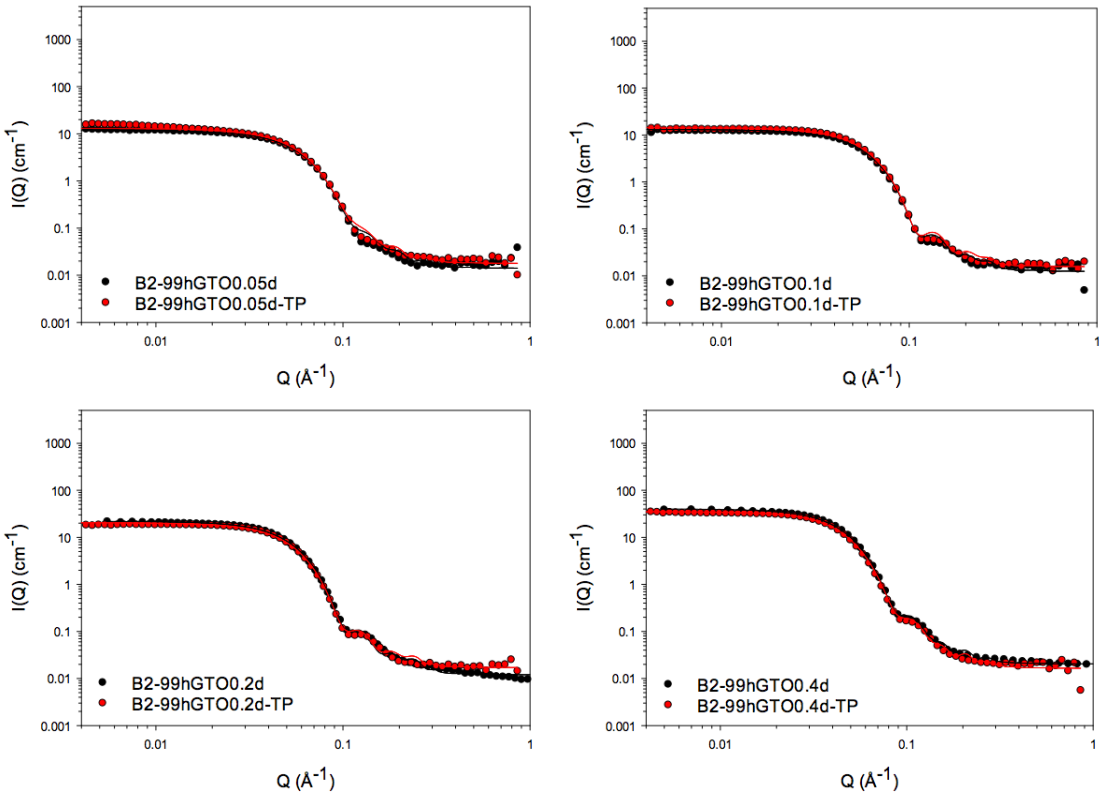

Figure B.24: SANS data and best fits to the drop contrast for 2 %w/w Brij O10 NE containing varying amounts of 99hGTO in the absence and presence of TP.

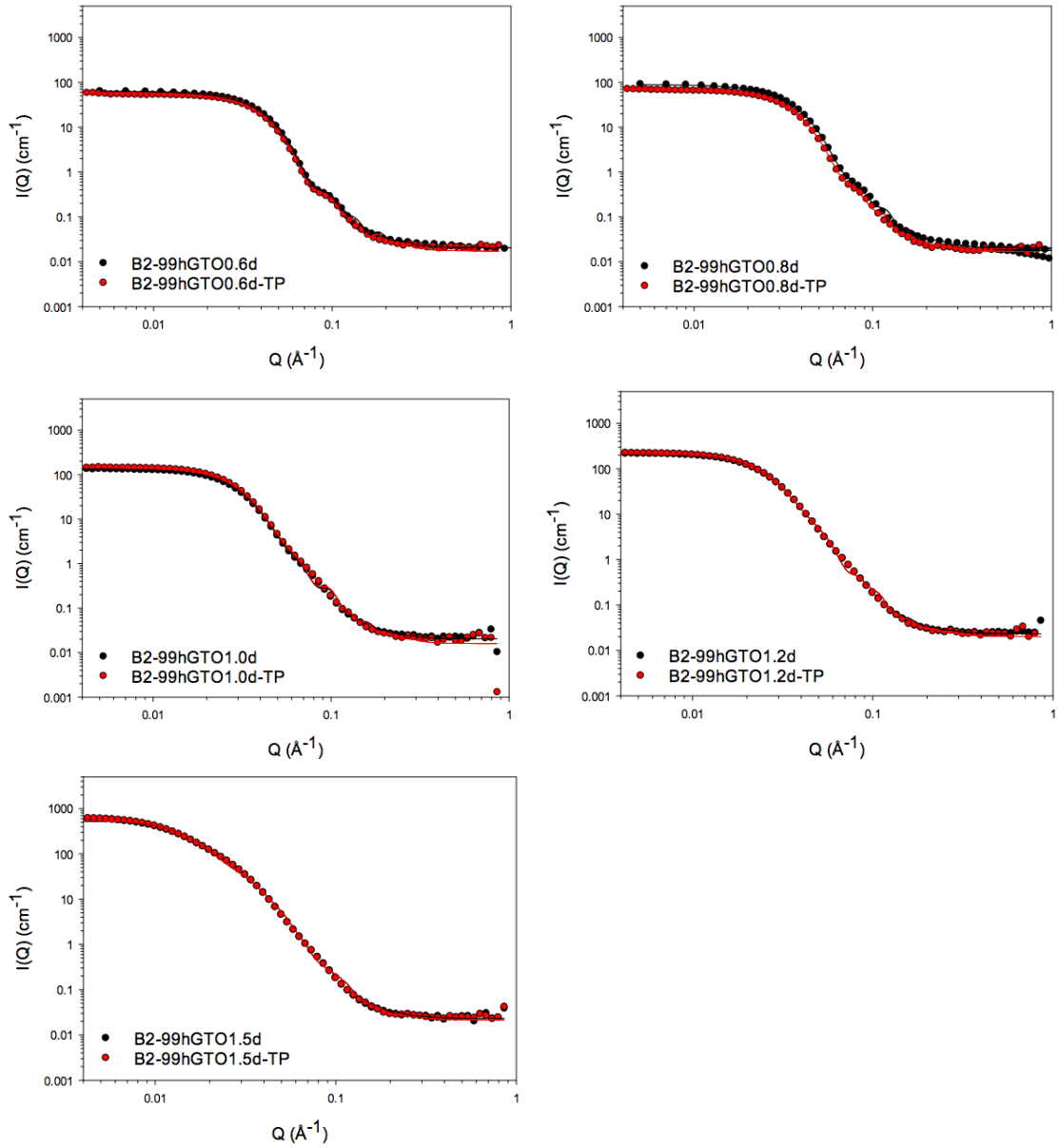

Figure B.25: SANS data and best fits to the drop contrast for 2 %w/w Brij O10 NE containing varying amounts of 99hGTO in the absence and presence of TP (cont.).

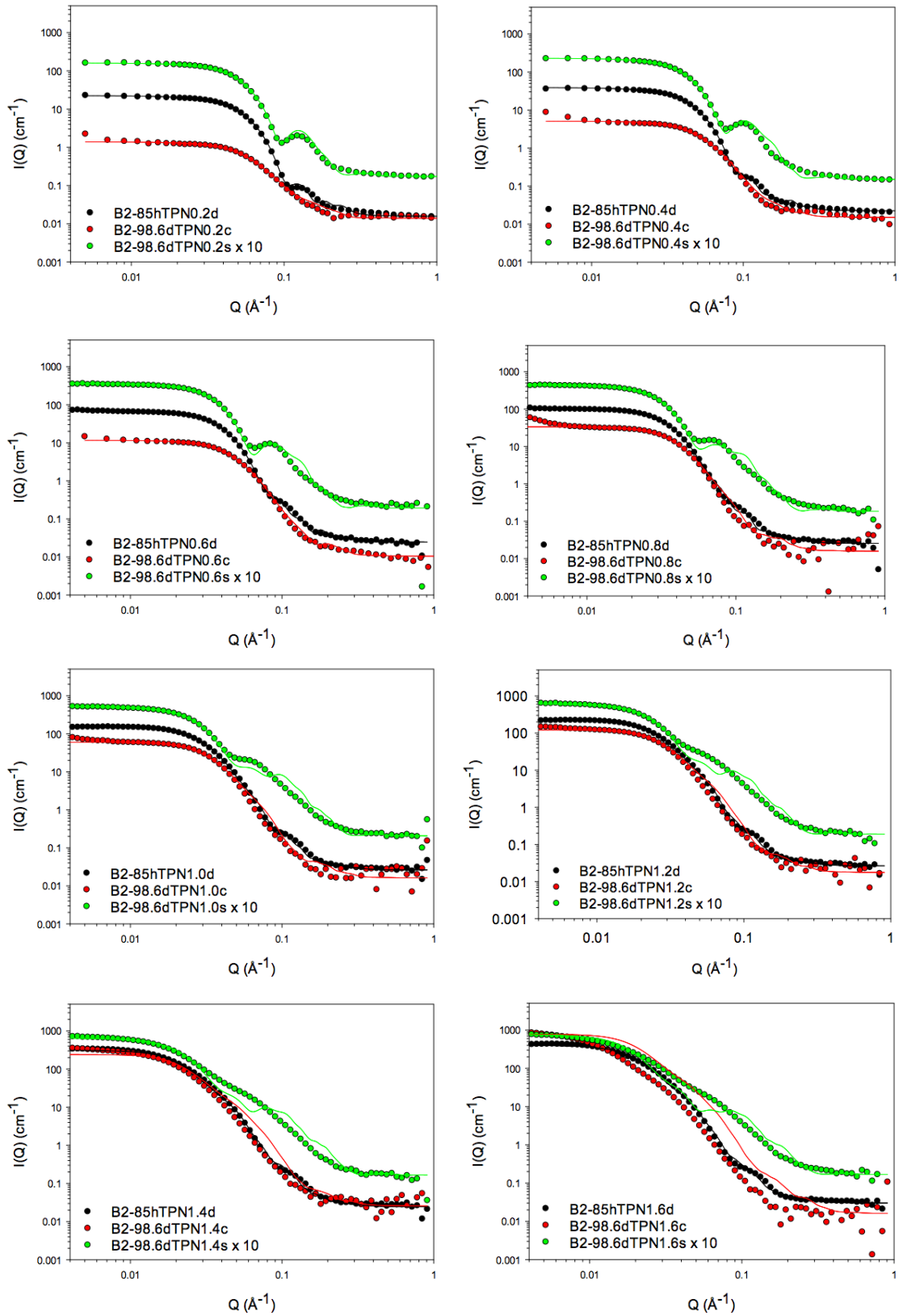

Figure B.26: SANS data and best fits to three contrasts for 2 %w/w Brij O10 NE containing varying amounts of 85hTPN in the absence of drug. The shell contrast for NE containing 98.6dTPN was multiplied by the factor of 10. Note that the best fits to the shell contrast for 2 %w/w Brij O10 NE containing 0.4 %w/w 98.6dTPN and higher concentrations of 98.6dTPN were not well fitted to SANS data and the best fits to the core contrast for 2 %w/w Brij O10 NE containing 0.8 %w/w 98.6dTPN and higher concentrations of 98.6dTPN were not fitted to SANS data.

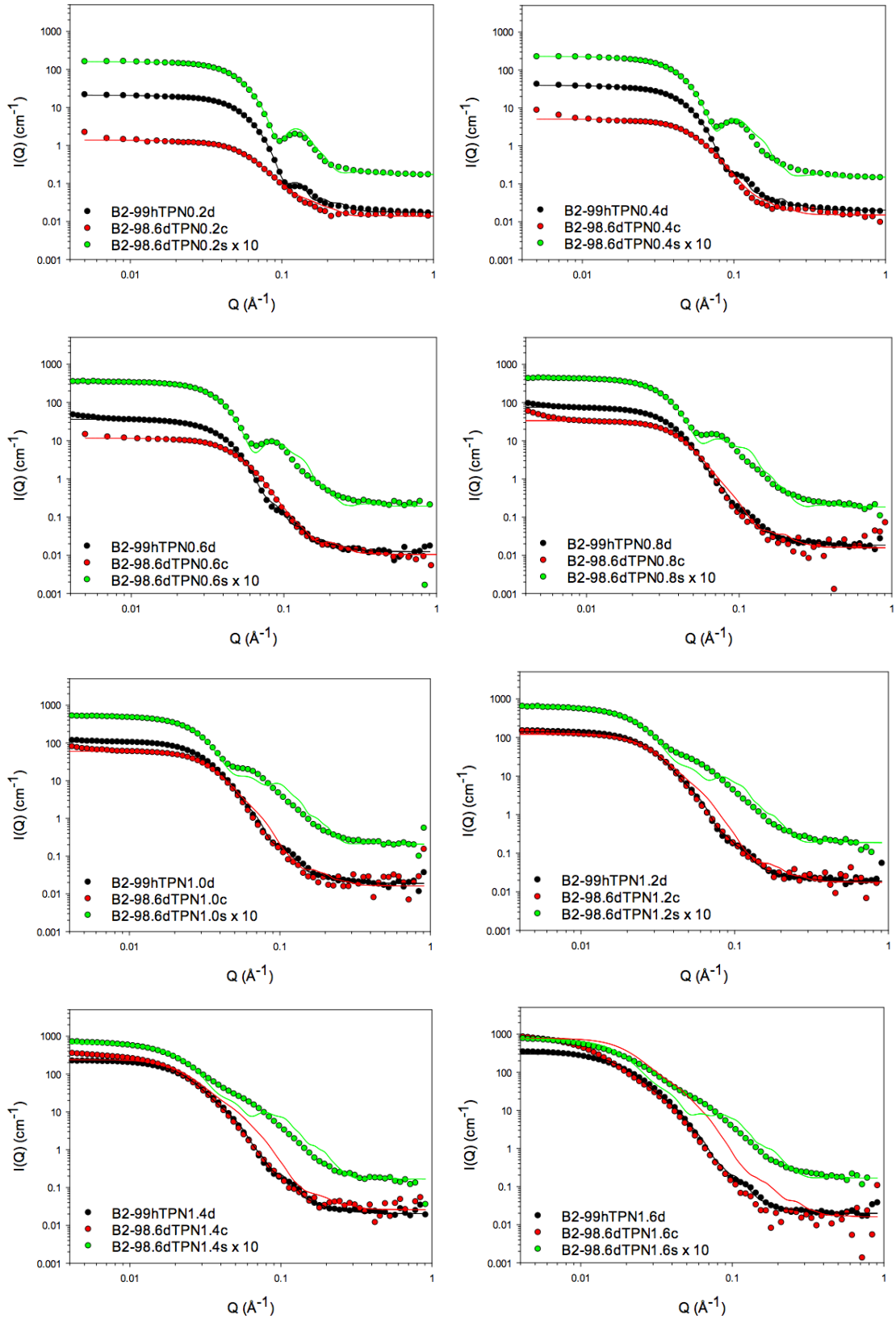

Figure B.27: SANS data and best fits to three contrasts for 2 %w/w Brij O10 NE containing varying amounts of 99hTPN in the absence of drug. The shell contrast for NE containing 98.6dTPN was multiplied by the factor of 10. Note that the best fits to the shell contrast for 2 %w/w Brij O10 NE containing 0.4 %w/w 98.6dTPN and higher concentrations of 98.6dTPN were not well fitted to SANS data and the best fits to core contrast for 2 %w/w Brij O10 NE containing 0.8 %w/w 98.6dTPN and higher concentrations of 98.6dTPN were not fitted to SANS data.

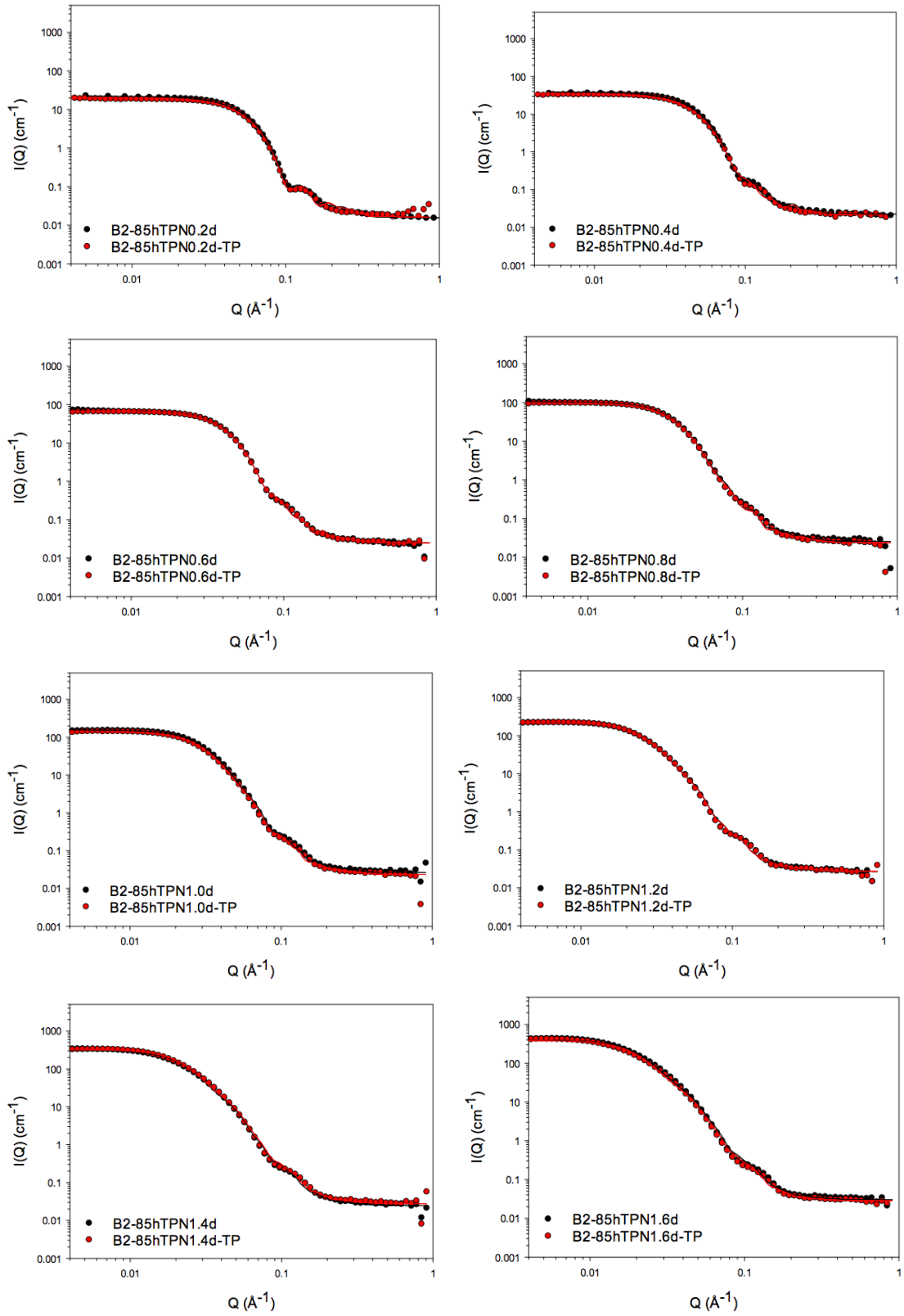

Figure B.28: SANS data and best fits to the drop contrast for 2 %w/w Brij O10 NE containing varying amounts of 85hTPN in the presence and absence of TP.

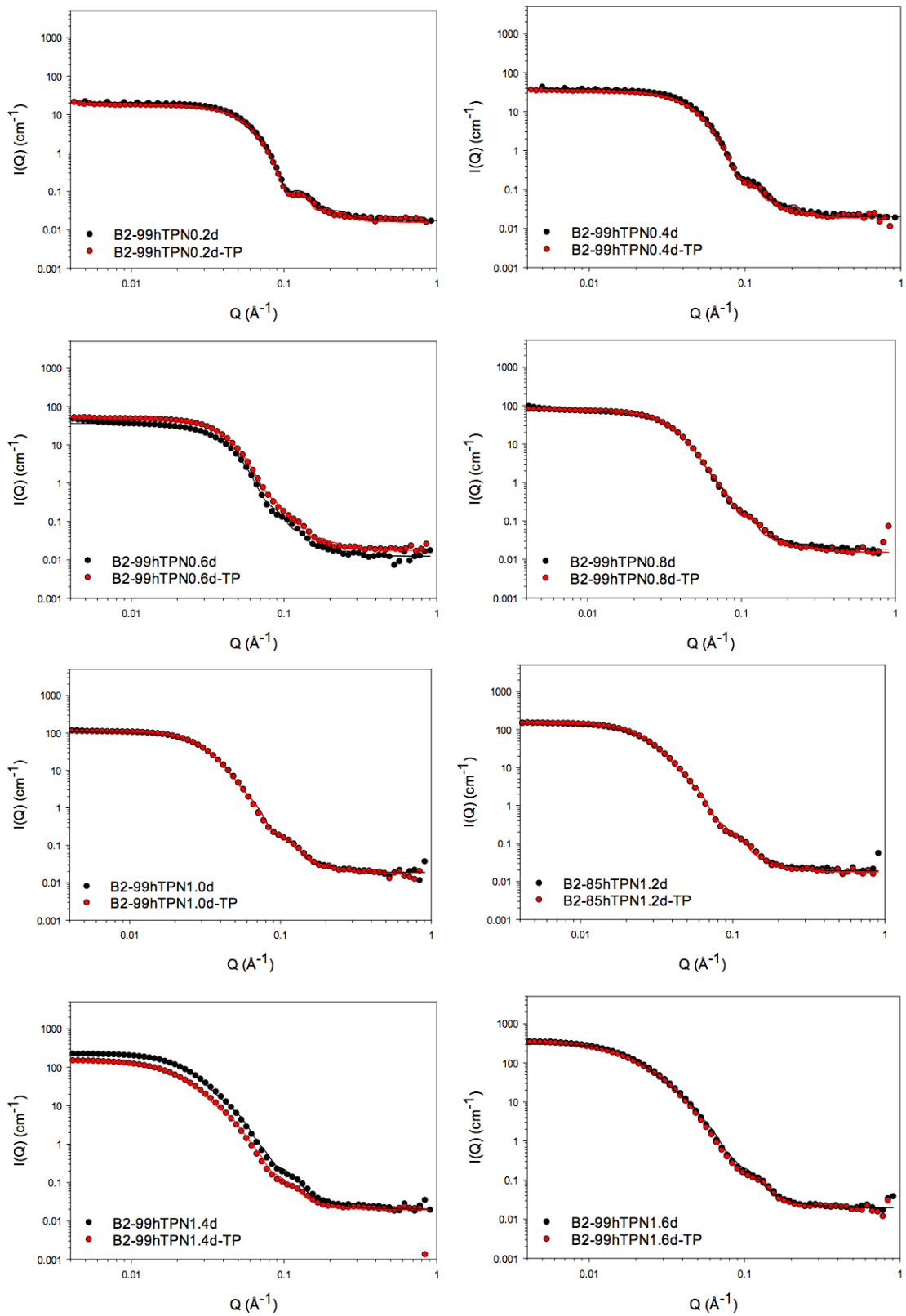

Figure B.29: SANS data and best fits to the drop contrast for 2 %w/w Brij O10 NE containing varying amounts of 99hTPN in the presence and absence of TP.

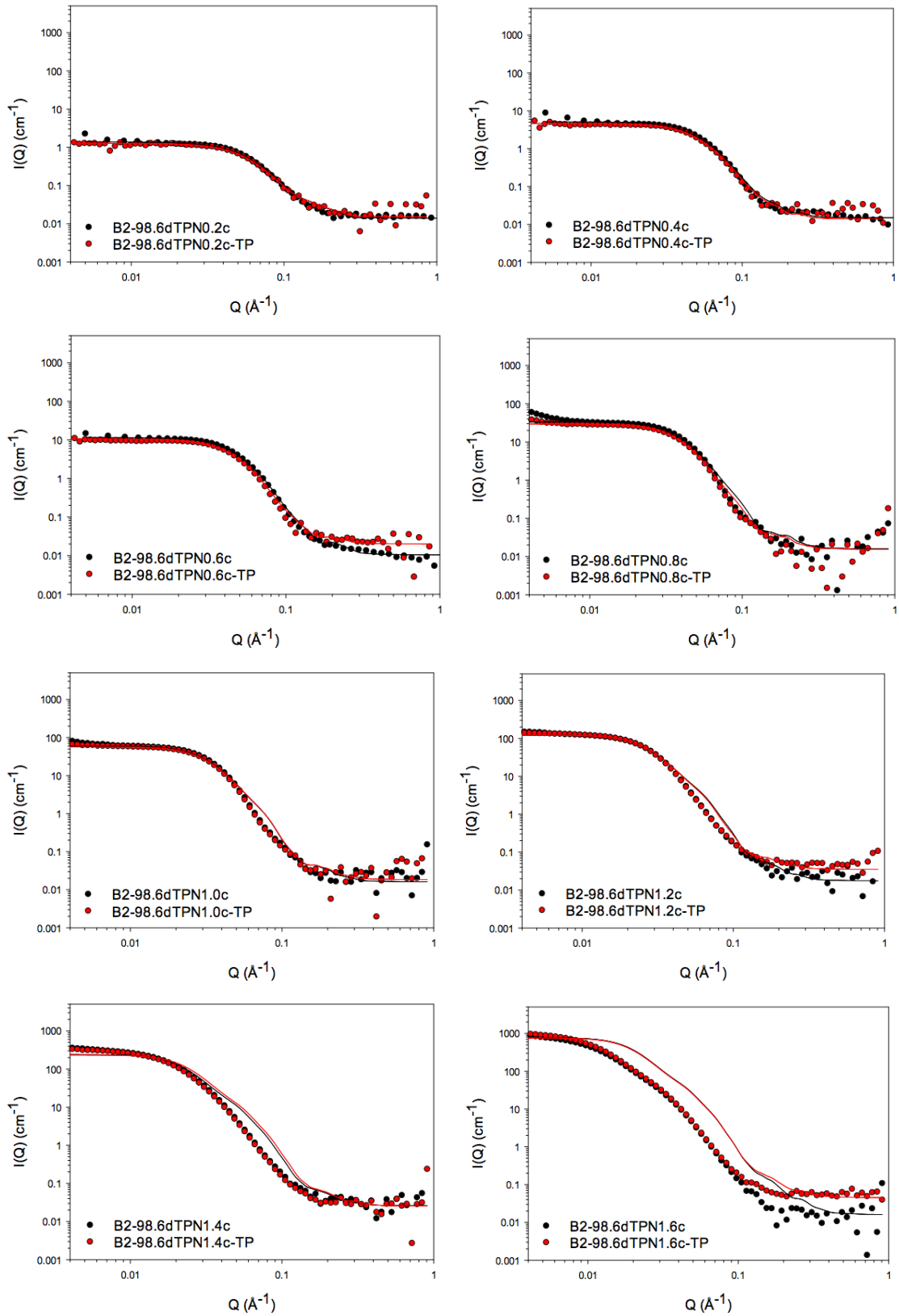

Figure B.30: SANS data and best fits to the core contrast for 2 %w/w Brij O10 NE containing varying amounts of 98.6dTPN in the presence and absence of TP. The best fits to the core contrast for 2 %w/w Brij O10 NE containing 0.8 %w/w 98.6dTPN and higher concentrations of 98.6dTPN were not well fitted to SANS data.

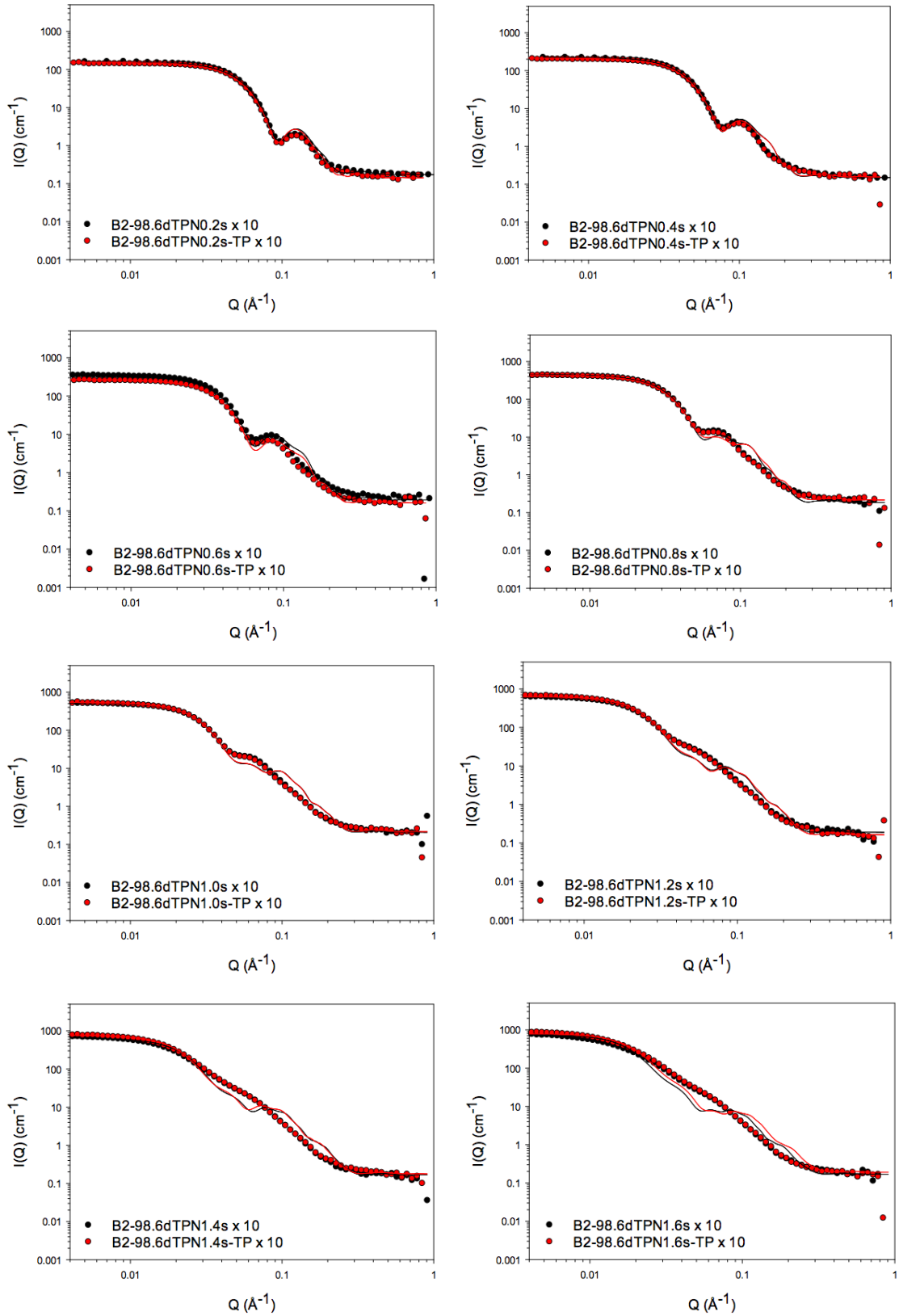

Figure B.31: SANS data and best fits to the shell contrast for 2 %w/w Brij O10 NE containing varying amounts of 98.6dTPN in the presence and absence of TP. The shell contrast for NE containing 98.6dTPN was multiplied by the factor of 10. Note that the best fits to the shell contrast for 2 %w/w Brij O10 NE containing 0.4 %w/w 98.6dTPN and higher concentrations of 98.6dTPN were not well fitted to SANS data.

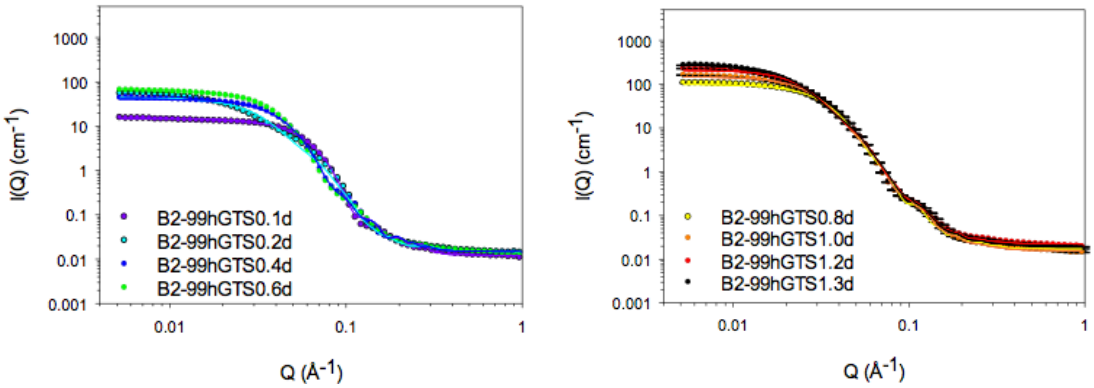

Figure B.32: SANS data and best fits to the drop contrast for 2 %w/w Brij O10 NE upon increasing concentration of 99hGTS from a) 0.1-0.6 %w/w and b) 0.8-1.3 %w/w.

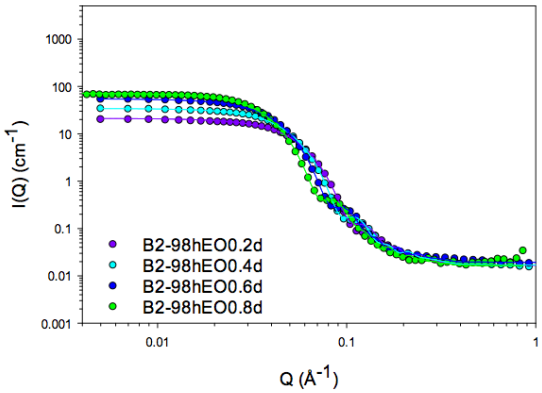

Figure B.33: SANS data and best fits to the drop contrast for 2 %w/w Brij O10 NE upon increasing concentration of 98hEO from 0.2-0.8 %w/w.

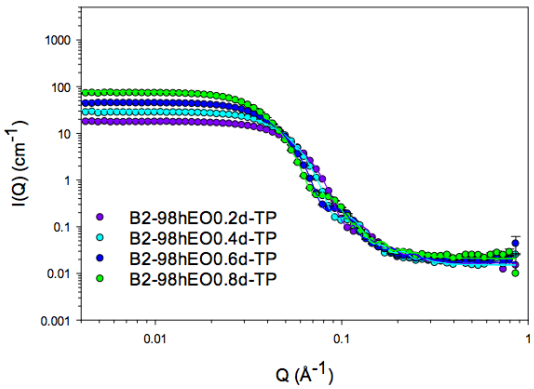

Figure B.34: SANS data and best fits to the drop contrast for 2 %w/w Brij O10 NE upon increasing concentration of 98hEO from 0.2-0.8 %w/w in the presence of drug.

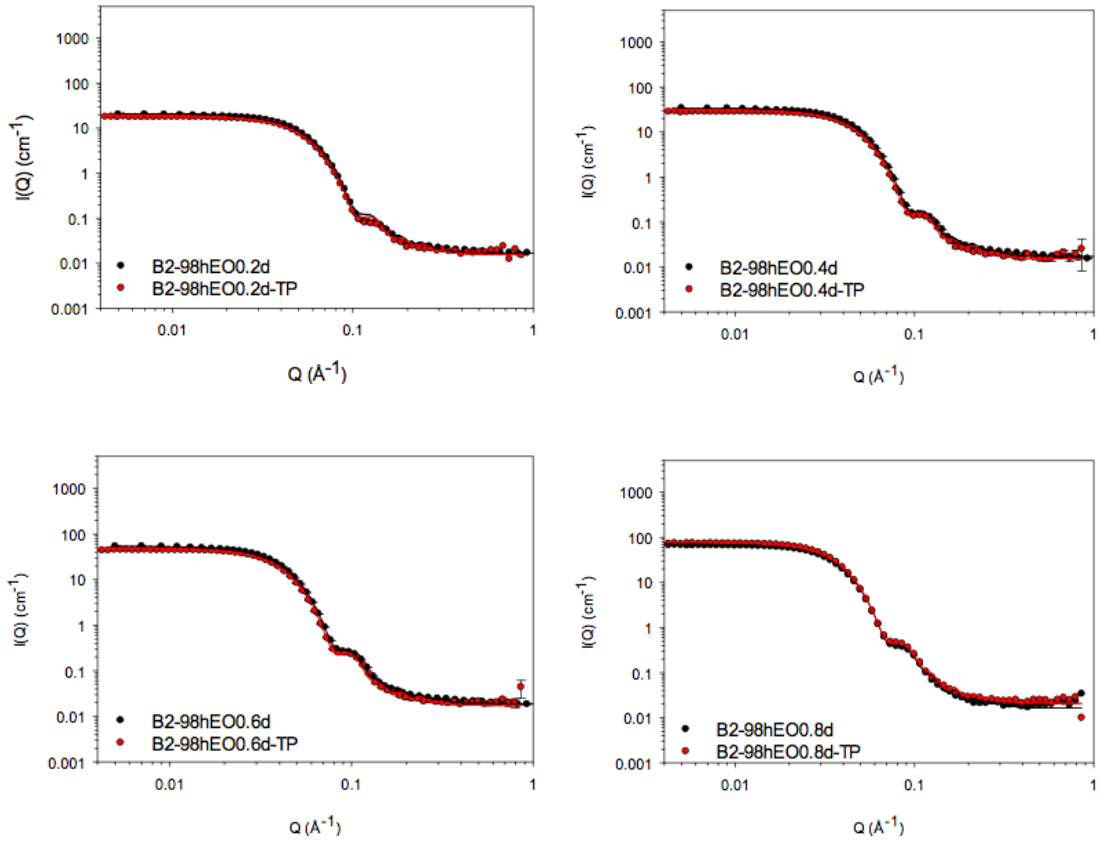

Figure B.35: SANS data and best fits to the drop contrast for 2 %w/w Brij O10 NE upon increasing concentration of 98hEO in the absence and presence of TP.

Appendix C: The results for the preparation of nanoemulsions with other nonionic surfactants in the absence and presence of cosurfactant

Table C.1 Variation in the cloud point of 20 %w/w Tween 80, 25 %w/w Tween 80:Dermosoft GMCY (weight ratio 3:1) and 25 %w/w Tween 80:Dermosoft GMCY:lecithin (weight ratio 7.5:2.5:1) micelle and the phase inversion temperature NE containing varying amounts of either hSBO or 98hEO (mean ± S.D., n = 3).

Oil concentration (%w/w)	Cloud point and phase inversion temperature (°C)			
	T20-hSBO NE in H_2O 1 month	T20-98hEO NE in H_2O 1 month	TD25-98hEO NE in H_2O 1 month	TDL25-hSBO NE in H_2O 1 month
0	87.8 ± 0.4	87.8 ± 0.4	60.9 ± 0.3	62.8 ± 0.5
1	95.0 ± 0.0	86.4 ± 0.5	-	-
2	95.0 ± 0.0	-	-	66.0 ± 0.7
3	-	-	-	70.4 ± 0.4
4	-	-	-	71.8 ± 0.4
8	-	-	60.0 ± 0.4	-
9	-	-	58.1 ± 0.4	-
10	-	-	56.0 ± 0.3	-

Table C.2 Variation in the apparent hydrodynamic size of micelle and nanoemulsions stabilised by either 20 %w/w Tween 80, 25 %w/w Tween 80:Dermosoft GMCY (weight ratio 3:1) or 25 %w/w Tween 80:Dermosoft GMCY:lecithin (weight ratio 7.5:2.5:1) and containing varying amounts of either hSBO or 98hEO after 1-month after preparation. All samples were diluted to 1 %w/w surfactant for measurement (mean ± S.D., n = 3).

Oil concentration (%w/w)	Hydrodynamic droplet size (nm)			
	T20-hSBO NE in H_2O 1 month	T20-98hEO NE in H_2O 1 month	TD25-98hEO NE in H_2O 1 month	TDL25-hSBO NE in H_2O 1 month
0	10.8 ± 0.4	10.8 ± 0.4	12.7 ± 0.1	23.5 ± 0.3
1	12.4 ± 0.2	12.6 ± 0.4	-	-
2	13.7 ± 0.4	-	-	13.9± 0.8
3	-	-	-	15.0 ± 0.1
4	-	-	-	16.2 ± 0.3
8	-	-	19.6 ± 0.4	-
9	-	-	20.8 ± 0.3	-
10	-	-	22.0 ± 0.6	-

Table C.3 Variation in the cloud point of 20 %w/w Tween 80, 25 %w/w Tween 80:Dermosoft GMCY (weight ratio 3:1) and 25 %w/w Tween 80:Dermosoft GMCY:lecithin (weight ratio 7.5:2.5:1) micelle and the phase inversion temperature of nanoemulsions stabilised by 20 %w/w Tween 80, 25 %w/w Tween 80:Dermosoft GMCY (weight ratio 3:1) and 25 %w/w Tween 80:Dermosoft GMCY:lecithin (weight ratio 7.5:2.5:1) and containing varying amount of either 98hEO or hSBO in H_2O and in the presence of either testosterone propionate (TP), curcumin (CUR) or docetaxel (DTX) (mean ± S.D., n = 3).

Oil concentration (%w/w)	Cloud point and phase Inversion Temperature (°C)								
	TD25-98hEO NE with TP in H_2O			T20-hSBO NE with CUR in H_2O	T20-98hEO NE with CUR in H_2O	TD25-98hEO NE with CUR in H_2O	TDL25-hSBO NE with CUR in H_2O	TD25-98hEO NE with CUR and TP in H_2O	TDL25-hSBO NE with DTX in H_2O
	7 days	10 days	14 days	7, 10 and 14 days					
0	55.3 ± 0.4 *	54.8 ± 0.4 *	55.2 ± 0.3 *	87.6 ± 0.4	87.6 ± 0.4	59.7 ± 0.6	57.7 ± 0.5 *	55.0 ± 0.7 *	56.5 ± 0.7 *
1	-	-	-	87.4 ± 0.5 *	85.8 ± 0.4	-	-	-	-
2	-	-	-	96.0 ± 0.0 *	-	-	63.4 ± 0.6 *	-	-
3	-	-	-	-	-	-	67.8 ± 0.5 *	-	66.4 ± 0.6 *
4	-	-	-	-	-	-	69.8 ± 0.6 *	-	-
8	55.2 ± 2.0 *	27.6 ± 0.6 *	29.0 ± 0.3 *	-	-	59.8 ± 0.3	-	33.5 ± 0.9 *	-
9	54.3 ± 0.5 *	31.1 ± 0.4 *	32.4 ± 0.4 *	-	-	61.7 ± 0.6 [a]	-	32.6 ± 0.6 *	-
10	44.3 ± 0.5 *	44.0 ± 0.8 *	43.3 ± 1.4 *	-	-	63.3 ± 0.4 [a]	-	38.5 ± 0.6 *	-

***** The CP or PIT of drug-saturated micelles or NE was significant lower than the CP or PIT of drug-free micelle or NE ($p<0.05$).
[a] The PIT of CUR-saturated NE was significant lower than the PIT of CUR-free NE ($p<0.05$).

Table C.4 The drug solubilisation in 20 %w/w Tween 80, 25 %w/w Tween 80:Dermosoft GMCY (weight ratio 3:1) and 25 %w/w Tween 80:Dermosoft GMCY:lecithin (weight ratio 7.5:2.5:1) micelles and nanoemulsions containing varying amounts of either 98hEO or hSBO in H_2O and in the presence of either testosterone propionate (TP), curcumin (CUR) or docetaxel (DTX) (mean ± S.D., n = 3).

Sample	Drug Solubilisation (%w/v)		
	7 days	10 days	14 days
TD25 with TP	0.45 ± 0.05	0.43 ± 0.05	0.45 ± 0.05
TD25-98hEO8 NE with TP	0.71 ± 0.03	1.49 ± 0.10	1.32 ± 0.09
TD25-98hEO9 NE with TP	0.73 ± 0.07	1.42 ± 0.08	1.46 ± 0.20
TD25-98hEO10 NE with TP	1.28 ± 0.15	1.11 ± 0.09	1.27 ± 0.18
CUR in TD25 with CUR and TP	0.22 ± 0.02	0.24 ± 0.02	0.23 ± 0.01
CUR in TD25-98hEO8 NE with CUR and TP	0.25 ± 0.01	0.24 ± 0.02	0.25 ± 0.01
CUR in TD25-98hEO9 NE with CUR and TP	0.25 ± 0.02	0.24 ± 0.02	0.24 ± 0.03
CUR in TD25-98hEO10 NE with CUR and TP	0.25 ± 0.02	0.23 ± 0.02	0.24 ± 0.02
TP in TD25 with CUR and TP	0.65 ± 0.02	0.69 ± 0.05	0.76 ± 0.02
TP in TD25-98hEO8 NE with CUR and TP	0.98 ± 0.06	0.98 ± 0.08	1.12 ± 0.06
TP in TD25-98hEO9 NE with CUR and TP	1.02 ± 0.05	0.98 ± 0.05	1.09 ± 0.06
TP in TD25-98hEO10 NE with CUR and TP	1.07 ± 0.06	1.05 ± 0.07	1.16 ± 0.03
TDL25 with DTX	0.20 ± 0.03	0.20 ± 0.06	0.19 ± 0.05
TDL25-hSBO3 NE with DTX	0.20 ± 0.05	0.29 ± 0.05	0.23 ± 0.03

References

Aboofazeli, R., Lawrence, M.J. (1993). Investigations into the formation and characterization of phospholipid microemulsions. I. Pseudo-ternary phase diagrams of systems containing water-lecithin-alcohol-isopropyl myristate. *Int J Pharm, 93*, 161-175.

Aboofazeli, R., Patel, N., Thomas, M., Lawrence, M.J. (1995). Investigations into the formation and characterization of phospholipid microemulsions. IV. Pseudo-ternary phase diagrams of systems containing water-lecithin-alcohol and oil; the influence of oil. *Int J Pharm, 125*, 107-116.

Ahmed, M., Ramadan, W., Rambhu, D., Shakeel, F. (2008). Potential of nanoemulsions for intravenous delivery of rifampicin. *Pharmazie, 64*, 806-811.

Ahyayauch, H., Bennouna, M., Alonso, A., & Goni, F. M. (2010). Detergent effects on membranes at subsolubilizing concentrations: transmembrane lipid motion, bilayer permeabilization, and vesicle lysis/reassembly are independent phenomena. *Langmuir, 26*(10), 7307-7313.

Almeida, C.P., Vital, C.G., Contente, T.C., Maria, D.A., Maranhao, R.C. (2010). Modification of composition of a nanoemulsion with different cholesteryl ester molecular species: effects on stability, peroxidation, and cell uptake. *Int J Nanomedicine, 5*, 679-686.

Amidon, G.L., Lennernas H., Shah, V.P., Crison, J.R. (1995). A theoretical basis for a biopharmaceutic drug classification: the correlation of in vitro drug product dissolution and in vivo bioavailability. *Pharmaceut Res, 12*(3), 413-420.

Anderberg, E.K., Nystrom, C., Artursson, P. (1992). Epithelial transport of drugs in cell culture. VII: Effects of pharmaceutical surfactant excipients and bile acids on transepithelial permeability in monolayers of human intestinal epithelial (Caco-s) cells. *Int J Pharm Pharm Sci, 81*, 879-887.

Anton N., Benoit J.-P., Saulnier P. (2008). Design and production of nanoparticles formulated from nano-emulsion templates—A review. *J Control Release, 128*(3), 185-199.

Anton, N., Gayet, P., Benoit, J.P., Saulnier, P. (2007). Nano-emulsions and nanocapsules by the PIT method: an investigation on the role of the temperature cycling on the emulsion phase inversion. *Int J Pharm, 344*(1-2), 44-52.

Anton, N., Vandamme, T.F. (2011). Nano-emulsions and micro-emulsions: clarifications of the critical differences. *Pharm Res, 28*(5), 978-985.

Arechabala, B., Coiffard, C., Rivalland, P., Coiffard, J.M., de Roeck-Holtzhauer, Y. (1999). Comparison of cytotoxicity of various surfactants tested on normal human fibroblast cultures using the neutral red test, MTT assay and LDH release. *J Appl Toxicol, 19*, 163-165.

Arleth, L., & Pedersen, J. S. (2001). Droplet polydispersity and shape fluctuations in AOT [bis(2-ethylhexyl)sulfosuccinate sodium salt] microemulsions studied by contrast variation small-angle neutron scattering. *Phys Rev E, 63*, 061406-061418.

Ashcroft, N.W., Lekner, J. (1966). Structure and Resistivity of Liquid Metals. *Physical Review, 145*(1), 83-90.

Aswal, V.K., Wagh, A.G. (2008). Small angle neutron scattering study of temperature-independent formulation of mixed micellar structures. *Pharmana, 71*(5), 1045-149.

Attwood, D. (1994). Microemulsions. In: Colloidal Drug Delivery Systems. Kreuter J (ed.) Dekker, New York.

Attwood, D., Mallon, C., Ktistis, G., Taylor, C.J. (1992). A study on factors influencing the droplet size in nonionic oil-in-water microemulsions. *Int J Pharm, 88*, 417-422.

Aungst, B.J. (2012). Absorption Enhancers: Applications and Advances. AAPS J, 14(1), 10-18.

Aveyard, R. Lawless, T.A. (1986). Interfacial tension minima in oil-water-surfactant systerms Systems containing pure non-ionic surfactants, alkanes and inorganic salts. *J Chem Soc, Faraday Trans 1, 82*, 2951-2963.

Aveyard, R., Binks, B.P., Fletcher, P.D.I. (1989b) Interfacial tensions and aggregate structure in $C_{12}E_5$/oil/water microemulsion systems. *Langmuir, 5*, 1210-1217.

Baker, R.C., Florence, A.T., Ottewill, R.H., Tadros, Th.F. (1984). Investigation into the formation and characterisation of microemulsions II. Light scattering conductivity and viscosity studies of microemulsions. *J Colloid Interface Sci, 100*(2), 332-349.

Balgavy, P., Devinsky, F. (1996). Cut-off effects in biological activities of surfactants. *Adv Colloid Interface Sci, 66*, 23-63.

Becker, R., Helenius, A., Simons, K. (1975). Solubilization of the Semliki Forest virus membrane with sodium dodecyl sulfate. *Biochemistry-US, 14*(9), 1835-1841.

Billman, J.F., Kaler, E.W. (1991). Structure and phase behavior in four-component nonionic microemulsions. *Langmuir, 7*, 1609-1617.

Binks, B.P., Meunier, J., Langevin, D. (1989). Characteristic sizes, film rigidity and interfacial tensions in microemulsion systems. *Prog Coll Pol Sci, 79*, 208-213.

Bivas-Benita, M., Oudshoorn, M., Romeijn, S., van Meijgaarden, K., Koerten, H., van der Meulen, H., Lambert, G., Ottenhoff, T., Benita, S., Junginger, H., Borchard, G. (2004). Cationic submicron emulsions for pulmonary DNA immunization. *J Control Release, 100*(1), 145-155.

Borhade, V., Nair, H., Hegde, D. (2008). Design and evaluation of self-microemulsifying drug delivery system (SMEDDS) of tacrolimus. *AAPS PharmSciTech, 9*(1), 13-21.

Brime, B., Moreno, M.A., Frutos, G., Ballesteros, M.P., Frutos, P. (2002). Amphotericin B in oil-water lecithin-based microemulsions: formulation and toxicity evaluation. *J Pharm Sci, 91*(4), 1178-1185.

Bunel, V., Ouedraogo, M., Nguyen, A. T., Stevigny, C., & Duez, P. (2014). Methods applied to the in vitro primary toxicology testing of natural products: state of the art, strengths, and limits. *Planta Med, 80*(14), 1210-1226.

Calligaris, S., Valoppi, F., Barba, L., Pizzale, L., Anese, M., Conte, L., Nicoli, M.C. *Food Biophysics, 12*(1), 45-51.

Chang, Y., Li, Y., Meng, X., Liu, N., Sun, D., Liu, H., Wang, J. (2013). Dendrimer functionalized water soluble magnetic iron oxide conjugates as dual imaging probe for tumor targeting and drug delivery. *Polym Chem, 4*(3), 789-794.

Charman, S.A., Charman, W.N., Rogge, M.C., Wilson, T.D., Dutko, F.J., Pouton, C.W. (1992). Self-emulsifying drug delivery systems: formulation and biopharmaceutic evaluation of an investigational lipophilic compound. *Pharmceut Res, 9*(1), 87-93.

Cheung, H.M. (1987). Light scattering study of oil-in-water microemulsions correlations for interactions. *Langmuir, 3*, 744-752.

Cho, Y.H., Kim, S., Bae, E.K., Mok, C.K., Park, J. (2008). Formulation of a cosurfactant-free O/W microemulsion using nonionic surfactant mixtures. *J Food Sci, 73*, E115-121.

Chodankar, S., Aswal, V.K., Kohlbrecher, J., Vavrin, R., Wagh, A.G. (2007). Surfactant-induced protein unfolding as studied by small-angle neutron scattering and dynamic light scattering. *J Phys: Condens Matter, 19*(32), 326102.

Conroy, J.P., Hall, C., Leng, C.A., Rendall, K., Tiddy, G.J.T., Walsh, J., Lindblom, G. (1990). Nonionic surfactant phase behaviour. The effect of CH3 capping of the terminal OH. Accurate measurements of cloud curves. *Prog Coll Pol Sci, 82*, 253-262.

Cornelis, M., Dupont, C., Wepierre, J. (1991). *In Vitro* cytotoxicity tests on cultured human skin fibroblasts to predict the irritation potential of surfactants. *ATLA-Altern lab anim, 19*, 324-336.

Cornwell, P.A., Tubek, J., van Gompel, A.H.P., Little, C.J., Wiecherrs, J.W. (1988). Glyceryl monocaprylate/caprate as a moderate skin penetration enhancer. *Int J Pharm, 171*, 243-255.

Corti, M., Minero, C., Degiorgio, V. (1984). Cloud point transition in nonionic micellar solutions. *J Phys Chem, 88*(2), 309-317.

Craig, P. N. (1990). Drug compendium. In Hansch, C., Sammes, P. G., Taylor, J. B. (eds). Comprehensive medicinal chemistry. VoL6: Cumulative subject inder anddrug compendium., Pergamon Press, New York, p. 237-991.

Date, A.A., Nagarsenker, M.S. (2007). Design and evaluation of self-nanoemulsifying drug delivery systems (SNEDDS) for cefpodoxime proxetil. *Int J Pharm, 329*(1-2), 166-172.

Date, A.A., Nagarsenker, M.S. (2008). Parenteral microemulsions: an overview. *Int J Pharm, 355*, 19-30.

Degiorgio, V. Corti, M. (1984). Laser-light scattering study of nonionic micelles in aqueous solution. In Mittal, K. L. & Lindman, B. (eds) Surfactants in solution. Vol. l. Plenum press, New York. p. 471-486.

Dimitrijevic, D., Lamandin, C., Uchegbu, I.F., Shaw, A.J. (1997). The effect of monomers and of micellar and vesicular forms of non-ionic surfactants (Solulan C24 and Solulan 16) on Caco-2 cell monolayers. *J Pharm Pharmacol, 49*, 611-616.

Dimitrijevic, D., Shaw, A.J., Florence, A.T. (2000). Effects of some non-ionic surfactants on transepithelial permeability in Caco-2 ccells. *J Pharm Pharmacol, 52*, 157-162.

Dixit, N., Kohli, K., Baboota, S. (2008). Nanoemulsion system for the transdermal delivery of a poorly soluble cardiovascular drug. *J Pharm Sci Technol, 62*: 46-55.

Djekic, L., Primorac, M. (2008). The influence of cosurfactants and oils on the formation of pharmaceutical microemulsions based on PEG-8 caprylic/capric glycerides. *Int J Pharm, 352*(1-2), 231-239.

Djekic, L., Primorac, M., Jockovic, J. (2011). Phase behaviour, microstructure and ibuprofen solubilization capacity of pseudo-ternary nonionic microemulsions. *J Mol Liq, 160*(2), 81-87.

Doke, S. K., & Dhawale, S. C. (2015). Alternatives to animal testing: A review. *Saudi Pharm J, 23*(3), 223-229.

Elsayed, M. M., Cevc, G. (2011). The vesicle-to-micelle transformation of phospholipid-cholate mixed aggregates: a state of the art analysis including membrane curvature effects. *Biochim Biophys Acta, 1808*(1), 140-153.

Ericsson, C.A., Soderman, O., Geramus, V.M., Bergstrom, M., Ulvenlund, S. (2004). Effects of temperature, salt, and deuterium oxide on the self-aggregation of alkylglycosides in dilute solution. 1. *n*-nonyl-*β*-D-glucoside. *Langmuir, 20*, 1401-1408.

Ericsson, C.A., Soderman, O., Geramus, V.M., Bergstrom, M., Ulvenlund, S. (2005). Effects of temperature, salt, and deuterium oxide on the the self-aggregation of alkylglycosides in dilute solution. 2. *n*-tetradecyl-*β*-D-maltoside. *Langmuir, 21*, 1507-1515.

Evans, D.F., Mitchell, D.J., Ninham, B.W. (1986). Oil, water, and surfactant: properties and conjectured structure of simple microemulsions. *J Phy Chem, 90*, 2817-2825.

Feng, J.L., Wang, Z.W., Zhang, J., Wang, Z.N., L.F. (2009). Study on food-grade vitamin E microemulsions based on nonionic emulsifiers. *Colloid Surface A, 339*(1-3), 1-6.

Forgiarini A., Esquena J., González C., Solans C. (2001) Formation and stability of nano-emulsions in mixed nonionic surfactant systems. In: Koutsoukos P.G. (eds) Trends in Colloid and Interface Science XV. Progress in Colloid and Polymer Science, vol 118. Springer, Berlin, Heidelberg

Forgiarini A., Esquena J., González C., Solans C. (2001b). Formation of Nano-emulsions by Low-Energy Emulsification Methods at Constant Temperature. *Langmuir, 17*(7): 2076-2083.

Gabizon, A.A. (1995). Liposome circulation time and tumor targeting: implications for cancer chemotherapy. *Adv Drug Deliver Rev, 16*, 285-294.

Gaikwad, S.G., Pandit, A.B. (2008). Ultrasound emulsification: effect of ultrasonic and physicochemical properties on dispersed phase volume and droplet size. *Ultrason Sonochem, 15*(4), 554-563.

General Medical Council. (2013). British Pharmacopoeia. London: The Stationery Office.

Girard, N., Tadros, Th.F., Bailey, A.I. (1997). Styrene and methylmethacrylate oil-in-water microemulsions. *Colloid Polym Sci, 275*, 698-704.

Goodwin, C.J., Holt, S.J., Downes, S., Maarshall, N.J. (1995). Microculture tetrazolium assays_a comparison between two new tetrazolium salts, XTT and MTS. *J Immunol Methods, 179*, 95-103.

Gould, L.A., Lansley, A. H., Martin, G.P. (1994). Phospholipid and surfactant mixed aggregates as penetration enhancers. *Proceed Intern Symp Control Rel Bioact Mater, 21*, 573-574.

Gradzielski, M., Hoffmann, H., Oetter, G. (1990). Ringing gels: their structure and macroscopic properties. *Colloid Polym Sci, 268*, 167-178.

Grant, R.L., Yao, C., Gabaldon, D., Acosta, D. (1992). Evaluation of surfactant cytotoxicity potential by primary cultures of ocular tissues: I. Characterization of rabbit corneal epithelial cells and initial injury and delayed toxicity studies. *Toxicology, 76*, 153-176.

Gulati, N., Gupta, H. (2011). Parenteral drug delivery: A review. *Recent Pat Drug Deliv Formul, 5*, 133-145.

Gull, N., Chodankar, S., Aswal, V.K., Din, K.U. (2008) Small angle neutron scattering studies on the interaction of cationic surfactants with bovine serum albumin. *Pramana, 71*(5), 1027-1031.

Gull, N., Chodankar, S., Aswal, V.K., Sen, P., Khan, R.H., Kabir ud, Din. (2009). Spectroscopic studies on the interaction of cationic surfactants with bovine serum albumin. *Colloids Surf B Biointerfaces, 69*(1), 122-128.

Gutiérrez, J.M., González, C., Maestro, A., Solè, I., Pey, C.M., Nolla, J. (2008). Nano-emulsions: New applications and optimization of their preparation. *Curr Opin Colloid In, 13*(4), 245-251.

Hamman, J., Steenekamp, J. (2012). Excipients with specialized functions for effective drug delivery. *Expert Opin Drug Deliv, 9*(2), 219-230.

Hauss, D. J. (2007). Oral lipid-based formulations. *Adv Drug Deliv Rev, 59*(7), 667-676.

Heenan, R.K. (1989). The "Fish" reference manual. Data fitting program for small angle neutron scattering (Revised 2005). *RAL Technical Reports***,** RAL 89–129.

Heenan, R.K., Rogers, S.E., Turner, D., Terry, A.E., Tredgold, J., King, S.M. (2011). Small angle neutron scattering using sans2d. *Neutron News, 22*(2), 19-21.

Heerklotz, H. (2008). Interactions of surfactants with lipid membranes. *Q Rev Biophys,* 41, 205–264.

Helenius, A., Simons, K. (1975). Solubilization of membranes by detergents. *Biochim Biophys Acta, 415*, 29-79.

Hoeller, S., Sperger, A., Valenta, C. (2009). Lecithin based nanoemulsions: A comparative study of the influence of non-ionic surfactants and the cationic phytosphingosine on physicochemical behaviour and skin permeation. *Int J Pharm, 370*, 181-186.

Hoffmann, H., Ulbright, W. (1989). Transition of rodlike to globular micelles by the solubilization of additives. *J Colloid Interf Sci, 129*(2), 388-405.

Hofland, H.E.J., Bouwstra, J.A., Ponec, M., Bodde, H.E., Spies, F., Verhoeff, C.J., Junginger, H.E. (1991). Safety aspects of non-ionic surfactant vesicles: a toxicity study related to the physicochemical characteristics of non-ionic surfactants. *J Pharm Pharmacol, 44*, 287-294.

Hofland, H.E.J., Bouwstra, J.A., Verhoeff, C.J., Buckton, G., Chowdry, B.Z., Ponec, M., Junginger, H.E. (1992). Interactions of non-ionic surfactant vesicles with cultured keratinocytes and human skin in vitro: a survey of toxicological aspects and ultrastructural changes in stratum corneum. *J Control Release, 16*, 155-168.

Huang Q., Yu H., Ru Q. (2010). Bioavailability and Delivery of Nutraceuticals Using Nanotechnology. *J Food Sci, 75*(1): R50-R57.

Huang, L. (1996). Folate-targeted, Anionic Liposome-entrapped Polylysine-condensed DNA for Tumor Cell-specific Gene Transfer. *J Biol Chem, 271*(14), 8481-8487.

Inoue, T., Yamakawa, H. (2011). Micelle formation of nonionic surfactants in a room temperature ionic liquid, 1-butyl-3-methylimidazolium tetrafluoroborate: surfactant chain length dependence of the critical micelle concentration. *J Colloid Interface Sci, 356*(2), 798-802.

Izquierdo, P., Esquena, J., Tadros, Th F., Dederen, C., Garcia, M. J., Azemar, N., & Solans, C. (2002). Formation and stability of nano-Emulsions prepared using the phase inversion temperature method. *Langmuir, 18*(1), 26-30.

Izquierdo, P., Esquena, J., Tadros, Th.F., Dederen, C., Feng, J., Garcia-celma, M.J., Azemar, N., Solan, C. (2004). Phase behavior and nano-emulsion formation by the phase inversion temperature method. *Langmuir, 20*, 6594-6598.

Izquierdo, P., Esquena, J., Tadros, Th.F., Dederen, C., Feng, J., Garcia-celma, M.J., Azemar, N., Solan, C. (2004). Phase behavior and nano-emulsion formation by the phase inversion temperature method. *Langmuir, 20*, 6594-6598.

Izquierdo, P., Feng, J., Esquena, J., Tadros, T.F., Dederen, J.C., Garcia, M.J., Azemar, N., Solans, C. (2005). The influence of surfactant mixing ratio on nano-emulsion formation by the pit method. *J Colloid Interface Sci, 285*(1), 388-394.

Jain, A., Yan, W., Miller, K. R., O'Carra, R., Woodward, J. G., & Mumper, R. J. (2010). Tresyl-based conjugation of protein antigen to lipid nanoparticles increases antigen immunogenicity. *Int J Pharm, 401*(1-2), 87-92.

Jasim, F., Ali, F. (1989). Measurements of some spectrophotometric parameters of curcumin in 12 polar and nonpolar organic solvents. *Microchem J, 39*(2), 156-159.

Jawhari, D.E. Monoglyceride containing nonionic oil-in-water miroemulsions : physico-chemical characterization using surface tension, light scattering and toxicity studies. PhD thesis, King's College London, 1999.

Jiao, J. (2008). Polyoxyethylated nonionic surfactants and their applications in topical ocular drug delivery. *Adv Drug Deliv Rev, 60*(15), 1663-1673.

Joyce, P., Barnes, Timothy J., Boyd, B.J., Prestidge, C.A. (2016). Porous nanostructure controls kinetics, disposition and self-assembly structure of lipid digestion products. *RSC Adv., 6*(82), 78385-78395.

Kale, N., Allen, L.V. (1989). Studies on microemulsions using Brij 96 as surfactant and glycerine, ethylene glycol and propylene glycol as cosurfactants. *Int J Pharm, 57,* 87-93.

Khoo, S.M., Shackleford, S.M., Porter, C.J.H., Edwards, G.A., Charman, W.N. (2003). Intestinal lymphatic transport of halofantrine occurs after oral administration of a unit-dose lipid-based formulation to fasted dogs. *Pharmaceut Res, 20*(9), 1460-1465.

Kim, S.L., Jeong, H.J., Kim, E.M., Lee, C.M., Kwon, T.H., Sohn, M.H. (2007). Folate receptor targeted imaging using poly (ethylene glycol)-folate: In vitro and in vivo studies. *J Korean Med Sci, 22,* 405-411.

King S.M. (1999). Small angle neutron scattering Vol. 171: John Wiley & Sons New York.

Kjellander, R. (1982). Phase separation of non-ionic surfactant solutions. A treatment of the micellar interaction and form. *J Chem Soc Faraday Trans, 2,* 2025-2042.

Klang, V., Valenta, C. (2011). Lecithin-based nanoemulsions. *J Drug Deliv Sci Tec, 21*, 55-76.

Klippstein, R., Wang, J. T., El-Gogary, R. I., Bai, J., Mustafa, F., Rubio, N., Al-Jamal, K. T. (2015). Passively Targeted Curcumin-Loaded PEGylated PLGA Nanocapsules for Colon Cancer Therapy In Vivo. *Small, 11*(36), 4704-4722.

Knothe, G., Kenar, J.A. (2004). Determination of the fatty acid profile by1H-NMR spectroscopy. *Eur J Lipid Sci Tech, 106*(2), 88-96.

Ko, C.J., Ko, Y.J., Kim, D.M., Park, H.J. (2003). Solution properties and PGSE-NMR self-diffusion study of $C_{18:1}E_{10}$/oil/water system. *Colloid Surface A, 216*(1-3), 55-63.

Kragh-hansen, U., le Maire, M., & Moller, J.P. (1998). The mechanism of detergent solubilization of liposomes and protein-containing membranes. *Biophys J, 75,* 2932-2946.

Kumar, A., Kaur, G., Kansal, S.K., Chaudhary, G.R., Mehta, S.K. (2016). (Cationic + nonionic) mixed surfactant aggregates for solubilisation of curcumin. *J Chem Thermodyn, 93,* 115-122.

Kumar, G.P., Rajeshwarrao, P. (2011). Nonionic surfactant vesicular systems for effective drug delivery—an overview. *Acta Pharm Sin B, 1*(4), 208-219.

Kunieda, H., Horii, M., Koyama, M., Sakamoto, K. (2001). Solubilization of Polar Oils in Surfactant Self-Organized Structures. *J Colloid Interface Sci, 236*(1), 78-84.

Kuntsche, J., Horst, J.C., Bunjes, H. (2011). Cryogenic transmission electron microscopy (cryo-TEM) for studying the morphology of colloidal drug delivery systems. *Int J Pharm, 417*(1-2), 120-137.

Kurien, B.T., Singh, A., Matsumoto, H., Scofield, R.H. (2007). Improving the solubility and pharmacological efficacy of curcumin by heat treatment. *Assay Drug Dev Technol, 5*, 567-576.

Lasch, J. (1995). Interaction of detergents with lipid vesicles. *Biochim Biophys Acta, 1241*, 269-292.

Lawrence, M.J. (1994). Surfactant systems:_microemulsions and vesicles as vehicles for drug delivery. *Eur J Drug Metab Ph, 3*, 257-269.

Lee, R., Low, P.S. (1994). Delivery of liposomes into cultured KB cells via folate receptor-mediated endocytosis. *J Biol Chem, 4*, 3198-3204.

Lee, R.J., Huang, L. (1996). Folate-targeted, anionic liposome-entrapped polylysine-condensed DNA for tumor cell-specific gene transfer. *J Biol Chem, 271*, 8481-8487.

Lee, R.J., Low, P.S. (1995). Folate-mediated tumor cell targeting of liposome-entrapped doxorubicin in vitro. *Biochem Biophys Acta, 1233*, 134-144.

Li, J.L., Bai, D.S., Chen, B.H. (2009). Effects of additives on the cloud points of selected nonionic linear ethoxylated alcohol surfactants. *Colloid Surface A, 346*(1-3), 237-243.

Li, X., Tian, X., Zhang, J., Zhao, X., Chen, X., Jiang, Y., Pan, W. (2011). In vitro and in vivo evaluation of folate receptor-targeting amphiphilic copolymer-modified liposomes loaded with docetaxel. *Int J Nanomedicine, 6*, 1167-1184.

Lichtenberg, D., Ahyayauch, H., Goni, F. M. (2013). The mechanism of detergent solubilization of lipid bilayers. *Biophys J, 105*(2), 289-299.

Lichtenberg, D., Robson, R.J., Dennis, E.A. (1983). Solubilization of phospholipids by detergents. Structural and kinetic aspects. *Biochim Biophys Acta, 737*, 285-304.

Lindman, B., Shinoda, K., Olsson, U., Anderson, D., Karlstrom, G., Wennerstrom, H. (1989). On the demonstration of bicontinuous structures in microemulsions. *Colloid Surface, 38*, 205-224.

Lipinski, C.A., Lombardo, F., Dominy, B.W., Feeney, P.J. (2001). Experimental and computational approaches to estimate solubility and permeability in drug discovery and development setting. *Adv Drug Deliv Rev, 46*, 3-26.

Lobenberg, R., Amidon, G.L. (2000). Modern bioavailability, bioequivalence and biopharmaceutics classification system. New scientific approaches to international regulatory standards. *Eur J Pharm Biopharm., 50*, 3-12.

Lu, Y., Low, P.S. (2002). Folate-mediated delivery of macromolecular anticancer therapeutic agents. *Adv Drug Deliver Rev, 54*, 675-693.

Luangwitchajaroen, Y. Preparation of nanosusponanoemulsion and nanosuspomicroemulsion: novel combination formulations suitable for personalised medicine. PhD thesis, King's College London, 2017.

Lund, W. (1994). The pharmaceutical codex: principles and practice of pharmaceutics. London: Pharmaceutical Press, 12th ed

Lundberg, B., Lovgren, T., Heikius, B. (1979). Simultaneous solubilization of steroid hormones II: androgens and estrogens. *J Pharm Sci, 68*(5), 542-545.

Luning Prak, D. J., Jahraus, W.I., Sims, J.M., MacArthur, A.H.R. (2011). An ^{1}H NMR investigation into the loci of solubilization of 4-nitrotoluene, 2,6-dinitrotoluene, and 2,4,6-trinitrotoluene in nonionic surfactant micelles. *Colloid Surface A, 375*(1-3), 12-22.

Lyons, C.J., Moore, B.P., Flbing, L.E., Coller, B.A.W., Wilson, I.R. (1990). Solubilization, microemulsions and surface chemistry of ethyl stearate in aqueous solutions of a nonionic emulsifier. *J Disper Sci Technol, 11*(2), 125-141.

Maali, A., Mosavian, M.T.H. (2013). Preparation and Application of Nanoemulsions in the Last Decade (2000–2010). *J Disper Sci Technol, 34*(1), 92-105.

Maestro, A., Sole, I., Gonzalez, C., Solans, C., Gutierrez, J.M. (2008). Influence of the phase behavior on the properties of ionic nanoemulsions prepared by the phase inversion composition method. *J Colloid Interface Sci, 327*(2), 433-439.

Malcolmson, C. The physicochemical properties of nonionic oil-in-water microemulsions. PhD thesis, King's College London, 1993.

Malcolmson, C., Lawrence, M.J. (1993). A comparison of the incorporation of steroids into nonionic micellar and microemulsion systems. *J Pharm Pharmacol. 45*, 141–143.

Malcolmson, C., Lawrence, M.J. (1995). Three-component non-ionic oil-in-water microemulsions using polyoxyethylene ether surfactants. *Colloid Surface B Biointerfaces, 4*, 97-109.

Malcolmson, C., Satra, C., Kantaria, S., Sidhu, A., Lawrence, M.J. (1998). Effect of oil on the level of solubilization of testosterone propionate into nonionic oil-in-water microemulsions. *J Pharm Sci, 87*(1), 109-116.

Manaargadoo-Catin, M., Ali-Cherif, A., Pougnas, J. L., & Perrin, C. (2016). Hemolysis by surfactants-A review. *Adv Colloid Interface Sci, 228*, 1-16.

Martin, A., Lesemann, M., Belkoura, L., Woermann, D. (1996) Slowing down of the mutual diffusion process approaching the liquid/liquid coexistence curve of a nonionic surfactant/deuterium oxide system: study of the system $C_{12}E_5/D_2O$. *J Phy Chem, 100*, 13760-13764.

Mason, T.G., Wilking, J.N., Meleson, K., Chang, C.B., Graves, S.M. (2006). Nanoemulsions: formation, structure, and physical properties. *J Phys: Condens Matter, 18*(41), R635-R666.

Mathias, C.J., Wang, S., Lee, R.J., Waters, D.J., Low, P.S., Green, M.A. (1996). Tumor-selective radiopharmaceutical targeting via receptor-mediated endocytosis of gallium-67-deferoxamine-folate. *J. Nucl Med, 37*, 1003-1008.

Matsuyama, T., Morita, T., Horikiri, Y., Yamahara, H., Yoshino, H. (2006). Enhancement of nasal absorption of large molecular weight compounds by combination of mucolytic agent and nonionic surfactant. *J Control Release, 110*(2), 347-352.

Mattei, B., Lira, R. B., Perez, K. R., & Riske, K. A. (2017). Membrane permeabilization induced by Triton X-100: The role of membrane phase state and edge tension. *Chem Phys Lipids, 202*, 28-37.

McClement, D.J. (2013). Nanoemulsion-based oral delivery systems for lipophilic bioactive components: nutraceuticals and pharmaceuticals. *Ther Deliv, 4*(7), 841-857.

McClements, D.J. (2012). Nanoemulsions versus microemulsions: terminology, differences, and similarities. *Soft Matter, 8*(6), 1719-1729.

Miyake, Y., Yokomizo, K., Matsuzaki, N. (1998). Determination of unsaturated fatty acid composition by high-resolution nuclear magnetic resonance spectroscopy. *JAOCS, 75*, 1091-1094.

Morales, D., Gutiérrez, J.M., García-Celma, M.J., Solans, Y.C. (2003). A study of the relation between bicontinuous microemulsions and oil/water nano-emulsion formation. *Langmuir, 19*(18), 7196-7200.

Morales, S., Solans, C., Gutiérrez, J.M., García-Celma, M.J., Olsson, U. (2006). Oil/water droplet formation by temperature change in the water-$C_{16}E_6$/mineral oil system. Langmuir, 22, 3014-3020.

Mosmann, T. (1983). Rapid colorimetric assay for cellular growth and survival: Application to proliferation and cytotoxicity assays. *J Immunol Methods, 65*, 55-63.

Mukherjee, P., Padhan, S.K., Dash, S., Patel, S., Mishra, B.K. (2011). Clouding behaviour in surfactant systems. *Adv Colloid Interface Sci, 162*, 59-79.

Muller, B.W., Muller, R.H. (1984). Particle size analysis of latex suspensions and microemulsions by photon correlation spectroscopy. *J Pharm Sci, 13*(7), 915-918.

Nagao, M., Okabe, S., Shibayama, M. (2005). Small-angle neutron-scattering study on a structure of microemulsion mixed with polymer networks. *J Chem Phys, 123*(14), 144909.

Nagarajan, R. (1997). Solubilization by amphiphilar aggregates. *Curr Opin Colloid In, 2*, 282-293.

Narang, A.S., Delmarre, D., Gao, D. (2007). Stable drug encapsulation in micelles and microemulsions. *Int J Pharm, 345*(1-2), 9-25.

Nilsson, K., Mosbach, K. (1981). Immobilization of enzymes and affinity ligands to various hydroxyl group carrying supports using highly reactive sulfonyl chlorides. *Biochem Bioph Res Co, 1*, 449-457.

Nilsson, K., Mosbach, K. (1984). Immobilization of ligands with organic sulfonyl chlorides. *Method Enzymol, 104*, 56-69.

Nilsson, P.G., Pacynko, W.F., Tiddy, G.J.T. (2004). 'Clouding' in Zwitterionic surfactant/water systems – the influence of additives on the upper consolute loop of the decyldimethylammonioethane sulfate/water system. *Curr Opin Colloid In,* 9(1-2), 117-123.

Nobbmann, U., Morfesis, A. (2009). Light scattering and nanoparticles. Mater Today,12(5), 52-55.

Ohnishi, M., Sagitani, H. (1993). The effect of nonionic surfactant structure on hemolysis. *J Am Oil Chem Soc, 70*(7), 679-684.

Ostertag, F., Weiss, J., McClements, D.J. (2012). Low-energy formation of edible nanoemulsions: factors influencing droplet size produced by emulsion phase inversion. *J Colloid Interf Sci, 388*, 95-102.

Pan, X.Q., Wang, H., Lee, R.J. (2003). Antitumor Activity of Folate Receptor-Targeted Liposomal Doxorubicin in a KB Oral carcinoma murine xenograft model. Pharmaceut Res, 20(3), 417-422.

Pandit, N.K, Carona, J. (1988). Comparison of the cloud point behavior of Triton X-lO0 in H_20 and D_2O. *J Colloid Interf Sci, 122*(1), 100-103.

Pantaler, E., Kamp, D., Haest, C.W.M. (2000). Acceleration of phospholipid flip-flop in the erythrocyte membrane by detergents differing in polar head group and alkyl chain length. *Biochim Biophys Acta, 1509*, 397-408.

Partearroyo, M.A., Pilling, S.J., Jones, M.N. (1991). The lysis of isolated fish (Oncorhynchus mykiss) gill epithelial cells by surfactants. *Comp Biochem Physiol, 100*(3), 381-388.

Pedersen, J.S. (1997). Analysis of small-angle scattering data from colloids and polymer solutions: modelling and least-squares fitting. Adv Colloid Interface Sci, 70, 171-210.

Petty, R.D., Sutherland, L.A., Hunter, E.M., Cree, I.A. (1995). Comparison of MTT and ATP-based assays for the measurement of viable cell number. *J Biolum Chemilumin, 10*, 29-34.

Praveen Kumar G., Divya A. (2015). Nanoemulsion based targeting in cancer therapeutics. *Med Chem, 5*(5), 272-284.

Preu, H., Zradba, A., Rast, S., Kunz, W., Hardy, E.H., Zeidler, M.D. (1999). Small angle neutron scattering of D_2O-Brij 35 and D_2O-alcohol-Brij 35 solutions and their modelling using the Percus-Yevick integral equation. Phys Chem Chem Phys, 1(14), 3321-3329.

Provost, C., Kinget, R. (1988). Transparent oil-water gels:_a study of some physicochemical and biopharmaceutical characteristics. Part I. Formation of transparent oil-water gels in the 4-component-system of Eumulgin B3, Cetiol HE, isopropyl palmitate, and water. *Int J Pharm, 44*, 75-85.

Ranganatha, N., Kuppast, I.J. (2012). A review on alternatives to animal testing methods in drug delivery development. *Int J Pharm Pharm Sci, 4*, 28-32.

Rao, J., McClements, D.J. (2010). Stabilization of phase inversion temperature nanoemulsions by surfactant displacement. *J Agric Food Chem, 58*(11), 7059-7066.

Ratner, B.D. (1995). Advances in the analysis of surfaces of biomedical interest. *Surf interface anal, 23*, 521-528.

Richtening, W.H., Burchard, W., Jahns, E., Finkelmann, H. (1988). Light scattering from aqueous solutions of a nonionic surfactant ($C_{14}E_8$) in a wide concentration range. *J Phys Chem, 92*, 6032-6040.

Rogers, S.E., Terry, A.E., Lawrence, M.J., Eastoe, J., Cabral, J.T., Chan, A. (2009). Soft matter at ISIS. *Mater Today, 12*(7-8), 92-99.

Ruckenstein, E. (1997). Phase inversion temperatures of macro- and microemulsions. Langmuir, 13, 2494-2497.

Saaka, Y. Effect of surfactant headgroup on the micellar solubilisation of poorly water soluble drugs. PhD thesis, King's College London, 2016.

Sadtler, V., Rondon-Gonzalez, M., Acrement, A., Choplin, L., Marie, E. (2010). PEO-Covered Nanoparticles by Emulsion Inversion Point (EIP) Method. Macromol Rapid Commun, 31(11), 998-1002.

Sadurni, N., Solans, C., Azemar, N., Garcia-Celma, M.J. (2005). Studies on the formation of O/W nano-emulsions, by low-energy emulsification methods, suitable for pharmaceutical applications. *Eur J Pharm Sci, 26*(5), 438-445.

Saint Ruth, H., Attwood, D., Ktistis, G., Taylor, C.J. (1995). Phase studies and particle size analysis of oil-in-water phospholipid microemulsions. *Int J Pharm, 116*, 253-261.

Saito, H., Shinoda, K. (1967). The solubilization of hydrocarbons in aqueous solutions of nonionic surfactants. *J Colloid Interface Sci*, 24,10-15.

Sanhai, W.R., Sakamoto, J.H., Canady, R., Rerrari, M. (2008). Seven challenges for nanomedicine. *Nat Nanotech, 3*, 242-244.

Satra, C.H. Physico-chemical studies on lecithin-based oil-in-water microemulsions. PhD thesis, University of London, 1998.

Savjani, K.T., Gajjar, A.K., Savjani, J.K. (2012). Drug solubility: importance and enhancement techniques. ISRN Pharm, 2012, 195727.

Schmiele, M., Gehrer, S., Westermann, M., Steiniger, F., Unruh, T. (2014). Formation of liquid crystalline phases in aqueous suspensions of platelet-like tripalmitin nanoparticles. *J Chem Phys, 140*(21), 214905.

Schmiele, M., Schindler, T., Unruh, T., Busch, S., Morhenn, H., Westermann, M., Steiniger, F., Radulescu, A., Lindner, P., Schweins, R., Boesecke, P. (2013). Structural characterization of the phospholipid stabilizer layer at the solid-liquid interface of dispersed triglyceride nanocrystals with small-angle x-ray and neutron scattering. *Phys Rev E, 87*(6), 062316.

Schmiele, M., Schindler, T., Westermann, M., Steiniger, F., Radulescu, A., Kriele, A., Gilles, R., Unruh, T. (2014). Mesoscopic structures of triglyceride nanosuspensions studied by small-angle X-ray and neutron scattering and computer simulations. *J Phys Chem B, 118*(29), 8808-8818.

Schön, W., Wiechers, R., & Woermann, D. (1986). Deuterium isotope effects in binary critical mixtures. *J Chem Phys, 85*(5), 2922-2928.

Schott, H., Royce, A.E. (1984). Effect of inorganic additives on solutions of nonionic surfactants VI: further cloud point relations. *J Pharm Sci, 73*(6), 793-799.

Schubert, K.V., Kaler, E.W. (1996). Nonionic microemulsions. Ber Bunsenges Phys Chem, 100(3), 190-205.

Schultz, S., Wagner, G., Urban, K., Ulrich, J. (2004). High-pressure homogenization as a process for emulsion formation. Chem Eng Technol, 4, 361-368.

Shafiq, S., Shakeel, F., Talegaonkar, S., Ahmad, F.J., Khar, R.K., Ali, M. (2007). Development and bioavailability assessment of ramipril nanoemulsion formulation. *Eur J Pharm Biopharm, 66*(2), 227-243.

Shah, N.H., Carvajal, M.T., patel, C.I., Infeld, M.H., Malick, A.W. (1994). Self-emulsifying drug-delivery systems (SEDDS) with polyglycolyzed glycosides for improving in vitro dissolution and oral absorption of lipophilic drugs. *Int J Pharm, 106*, 15-23.

Shah, P., Bhalodia, D., & Shelat, P. (2010). Nanoemulsion: A pharmaceutical review. Sys Rev Pharm, 1(1), 24-32.

Sharma, S.C., Warr, G.G. (2012). Phase behavior, self-assembly, and emulsification of Tween 80/water mixtures with limonene and perfluoromethyldecalin. *Langmuir, 28*(32), 11707-11713.

Shigeta, K., Olsson, U., Kunieda, H. (2001). Correlation between micellar structure and cloud point in long poly(oxyethylene)$_n$ oleyl ether systems. *Langmuir, 17*, 4717-4723.

Shinoda, K., Arai, H. (1964). The correlation between phase inversion temperature in emulsion and cloud point in solution of nonionic emulsifier. 68(12), 3485-3490. *J Phy Chem*, 68(12), 3485-3490.

Sigma Aldrich. Product information of testosterone propionate.

Singh, K.K., Vingkar, S.K. (2008). Formulation, antimalarial activity and biodistribution of oral lipid nanoemulsion of primaquine. *Int J Pharm, 347*(1-2), 136-143.

Singh, R.K., Rai, D., Yadav, D., Bhargava, A., Balzarini, J., De Clercq, E. (2010). Synthesis, antibacterial and antiviral properties of curcumin bioconjugates bearing dipeptide, fatty acids and folic acid. *Eur J Med Chem, 45*, 1078-1086.

Solan, C., Izquierdo, P., Nolla, J., Azemar, N., Garcia-celma, M.J. (2005). Nano-emulsions. *Curr Opin Colloid In, 10*, 102-110.

Sood, S., Jain, K., Gowthamarajan, K. (2014). Optimization of curcumin nanoemulsion for intranasal delivery using design of experiment and its toxicity assessment. *Colloid Surface B, 113*, 330-337.

Stockert, J. C., Blazquez-Castro, A., Canete, M., Horobin, R. W., Villanueva, A. (2012). MTT assay for cell viability: Intracellular localization of the formazan product is in lipid droplets. *Acta Histochem, 114*(8), 785-796.

Strey, R., Glatter, O., Schubert, K.-V, Kaler, E.W. (1996). Small-angle neutron scattering of D_2O–$C_{12}E_5$ mixtures and microemulsions with *n*-octane: Direct analysis by Fourier transformation. *J Chem Phys, 105*(3), 1175-1188.

Strickley, R.G. (2004). Solubilizing excipients in oral and injectable formulations. *Pharm Res, 21*(2), 201-230.

Stuart, M.C.A., Boekema, E.J. (2007). Two distinct mechanisms of vesicle-to-micelle and micelle-to-vesicle transition are mediated by the packing parameter of phospholipid–detergent systems. *Biochim Biophys Acta, 1768*, 2681-2689.

Swenson, E.S., Curatolo, W.J. (1992). (C) Means to enhance penetration (2) Intestinal permeability enhancement for proteins, peptides and other polar drugs: mechanisms and potential t oxicity. *Adv Drug Delivery Rev, 8*, 39-92.

Tadros, T., Izquierdo, P., Esquena, J., Solans, C. (2004). Formation and stability of nano-emulsions. Adv Colloid Interface Sci, 108-109, 303-318.

Talegaonkar, S., Azeem, A., Ahmed, F.J., Khar, R.K., Pathan, S.A., Khan, Z.I. (2008). Microemulsions: a novel approach to enhanced drug delivery. *Recent Pat Drug Deliv Formul, 2*, 238-257.

Tanford, C. (1972). Hydrophobic free energy, micelle formation and the association of proteins with amphiphiles. *J Mol Biol, 67*, 59-74.

Tanford, C., Nozaki, Y., Rohde, M.F. (1977). Size and shape of globular micelles formed in aqueous solution by n-alkyl polyoxyethylene ethers. *J Phys Chem, 81*(16), 1555-1560.

Tang, X., Wang, G., Shi, R., Jiang, K., Meng, L., Ren, H., Wu, J., Hu, Y. (2016). Enhanced tolerance and antitumor efficacy by docetaxel-loaded albumin nanoparticles. *Drug deliv, 23*, 2686-2696.

Thakkar, A.L. Kuehn, P.B. (1969). Solubilization of some steroids in aqueous solutions of a steroidal nonionic surfactant. *J Pharm Sci, 58*(7), 850-852.

Thakkar, A.L., Hall, N.A. (1967). Micellar Solubilization of Testosterone I In aqueous solutions of polysorbates. *J Pharm Sci, 56*(9), 1121-1125.

The Human Metabolome Database (HMDB). http://www.hmdb.ca/ (last accessed date September 13, 2017).

Tije, A.J., Verweij, J., Loos, W.J., Spareboom, A. (2003). Pharmacological effects of formulation vehicles implications for cancer chemotherapy. *Clin Pharmacokinet, 42*, 665–685.

Tomida, H., Yotsuyananagi, T., Ikeda, K. (1978). Solubilization of steroid hormones by polyoxyethylene lauryl ether. *Chem Pharm Bulk, 26*(9), 2832-2837.

Trotta, M., Pattarino, F., Gasco, M.R. (1996). Behaviour of erythrocytes in the presence of monoalkylphosphates. Pharmazie, 51(3), 192-193.

Tscharnuter, W. (2006). Photon Correlation Spectroscopy in Particle Sizing. In: Meyers, R.A. ed. Encyclopedia of analytical chemistry. Chichester: Willey. p. 5469-5485.

Ujhelyi, Z., Fenyvesi, F., Varadi, J., Feher, P., Kiss, T., Veszelka, S., Bacskay, I. (2012). Evaluation of cytotoxicity of surfactants used in self-micro emulsifying drug delivery systems and their effects on paracellular transport in Caco-2 cell monolayer. *Eur J Pharm Sci, 47*(3), 564-573.

Vezocnik, V., Rebolj, K., Sitar, S., Ota, K., Tusek-Znidaric, M., Strus, J., Sepcic, K., Pahovnik, D., Macek, P., Zagar, E. Size fractionation and size characterization of nanoemulsions of lipid droplets and large unilamellar lipid vesicles by asymmetric-flow field-flow fractionation/multi-angle light scattering and dynamic light scattering. *J Chromatogr A, 1418*, 185-191.

Vortherms, A.R., Doyle, R.P., Gao, D., Debrah, O., & Sinko, P.J. (2008). Synthesis, characterization, and in vitro assay of folic acid conjugates of 3'-azido-3'-deoxythymidine (AZT): toward targeted AZT based anticancer therapeutics. *Nucleosides Nucleotides Nucleic Acids, 27*(2), 173-185.

Wade, A., Weller, P.J. (1994). Handbook of Pharmaceutical excipients. 2nd edition, Vol. 1. The Pharmaceutical Press, The American Pharmaceutical Association, London.

Wan, H., Willians, R., Doherty, P., Williams, D.F. (1994). A study of the reproducibility of the MTT test. *J Mater Sci-Mater M, 5*, 154-159.

Wang, S., Lee, R.J., Cauchon, G., Gorenstein, D.G., Low, P.S. (1995). Delivery of antisense oligodeoxyribonucleotides against the human epidermal growth factor receptor into cultured KB cells with liposomes conjugated to folate via polyethylene glycol. *Proc Natl Acad Sci, 92*,3318-3322.

Waranyoupalin, R., Wongnawa, S., Wongnawa, M., Pakawatchai, C., Panichayupakaranant, P., Sherdshoopongse, P. (2009) Studies on complex formation between curcumin and Hg(II) ion by spectrophotometric method: A new approach to overcome peak overlap. *Central Eur J Chem, 7*(3), 388-394.

Warisnoicharoen, W., Lansley, A.B., Lawrence, M, J. (2003). Toxicological evaluation of mixtures of nonionic surfactants, alone and in combination with oil. *J Pharm Sci, 92*(4), 859-868.

Warisnoicharoen, W., Lansley, A.B., Lawrence, M.J. (2000a). Nonionic oil-in-water microemulsions: the effect of oil type on phase behaviour. *Int J Pharm, 198*, 7-27.

Warisnoicharoen, W., Lansley, A.B., Lawrence, M.J. (2000b) Light-scattering investigations on dilute nonionic oil-in-water microemulsions. *AAPS Pharmsci, 2*(2), 1-11.

Wasutrasawat P. Formation and physicochemical properties of nonionic oil-in-water nanoemulsions containing liquid and solid triglyceride. PhD Thesis, Chulalongkorn University, 2011.

Wasutrasawat, P., Al-Obaidi, H., Gaisford, S., Lawrence, M. J., Warisnoicharoen, W. (2013). Drug solubilisation in lipid nanoparticles containing high melting point triglycerides. *Eur J Pharm Biopharm, 85*(3 Pt A), 365-371.

Whiddon, C., Soderman, O. (2001). Unusually large deuterium isotope effects in the phase diagram of a mixed alkylglucoside surfactant/water system. Langmuir, 17(6), 1803-1806.

Wooster, T., Golding, M., Sanguansri, P. (2008). Impact of oil type on nanoemulsion formation and Ostwald ripening stability. *Langmuir, 24*, 12758-12765.

Yao, J., Wang, D., Zhang, X., Booth-Genthe, C., Zhu, P., He, L. (2012). Development of docetaxel self-microemulsifying drug delivery system (SMEDDS) for parenteral delivery: preparation, characterization and in vivo evaluation. *Asian J Pharm Sci, 7*(4), 18-27.

Yilmaz, E., Borchert, H.H. (2005). Design of a phytosphingosine-containing, positively-charged nanoemulsion as a colloidal carrier system for dermal application of ceramides. *Eur J Pharm Biopharm, 60*, 91-98.

Yin, Y.M., Cui, F.D., Mu, C.F., Choi, M.K., Kim, J.S., Chung, S.J., Shim, C.K., Kim, D.D. (2009). Docetaxel microemulsion for enhanced oral bioavailability: preparation and in vitro and in vivo evaluation. . *J Control Release, 140*, 86-94.

Yuan, Y., Gao, Y., Zhao, J., Mao, L. (2008). Characterization and stability evaluation of β-carotene nanoemulsions prepared by high pressure homogenization under various emulsifying conditions. *Food Res Int, 41*(1), 61-68.

Zargar-Shoshtari, S., Wen, J., Alany, R.G. (2010). Formulation and physicochemical characterization of Imwitor 308 based self microemulsifying drug delivery systems. *Chem Pharm Bull, 58*(10), 1332-1338.

Zielinski, R.G., Kaler, E.W., Paulaitis, M.E. (1995). Microstructure in D_2O/*n*-hexaethylene glycol monododecyl ether ($C_{12}E_6$)/CO_2 mixtures determined by small-angle neutron scattering. *J Phy Chem, 99*, 10354-10358.

Zsila, F., Bikádi, Z., Simonyi M. (2003). Unique, pH-dependent biphasic band shape of the visible circular dichroism of curcumin–serum albumin complex. *Biochem Biophys Res Commun, 301*(3), 776-782.

Zulauf, M., Weckstrom, K., Hayter, J.B., Degiorgio, V., Corti, M. (1985). Neutron scattering study of micelle structure in isotropic aqueous solutions of poly(oxyethylene) amphiphiles. *J Phys Chem, 89*(15), 3411-3417.